

**MOLECULAR CHARACTERIZATION OF LYTIC
BACTERIOPHAGE SPECIFIC TO MULTI DRUG
RESISTANT BACTERIA AND
PHARMACOKINETICS OF PHAGE IN
BIOLOGICAL MODEL**



**A THESIS SUBMITTED TO THE
CENTRAL DEPARTMENT OF BIOTECHNOLOGY
INSTITUTE OF SCIENCE AND TECHNOLOGY TRIBHUVAN
UNIVERSITY NEPAL**

**FOR THE AWARD OF
DOCTOR OF PHILOSOPHY
IN BIOTECHNOLOGY**

**BY
GUNARAJ DHUNGANA**

SEPTEMBER 2022

RECOMMENDATION

This is to recommend that **Gunaraj Dhungana** has carried out research entitled **“MOLECULAR CHARACTERIZATION OF LYTIC BACTERIOPHAGE SPECIFIC TO MULTI DRUG RESISTANT BACTERIA AND PHARMACOKINETICS OF PHAGE IN BIOLOGICAL MODEL”** for the award of Doctor of Philosophy (Ph.D.) in Biotechnology under my supervision. To my knowledge, this work has not been submitted for any other degree.

He has fulfilled all the requirements laid down by the Institute of Science and Technology (IOST), Tribhuvan University, Kirtipur for the submission of the thesis for the award of Ph.D. degree.

Prof. Dr. Rajani Malla

Supervisor

Designation: Professor of Microbiology

Central Department of Biotechnology

Tribhuvan University

Kirtipur, Kathmandu, Nepal

November 2021

LETTER OF APPROVAL

Date:

On the recommendation of Prof. Dr. Rajani Malla this Ph. D. thesis submitted by Gunaraj Dhungana entitled **“MOLECULAR CHARACTERIZATION OF LYTIC BACTERIOPHAGE SPECIFIC TO MULTIDRUG RESISTANT BACTERIA AND PHARMACOKINETICS OF PHAGE IN BIOLOGICAL MODEL”** is forwarded by Central Department Research Committee (CDRC) to the Dean, IOST, T.U.

.....

Prof. Dr. Krishna Das Manandhar.

Professor,

Head, Central Department of Biotechnology,

Tribhuvan University

Kirtipur, Kathmandu

DECLARATION

Thesis entitled **“MOLECULAR CHARACTERIZATION OF LYTIC BACTERIOPHAGE SPECIFIC TO MULTIDRUG RESISTANT BACTERIA AND PHARMACOKINETICS OF PHAGE IN BIOLOGICAL MODEL”** which is being submitted to the Central Department of Biotechnology, Institute of Science and Technology (IOST), Tribhuvan University, Nepal for the award of the degree of Doctor of Philosophy (Ph.D.), is a research work carried out by me under the supervision of Prof. Dr. Rajani Malla, Central Department of Biotechnology, Tribhuvan University.

This research is original and has not been submitted earlier in part or full in this or any other form to any university or institute, here or elsewhere, for the award of any degree.

Gunaraj Dhungana

ACKNOWLEDGEMENTS

With immense delight, I record my sincerest gratitude and indebtedness to my supervisor **Prof. Dr. Rajani Malla**, who has supported me throughout my Ph.D. life with her patience, expertise, and keen supervision. She had granted me enough freedom to explore on my own and at the same time, the guidance to pull through when my steps faltered. Thank you, Madam! for everything and your kind support throughout my Ph.D. career.

I sincerely thank **Prof. Dr. Krishna Das Manandhar**, Head, Central Department of Biotechnology, for his advice and valuable suggestions during animal model experiments and for providing a delightful environment to conduct research projects smoothly. I am also thankful to all faculty members Prof. Dr. Tribikram Bhattarai, Prof. Dr. Mohan Kharel, Prof. Dr. Tilak Ram Shrestha, Prof. Dr. Ganga Kharel, Dr. Gauri Shankar Manadhar, Dr. Jarina Joshi, Dr. Suresh Subedi, Dr. Smita Shrestha, Miss Pragati Pradhan, Mrs. Preeti Regmi and Mrs. Alina Sapkota for their support and feedback. I would also like to express my sincere gratitude to Dr. Pramod Aryal for his valuable suggestion and guidance.

I am grateful to **Dr. Sankar Adhya**, Laboratory of Molecular Biology, NCI, National Institute of Health, USA, who believed me and granted me an opportunity to work in his prestigious lab. Without his support, collaboration and guidance, I would not succeed in all the works especially electron microscopy, genome sequencing, and molecular cloning that are presented in this dissertation. **Dr. Manoj Rajaure, NCI, NIH** was the backbone of my Ph.D. project. I have learned a lot from him during my NIH stay. He has instilled in me the fundamentals of basic science and the importance of understanding the concept before launching into any research. Without his time and effort, this project could not have been a reality. He has encouraged and mentored me right from the basics to the advanced knowledge required to accomplish the tasks. I am indebted to both Dr. Adhya and Dr. Rajaure for allowing me to be a part of their group, leading me in the completion of my Ph.D. project, and providing me with a life-changing experience of working and living in the USA. A huge debt is owed to lab members of Adhya's lab, NIH, for providing a stimulating and fun-filled working environment in the lab which is envied by many. My thanks to Dr. Subash Verma, Dr.

Dale Lewis, Dr. Shayla Hesse, Dr. Xiaoli Weng, Joy Johnson, Andrei Trostel, and Phuoc le.

I am grateful to **Dr. Roshan Lal Shrestha**, NCI, NIH, for his every help and support for NIH pre-doctoral fellowship. My bunch of good words of appreciation to **Mr. Roshan Nepal**, (Ph.D. Candidate, The University of Adelaide, Australia) who first started the phage research in the department and helped me effortlessly in every aspect of the research and publications. I would also like to extend my appreciation to the phage research team at CDBT, TU, particularly, Apshara Parajuli, Archana Maharjan, Madhav Regmi, Prashant Poudel, Elisha Upadhyay, Indu Gyanwali, Himani Upreti, Yujeeen Chapagain. My special thanks to Mr. Kapil Dev Neupane for his generous support during the animal trials. Though I cannot thank every colleague who has helped me through my Ph.D. work; however, special mention goes to Mr. Rajindra Napit for qPCR analysis and National Public Health Laboratory (NPHL), Teku, for providing clinical strains.

I would also like to express my sincere appreciation to the University Grant Commission (UGC), Nepal, and Nepal Academy of Science and Technology, for Ph.D. fellowship and research grants. This research would not have come this far without support from NIH Pre-doctoral Intramural Research Training Award provided by the NIH, USA.

Last but not the least, I owe and dedicate my Ph.D. degree to my loving wife Sunita and my wonderful daughter Shriyana and son Shriyam. They have silently endured all the pain and anguish of my inability to be with them due to my work. My wife has done everything she could to facilitate my studies from the very beginning of my academic/professional carrier. She has been a true and great supporter and has unconditionally loved me during my good and bad times. The final stages of my Ph.D. have not been an easy ride personally. She has been a pillar of strength for me. I am also thankful to my late parents and my in-laws for their unconditional support and understanding since my early academic carrier. There are innumerable others whom I may unknowingly have not mentioned, I sincerely thank all of them for their help.

Gunaraj Dhungana
September 2022

ABSTRACT

The resistance developed by the *Enterobacteriaceae* family towards nearly all antibiotics including carbapenem has been intensely increasing worldwide with a higher prevalence in European and Asian countries. Thus, there is an urgent need for research and the development of new antimicrobial agents. Among various alternatives, a century-old treatment modality called bacteriophage therapy has recently resurfaced to mitigate the antibiotic crisis. Bacteriophages (or phages in short) are viruses that prey on specific bacteria and thus bear therapeutic potential. Phages are the most abundant entity in this biosphere, relatively easy to isolate, and a limited number of phages have been characterized for their therapeutic utility. Because of the poor understanding of newly isolated phages and the significant knowledge gap on phage-pathogen interaction in animal or human hosts, phage therapy is yet to be adopted in mainstream medicine. This research aimed to isolate, characterize and assess the therapeutic potential of novel lytic phages against multidrug-resistant clinical strains circulating in Kathmandu, Nepal. A total of twenty river water and sewage samples were collected from different locations in the Kathmandu valley and screened for the presence of phages against three carbapenem-resistant *Escherichia coli* and two *Klebsiella pneumoniae* clinical isolates (CIs). A total of three different phages of carbapenem-resistant *E. coli* and two different phages of carbapenem-resistant *K. pneumoniae* were fully characterized to their genomic level. Following isolation, a novel virulent *Klebsiella* phage named ϕ Kp_Pokalde_002 was evaluated for its therapeutic efficacy in clearing infection in a mouse model. The pharmacokinetics and pharmacodynamics along with immune response due to phage inoculation in mice were studied to underpin the safety and efficacy of phage therapy. Based on the morphological features of electron microscopy and whole-genome analysis, all of the *Escherichia* phages belonged to the *Myoviridae* family, and both *Klebsiella* phages belonged to the *Podoviridae* family. All of the isolated phages showed similar pH and thermal stability. The phage titer did not reduce significantly between pH 7 to 8 and temperature at 25 °C and 37 °C for up to 180 minutes. The isolated phages showed a similar short latent period (15-20 minutes) with a higher burst size of 74 to 127. All of the *Escherichia* phages were found to be a wide host range. However, both *Klebsiella* phages were found to be strictly host-specific. The genomes of all the phages were composed of linear, double-stranded DNA. The genome size of the *Escherichia* phages ranged from

162 to 164 kb in length with an average G+C content of about 40.6%. Similarly, both *Klebsiella* phages consisted of a small 42kb genome size with an average 53% G+C content. All of the five phage genomes were free from virulence factors and antimicrobial resistance genes. While characterizing the phages, we found that ϕ Kp_Pokalde_001 showed a mixture of plaque phenotypes with or without a halo surrounding the clear center. Interestingly, these two plaque phenotypes were reversible between phage generations regardless of their origin. We focused our attention to understand this dynamic. Genome sequencing led us to identify independent spontaneous mutations that were specific to the tail spike gene (gp53) responsible for modulating such phage behavior under laboratory conditions. We found that mutation in the tail spike protein had a dual effect influencing the depolymerase enzymatic activity and the phage adsorption kinetics.

In phage therapy experiments, both concurrent and one-hour delayed intraperitoneal (IP) treated mice were rescued with a survival rate of 100%, while mouse survivability was decreased to 40% via the oral route. The ϕ Kp_Pokalde_002 was disseminated into the systemic circulation within 1hr. of administration through both oral and IP routes. A higher phage count in blood was found after 4 hr. (2.3×10^5 PFU/mL) and 8 hr. (7.3×10^4 PFU/mL) of administration via IP and oral routes respectively. In the infection model, the bacterial load significantly decreased in the blood and other organs by 4-7 \log_{10} CFU/mL after 24 hr of phage therapy. The half-life of the ϕ Kp_Pokalde_002 was found to be shorter in presence of host bacteria suggesting rapid clearance of the phage. Similarly, administration of the ϕ Kp_Pokalde_002 alone in healthy mice did not increase the expression of pro-inflammatory cytokines (TNF- α and IL-6) mRNA levels in the blood. However, treatment with the phage showed a significant reduction of TNF- α and IL-6 mRNA expression caused by bacterial infection thus reducing the tissue inflammation. This result was also supported by histological examination of the lung tissues, where interstitial infiltration of inflammatory cells were remarkably reduced in the phage treatment group.

TABLE OF CONTENTS

DECLARATON	ii
RECOMMENDATION	iii
LETTER OF APPROVAL	iv
ACKNOWLEDGEMENTS	v
ABSTRACT	vii
LIST OF ACRONYMS AND ABBREVIATIONS	ix
LIST OF TABLES	xii
LIST OF FIGURES	xiii
TABLE OF CONTENTS	xvi
CHAPTER 1	1
INTRODUCTION	1
1.1 Introduction	1
1.2 Enterobacteriaceae	3
1.3 Alternative approaches to antibiotics	5
1.4 Bacteriophage	6
1.4.1 Caudovirales	7
1.5 Phage biology	9
1.5.1 <i>Life cycle</i>	9
1.5.2 <i>Lytic cycle</i>	9
1.5.3 <i>Lysogenic cycle</i>	10
1.6 Mechanism of bacteriolysis	11
1.7 Phage classification	12
1.8 Phage therapy	13
1.9 Rationale	15
1.10 Importance and national status of the phage research	16

1.11 Objectives	18
1.11.1 General objective	18
1.11.2 Specific objectives	18
CHAPTER 2	19
LITERATURE REVIEW	19
2.1 History of phage research	19
2.2 Phage ecology, evolution and genetic diversity	20
2.3 Bacterial defense against phage infection	22
2.4 Tail spike and tail fiber proteins	24
2.4.1 Phage encoded depolymerases	25
2.4.2 Structure of depolymerase enzyme	26
2.5 Reappraisal of phage therapy in the western countries	28
2.6 Phage therapy research in an animal model	28
2.7 Phage therapy research in human	30
2.8 Routes of phage application	33
2.9 Pharmacokinetics and pharmacodynamics of phage therapy	34
2.10 Host immunity against the phage	37
2.11 Limitations of phage therapy	38
2.11.1 Endotoxins:	38
2.11.2 Activity against intracellular pathogens:	38
2.11.3 Phage specificity:	39
2.11.4 Phage-induced bacterial evolution:	39
2.11.5 Phage resistance:	39
2.12 Recent advancement of phage therapy and commercial products	39
2.13 Challenges in the clinical use of phage therapy	42
2.14 Concluding remarks on literature review	44
CHAPTER 3	45

MATERIALS AND METHODS	45
3.1 Media and Bacterial strains	45
3.2 Sample collection and processing	45
3.3 Phage isolation and clonal purification	48
3.4 High titer phage lysate preparation	50
3.5 Phage concentrated by centrifugation method	50
3.6 Purification of phage lysate	51
3.7 Transmission electron microscopy (TEM)	51
3.8 Phage protein profiles by SDS-PAGE	51
3.9 One-step growth curve	52
3.10 Temperature and pH stability	52
3.11 Host range analysis	53
3.12 Genomic DNA extraction and sequencing	53
3.13 Safety Evaluation	54
3.14 Genome comparison and phylogenetic analysis	55
3.15 Assessment for depolymerase activity of ϕ Kp_Pokalde_001	55
3.16 Identification of the polysaccharide depolymerase gene	56
3.17 Plaque selection, PCR amplification of tail spike gene, and analysis	56
3.18 Cloning of tail spike gene (gp53) of ϕ Kp_Pokalde_001	56
3.19 Preparation of a Gibson assembly mix	57
3.20 Target tail spike gene (gp53) preparation	58
3.21 Expression constructs and cloning confirmation	58
3.22 Purification of the depolymerase enzyme and activity assay	59
3.23 Phage adsorption efficiency and adsorption kinetic assay.	60
3.24 Phage therapy experiments	60
3.24.1 Ethical clearance and animal model	60

3.24.2 Bacterial strain and phage used in an animal model experiment	61
3.24.3 Preparation of bacterial inoculums	62
3.24.4 Blood and Tissue Collection	62
3.24.5 Enumeration of the bacterial count	62
3.24.6 Enumeration of the phage count	63
3.24.7 Determination of minimum lethal Dose (MLD)	63
3.24.8 Pharmacokinetics (PK) of phage ϕ Kp_Pokalde_002	64
3.24.9 Cytokine quantification by qPCR	65
3.24.10 qPCR validation	67
3.24.11 Histological examination	67
3.24.12 Assessment of phage therapy in a mouse model	67
3.24.13 Positive control group	69
3.24.14 Data availability and statistical analysis	69
CHAPTER 4	71
RESULTS AND DISCUSSION	71
4.1 Phage isolation	71
4.2 Naming of the phages	73
4.3 Morphological characterization	76
4.4 Biological characterization of isolated phages	79
4.4.1 Host range profiles	79
4.4.2 Thermal and pH stability	82
4.4.3 One-step growth curve	84
4.4.4 Structural protein analysis	87
4.5 Genomic characterization	89
4.5.1 Genome properties and annotation of <i>Escherichia</i> phages	89
4.5.3 Toxins, virulence factors, or antimicrobial resistance genes	93
4.5.4 Phylogenetic analysis	95

4.5.5 Genome properties and annotation of <i>Klebsiella</i> phages	98
4.5.6 Phylogenetic analysis	102
4.5.7 Heterogeneity in plaque morphology of ϕ Kp_Pokalde_001	104
4.5.8 Bidirectional conversion in plaque phenotype	107
4.5.9 Change in plaque phenotype is linked to the amino acid substitution	110
4.5.10 Activity assay of spontaneous and selected mutations of the tail spike protein	113
4.5.11 Mutation in the tail spike merely affects the phage adsorption rate	116
4.6 Phage therapy experiments	120
4.6.1 Minimum lethal dose (MLD) determination	120
4.6.2 Efficacy of phage therapy in the mouse model	121
4.7 Pharmacokinetics	123
4.8 Pharmacodynamics	131
CHAPTER 5	137
CONCLUSION AND RECOMMENDATIONS	137
5.1 Conclusion	137
5.2 Recommendations and future perspectives	138
5.3 Limitations	139
CHAPTER 6	141
SUMMARY	141
REFERENCES	147

LIST OF TABLES

	Page No.
Table 1: Classification of principal categories of the phages	13
Table 2: The summary of clinical trials	33
Table 3: List of companies that are preparing phage and phage products	40
Table 4: Major challenges and possible solutions of phage therapy	43
Table 5: List of bacteria used in this study	46
Table 6: Water and sewage sample collection sites	47
Table 7: Dose of bacteria (Kp56) given to the mice to find out the lethal dose	64
Table 8: Real-Time PCR thermal cycler conditions for β -actin, IL-6, and TNF α	66
Table 9: Isolation of phages from different water/sewage samples	74
Table 10: Nomenclature of the novel phages	75
Table 11: Morphological characteristics and classification of isolated phages	78
Table 12: The latent periods and burst sizes of the phages	87
Table 13: Genome alignment of Myophages	92
Table 14: EMBL-EBI, HMMER analysis of ϕ Kp_Pokalde_001 gp 53	105
Table 15: Mutation and associated phenotype of the tail spike protein	112
Table 16: Additional mutation in the genome	112
Table 17: The effect in enzymatic activity of the protein	115
Table 18: Estimated pharmacokinetic parameters of virulent phage	127
Table 19: Inter mice variability (%CV) between the IP and oral routes	129

LIST OF FIGURES

	Page No
Figure 1: Deaths due to antimicrobial resistance every year by 2050	2
Figure 2: Alternative non-antibiotic approaches for bacterial infections	5
Figure 3: The founding fathers of phage research	7
Figure 4: Basic morphology of the three families of the Caudovirales	8
Figure 5: Schematic representation of the phage's life cycle	10
Figure 6: Bacterial defense mechanisms to phage infection	23
Figure 7: Phage depolymerase	25
Figure 8: Structure of the tail spike protein of KP32gp38	27
Figure 9: A timeline of important events of phage therapy	29
Figure 10: Map of sample collection sites	48
Figure 11: Representative pictures of water collection sites	49
Figure 12: Map of the cloning vector pBAD33	57
Figure 13: Schematic representation of the mouse model experiment design	61
Figure 14: Schematic representation of the PK/PD experiment design	65
Figure 15: Schematic representation of phage therapy in a mouse model	68
Figure 16: Different plaques morphology of phage observed in DLAA plates	72
Figure 17: Zoomed view of plaques morphology of isolated phages	73
Figure 18: Morphological characterization of <i>Escherichia</i> phages	77
Figure 19: Morphological characterization of isolated <i>Klebsiella</i> phages	78

	Page No
Figure 20: Host range profile of the <i>Escherichia</i> phages	80
Figure 21: Thermal stability of <i>Escherichia</i> and <i>Klebsiella</i> phages	83
Figure 22: pH stability of the phages	84
Figure 23: One-step growth curve of <i>Escherichia</i> and <i>Klebsiella</i> phages	86
Figure 24: SDS- polyacrylamide gel electrophoresis of phages	88
Figure 25: Circular genome view of <i>Escherichia</i> phages	91
Figure 26: Multiple genome alignment <i>Escherichia</i> phages by MAUVE	94
Figure 27: Phylogenomic trees of <i>Escherichia</i> phages	96
Figure 28: Circular genome view of <i>Klebsiella</i> phages	99
Figure 29: Multiple genome alignment of <i>Klebsiella</i> phages by MAUVE	101
Figure 30: Phylogenomic trees of the <i>Klebsiella</i> phages	102
Figure 31: Predicted 3D-model of <i>Klebsiella</i> phages' tail spike protein	103
Figure 32: Evolutionary analysis using tail spike protein	104
Figure 33: The BLASTN comparison of the ϕ Kp_Pokalde_001 genome	106
Figure 34: Predicted secondary structure of ϕ Kp_Pokalde_001TSP (gp53)	106
Figure 35: Halo and clear plaques of ϕ Kp_Pokalde_001	107
Figure 361: The bidirectional conversion of plaque phenotype	109
Figure 37: Lysis curve of <i>K. pneumoniae</i> (TUKP1) by the ϕ Kp_Pokalde_001	110
Figure 38: Genome of ϕ Kp_Pokalde_001 showing tail spike gene	110
Figure 39: Tail spike protein (gp53 of Pokalde_001) feature	111
Figure 40: Purification of the tail spike protein (Gp53)	114

	Page No
Figure 41: Alignment of residues in the segment of pectin lyase fold	116
Figure 42: Adsorption efficiency and adsorption kinetics	117
Figure 43: Determination of minimum lethal dose (MLD) of Kp56	121
Figure 44: Efficiency of phage therapy in a mouse model	122
Figure 45: Pharmacokinetics of ϕ Kp_Pokalde_002 in vivo	124
Figure 46: Area under the curve (AUC)	125
Figure 47: Half-life of ϕ Kp_Pokalde_002	126
Figure 48: Histology of mouse lung tissue sections	132
Figure 49: Pro-inflammatory cytokine TNF- α and IL-6 levels	134
Figure 50: Bacterial load in the blood and lung tissue	135

LIST OF ACRONYMS AND ABBREVIATIONS

AMR	: Antimicrobial Resistant
AST	: Antibiotic Susceptibility Test
BLAST	: Basic Local Alignment Search Tool
BLASTN	: Basic Local Alignment Search Tool – Nucleotide
bp	: Base pairs
CCR	: Center for Cancer Research
CDBT	: Central Department of Biotechnology
CDC	: Centers for Disease Control and Prevention
CDS	: Coding DNA Sequence
CFU	: Colony Forming Units
CRISPR	: Clustered Regularly Interspaced Short Palindromic Repeats
DDCT	: Delta Delta Cycle Threshold
DLAA	: Double Layer Agar Assay
DNA	: Deoxy Ribonucleic Acid
dsDNA	: Double-Stranded Deoxy Ribonucleic Acid
dsRNA	: Double-Stranded Deoxy Ribonucleic Acid
dpi	: Days post infection
EDTA	: Ethylene Di-amine Tetra acetic acid
EPA	: Environmental Protection Agency
EOP	: Efficiency of Plating
ESBL	: Extended Spectrum Beta Lactamase
FDA	: Food and Drug Administration
gDNA	: Genomic Deoxy Ribonucleic Acid
GC or G+C content	: Guanine – Cytosine content
GDP	: Gross Domestic Product
Gp	: Gene product
GPS	: Global Positioning Service
GRAS	: Generally Recognized as Safe
hpi	: Hours post infection
ICTV	: International Committee for Taxonomy of Viruses
IP	: Intraperitoneal
KDa	: Kilodalton

Kbp	: Kilo Base Pair
KPC	: Carbapenemases producing <i>K. pneumoniae</i>
LB	: Luria Bertani Broth
MBL	: Metallo Beta Lactamase
MDR	: Multi Drug-Resistant
MEGA	: Molecular Evolutionary Genetic Analysis
µg	: microgram [one billionth (1×10^{-9}) of a kilogram]
µL	: microliter [one millionth (1×10^{-6}) of a liter]
MHR	: Multiple Host Range
MTB	: <i>Mycobacterium tuberculosis</i>
mm	: Millimeter
MOI	: Multiplicity of Infection
MRSA	: Methicillin-Resistant <i>Staphylococcus aureus</i>
NA	: Nutrient agar
NCBI	: National Center of Biotechnology Information
ng	: Nanogram
NGS	: Next Generation Sequencing
NIH	: National Institute of Health
nm	: Nanometer
NPHL	: National Public Health Laboratory
OD	: Optical Density
ORF/ORFans	: Open Reading Frame
PBS	: Phosphate Buffer Saline
PHASTER	: Phage Search Tool Enhanced Release
PCR	: Polymerase Chain Reaction
PFU	: Plaque Forming Units
RBP	: Receptor Binding Protein
RNA	: Ribo Nucleic Acid
RPM	: Revolutions per Minute
SD	: Standard deviation
SDS-PAGE	: Sodium Dodecyl Sulfate Polyacrylamide Gel Electrophoresis
SM	: Sodium Chloride and Magnesium Sulfate
ssDNA	: Single-Stranded Deoxy Ribonucleic Acid
ssRNA	: Single-Stranded Ribonucleic Acid

TAE	: Tris-Acetate EDTA buffer.
TE	: Tris-Chloride EDTA buffer.
Tm	: Melting temperature
TSA	: Tryptic Soya Agar
TSB	: Tryptic Soya Broth
TEM	: Transmission Electron Microscopy
TUTH	: Tribhuvan University Teaching Hospital
UPGMA	: Unweighted Pair Group Method with Arithmetic mean
UTI: Urinary Tract Infections	
WGS	: Whole Genome Sequencing
WHO	: World Health Organization
XDR	: Extensively Drug-Resistant

CHAPTER 1

INTRODUCTION

1.1 Introduction

Antimicrobial resistance has now become one of the major challenges to the modern medicine globally. According to the World Health Organization (WHO), the world is heading towards a post-antibiotic era. By 2030, antimicrobial resistance (AMR) would be the cause of up to 24 million people being forced into extreme poverty (World Health Organization [WHO], 2017). A review on Antimicrobial Resistance presented by the British economist Jim O'Neill (2014) stated that by 2050, antibiotic resistance can cause 10 million deaths every year world-wide (Figure 1). It is reported that more than 2.8 million cases of antibiotic-resistant infections and 35,000 deaths due to the infections in the United States each year (Centers for Disease Control and Prevention [CDC], 2019).

Many new classes of antibiotics were developed after the discovery of penicillin in 1928 by Alexander Fleming and this period is often referred to as the “golden era” of antibiotic development. The infections were effectively controlled with the antibiotics in this era. However, over time, bacteria became resistant to all of the developed antibiotics (Dhingra et al., 2020). The discovery of a new class of antibiotics is time-consuming, and requires a huge fund. However, bacteria quickly become resistant to antibiotics, and will shortly be ineffective (Spellberg, 2014). The rate of developing a new class of antibiotics is much slower than that of the development of bacterial resistance today.

Antibiotic resistance is even more catastrophic in developing countries like Nepal due to the lack of diagnostic tools, indiscriminate use of antibiotics in humans, and unguided prophylactic use of antibiotics in the food and animal industry for profit. This leads to a high risk for the emergence and spread of antibiotic-resistant bacteria in humans in this region (Ayukekbong et al., 2017; Chereau et al., 2017; Yam et al., 2019). Moreover, the prevalence of low-quality antibiotics, clinical misuse, and over-the-counter antibiotics which is readily accessible as self-medication for the treatment of disease that does not essentially need antibiotics. Such activities may enhance the development of antibiotic resistance (Chokshi et al., 2019; Nepal & Bhatta, 2018).

AMR possesses a significant threat to human health so that the treatments become unsuccessful particularly in carbapenem-resistant *Enterobacteriaceae* (CRE), methicillin-resistant *Staphylococcus aureus* (MRSA), multidrug-resistant (MDR), and extensively drug-resistant (XDR) pathogens. WHO (2017) has also categorized these pathogens as a high priority for research and development of new antimicrobial agents. At the same time, a group of pathogens is often referred to as “ESKAPE” (*Enterococcus faecium*, *Staphylococcus aureus*, *Klebsiella pneumoniae*, *A. baumannii*, *Pseudomonas aeruginosa*, and *Enterobacter* species) are known to be the most common causes of life-threatening nosocomial infections globally. These bacteria have remarkable genomic plasticity enabling them to acquire antibiotic-resistant determinants which leads to several AMR outbreaks (Kempf & Rolain, 2012; Rice, 2008). The infections caused by these bacteria are once again becoming the second highest cause of death globally (Martens & Demain, 2017).

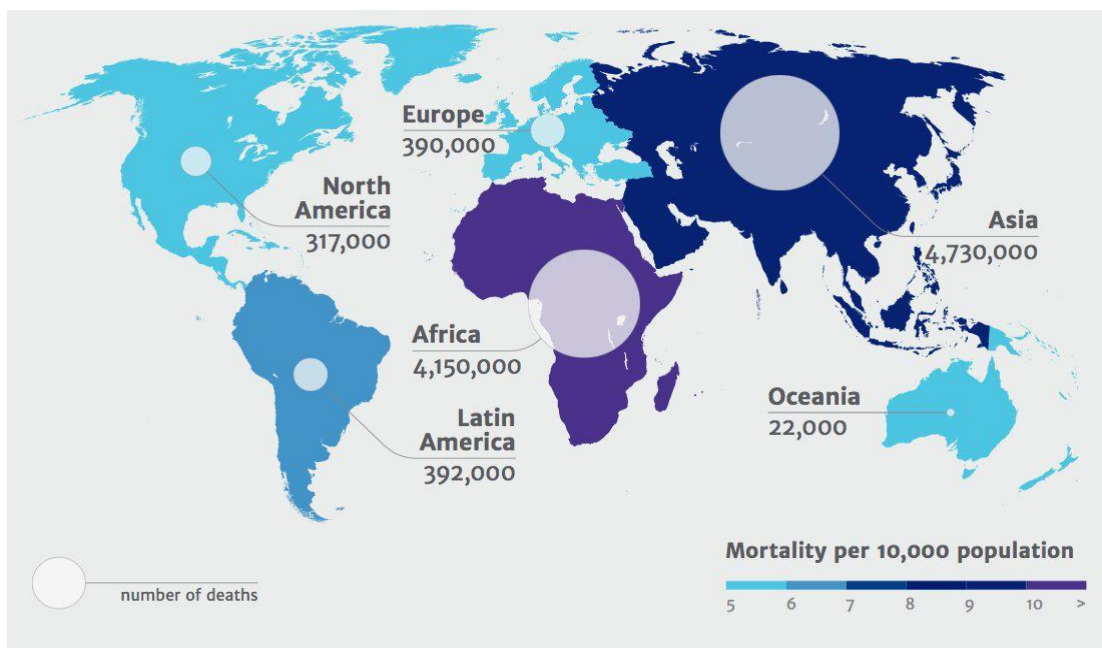


Figure 1: Deaths due to antimicrobial resistance every year by 2050. (Source: Review on Antimicrobial Resistance (O’Neill, 2014).

AMR is the ability of microorganisms to withstand the antimicrobial agents intended to kill them and thereby render those antibiotics ineffective. Bacterial resistance to antibiotics is both natural and inevitable (Ventola, 2015). The intrinsic factors like efflux pumps, biofilm formation, low outer membrane permeability, etc., and acquired

factors such as mutation, horizontal gene transfer, phenotypic changes, etc. are the main mechanisms leading to antibiotic resistance (Hawkey, 1998).

Multidrug-resistant infections lead to more severe illness, require extended hospitalization, and are associated with higher morbidity and mortality (Zhen et al., 2019). This increases the cost of treatments, impacts on overall public health condition, and increases substantial economic burden of the society (CDC, 2019). It is estimated that a total of \$100.2 trillion in world GDP will be lost by 2050 if appropriate measures are not taken (O'Neill, 2014). This implies that the achievement of modern medicine has already been threatened and the magnitude of AMR is increasing at an alarming rate. WHO has already stated that “The world is running out of antibiotics” (WHO, 2017), and the development of a cheap and reliable alternative to antibiotics is needed as there are only a few antibiotics are left. Sixteen new antibiotics were discovered and approved by the US FDA from 1983 to 1987. However, the discovery was dropped remarkably from 2008 to 2012, when only two antibiotics were approved for the treatment (Li & Webster, 2018). The discovery of new antimicrobial drug compounds is a challenging task. It is more complex and costly process and takes several decades for target identification. This has caused large pharmaceutical companies around the world to stop their investments in the field.

1.2 Enterobacteriaceae

Enterobacteriaceae comprises a large family of rod-shaped, gram-negative, and facultative anaerobic bacteria, with potential to cause human infections such as *Escherichia* spp., *Klebsiella* spp., *Salmonella* spp., *Shigella* spp., etc. Resistance developed by this family (also known as the “nightmare bacteria”) towards nearly all antibiotics have been intensely increasing worldwide with a higher prevalence in European and Asian countries including Nepal (Hsu et al., 2017; Nepal et al., 2017; Yam et al., 2019). These bacteria produce various enzymes such as *K. pneumoniae* carbapenemase (*KPC*), Metallo- β -Lactamases (*MBL*), and *OXA-48*-like, etc. which are capable of hydrolyzing carbapenem antibiotics rendering them to be ineffective for treatment (Suay-García & Pérez-Gracia, 2019). Within the *Enterobacteriaceae* family *Escherichia* and *Klebsiella* are the most commonly isolated as multi-drug resistant, and which caused about 0.5 million bloodstream infections and about 3.0 million serious infections globally (Tacconelli et al., 2018; Temkin et al.,

2018). Falagus et al. (2014) has also reported that the death due to carbapenem-resistant infections was 26% to 44%, which was significantly higher as compared to carbapenem-sensitive infections.

Klebsiella pneumoniae (*K. pneumoniae*) is a gram-negative, facultative anaerobic rod-shaped bacteria of genus *Klebsiella* within the family *Enterobacteriaceae*. *Klebsiella* spp. are one of the most frequently occurring pathogens in nosocomial and community-acquired infections and are often multidrug-resistant. About 6 to 7% of all nosocomial urinary tract infections (UTI) are caused by the *Klebsiella* spp. (Podschun & Ullmann, 1998). Most *Klebsiella* spp. can produce a thick capsule layer around the cell, which protects the bacteria from host defense system such as phagocytosis. The capsule is made up of a wide-ranging acidic polysaccharide, of which 77 different capsular serotypes have been described so far. Some capsular antigens, named K-antigens, have been identified as a higher pathogenicity and are frequently isolated from the clinical samples (Simoons-Smit et al., 1984). The pathogenicity of *K. pneumoniae* is multifactorial including capsular serotype, lipopolysaccharide, iron-scavenging systems, and fimbrial and nonfimbrial adhesions urease, outer-membrane proteins, and biofilms. Because of the collective threat of several virulence factors, *K. pneumoniae* has attained superbug status and is one of the most common antibiotic-resistant bacteria (Wu & Li, 2015).

Escherichia coli (*E. coli*) is the most common pathogen causing diarrhea, neonatal septicemia, urinary tract infection (UTI), bacteremia, and urosepsis. It is responsible for 80% of community-acquired UTIs and 30% of nosocomial infections (Lee et al., 2018). Extraintestinal *E. coli* is one of the leading causes of bloodstream infections and comprises 17–37% of all bacteria isolated from patients with bloodstream infections (Poolman & Wacker, 2016). Such strains have also been associated with ventilator-associated pneumonia (VAP), a most common life-threatening hospital-acquired infection (Messika et al., 2012). Bloodstream infections with extraintestinal *E. coli* are frequently associated with patients who have undergone major surgeries and were admitted for a long time in hospital (Johnson & Russo, 2002). Virulence is multifactorial and based on functional groups, the *E. coli* virulence factors can be categorized as adhesins, toxins, iron uptake, protectins, biofilms, and others, such as pathogenicity-associated islands (Nagarjuna et al., 2015).

1.3 Alternative approaches to antibiotics

Several alternative approaches have been made to mitigate this global AMR crisis in the present day (Figure 2). Along with a new class of antibiotic pipelines, several non-traditional alternative approaches such as direct-acting molecules (antibodies and phage endolysins), antimicrobial peptides, synthetic microbiota (engineered live bacteria), bacteriophages, herbal medicine, essential oils, heavy metals, CRISPR (clustered regularly interspaced short palindromic repeats) gene-editing techniques, etc. are gaining traction in the modern scientific community (Low et al., 2017; Reardon, 2015; WHO, 2019a).

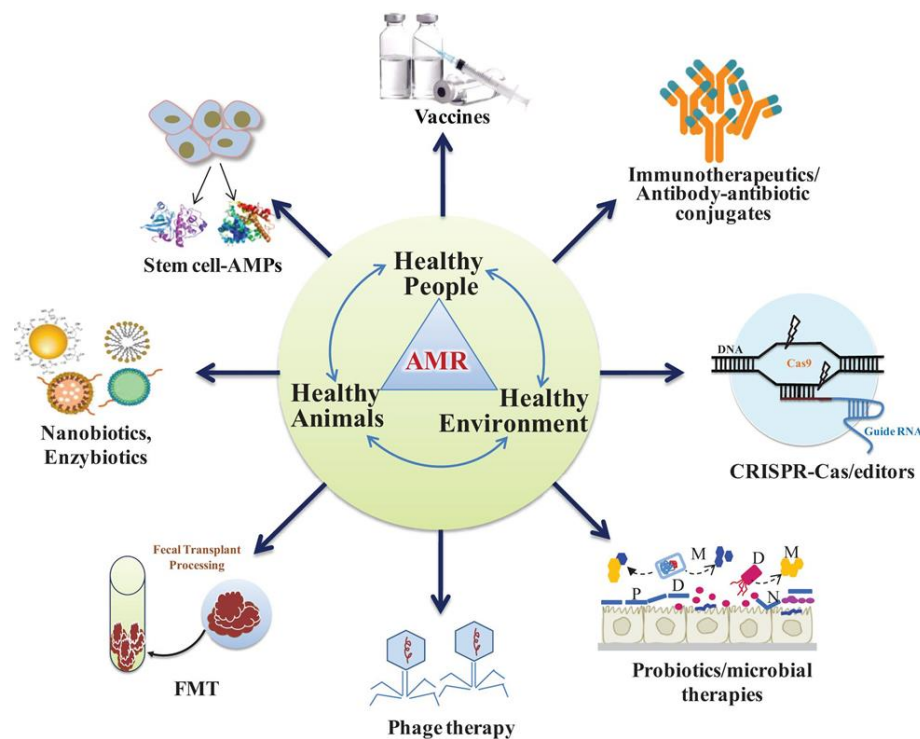


Figure 2: Alternative non-antibiotic approaches for bacterial infections. (Source: <https://www.frontiersin.org/articles/10.3389/fmicb.2021.609459/full>)

Antimicrobial peptides (AMPs) such as hepcidin, and LL-37 showed antibacterial properties against drug-resistant clinical pathogens (McCarthy et al., 2020). Another approach is to use immunotherapeutic biomolecules (such as pegfilgrastim, a granulocyte colony-stimulating factor) to bust and confer the host immunity against infections (Molineux, 2004). Gene editing using CRISPR-Cas9 technology has now been utilized to edit prokaryotes and eukaryotes genomes in recent years. Studies have shown that antibiotics resistant genes can be selectively removed from the bacteria with

the use of the CRISPR-Cas9 system (Bikard et al., 2014). Similarly, fecal microbiota transplant (FMT) is also considered an effective strategy to treat infections in gastrointestinal diseases (Suez et al., 2018). However, the use of FMT has a lot of ethical issues to get approval. The metal oxide-based nanoparticles are also being used as a promising antimicrobial agent. They act as a carrier for targeted drug delivery and at the same time they may have antibacterial properties of their own and are likely to be effective against antibiotic-resistant bacteria (Muzammil et al., 2018). The use of probiotics to control the gut microbiome is regarded as an alternative strategy. However, there is a lack of understanding of bacterial interaction with each other and with host animals (Aguilar-Toalá et al., 2018). Recombinant vaccines are also being used in highly pathogenic bacteria like *Clostridium difficile*, *Mycobacterium tuberculosis*, Group B *Streptococcus*, etc. (Kumar et al., 2021). Unfortunately, none of the above-mentioned approaches have been approved in the mainstream of medicine so far due to a lack of clinical data and consistent results.

Among many options, bacteriophages (phages in short) have now been recognized as potential candidates to combat AMR. The use of phages and their products for the treatment of bacterial infections is known as phage therapy and has been known for more than 100 years. About a decade before the discovery of the miracle drug penicillin, phage therapy was being practiced for the treatment of infections like *Shigella dysenteriae* (Chanishvili, 2012). However, following the discovery and wide applications of antibiotics during and after the second world war, interest and enthusiasm towards phage therapy declined in the western world. Limited knowledge of phage biology and poor documentation of phage therapy with a controversial success rate led to subsequent displacement of phage therapy by antibiotics (Abedon et al., 2011). However, it is regaining attention in the western scientific community as the modern knowledge of phage biology at genomic level recognize its use in mitigating the antibiotic resistance crisis (Young & Gill, 2015).

1.4 Bacteriophage

Bacteriophages are virus, obligatory intracellular parasites of bacteria. They exist as the most profuse and ubiquitous biological entities on the planet. It is reported that there are more than 10^{31} phage particles (virions) present in the biosphere (Clokier et al., 2011). Phages play a significant role in bacterial evolution and maintaining the

ecosystem (Clokie et al., 2011; Hendrix, 2002). They were co-discovered independently by Frederick William Twort in 1915, and Félix Hubert d’Hérelle in 1917 (Duckworth, 1976) (Figure 3) and named as bacteriophage by d’Hérelle, short for the Greek word "*phagein*", which means “to eat”. Structurally phages are made up of two biomolecules: proteins and nucleic acid or genome. The proteins, also known as capsid or head enclosed the nucleic acid within it and provides structure to the phage. Some of the phages may contain envelopes made up of lipid. The genome of the phages contains either DNA or RNA, which may be single or double-stranded size ranging from 3.5 kb (of MS2) to 500 kb (of phage G) (Kutter & Sulakvelidze, 2004). In addition to these, many phages contain other protein components like neck, tail tube, tail fibers, baseplates, etc., that are required for host recognition and infection. Approximately 96% of well-characterized phages are assigned to the *Caudovirales* order or tailed dsDNA phages (Ackermann, 2007). According to the International Committee on Taxonomy of Viruses (ICTV), “Virus Taxonomy: 2019 Release”, the *Caudovirales* comprises nine families, 44 subfamilies, 671 genera, and 1,967 species (Walker et al., 2019).



Figure 3: The founding fathers of phage research. Felix d'Herelle (1873-1949, left) and Frederick Twort (1850-1922, right). (Source: Wikipedia)

1.4.1 *Caudovirales*

As the name suggests *Caudovirales* (in Latin *cauda* means "tail") are tailed phages composed of the capsid (head) and tail with a similar overall organization. The capsid is exclusively filled with double-stranded DNA (dsDNA) as a genome that is connected to a tail by connector protein. The capsid is icosahedral symmetry (20 sides/12 vertices)

and composed of a single or double layer of morphological subunits called capsomeres. The size of the capsid ranges between 10 to 100 nm in diameter and genome size in between 17,000 to 725, 000 base pairs (bp) in length (Ackermann, 1998). *Caudovirales* are subdivided into three families, on the basis of tail morphology on the electron microscope. Among *Caudovirales*, 60% of phages with long, flexible tails are categorized as *Siphoviridae* family, 25% as *Myoviridae* family having contractile tails; and 15% are *Podoviridae* family with short, and stubby tails (Ackermann, 2007; Veesler & Cambillau, 2011).

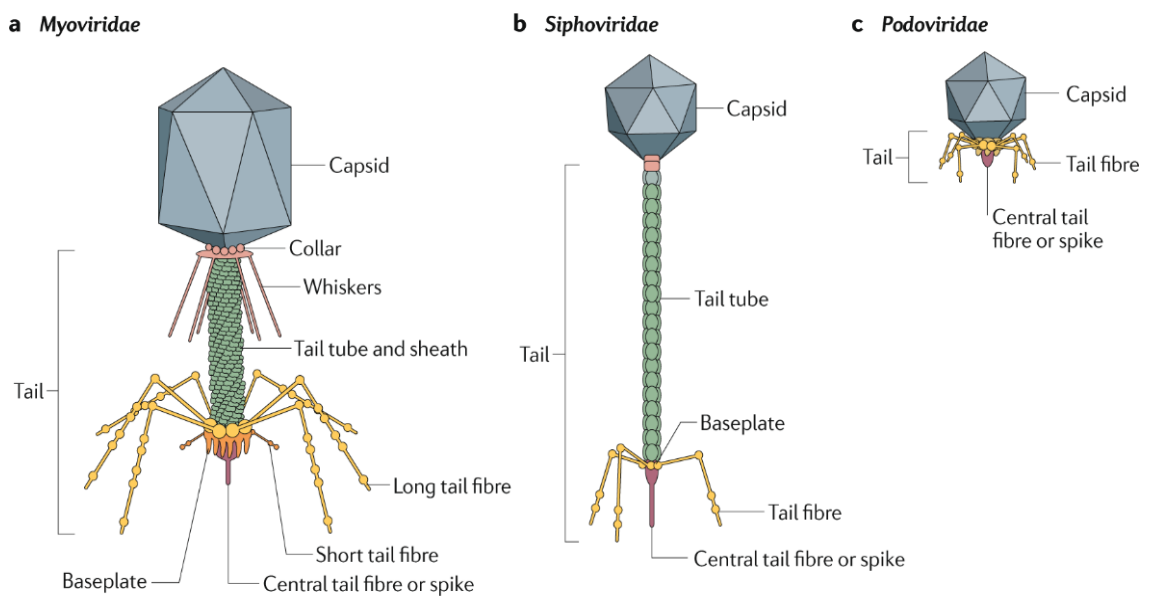


Figure 41: Basic morphology of the Caudovirales families: a) Myovirus (long, contractile tail) b) Siphovirus (long, non-contractile tail), and c) Podovirus (short tail). (Source: Nobrega et al.,2018)

The *Myoviridae* family comprises a long tail surrounded by a contractile sheath which is connected to the neck for instance phage T4 (Figure 4 a). Similarly, the *Siphoviridae* family contains a long and flexible but noncontractile tail eg. Coliphage T5 (Figure 4 b). The *Podoviridae* family has a very short non-contractile central tubular tail eg. phage T7 (Figure 4 c) with 6 or 12 tail fibers. The tail spikes/tail fiber protein present in this family usually exhibits a depolymerase activity that digests the capsular polysaccharides allowing the phage to attach with the receptor-binding protein of the host cell during infection (Hu et al., 2013).

1.5 Phage biology

1.5.1 Life cycle

Like other viruses, phages are obligatory parasites of bacteria. They essentially hijack the molecular machinery of the host bacteria to multiply within it. Based on the mode of replication, the phages are roughly categorized into lytic (virulent) and lysogenic (temperate) phages. The initial step in the replication process is the attachment of phage particle to their host specifically via receptors present in the host cell surface that determines its host specificity (Clokic et al., 2011). The receptor can either be capsular polysaccharides, protein (OmpA and OmpC), lipopolysaccharides (LPS), or flagella and pili of the host cell. Requirements of the highly specific receptors for adsorption make the phage unable to infect or multiply in eukaryotic cells. Initially, the attachment is reversible. Irreversible binding occurs with the help of other components present on the base plate of the phage (Rakhuba et al., 2010). After successful binding, the base plate undergoes conformational changes causing contraction and injection of the phage genome into the host cell known as penetration. Phage encoded enzymes such as lysozymes that are present on the tail fiber, hydrolyze β -1,4-linkages present in the N-acetylmuramic acid and N-acetyl-D-glucosamine of the peptidoglycan facilitates the penetration of bacteria cell envelope. After phage genome injection into the cells, it can go through different pathways such as lytic, lysogenic, pseudolysogeny, and chronic infections cycles as shown in Figure 5.

1.5.2 Lytic cycle

If the phage progeny is released by the lysis of its host bacteria, it is called a lytic cycle. Soon after the entrance of the genome into the bacterial cell, infectious phage particles undergo a dormant stage and are not found in and outside of the host, this period is called the eclipse period. In the lytic cycle, the eclipse period is very short (only several minutes). The phage genome takes over the cellular machinery (such as RNA polymerase) of the host bacterium immediately and arrests the gene expression of the host, followed by expression of phage genes and synthesizes viral proteins (Hausmann, 1988; Storms et al., 2014). The phage gene expression is highly coordinated and regulated by the phage promoters. Early genes encode mRNA, which is translated into the early proteins and required for DNA metabolism and shut off/destroy the host nucleic acids and protein synthesis. The middle and late genes are responsible for viral

replication and synthesis of the structural and lysis proteins. The synthesized structural proteins are then assembled and the nucleic acid is incorporated into a capsid forming new progeny phages finally, the viral particles are released from the host cell by rupturing it with the help of lysis proteins (Desplats & Krisch, 2003).

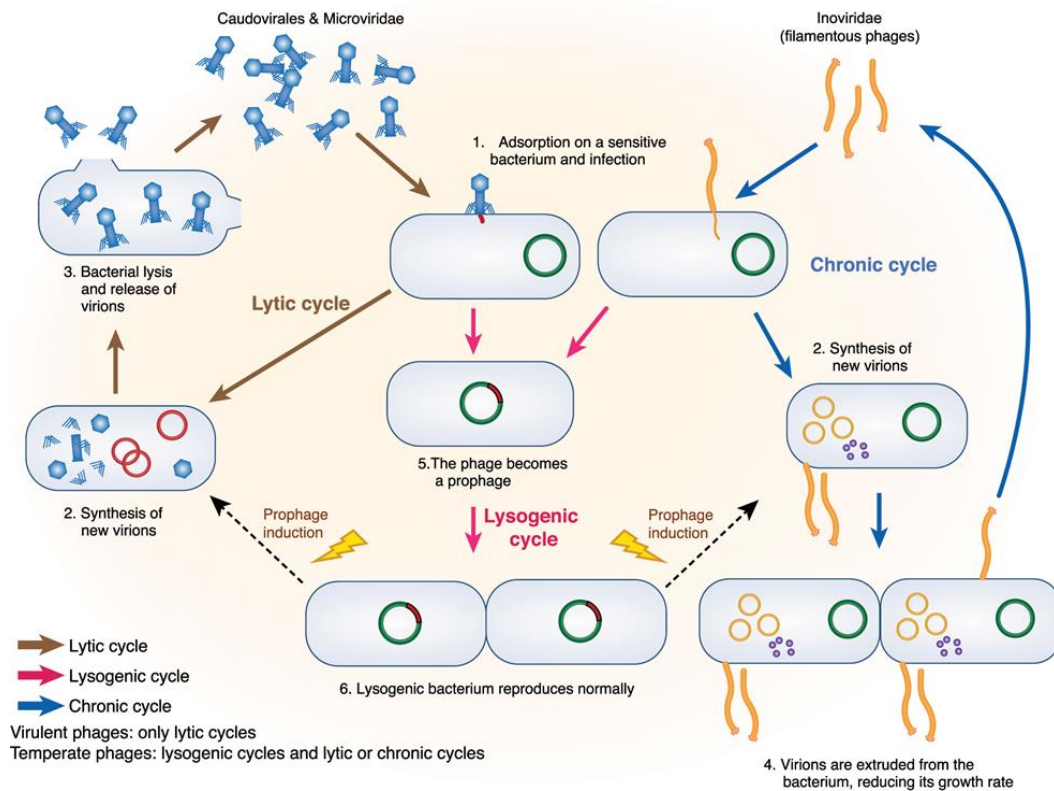


Figure 5: Schematic representation of the phage life cycle. New phage particles either go through the lytic cycles (left side in the Figure) or through chronic infection (blue arrows). When phage recognize and infect the targeted bacteria (1), followed by phage DNA replication and synthesis of new virions (2). In lytic cycles, new virions are released through bacterial lysis (3), while new virions of filamentous phages exit bacteria without bacterial lysis (4). Temperate phages, enter a dormant (prophage) state in the infected bacteria (5). The prophage, either integrated within the bacterial genome or in an episomal state, is replicated with the bacterial chromosome as long as bacteria divide (6).

(Source: <https://www.nature.com/articles/s41385-019-0250-5>)

1.5.3 Lysogenic cycle

During the lysogenic cycle, new phage particles are not produced, and the host cell is not lysed immediately. Instead, the phage genome is integrated into the host genome by transduction and stays as a prophage. The phage genome is multiplied cooperatively with the bacterial cell. Initially, the phage genome is circularized with the help of *cos*

sites present at both ends of the genome to prevent its degradation from the host. This circularized phage genome gets integrated into the host chromosome by site-specific recombination at the specific site (eg. lambda phage: attP of the phage DNA and attB of the bacterium). Transcription of the phage genome is shut down by the repressor protein which binds to the operator of the phage DNA. This integrated phage genome is known as prophage and the host cell is called a lysogen. The prophage remains dormant and replicates indefinitely as a segment of the host genome and makes the bacteria immune to superinfection. Under certain unfavorable, physiological, and chemical conditions such as UV radiation, temperature, mitomycin C, etc, the prophage can trigger the termination of the lysogenic state and cause the expression of the phage genome and the start of the lytic cycle (Ackermann, 1998; Campbell, 2003; Howard-Varona et al., 2017). When the host bacterium is exposed to starvation, the phage genome becomes unstable and inactive within the bacterial cytoplasm. This state is called pseudolysogeny. Under sufficient nutritional conditions, the pseudolysogeny may start lysogeny or lytic cycle (Ripp & Miller, 1997). Prolonged infecting phage may release the virus progeny from the host cell without lysing the host is called chronic or continuous infection. Filamentous phages may exhibit this phenomenon (Abedon, 2009). Some prophages may encode certain virulent genes such as botulinum neurotoxins C1, Shiga toxin, *Vibrio cholera* toxins, etc. This causes the host bacteria to become a virulent pathogen (Brüssow et al., 2004).

1.6 Mechanism of bacteriolysis

Lytic phages release phage progeny by lysing host bacteria at the end of their infection cycle. Following phage adsorption to the host bacteria, genomic material is injected into the host cell and the DNA undergoes replication, transcription, and translation into the virion proteins. Newly assembled phage progeny are ultimately released with the lysis of the host cells in the lytic cycle. Phage encoded proteins such as holin and endolysin are responsible for cell lysis. At the beginning of the lysis process, the holin accumulates in the cytoplasmic membrane to form large pores on it, which are called “holes”. This enables another protein endolysin, to escape from the cytoplasm which degrades the peptidoglycan layer. The endolysin act as a as a peptidoglycan-degrading enzyme (peptidoglycan hydrolase), hydrolyzes the glycosidic bonds of the amino-sugars and peptide bonds of the oligopeptide cross-linking chains of the peptidoglycan layer (Young, 1992). Another type of holin protein is called pinholin, which forms

small pores on the cell membrane and is associated with Signal-arrest-release (SAR) endolysins. The cell envelope of gram-negative bacteria comprises an additional membrane layer called the outer membrane. The lysis of this outer membrane is achieved by a spanin complex (i-spanin and o-spanin) (Young, 2014). This spanin complex connects the inner membrane (IM) and the outer membrane (OM) to cause fusion of these membranes and disruption of the outer membrane (with unknown mechanism) allowing the release of phage progeny from the host cell (Rajaure et al., 2015).

1.7 Phage classification

Phages are enormously diverse based on structural, physicochemical, and biological properties. Several schemes have been employed for the classifications of phages in the early days. Classification of phages is essential for understanding the relatedness of the phages to each other, identification of novel phages, and phylogenetic comparison. Soon after the discovery of the phages, they were classified based on host specificity. After the discovery of the electron microscope, morphological classification has been established. With the advent of molecular techniques, the phages were classified according to types of nucleic acid (RNA and DNA) (Nelson, 2004; Thomas & Abelson, 1966). The systemic and universally acceptable virus classification and taxonomy have been developed by the International Committee on Taxonomy of Viruses (ICTV), which was established in 1966. The first viral classification and taxonomy report was issued by ICTV in 1971. This report classified phages in six genera based on morphology and types of nucleic acid types (eg: T4, λ , T7, ϕ X174, MS2, and fd.). Over time, the ICTV has regularly updated the reports with many new orders, families, genus, species, etc. based on the phage morphological character, genome type, mode of replication, sequence similarity, pathogenicity, and host range (<https://talk.ictvonline.org/taxonomy/>). Classification of the principal categories of the phages based on morphology and genome type are summarized in Table 1. Phages are very diverse. Several thousands of phages have been studied under electron microscopy. Every year, 400-600 whole phage genome sequences are submitted to genebank. Types of the genome of the phage include single-stranded (ss) RNA, double-stranded (ds) RNA, ssDNA, and dsDNA. The shape and size of the phage capsid are determined by the size of the genome incorporated within it. In 2018, the ICTV report classified the phages into five families, 26 subfamilies, 363 genera, and 1,320

species. The most recent report issued by ICTV in July 2019 “Virus Taxonomy: 2019 Release” and ratified in march 2020, proposed a new order (Tubulavirales); 10 new families, 22 new subfamilies, 424 new genera and new 964 species (Adriaenssens et al., 2020).

Table 1: Classification of principal categories of the phages based on morphology and genome type according to the International Committee on Taxonomy of Viruses (ICTV).

Order	Family	Morphology	Genome	Examples
Caudovirales	Myoviridae	Non enveloped, long contractile tail	Linear dsDNA	T4, Mu, P1, P2
Caudovirales	Siphoviridae	Non enveloped, long noncontractile tail	Linear dsDNA	A, TS, HK97, N1S
Caudovirales	Podoviridae	Non enveloped, short noncontractile tail	Linear dsDNA	17,13, 029, P22
Levivirales	Leviviridae	Nonenveloped, isometric	Linear ssRNA	MS2 phage, Op
Petitvirales	Microviridae	Nonenveloped, isometric	Circular dsDNA	0X174
Tubulovirales	Inoviridae	Nonenveloped, filamentous	Circular ssDNA	M13 phage
Vinavirales	Corticoviridae	Nonenveloped, isometric	Circular dsDNA	PM2

1.8 Phage therapy

Phage therapy (PT) is the use of phages or their components for the treatment of bacterial infection as therapeutic agents. Phages naturally infect the bacteria and kill them in course of their lytic life cycles. Phage therapy exploits this lytic nature of the phage in the treatment of bacterial infection. Phages has been used in the treatment of infections soon after their discovery. The first therapeutic application of the phage was accomplished by Felix d’Herelle himself. He successfully treated a 12-year-old boy severely suffering from dysentery. Subsequently, he treated other patients having the same disease with successful results. D’Herelle mentioned in his book about the commercial production of phage for the treatment of cholera in India. During World

War II, phages were used among soldiers of the Soviet Union, German and Japanese armies particularly gangrene and dysentery (Sulakvelidze et al., 2001; Summers, 2012). About five D'Herelle, Hutinel's phage preparations namely Bacte´-coliphage, Bacte´-rhino-phage, Bacte´-intesti-phage, Bacte´-Pyo-phage, and Bacte´-staphy-phage against the various diseases were available commercially at that time (Sulakvelidze et al., 2001; Summers, 1999). In 1924, the Oswaldo Cruz Institute in Brazil initiated the production of phage as the medication for dysentery in Latin American countries. The phage preparations were also sent to the hospitals around Brazil too (Dublanchet & Bourne, 2007). After successful treatment of various infections in humans, the phage preparations were prepared and sold commercially by various companies such as Eli Lilly during the 19th century. The company produced phage therapeutics against bacterial pathogens such as *Staphylococci*, *Streptococci*, and *E. coli* (Sulakvelidze et al., 2001).

Despite the success and commercialization of phage preparation, phage therapy was not admired from the beginning. This was due to the lack of information about the phage itself, the inconsistent result in the treatment, and the lack of reproducibility (Wittebole et al., 2014). In the past, the use of phage as an antimicrobial agent was limited owing to a lack of extensive knowledge and research of phage biology, its molecular organization, and its application as a therapeutic agent. They used randomly uncharacterized phages in terms of lytic or lysogenic and most of the studies lacked standardized protocols. After Fleming's historic discovery of penicillin, antibiotics became popular due to their broad spectrum of killing and greater potency, and phage therapy was unfortunately marginalized in western countries (Fischetti et al., 2006). However, the rigor in phage-based research and its clinical application continued to persist in Eastern Europe like Poland, the former Soviet Republic of Georgia, and Russia (Wittebole et al., 2014).

The emergence of multi-drug resistant bacterial pathogens and their continuous spread in recent years has brought an urgency to search for a fast, reliable, and economic alternative to antibiotics (Sulakvelidze, 2011). Phages have been widely exploited and extensively studied with the advancement in sophisticated tools and technology to provide clear and concrete insights about phage therapy. Scientists are trying to implement the advancements of technology such as genetic engineering to give phage

therapy a new perspective and to overcome the problems it had in the past. Genetically engineered phage and purified phage lytic enzymes such as depolymerases, endolysin, etc. have shown a remarkable effect against multidrug resistance pathogen which gives a new direction to phage therapy. Two most prominent cases that were recently highlighted were the application of naturally isolated phages to treat necrotizing pancreatitis caused by multidrug-resistant *A. baumannii* and the application of engineered phage to treat the lung transplant patient with cystic fibrosis suffering from *Mycobacterium abscessus* infection (Dedrick et al., 2019; Schooley et al., 2017).

1.9 Rationale

In recent years, the treatment of bacterial infections has become complicated due to the resistance towards most of the available antibiotics including third and fourth generation cephalosporins and even colistin which is considered as the last resort drug (Johura et al., 2020; Sidjabat & Paterson, 2015; Thaden et al., 2016). As no new class of antibiotics has been developed since the 1980s, there is a necessity to investigate new antimicrobial agents. The WHO has also highlighted the carbapenem-resistant *Enterobacteriaceae* as a critical pathogen and urged to prioritize research and development of new antimicrobial agents (WHO, 2019b).

Among various alternatives, such as the use of antimicrobial peptides (AMP) and preventive probiotics (Ghosh et al., 2019), recently there has been a new excitement in the west due to the successful outcome of phage application to treat antibiotic-resistant bacterial infections (Schmidt, 2019). Though, there are several successful phage therapy cases reported over the last 10 years (Dedrick et al., 2019; Petrovic Fabijan et al., 2020; Pirnay, 2020; Schooley et al., 2017; Sybesma et al., 2018;); however, it is not adopted in the medicine. Besides regulatory hurdles, one of the possible reasons is lack of pharmacokinetics (PK) and pharmacodynamics (PD) knowledge of the phages *in-vivo*. Understanding of PK/PD of the phages to know the biodistribution, bioavailability, and immune response to phages *in-vivo* is necessary (Caflisch et al., 2019). Phage administration route and dosage must be evaluated and standardized for successful phage therapy (Dąbrowska, 2019; Nilsson, 2019; Payne & Jansen, 2003).

Phages from the different natural environments may conserve genetic identity and diversity regardless of their host (Hambly & Suttle, 2005). The complete sequence of the phage genome not only facilitate studies of phage ecology, evolution, biodiversity,

and genetic novelty (Hatfull & Hendrix, 2011) but also plays an important role in the development of modern molecular biology as well as a foundation of phage repository for future use in phage therapy and as a biocontrol agent. A large number of sequenced phage genomes have been deposited into public databases such as National Center for Biotechnology Information (NCBI). However, there are still some genomic orphans yet to be discovered. Furthermore, most of the well-studied phages were isolated and sequenced from the western world like America, Europe but very few numbers of phages that infect pathogenic strains have been well characterized and studied at a molecular level from southeast Asia, particularly from Nepal. This study provides insight into the enormous genetic and biological diversity of the *Escherichia* and *Klebsiella* phages via morphology and genome-based analysis. The present work is expected to provide information on the genome architecture, functional annotation as well as sequence homology of newly isolated *Myophages* (N=3) and *Podophages* (N=2) with other phage genomes isolated elsewhere. Sequence analysis also conformed the phage lifestyle, harboring virulent/toxic genes and antimicrobial-resistant genes, an important consideration for the possibility of phage in therapeutics and biocontrol. In addition, this study may help to carry out a deeper mechanistic study to identify the putative catalytic domain of the phage depolymerase enzyme. In this study, we evaluated the therapeutic efficacy along with PK/PD of a newly isolated *Klebsiella* phage (Kp_Pokalde_002) that infects carbapenem-resistant *K. pneumoniae* in a mouse model. The study provides the required data that can further be used to assess the possibility of phage therapy to treat multidrug-resistant infections in animals and probably in humans in future days.

1.10 Importance and national status of the phage research

Fifteenth Plan (Fiscal Year 2019/20 – 2023/24) Government of Nepal, National Planning Commission (2020) has stated that studies and research will be conducted in the fields of science and technologies, nanotechnologies, and biological sciences to make innovation consistent with the sustainable development goals by encouraging and promoting the use of emerging technologies. This work fits under these strategies and working policies. As phages can be used efficiently in modern biotechnology tools such as vehicles for DNA/protein vaccines, detection of bacterial pathogens, and as a phage display system. Moreover, they now have been proposed as an alternative strategy to treat antibiotic-resistant infections. Fighting antimicrobial resistance is not only our

national problem but a global crisis. We, people of developing countries, are facing burdens of drug resistance more than any other developed nation and thus we are obliged to search for an affordable and long-term solution to the problem. Phage therapy has been long neglected in the Western world because of long and strict guidelines. However, the use of phages in countries like Georgia and Poland has boosted our hope in our context. There are only a very few research works on phages in Nepal. The Central Department of Biotechnology, Tribhuvan University, has been leading phage research under Prof. Dr. Rajani Malla for the first time in Nepal since 2015. The focus of their research is the isolation, characterization, and application of therapeutic potential phage against multidrug-resistant clinical isolate and the establishment of a well-characterized phage repository in Nepal. Before starting this study, there were no published reports on phage at a molecular level from Nepal. Only a study conducted by Bhetwal et al. (2017) described isolation and host range analysis of potential phages against pathogenic bacteria. However, they did not characterize the isolated phages morphologically and genomically and did not ensure the phages were strictly lytic and safe for therapeutic application. Nepal is a virgin land for phage research. Some other institutions like Kathmandu University and the Institute of Medicine (IOM) have also been started phage research. The major obstacles in phage research in Nepal are a huge shortage of sophisticated instruments like electron microscopy facility and well-established molecular lab set-up till date.

1.11 Objectives

The main aim of this Ph.D. thesis has been isolation, purification, and characterization of lytic phages against multidrug-resistant clinical isolates circulating in Kathmandu, Nepal, and evaluation of the phage therapy efficacy, pharmacokinetics and pharmacodynamics *in-vivo*. The long-term goal is to establish a phage repository for the treatment of multidrug-resistant bacterial infections.

1.11.1 General objective

Isolation and characterization of lytic phages against multidrug-resistant clinical isolates and assess their therapeutic efficiency *in-vivo* model.

1.11.2 Specific objectives

1. Isolation of lytic phages against carbapenem-resistant *E. coli* and *K. pneumoniae* clinical isolates from the rivers/sewages of Kathmandu Valley
2. Characterization of the isolated phages based on their morphological, physicochemical, biological, and genomic properties to select the phages for therapeutic potential
3. Confirmation of the phages to be strictly lytic and identify possible toxins, and other virulent /antibiotic-resistant genes by the annotation and bioinformatic analysis of the phage genomes
4. Characterization of phage tail spike protein (phage depolymerase) potential use as an antimicrobial agent
5. Assessment of safety and efficacy of phage therapy, pharmacokinetics, and pharmacodynamics along with the immune response of the phage in a mouse model

CHAPTER 2

LITERATURE REVIEW

2.1 History of phage research

English bacteriologist Ernest Hanbury Hankin in 1896 had made the early presumptions of anti-bacterial properties against *Vibrio cholera* in the water of Ganges and Yamuna rivers in India (Abedon et al., 2011; Wittebole et al., 2014). Two decades later, Frederick Twort, a British bacteriologist, explained the interesting “glossy formation” of the micrococcus colonies in 1915. He stated that the “filterable agent” can kill the bacterial cultures and multiply in the presence of the bacteria. Despite his observation, he could not propose the exact mechanism and the exact name of that antibacterial substance as a bacterial virus at that time. Two years later, a French-Canadian microbiologist, Felix d'Herelle discovered a phage at the Institute Pasteur in Paris. He independently described a similar phenomenon during his study on bacillary dysentery. He observed that bacteria-free filtrate collected from sewage formed a clear circular area on the bacterial lawn, which he named ‘*taches verges*’ meaning ‘clear spots’. The scientific community around the world has accepted that both Frederick Twort and Felix d'Herelle independently discovered the phage. Soon after the discovery, Felix d'Herelle had also proposed the use of phages for therapeutic use in human and animal bacterial infections at the beginning of the 20th century.

After the discovery of phage, the scientific community around the world became interested to define its nature and biology. Felix d'Herelle himself first started the use of phage in the therapeutic purpose and expanded all over the world. The temperate phage was introduced by Bordet in 1925. Bail explained the insertion of hereditary material into the host bacteria. Several scientists studied the viral nature of the phage, interaction with the host, biochemical nature of the nucleoprotein, etc. This ultimately drove the development of modern molecular biology (Wittebole et al., 2014). After the discovery of the electron microscope (EM) in 1939, Dr. Helmut Ruska first visualized the image of the phage and described it as “sperm-shaped” particles attached to the bacterial membrane (Ruska, 1940). In the early 1940s, a group of scientists Viz: Max Delbrück, Emory Ellis, Salvador Luria, Alfred Hershey, and their colleagues, called “Phage Group” were very interested and continued their research on the phage. They

worked on the phage life cycle, replication and started using T- series phages of *E. coli* as model organisms. Finally, the legacy of the early scientists towards the phage research has made a dramatic revolution in the understanding of fundamental biology (Keen, 2015; Sulakvelidze et al., 2001). In recent years, phage and their products are being used as a molecular and diagnostic tool, in the food industry, vaccine delivery vehicles, phage display, antimicrobial drug discovery as well as in the treatment of multidrug-resistant infections.

2.2 Phage ecology, evolution and genetic diversity

Phages are found in every environment where their host is found. They play important roles in balancing bacterial population densities. Bacterial density determines the phage population. It is estimated total of 10^{31} phage population in the ocean and high titer in marine (10^9 particles/g), whey (10^9 particles/mL), animal feces (10^7 particles/g), terrestrial soil (10^7 particles/g), and in the air (10^5 particles/m³) (S. Chibani-Chennoufi et al., 2004). Several environmental factors affect phage's survival like the association with bacteria in solids or liquid environments, presence of organic matter, temperature, biofilms, pH and UV radiation, etc. Another aspect of phage ecology is a competition of phages for host and their lifestyle. Lytic phages rapidly increase their population as hosts continue to multiply. Temperate phages maintain the phage and host population balance. Thus, the phage plays a significant role in the bacterial ecology. Phages can alter the gene expression of the host which affects the bacterial phenotype, such as transduction of virulent/toxic genes that convert the host bacteria into nonpathogenic to pathogenic (Abedon, 2009; Gill & Abedon, 2003; Pantastico-Caldas et al., 1992). Phage-host interaction govern the evolution of both phage and bacteria. Bacteria evolve to be resistant phages as phages always provide a selective pressure to its host (Clokic et al., 2011). Phages have diverse genetic material with mosaic architectures due to complex evolutionary processes. The phage evolution is driven by several factors such as mutation, genetic drift, natural selection, recombination, horizontal gene transfer, and nonrandom mating (Gregory et al., 2016; Sanjuán & Domingo-Calap, 2019). The phage genome generally shares a common gene architecture. To date, most of the sequenced phage genomes comprise of double-stranded DNA displaying a mosaic composition of genes (Hatfull & Hendrix, 2011). Bacteria comprise up to 20% of prophage elements into their genome (Casjens, 2003). During evolution, the phage genes transfer by homologous recombination between a prophage and a lytic phage

within the host bacteria. Temperate phages may acquire novel genes during imprecise prophage excision which provides a diverse genetic pool for the homologous recombination triggering the phage genome evolution. Thus, the temperate phages are more diverse than the lytic phages (Abedon, 2009; Mavrich & Hatfull, 2017). Though the phages are very tiny, they play important roles in the ecosystems of the planet. They control the bacterial and other microorganisms' population, maintenance of biogeochemical cycles like carbon cycles, nitrogen cycles, and phosphorus cycles, which helps higher organism to live. Phages play an important role in understanding bacterial population dynamics, fundamental molecular biology, and evolution. They can be used as a source of diagnostic and genetic tools and also as a therapeutic agent (Clokie et al., 2011).

In recent years, with the advancement of new technology like genome sequencing, phage research has been moved towards genomic study. Based on the data deposited to the NCBI GenBank, phage genomes are significantly diverse. Each phage genome has a difference in nucleotide similarity with others even they infect the same host. It is estimated that approx. 10^{25} phages infect the host every second. Each infection possibly recombines with the bacterial and prophage DNA resulting in a novel genetic identity (Pedulla et al., 2003). Genomes of the Caudovirales encode 27 to 600 genes that are highly packed and clustered according to function. The gene expression is highly timed manner and expressed accordingly. Soon after the appearance of the phage genome into the bacterial cell, the host RNA polymerase (RNAP) binds to the promoter region of the phage genome. This initiates the transcription of the early genes that are involved in the modification of the host cells machinery and replication of the phage DNA. Replication of DNA is a semi-conservative model which may be unidirectional or bidirectional forming a long concatemer. The early proteins are highly phage-specific having no sequence similarity to the closely related phages (Roucourt & Lavigne, 2009). Some phages entirely depend on host RNAP while some phages encode their own RNAP such as *Autographiviridae*. The middle mRNA encodes proteins responsible for DNA metabolism and replication and are transcribed with the host or phage RNAP. Late mRNA encodes late structural proteins such as capsid, tail fibers, baseplates, etc. The genomes of the Caudovirales have different types of terminal structures such as (a) direct terminal repeat (e.g., phage T3/T7), (b) circularly permuted (e.g., phages T4, SPP1, P1, and P22), (c) host DNA containing to both ends

(e.g., phage Mu), (d) single-stranded cohesive ends (e.g., phages λ and P2). Some phage genomes such as T4-like genomes have conserved and hyperplastic regions. A large DNA segment that encodes structural proteins and DNA replication is highly conserved. These genomes consist of early, middle, and late promoters indicating a conserved transcriptional regulation (Nolan et al., 2006). The hypervariable regions are located between the conserved gene segments. Gene encoding tail fiber proteins significantly diverge in the T4-like genomes. Most of the sequenced phage genomes revealed one or more novel ORFans with no sequence similarity to the other genomes and are annotated as hypothetical proteins. These ORFans are thought to be responsible for controlling host activities and may be modified by the bacteria for their benefit (Comeau & Krisch, 2005).

When we consider the phage as a therapeutic agent, it is necessary to evaluate its genome to rule out the harmful genes such as toxins, antimicrobial resistant genes, and lysogeny markers (Barrow & Soothill, 1997; Skurnik et al., 2007). Well-characterized phages are needed for phage therapy to ensure genomic safety of the phage candidate as some phages may encode toxins producing genes (Shiga toxin (stx) by Stx phages, cholera toxin (ctx) in by CTX phages), AMR genes, and other VFs (Philipson et al., 2018). Phages are also associated with transduction which can transfer antibiotic resistant genes to the host bacteria (Abedon et al., 2011). Sequence analysis will determine the phage lifestyle, harboring virulent/toxic genes and antimicrobial-resistant genes, an important consideration for a possible phage in therapeutics and biocontrol. The USFDA has also specifically mentioned that the genomes should be free from genes which encode harmful toxins, for potential phage therapy candidates.

2.3 Bacterial defense against phage infection

There is a dynamic relationship between bacteria and phages. The phage infects the susceptible host bacteria to produce progeny phage. At the same time, bacteria evolve to defend themselves. Phage again counters evolved against these defenses resulting in the evolution and diversification of both phage and bacteria (Emond et al., 1998). Bacteria have some tactics to counter each step of the phage infection process such as adsorption, synthesis of phage protein, assembly, and release into the environment. These interactions and defense mechanisms can be categorized into three types: 1. Adsorption inhibition, 2. Restriction and 3. Abortive infections (Hyman & Abedon,

2010) as shown in Figure 6. The first line defense of the bacteria against phage infection is adsorption inhibition where the phage is prevented from attachment to inject the genomic material into the host cell. Phage surface structures such as tail fiber/spike proteins bind to different surface structures of the bacterial cell wall eg. ferrichrome membrane transport protein, FhuA, etc. during adsorption. Another strategy of bacteria to protect from phage infection is the blockage of phage receptors. (Labrie et al., 2010). Some bacteria such as *E. coli* and *K. pneumoniae* may have an exopolysaccharide capsular coat around the cell. Phages such as K1E and K1-5 have ability to degrade these polysaccharide capsules by virion-associated depolymerase enzymes to reach the cellular wall for infection (Leiman et al., 2007).

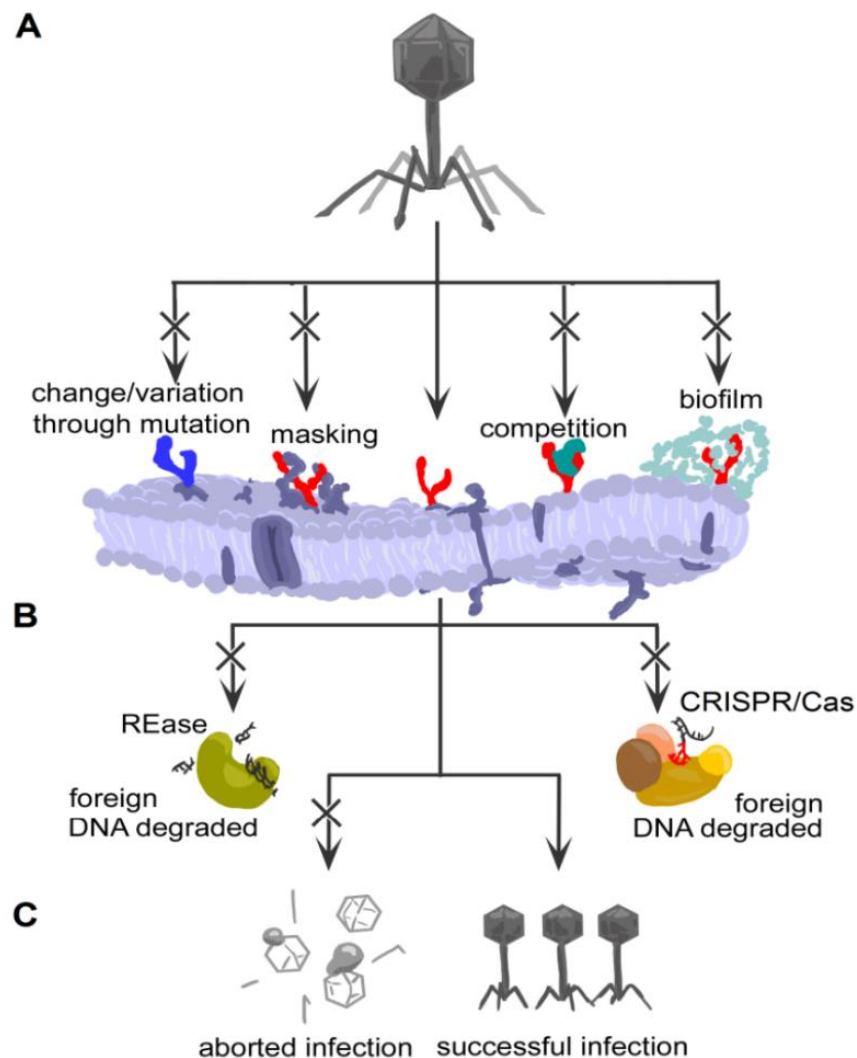


Figure 6: Bacterial defense mechanisms to phage infection. A) Adsorption inhibition, B) Restriction, C) Abortive infection. (Source: Harald Eriksson (2015)).

Biofilm, an external protective barrier, is produced by some bacteria which is a powerful defense mechanism for bacteria. These biofilms consist of secreted lipopolysaccharides, proteins, and DNA that protect the bacteria from phages and antibiotics (Hall-Stoodley et al., 2004). Bacteria can survive for a long time on the surfaces such as prosthetics, catheters, artificial implants, etc. which is often problematic in hospital settings (Kostakioti et al., 2013). Some phages have been encoded with tail-associated biofilm degrading enzymes called depolymerases. These enzymes can disrupt the biofilm and subsequently infect and replicate within the host cells (Cornelissen et al., 2011). Restriction modification (RM) is another bacterial defense system where foreign DNA is prevented from invading the cell. Phages have evolved through different strategies to escape degradation by host defense systems for instance base modification to prevent recognition, DNA masking, and blocking of the endonuclease (Samson et al., 2013). Similarly, the CRISPR-Cas system consists of genes encoding proteins such as Cas proteins, and a nucleotide array of clustered regularly interspaced short palindromic repeats (CRISPR) (Bondy-Denomy et al., 2013). The abortive infection systems typically allow a successful phage infection to progress normally and suddenly aborted, usually before the release of progeny viruses (Samson et al., 2013). During abortive infection, the infected cell arrest the phage infection and induce autolysis of the bacteria. Phage infection disrupts this homeostasis, and cell death follows (Blower et al., 2012).

2.4 Tail spike and tail fiber proteins

Phages belonging to the order of *Caudovirales* possess a tail complex attached to their capsid (Ackermann, 1998; Fokine & Rossmann, 2014). The remarkable diversity of phage tail structures is the key determinant of phage specificity to their host. This specificity is particularly driven by the receptor-binding domain (RBD) at the distal end of the tail structure necessary to recognize the host receptors. Phage tail complexes are the special molecular machines that are needed to recognize bacterial host cells to penetrate the cell envelope, and deliver its genome into the cytoplasm (Veesler & Cambillau, 2011; Xu & Xiang, 2017). Tail spike and tail fiber proteins recognize the bacterial cell surface ligands such as lipopolysaccharide (LPS), capsule polysaccharide (CPS), exopolysaccharide (EPS), teichoic acids, and surface porins and attached to it. These spikes and fiber proteins are composed of parallel homotrimers. The structure can be divided into three parts: 1. An amino-terminal containing three-helix bundles,

which connects to the base plate, 2. Middle slender shaft of β -helical domain and 3. Carboxy-terminal intertwined domain. In general, tail fibers do not have enzymatic activities (with exceptions). In contrast to tail fibers, tail spikes have an enzymatic activity to penetrate the thick layers of capsular polysaccharides (CPS), lipopolysaccharides (LPS), and exopolysaccharides (EPS) present in the outer surface of several pathogenic bacteria. These depolymerase enzymes depolymerize or degrade the bacterial surface polysaccharides to get access to the phage receptors located in the bacterial outer membrane allowing phage to access the underneath bacterial surface to initiate infection (Drulis-Kawa et al., 2015).

2.4.1 Phage encoded depolymerases

A depolymerase enzyme essentially cleaves and disintegrates the polysaccharide chain. It also acts as a structural component that facilitates phage adsorption to the bacterial cell surface (Figure 7). We can observe the activities of the phage-encoded depolymerase as a peripheral halo-like appearance around the plaque. Depolymerases are of two types: lyases and hydrolases. Both enzymes have high specificity to cleave the bacterial polysaccharides (CPS, LPS, EPS) into soluble oligosaccharides which may also determine the phage host range.

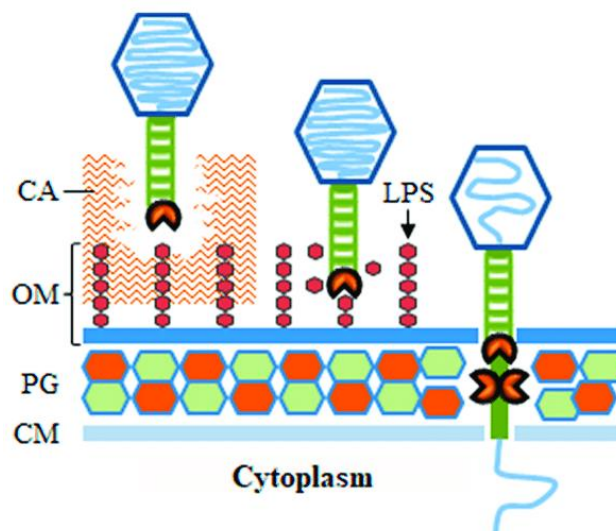


Figure 7: Phage depolymerases recognize and penetrate the bacterial cell envelope (Gram-negative bacteria used as an example). Depolymerase activity is generically depicted as a Pacman symbol. CM, cytoplasmic membrane; PG, cell wall peptidoglycan; OM, outer membrane; LPS, lipopolysaccharide; CA, capsule. (Source: Fernandes & São-José, 2018).

Well-characterized phage depolymerase active against EPS and LPS are lyases. The lyases cleave a glycosidic bond of the polysaccharides without using a water molecule. Lyases include hyaluronate, pectate/pectin, and alginate lyases. The pectin lyases degrade extracellular polysaccharides and hyaluronidases degrade hyaluronate of the bacterial capsules. While the hydrolases are members of the O-glycosyl hydrolases group which use a water molecule to cleave the O-glycosidic bonds of the polysaccharide. The hydrolase group includes sialidases, levanases, rhamnosidases, xylanases, and dextranases (Knecht et al., 2019; Latka et al., 2017).

One of the most well-characterized tail spike proteins is that of *Salmonella* phage P22, a model to study protein folding and stability (Betts & King, 1999; Seckler, 1998). It is a stable homotrimer comprised of three domains: an amino-terminal domain for capsid binding, a central catalytic domain containing right-handed helical turns, and a carboxy-terminal domain for trimerization. Structural comparison of tail spike protein from other phage members has indicated the conservation of protein scaffolds similar to that of the tail spike of P22 suggesting the modular exchange of receptor binding domains among phages of various groups has occurred in the course of phage evolution (Casjens & Molineux, 2012). Beyond the common structural scaffold of enriched α -helical turns present in the tail spikes, the mechanistic detail of the catalytic domain of the tail spike is not well understood. Recently, Squeglia et al. (2020) characterized the tail spike protein of phage KP32. They identified the important catalytic residues of a KP32gp38 (YP_003347556.1) tail spike protein based on the structural and *in silico* analysis. Phage KP32 is comprised of branched dual tail spikes gp37 and gp38 and can infect a *Klebsiella* host of serotypes K3 and K21, respectively (Majkowska-Skrobek et al., 2018).

2.4.2 Structure of depolymerase enzyme

The tail spike proteins are structurally complex fibrous proteins composed of parallel β -helix orthogonal to the long axis. They are highly stable maintaining their conformation in drastic conditions such as extreme heat, pH, and other biochemical environments (Jonczyk et al., 2011; Walter et al., 2008). The structure of the tail spike protein of phage KP32 gp38 (tail spike protein) is depicted in Figure 8. The proximal N-terminal domain connects to the tail fiber or base plate and the C-terminal domain works as a molecular chaperone and for receptor recognition. The middle domain is a

critical part of the enzyme which works as a host receptor and enzymatic activities to cleave the host polysaccharide. This structure consists of an enzymatic active site that recognizes the specific polysaccharide substrate. Specific catalytic pockets are formed in an elongated and highly interwoven β -helical domain of the enzyme. The N-terminal and C-terminal domains are remarkably conserved regions in the phages of similar families. However, the middle domain is extremely variable (Latka et al., 2019; Schwarzer et al., 2012; Stummeyer et al., 2006). Tail spike proteins with depolymerase activity are most prevalent among *Podophages* but are also identified among the Siphophages and *Myophages* (Pires et al., 2016). As such tail spikes associated with depolymerase specific to capsular types across bacterial genera of *Pseudomonas spp.*, *E. coli*, *A. baumannii*, and *K. pneumoniae* have been isolated and characterized (Hernandez-Morales et al., 2018; Knecht et al., 2019; Olszak et al., 2017; Wu et al., 2019). Owing to the great diversity of phages, some have even more than one tail spike protein in their tail machinery. For example, phage K1-5, a *Podovirus*, contains two tail spikes infecting two different capsular *E. coli* strains whereas a *Myophage* ϕ K64-1 encodes 11 tail fiber/spikes or lyase genes, out of which nine were functionally active against 10 different capsular types of *Klebsiella* species (Pan et al., 2017; Scholl et al., 2001). This suggests some phages have evolved by acquiring multiple genes encoding tail spike protein to broaden their host range.

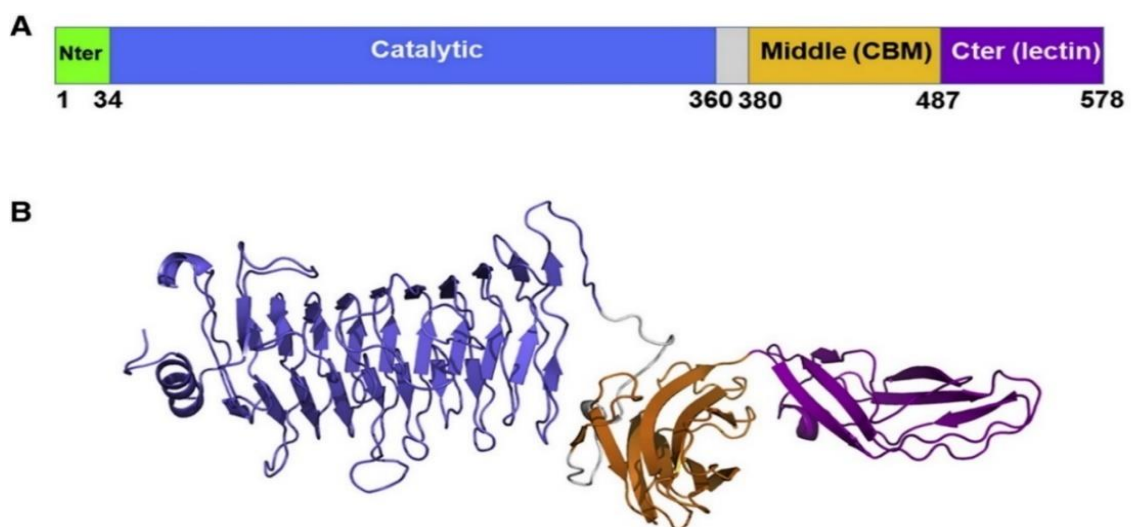


Figure 8: Structure of the tail spike protein of KP32gp38. A) Domain boundaries based on the crystal structure. B) Cartoon representation of the structure of a KP32gp38 monomer, representing the fold of each of the four protein domains, according to the color code in (A). Source: Squeglia et al. (2020).

2.5 Reappraisal of phage therapy in the western countries

In the mid twentieth century, with a poor understanding of phage biology and subsequent discovery of broad-spectrum antibiotics, interest in the therapeutic use of phage had declined. Phages were used only as a research tool in molecular biology (Clark & March, 2006). Presently, lytic phages have received keen attention as a potent antimicrobial agent to treat antibiotic-resistant bacterial infections (Clokie et al., 2011). Phage therapy has been recognized for more than a century. Recent knowledge of phage biology at molecular level, host immunology, and PK/PD have recognize its use to tackle the antibiotic resistance crisis (Young & Gill, 2015). Continuous research on phage and its understanding explores the application of phage in diverse fields such as food safety, agriculture, veterinary applications, environment sanitation, industry, and diagnostic purposes such as identification and typing of bacteria in human infections. Phages are not only used in humans to treat infections but they are also being developed for environmental prophylaxis; for example, to get rid of the pathogens in the environment and animals that could contaminate food supplies, to control infections in poultry production for the treatment of fish pathogens in aquaculture (Wernicki et al., 2017). Different studies have already showed the efficacy and safety of phage therapy in both animals and humans (Furfaro et al., 2018; Kumari et al., 2011; Pouillot et al., 2012; Vinodkumar et al., 2008; Wang et al., 2018). Phage therapy in humans is being used in countries like Poland, Russia, and Georgia. Other western countries like the USA, UK, Belgium, France, and Germany are also practicing the phage therapy sporadically as a personalized or compassionate use to treat antibiotic resistant infections (Pirnay et al., 2018; Romero-Calle et al., 2019). The timeline of the development of phage as a therapeutic agent to treat antibiotic-resistant infections is depicted in Figure 9.

2.6 Phage therapy research in an animal model

In recent years, phage research is mainly focused on cell line infection protection and phage rescue in an animal model. In the late twentieth century, H. Williams Smith and his colleagues started rigorous clinical phage therapy experiments in animal models to treat the infections of enterotoxigenic *E. coli* (ETEC). They successfully treated the infections in mice with phage as compared to antibiotics (Smith & Huggins, 1982). Similar successful studies have been performed to treat septicemia and meningitis caused by *E. coli* in chickens and colostrum-deprived calves (Barrow et al., 1998). They

had shown the phage can cross the blood-brain barrier. Experimental phage therapy using the mouse model had reported efficacy against up to 95% of all tested *S. aureus* (Golkar et al., 2014).

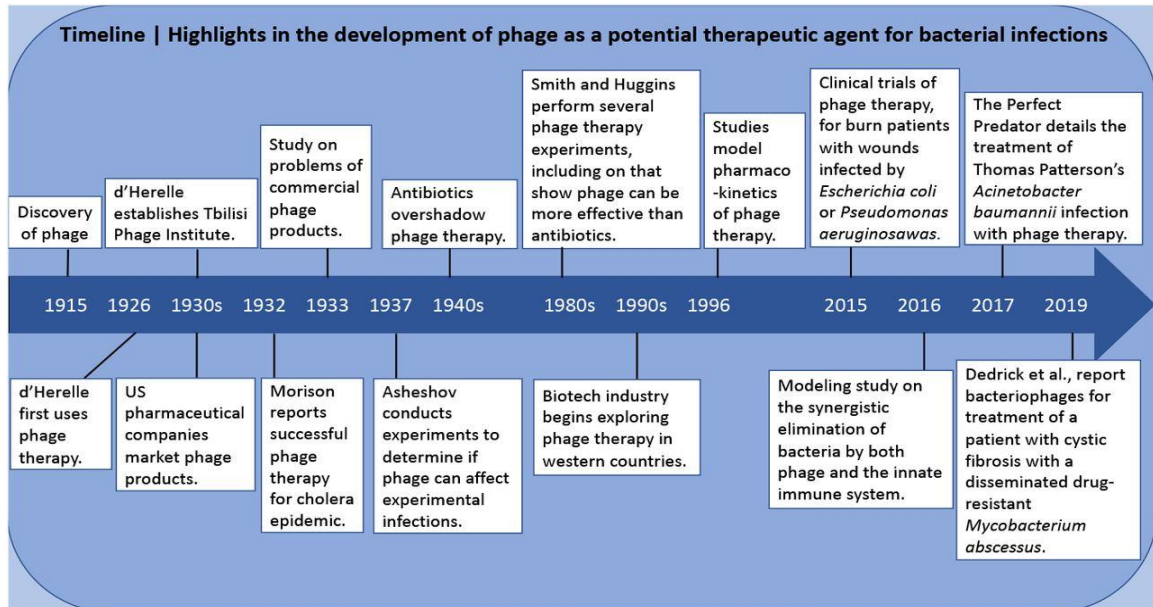


Figure 9: A timeline of important events in the history of phage therapy. (Source: Banuelos et al., 2020)

A study conducted in a HeLa cell line and BALB/c mice showed that the phage possesses no cytotoxicity and the phage was safe to use *in-vivo*. The HeLa cells were successfully rescued from the pan drug-resistant *A. baumannii* infection and the survival rate was similar to negative control even when the phage is applied after two hours of bacterial infection. Similarly, BALB/c mice have also accelerated the healing from localized infection of multi-drug-resistant *A. baumannii*. When a mouse challenged with *P. aeruginosa* developed gut-derived sepsis, phage therapy through oral route successfully rescued 66.7% of mice from mortality compared to the control group (Watanabe et al., 2007). In another study carried out in hamster model infected by *Clostridium difficile* a single dose of the phage reduced colonization of *C. difficile* after 36 hours of administration of the phage whereas control hamster treated with clindamycin died within 96 hours (Nale et al., 2015). In another study, it was also reported that phage administration restores the antibiotic sensitivity in multidrug-resistant *P. aeruginosa* (Chan et al., 2016). In addition, a group of mice treated with phage survived from the systemic infection of multidrug-resistant *A. baumannii* whereas untreated were died within a day of infection (Yin et al., 2017). Phages were

used as a singly and/or in a combination with phages as a cocktail, to ensure the phage's ability to cover the phage-resistant bacteria.

The immunogenicity of the phage candidate in animal models has been studied by several researchers. Capparelli et al. (2007), conducted an immune response of the *S. aureus* phage in a mouse model with an intravenous dose of 10^7 PFU at the interval of two weeks. They have found that the phages were present in the blood circulation for 21-25 days without neutralization of the phage activity. A similar result was reported by Roach et al. (2017) in a mouse model. They observed a high phage titer in the airways of the mice in the four days of phage administration with a single dose of (10^9 PFU) *Pseudomonas* phage. These reports suggest that animals could elicit phage-specific humoral immunity dependent on the route, dose, and time of administration.

The data presented above indicate that most of the phage therapy experiments were done using a mouse model and it is a logical choice to use the mouse model for this project. The mouse model has a high similarity with humans. They have been demonstrated that they can be easily handled and similar immune profile to humans.

2.7 Phage therapy research in human

Phage therapy research is not only limited to the animal model, many healthcare centers around the world provide phage therapy to patients infected with multidrug-resistant superbugs where antibiotics no longer work. Phage therapy centers in Georgia and Poland have been treating a patient having chronic infections caused by antibiotic-resistant bacteria for over 80 years with a 95% success rate (Kutter et al., 2010). In Poland, thousands of people have been treated with phages. With safety trials completed in 1959, Staphylococcal phage lysate (SPL) was licensed for human therapeutic usage and was successfully administered using different routes (intranasal by aerosol, topically, orally, subcutaneously, and also intravenously) (Golkar et al., 2014). Studies have also reported treatment of MRSA using phages which can be accomplished by local application for local infection or, if necessary, and with substantially more caution, more systemic dosing, including intra-peritoneally for systemic infections (Straub & Applebaum, 1933). Since phages can be applied as spray and MRSA resides on skin and nasal epithelial linings, phage therapy may work most efficiently without harming gut commensals. Also, in hospitals, as MRSA is transmitted by the use of contaminated equipment, phage spray may be a handy and

effective method to curb MRSA wherever it is most prevalent. A Soviet literature has shown that the phage therapy was used widely to treat bacterial infections of dermatology, ophthalmology, urology, stomatology, pediatrics, otolaryngology, and surgery (Chanishvili, 2012). While West and Europe halted the phage research Soviet Union 1940s, phage research was diverted to a more fundamental level. At the same time, phage continued development in the 1920s' and former Soviet Union countries like Russia, Georgia, and other Eastern European nations continually used phages therapeutically for the treatment of pathogenic bacterial infections that are resistant to antibiotics (Reardon, 2015).

Phage therapy is a century-old technique that fell out of its favor worldwide with the advent of antibiotics in the 1940s (Hume 1951). Phage therapy in humans is being considered a potential alternative as the bacteria become resistant to the last resort of available antibiotics. Several clinical trials have been reported in recent years. A randomized control trial (RCT) with phage therapy in 42 patients with chronic venous ulcers in leg showed that the phage has not been associated with any kind of harmful effect (Rhoads et al., 2009). Another randomized, double-blind, Phase I/II clinical trial was conducted in the UK. The result showed the phage significantly lowered the bacterial count without any adverse effect in chronic otitis caused by antibiotic-resistant *P. aeruginosa* (Wright et al., 2009).

A multinational company Nestle' funded a study on a randomized trial of phage therapy in children in Bangladesh in 2012. The study focused on the evaluation of the safety of oral phage therapy in children with acute bacterial diarrhea using commercial Russian coliphage products. They reported a safe gut transit of coliphage in children (Sarker et al., 2016). A project called PHAGOBURN funded by the European Union launched a Phase I-II clinical trial on the "Evaluation of phage therapy for the treatment of *E. coli* and *P. aeruginosa* burn wound infections" from 2013 to 2017. This was the world's first multicentric, randomized, single-blind, and controlled clinical trial of phage therapy. They included the burn patients hospitalized in Belgium, France, and Switzerland. They concluded that phage products were safe and significantly reduced the bacterial burden in burn wounds (Jault et al., 2019). An interventional clinical trial in Poland targeting bacterial infections where antibiotic treatment has failed (Górski et al., 2016).

A case study in a 68-years-old diabetic patient with necrotizing pancreatitis complicated by MDR *A. baumannii* infected pancreatic pseudocyst, who was in a comma for several weeks when received phage therapy as a cocktail of phages, woke up from coma after two days, and recovered fully in 245 days and returned to his work after recovery (Schooley et al., 2017). After the successful phage therapy, the University of California San-Diego School of Medicine in collaboration with national research institutions has established a Center for Innovative Phage Applications and Therapeutics (IPATH). Phages are being used as magistral preparations and/or compassionate use to treat antibiotic resistant bacterial infections (Pirnay et al., 2018; Romero-Calle et al., 2019). More recently, there are many case reports published on phage therapy (Pirnay, 2020; Sybesma et al., 2018), and most of them showing inspiring results (Dedrick et al., 2019; Petrovic Fabijan et al., 2020; Schooley et al., 2017). A remarkable clinical improvement was reported in a patient infected with multi-drug-resistant *P. aeruginosa* using IV and nebulized phages (Maddocks et al., 2019).

In recent years, several phage-based companies have been established in western countries. Some of them are emphasizing pre-clinical phage therapy research and development, some provide phage-mediated biocontrol, some manufacture enzybiotics and some are well-established phage therapy centers. The above-mentioned research has concerned the application of phage therapy in systemic infection and the persistence of the phage in vivo. But still, phage therapy is not accepted and adopted worldwide due to a few drawbacks such as the narrow host range of phages and the possibility of phage-mediated horizontal gene transfer. Advancements in biotechnology have further expanded the promising aspects of phage therapy such as bio-engineered phages and the recombinant phage lytic enzymes such as depolymerases, holin, endolysins, etc. (Lin et al., 2017). Recent clinical trials of human phage therapy have been summarized in Table 2.

Table 2: The summary of clinical trials specified as completed in Global Clinical Trials Data websites.

Title	Description	Date	Count	Sources
-------	-------------	------	-------	---------

ry

Study of the safety of AB-SA01	Three phages against <i>Staphylococcus aureus</i> are topically applied to the intact skin.	2016	U.S. A	https://globalclinicaltrialsdata.com/trial/GCT0102757755
Phages as Novel Prebiotics	PreforPro; a mixture of phages given to improve gut bacteria profiles.	2017	U.S. A	https://globalclinicaltrialsdata.com/trial/GCT0103269617
Phage effects on <i>Pseudomonas aeruginosa</i>	Evaluation of the efficacy of phages in <i>P. aeruginosa</i> in sputum samples of cystic fibrosis patients	2013	France	https://globalclinicaltrialsdata.com/trial/GCT0101818206
Evaluation of Phage Therapy	Topical applications of PP1131 phage cocktail (PHAGOBURN) in <i>P. aeruginosa</i> infected burn wounds (Phase I–II clinical trial).	2017	France	https://globalclinicaltrialsdata.com/trial/GCT022014-000714-65
Study of WPP-201 for the Safety and Efficacy	A randomized, double-blind controlled trial to assess the safety of WPP-201	2015	USA	https://globalclinicaltrialsdata.com/trial/GCT0100663091
Phages for Treating Urinary Tract Infections	Phage treatment in urinary tract infected patients	2019	Georgi a	https://clinicaltrials.gov/ct2/show/NCT03140085?cond=phage&draw=1&rank=1
PHAGE Study: Phages as Novel Prebiotics	The study investigated the utility of four supplemental phages to modulate the gut microbiota	2019	USA	https://clinicaltrials.gov/ct2/show/NCT03269617?cond=phage&draw=1&rank=13

2.8 Routes of phage application

Effective phage therapy depends on sufficient bioavailability of the phages in the body (Dąbrowska & Abedon, 2019). The routes of phage administration in phage therapy

depend on the type and site of the infection. Human clinical trials and case, reports revealed three main routes had been employed viz: topical, intravenous, and oral route.

To establish a standard phage therapy, ideal routes must be identified. Animal model experiments will be a useful tool to examine and optimize these aspects for future human therapy. Recently, diabetic foot ulcers have been successfully cured using a phage as compassionate treatment. For the treatment of skin or superficial infections like ulcers, burn wounds; topical application has been largely applied safely and without adverse effects (Chadha et al., 2016; Kumari et al., 2011; Trigo et al., 2013). Although there is a difference in size and immune response of mice and humans, pre-screening of phage in animals will be helpful to optimize and evaluate any adverse effects that possibly elicited in topical application.

Injection of phage particles directly into the bloodstream through the vein is called intravenous (IV) route of administration. It is the most common and ideal route to treat widespread infections and bacteremia. Several studies have been done using this route. Speck and Smithyman (2015) reported the IV route as safe and effective. Although there were some concerns like phage lysis in the bloodstream could lead to the release of an excessive amount of endotoxins which triggers hypersensitivity and anaphylaxis (Speck & Smithyman, 2016). A study of IV phage therapy in pediatric patients with an anaphylactic response by releasing endotoxins had been reported (Duplessis et al., 2017). However, the effectiveness of the phage therapy could be lower due to rapid clearance by the reticuloendothelial system when administered through the IV route and this should be concerned before IV phage therapy. Studies showed that the phages were able to cross the intestinal barrier to reach into the systemic circulation and were found to be viable even in fecal samples after oral administration. (Brix et al., 2020; Heo et al., 2009). Phage pretreated with sodium bicarbonate significantly increases the phage viability and also decreased the diarrheal symptoms in the pig model (Jamalludeen et al., 2009). Colom et al. (2017) reported microencapsulation protects the phage from degradation in the acidic environment in the gut, which also increases the phage efficacy in a chicken model of *S. enterica* infection.

2.9 Pharmacokinetics and pharmacodynamics of phage therapy

Several studies have been reported regarding the pharmacokinetics of phage therapy previously. Abundant data can be found related to phage therapy but when it comes to

the pharmacology of phage in an animal model, there is a limited number of data available to date. Pharmacology mainly deals with the drug and body interactions; it can be further subdivided into pharmacokinetics- the body's impact on drugs- and pharmacodynamics-drugs impact on the body (Dąbrowska, 2019). Pharmacokinetics deals with a drug's ability to reach desirable concentrations in the locality of targeted tissues, as it is necessary to bring about the desirable effect of the drug. Pharmacokinetics focuses on the absorption, distribution, metabolism, and excretion of drugs. Absorption is drug dissemination into the bloodstream. From the bloodstream, the drug is transported to the body tissues this process is known as distribution. Once the drug reaches the target tissues, it is metabolized and modified into its active form; the last step is the excretion of drugs from the body. All these processes of pharmacokinetics play their role in both increasing and decreasing drug concentration. For instance, both absorption and distribution result in the decrease in drug concentration resulting in drug dilution, which on the other hand increases drug density in the particular body organ or tissue (Abedon et al., 2011).

Phages possess a unique three-party relationship between their host bacteria and the immune system of human (Wahida et al., 2021). They co-evolve and self-replicate in the presence of host bacteria within the human body (Payne & Jansen, 2003) resulting the PK/PD of phages are different from antibiotics. Similarly, the phages can pass through the body walls thus, potential to elicit the immune response (Barr et al., 2013; Dąbrowska & Abedon, 2019). It is essential to know the rate of biodistribution, bioavailability, and clearance of the phage by the immune system (Caflisch et al., 2019). The route and dosage of phage administration must be evaluated and standardized for successful phage therapy (Dąbrowska, 2019; Nilsson, 2019; Payne & Jansen, 2003). Based on the pharmacokinetics, different routes of drug delivery are approved. The route of administration is designated taking consideration of several factors such as targeted tissue, the sensitivity to body enzymes, intake route, patient's convenience, etc. In phage therapy, metabolism may work two ways; either inactivation of phage particles by the patient's immune system or activation followed by replication of phages. Furthermore, excretion results in decreased drug concentration, on the other hand, it can lead to an increase in phage concentration in organs like kidneys and bladder, which can be therapeutically beneficial (Vandenheuvel et al., 2015). The pharmacokinetics of phages defines the number of phage particles available in the body

while pharmacodynamics is the physiological effects exert by the phages in a living system. The terms phage kinetics and dynamic are interrelated and represent reciprocal interactions and impact that the human or animal body may have with phage in a therapeutic action. Which is crucial for understanding of therapeutic failures or successes. The phage kinetics and dynamic are more complex than classical drug. Phages proliferate throughout bacterial host populations. Mode of the phage dispersion throughout microbial populations is same as epidemic. The rate of phage propagation totally depends on the host population, and the phage population only increase in the presence of a high number of host cell (Cairns et al., 2009). The phage kinetics relies on several factors such as (i) adsorption; (ii) latency; (iii) phage dosage; (iv) time; (v) clearance of the phage particles from the body; (vi) ability of the phage replication and phage resistance; (vii) animal or human anatomy/physiology; (viii) environmental situations; and (ix) phage distribution in the human body, including immune response. These all parameters determine the effective routes of phage administration such as topical or parenteral, intraperitoneal, intravenous, oral etc. (Hodyra-Stefaniak et al., 2015)

Publications on phage pharmacokinetics recommend that phages can get into the bloodstream of animals within 2 to 4 hours and are found in internal organs such as liver, spleen, kidney, lungs etc. within approx. 10 hours (Dąbrowska, 2019). Also, data showed that the persistence of administered phages indicate that the phages can remain in the human body for prolonged periods - up to several days (Rashel et al., 2007). This property suggests that phages can also be used to treat systemic infections. Another study used four types of phages to treat 72 strains of MRSA and reported that injections of 8×10^8 CFU bacteria intra-peritoneally caused bacteremia and eventual death in mice, but when administered simultaneously with purified phage ϕ MR11 ($\text{MOI} \geq 0.1$) they suppressed *S. aureus* induced lethality (Matsuzaki et al., 2003). Further, high doses of phage ϕ MR11 used on uninfected mice showed no adverse effects. Similar effects of anti-staphylococcal phage were demonstrated while dose-related phage treatment was studied (Capparelli et al., 2007). Phages were administered intravenously and reported that the minimal effective dose was 10^9 PFU/mL per mouse and also showed that lower doses were ineffective. Phages were active against systemic as well as local infections and within 4 days, bacteria in the bloodstream were completely eradicated (97% of mice survived) (Capparelli et al., 2007). Most importantly, according to Capparelli et

al. (2007), the phages also successfully lysed MRSA. A study in BALB/c mice suggests combination therapy (mupirocin+phage) represents a more attractive option in decolonizing MRSA from nasal cells (Capparelli et al., 2007; Chhibber et al., 2014)

The successful phage therapy relies on ample phage concentration within the site of target tissue to eradicate pathogen bacteria from the body. The increase in the number of phages up to an adequate level can be achieved by two means. One with *in-situ* replication is also called active treatment, and second approach is the passive treatment. The administration of phage should be in such dose which compensates for the mechanism of phage reduction. Thus, the goal is to achieve minimum phage concentration at the target organ or site, which is enough for the reduction of the bacterial cells to the desired level. Moreover, the phage preparations should be purified to remove bacterial debris and other components, including endotoxins, when phages are administrated directly to an animal's systemic circulation (Chan & Abedon, 2012). The study done so far suggests that the phage when administered orally can reach the bloodstream of animals 2-4 hours after a single dose. Phages are found in an internal organ such as the liver spleen and kidney approximately after 10 hours of administration (Dąbrowska, 2019). A study showed that the phage can persist for up to several days in the subject's body (Jassim & Limoges, 2014).

2.10 Host immunity against the phage

The immune system human may recognize the phages as a foreign particle and elicit an immune response (Sulakvelidze et al., 2001). Neutralizing antibodies have been reported after 10 to 12 days of administration of phages in the mice model (Kutter et al., 2010). The phages influence the animal microbiome thus impact on host immunity indirectly (De Paepe et al., 2014). Moreover, the phages also activate the innate and adaptive immunity directly itself (Van Belleghem et al., 2019). However, the role of phage to activate immune response during phage therapy is inconsistent and unclear (Liu et al., 2021). Cytokines are mediators of host responses to infection, inflammation, immune responses, and trauma. Cytokines are regulatory proteins, which play a key role in inflammatory responses either directly or by their ability to induce the synthesis of cellular adhesion molecules or other cytokines in numerous cell types. Cytokine pattern is essential to elucidate the immune and pathological pathways involved in many inflammatory responses such as infectious diseases, autoimmune reactions.

Quantification of cytokine gene expression is essential for analyzing immune responses (Giulietti et al., 2001). Some cytokines may make the disease worse called proinflammatory cytokines, whereas others help to reduce inflammation and promote healing called anti-inflammatory cytokines. Interleukin (IL-6) and tumor necrosis factor (TNF α) are pro-inflammatory cytokines, and when they are expressed in abnormal amounts, they produce fever, inflammation, tissue destruction, and shock in some cases (Stenvinkel et al., 2005). The expression of IL-6 during infection is reported from 6 to 24-fold during inflammation (Berti et al., 2002).

The host adaptive immune responses may elicit by the phages as they are immunogenic biological entities (Gorski et al., 2012). Clinical studies have shown that phage triggered both specific IgG and IgM antibodies when administered via the IP route (Aslam et al., 2019; Gainey et al., 2020). Immune response towards phages may depend on the route, dose, phage type, and time of administration (Liu et al., 2021). Presently, it is assumed that antibody production by phage itself may affect the efficacy of phage therapy. Though, the role of phages in therapeutic safety is not clear to date. There is a lack of data on phage-induced immunity including phage-specific antibodies and inflammatory cytokines, and are the underexplored area in the field.

2.11 Limitations of phage therapy

Despite all advantages of the phages to treat any type of infection, there are some major disadvantages or drawbacks associated with phage therapy.

2.11.1 Endotoxins:

The component of the cell wall of Gram-negative bacteria (e.g., lipopolysaccharides) are released during cell lysis by phage. If it is present in sufficient quantities, lipopolysaccharides (endotoxins) could cause a variety of biological effects including fever, hypotension, and endotoxic shock (Rietschel, 1982). Using different techniques such as ultrafiltration, chromatography, etc. can provide endotoxin-free preparations during phage purification (Boratyński et al., 2004).

2.11.2 Activity against intracellular pathogens:

Phages should be able to enter the eukaryotic cells during phage therapy. However, phages are shown to be less effective against intracellular bacteria, such as,

Mycobacterium tuberculosis, and other intracellular persistent clones of extracellular bacteria (Sulakvelidze et al., 2001).

2.11.3 Phage specificity:

The specificity of phage for its host is an advantageous part of therapy but sometimes it may lead to limiting of phage therapy and biocontrol because during infection usually a mixture of various species and strains of bacteria is found. Broad host range phages can be a solution to this problem (Jensen et al., 1998). Using a mixture of phages as ‘phage cocktails’ is another proposed approach to overcome this limitation (Chan & Abedon, 2012).

2.11.4 Phage-induced bacterial evolution:

Another major concern of phage therapy is ability of phages to transfer bacterial DNA among bacterial population. The transfer of DNA/RNA, or transduction, may cause the development of a new microbe or even more resistant bacteria (Brabban et al., 2005). There is evidence pointing to the origin of some bacteriocins and even the bacterial pili to phages (Karaolis et al., 1999).

2.11.5 Phage resistance:

Another major drawback of phage is that phage-mediated lysis can drive the evolution of the target population resistant mutants (Rice et al., 2009). The development of phage-resistant mutation makes phage therapy unproductive. It is reported that the rate of resistance develop by phages is about 10-fold lower as compare to antibiotics (Carlton, 1999). Use of a mixture of phage (cocktails) may deal with the problem of resistant mutants (Tanji et al., 2004).

2.12 Recent advancement of phage therapy and commercial products

Conventionally, phage therapy relied on the use of phages that are naturally isolated to kill the specific host bacteria. Due to the very narrow host range of the naturally occurring phages, a large phage library is needed. With the advancement of many biotechnological tools and techniques, phages can be engineered to expand the host range and overcome phage resistance. Phages are also being used as a delivery vehicle for gene therapy, as biocontrol agents, development of the phage-derived vaccine, and in phage display techniques and use of bioengineered phages and purified phage lytic

proteins in phage therapy. These preparations consist of phage-lysed, bacteriologically sterile broth culture of targeted pathogen and water-soluble jelly base. The product was used for the treatment of infections such as abscesses, wounds, vaginitis, acute and chronic infections of the upper respiratory tract, and mastoid infections etc. The advent of antibiotics and the controversial efficacy of phage preparation led to the cessation of commercial phage production in most of the Western worlds (Eaton & Bayne-Jones, 1934) although phage products were used continuously as therapeutic together with antibiotics or instead of it in the Europe and former Soviet Union. Many institutions in these countries were continuously involved in research and production of therapeutic phages. The Eliava Institute of Phage, Microbiology, and Virology (EIBMV) of the Georgian Academy of Sciences, Tbilisi, Georgia, and the Hirsfeld Institute of Immunology and Experimental Therapy (HIET) of the Polish Academy of Sciences, Wroclaw, Poland (Kutter et al., 2010). The list of companies that are preparing phage and phage products for biocontrol of bacteria in animals, plants, or food products is listed in Table 3.

Table 3: List of companies that are preparing phage and phage products for biocontrol of bacteria in animals, plants, or food products. (Source: Moradpour & Ghasemian, 2020).

Company Name	Products	Description
Omnilytics (USA)	AgriPhage	For biocontrol several bacterial pathogens in plant
ACD Pharma	CUSTUSYRS	For the treatment of enteric red mouth disease (ERM) caused by the <i>Yersinia</i>
CheilJedang Corp. (Korea)	BioTector	For control of Salmonella in poultry
Intralytix (USA)	Eco-Shield List-Shield Salmo-Fresh Shiga-Shield Salmo Lyse etc	For <i>Listeria monocytogenes</i> , <i>Escherichia coli</i> (O157:H7), <i>Shigella</i> spp., and <i>Salmonella</i> .
APS Biocontrol (UK)	Biolyse-PB	For biocontrol of the soft-rot bacteria of potatoes.
Biotech Laboratories (Israel)	FAST Plaque-response FAST Plaque TB	For rapid detection of rifampicin resistance in smear-positive sputum specimens containing <i>Mycobacterium tuberculosis</i> . For rapid detection of <i>Mycobacterium tuberculosis</i> in human sputum samples

EBI Food Safety (The Netherlands)		LISTEX P100	A food-processing aid that targets <i>Listeria monocytogenes</i> strains on food products
Microphage (USA)		MRSA/MSSA blood culture test MRSA screening test Micro Phage MRSA/MSSA test	Determining of <i>Staphylococcus aureus</i> methicillin resistance or susceptibility directly from blood cultures. Differentiation of methicillin-resistant (MRSA) and methicillin-susceptible (MSSA) <i>Staphylococcus aureus</i>
Biocontrol (United Kingdom)		Phage products to combat otitis and lung infections	Clinical trials on phage products to combat <i>P. aeruginosa</i> infections have been completed
Novolytics (United Kingdom)		In development—gels for targeting MRSA and <i>Clostridium difficile</i>	A gel containing a cocktail of phages targeted at MRSA to treat nasal carriage of MRSA. Also in development are gels for skin infections and indwelling medical devices
New Diagnostics Corporation (USA)	Horizons	In development—phage-associated enzymes	Lysins to be applied directly to the designated area (limited information available)
Biophage Inc. (Canada)	Pharma	Phage-based products for a range of applications	A large bank of phages is being isolated from natural sources for use in phage therapy applications.
Phico (United Kingdom)	Therapeutics	SASPject	Phico modifies a fully characterized phage for each type of target bacterium
Biocontrol (United Kingdom)		Phage products to combat otitis and lung infections	Clinical trials on phage products to combat <i>P. aeruginosa</i> infections
GangaGen Biotechnologies Ltd. (India)		Ecto-Lysin P128	P128 phage lysin for <i>Staphylococcal</i> spp. including methicillin-resistant <i>Staphylococcus aureus</i> (MRSA), vancomycin-resistant <i>Staphylococcus aureus</i> (VRSA), and coagulase-negative <i>Staphylococci</i> .
Pherecydes (Romainville, France)	Pharma	Phage cocktail: PP1131	Phagoburn project intended for assessing phage therapy (phase I/II randomized and controlled double-blind study) for the treatment of burn wounds infected with bacteria <i>E. coli</i> and <i>Pseudomonas aeruginosa</i>
Locus (USA)	Biosciences	CrPhage develops CRISPR-engineered antibacterial products	crPhage designed to kill urinary tracts <i>E. coli</i> , <i>Clostridium difficile</i> , undisclosed bacterial relevant for inflammatory bowel disease (IBD) and other disorders causes

2.13 Challenges in the clinical use of phage therapy

The phage therapy is highly relying on the safety of phage preparation, route of application, mode of action, immune response, etc. In the current scenario, there are some challenges in the use of phage therapeutically among which the main challenge is the safety of phage production. For extensive medical applications, phages should be produced on large scale with Good Manufacturing Practices (GMP) that are approved by the authorized agency (Regulski et al., 2021). The production of phages usually applied for pharmaceutical purposes should ensure high standard quality. But there is no clear guideline yet developed for the manufacturing of therapeutic phage (Mutti & Corsini, 2019). Several purification methods have been developed for optimization and removal of toxins from phage preparations but none of the methods has reached its optimal result so far (Hietala et al., 2019). The stability of phage preparations is a crucial prerequisite for successful phage treatment. Phage should have a good shelf life and should be stored in a formulation that ensures optimal activity without a significant drop in phage titer during processing and long-term storage (Malik et al., 2017). Several approaches have been developed and optimized to expand stability of phage. Most commonly used are freeze-drying, spray-drying, extrusion dripping methods, emulsion, polymerization, and encapsulation (Gonzalez-Menendez et al., 2018).

The most challenging issue of phage stability is the occurrence of natural mutations in phage stocks kept for long time which can impair viral fitness (Tibor et al., 2019). Lack of regulatory approval for phage therapy is also an issue. In 2015, the European Medicines Agency (EMA) conducted a workshop to identify possibilities for the development of phage-based therapies against antibiotic resistant bacterial infections (Wienhold et al., 2019). The most promising approval pathway has not been identified and EMA also has not licensed the phage products so far. Presently, new time and cost-intensive re-production and re-approval under GMP conditions would be required (Hill et al., 2018). If a phage product should be employed in clinical uses as an emerging case of antibiotic-resistant, the process of developing an approval of phage as therapeutic needs to shorten with well-structured guidelines of GMP, and it must be clarified whether each phage of a cocktail is considered a medicinal product that needs regulatory approval. The main challenges of phage therapy to the clinician is the delivery of phages and the lack of methodology for the rapid identification of patient-specific phage.

Nevertheless, of the several known advantages of phages, there are many challenges and unaddressed boundaries to this approach that must be addressed and further investigated. These might be principally due to gaps in knowledge and regulations, which may be addressed in the future. The major challenges and possible solutions have been summarized in Table 4.

Table 4: Major challenges and possible solutions of phage therapy

Challenges	Possible solutions
Nature of infection	As phages can multiply only in the presence of host bacteria or at the site of infection, we need to choose the correct administration routes and dose so that the phage can reach the site of infection. A better understanding of the pharmacokinetics and pharmacodynamics of the phage.
Host immune against phage	Phage can be engineered to express certain proteins on their capsids that can prevent antibodies from recognizing and subsequently clearing the phage.
Temperate phages (Transducing AMR/virulent genes)	Whole-genome sequencing and bioinformatic analysis to rule out any lysogens, toxic genes, and AMR genes.
Narrow host range	Isolation and characterization of novel phages to have large collections of the phage repository. Using a mixture of phages as ‘phage cocktails’ is another proposed approach to overcome this limitation Modifications of the phage genome using phage engineering
Phage inactivation/encapsulation	Phage encapsulation like Nanoparticle delivery systems, like polyethylene glycol (PEG)-based or liposome platforms is another possible approach to avoid human immune system recognition and enable phage-bacterial interactions.
Intellectual property	Although a patent cannot be obtained for the concept of phage therapy itself, many aspects related to phage therapy are patentable if companies invest in research to develop a genetically engineered phage strain.
Regulatory issues	Regulatory agencies such as U.S. FDA, European Medicines Agency (EMA), and other countries, need to modify policies for managing phage-based therapeutics.

Lack of awareness	The best strategy is to heighten the awareness of phages and their therapeutic potential among both scientists and the general public.
-------------------	--

2.14 Concluding remarks on literature review

After reviewing the research done so far in the field of phage and phage therapy, it can be said that in the era where people are dying due to the infection of MDR superbugs, the phage is a bright ray of hope. Isolation of new phage is fast and cheap compared to the antibiotic. It can also be a personalized therapy as phages can be host-specific. Phage can be used to treat any type of infection, either localized or systemic. The doubts people had in the past have been cleared by the recent research and the world is slowly attracted towards the application of phages in therapeutics. It is obvious that people still have some insecurity using a live virus as a drug and doubt on horizontal gene transfer. It is important to isolate a large number of novel phages and analyze their genomes to rule out a more complete set of toxicity genes and work towards a better understanding of phage genomics and phage biology. The recent studies in genetically modified phages and the phage-derived enzymes such as depolymerase, lysins, etc. will solve many problems in phage therapy. The main obstacle of phage therapy is the lack of well-control clinical trials. With the lack of data on randomized controlled trials (RCT) and regulatory hurdles, most of the human phage therapy data are limited in the form of compassionate phage therapy. Selection of appropriate phages or their components, dose, route of administration, pharmacokinetic and pharmacodynamic properties must be optimized for successful phage therapy.

CHAPTER 3

MATERIALS AND METHODS

3.1 Media and Bacterial strains

Bacterial cultures were sub-cultured into freshly prepared nutrient agar and MacConkey agar (HiMedia, India) plates, and incubated at 37°C for overnight. From these plates, a single isolated colony was propagated in Luria-Bertani (LB) broth (HiMedia, India) at 37°C until the log phase was obtained (OD_{600nm} of 0.3). For long-term storage, a single colony of the bacteria was sub-cultured in nutrient broth (HiMedia, India) and incubated at 37°C for 24 hours and 0.5 mL of overnight broth culture was added to 0.5 mL of sterile 50% glycerol (HiMedia, India) in 1.5 mL tubes. The tubes were then cooled at 4°C for an hour, chilled at -20°C for an hour, and finally transferred to -80°C. Tryptic soy broth (TSB) (HiMedia, India) was used for phage isolation, purification, and amplification. Agar was separately added to TSB in an appropriate concentration whenever required.

A total of five carbapenem-resistant clinical isolates (CIs) (molecularly confirmed for the presence of *bla*-NDM and *bla*-KPC genes) were recovered from the glycerol stock at the Central Department of Biotechnology, Tribhuvan University. They were used as a primary host for phage isolation. Among them, three were confirmed as *E. coli* and two were confirmed as *K. pneumoniae* by Bruker MALDI Biotyper at the National Institute of Health (NIH). All other CIs used for the phage host range analysis (n = 45) were obtained from the Department of Microbiology, National Public Health Laboratory (NPHL), Kathmandu. These isolates were identified by their biochemical and morphological characteristics at the NPHL. A laboratory strain of *E. coli* MG1655 was used for the propagation and purification of isolated phages. Bacterial isolates used in this study are listed in Table 5.

3.2 Sample collection and processing

Water samples (n = 20) were collected from different rivers and sewage of Kathmandu valley. Stagnant water was preferred rather than running water. The detailed information of location and water sample type is elaborated in Table 6. The map of the

sample collection sites is depicted in Figure 10 and representative pictures of water collection sites in Figure 11.

Table 5: List of bacteria used in this study

Sample sources	Bacteria (clinical isolates) *	Application in this study
Laboratory strain	<i>E. coli</i> MG1655	Phage propagation, and purification
Urine	<i>E. coli</i> M1, <i>E. coli</i> M2, <i>E. coli</i> M3, <i>K. pneumoniae</i> TUKp1, <i>K. pneumoniae</i> Kp56	The primary host of phage isolation
	<i>E. coli</i> M5, <i>E. coli</i> M6, <i>E. coli</i> A6 <i>E. coli</i> A7, <i>E. coli</i> A8, <i>E. coli</i> A11 <i>E. coli</i> A14, <i>E. coli</i> A17, <i>E. coli</i> Ab21 <i>E. coli</i> Ab22, <i>E. coli</i> Ab23, <i>E. coli</i> Ab24, <i>E. coli</i> Ab32, <i>E. coli</i> Ab35, <i>E. coli</i> Ab38, <i>E. coli</i> Ab47, <i>E. coli</i> Ab49, <i>E. coli</i> Ab50, <i>E. coli</i> Ab56, <i>E. coli</i> Ab58, <i>E. coli</i> Ab59, <i>E. coli</i> Ab70, <i>P. aeruginosa</i> P42, <i>K. pneumoniae</i> K12, <i>K. pneumoniae</i> K27, <i>K. pneumoniae</i> K41, <i>K. pneumoniae</i> K42, <i>K. pneumoniae</i> K57, <i>K. pneumoniae</i> K70	Phage host range
Wound swab	<i>E. coli</i> M4, <i>E. coli</i> A1, <i>E. coli</i> A4, <i>E. coli</i> A5 <i>E. coli</i> A13, <i>E. coli</i> A15, <i>E. coli</i> Ab25 <i>E. coli</i> Ab53, <i>P. aeruginosa</i> P4, <i>P. aeruginosa</i> P19, <i>P. aeruginosa</i> P43 <i>P. aeruginosa</i> P53	Phage host range
Sputum	<i>E. coli</i> A12, <i>K. pneumoniae</i> K13 <i>K. pneumoniae</i> K23	Phage host range

* All bacteria used in this study were uncharacterized (isolated from the clinical samples) and were named as per our convenient except a laboratory strain *E. coli* MG1655.

Table 6: Water and sewage sample collection sites

Sample no.	Location	Date	GPS co-ordinates	Remarks
1.	Karmanasa river	18/01/2017	27°39'06.7"N 85°20'09.2"E	Near Little angle school, Lalitpur
2.	Manohara river	22/01/2017	27°40'23.8"N 85°20'29.8"E	Near balkumari bridge, Lalitpur
3.	Hattiban sewage	23/01/2017	27°38'36.2"N 85°20'19.4"E	Near Cancer Hospital Harishiddi, Lalitpur
4.	Basundhara Sewage	26/01/2017	27°44'32.4"N 85°19'57.5"E	Near Ishan Hospital Basundhara chowk, Kathmandu
5.	Sewage from Shankhamul area	29/01/2017	27°40'49.1"N 85°19'49.8"E	Near Shankhamul bridge, Kathmandu
6.	Sali Nadi	01/02/2017	27°43'40.2"N 85°28'08.9"E	Near Chandrawati Bridge, Kathmandu
7.	Balkhu river	10/02/2017	27°41'01.7"N 85°17'57.1"E	Downstream of Balkhu tarkari bazaar, Kathmandu
8.	Bishnumati river	11/02/2017	27°44'06.9"N 85°18'25.6"E	Near Nayabuspark bridge , Kathmandu
9.	Bisnumati river	15/02/2017	27°42'01.1"N 85°18'10.6"E	Near Teku bridge, Kathmandu
10.	Bisnumati river	19/02/2017	27°41'55.3"N 85°18'09.9"E	Near Kalimati Bridge, Kathmandu
11.	Teku Sewage	20/02/2017	27°41'59.5"N 85°18'10.9"E	Near slaughterhouse, Teku, Kathmandu
12.	Kalimati Sewage	05/03/2017	27°41'54.0"N 85°17'58.2"E	Near Kalimati Tarkari bazar, Kathmandu
13	Balkhu river	09/03/2017	27°41'07.7"N 85°17'59.7"E	Downstream of Balkhu tarkari bazaar, Kathmandu
14	Balkhu river	13/03/2017	27°40'58.4"N 85°17'56.4"E	Downstream of Balkhu tarkari bazaar, Kathmandu
15	Mahadev Khola	19/03/2017	27°45'09.8"N 85°18'09.8"E	Tarkeshwor, Kathmandu

16	Bagmati river	19/03/2017	27°42'36.9"N 85°20'56.6"E	Near Pashupatinath temple, Kathmandu
17	Sewage from Lainchaur	02/04/2017	27°43'02.6"N 85°18'54.7"E	Lainchaur chowk, Kathmandu
18	Sewage from Kirtipur	02/04/2017	27°40'44.4"N 85°17'03.8"E	Near TUTH, Kathmandu
19	Sewage from Teku	09/04/2017	27°41'42.3"N 85°18'25.7"E	Near Teku Hospital, Kathmandu
20	Sewage from Maharajgunj	09/04/2017	27°44'06.6"N 85°19'50.4"E	Near TU Teaching Hospital, Kathmandu



Figure 10: Map of sample collection sites. Markings indicate the sample collection area. Sampling sites were selected to cover the different geographical areas of Kathmandu valley. Water (50 mL from each of the sites) samples were collected in a sterile falcon tube. Stagnant water was preferred rather than running water.

3.3 Phage isolation and clonal purification

Phages were recovered from the collected samples using the double-layer agar assay (DLAA) method described previously with some modification (Kropinski et al., 2009; Swanstrom & Adams, 1951). Briefly, 50 mL of sewage/water sample was centrifuged at 4000 RPM for 30 min at room temperature. The supernatant was then filtered through 0.22

μm syringe filters (Whatman™ syringe filter (Sigma-Aldrich, Missouri, United States)). One mL of filtrate was mixed with 100 μL log phase host bacteria and left for 10 minutes for phage attachment. Three-milliliter soft agar (TSB with 0.5% agar), maintained at 50°C, was added to the mixture and poured onto the surface of previously prepared TSA plates. The plates were left at room temperature (RT) until soft-agar was completely solidified (1-2 hr.) and incubated at 37 °C overnight. The next day, the plates were examined for the presence of phage in the form of plaques. A single isolated clear plaque was picked with the help of a 200 μL pipette tip and suspended in one-milliliter sodium chloride-magnesium sulfate (SM) buffer (10 mM Tris-HCl, pH 7.5, 10 mM $\text{MgSO}_4 \times 7 \text{H}_2\text{O}$, 2% gelatin, and 100 mM NaCl). A 50 μL of chloroform was added to the phage suspension and vortexed. Then the suspension was centrifuged at 10,000 rpm for 5 minutes at 4 °C. The supernatant was serially diluted plated against respective host bacteria using DLAA. Clonal purification of a single isolated plaque was done by the subsequent five rounds of DLAA.



Figure 11: Representative pictures of water collection sites. Sample collection sites of Teku river and Bagmati river (behind the Vayodha hospital and Balkhu Tarkari Bazar) in Figures A and B respectively. Similarly, Figures C and D are sewage from Basundhara and Maharajgunj respectively. Water samples were specifically collected from the place where immobile water was there. Water was collected in 50mL falcon tubes.

3.4 High titer phage lysate preparation

High titer phage lysates were prepared by mixing host bacteria ($OD_{600\text{ nm}}$ of 0.25) in 10 mL of LB broth medium with 50 μL of purified phage lysate and incubated in shaking incubator maintained at 37 °C for 3 to 4 hr. (or until the clear appearance of the LB media) with shaking (220 rpm). The culture was mixed with 1% chloroform and centrifuged at 10,000rpm for 10 minutes at 4°C then filtered through a 0.22 μm syringe filter (Whatman™ syringe filter (Sigma-Aldrich, Missouri, United States) to remove cell debris. The phage titer in PFU/mL was obtained through plaque assays using the DLAA method as described earlier. Briefly, phage lysate was serially diluted up to 10^{-12} dilutions using SM buffer. Nine hundred microliters of SM buffer were aliquoted in Eppendorf tubes (labeled 10^{-1} to 10^{-12}) and 100 μL of phage was mixed with the first dilution (10^{-1}) tube. Subsequently, 100 μL of the dilution was transferred to the next dilution (eg. 10^{-2}) tube and so on to make two-fold serial dilution. DLAA was performed from each of the dilution and phage titers in PFU/ mL were calculated using the formula given below:

$$\text{PFU/mL} = \frac{\text{Number of plaques observed}}{\text{Dilution factor} \times \text{Volume}}$$

3.5 Phage concentrated by centrifugation method

Two milliliters of high titer phage lysate ($>10^9$ PFU/mL) was added to 500 mL of mid-log host cell culture ($OD_{600} = 0.25$) in LB broth and incubated at 37 °C water bath with shaking 250 rpm until the clear appearance of the broth (2 to 3 hr.). The lysate was transferred to the 50 mL centrifuge tube and centrifuged at 10,000rpm for 10 minutes. The supernatant was centrifuged at 6,500 rpm for 18 hr. at 4 °C in a Sorvall RC5B plus centrifuge (Thermo Scientific, USA) using SLA-3000 rotor. The supernatant was carefully poured off and one milliliter of gelatin-free SM buffer was added to the pellets. The pellet was left overnight at 4 °C to loosen up. Then gently resuspended the pellet with the help of a micropipette. The phage suspension was centrifuged again at 10,000 rpm for 10 min. at 4 °C to remove any remaining cell debris. The titer of the concentrated lysate was determined by the double-layer agar overlay method. This lysate was purified by cesium chloride (CsCl) gradient centrifugation.

3.6 Purification of phage lysate

Phages were purified by isopycnic CsCl density-gradient ultracentrifugation as described previously with modification (Sambrook & Russell, 2001). Two milliliters of concentrated phage ($>10^{12}$ PFU/mL) lysate overlaid onto a three-step cesium chloride (CsCl) gradient containing 1.5 mL each of 1.6 p, 1.5 p, and 1.4 p density CsCl in a 16x76 mm polymer quick seal ultracentrifuge tube (Beckman Coulter, USA). SM buffer was added on the top to fill up to the neck of the tube. The tube was sealed using a Beckman tube sealer and centrifuged for 5 hr. at a speed of 45,000 rpm at 4°C in an ultracentrifuge (Beckman Coulter, L8-M with Ti 70.1 fixed angle rotor). The grey-white band containing the phage was collected by puncturing the wall of the ultracentrifuge tube using a 23 G needle. The phage sample was transferred into a slide-A-Lyzer dialysis cassette (10,000 MWCO, Thermo Scientific, USA) and dialyzed overnight against 1000 mL of gelatin-free SM buffer containing 1 M sodium chloride at 4 °C. The dialysis cassette was transferred to one liter of normal gelatin-free SM buffer and dialyzed for 4 hr. This process was repeated twice. The phage preparation was filter sterilized with a 0.22 µm syringe filter (Whatman™) and the phage titer was determined by DLAA. The purified phage stock was stored at 4 °C until further use.

3.7 Transmission electron microscopy (TEM)

The purified phage lysate was fixed with 2% paraformaldehyde and 2.5 % glutaraldehyde. Ten microliters of fixed phage lysate were spread on a carbon-coated copper grid and after 2 minutes, excess phage lysate was soaked-off using blotting paper. The copper grid was negatively stained with 2% (w/v) uranyl acetate (pH 4.5) and after two minutes, the excess stain was soaked-off with blotting paper. The copper grid was dried and finally examined in an FEI Tecnai T12 transmission electron microscope at the Electron Microscopy Unit of the National Institute of Biomedical Imaging and Bioengineering, NIH, USA.

3.8 Phage protein profiles by SDS-PAGE

Sodium dodecyl sulfate-polyacrylamide gel electrophoresis (SDS-PAGE) analysis was performed as described by Laemmli (1970) with modifications. The phage proteins were extracted from the CsCl purified phage lysates using the acetone precipitation method. Briefly, 500µL of CsCl purified phage lysate ($\sim 10^{10}$ PFU/mL) was precipitated

with four times the volume of ice-cold acetone for 90 minutes and the supernatant was decanted. The phage protein pellet was resuspended in SDS-PAGE loading buffer and boiled for 5 min before loading onto a 12% polyacrylamide gel. Separation was carried out in 12% resolving gel (Tris–HCl buffer with pH 8.8), and 4% polyacrylamide in Tris–HCl buffer (pH 6.8) was used as a stacking gel. Electrophoresis was carried out in Tris-glycine buffer at a constant current of 400 mA till the tracking dye reached the bottom of the gel. A molecular weight standard (Protein Ladder, GeNei labs, India) with a molecular weight ranging from 7 to 240 kDa was used as a protein marker. After electrophoretic separation, the gels were stained with Bio-Safe Coomassie brilliant blue (Bio-Rad, USA) solution for 6 to 8 hours in a shaker and then suitably destained with destaining solution (Appendix - A). The gel was scanned in a scanner and a photograph of separated protein bands was taken.

3.9 One-step growth curve

A one-step growth curve experiment was done as described previously (Merabishvili et al., 2014) with modification. Briefly, log phase bacterial culture in LB broth (OD_{600nm} of 0.3) was mixed with the phage lysates at a multiplicity of infection (MOI) 0.01 and incubated at 37 °C for 10 min. for adsorption of phages to the host bacteria. The mixture was centrifuged at 11,000 rpm at 4°C for 10 minutes to remove un-adsorbed phage particles. The supernatant was titrated by DLAA to count unadsorbed phages. Then, the pellet was resuspended in LB broth and incubated at 37°C. Aliquots of 0.1mL were taken for the phage titration at intervals of 5 minutes for up to 70 minutes. Assays were carried out in triplicate. The burst size was calculated as the ratio of the number of phage particles liberated and the initial count of infected bacterial cells.

3.10 Temperature and pH stability

The stability of phages at different temperatures and pH was determined as described earlier with modification (D'Andrea et al., 2017). Briefly, 1.5mL of SM buffer was aliquoted in a microcentrifuge tube and adjusted different pHs ranging from 2 to 12 with 1M HCl and 0.5 M NaOH. The stability of the phages at different pHs was determined by mixing 100 μ L phages lysate (10^8 PFU/mL) with the previously pHs adjusted SM buffer. Phage suspensions were incubated at 37 °C for 60 minutes in a

water bath and viable phages were counted by the double-layer agar assay (DLAA) as described earlier. For temperature stability, two milliliters of the phage lysates (10^8 PFU/mL) were aliquoted into the microcentrifuge tube. The aliquots were incubated at 25 °C, 37 °C, 50 °C, 60 °C, and 70 °C in a dry-bath incubator for up to 180 minutes and the surviving phages were immediately counted by DLAA. The assays were carried out in triplicate and the data were analyzed under an ordinary one-way and two-way analysis of variance (ANOVA).

3.11 Host range analysis

A total of 50 different multidrug-resistant clinical bacterial isolates (35 *E. coli*, 5 *P. aeruginosa*, and 10 *K. pneumoniae*) including a laboratory strain of *E. coli* MG1655 were used to evaluate the phage host range. Initially, a spot test was done to determine the host range of the phages as described previously (Kutter, 2009). Based on the spot test result, the killing efficacy of the phage on the bacterial strains was assessed by the efficiency of plating (EOP) with modifications. Briefly, 100 μ L of an overnight culture of each isolate was mixed individually with 3.0 mL of 0.5% molten TSA top agar (temperature 50 °C). The inoculated agar was spread onto 1% tryptic soy (TSA) agar plates. Top agar was allowed to cool at room temperature, then 10 μ L of 10-fold serial dilutions of the phage lysate (10^8 PFU/mL) were spotted on the bacterial lawn. All spots were allowed to fully absorb on the top agar and incubated overnight at 37 °C for plaque formation. After incubation, the lowest titer of the phage that gives countable plaques was determined and a double-layer agar assay was done as described above. The number of plaques was counted in each bacterial strain. The EOP was determined by dividing the average number of plaques (PFU) formed on the tested bacterial strain with the average PFU of the original host bacterium. The test was performed in triplicates to obtain a consistent result.

3.12 Genomic DNA extraction and sequencing

The genomic DNA of the phages was extracted using the standard phenol-chloroform extraction method as described previously (Sambrook, 1989). The phage genomic DNA concentrations and the quality check was carried out using a NanoDrop 8000 (Nanodrop Technologies Inc., Wilmington, USA). Whole-genome sequencing was performed by Illumina Nextseq500 platform at the CCR Genomics Core Facility,

and *de novo* sequence assembly was performed utilizing the computational resources of the NIH High-Performing Computation Biowulf Cluster genomic core facility, NIH. DNA library was prepared using the Illumina NexteraXT kit. Raw reads generated by the paired-end library and overall quality were checked by using FastQC (<http://www.bioinformatics.babraham.ac.uk/projects/fastqc/>) and the adaptor sequence was trimmed by Trimmomatic (Bolger et al., 2014), and *de novo* sequence assembly was done using SPAdes 3.13.1 (Bankevich et al., 2012). The assembled contigs of each of the phages were closed by PCR followed by Sanger sequencing using primers facing opposite directions at both ends, and the sequence reads were manually inspected/corrected wherever necessary. Structural and functional annotation was done using tools available at the Galaxy and Web Apollo available at the Center for Phage Technology (<https://cpt.tamu.edu/galaxy-pub/>) (Afgan et al., 2018; Lee et al., 2013). Gene prediction was done by GLIMMER v3.0 (Delcher et al., 1999) and MetaGeneAnnotator 1.0 (Noguchi et al., 2008). Similarly, tRNA was predicted by ARAGORN 2.36 (Laslett & Canback, 2004) and transcriptional terminators were manually analyzed that were called by *TransTermHP* (Kingsford et al., 2007). Promoter sequences were predicted using *PhagePromoter* available in the Galaxy framework setting threshold at 0.8 (Sampaio et al., 2019). Functional annotations were done by InterProScan (Jones et al., 2014) and BLASTp similarity search to Canonical Phages database (Camacho et al., 2009) and/or confirmed TMHMM (Krogh et al., 2001), at default settings in the WebApollo interface (Lee et al., 2013). The functional domain of the predicted protein was accessed by the Pfam and HHpred databases (Finn et al., 2016; Soding, 2005). Phage genome annotation was visualized by using CGview (Stothard & Wishart, 2005).

3.13 Safety Evaluation

The phage genomes were screened for the presence or absence of pathogenic bacterial toxins/virulence factors and antimicrobial resistance genes. Virulence Factors of Pathogenic Bacteria (VFDB) (Liu et al., 2018) and Comprehensive Antibiotic Resistance Database (CARD 3.0.7), Resistance Gene Identifier (RGI, v5.1.0) (Jia et al., 2017) databases were used to detect such problematic/toxic genes. PHAge Search Tool Enhanced Release (PHASTER) was used to rule out the lytic and lysogenic lifecycle based on integrase genes (Arndt et al., 2016). Default parameters were used for all tools.

3.14 Genome comparison and phylogenetic analysis

Basic Local Alignment Search Tool (BLAST) online tool from the NCBI website (<https://blast.ncbi.nlm.nih.gov/Blast.cgi>) was used to identify high nucleotide homology with the phages ϕ Ec_Makalu_001, ϕ Ec_Makalu_002 and ϕ Ec_Makalu_003 genomes (>90% query cover and > 90% identical genome). Progressive MAUVE (Darling et al., 2010) was used to compare highly homolog genomes available at NCBI. EMBOSS (The European Molecular Biology Open Software Suite) Stretcher software was used for pairwise sequence alignment of amino acids, with the parameters set at default values (Madeira et al., 2019). Phylogenetic analysis of the 17 highly similar (>90% coverage and >90% identity) phage genomes belonging to subfamily Tevenvirinae, a genus of Krischvirus was carried out using the VICTOR tool under the parameter recommended for prokaryotic viruses (Meier-Kolthoff & Goker, 2017). All pairwise comparisons of the amino acid sequences were conducted using the Genome-BLAST Distance Phylogeny (GBDP) method (Meier-Kolthoff et al., 2013). The resulting intergenomic distances were used to infer a balanced minimum evolution tree with branch support via FASTME including SPR post processing (Lefort et al., 2015). Branch support was inferred from 100 pseudo-bootstrap replicates each. Trees were rooted at the midpoint (Farris, 1972). and visualized with Fig Tree software. Taxon boundaries at the species, genus, and family level were estimated with the OPTSIL program the recommended clustering thresholds, and an F value of 0.5 (Meier-Kolthoff & Goker, 2017).

3.15 Assessment for depolymerase activity of ϕ Kp_Pokalde_001

When the phage is plated on the lawns of its host bacteria, clear plaques surrounded by an expanding turbid halo were assumed to be depolymerase activity of the phage (Sutherland, 1976). The clear central region of the plaque represents the area where the phage has lysed all phage-sensitive host bacteria, and the turbid halo corresponds to clearing of the bacterial capsule, but not lysis of the cells. Here “depolymerase activity” means any activity that cleaves polysaccharide chains into smaller subunits, regardless of the precise catalytic mechanism. We observed a unique plaque morphology conversion into a halo and clear edge originating from the same plaque during clonal purification. The plaque in query was cored at the center and/or periphery by a 200 μ L pipette tip and the chunk of solid agar was resuspended in the SM buffer.

A drop of chloroform was added, vortexed, and centrifuged to obtain the phage suspension. It was then serially diluted and 50 μ L of the diluted phage suspension was mixed with 100 μ L of an overnight culture of host strain and incubated for 10 minutes at room temperature. The mixture was added in 3 mL of LB soft agar and poured onto TB plates. The clear-edged plaques and those with halo surrounding were counted for percentage.

3.16 Identification of the polysaccharide depolymerase gene

It was hypothesized that a putative tail spike gene in phage Kp_Pokalde_001 was responsible for the observed putative depolymerase activity. Gene product 53 (gp53) having a 1716-bp length (571 amino acid) from the phage Kp_Pokalde_001 was selected as the most likely candidate due to its protein sequence similarity to other known depolymerases. Gene 53, encoding the predicted depolymerase, was cloned, expressed, and partially purified.

3.17 Plaque selection, PCR amplification of tail spike gene, and analysis

Each clear phage mutant and revertant with halo surrounding was subjected to three rounds of plaque purification for clonality. Each plaque was picked and purified soon after its appearance on the bacterial lawn, usually within 4 to 6 hr. depending on the plaque size, to maximize the selection of the clonal population. The tail spike gene (gp 53) of the phage ϕ Kp_Pokalde_001 wild type and revertant phages was PCR amplified using the primer pair TS_Forward 5'GACTGGCGCTATATTAGCAAGTAC 3' and TS_Reverse 5' TCTGTGCGTTAGAAGTGCAGCAC 3'. The 1950-bp amplified product was purified by gel-extraction and sequenced by the Sanger method using three primers covering the entire gene, Seq1 5' GTGGCAGAGCAAAGCCATTG 3', Seq2 5' GAACTTGTTCCGTAGGATGGGTG 3', and Seq3 5' ATAGTCCGTTCCGGCCCTG 3'. Sanger sequencing was performed at the CCR, Genomics Core Facility, NIH, USA. Nucleotide changes in the tail spike gene were identified by sequence alignment using SnapGene software.

3.18 Cloning of tail spike gene (gp53) of ϕ Kp_Pokalde_001

The full-length tail spike gene (gp53) was PCR amplified directly from the phage lysates designed to incorporate His6-tag at the C-terminal end for downstream Ni²⁺ - NTA purification of the protein product. The linear plasmid was purified by GeneJET

Genomic DNA Purification Kit (Thermofisher Scientific™ USA). PCR products of both vector and insert were separated on a 1.0% agarose gel in TAE electrophoresis buffer (40 mM Tris -HCl pH 7.2, 500 mM sodium acetate and 50 mM EDTA, stained with SYBR® Safe DNA Gel Stain (Thermofisher Scientific™ USA) and visualized with blue light. Each fragment was cloned into the pBAD expression vector (Figure 12) available in Adhya's lab, NCI, NIH using the Gibson assembly technique. The PCR products of both vector and insert were purified by GeneJet Gel-Extraction kit (Thermofisher Scientific™ USA) and extracted DNA fragments were quantified by NanoDropOnec (Thermofisher Scientific™ USA).

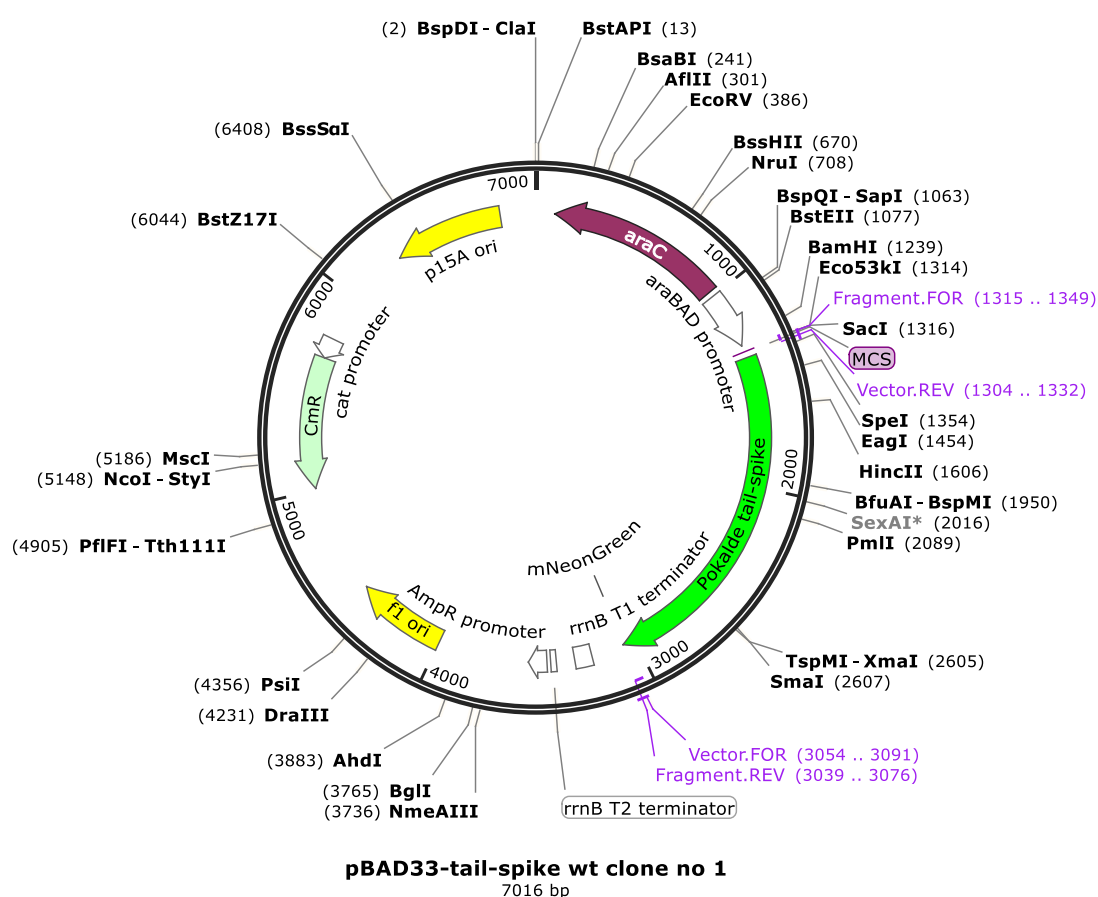


Figure 12: Map of the cloning vector pBAD33. The vector has a chloramphenicol-resistant gene. The araBAD promoter drives the expression of inserted genes. The Tail-spike gene of the ϕ Kp_Pokalde_001 (gp53) is inserted into the multiple cloning site (green region).

3.19 Preparation of a Gibson assembly mix

The reagent mix was prepared for Gibson assembly as described before (Gibson et al., 2009). The Master Mix (1.33x) was prepared by mixing 100 μ L of 5x isothermal

reaction buffer (500 mM Tris-HCl, pH 7.5, 250 mg/mL PEG 8000, 50 mM MgCl₂, 50 mM DTT, 1.0 mM of each dNTPs and 5 mM NAD), 50 µL Taq ligase (40 U/µL), 2 µL T5 exonuclease (1.0 U/µL), 6.25 µL Phusion polymerase (2 U/µL) to a final volume of 375 µL. This solution mix was aliquoted into 15 µL aliquots and stored at -20 °C.

3.20 Preparation of the Tail spike gene (gp53) of ϕ Kp_Pokalde_001

Gene-specific primers were designed using SnapGene software. To create an insert with complementary overhangs with the pBAD vector, specific primers 5' GCCAATTCGAGCTCGGTACCGAAACGATAAGAGGGGACACATGG 3' and 5' AATTTAATGGTGATGGTGATGGTGGAAGTGCAGCACCAAGCTAGCCCGAG 3' were added to the both forward and reverse primers, respectively. These extensions allowed to remove the stop codon to clone the ORF in frame with both the multiple cloning sites (MCS) and the C-Terminal His6-tag encoding sequences. Phage genomic DNA was used as templates for the PCR reactions. The forward or reverse primers were designed with 5' and 3' overhangs sequences overlapping with the plasmid pBAD as described earlier. All primers used in this research to amplify the target genes are tabulated in Appendix-E. The gene was amplified with a NEBNext® High-Fidelity 2X PCR Master Mix (New England Biolabs). Briefly, a 50 µL reaction mix containing 30 ng of gDNA, or 10 ng of plasmid as templates, 25 pmol of each primer, 0.2 mM dNTP Mix, one unit of the polymerase, and 1X polymerase buffer was used in the following PCR reaction steps: (1) 98 °C for 3min, 1 cycle; (2) 98 °C for 30 s, 60°C for 30 s, followed by 72 °C for 2min; 30 cycles; (3) 72 °C for 5 min, a cycle. PCR products were purified by GeneJET Genomic DNA Purification Kit (ThermoFisher Scientific™ USA) according to the manufacturer's instruction, and DNAs were quantified using Nanodrop™ spectrophotometer (ThermoFisher Scientific™ USA).

3.21 Expression constructs and cloning confirmation

The assembly of the pBAD vector and gene insert was performed by a one-step isothermal DNA recombination method. Vector and fragment were mixed in 1:1 equimolar concentration then added to the 10 µL Gibson assembly master mix (2X) and distilled water was added to a final volume of 20 µL. The mixture was incubated at 50 °C for 1 hr, and 5 µL was transformed into a chemically competent laboratory strain of *E. coli* XL-1 blue cells by electroporation using 2 mm diameter cuvettes and

the GenePulser XCell system (Bio-Rad, Hercules, CA, USA) with 1.8 kV voltage and 800 Ω resistance. Immediately after electroporation, SOC media (1 mL) was added and the suspension was transferred to a 1.5 mL microcentrifuge tube and incubated at 32°C for an hour in a roller incubator. One hundred microliters of the suspension were spread onto the LB media containing chloramphenicol and incubated overnight at 32°C. Colony having positive clones was confirmed using colony PCR by growing on chloramphenicol LB plates using the gene (insert)specific primer. PCR products were analyzed in 1% (w/v) agarose gel electrophoresis. The remaining liquid media containing the positive clones were inoculated in 10 mL LB with 25 μ g/mL chloramphenicol overnight at 37°C for further plasmid extraction by GeneJET Plasmid Miniprep Kit (Thermo Fisher Scientific).

3.22 Purification of the depolymerase enzyme and activity assay

Each fragment was cloned into the pBAD expression vector available in the lab using the Gibson assembly method. After verification of individual clones by DNA sequencing, the clone was transformed into NM397 (*DaraEp Pcp6genta::Pcp18-araE*) strain, a derivative of *E. coli* K-12. The culture was grown in regular LB at 37 °C in the presence of 25 μ g/mL chloramphenicol, induced with 0.2% arabinose at OD_{600nm} of 0.3 for the expression of a protein. The following induction for 3 hr., cells were harvested by centrifugation; the pellet was resuspended in a buffer (20 mM sodium phosphate, 250 mM NaCl, pH8.0 plus 10 mM imidazole and protease inhibitor cocktail) and subjected to French press for lysis (pressure stabilized at 1500 psi). The protein in the lysate was then affinity purified using immobilized nickel-nitrilotriacetic acid (Ni-NTA) resin (GE Healthcare, USA) in a gravity column and dialyzed to remove excess imidazole from the elution buffer. The eluted protein was concentrated by centrifugation using a 30 kDa MWCO Amicon Ultra-15 column. The protein was further purified by size exclusion chromatography using a Superdex 200 pg 16/600 HiLoad Column in an AKTA system (GE Healthcare, USA). The protein concentration was measured using a NanoDropOnec (Thermo Scientific, USA). The protein purity was analyzed by SDS-PAGE. To measure the activity of a protein, a bacterial host was mixed on a top agar and layered on top of the LB plate. The protein of 2-fold serial dilution from 100 μ g/mL was spotted on the plate and incubated at 37°C for 6 to 8 hours. The lowest concentration of protein with a visible clearing of the bacterial lawn was noted as the minimal inhibitory concentration (MIC).

3.23 Phage adsorption efficiency and adsorption kinetic assay.

A small volume (100 µL) of a bacterial culture grown to an optical density (OD_{600nm}) of 0.3 was mixed with phage at MOI of 0.01 and incubated at room temperature for 15 minutes. A drop of chloroform was immediately added to stop the phage production. After centrifugation at 11,000 rpm for 10 minutes, the supernatant was serially diluted, and spot tittered to calculate the number of free phages. A phage-host mixture was serially diluted, and spot tittered without chloroform treatment to calculate the input phage. Adsorption efficiencies were calculated using the following equation:

$$\text{Adsorption efficiency (\%)} = 1 - \frac{\text{PFU of free phage (Pt)}}{\text{PFU of host and phage mixture (Po)}} \times 100$$

For the adsorption kinetics, ~25 mL culture at OD_{600nm} of 0.3 was infected with phage at MOI of 0.01 and kept shaking the culture at 37 °C water bath. The sample was withdrawn (1.0 mL), chloroform treated, and centrifuged to collect the supernatant at 4, 6, 8, and 12 minutes. The supernatant was plated for free phage counting. The ratio of free phage (Pt) and input phage (Po) was plotted against time.

3.24 Phage therapy experiments

3.24.1 Ethical clearance and animal model

Ethical approval for the use of animals in this study was obtained from Nepal Health Research Council (NHRC), Kathmandu, Nepal (Ethical approval No.161/2018). Animal experiment protocol was also approved by the Ethical Review Board, NHRC. Six to eight weeks old female Swiss Albino mice weighing 23 ± 2.5 g were bought from Natural Products Research Laboratory (NPRL), Department of Plant Resources, Thapathali, Kathmandu. The animals were kept in an animal room at the Central Department of Biotechnology (CDBT), Tribhuvan University, and fed with a normal antibiotic-free diet. Chloroform vapor was used to anesthetize the mice and then euthanized by cervical dislocation before any invasive procedures. Each experiment was performed in triplicates. Schematic representation of mouse model experiment design is depicted in Figure 13.

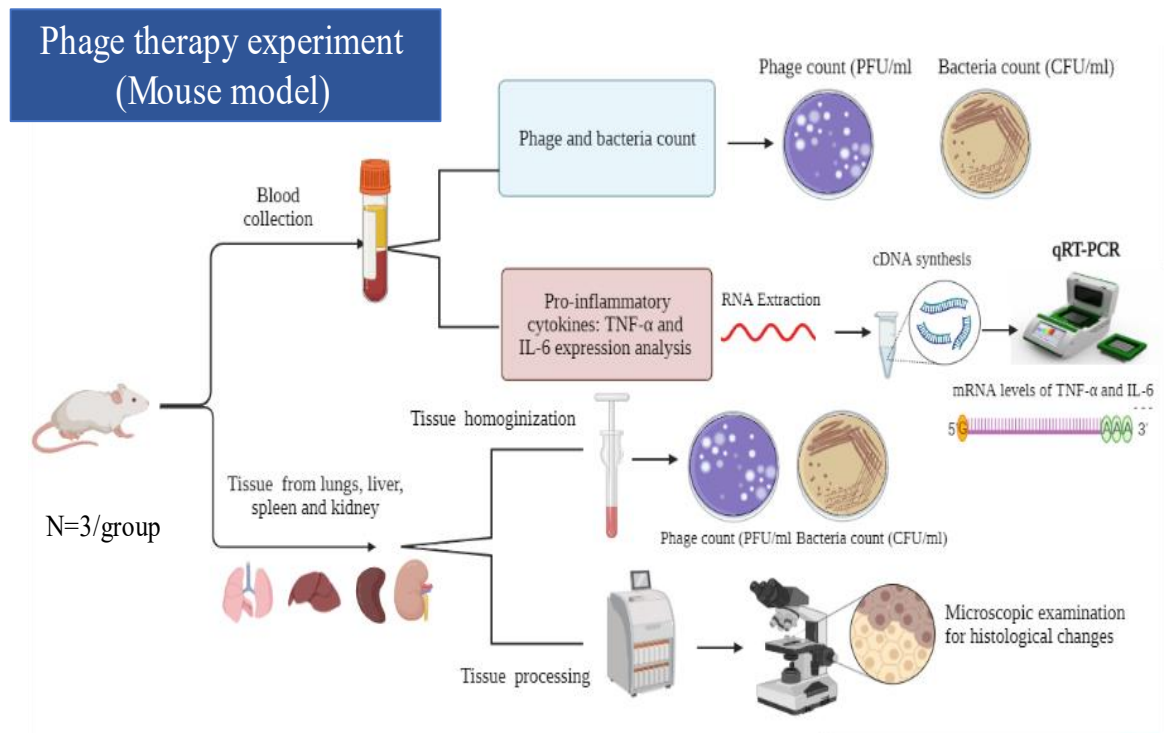


Figure 13: Schematic representation of the mouse model experiment design. The bacteria and phage numbers were enumerated from the blood and tissue samples (lungs, liver, spleen, and kidney) from the mouse under test. The expression of pro-inflammatory cytokines (TNF- α and IL-6) levels was evaluated by qRT-PCR from the blood sample. The lung tissue sample was processed for histological examination. Figure made in BioRender.com.

3.24.2 Bacterial strain and phage used in an animal model experiment

The virulent ϕ Kp_Pokalde_002 (*Podoviridae*, C1 morphotype) was selected for phage therapy experiment which was isolated against a clinical isolate of *K. pneumoniae* (hereafter mentioned to as Kp56) molecularly confirmed as a carbapenem-resistant from previous study. Owing to the phage suitability in terms of its lytic lifestyle, good thermal and pH stability, a large burst size, and genomic properties as discussed in the result section. The ϕ Kp_Pokalde_002 was amplified from glycerol stocks and phage lysate was prepared. Briefly, eight to ten hours culture of the host bacteria (1.0 mL) was mixed with 100 mL LB broth and incubated at 37°C for two hours with agitation (100 rpm) to reach an exponential growth phase (OD_{600nm} of 0.25). The phage stock, adjusted to room temperature, then host bacteria Kp56 was added at a multiplicity of infection (MOI) of 10, and the culture was further incubated at 37°C in a shaking incubator (250 rpm) for 5.0 hr. until the media was visually clear. The phage lysate was

centrifuged at 8000 rpm (Eppendorf, Germany) for 15 min at 4°C, and the supernatant was filtered through a 0.22 mm pore-size Whatman™ syringe filter (Sigma- Aldrich, United States). The phage lysate then further purified by isopycnic cesium-chloride (CsCl) density-gradient ultracentrifugation as described earlier.

3.24.3 Preparation of bacterial inoculums

An isolated colony of Kp56 was picked with a pointed wire loop and diluted in 3.0mL LB broth and incubated overnight at 37 °C. The next day, visible turbidity of the bacterial growth was observed and diluted 1:100 in LB broth and incubated in a shaking incubator (200 rpm) at 37 °C till mid-log phase is attained (OD_{600nm} of 0.25). Then the bacterial suspension was centrifuged at 4100rpm for 10 minutes and the pellet was washed with normal saline three times. The cell pellet was then dissolved in normal saline solution to make up a final volume of one milliliter. This bacterial suspension was used to infect the mouse in a phage therapy experiment.

3.24.4 Blood and Tissue Collection

Blood was collected from anesthetized animals in tubes containing anticoagulant (EDTA) through cardiac puncture. Blood samples were used for enumeration of bacteria and phage count as well as to access the level of the pro-inflammatory cytokine. After blood collection, the anesthetized mice were euthanized by cervical dislocation. The blood samples were centrifuged at 10,000 rpm for 5 min., and the plasma was collected with sterile pipettes. Plasma from these samples was serially diluted with PBS up to 10⁻⁶ for bacterial CFU and phage plaque-forming units (PFU) count. Lungs, Liver, spleen, and kidney tissue samples were removed aseptically from the animals. The tissues were weighed, suspended in 2.0 mL of PBS, homogenized with sterile Dounce homogenizer, and then serially diluted with PBS for the enumeration of bacterial CFU and phage PFU count per gram of tissue.

3.24.5 Enumeration of the bacterial count

Blood and tissue samples (homogenized) were serially diluted up to 10⁻⁶ in 1.5 mL Eppendorf tubes. A 100 µL aliquot of the dilutions was spread-plated on nutrient agar plates using glass beads and incubated at 37°C for overnight. The bacterial counts were

corrected to determine bacterial counts in CFU/gm of tissue using the following formula:

$$\frac{\# \text{ colonies/mL plated} \times \text{Dilution Factor}}{\# \text{ grams tissue/mL original homogenate}} = \text{CFU/gm}$$

3.24.6 Enumeration of the phage count

Blood and Homogenized tissue samples were centrifuged at 10,000 rpm for 10 minutes at 4°C in (Centrifuge 5810 R, Eppendorf, Hamburg, Germany) and filtered with a 0.22 µm pore size syringe filter (Whatman™, Sigma-Aldrich, United States). The filtrate was serially diluted to up to 10⁻⁸ and phage titer was determined by Double Layer Agar (DLA) assay as described above. The phage counts were calculated for tissue/fluid weights using following formula:

$$\frac{\# \text{ plaques/mL plated} \times \text{Dilution Factor}}{\# \text{ grams tissue/mL original homogenate}} = \text{PFU/gm tissue}$$

3.24.7 Determination of minimum lethal Dose (MLD)

The minimum lethal dose (MLD) of Kp56 in mice was obtained as described before with modifications (Saganuwan, 2011). One milliliter of mid-log phase bacterial suspension in LB broth (OD_{600nm} of 0.3) was centrifuged at 4,000 rpm for 10 minutes and washed with 1.0 mL sterile phosphate buffer saline (PBS) three times. The bacterial pellet was resuspended in normal saline (1.0 mL) and serially diluted to obtain different concentration of bacterial count (~1×10⁵, ~1×10⁶, ~1×10⁷, ~1×10⁸, and ~1×10⁹ CFU/mL). Mice were divided into six groups (n=30). Two hundred microliter of diluted bacterial cell suspensions from each of the dilutions (~1×10⁵, ~1×10⁶, ~1×10⁷, ~1×10⁸, and ~1×10⁹ CFU/mL) was injected into one to five groups of the mice through the IP route. Two hundred microliter of normal saline was injected into the sixth (control) group (Table 7). The mice were kept in a animal room at CDBT, TU and observed for signs of illness and survivability for up to 7 days.

Table 7: Dose of bacteria (Kp56) given to the mice to find out the lethal dose.

Group of mice	Number of mice	Bacterial (Kp56) dose (CFU)	Normal saline
Control Group A	5	-	200 μ L
Experiment Group B	5	2×10^8	-
Experiment Group C	5	2×10^7	-
Experiment Group D	5	2×10^6	-
Experiment Group E	5	2×10^5	-
Experiment Group F	5	2×10^4	-

3.24.8 Pharmacokinetics (PK) of phage ϕ Kp_Pokalde_002

Pharmacokinetics (PK) assessment *in-vivo* was performed as described before (Pouillot et al., 2012; Verma et al., 2009) with some changes. Mice were divided into four groups (n=72) [2 phage only and 2 vehicles (SM buffer) control, 18 mice in each group] (Figure 14). In a phage-only control group, the first group of mice were administered 200 μ L (1.2×10^8 PFU/mL) of the purified ϕ Kp_Pokalde_002 through oral route and the same dosage of phage lysate was injected through IP route in another group. The third and fourth (vehicle control group) received 200 μ L of SM buffer only by oral and IP routes respectively. Three mice from each group were euthanized by cervical dislocation at 1hr, 4hr, 8hr, 24hr, 48hr, and 72 hr., after phage administration. Blood samples were collected in tubes containing anticoagulant (0.05 M EDTA) by cardiac puncture. Tissue samples from lungs, liver, spleen, and kidneys were collected aseptically from the euthanized mice and further divided into two parts. One part of each tissue was fixed in 10% formalin for histopathological examinations. Another part of the tissue was weighed and homogenized in 2.0 mL PBS aseptically as described earlier. The homogenized tissue was centrifuged at 10,000 rpm for 10 minutes at 4 °C and the supernatant was filtered through a 0.22 μ m pore size (WhatmanTM syringe filter, Sigma-Aldrich, Missouri, United States) syringe filter. The phage titer was determined by DLAA method as described earlier.

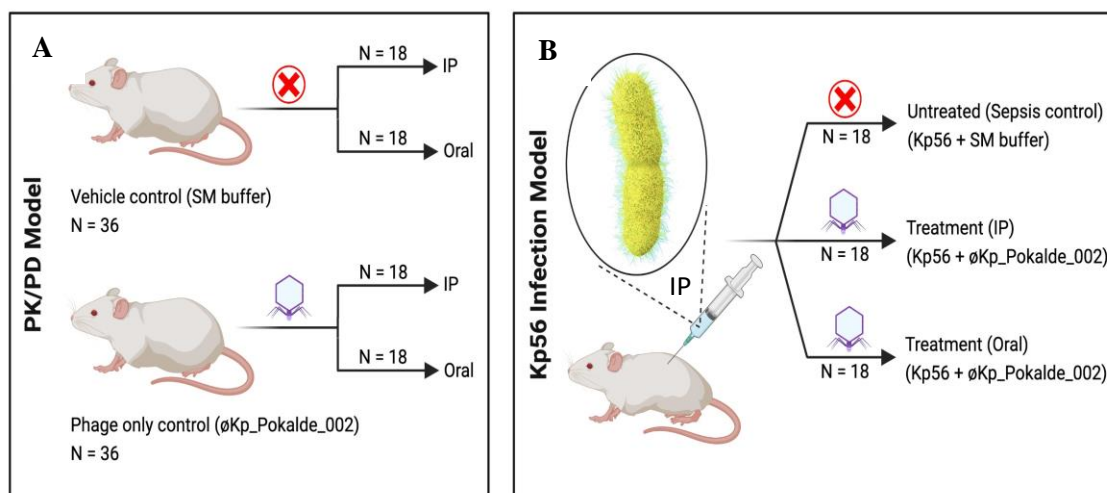


Figure 14: Schematic representation of the PK/PD experiment design. In Figure: A) In PK/PD model, SM buffer (vehicle control) and the same dose of purified ϕ Kp_Pokalde_002 (phage only control) were administered via both IP and oral routes. B) In the bacteria infection model, bacteria (Kp56) was administered through IP route only, and the phage ϕ Kp_Pokalde_002 was administered through both IP and oral routes. PK: pharmacokinetics; PD: pharmacodynamics; SM: Sodium Magnesium; IP: intraperitoneal. Figure created in BioRender.com.

In another study, mice ($n=54$) (3 groups, 18 in each group) were inoculated with 200 μL (1×10^8 CFU/mL) of exponentially growing Kp56 intraperitoneally. Immediately after bacterial injection, a 200 μL of SM buffer was injected into all mice in the first group (as a sepsis control) and 200 μL of ϕ Kp_Pokalde_002 (1.2×10^8 PFU/mL) was administered to all mice in second and third groups (treatment) through IP and oral routes. Three mice from each group were euthanized by cervical dislocation at 1hr, 4hr, 8hr, 24hr, 48 hr, and 72 hr. post bacterial inoculation. Blood and tissue samples were collected and processed as described earlier to determine the phage titer and the levels of pro-inflammatory cytokines.

3.24.9 Cytokine quantification by qPCR

Pro-inflammatory cytokines: tumor necrosis factor-alpha (TNF- α) and interleukin 6 (IL-6) mRNA expression levels were measured in all bacteria infected and phage treated mice. Total RNA was isolated from the blood samples using Direct-zol™ RNA MiniPrep Plus Kits (Zymo Research, USA) and cDNA was synthesized using iScript™ cDNA Synthesis Kit (Bio-Rad Laboratories, USA) following the manufacturer's instruction. DNase I (6 U/ μL) was used to digest any residual DNA. Total RNA concentration was measured using NanoDrop 8000 (Thermo Fisher Scientific, USA) by spectrophotometric optical density measurement at 260/280 nm. The mRNA levels

of TNF- α and IL-6 were measured by two-step relative qRT-PCR. The β -actin housekeeping gene was amplified as an internal control. Gene expressions were normalized to the expression of the β -actin gene. The sequences of primers used for IL-6: F-5'-GAGGATACCACTCCCAACAGACC-3', R-5'-AAGTGCATCATCGTTGTTTCATACA-3' for TNF- α , F-5'-CATCTTCTCAAAATTCGAGTGACAA-3, R-5'-TGGGAGTAGACAAGGTACAACCC-3' and for β -actin: F-5'-CTGTCCCTGTATGCCTCTG-3', R-5'-ATGTCACGCACGATTTCC-3'. The real-time PCR was performed using SYBR®Green Master Mix(2x) Kit in CFX Connect™ RT-PCR system (Bio-Rad Laboratories, USA). Real-time PCR thermal cyclers conditions for β -actin, IL-6, and TNF α amplification are shown in Table 8. Melting curve analysis was performed after the amplification phase to eliminate the possibility of nonspecific amplification or primer-dimer formation. All samples were processed in duplicate, and output level was reported as an average. The comparative CT method was used to calculate the relative expression ratio from the real-time PCR efficiency and the CT (Jain et al., 2006; Livak & Schmittgen, 2001). The fold of cytokines mRNA expression level change was calculated using the double delta Ct (DDCT) method and the change in mRNA expression levels of cytokines were expressed as fold change.

$$\text{Fold change} = 2^{-\Delta\Delta Ct}$$

where $2^{-\Delta\Delta Ct} = [(Ct \text{ of the gene of interest} - Ct \text{ of internal control}) \text{ sample A} - (Ct \text{ of the gene of interest} - Ct \text{ of internal control}) \text{ sample B}]$

Table 8: Real-Time PCR thermal cyclers conditions for β -actin, IL-6, and TNF α

Steps	Temperature (°C)	Time
Enzyme Activation	95	10 minutes
Initial Denaturation	94	15 seconds
Annealing	55 (58 for TNF α)	30 seconds (55 seconds for TNF α)
Extension	72	1 minute
Melt curve	85	10 minutes
Total cycle = 45		

3.24.10 qPCR validation

Samples collected from normal uninfected mice were used as reference samples (calibrators) to validate the primers. Primer concentrations were optimized to determine the minimum primer concentrations giving the lowest threshold cycle (ct) and the maximum signal-to-noise fluorescence ratio while minimizing nonspecific amplification. To address the question of whether contaminating gDNA present in the total RNA samples could influence the cytokine cDNA quantitation, RNA preparations without prior cDNA synthesis were subjected to PCR. None of the samples gave a signal for any of the cytokines. To investigate whether contaminating gDNA was co-amplified or could have interfered with the quantitation of cytokine cDNAs, both cDNA and 100 ng of genomic DNA were subjected to PCR. All cytokine sequences were amplified with cDNA but not with gDNA as a template. Therefore, all reactions were able to differentiate between cDNA and gDNA, confirming the specificity of the primer combinations used for the selective amplification of cDNA. The primer pairs amplified PCR products with high specificity for each target gene with the respective melting curve.

3.24.11 Histological examination

The lung tissue was examined for histological changes as described elsewhere (Singla et al., 2015) with modification. Briefly, pieces of tissues were fixed in 10% formal saline. After proper fixation, the tissues were dehydrated in ascending grades of ethyl alcohol (70, 80, 90, and 100%), cleared in xylol, then impregnated and embedded in paraffin wax. Serial sections of 4 μm - 6 μm thickness were cut using a rotary microtome and sections were deparaffinized, rehydrated, and stained with hematoxylin and eosin (H&E) stain. The tissue sections were examined under the light microscope for histological changes.

3.24.12 Assessment of phage therapy in a mouse model

The efficacy of phage therapy in a mouse model was assessed as described previously with some modifications (Capparelli et al., 2006; Gill et al., 2006; Jeon et al., 2016; Merrill et al., 1996; Singla et al., 2015). Briefly, 40 mice were divided into eight groups (Figure 15). A lethal dose, 200 μL of ($\sim 1 \times 10^8$ CFU/mL) Kp56 was injected through the IP route into five of the eight groups. The first group was injected with 200 μL of SM buffer through the IP route for a sepsis-positive control. The second and third groups

of mice were treated with a single dose of ϕ Kp_Pokalde_002 at MOI=1 (200 μ L of 1.2×10^8 PFU/mL) via either oral or IP route immediately after bacterial injection. The phage was injected through the IP route after 1hr. of bacterial challenge in the fourth group. In the fifth group, the phage was injected intraperitoneally 24 hours before bacterial infection (pre-phage therapy group), and the sixth group was treated with the phage via IP route after 24 hr. of bacterial infection. Similarly, the seventh group was served as a vehicle control group which was injected with a 200 μ L of SM buffer only. The last, phage-only group, mice were injected with 200 μ L of the phage (MOI=1) via IP route. The bacterial count was enumerated from the blood and homogenized lung tissues samples. Animals were observed for their health conditions and survivability for 15 days.

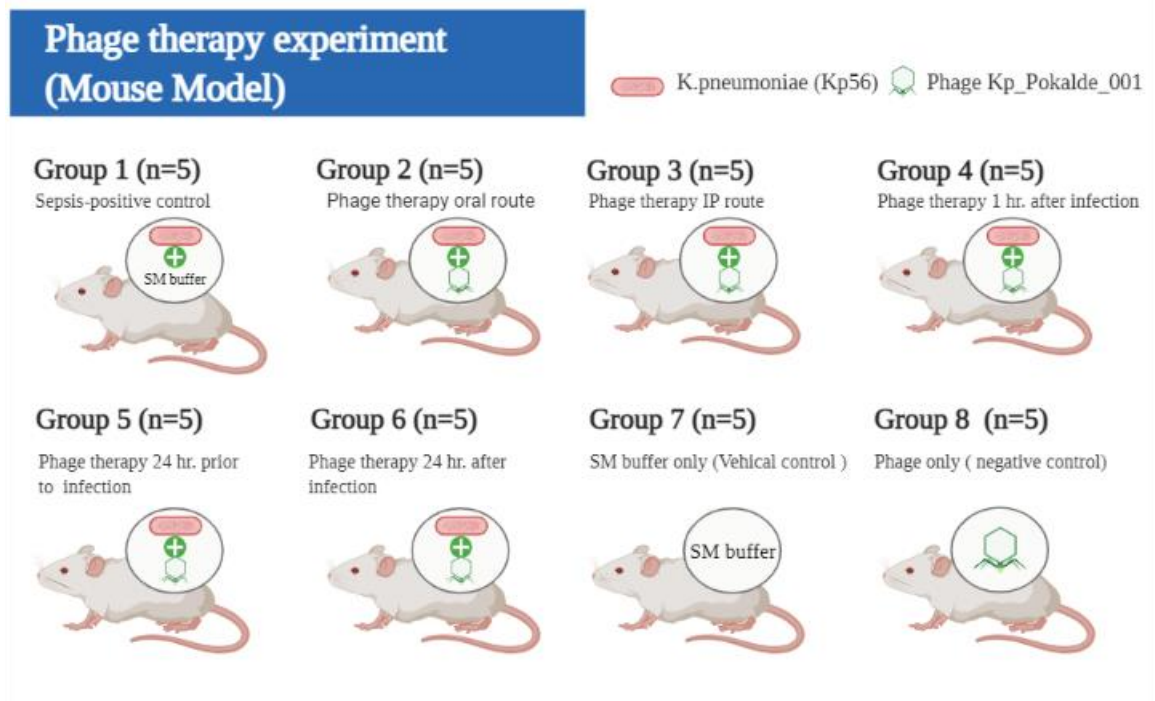


Figure 15: Schematic representation of phage therapy in a mouse model. Mice were divided into eight groups (n=40). Mice were infected with a lethal dose (200 μ L of $\sim 1 \times 10^8$ CFU/mL) of Kp56 through the IP route. In phage therapy groups, infected mice were treated with 200 μ L of ϕ Kp_Pokalde_002 (1.2×10^8 PFU/mL) at MOI=01 through either oral or IP routes. SM buffer was administered via IP route in sepsis positive control group. The vehicle control and negative control groups were injected with 200 μ L of SM buffer and ϕ Kp_Pokalde_002 (1.2×10^8 PFU/mL) via IP route respectively. SM = Sodium Magnesium buffer, IP = intraperitoneal, MOI = multiplicity of infection. Figure made in BioRender.com.

3.24.13 Positive control group

In the sepsis control group, mice (n=24) were infected with a lethal dose of Kp56 (2×10^8 CFU/mL) through the intraperitoneal (IP) route. Mice were then divided into two groups. A 200 μ L of SM buffer was administered through the oral route in one group. Similarly, 200 μ L of SM buffer was injected through the IP route. After 1hr, 4hr, 8hr and 24hr. three mice from each group were processed for blood and tissue samples from liver, spleen, and kidney collection. Blood and tissues were used to determine bacterial count (CFU/mL), cytokine expression, and histopathological examination.

3.24.14 Data availability and statistical analysis

The genome sequence data are deposited in NCBI under Bio-project accession *PRJNA594990* and is publicly available through the following GenBank accession numbers: *Escherichia* virus Ec_Makalu_001 (MN894885), *Escherichia* virus Ec_Makalu_002 (MN709127), and *Escherichia* virus Ec_Makalu_003 (MN882349) for *Myophages* and *Klebsiella* virus Kp_Pokalde_001 (MW590329.1) and *Klebsiella* virus Kp_Pokalde_002 (MT425185.1) for Podophages. All statistical analysis was performed using GraphPad Prism 8 (Version 8.3.0) and differences with $p < 0.05$ were considered statistically significant. The data were expressed as a mean, standard deviation (SD) of the mean and analyzed under an ordinary one-way and two-way analysis of variance (ANOVA) with Dunnett's multiple comparisons test and student's t-test.

For pharmacokinetic analysis, non-compartmental PK parameters: the peak plasma concentration (C_{max}) and the time to reach peak plasma concentration (T_{max}) were obtained by visual inspection of the data. The area under the plasma concentration-time curve (AUC) was calculated according to the linear trapezoidal rule up to the T_{last} phage concentration using GraphPad Prism 8 (Version 8.3.0). The half-life ($T_{1/2}$) was calculated from the one-phase exponential regression equation ($T_{1/2} = 0.693/K_{el}$) (Chow et al., 2020; Dufour et al., 2018). The elimination rate constant (K_{el}) was estimated from the slope of the elimination phase of the log-transformed plasma concentration-time curve fitted by the method of least squares. All elimination phase data with associated variability were included in the estimation. Data were expressed as mean \pm

standard error of the mean (SEM). Comparisons of phage count and cytokine levels were performed by one-way ANOVA with Tukey's multiple-comparison test and Student's t-test. Inter mice variability was expressed as coefficient of variation (%CV). For the phage therapy experiment, survival curves were compared for significance using the log-rank (Mantel-Cox) test. Differences with $p < 0.05$ were considered statistically significant. Each of the experiments was performed three times. All statistical analyses were performed using GraphPad Prism 8 (Version 8.3.0).

CHAPTER 4

RESULTS AND DISCUSSION

4.1 Phage isolation

Isolation and characterization of the potent lytic phages and their therapeutic application against drug-resistant infections is the main aim of this Ph.D. project. A total of twenty river water and sewage samples were collected and screened for the presence of phages. Samples were collected from different locations of the Kathmandu valley assuming the water in these areas were heavily polluted with solid waste originating from household as well as from the hospital area assuming the samples were contaminated with pathogenic bacteria. The water samples from the river appeared to be clear with some sediment and samples from sewage were largely turbid with an abundant number of algae floating on the surface.

In this study, a total of three carbapenem-resistant *Escherichia coli* (*E. coli* M1, *E. coli* M2, and *E. coli* M3). and two *Klebsiella pneumoniae* (*K. pneumoniae* TUKp1 and *K. pneumoniae* Kp56) recovered from the clinical samples were used as a host for the isolation of the phage. These bacteria were confirmed as carbapenem-resistant harboring MBL genes: *blaNDM*, *blaOXA*, *blaKPC*, *blaIMP*, and *blaVIM* in a previous study (unpublished data). Among 20 water samples, 75% of the samples (15/20) were positive for visible plaques in double-layer agar assay (DLAA) indicating the presence of phages in those samples. Round, clear, and transparent lysis zones of variable sizes in the form of plaques were observed on the surface of the plates, signifying that the samples collected from different sites contained phages that were infectious against the tested bacterial hosts. The phages produced clear, variable-sized (ranging 1.0-14.0 mm in diameter) plaques with well-defined edges in the bacterial lawn, showing that the isolated phages have a lytic effect against the bacterial strains (Figure 16). The size of the plaque depends on the adsorption efficiency of the phage, latent time, and burst size. A difference in adsorption time of the phage particles to host cells also may lead to variables in plaque size. The physical size of the phage also influences the overall size of plaques. A smaller phage can diffuse more easily and quickly through semi-solid agar resulting formation of larger plaques as compared to larger phages (Figure 17). Different plaque morphology was observed in the plate of a single host lawn. This

indicates the presence of both lytic and temperate phages as they produce plaques with different degrees of transparency and sizes. Plaques with a turbid center surrounded by a clear ring particularly appeared as a “bulls-eye” shape suggesting temperate phages. The halo around the plaque indicates that decapsulation of the bacterial host cell by phage produced soluble enzymes such as depolymerases (Figure 17 A). The hazy ring suggests that the phage produced a depolymerase enzyme that diffuse through the agar layer and degraded the bacterial capsular polysaccharide (CPS) into different oligosaccharide components. Early studies showed that certain *K. pneumoniae* phages produced depolymerase during phage proliferation and released the enzyme from infected bacteria that targeted another bacteria’s CPS (Adams & Park, 1956).

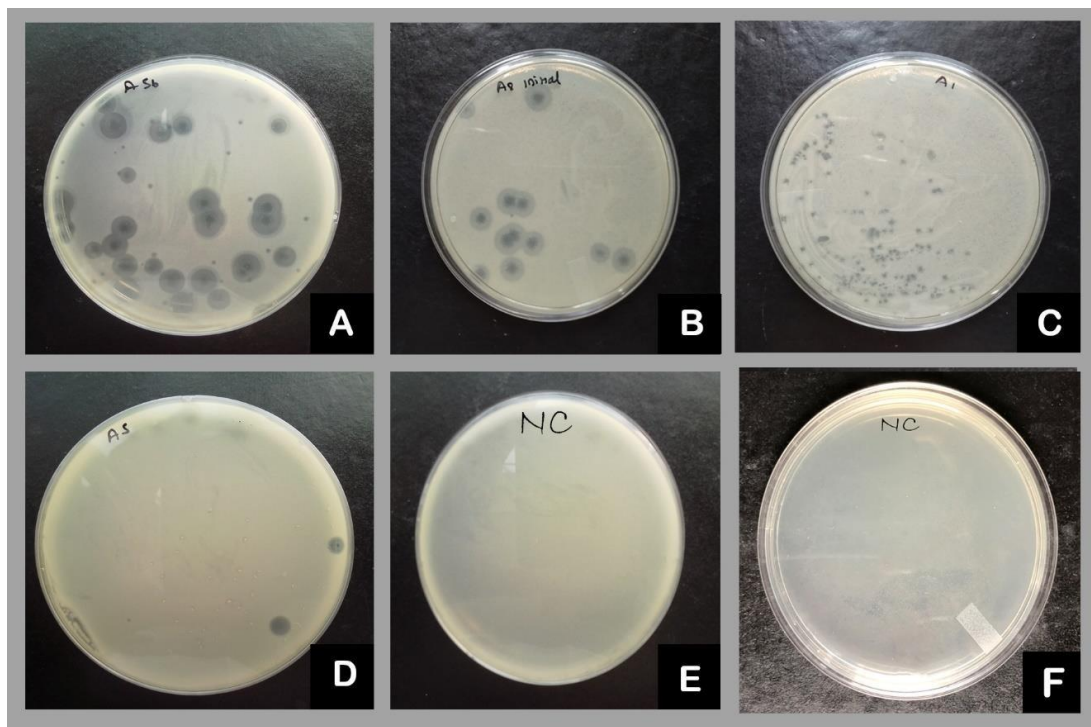


Figure 16: Different plaques morphology of phage observed in DLAA plates. In Figure A) Mixed plaques B) plaques with peripheral halo C) and D) pinhead and bull's eye plaques respectively. Figure E) Negative control (bacteria only) and F) Negative control (water sample only)

In this research, we intentionally omitted the ‘visually suspected’ temperate phages as our objective was to isolate strictly lytic phages that have therapeutic potential. As shown in Table 9 morphologically different plaques were observed in the same host cell suggesting the presence of both temperate and lytic phage from a single sample source. Among numerous plaques, a single clear plaque per plate/host was selected for

further experiment. The selected plaques were purified clonally before further characterization of the phages.

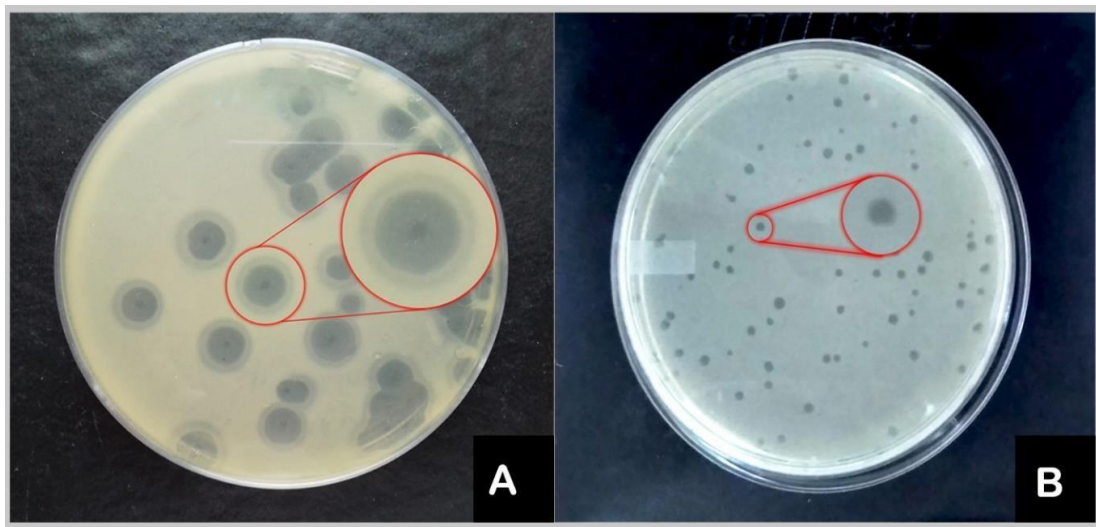


Figure 17: Zoomed view of plaques morphology of isolated phages. Figure A) 50% zoomed view of *Klebsiella* phage showing a large plaque with a clear center and halo periphery suggesting complete lysis of the host cells at the center and partial lysis at the periphery indicating a capsular depolymerase activities, and Figure B) 50% zoomed view of *Escherichia* phage showing a pin headed plaque with complete lysis in the small area suggesting a larger phage size.

A high titer of phage stock was prepared from the clonally purified plaques. Altogether, 22 phages were isolated from 15 samples using five different bacterial hosts. Among them, seven phages were isolated against *E. coli* M1, three phages against *E. coli* M2, and four phages against *E. coli* M3. Similarly, four phages were isolated against each of the *K. pneumoniae* TUKP1 and *K. pneumoniae* Kp56. Two to three different phages against different hosts were isolated from some of the samples such as Basundhara sewage, Bisnumati river, Kalimati sewage, sewage from Kirtipur, sewage from Teku, and sewage from Maharajgunj. The presence of high titer phages against both bacterial genera without enrichment implies that the sample sources were heavily contaminated with the pathogenic bacteria.

4.2 Naming of the phages

For the naming of the isolated phages, the word “Makalu” is used for *Myophages* and “Pokalde” for *Podophages*. A numerical serial code was given which will be used for future phage repository of Nepal. In the present study, only five phages isolated against

each of the bacterial hosts were selected for further experiment. Among them, three phages were from each of the *E. coli* hosts and two from each of the *K. pneumoniae* hosts. Based on the morphological features on electron microscopy and as per the International Committee on Taxonomy of Viruses (ICTV) classification guideline, all of the *E. coli* phages belonged to the *Myoviridae* family and both *K. pneumoniae* phages belonged to the *Podoviridae* family. We named them as ϕ Ec_Makalu_001, ϕ Ec_Makalu_002, ϕ Ec_Makalu_003 for *E. coli* phages and ϕ Kp_Pokalde_001, ϕ Kp_Pokalde_002 for *K. pneumoniae* phages (Table 10).

Table 9: Isolation of phages from different water/sewage samples. The presence of different sizes and morphology of plaques suggests the existence of varieties of phages infecting pathogenic bacteria.

Sample Sources	Host bacteria	Initial plaque count (PFU/mL)	Types of plaques	Size of plaques (mm)
Karmanasa river	<i>E. coli</i> M2	2.3x10	Clear&Turbid	1- 8
Manohara river	<i>K. pneumoniae</i> Kp56	2.6x10	Clear&Turbid	3 - 5
Hattiban sewage	<i>E. coli</i> M1	4.6x10	Clear&Turbid	2 - 7
Basundhara Sewage	<i>K. pneumoniae</i> TUKp1	1.65x10 ²	Clear with peripheral halo	6 - 14
	<i>E. coli</i> M1	1.32x10 ²	Turbid, Bull's eye & Clear	1 - 7
Shankhamul river	<i>E. coli</i> M3	> 4x10 ²	Turbid to Clear	1 - 6
Sali Nadi	No phage isolated			
Balkhu river	<i>E. coli</i> M1	8.7x10	Turbid & Clear	1 - 6
Bishnumati river	<i>K. pneumoniae</i> Kp56	3.6x10	Turbid & Clear	1 - 4
Bisnumati river	No phage isolated			
Bisnumati river	<i>E. coli</i> M1	0.8x10	Bull's eye	5 - 10

	<i>K. pneumoniae</i> TUKp1	1.8x10	Plaques with halo	4 - 9
Teku Sewage	<i>E. coli</i> M2	7.3x10	Clear	2 - 4
Kalimati Sewage	<i>K. pneumoniae</i> Kp56	> 4x10 ²	Turbid & Clear	1 - 6
	<i>E. coli</i> M1	1.18x10	Turbid & Clear	2 - 6
Balkhu river	No phage isolated			
Balkhu river	<i>E. coli</i> M3	0.9x10	Clear	4 - 8
Mahadev Khola	<i>E. coli</i> M1	1.08x10	Turbid, Bull's eye & Clear	2 - 8
Bagmati river	No phage isolated			
Sewage from lainchaur	No phage isolated			
	<i>E. coli</i> M2	> 4x10 ²	Clear & Turbid	1 - 4
Sewage from Kirtipur	<i>K. pneumoniae</i> TUKp1	2.56x10 ²	Clear & Turbid	1 - 6
	<i>K. pneumoniae</i> Kp56	0.8x10	Clear	4 - 6
Sewage from Teku	<i>E. coli</i> M3	1.74x10 ²	Clear	3 - 6
Sewage from	<i>K. pneumoniae</i> TUKp1	3.9x10	Plaques with halo	3 - 8
Maharajgunj	<i>E. coli</i> M3	> 4x10 ²	Clear & Turbid	1 - 8

Table 10: Nomenclature of the novel phages.

Source of Sample	Host	Name of the phage
Sewage from Maharajgunj	<i>E. coli</i> M1	ϕ Ec_Makalu_001
Sewage from Kirtipur	<i>E. coli</i> M2	ϕ Ec_Makalu_002
Sewage from Teku	<i>E. coli</i> M3	ϕ Ec_Makalu_003
Basundhara sewage	<i>K. pneumoniae</i> TUKp1	ϕ Kp_Pokalde_001
Bishnumati river	<i>K. pneumoniae</i> Kp56	ϕ Kp_Pokalde_002

The presence of phages depends upon the availability of their host bacterium. River water, sewage, soil, poultry manure, stagnant water, and seawater are profound sources of the phage as they usually have bacteria in them. We primarily choose river water as a phage source as the water is heavily contaminated with sewage from industries, hospitals, and households. The abundance isolation of phages may be because the rivers of Kathmandu valley are heavily polluted with human/animal excreta as well as waste produced by the nearby hospitals, industries, and households without treatment. This result is somewhat similar to the study conducted by Bhetwal et al. (2017) from Nepal, in which a total of 67 phages were isolated from 8 samples. Similarly, Kęsik-Szeloch et al. (2013) from Poland isolated 32 lytic phages using 11 ESBL-producing clinical *K. pneumoniae* from 8 aquatic samples. Similarly, Carey-Smith et al. (2006) isolated 8 phages from sewage against *Salmonella* serovars (Carey-Smith et al., 2006). The difference in the phage isolation might be due to the difference in samples types, host bacteria, and geographic location.

4.3 Morphological characterization

Transmission electron microscopy (TEM) of three *Escherichia* phages (ϕ Ec_Makalu_001, ϕ Ec_Makalu_002, and ϕ Ec_Makalu_003) and *Klebsiella* phages (ϕ Kp_Pokalde_001 and ϕ Kp_Pokalde_002) was done at Electron Microscopy Unit, National Institute of Biomedical Imaging and Bioengineering, National Institutes of Health (NIH), Bethesda, MD, USA. The result revealed that all phages are tailed having isometric capsids. The morphometry and classification of phages under study as per the International Committee on Taxonomy of Viruses (ICTV) classification are summarized in Table 11. All of the isolated *Escherichia* phages had a long tail with contractile sheath, a baseplate, and tail fibers carrying morphologically undistinguishable with T4 like phages (Figure 18). According to ICTV guidelines, these phages belonged to the *Myoviridae* family; *Caudovirales* order (King et al., 2018) which comprises a major portion of tailed phages including Coliphage T4 (Comeau et al., 2012). All of the *Myoviridae* phages had almost similar head diameters ranging from 83-88 nm in diameter and tail lengths between 94-109 nm. The head and tail measurements of our *Myophages* match those of previous researchers. According to reports, the typical dimensions of Caudovirals head diameter range from 30-160 nm and tail length 80-800 nm (Ackermann, 2005). Similarly, both *Klebsiella* phages viz. ϕ Kp_Pokalde_001 and ϕ Kp_Pokalde_002 had an icosahedral head measuring

approximately 53 -54 nm in diameter with a short non-contractile tail measuring approximately 13- -16 nm in length (Figure 19). These *Klebsiella* phages are identical to the widely-studied phage T7 and have a similar genome size. Average dimensions of the *Podophages* in this study are in agreement with the average dimensions reported earlier for *Podoviridae* phages infecting *Klebsiella* spp. (Domingo-Calap et al., 2020). Other published reports showed that the *K. pneumoniae* phages belonging to the *Siphoviridae*, *Myoviridae*, and *Podoviridae* families (Zurabov & Zhilenkov, 2021). However, in our study, we have found *Podophages* infecting both *K. pneumoniae* (*K. pneumoniae* TUKp1 and *K. pneumoniae* Kp56) clinical isolates. To date, most of the published literature reported ‘tailed virus’ to be abundant in nature and our result is also coherent with this.

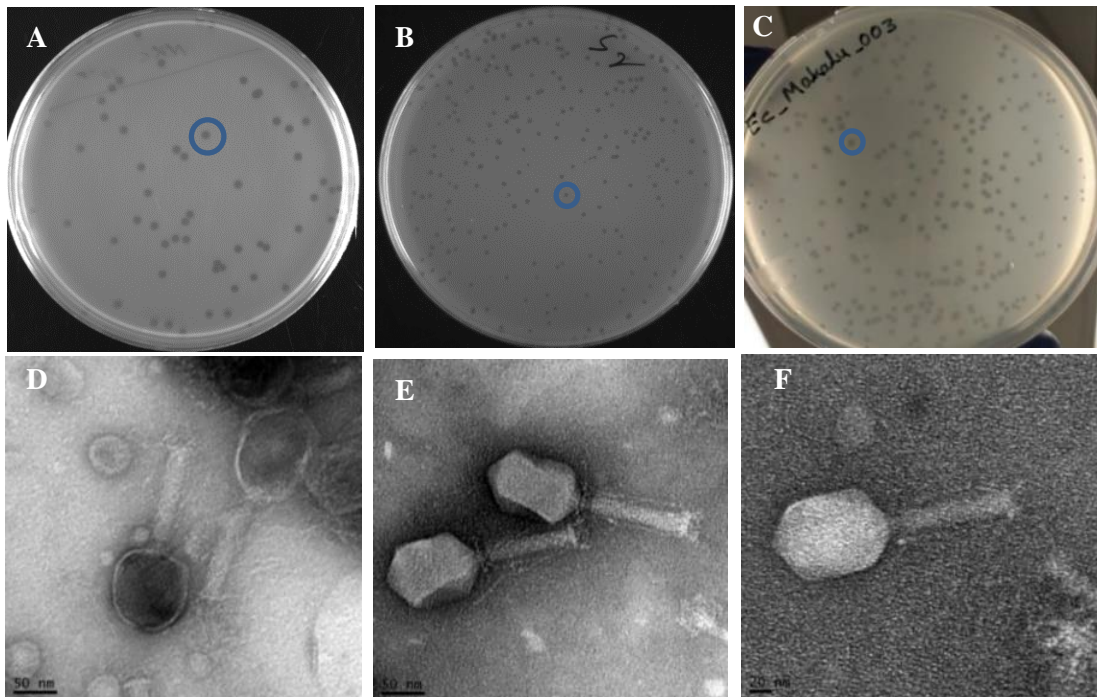


Figure 18: Morphological characterization of *Escherichia* phages ϕ Ec_Makalu_001, ϕ Ec_Makalu_002, and ϕ Ec_Makalu_003. In Figures A), B) and C): plaque of the three phages. Plaques were allowed to develop in soft agar media at 37°C for 24 hr. Notice that the plaques are the small, clear, and transparent small size of the plaques also correlates with the large physical size of the phage. D), E) and F): Transmission electron micrographs (TEM) of the *Escherichia* phages ϕ Ec_Makalu_001, ϕ Ec_Makalu_002, and ϕ Ec_Makalu_003 respectively. All three phages show an icosahedral capsid with a long contractile tail suggesting Myovirus. Scale bar: 50 nm.

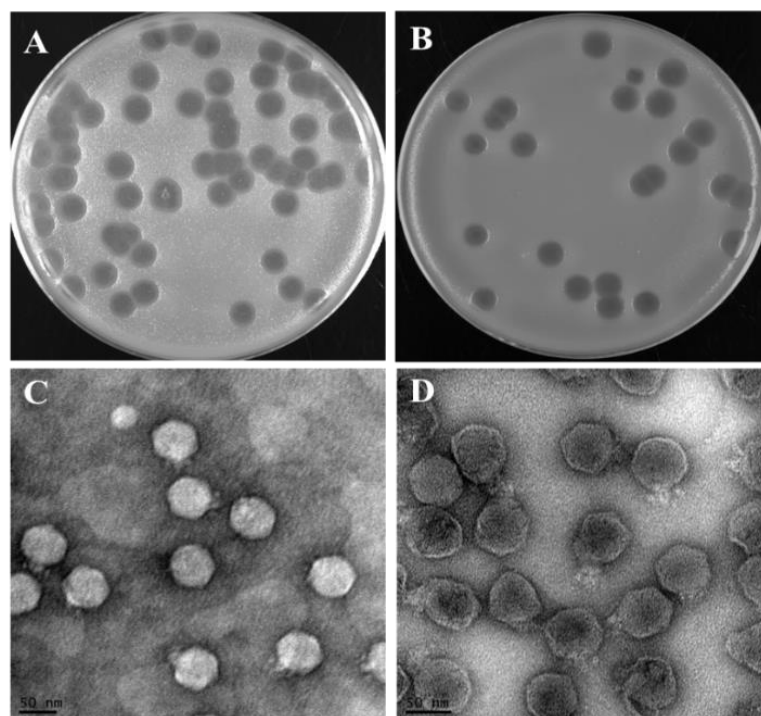


Figure 19: Morphological characterization of isolated *Klebsiella* phages. Clear plaques with a surrounding halo formed by the *Klebsiella* phages ϕ Kp_Pokalde_001 and ϕ Kp_Pokalde_002 in Figures A and B respectively. Transmission electron micrograph (TEM) images of *Klebsiella* phages ϕ Kp_Pokalde_001 and ϕ Kp_Pokalde_002 showing icosahedral capsid with a short tail in Figures C) and D) respectively. Scale bar = 50 nm

Table 11: Morphological characteristics and classification of isolated phages based on a transmission electron micrograph. Head diameter was calculated for isometric capsids. All measurements were made with ImageJ software, 3 to 5 phage particles were measured for each phage and standard deviation was calculated (\pm SD), nm = nanometer.

Phage and (GenBank Acc.)	Capsid (nm) \pm SD	Tail (nm) \pm SD		Shape of capsid	Order	Family
		Width	Length			
Ec_Makalu_001 (MN894885.1)	88.9 \pm 12.2	19.1 \pm 1.0	109 \pm 1.0	Icosahedral	Caudovirales	<i>Myoviridae</i>
Ec_Makalu_002 (MN709127.1)	88.5 \pm 16.2	18.6 \pm 1.4	97.4 \pm 1.4	Icosahedral	Caudovirales	<i>Myoviridae</i>
Ec_Makalu_003 (MN882349.1)	83.7 \pm 13.0	16.7 \pm 1.1	94.3 \pm 1.5	Icosahedral	Caudovirales	<i>Myoviridae</i>
Kp_Pokalde_001 (MN882349.1)	54.6 \pm 2.24	11.2 \pm 1.16	16.9 \pm 1.80	Icosahedral	Caudovirales	<i>Podoviridae</i>
Kp_Pokalde_002 (MT425185.1)	53.7 \pm 2.15	11 \pm 1.41	13.6 \pm 1.9	Icosahedral	Caudovirales	<i>Podoviridae</i>

4.4 Biological characterization of isolated phages

4.4.1 Host range profiles

Host range spectrum of all of the selected *Escherichia* phages (ϕ Ec_Makalu_001, ϕ Ec_Makalu_002, and ϕ Ec_Makalu_003) and *Klebsiella* phages (ϕ Kp_Pokalde_001 and ϕ Kp_Pokalde_002) was evaluated using 50 different multidrug-resistant clinical isolates (35 *E. coli*, 10 *K. pneumoniae*, and 5 *P. aeruginosa*) (Figure 20). Among 3 *Escherichia* phages, ϕ Ec_Makalu_001 lysed 28.5% (10/35) *E. coli* strains only, while ϕ Ec_Makalu_002 and ϕ Ec_Makalu_003 could infect and lyse 34.2% (12/35) *E. coli* strains as well as 20% (2/10) *K. pneumoniae* strains. All three phages did not show any lysis on *P. aeruginosa* strains.

Contrary to this, both *Klebsiella* phages were unable to lyse other bacterial isolates besides their primary host. Thus, both *Klebsiella* phages are strictly host-specific and did not possess multiple host-range. This variation was expected, which signified the vast diversity among both phages. Further, the efficiency of plating (EoP) among *Escherichia* phages was performed to evaluate the ability of phages to produce plaque in bacterial strains other than its primary host. The EoP analysis revealed that the phages had low to high lysis ability (EoP = 0.1 to 1) among all the spot test positive *E. coli* strains. Phages ϕ Ec_Makalu_002 and ϕ Ec_Makalu_003 also showed inter-genus lysis activity in two of the *K. pneumoniae* isolates but the plating efficiency was low (EoP = 0.0 to 0.2) (Figure 20). All three *Escherichia* phages produced plaques on the laboratory strain of *E. coli* MG1655 (EoP=0.9 to 1.0).

Further, the host range spectrum of a phage is considered cardinal in the selection of phage for therapeutic applications and usually, phages with a broad host range are preferred. Though phages are conventionally regarded as extremely specific to their host which limits its application in phage therapy, occasionally broad host range (including intergeneric lysis) phages have been reported. Although phages are quite specific, recent findings have shown that some phages possess the ability to infect a wide range of bacterial strains, (Fernandez et al., 2019). Thus, the host range of all of the isolated phages was screened by spot test followed by EoP to determine the relative EoP on 50 clinical isolates in three different genera (*Escherichia*, *Klebsiella*, and *Pseudomonas*).

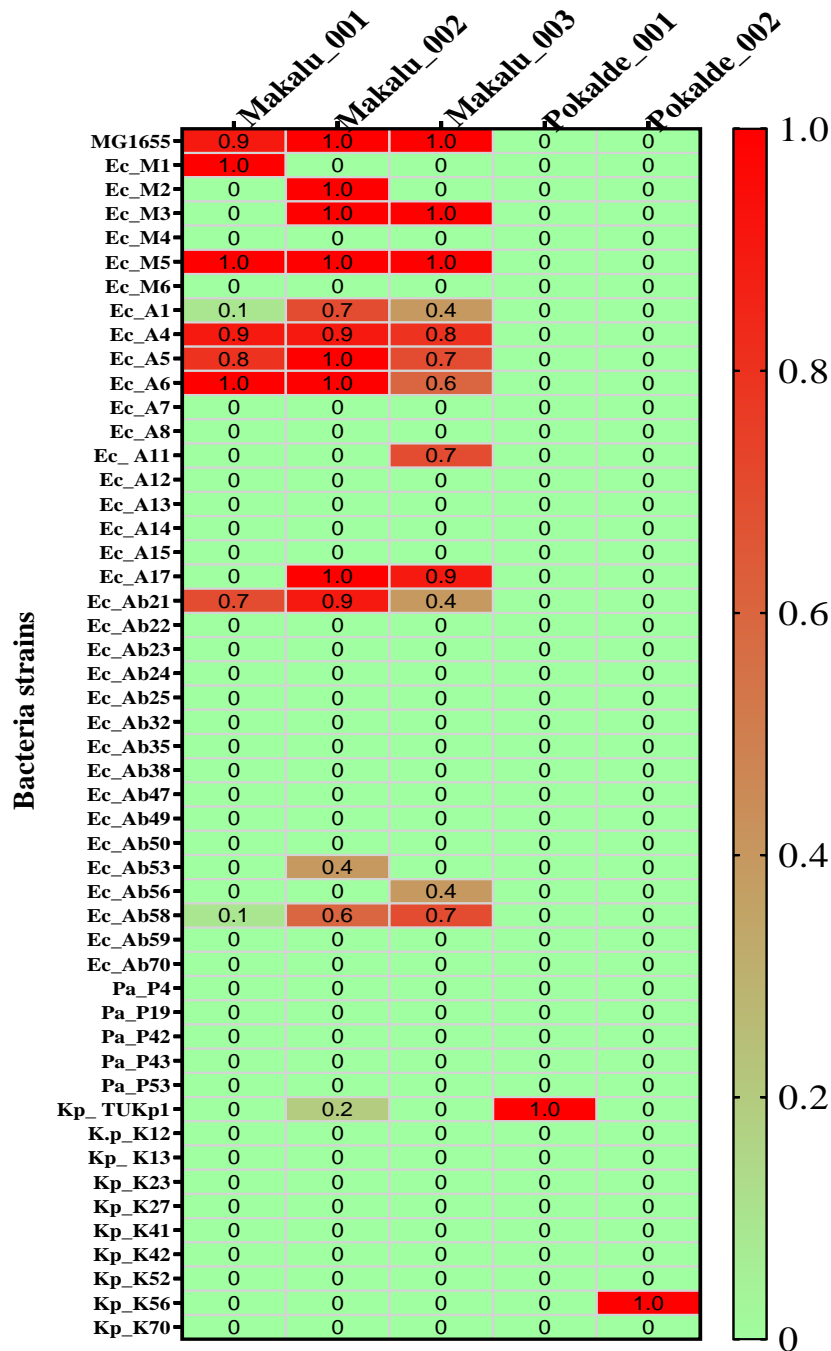


Figure 20: Host range profile of the *Escherichia* phages (ϕ Ec_Makalu_001, ϕ Ec_Makalu_002 and ϕ Ec_Makalu_003) and *Klebsiella* phages (ϕ Kp_Pokalde_001 and ϕ Kp_Pokalde_002). The heat map of host range results was produced using GraphPad Prism v8. The red color indicates lysis of tested bacteria and no lysis of bacteria in light green color. The phage Ec_Makalu_001 lysed 28.5% (10/35) *E. coli*, ϕ Ec_Makalu_002 and ϕ Ec_Makalu_003 could infect and lyse 34.2% (12/35) *E. coli* as well as 20% (2/10) *K. pneumoniae* while both *Klebsiella* phages were unable to lyse other bacterial isolates beside their primary host. EOP= Efficiency of plating. Plating ability (EOP) ranges from 0-1.

Based on spot assay and EoP, all three phages showed multi-host range within their host genus. Interestingly, ϕ Ec_Makalu_002 and ϕ Ec_Makalu_003 also showed intergeneric lysis ability producing lysis zone on the lawn of *K. pneumoniae* isolates (EoP= 0.0-0.2) suggesting property of polyvalent phages displaying remarkable host diversity by *Myophages*. The low EoP on *K. pneumoniae* isolates probably is due to the release of bacteriocin or breakdown of cellular energetics leading to abortive infection (Kutter, 2009). Similar polyvalent wide host range (WHR) phages have also been reported in past.

Bielke et al. (2007) showed that lytic phage isolated using *Salmonella enteritidis* was also successfully amplified in *Escherichia*, *Klebsiella*, and other strains of *Salmonella*. Similarly, Sui et al. (2021) reported that polyvalent phage isolated using *E. coli* could also infect *Salmonella enteritidis* and Jensen et al. (1998) reported phages capable of intergeneric replication in *Sphaerotilus natans*, *E. coli*, and *P. aeruginosa* that could cross-infect each other. Similarly, Greene & Goldberg (1985) were able to isolate phages capable of lysing more than one species of *Streptomyces*. Further, a polyvalent *E. coli* phage having WHR (infecting enterotoxigenic *E. coli*, enteroaggregative *E. coli*, enterohemorrhagic *E. coli*, *Shigella flexneri*, and *Shigella sonnei*) has been used as a phage-based probiotic dietary supplement to treat Traveler's diarrhea (Aleshkin et al., 2015).

In this study, we reported WHR *Escherichia* phages. We assumed that phages regularly interact with multiple host genera in nature and evolve over time showing different phenotypic plasticity suggesting complex co-evolutionary relationships between bacteria and phages. In phage therapy, a phage that can infect multiple genera of bacteria effectively is equivalent to a broad spectrum of antibiotics (Ross et al., 2016) and is an extremely desirable property because phages would not have to be isolated for individual isolates. This evidence suggests that WHR phages exist in nature and a small library of such phages could potentially treat a wide range of infections. Additionally, amplification of phages in a nonpathogenic alternative host eliminates the possibility of incorporating detrimental accessory genes during phage amplification.

4.4.2 Thermal and pH stability

Thermal stability of all of the *Escherichia* phages (ϕ Ec_Makalu_001, ϕ Ec_Makalu_002, and ϕ Ec_Makalu_003) and *Klebsiella* phages (ϕ Kp_Pokalde_001 and ϕ Kp_Pokalde_002) was determined by incubating the phage lysate at different temperatures (25, 37, 50, 60 and 70 °C) up to 180 minutes. The titer of all of the phages did not decrease significantly ($p > 0.05$) at 25 °C and 37 °C for up to 180 minutes while the phage titer decreased rapidly after 60 minutes when incubating at 50 °C and lost its viability completely after 180 minutes. The phage titer decreased significantly at or above 60°C within 30 minutes. Interestingly, a similar pattern of thermal stability was observed in all of the *Myophages* and *Podophages* under study. A graphical representation of the thermal stability of the phages is depicted in Figure 21.

The phage viability was studied over a range of pH 2 to 12. Figure 22 elucidates the pH tolerance of the phages under study. The optimum pH was between 7 to 8 for all of the *Escherichia* and *Klebsiella* phages. The phage viability was unaffected within pH 6 to 9, while viability decreased below pH 5 and above pH 10. However, phage viability was completely lost below pH 2 and above pH 12. The result indicates that all of the phages shared a similar pH affinity.

The stability of therapeutic phages in the different physiochemical conditions is important for storage and applications (Jonczyk et al., 2011). In this study, all of the *Myophages* (ϕ Ec_Makalu_001, ϕ Ec_Makalu_002, and ϕ Ec_Makalu_003) and *Podophages* (ϕ Kp_Pokalde_001 and ϕ Kp_Pokalde_002) were stable at 25 °C and 37 °C temperature and pH 6 to 9 without significant loss of phage titer ($p > 0.05$).

Tailed phages (T4, T5, and T7) are known to be robust, survive in adverse conditions for several years, and thus are preferred in therapeutics (Jonczyk et al., 2011). The findings support observations reported earlier that vB_EaeM_ ϕ Eap-3 (a tailed *Myophage*) remained stable at 4-37 °C and decreased infectivity at 60-70 °C within 15 min and completely inactivated at 50 °C for 60 min or 80 °C for 15 min (Zhao et al., 2019). Similarly, T4 phage showed optimum stability at pH 6.0 to 7.4 and decreased its titer at above pH 9.2 and below pH4.0 (Jonczyk et al., 2011).

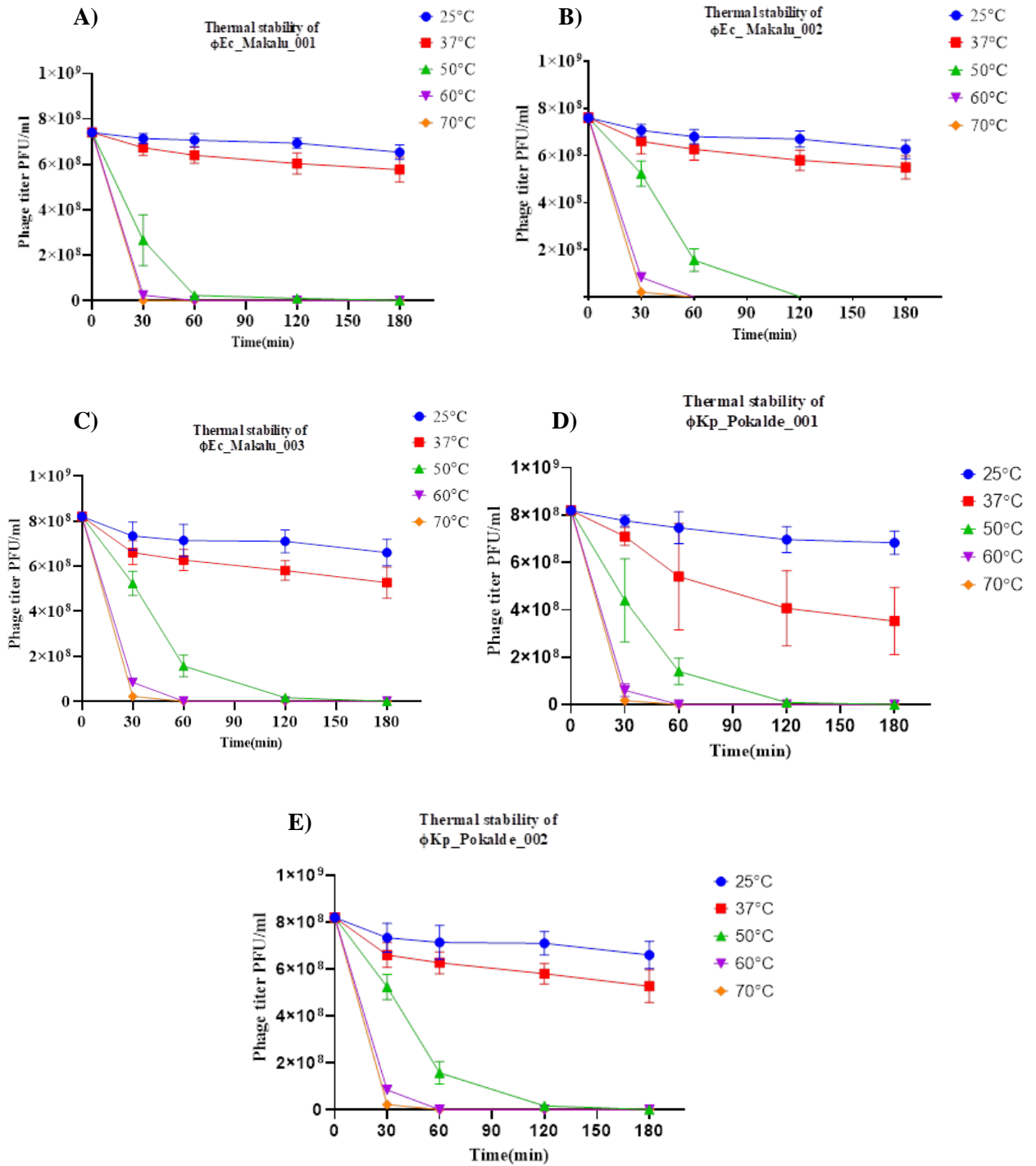


Figure 21: Thermal stability of *Escherichia* and *Klebsiella* phages. In Figure A), B), and C) are thermal stability of phages ϕ Ec_Makalu_001, ϕ Ec_Makalu_002 and ϕ Ec_Makalu_003 respectively. Similarly, ϕ Kp_Pokalde_001 and ϕ Kp_Pokalde_002 in Figures D) and E) respectively. The thermal stability of the phages was determined by incubating the phage lysate at different temperatures (25, 37, 50, 60, and 70°C) for up to 180 minutes. The titer of all of the phages did not decrease significantly ($p > 0.05$) at 25°C and 37°C for up to 180 minutes. Error bars indicate standard deviations of the mean ($n=3$) of three independent experiments. Results were expressed as PFU/mL.

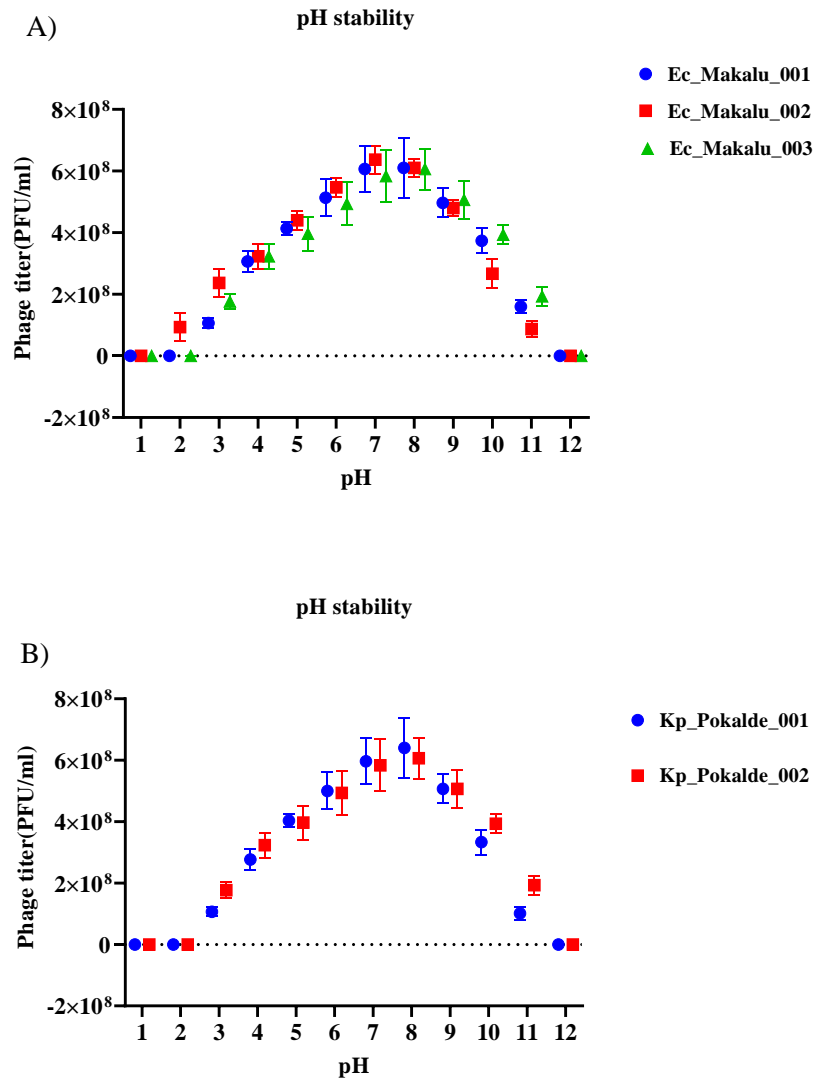


Figure 22: pH stability of the phages. In Figure A: pH stability of *Escherichia* phages (ϕ Ec_Makalu_001, ϕ Ec_Makalu_002 and ϕ Ec_Makalu_003) and B: pH stability of *Klebsiella* phages (ϕ Kp_Pokalde_001 and ϕ Kp_Pokalde_002). The stability of phages in different pH ranges from pH 2 to 12 was evaluated by pre-incubating the phage suspensions in different pHs. All of the phages were found to be stable at pH 6 to 9 without significant loss of phage titer ($p > 0.05$). Error bars indicate standard deviations of the mean ($n=3$) of three independent experiments. Results are expressed as PFU/mL.

4.4.3 One-step growth curve

The one-step growth curve experiment was performed to determine the latent period and burst size of the phages under study. The graph of the one-step growth curve of the phages is depicted in Figure 23. Among *Escherichia* phages, the latent period of the phages ϕ Ec_Makalu_001 and ϕ Ec_Makalu_003 was found to be 15-20 minutes, while

ϕ Ec_Makalu_002 had a shorter latent period of 15 minutes. The latent period is the time taken by the phage to begin the lysis of the host bacterium after adsorption of the phage. Similarly, the growth of ϕ Ec_Makalu_002 and ϕ Ec_Makalu_003 reached its plateau at 50 minutes while the plateau of ϕ Ec_Makalu_001 was 55 minutes. The burst size was calculated based on the final titer of the phage and the number of infected bacterial cells. The average burst size of ϕ Ec_Makalu_001, ϕ Ec_Makalu_002, and ϕ Ec_Makalu_003 was approximately 127, 74, and 120 phage particles per bacterium respectively. Similarly, the one-step growth curve of *Klebsiella* phages, ϕ Pokalde_001 and ϕ Pokalde_002 clearly showed the same latent period of about 15-20 minutes. The calculated burst size of the phages was found to be 93 and 121 phage particles per infected cells in ϕ Kp_Pokalde_001 and ϕ Kp_Pokalde_002 respectively. The burst size is an important parameter while selecting phages for efficient and effective phage therapy (Khan Mirzaei & Nilsson, 2015). The burst size of the phage is determined as the ratio of the final number of plaques to the number of infected host cells. We determined the burst size and latent period of all three *Escherichia Myophages* and two *Klebsiella* Podophages. Latent periods of these phages were relatively short between 15-20 minutes with burst sizes of 74 to 127 (Table 12).

The growth kinetics of the *Myophages* shared a similar pattern with those *Escherichia* phages reported previously (Duc et al., 2018; Litt & Jaroni, 2017; Montso et al., 2019). They reported the latent period of 10 to 25 minutes and burst size of 80 to a maximum of 631 virions per infected cell. However, a lower burst size of *Myophages* with 10-15 PFU per infected cells had been reported earlier (Kęsik-Szeloch et al., 2013). Some phages such as phage P1_{vir} had been reported with a long latent period of 60 minutes (Eriksen et al., 2018). A long latent period suggests slow adsorption of phages to host bacteria resulting in slow release of the virus particles (Cohen et al., 2013). Similarly, less than 10 minutes latent period of the well-studied *Podophage* i.e., *E. coli* phage T7 (You et al., 2002) and other *Klebsiella* phages such as phage TUN1 which had a 10 min latent period and a burst size of 76 phage particles/cell (Eckstein et al., 2021). Recently, a *Klebsiella* phage B1 which had 9 minutes latent period and 20 minutes of the plateau with a large burst size of \approx 2200 phage particles per infected bacteria have been reported (Pertics et al., 2021). The latent period is the time of phage that induces the lysis of the host cell and depends on multiple factors like host physiology, phage lytic protein complex like a holin, endolysin, spanin (Abedon et al., 2001; Rajaure et al., 2015).

Phage having a short latent period and high burst size is crucial in eliminating infecting bacteria as well as overcome to the risk of development of phage resistant mutants. Here, all phages showed a similar short latent period with high burst size clearly showing potential for phage therapy.

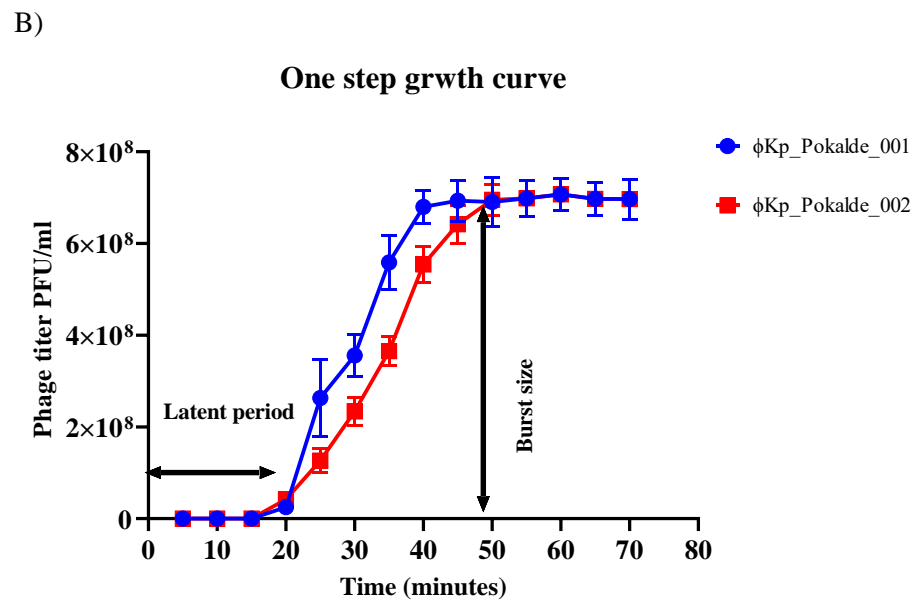
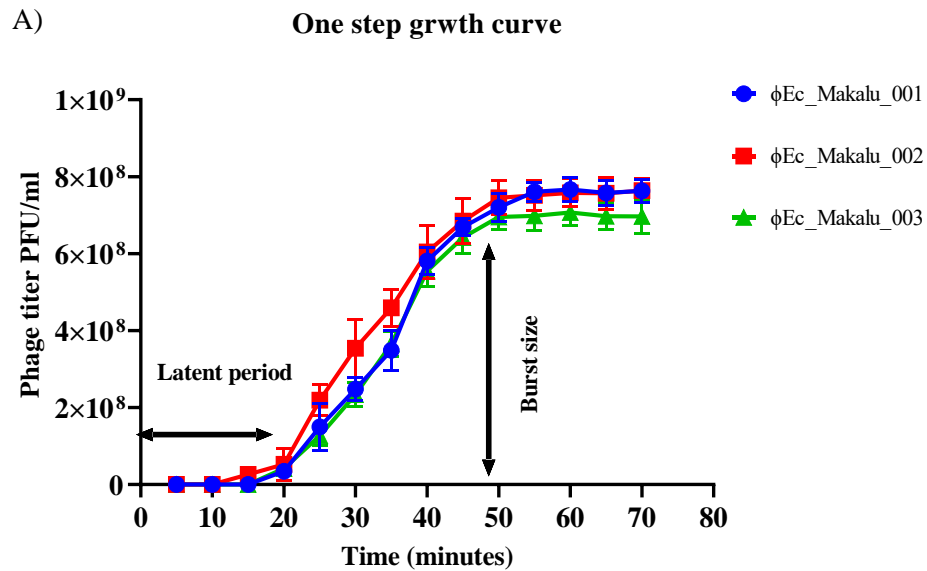


Figure 23: One-step growth curve of *Escherichia* phages (ϕ Ec_Makalu_001, ϕ Ec_Makalu_002, and ϕ Ec_Makalu_003) and *Klebsiella* phages (ϕ Pokalde_001 and ϕ Pokalde_002) in Figure A and B respectively. Phages were grown in an exponential phase culture of their respective host strains. Data points indicate the PFU/mL at different time points. Error bars indicate standard deviations of the mean (n=3) of three independent experiments.

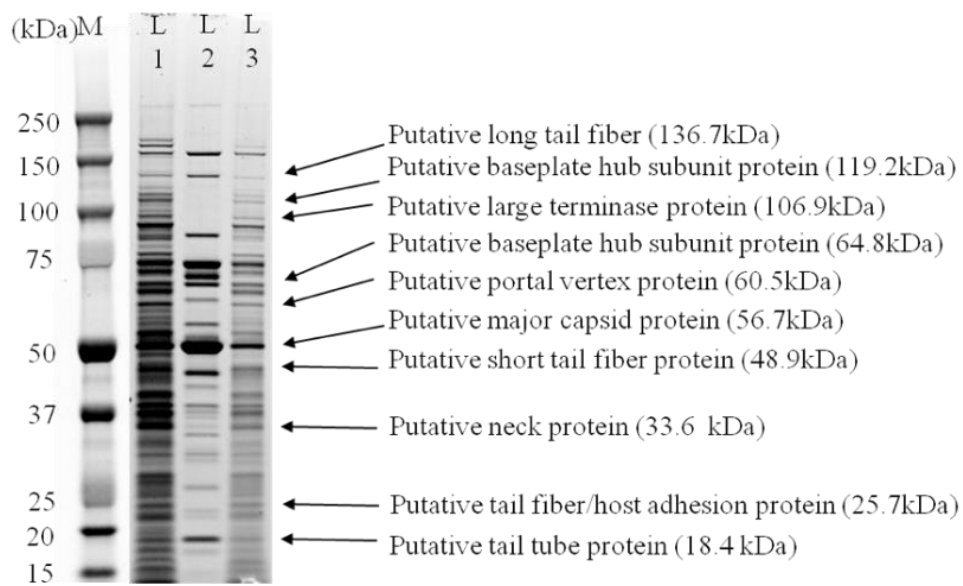
Table 12: The latent periods and burst sizes of the phages.

Phage	Latent period (minutes)	Burst size (PFU/cell)
<i>Escherichia</i> phage ϕ Ec_Makalu_001 (MN894885.1)	20	127
<i>Escherichia</i> phage ϕ Ec_Makalu_002 (MN709127.1)	20	74
<i>Escherichia</i> phage ϕ Ec_Makalu_003 (MN882349.1)	15	120
<i>Klebsiella</i> phage ϕ Kp_Pokalde_001 (MN882349.1)	20	93
<i>Klebsiella</i> phage ϕ Kp_Pokalde_002 (MT425185 .1)	20	121

4.4.4 Structural protein analysis

The protein profiling of the phages was done by sodium dodecyl sulfate-polyacrylamide gel electrophoresis (SDS-PAGE). Multiple bands that correspond to predicted proteins were analyzed. These proteins bands were compared with phage proteins of known phage protein profiles. At least 12 prominent bands of both *Myophages* and *Podophages* were observed in the gel ranging from approximately 12 to 200 kDa. In the *Myophages*, the most predominant polypeptide band appeared at a size of approximately 56 kDa. This band could be assigned as major capsid protein by its size and by its initial 60 amino acid residues at the N-terminal region (amino acid sequence data obtained from whole-genome sequencing and annotation of the *Myophages*) as it was shown earlier for phage RB49 (Desplats et al., 2002). Further, pairwise sequence alignment using EMBOSS Stretcher showed 100% amino acid sequence homology with Enterobacteria phage RB49, extensively studied model of pseudo-T-even phage, which is a member of the *Myoviridae* family, has a contractile tail, linear double-stranded DNA, and similar genome size of 164 Kbp. Likewise, based on the protein size and sequence similarity at the initial N terminal amino acid residues, other prominent bands could be correlated with other T4 like phage's structural proteins such as *Escherichia* phage Phi1, *Escherichia* phage JSE, *Escherichia* phage ECD7 etc.

A) Protein profile of *Escherichia* phages



B) Protein profile of *Klebsiella* phages

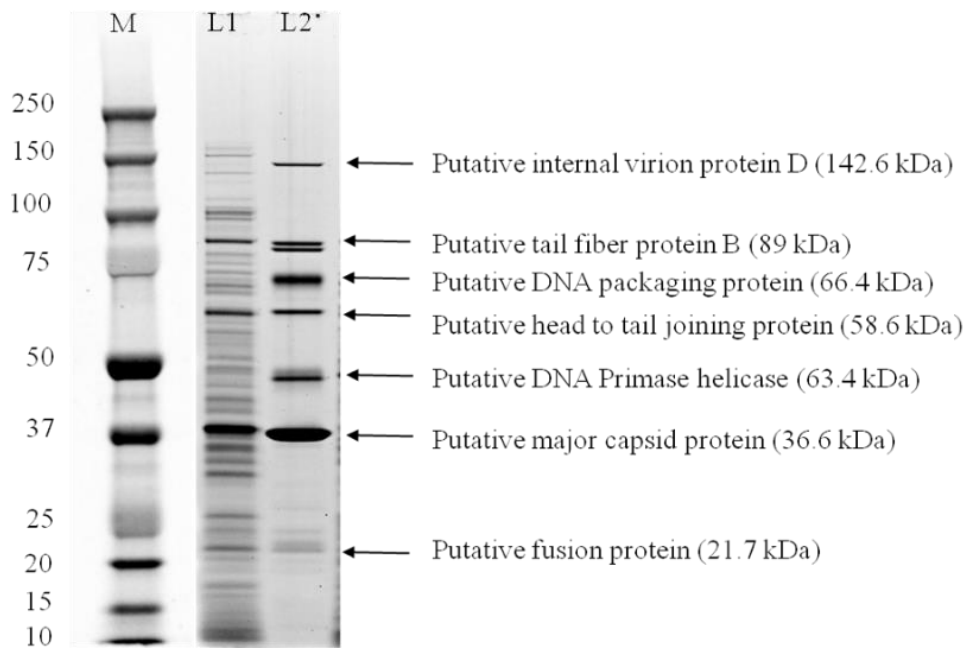


Figure 24: SDS- polyacrylamide gel electrophoresis analysis of the phages of *Myophages* and *Podophages* in Figures A) and B) respectively. Phage lysate was mixed with LaemmLi buffer containing SDS, boiled for 10 min, and loaded on a 4-20% gradient gel that was electrophoresed with Tris-glycine running buffer. M: Protein marker, L1: Phage Ec_Makalu_001, L2: Phage Ec_Makalu_002, and L3: Phage Ec_Makalu_003-mark sizes of typical phage structural proteins. B) SDS-polyacrylamide gel electrophoresis analysis of Podophages. Lane M: Protein marker, L1: Phage_Kp_Pokalde_001, and L2: phage_Kp_Pokalde_002-mark sizes of typical phage structural proteins.

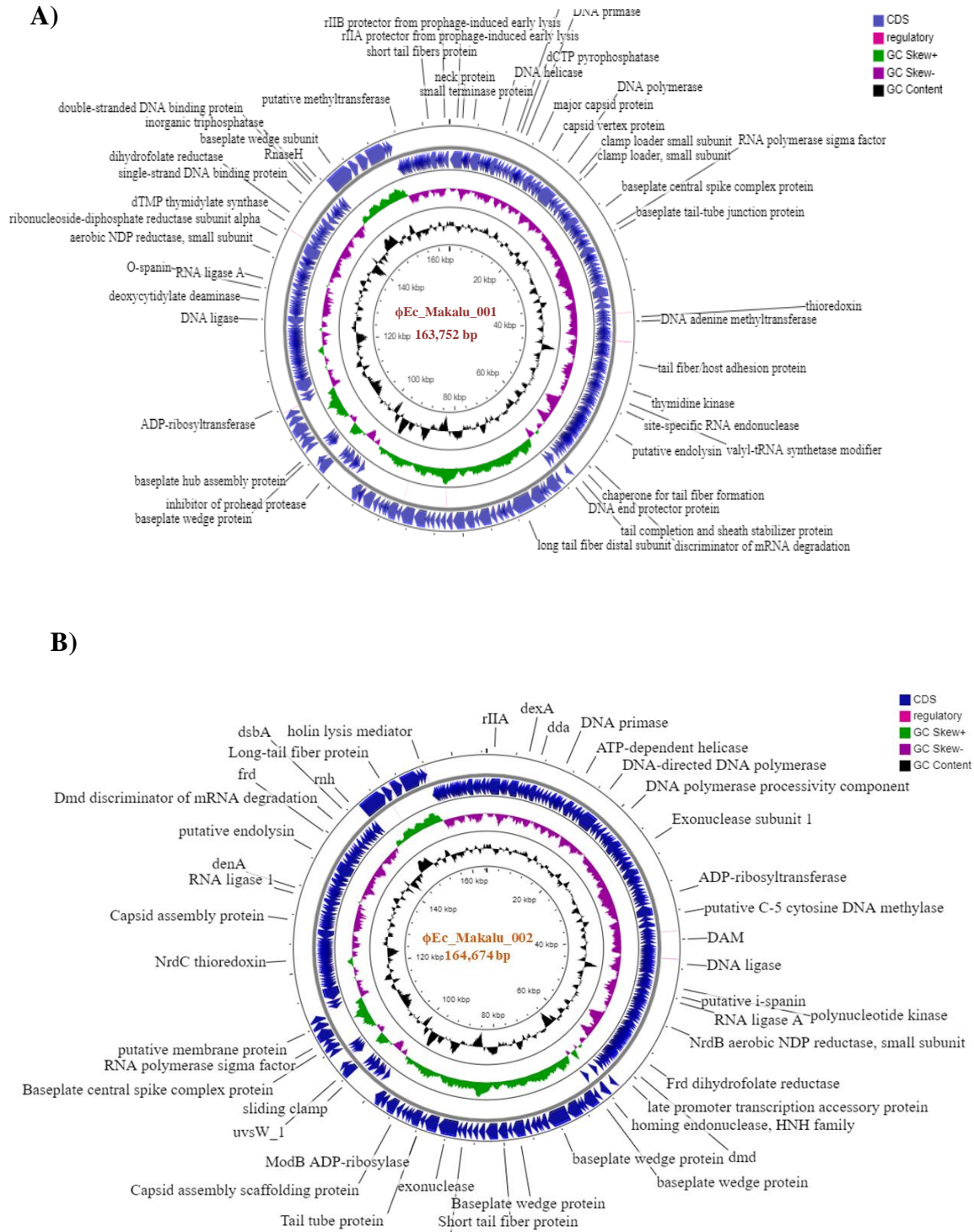
The protein bands with the putative structural protein of the *Escherichia* phages have been depicted in Figure 24 A. Similarly, the most prominent band of the *Podophages* resolved at a size of approximately 36 kDa, which is suggestive of major capsid protein. The protein shares 100% amino acid sequence (amino acid sequence data obtained from whole-genome sequencing and annotation of the *Podophages*) similarity on EMBOSS Stretcher with the amino acid sequence of the N-terminal region of the major capsid protein of a well-studied phage *Klebsiella* virus KP32 (Pyra et al., 2017), a member of T7 like virus. Other prominent bands that also could be correlated with putative structural proteins of genus *Drulisvirus* are shown in Figure 24 B.

4.5 Genomic characterization

4.5.1 Genome properties and annotation of *Escherichia* phages

The genomes of ϕ Ec_Makalu_001 (GenBank: MN894885.1), ϕ Ec_Makalu_002 (GenBank: MN709127.1) and ϕ Ec_Makalu_003 (GenBank: MN882349.1) were composed of a linear, double-stranded DNA of 163,752 bp, 164,674bp and 162,966 bp in length respectively and had a same G+C content about (40.6%). The complete annotation of the phage ϕ Ec_Makalu_001 genome revealed the existence of 272 open reading frames (ORF), 242 predicted promoters, and 45 Rho-independent terminator sequences. Forty percent of the ORFs (110 ORFs) have predicted function and the remaining 162 ORFs encode for protein assigned as hypothetical function (Figure 25A). The complete genome of phage ϕ Ec_Makalu_002 was 164,674 bp long. This phage encodes 274 predicted ORFs, 244 promoters, and 38 rho-independent terminators. Among them, 110 ORFs (40%) were predicted to be functional proteins and 164 ORFs (60 %) were hypothetical proteins (Figure 25B). Similarly, the genome of phage ϕ Ec_Makalu_003 contains 273 predicted ORFs with 227 promoters and 48 rho-independent terminators. Among them, 112 ORFs (41%) were predicted to be functional proteins and 161 ORFs (59%) were hypothetical proteins (Figure 25C). The majority of the ORFs (80%) of all phages (ϕ Ec_Makalu_001, ϕ Ec_Makalu_002, and ϕ Ec_Makalu_003) were located on the reverse strand of the DNA and none of them encode any predicted tRNA gene throughout the genome. On BLASTP analysis, all of the three phage genomes revealed no sequence similarity to the genes encoding lysogenic markers such as integrase, recombinase, repressor/ anti-repressor protein, and excisionase (Oakey et al., 2002). Thus, we can consider the phages to be a strict

virulent phage. Besides the predicted protein functions, the predicted amino acid size, the genomic position, the transcriptional orientation, and the GenBank protein identification numbers of all three genomes have been summarized in the appendix- F



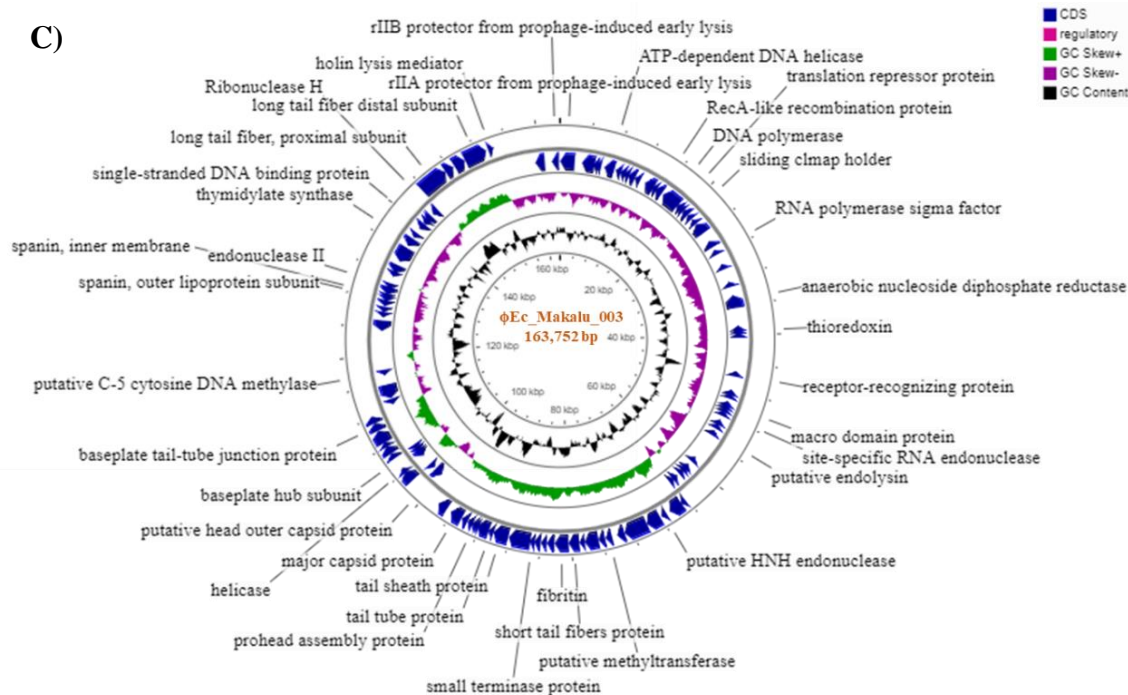


Figure 25: Circular genome view of *Escherichia* phages ϕ Ec_Makalu_001, ϕ Ec_Makalu_002, and ϕ Ec_Makalu_003 in Figure A, B and C respectively, produced from CG view software. The most external rings with arrow-headed bands represent the predicted open reading frames (ORFs) in the positive strand (blue arrows) and adjacent rings show ORFs in the negative strand and annotated genes. The inner rings show genome locations and the middle ring represents the GC content (black ring) and GC skew (green and (purple)). The predicted gene functions of the CDSs are labeled.

Further, multiple genome alignment of the *Myophages* (ϕ Ec_Makalu_001, ϕ Ec_Makalu_002, and ϕ Ec_Makalu_003) using Progressive MAUVE software revealed a significant nucleotide homology with each other (Figure 26). Moreover, a high degree of nucleotide similarity (>95% coverage and >96% identity) was found on BLASTn search (database Nucleotide collection (nr/nt) using Megablast) to other 16 *Myophage* genomes available in the NCBI database (Table 13). Based on the specific locations of the predicted genes, associated functions, and overall organization of the genomes, typically comprising DNA packaging mechanism, GC content, DNA replication-transcription, and structural genes, all three phages share modular structure with many phages within the *Myoviridae* family, more specifically, with phages belonging to the genus of T4-like viruses with high similarity to the RB49 group virus (Petrov et al., 2010). Genes encoding putative holin, endolysin, and spanin complex (i-spanin/o-spanin) that involve in the lysis of the host bacteria were scattered throughout

the genomes of all three phages. On protein BLAST and PHASTER analysis, all the three phage genomes revealed no sequence similarity to the genes encoding lysogenic markers such as integrase, recombinase, repressor/anti-repressor protein, and excisionase. Thus, we confidently predicted all of the isolated *Myophages* to be strictly virulent phages. Moreover, the genomes of all phages did not encode the lysogeny modules and any known harmful genes such as toxins, ARGs and VFs. Hence, we consider all three *Myophages* to be the excellent candidates for therapeutical application against *E. coli* infections. Multiple genome alignment of the phage genomes with all 16 similar phages conserved the similar synteny and revealed high homologous regions at protein levels, typically genes encoding DNA packaging/replication/transcription regulation, structural proteins like head, tail fiber, and lytic cassettes. All three *Myophages* were most closely identical to Enterobacteria phage Phi1 (GenBank: EF437941.1).

Table 13: Genome alignment of Myophages. Basic Local Alignment Search Tool (BLAST) online tool from the NCBI website (<https://blast.ncbi.nlm.nih.gov/Blast.cgi>) was used to identify high nucleotide homology with the newly isolated Escherichia phage genomes (>90% query cover and > 90% identical). As of March 2020.

Description	Query Cover	E-value	Per. Ident	Accession no	Country of origin	Genome size (bp)	No. of ORF
Ec_Makalu_001, complete genome	100%	0	100.0 0%	MN894 885.1	Nepal	163752	272
Ec_Makalu_002, complete genome	98%	0	98.49 %	MN709 127.1	Nepal	164674	274
Ec_Makalu_003, complete genome	98%	0	98.79 %	MN882 349.1	Nepal	162966	273
Enterobacteria phage Phi1, complete genome	96%	0	97.07 %	EF4379 41.1	Georgia	164270	274
<i>Escherichia</i> phage kvi, complete genome	94%	0	96.74 %	MN850 615.1	Denmark	163673	263
vB_EcoM_PHB13, partial genome	96%	0	97.31 %	MK573 636.1	China	165641	277

Enterobacteria phage GEC-3S complete genome	97%	0	95.04 %	<i>HE978</i> <i>309.1</i>	Georgia	163424	276
<i>Escherichia</i> phage ECD7, complete genome	97%	0	97.29 %	<i>NC_04</i> <i>1936.1</i>	Russia	164706	264
<i>Escherichia</i> virus KFS-EC, genome	94%	0	93.29 %	<i>MH560</i> <i>358.1</i>	South Korea	164715	262
Enterobacteria phage RB49, complete genome	96%	0	97.33 %	<i>AY3433</i> <i>33.1</i>	USA	164018	280
<i>Escherichia</i> phage kaaroe, complete genome	96%	0	96.94 %	<i>MN850</i> <i>574.1</i>	Denmark	163719	263
<i>Escherichia</i> phage E26, complete genome	96%	0	96.43 %	<i>MN655</i> <i>998.1</i>	China	164572	276
vB_EcoM_G2248, complete genome	93%	0	95.48 %	<i>MK327</i> <i>932.1</i>	Germany	170678	279
Shigella phage JK32, complete genome	93%	0	93.65 %	<i>MK962</i> <i>753.1</i>	Ireland	176009	271
vB_EcoM_G37-3, complete genome	94%	0	96.00 %	<i>MK327</i> <i>941.1</i>	Germany	167832	281
Shigella phage Sf20, complete genome	96%	0	97.75 %	<i>MF327</i> <i>006.1</i>	USA	163982	272
vB_EcoM_G5211, complete genome	93%	0	96.21 %	<i>MK327</i> <i>947.1</i>	Germany	164278	272
vB_EcoM_G2494, complete genome	94%	0	97.15 %	<i>MK327</i> <i>935.1</i>	Germany	168327	278
Enterobacteria phage JSE, genome	95%	0	96.97 %	<i>EU863</i> <i>408.1</i>	Switzerl and	166418	279

4.5.3 Toxins, virulence factors, or antimicrobial resistance genes

Toxins or virulence factors (VFs) of bacterial pathogens were screened by the virulence factor database (VFDB) and antibiotic-resistant genes were predicted through the Comprehensive Antibiotic Resistance Database (CARD), Resistance Gene Identifier (RGI). The genomes of phages ϕ Ec_Makalu_001, ϕ Ec_Makalu_002, and ϕ Ec_Makalu_003 encode zero hits to any known such target genes.

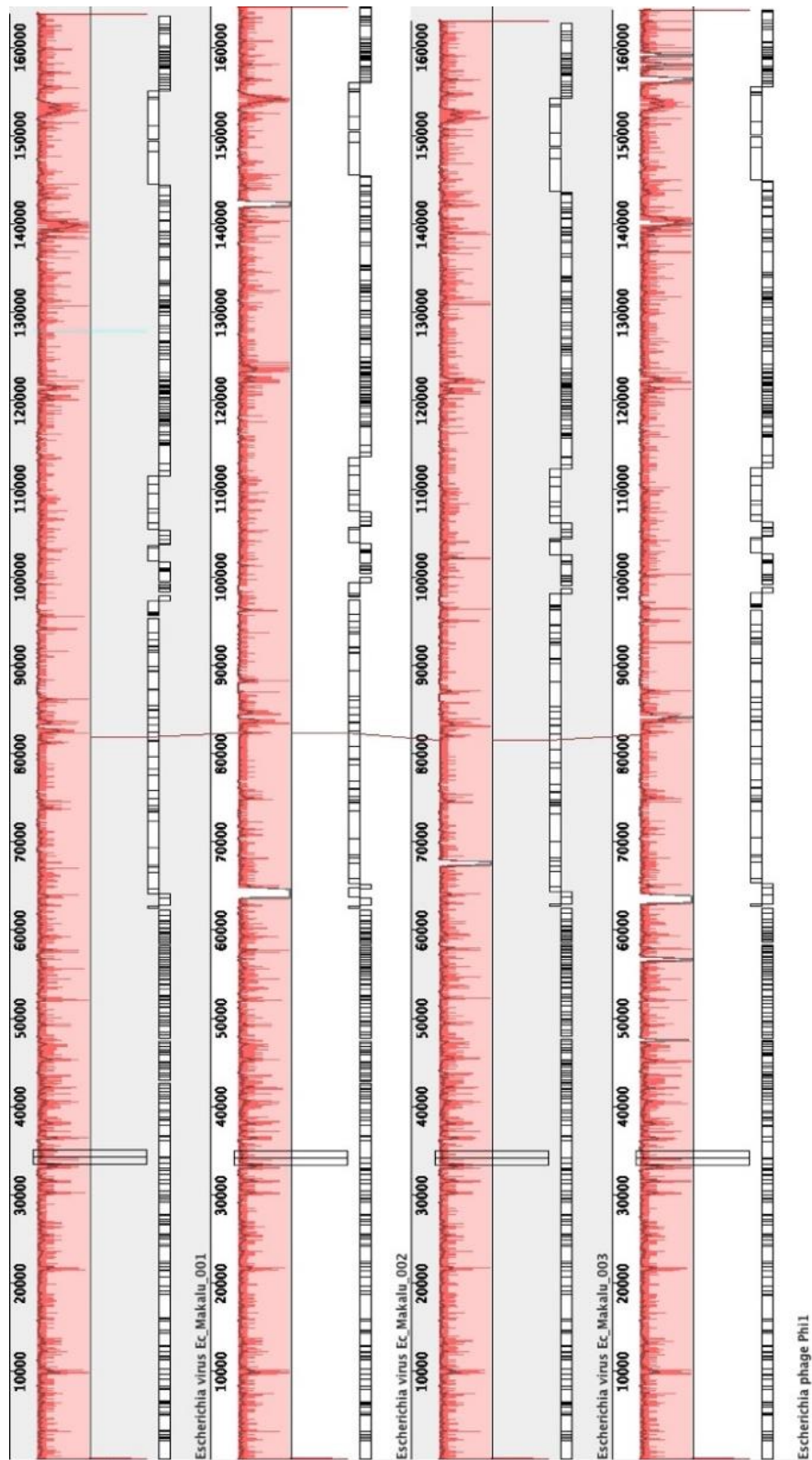


Figure 26: Multiple genome alignment using Progressive MAUVE of isolated *Escherichia* phages with Enterobacteria phage Phi1. The height of the similarity profile corresponds to an average level of conservation in that particular region of the genome. Blank regions (white) represent fragments that are not aligned or conserved in a particular genome sequence.

4.5.4 Phylogenetic analysis

Genome-BLAST Distance Phylogeny (GBDP) analysis showed the close relatedness of the phage genomes to the other similar phages available in the NCBI database (Figure 27). The analysis of 19 highly similar genome sequences (>90% sequence similarity on NCBI BLAST search) yielded one family-level cluster (F1), one genus level cluster (G1), and seven species-level clusters (S1–S7). All three phages (ϕ Ec_Makalu_001, ϕ Ec_Makalu_002 and ϕ Ec_Makalu_003) which were isolated from Nepal, fall within the same family (F1), and genus (G1) but different species level clusters S18, S14 and S17 for ϕ Ec_Makalu_001, ϕ Ec_Makalu_002 and ϕ Ec_Makalu_003 respectively.

The phage genome must be screened to ensure genetic safety before getting approval from the regulatory agency (like USFDA) (Philipson et al., 2018). Whole-genome sequencing is essential for functional genomics as well as to rule out detrimental outcomes of therapeutic phages as it may carry toxic genes, ARGs and VFs. Computational analysis of the genomes revealed that all three phages were confidently virulent and free from known toxic genes such as ARGs and VFs of bacterial origin. Further, ϕ Ec_Makalu_001, ϕ Ec_Makalu_002, and ϕ Ec_Makalu_003 genomes were highly homologous with the genomes of known members of T4-like viruses (representatives of the RB49 group, genus *Krischvirus*) (Walker et al., 2019).

The RB49 group of viruses are pseudo-T-evens phages primarily infecting Enterobacteria and environmentally important as they are found ubiquitously (Monod et al., 1997) and till date, 19 members of phage genomes having more than 96% sequence identity with Enterobacteria phage RB49 have been sequenced and deposited to NCBI GenBank database. The genome size of all these phages ranges from 162,966 bp to 176,009 bp with a very small window of G+C content (40.32% to 40.68%) and was isolated using *E. coli* as a primary host except two Shigella phages JK32 and Sf20. Enterobacteria phage RB49 has been extensively studied as a model of pseudo-T-even phage (Desplats et al., 2002).

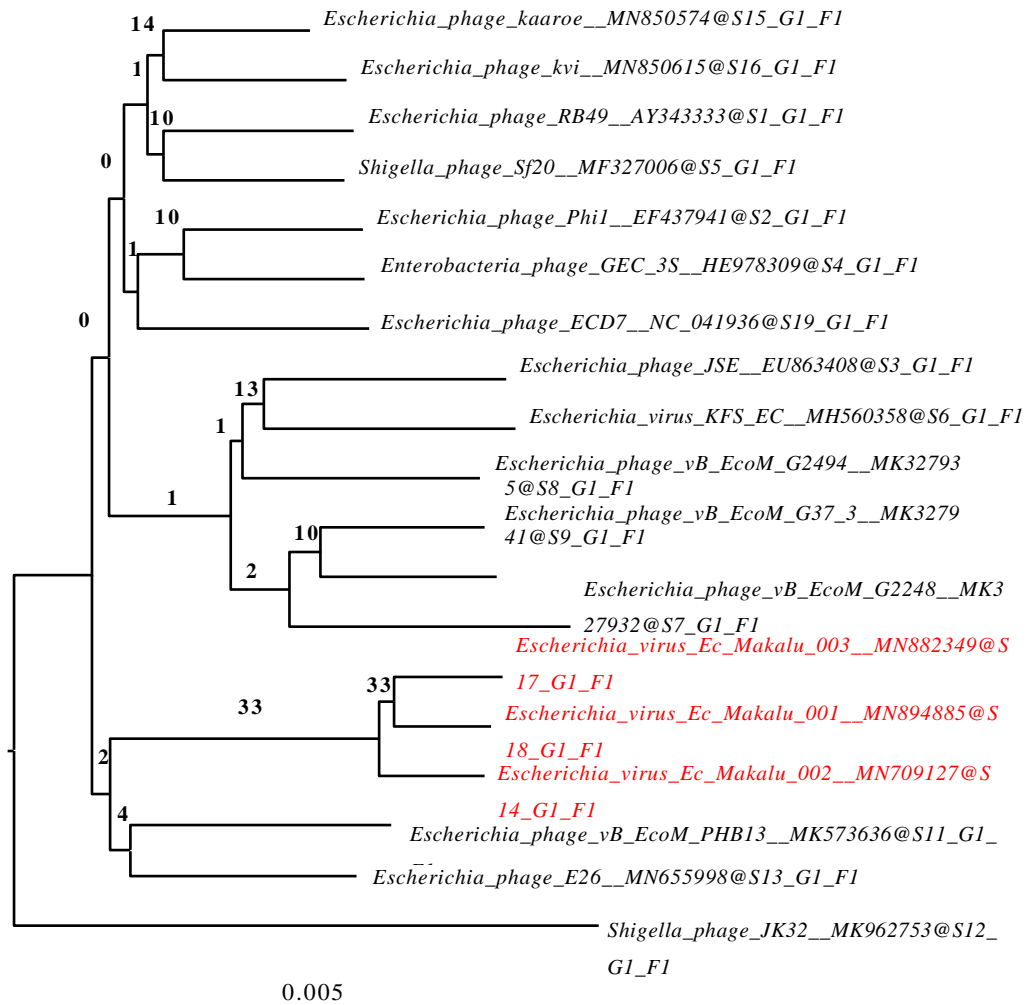


Figure 27: Phylogenomic tree of *Escherichia* phages (ϕ Ec_Makalu_001, ϕ Ec_Makalu_002, and ϕ Ec_Makalu_003) inferred using the formulas D4 and yielding average support of 8 %. The numbers above branches are GBDP pseudo-bootstrap support values from 100 replications. The branch lengths of the resulting VICTOR trees are scaled in terms of the distance formula used.

The genome size and G+C content of all three phages were also highly consistent with other phage genomes of the RB49 group and shared >96% ORF homology with each other. All three phage genomes in this study showed a close phylogenetic relationship with each other and with other phages from the RB49 group although they were isolated using different hosts and in different continents. The high degree of sequence similarity and identity probably may be due to the horizontal exchange of genes from a shared pool among the ancestors of contemporary phages during co-evolution (Hendrix et al., 1999). Thus, we assume that ϕ Ec_Makalu_001, ϕ Ec_Makalu_002, and ϕ

Ec_Makalu_003 and its relatives may have co-evolved with their host through extensive gain, loss, and exchange of their genes under different selection pressures and diverged from a common ancestor. However, there are differences observed in ORFs particularly encoding large terminase protein, HNH endonuclease, and tail fiber protein. Terminase enzymes are specifically associated with the recognition and cleavage of the cohesive end sites (*cos*) of the phage genome. HNH protein is a nuclease-associated protein required as a co-factor of phage terminase responsible for DNA packaging to the prohead. Terminase-associated HNH proteins are commonly found in long-tailed phage genomes (Kala et al., 2014). Tail fiber protein is associated with host specificities and is a more divergent and plastic structural region of the hypervariable region of the T4-like phage genomes whose primary function is to adapt the phage to its host (Comeau et al., 2007). The long tail fiber of the phage initially recognizes the receptors present on the host cell surface and facilitates the initial binding which determines host specificity (Hyman & van Raaij, 2018). Comparative sequence analysis of tail fiber protein at the amino acid level using pairwise sequence alignment EMBOSS Stretcher revealed that ϕ Ec_Makalu_002 and ϕ Ec_Makalu_003 shares 80.1% sequence similarity. Both phages have highly conserved identical amino acid sequences (100% identical) in N-terminus (up to 371 residues) and low identity in the C-terminus region. N-terminal residues of the tail fiber protein are responsible for attachment towards the baseplate, so this region may be highly consistent while the C-terminal region recognizes the host receptors protein where the receptor-binding domain is located. Significant differences in the host range and other biological properties could be observed with subtle changes in the sequence in tail fiber proteins (Yosef et al., 2017). The putative long tail fiber tip protein of each phage is comparatively different from each other at the nucleotide level may make a different host range. It is further hypothesized that phages capable of intergeneric lysis may use receptors, intermediary functions, or both common to a wide range of bacteria to achieve a wide host range.

MAUVE comparison of all three *Myophages* with the reference *Enterobacteria* phage Phi1 revealed that all these genomes are highly co-linear and related except for the deletion of seven genes of the *Enterobacteria* phage Phi1 (ORF84.1, ORF110, ORF111, ORF130.1, ORF131.1, ORF257, and ORF263.1) in the genomes of ϕ Ec_Makalu_001, ϕ Ec_Makalu_002 and ϕ Ec_Makalu_003 phages. Likewise,

hypothetical protein-coding genes; ORF 232, ORF237 of ϕ Ec_Makalu_001 homolog to ORF233, ORF238 of ϕ Ec_Makalu_002 and ORF233, ORF239 are absent in the genome of the *Enterobacteria* phage Phi1. Further, ORF238 of ϕ Ec_Makalu_001 and its homolog ORF240 of *Enterobacteria* phage Phi1 encoding a hypothetical protein is deleted in the genomes of ϕ Ec_Makalu_002 and ϕ Ec_Makalu_003. Interestingly, ϕ Ec_Makalu_002 genome possess two alleles of HNH-type homing endonucleases (ORF131 and ORF240) which are absent in phage ϕ Ec_Makalu_001 and *Enterobacteria* phage Phi1 but only one HNH-type endonuclease (ORF136) is conserved in ϕ Ec_Makalu_003. Homing endonucleases play important role in homologous recombination between phages during co-infection to the same host. A variable number of HNH-type endonuclease found in these genomes possibly mediates the genome evolution. Despite the diversity of genes of T4-like phages, they share a highly conserved core genome orientation and order that determines the structural design or phage morphogenesis. However, there is a highly variable hyperplastic region outside of this core genome primarily composed of genes of unknown function and origin providing a high degree of genetic heterogeneity. Although it is suspected that the lateral/horizontal gene transfer during evolution plays a major role in the evolution of the T4-like phages causing diversification of the phage pangenome (Petrov et al., 2010) there are few clues about the agents that might mediate such transfer.

4.5.5 Genome properties and annotation of *Klebsiella* phages

The genomes of the *Klebsiella* phages viz: ϕ Kp_Pokalde_001 (Accession number GenBank: MW590329.1) and ϕ Kp_Pokalde_002 (Accession number GenBank: MT425185 .1), were composed of a linear, double-stranded DNA of 44,535 bp and 41,816 bp in length with an average G+C content of 54% and 53% respectively. The complete annotation of the phage ϕ Kp_Pokalde_001 genome revealed that the genome contained 53 open reading frames (ORFs), 13 predicted promoters, and 2 Rho-independent terminator sequences. Among them, 32 ORFs have been assigned with predicted function and the remaining 21 ORFs with unknown function. The genome had 247 bp direct terminal repeats at both ends (Figure 28 A). Similarly, the phage ϕ Kp_Pokalde_002 contained 180 bp direct terminal repeats at both ends. The phage genome comprised 45 open reading frames (ORF) with 35 predicted functional, one host RNAP promoter, and 12 phage promoters. Two Rho-independent terminator sequences and no tRNA genes were predicted throughout the genomes of both phages.

All the predicted ORFs were located on the same forward strand of the DNA (Figure 28 B).

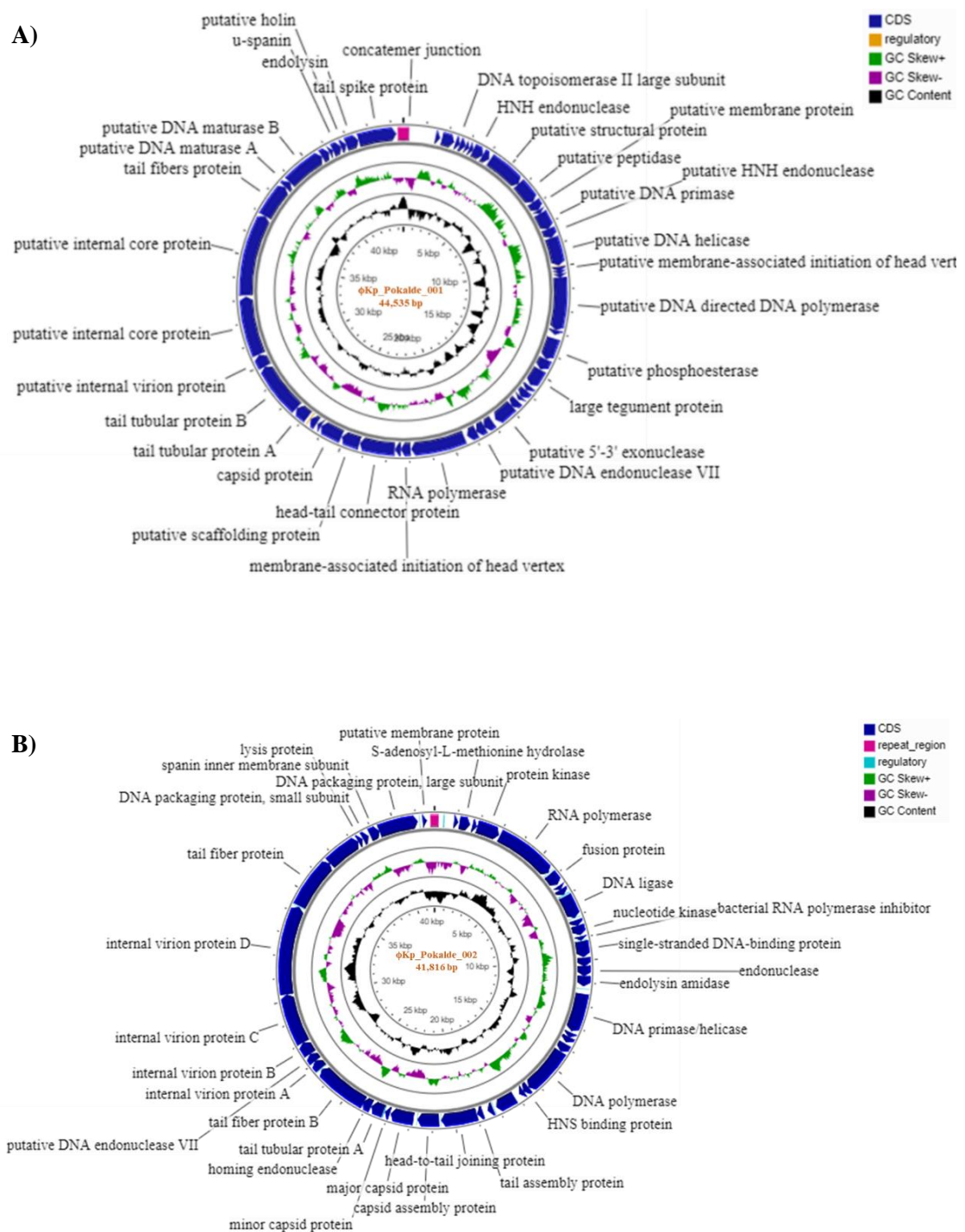


Figure 28: Circular genome view of *Klebsiella* phages ϕ Kp_Pokalde_001 and ϕ Kp_Pokalde_002 in Figures A and B respectively, produced from CG view software. The inner rings show genome location, GC content (black ring) GC skew + (green) and-(purple), and the most external rings show predicted open reading frames (ORFs) (blue arrows) and annotated genes.

On protein BLASTp and PHASTER analysis, both phage ϕ Kp_Pokalde_001 and ϕ Kp_Pokalde_002 genomes revealed no sequence similarity to the genes encoding lysogenic markers such as integrase, recombinase, repressor/anti-repressor protein, and excisionase. Thus, we predict both phages to be strictly lytic in lifestyle. Moreover, the genomes of both phages did not encode the lysogeny module and any known harmful genes such as toxins, ARGs and VFs. Hence, we consider both phages to be an excellent candidate for therapeutical application against *K. pneumoniae* infections. The complete list of predicted protein functions, genomic position, the transcriptional orientation of the genomes is depicted in Appendix-F

The morphological and genomic features of both of the phages indicate that the phages belong to the same *Podoviridae* family. Initial whole-genome BLAST (database Nucleotide collection (nr/nt) using Megablast) of the phages against the NCBI database showed that the phages were related to several *Podophages* isolated against *K. pneumoniae*. The result revealed that the phage ϕ Kp_Pokalde_001 was 90% genome identity with *Klebsiella* phage KP34 (GenBank: GQ413938). Similarly, the phage ϕ Kp_Pokalde_002 shares 96% of the genomic identity with the *Klebsiella virus* KP32 (GenBank: NC_013647). Multiple genome alignment using Progressive MAUVE software of the *Klebsiella* phages ϕ Kp_Pokalde_001 and ϕ Kp_Pokalde_002 with *Klebsiella* phages KP34 and KP32 is shown in Figure 29. The result showed the phages conserved similar synteny and homologous regions at the protein levels of the genes. Based on the specific locations of the predicted genes, associated functions, overall genomic organization, G+C content, DNA replication-transcription, and structural genes, both phages shared a modular structure with many other phages within the *Podoviridae* family, T7-like viruses. The predicted ORFs were assigned functional or hypothetical based on the amino acid sequences and homology to functional domains of known phage proteins such as proteins involved in DNA replication, transcription, DNA packaging into capsid, bacterial cell lysis, and phage structural proteins. Both of the phages induced a halo zone around the clear lysis region (plaque) on the lawn of host cells, suggestive of capsular depolymerase activity which is responsible for degrading capsular exopolysaccharides and biofilm produced by *K. pneumoniae* (Hatfull, 2008; Majkowska-Skrobek et al., 2018). The lysis cassette genes encoding putative class II holin, endolysin, and spanin complex (i-spanin/o-spanin) that involve in the lysis of the host bacteria were scattered throughout the genomes.

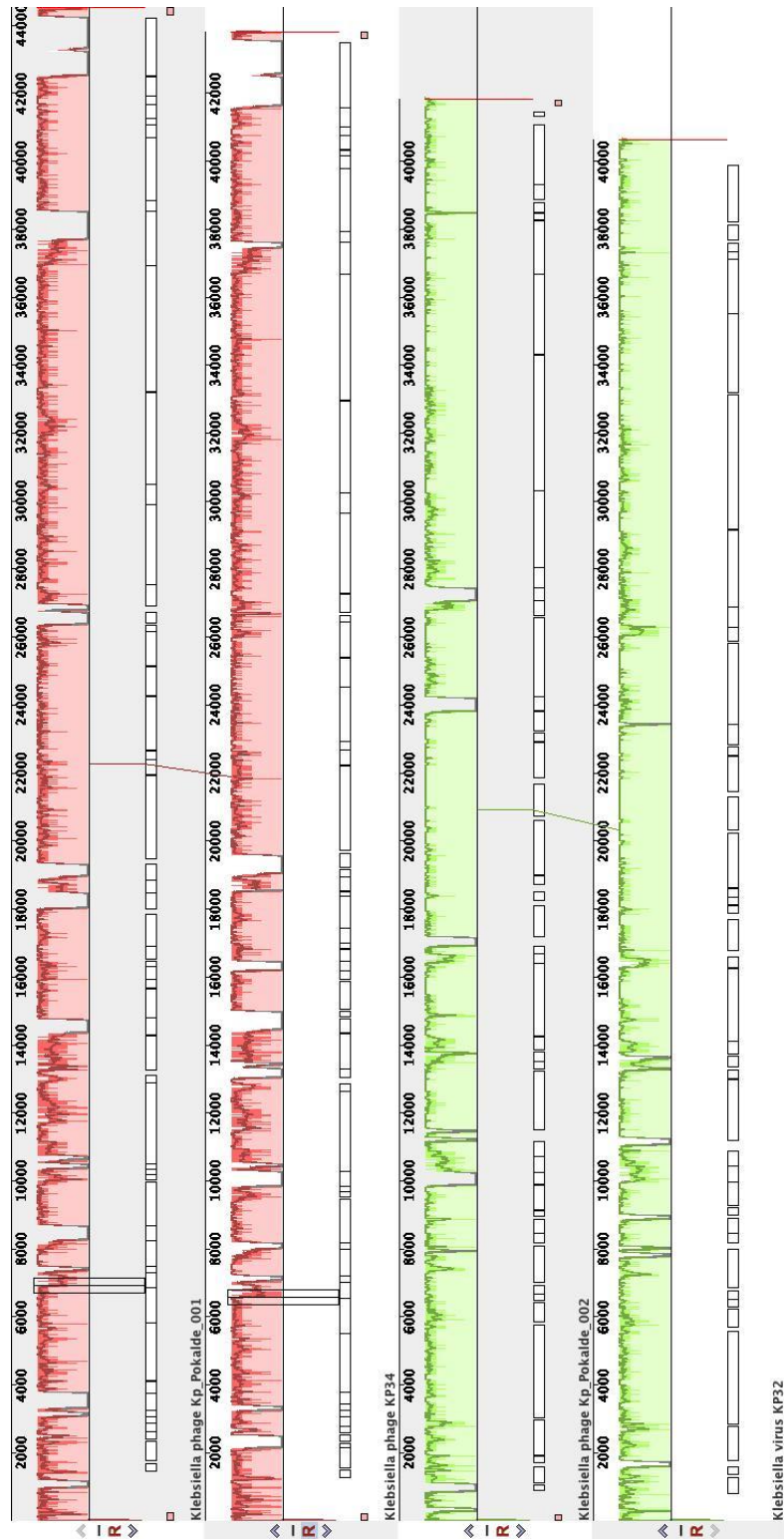


Figure 29: Multiple genome alignment using Progressive MAUVE of isolated *Klebsiella* phages Kp_Pokalde_001 and Kp_Pokalde_002 with other highly homologue *Klebsiella* phages KP34 (GenBank: GQ413938) and KP32 (GenBank: NC_013647). The height of the similarity profile corresponds to an average level of conservation in that particular region of the genome. Blank regions (white) represent fragments that are not aligned or conserved in a particular genome sequence.

4.5.6 Phylogenetic analysis

Genome-BLAST Distance Phylogeny (GBDP) analysis showed the close relatedness of the phage genomes to the other phages available in the NCBI database (genomes having more than 90% sequence similarity). The analysis yielded two family-level clusters (F1 and F2), nine genus-level clusters (G1-G9), and thirty-four species-level clusters (S1–S34). Both *Klebsiella* phages isolated against *K. pneumoniae* from Nepal, fall in the different family, genus, and species-level clusters. The phage ϕ Kp_Pokalde_001 falls in family-F2, genus-G5, and species-S23. Likewise, the phage ϕ Kp_Pokalde_002 lies in family-F1, genus-G7, and species-S20 as shown in Figure 30.

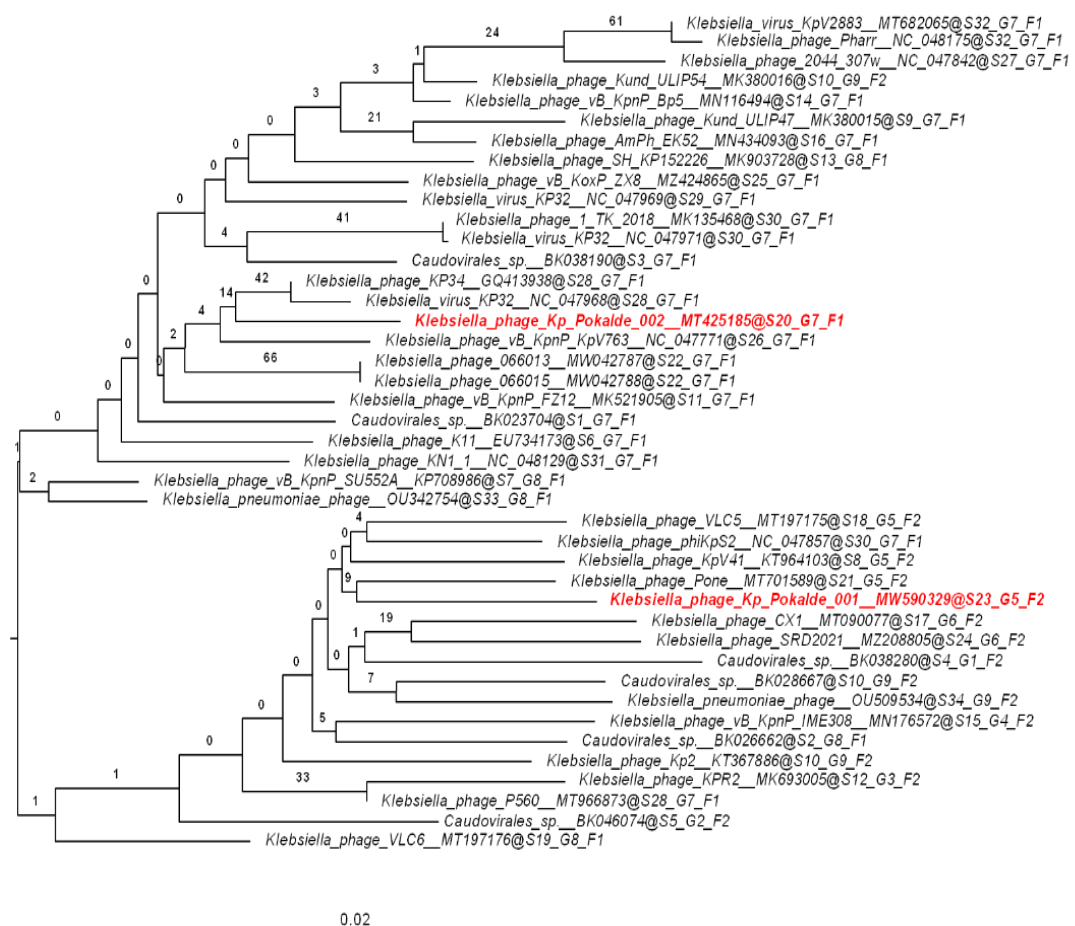


Figure 30: Phylogenomic trees of the *Klebsiella* phages inferred using the formulas D4 and yielding average support of 9 %. The numbers above branches are GBDP pseudo-bootstrap support values from 100 replications. The branch lengths of the resulting VICTOR trees are scaled in terms of the distance formula used. The OPTSIL clustering yielded 34 species clusters. At the genus level, nine clusters resulted and the number of clusters determined at the family level was two.

Both phages produced a halo zone surrounding plaques suggesting the presence of active depolymerase. We found a tail spike protein encoded by gp53 (ORF53) of Kp_Pokalde_001 to be similar to that of gp38 of phage KP32 (Squeglia et al., 2020) and gp39 (ORF39) of Kp_Pokalde_002 which encodes putative tail fiber protein identical (77%) with conserved N- terminal region of Phage T7 tail fiber protein (gp17) on HMMER and HHPRED analysis. The predicted three-dimensional structure model of gp53 (ORF53) of ϕ Kp_Pokalde_001 and gp39 (ORF39) of the ϕ Kp_Pokalde_002 by Protein Homology/analogy Recognition Engine V 2.0 (Phyre2) are presented in Figure 31. Furthermore, the phylogenetic tree of the tail spike proteins of phage Kp_Pokalde_001 (gp53) and phage Kp_Pokalde_002 (gp39) with other similar tail fiber/ spike proteins encoded by *Klebsiella* phages is shown in Figure 32.

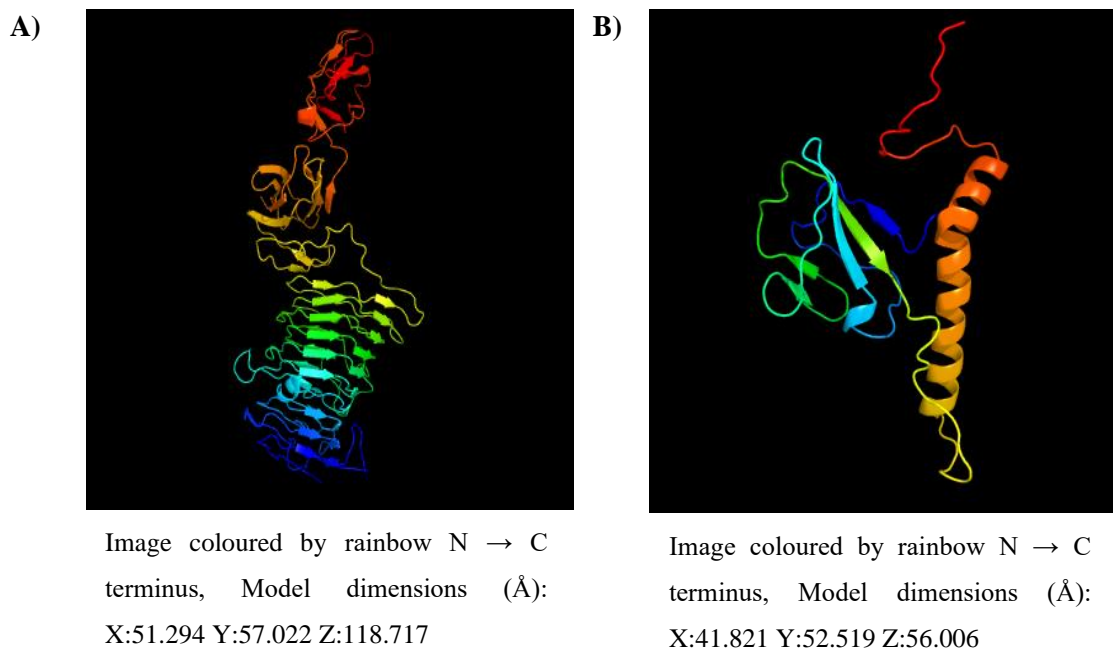


Figure 31.: Predicted three-dimensional structure model of gp53 (ORF53) of ϕ Kp_Pokalde_001 and gp39 (ORF39) of the ϕ Kp_Pokalde_002 by Protein Homology/analogy Recognition Engine V 2.0 (Phyre2) in Figure A and B respectively. The tail spike protein (gp53) of ϕ Kp_Pokalde_001 showed a top template with a crystal structure of a capsule-specific depolymerase produced by *Klebsiella* phage Kp32gp38. (Confidence in the model: 100% and coverage: 87%). Total 498 residues (87% of sequence) have been modeled with 100% confidence by the single highest scoring template. The tail spike protein (gp39) of ϕ Kp_Pokalde_002 protein had a top template with a n-terminal of mature phage T7 tail fiber protein gp17. (Confidence in the model: 99.9% and coverage: 17%). Total 132 residues (17% of sequence) have been modeled with 99.9% confidence by the single highest scoring template.

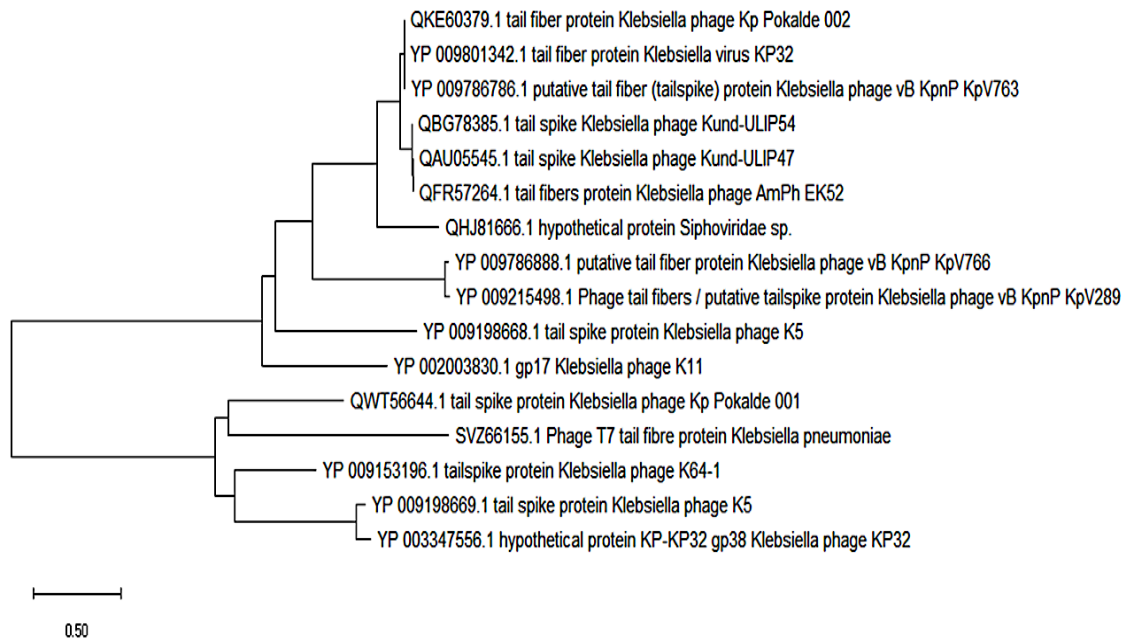


Figure 32: Evolutionary analysis using tail spike protein by Maximum Likelihood method. The evolutionary history was inferred by using the Maximum Likelihood method and JTT matrix-based model. The tree with the highest log likelihood (-17642.08) is shown. Initial tree(s) for the heuristic search were obtained automatically by applying Neighbor-Join and BioNJ algorithms to a matrix of pairwise distances estimated using the JTT model, and then selecting the topology with a superior log-likelihood value. This analysis involved 16 amino acid sequences. There were a total of 1106 positions in the final dataset. Evolutionary analyses were conducted in MEGA X.

Peculiar to this study is that during phage purification, we observed the spontaneous loss and then recovery in the halo plaque phenotype by one of the *Klebsiella* phages ϕ Kp_Pokalde_001, isolated against a clinical isolate *K. pneumoniae* (TUKP1). We parsed out the plaque morphology and carried a forward genetic screen which allowed us to identify multiple residues clustered in the putative catalytic domain of the tail spike protein responsible for this phenotype switching. The protein sequence matches associated with the predicted pectate lyase catalytic domain which is associated with depolymerase activity. Thus, it is suggested that the halo phenotype must have resulted from its depolymerase activity.

4.5.7 Heterogeneity in plaque morphology of ϕ Kp_Pokalde_001

The structural arrangement of its genome indicated its relatedness to several other independently isolated *Klebsiella* phages in the public database including its identity to

phage KP34 that has been previously characterized (Drulis-Kawa et al., 2011). Despite the close relatedness among these phages (CX1, vB_Kp2, Pone, and KP34; 90-92% identity with ~82% genome coverage), an outstanding difference was in their tail structures indicating the essentiality of phage to recognize a precise host (Figure 33). The amino acid sequence similarity of the tail spike protein (gp53) of ϕ Kp_Pokalde_001 was done using EMBL-EBI, HMMER analysis to understand the protein of known structure. The protein sequence matches associated with the predicted pectate lyase catalytic domain which is associated with depolymerase activity (Table 14). Thus, it is suggested that the halo phenotype must have resulted from its depolymerase activity. The protein sequence and its structure primarily decide the function and stability of the protein. Therefore, the secondary structure of ϕ Kp_Pokalde_001 tail spike protein (gp53) was predicted using PSIPRED Workbench. According to the PSIPRED analysis, the protein was dominated by Beta strand (56%) followed by the random coil (24%) and Alpha helix (7%). The secondary structure of ϕ Kp_Pokalde_001 tail spike protein (gp53) as generated by the PSIPRED server is given in Figure 34.

Table 14: EMBL-EBI, HMMER analysis of ϕ Kp_Pokalde_001 tail spike protein (gp53) for amino acid sequence similarity with protein of known structure.

Name of predicted similar protein	Identity	Protein Family
Tail spike protein (<i>Klebsiella</i> phage K64-1)	36.6%	Pectin lyase-like
Tail spike protein (<i>Klebsiella</i> phage K5)	36.4%	Pectin lyase-like
Depolymerase KP32gp38 [<i>Klebsiella</i> phage KP32]	35.9%	Pectin lyase-like

Phage ϕ Kp_Pokalde_001 formed a plaque with a halo surrounding. What struck our attention was the secondary ring around the halo zone of each plaque. When we cored the individual plaque and performed subsequent analysis, a mixture of two types of plaques, clear with a sharp edge and a clear plaque with halo surrounding, appeared in the bacterial lawn. This heterogeneity of plaque morphology that emerged from a single plaque could be separated into distinct and uniform plaque morphology if one would subsequently purify the selected plaque without prolonging co-incubation with the host (Figure 35).

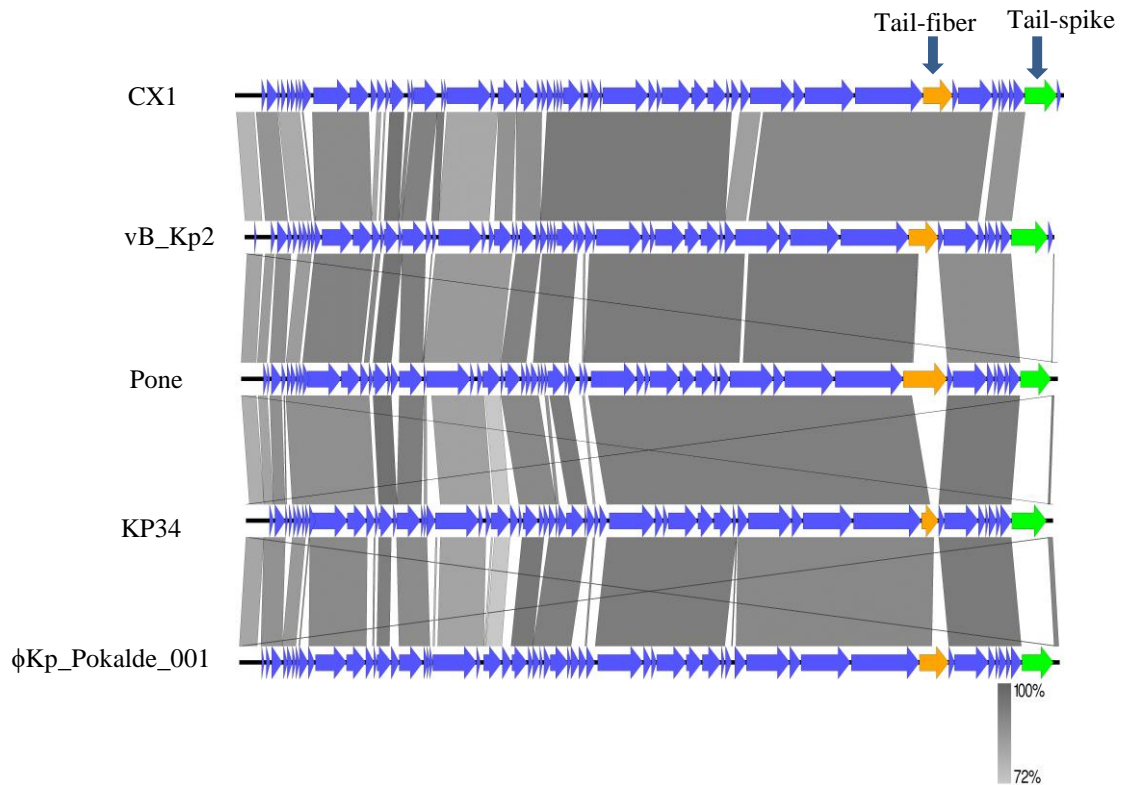


Figure 33: The BLASTN comparison of the whole genome sequence of the ϕ Kp_Pokalde_001 with other Klebsiella phages CX1, vB_Kp2, Pone, and KP34 using Easyfig software. The intensity of gray shading represents identity levels. ORFs are presented by arrows highlighting the difference in the tail fiber (yellow) and the tail spike protein (green).

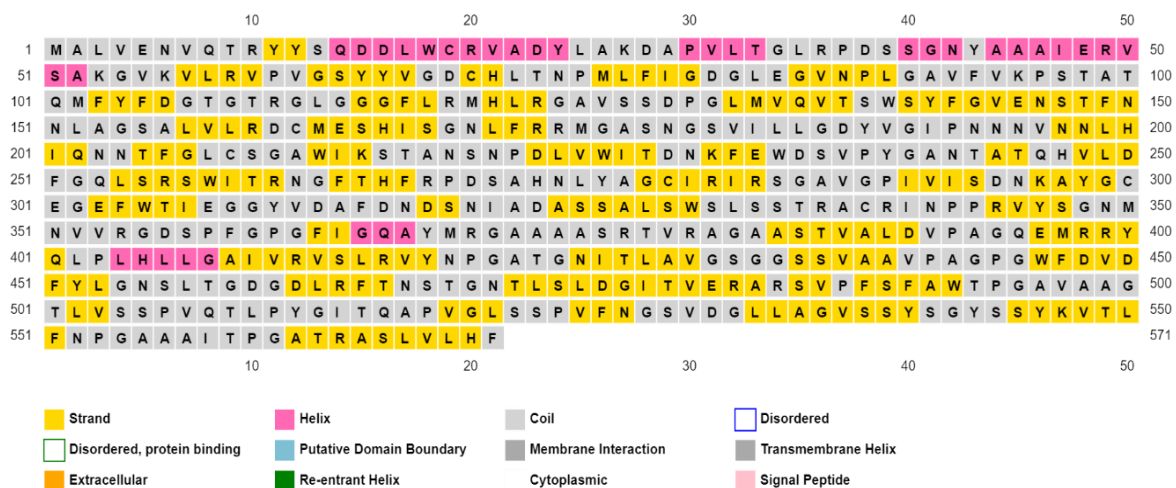


Figure 34: Secondary structure prediction of ϕ Kp_Pokalde_001 tail spike protein (gp53) using PSIPRED Workbench. The protein was dominated by the Beta strand (56%) followed by the random coil (24%) and Alpha helix (7%).

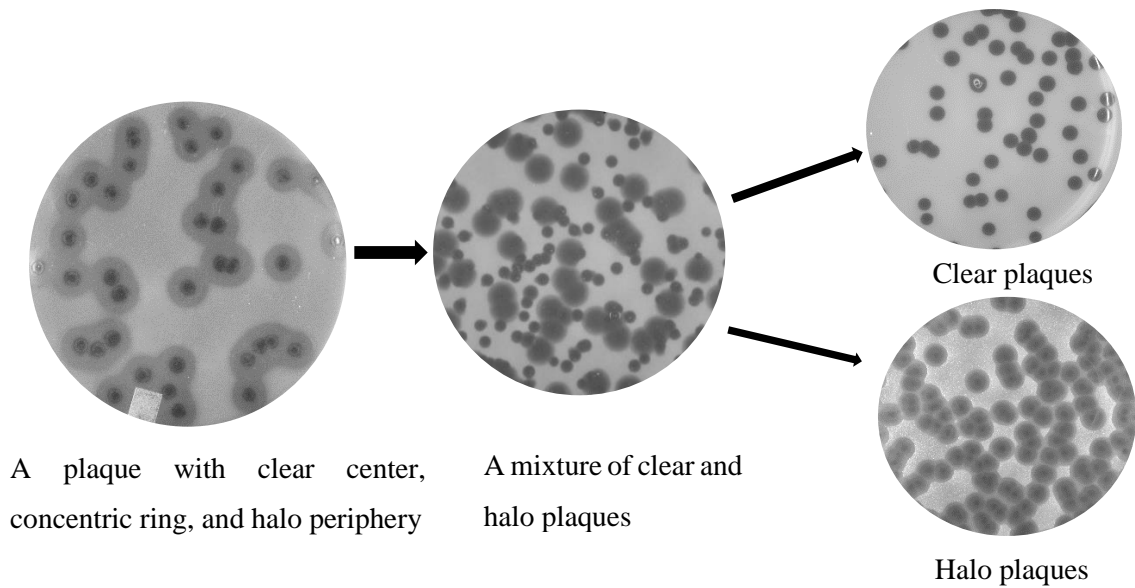
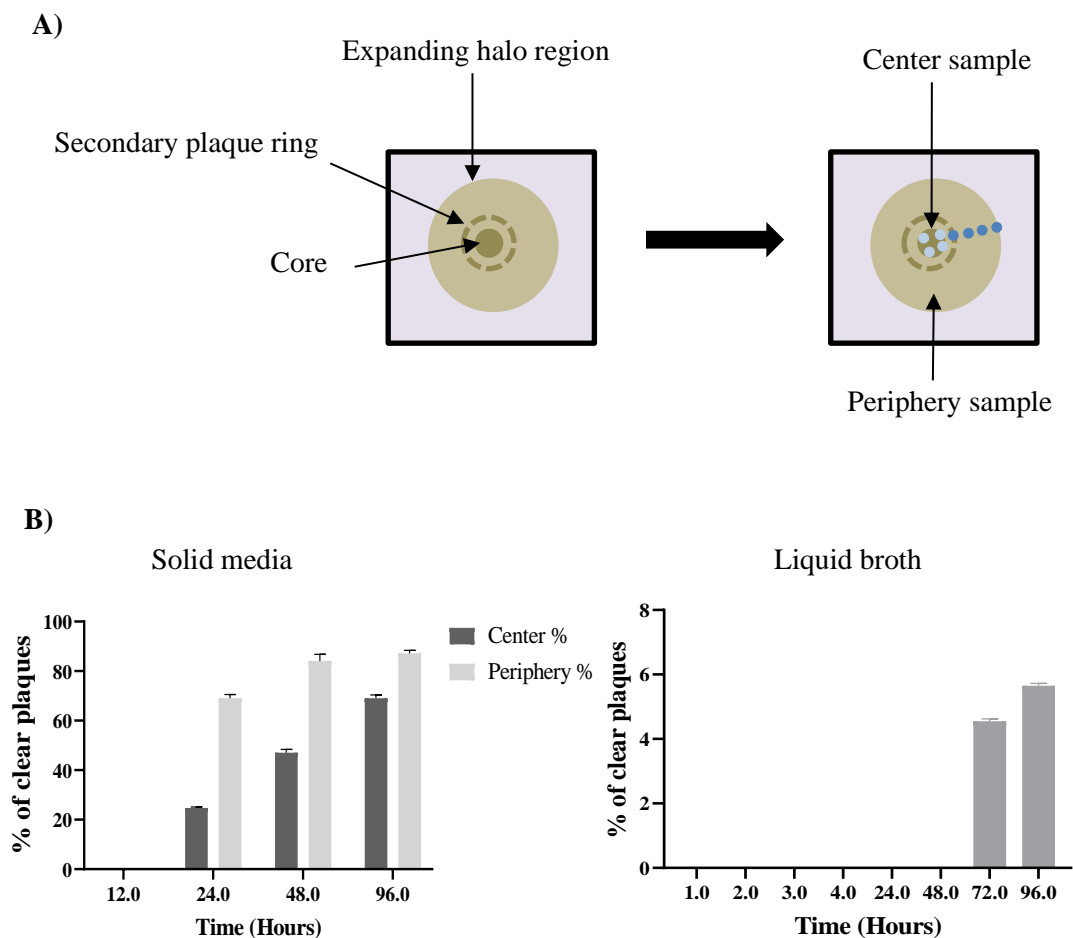


Figure 35: Halo and clear plaques of ϕ Kp_Pokalde_001. Representation of successive plating from a single halo plaque giving rise to a mixture of clear and halo plaques that are separated by plaque purification.

4.5.8 Bidirectional conversion in plaque phenotype

The origin of clear plaques from the periphery of halo plaques after prolonged incubation led us to quantify the percentage of plaque types over time and space. We cored the central and peripheral regions of the individual plaque at different time points and calculated the percentage of plaque types (Figure 36). As the time of incubation progressed, the clear phenotype started to accumulate more in the peripheral region of the plaque compared to the central region (Figure 36 B left panel). The percentage of clear plaques not only steadily increased over time but surprisingly took over the population of the halo surrounding plaques reaching 87% on average. Conversely, we followed the reversion of one independent clear plaque (*Clr1*) if it could restore its halo phenotype. Applying the same method, we cored the central and peripheral regions of this clear plaque at various times of incubation and calculated the percentage of halo-generating plaques. The reversion rate was slower and less frequent giving rise to 4% of halo plaques on average on the agar surface, significantly less compared to the accumulation of clear phenotype (compare Figure 36 B left panel & C). We tested if the emergence of the clear type is as frequent in the liquid broth condition by infecting an actively grown dense culture (OD = 0.4) of TUKP1 with an MOI of 0.00001. The liquid culture did not become clear due to lysis, but the active phage started to accumulate reaching the titer of $\sim 10^8$ pfu/mL in about six hours. The detectable clear

type started to accumulate from 72 hours of incubation which was significantly slower compared to its detection from the single virion infective center on the agar surface (Figure 36 B, right panel). In the same time frame of the liquid culture condition, the reversion of the clear to halo phenotype of *Clr1* did not occur. To test the generality of individual clear types in their reversion ability, we then purified 11 additional phage isolates (*Clr2* to *Clr12*) that formed clear plaques, totaling 12 parallel independent experiments. Most of these new isolates easily reverted to halo phenotype with variable percentage within 12 hours of co-incubation with its host in the liquid condition described before (Figure 36 E). For example, *Clr1* did not give rise to a halo phenotype under this condition whereas *Clr10* gave 20.5% and 48.7% of halo plaques in two separate experiments. The random appearance of irregular boundaries in the spot dilution series due to phenotypic conversation was also observed in the solid agar surface (Figure 36 D). Overall, the bidirectional switching of phage phenotype was easily tractable.



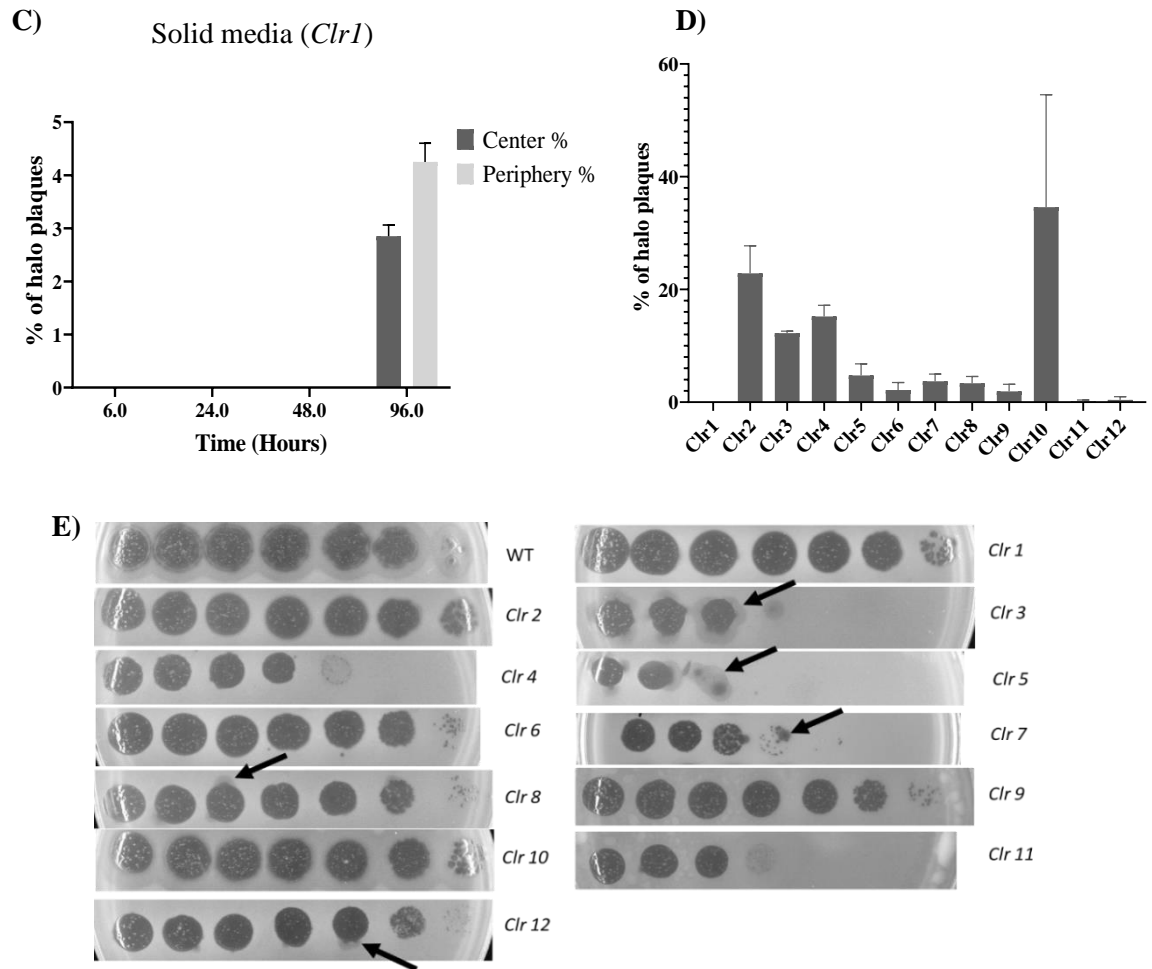


Figure 36: The bidirectional conversion of plaque phenotype. A) the diagram represents the sampling site at the center and successive adjacent points along the radii of the periphery of a single plaque or sampling from the liquid lysate to identify plaques of different morphology. B) Percentage of clear plaques evolved at the center and periphery of a single halo plaque on a solid agar surface (left) and in the liquid media (right) at indicated time points throughout incubation up to 96 hours. C) Percentage of halo plaques originated from the center and edge of a single clear plaque on a solid agar surface at indicated time point. D) Percentage of halo plaque formers evolved from the coincubation of clear types and the host in liquid broth for 12 hours. Error bars are standard deviations (SD) of the means of data obtained from duplicate experiments. E) spontaneous emergence of halo plaques (black arrows) on the edges of serial dilution spots of purified clear plaque formers.

We further analyzed the lysis efficiency of the ϕ Kp_Pokalde_001 wild type (halo plaque former) and clear plaque former mutant (*Clr1*) to the same *K. pneumoniae* (TUKP1) host bacteria in LB medium. The *Clr1* mutant phase showed a slower lysis rate as compared to the wild-type phage (WT) (Figure 37).

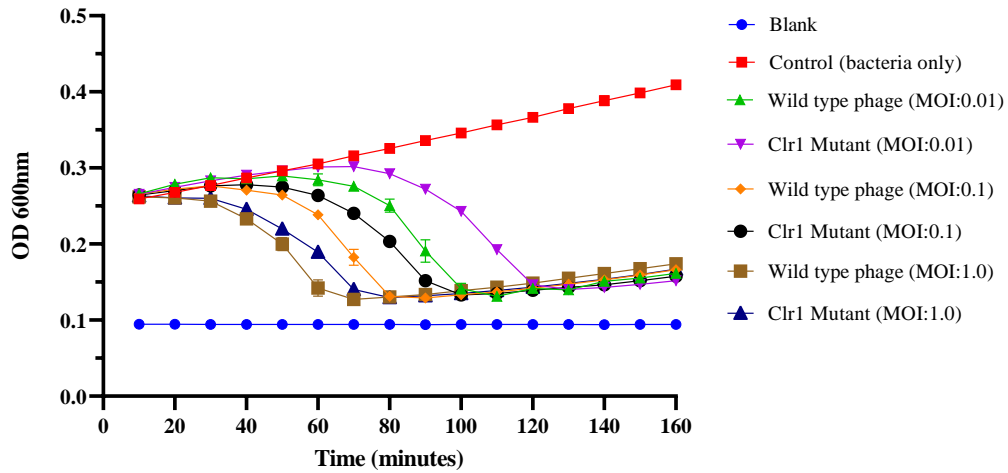


Figure 37: Lysis curve of *K. pneumoniae* (TUKP1) by the ϕ Kp_Pokalde_001 wild type (halo plaque former) and clear plaque former mutant (Clr1) in LB medium. The Clr1 mutant phage showed slower lysis of the host bacteria as compared to the wild-type phage.

4.5.9 Change in plaque phenotype is linked to the amino acid substitution

During this study, 12 independent clear plaque types were isolated and purified until true-breeding was confirmed. Of note, the prolonged incubation was abstained to restrict the spontaneous reversion of plaque morphotype. The whole-genome sequence of each independent isolate was compared with the original phage. The clear plaque formers had a mutation in a tail-spike gene (gp53) (Figure 38).

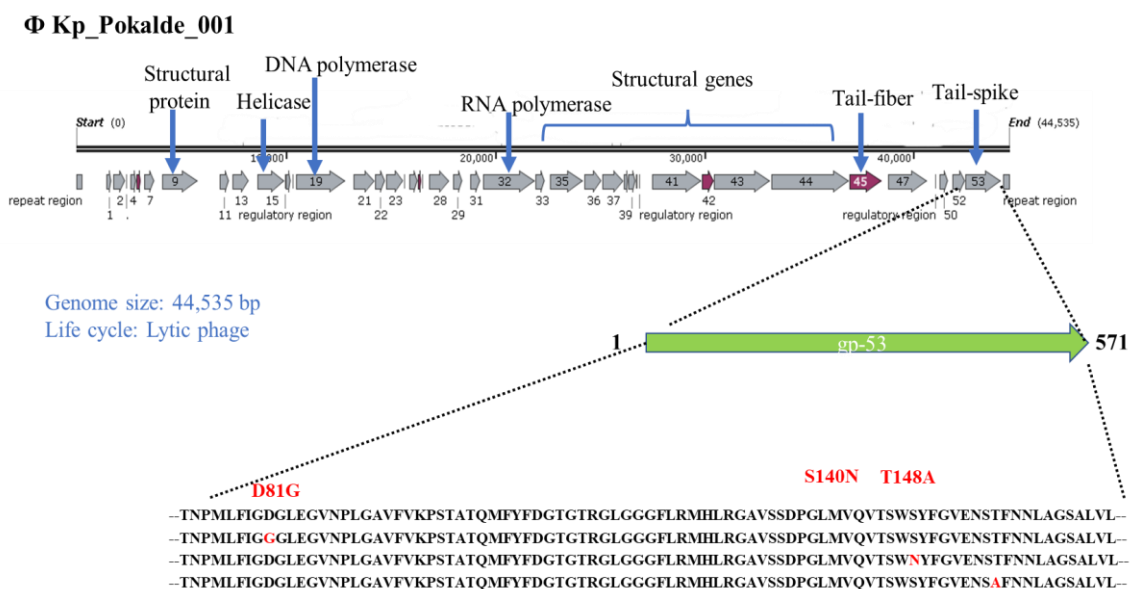
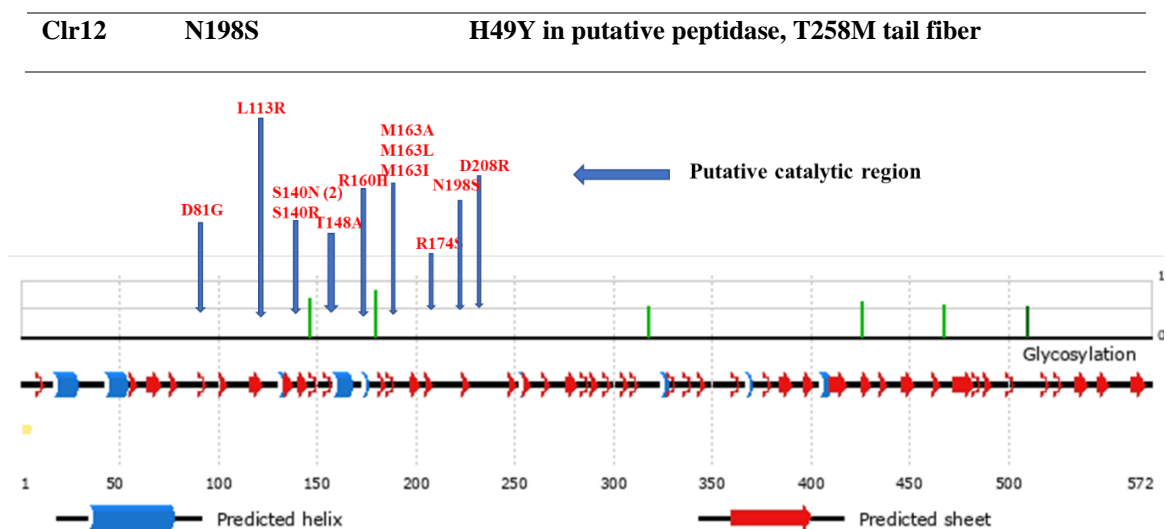


Figure 38: Genome of ϕ Kp_Pokalde_001 showing tail spike gene. Clear plaque formers had a mutation in a tail-spike gene (gp53).

Although, synonymous (2 out of 12 candidates) and non-synonymous (7 out of 12 candidates) (Table 15) additional changes were found elsewhere in the phage genome (Table 16). All phages had a missense change within the small region of the tail spike protein (residue 81 to 208 of 571 residues long polypeptide) suggesting a critical domain for the protein function (Figure 39). Two of these candidates, *Clr3* and *Clr5*, had a double mutation in their tail spike (T148A M163T and E48G L113R, respectively). The collection of spontaneous mutants in this study is inadequate to assign the functional domain boundary that participates in the halo phenotypic occurrence. However, twice and four-times independent isolation of mutants for a single position Ser140 and Met163, respectively, in such a small-scale experiment underpins the functional region of this protein.



Spontaneous Mutations (halo to clear phenotype)

S140N polar to polar	R160H basic to basic	L113R non-polar to basic
T148A polar to non-polar	M163A non-polar to non-polar	S140N polar to polar (twice)
D81G acidic to non-polar	R174S basic to polar	N198S polar to polar
L208R non-polar to basic	S140R polar to basic	M163I non-polar to non-polar

Figure 39: Tail spike protein (gp53 of Pokalde_001) feature predicted by PSIPRED. Clear plaque-forming mutants showing mutations cluster around the putative catalytic domain.

We were then interested to understand the changes needed in the spike protein of these 12 specific mutants to convert back to its original halo phenotype. After successful isolation of the revertants, the tail spike gene was sequenced for analysis. To our surprise, we found that 6 out of 12 were true revertants with no intracodon change

whereas one at position 174 appeared to be pseudo-revertant with the synonymous change of degenerate codon (revertant of Clr8).

Table 15: Mutation and associated phenotype of the tail spike protein of each isolate. Arrows (→) indicate transitions and double greater-than (>>) signs indicate transversions changes.

Mutants	Clear plaque (Codon changes)	Halo restored (Codon changes)	Mutation type
Clr1 & Clr9	S140N (AGC →AAC)	N140S (AAC→AGC)	True revertant
Clr2	D81G (GAT→ GGT)	G81D (GGT→GAT)	True revertant
Clr3	T148A (ACC→GCC)	A148T (GCC→ ACC)	True revertant
Clr4	L208R (CTG >>CGG)	R208L (CGG >>CTG)	True revertant
Clr5	L113R (CTT >>CGT)	R113C (CGT →TGT)	Pseudo revertant
Clr6	S140R (AGC >> AGA)	R140S (AGA >> AGC)	True revertant
Clr7	M163I (ATG→ATA)	I163M (ATA→ATG)	True revertant
Clr8	R174S (AGG >>AGT)	S174R (AGT>>CGT)	Pseudo revertant
Clr10	M163L (ATG >> TTG)	T265A (ACG →GCG)	Intragenic suppressor
Clr11	R160H (CGT→ CAT)	I191T (ATC→ACC)	Intragenic suppressor
Clr12	M163A (ATG →GCG)	T265A (ACG →GCG)	Intragenic suppressor
Clr13	N198S (AAC→AGC)	S198N (AGC→AAC)	True revertant

Table 161: Additional mutation in the genome associated with individual tail spike mutant.

Isolate No	Mutation in the tail spike	Additional mutation in the genome
Clr1	S140N	A89D HNH endonuclease, T256P putative peptidase, A255V large tegument protein
Clr2	D81G	No additional change
Clr3	T148A, M163T	A172V large tegument protein
Clr4	L208R	R18G in tail-tubular protein A
Clr5	E48G, L113R	No additional mutation
Clr6	S140R	S175S synonymous change in tail-tubular B
Clr7	M163I	M128I in internal virion protein
Clr8	R174S	R50R synonymous change in tail-fiber
Clr9	M163L	No additional mutation
Clr10	R160H	No additional mutation
Clr11	M163A	G609S in DNA maturase B
Clr12	N198S	H49Y in putative peptidase, T258M tail fiber

Of the remaining, one was pseudo-revertant with non-synonymous change where the mutant L113R restored the halo phenotype by replacing the *Arg* at position 113 with *Cys* but without reversion of the accompanying E48G mutation (revertant of Clr5). Similarly, another candidate was the true-revertant type where M163T restored its original codon for Met but without any changes to the accompanying mutation T148A (revertant of Clr3). The remaining three mutants restored the phenotype by picking up additional intragenic compensatory mutations to restore the protein function. Two out of these three compensatory mutations were identical, i.e, T265A for a different change in the same position i.e M163L and M163A (revertant of Clr9 and Clr11) whereas for R160H mutation an additional mutation at a different position, I191T, was acquired (revertant of Clr10).

4.5.10 Activity assay of spontaneous and selected mutations of the tail spike protein

Mutation in the tail spike protein manifesting the clear phenotype with sharp edges initially led us to hypothesize that each mutant is null in hydrolyzing the capsular polysaccharide. To test this idea, we first chose to purify the *ClrI*_(S140N) mutant that formed the robust clear edge plaque and compare its activity with the wild-type tail spike protein. The purification profile and SDS page analysis indicated both proteins were equally stable and of the expected molecular mass of ~62 kDa (Figure 40 A and B). Both wild type and *ClrI*_(S140N) mutant eluted as a higher-order oligomer and of trimeric composition from the size-exclusion-chromatography.

The relative difference in partitioning between the higher-order oligomer and the trimeric form is not yet established. The N-terminal domain of the protein that is responsible for assembly onto the virion structure is suspected to cause this concentration-dependent higher-order oligomerization. Nevertheless, the purification profile confirmed the trimeric nature of the tail spike protein as expected. We then compared the minimal concentration of protein required for bacterial clearing activity by spotting a dilution series on the bacterial lawn (Figure 40 C), a method that has been adopted in the field (Squeglia et al., 2020). We found an approximately eight-fold reduction in the activity of the *ClrI*_(S140N) mutant from the wild-type tail spike protein. A recent analysis of the tail spike structure of phage KP32 (gp38) had revealed the acidic residues in the intermolecular cleft of the catalytic pocket responsible for capsule degradation (Squeglia et al., 2020).

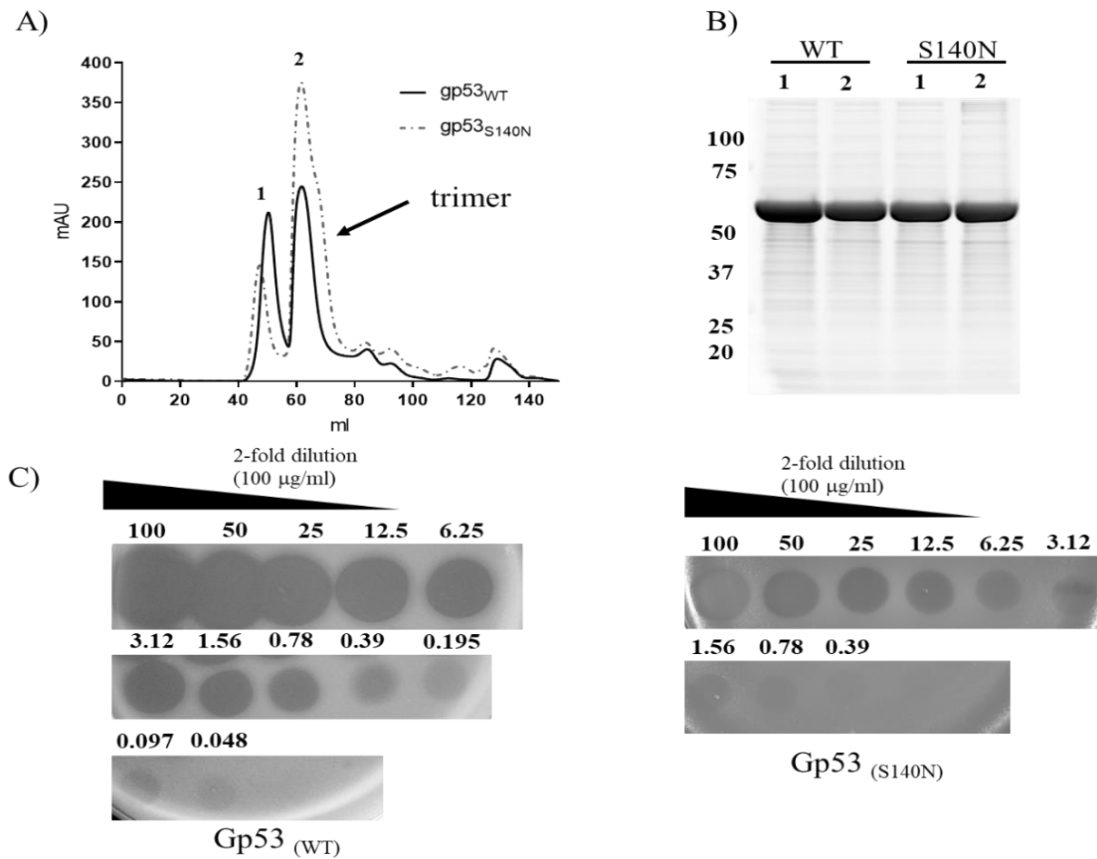


Figure 40: Purification of the tail spike protein (Gp53) and mutant variant encoded by Kp_Pokalde_001, their antibacterial activity, and conserved catalytic residues. In Figure A) Size exclusion chromatography of a Ni-NTA affinity-purified Gp53_{WT} and a mutant protein Gp53_{S140N} using Hi-load superdex 200 16/600 column. Two peaks reflecting an aggregation and a trimer were observed in both elution profiles. B) Purity of the protein sample from each peak was analyzed by SDS-PAGE (4-15%) and sypro-ruby staining. A monomer of anticipated protein size (~62kDa) was observed. A molecular ladder is indicated on the left. C) The depolymerase activity of Gp53 (WT and S140N mutant) was determined by spot assay using a serial dilution of the enzyme on a lawn of the host bacterium. 5 μ L spot series of 2-fold dilution starting from 100 μ g/mL concentration was used.

We found an approximately eight-fold reduction in the activity of the *Clr1*_(S140N) mutant from the wild-type tail spike protein. A recent analysis of the tail spike structure of phage KP32 (gp38) had revealed the acidic residues in the intermolecular cleft of the catalytic pocket responsible for capsule degradation (Squeglia et al., 2020). The mutational analysis of these residues also demonstrated the reduced activity of the KP32gp38 but did not completely abrogate the hydrolyzing property. Despite the phage diversity, these acidic residues in KP32gp38 were also conserved in the tail spike of

Kp_Pokalde_001 (gp53) but were not among the isolated spontaneous mutant pool of clear plaque phenotype (Figure 41). Taking a similar approach as described by Squeglia et al. (2020), we purified and tested the activity of all the mutants in our pool including mutants generated by site-directed mutagenesis of the conserved acidic residues (Table 17).

Table 17: The effect in enzymatic activity of the protein due to various spontaneous mutations and site-directed point mutation. ‘*’ and ‘‡’ symbols indicate different mutations for the same position.

Mutation	Minimum enzyme concentration for activity (mg/mL)	Activity reduction fold
Pokalde_001(gp53) wild type	0.048	-
Clr1 (S140N) *	0.39	8
Clr2 (D81G)	1.56	32
Clr3 (M163T) ‡	0.195	4
Clr4 (L208R)	0.39	8
Clr5 (L113R)	0.78	16
Clr6 (S140R)*	3.12	64
Clr7 (M163I) ‡	0.78	16
Clr8 (R174S)	0.195	4
Clr9 (M163L) ‡	0.39	8
Clr10 (R160H)	0.39	8
Clr11 (M163A) ‡	0.097	2
Clr12 (N198S)	0.39	8
SDM (D161N)	0.048	-
SDM (E164Q)	200	4166
SDM (D223N)	0.39	8
SDM (E233Q)	100	2083
SDM (D235N)	1.56	32

Among the site-directed mutations, the single mutation in the conserved Asp223 and Asp235 reduced the enzyme activity by eight and thirty-two-fold respectively whereas mutation in Glu164 and Glu233 displayed at least three orders of reduced activity. Mutation at position Asp161 had no observable effect. The difference in activity reduction did not precisely mirror the mutations in KP32 gp38 presumably owing to

their diversity. Contrary to our anticipation, the reduction in enzymatic activity was subtle among the spontaneous mutants (Table 17). However, a dramatic difference in activity depending on the type of replaced residue was observed. For instance, replacement with Arg instead of Asn at position 140 had more effect on protein activity.

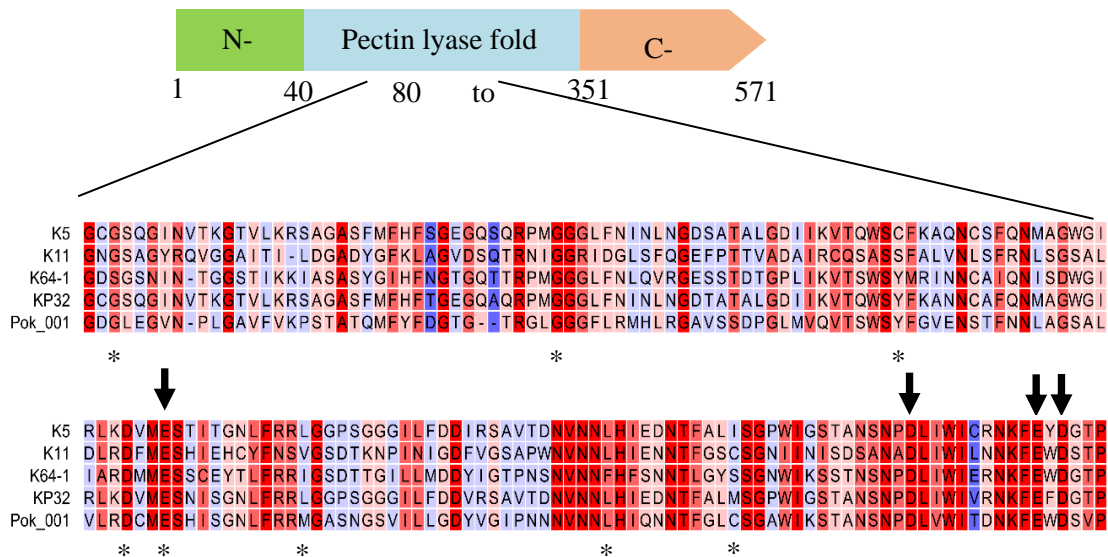


Figure 41: Alignment of residues in the segment of pectin lyase fold identified by InterproScan5 that is depicted arbitrarily with flanking N- and C-terminal domains. The residues of the suggested catalytic pocket by Squeglia et al., 2020 (Squeglia et al., 2020) (down arrow) and all eight target positions of spontaneous mutation (asterisk symbol) are highly conserved among aligned tail spikes of other phages.

4.5.11 Mutation in the tail spike merely affects the phage adsorption rate

The subtlety in the enzymatic activity reduction due to mutation without completely abrogating the enzymatic property of the tail spike protein suggested the alternative hypothesis where the mutation modulates the adsorption efficiency as well. Therefore, we first measured the adsorption efficiency of selective mutants to the TUKP1 host after co-incubation for 15 minutes. We first chose two sets of phage mutants that had similar fold reduction in enzymatic activity (set of R160H, S140N, L208R, and M163L with 8-fold reduction and set of L113R and M163I with 16-fold reduction). The adsorption efficiency of mutants from either category was poor compared to the wild-type phage but did not necessarily correlate with the severity in enzymatic activity reduction. For example, the adsorption efficiency of mutant S140N and R160H with 8-fold reduction was 86% and 93% respectively, almost close to 99% adsorption efficiency of the wild-type phage. On the other hand, the mutants of similar 8-fold

reduction, L208R, and M163L were below 70% efficiency. The adsorption efficiency and adsorption kinetics of tail spike mutant phages are depicted in Figure 42.

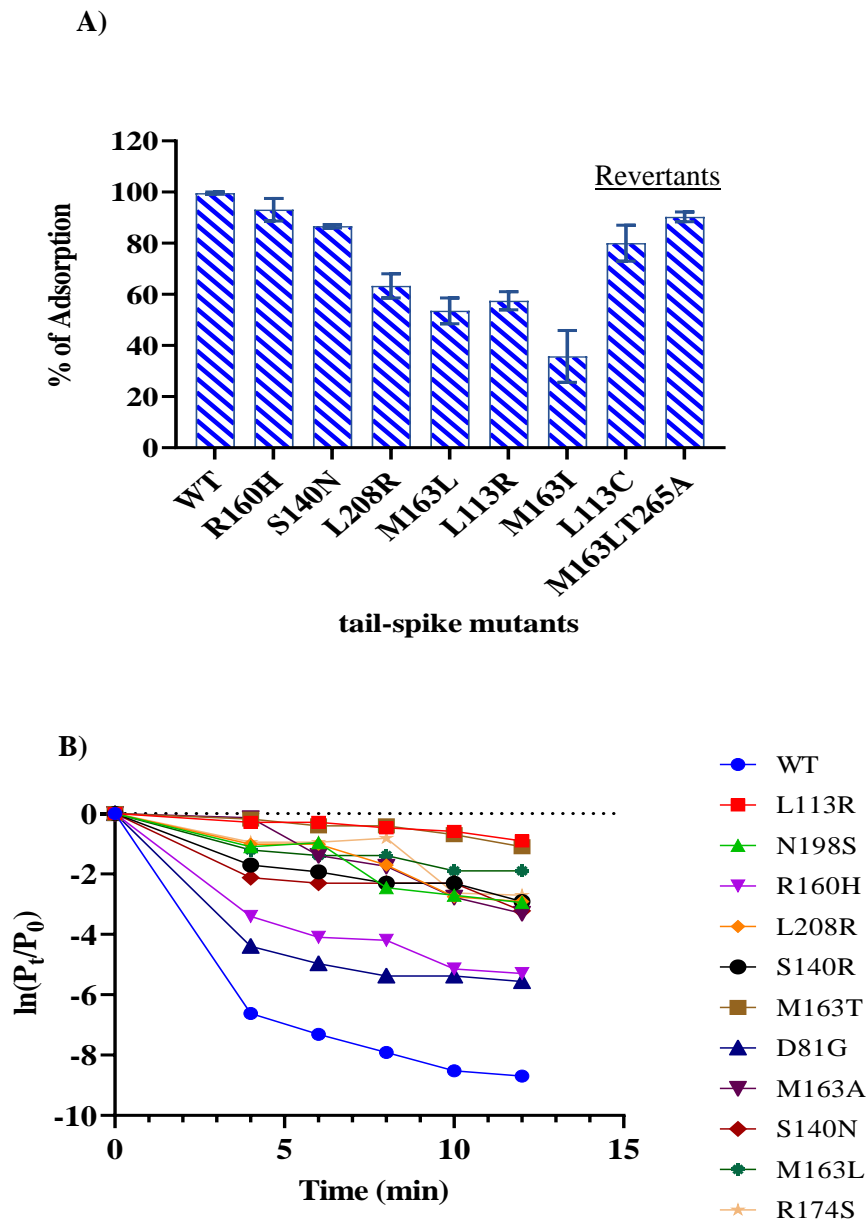


Figure 42: Adsorption efficiency and adsorption kinetics of tail spike mutant phages. In Figure: **A)** Wild type, a subset of phage with the 2-fold difference in enzymatic activity, and revertants were incubated with the host for 15 mins. Free unadsorbed phages were quantified to determine their adsorption efficiency. Error bar represents SDs (n=2). **B)** The adsorption kinetics of all mutants was compared to the wild type. The ratio of unadsorbed to input phages was calculated at 4-, 6-, 8-, and 12-minutes post-infection. The natural log of the ratio was plotted against time for adsorption kinetics. Legends for corresponding symbols are shown on the right.

In response to the immense evolutionary pressure from phage infection, bacteria deploy the innate and adaptive immune response such as restriction-modification, abortive infection, CRISPR-Cas, BREX, DISARM, and others for their survival (Bikard & Marraffini, 2012; Hampton et al., 2020). The most common of all, as the first line of defense, is the alteration of host surface receptors prohibiting phage infection (Azam & Tanji, 2019; Hesse et al., 2020; Labrie et al., 2010). Phages acquire mutations or generate variations in the receptor binding proteins such as tail fibers or tail spikes to counter-adapt with altered host receptors. For example, members of phiKMV viruses are known to utilize error-prone polymerase to accumulate mutation in the phage adsorption apparatus (Magill et al., 2017). *Bordetella* phage BPP-1 recruits the diversity-generating retroelement to generate variation in the major tropism determinant protein leading to host switching (Liu et al., 2002). Similarly, Mu and P1 phages undergo DNA inversion at the C-terminal regions of tail fiber leading to host range alteration (Iida, 1984; Kamp et al., 1978). Here we identified a high rate of spontaneous mutation in the tail spike protein of a *Klebsiella* phage ϕ Kp_Pokalde_001 without losing its infectivity to the original host. What is the mechanism resulting in a selective advantage to the mutants once formed is unclear at this point. Remarkably, the mutation in the tail spike protein was not fixed indefinitely to alter the plaque morphology because each mutant reverted to restore the original plaque morphology under similar conditions. To our knowledge, this is the first follow-up study of the progeny virions in the vicinity of halo plaque surrounding to understand the plaque morphology dynamics. The closest study to look for genetic changes in the progeny virion present in the plaque surroundings was performed by providing a conducive environment for irreversible adaptation of T7 phage (Yin, 1993).

In this study, we revealed multiple residues clustered around the putative catalytic domain of the tail spike protein of ϕ Kp_Pokalde_001 that modulated the plaque phenotype. These residues were also conserved in the tail spike proteins of K5, K11, K64-1, and KP32 phages in addition to the conserved catalytic residue arrangement of E(58aa gap)D(9aa gap)E(1aa gap)D described by Squeglia et al. (2020). Out of 12 tail spike mutants that had missense change in the eight locations, four residues were identical and the other four were either similar or identical among these phages. Our finding strongly suggests that these conserved residues in the vicinity of the catalytic pocket somehow influence the substrate catalysis as observed from the fold reduction

in enzymatic activity due to mutation. Although our study was of limited observation, none of the isolated spontaneous mutants had changes in the positions D161, E164, D223, E233, and D235 – conserved residues of E (58)D(9)E(1)D arrangement in the catalytic pocket. Presumably mutation in these residues could have a more deleterious effect on the phage infection process and thus were not visible on our screen. Our *in-vitro* enzymatic analysis derived from a purified protein of single point mutation in D223 and D235 however had a similar effect as that of other spontaneous mutants. These specific mutations in the context of the phage genome could have a different outcome that needs to be tested.

Remarkably, after a generation of phage growth, each mutant was able to return to its original phenotype either by codon reversion or by acquiring compensatory intragenic mutation. The reversion also occurred only in the critical residues paring the additional missense change that was present in mutant *Clr3* and *Clr5*. (Table 15). Furthermore, there was a reduction in the adsorption efficiency and the adsorption rate of the mutants compared to the wild-type phage. The adsorption efficiency, adsorption rate, burst size, and diffusion rate are known to influence the plaque size and plaque phenotype (Gallet et al., 2011). Our study suggests that halo plaque phenotype is manifested by the pleiotropy of specific mutation in the tail spike protein affecting adsorption rate, adsorption efficiency, and the enzymatic activity of the protein. This probably culminates in slowing down the infection and lysis rate in the periphery of the active center contributing to a halo appearance. Our evidence should be interpreted differently from the inconclusive remarks where the halo phenotype is often postulated to appear by diffusion of excessive free depolymerase surrounding the infective center (Knecht et al., 2019). Whether the halo plaques are due to the activity of a heterogeneous population of wild-type phages and depolymerase mutants to slower the infection kinetics now must be properly scrutinized.

The arms race between phages and their surrounding bacteria is what ultimately shapes the ecology of the community (Diaz-Munoz & Koskella, 2014; Koskella & Brockhurst, 2014). It is plausible to think that some phages or viruses, in general, are evolved to undergo autonomous mutation in the receptor-binding protein (a tail spike in this study) to slow down its spread when the host in its vicinity becomes limiting, such as in the halo region. But they revert with full potential once the host supply becomes abundant and may get a chance to evolve to target resistant hosts with altered phage receptors.

One can imagine that the selective benefit provided by tail spike reversible mutation in the environment could be substantial for both the phage and its surrounding host. Lastly, our method of isolating mutants associated with the phenotypic change is more physiologically relevant and an easier way to identify critical residues for protein function. Our forward genetic screen approach could reveal a clearer picture of the catalytic domain and foster the mechanistic understanding of other phage tail spike proteins. This could become a valuable resource for engineering tail spikes for a broader host range application.

4.6 Phage therapy experiments

In this study, we evaluated the therapeutic efficacy and pharmacokinetics/pharmacodynamics of a novel virulent *Klebsiella* phage ϕ Kp_Pokalde_002 (GenBank ID: MT425185) a mouse model.

4.6.1 Minimum lethal dose (MLD) determination

Swiss albino mice were injected with 200 μ L of *K. pneumoniae* (Kp56) cell suspension via intraperitoneal (IP) route at different concentrations ($\sim 1 \times 10^5$, $\sim 1 \times 10^6$, $\sim 1 \times 10^7$, $\sim 1 \times 10^8$ and $\sim 1 \times 10^9$ CFU/mL) and survival of the mouse was observed up to 10 days. A group of mice (n=8) injected with $\sim 1 \times 10^5$ CFU/mL of Kp56 suspension showed no clinical signs of sickness up to 10 days, suggesting animals had negligible immune response towards the bacteria. While the concentration of bacterial suspension increased to 10-fold (eg. $\sim 1 \times 10^6$ CFU/mL) and so on, the survival rate of mice has reduced in dose-dependent manner with noticeable clinical signs such as lethargy, ruffled fur, higher respiration rate, and laying on sides, etc. After injections of $\sim 1 \times 10^6$ CFU/mL, the survival rate was observed to be 100% while $\sim 1 \times 10^7$ CFU/mL showed decreased mice survivability to 60%. Similarly, two groups of mice infected with $\sim 1 \times 10^8$ CFU/mL and $\sim 1 \times 10^9$ CFU/mL of Kp56 were dead within 48 hours. Therefore, $\sim 1 \times 10^8$ CFU/mL was considered as a lethal dose (LD₁₀₀) in the Swiss albino mouse used in this study (Figure 43). A similar result was observed by Wang Z et. al. (2021). They reported the MLD of intranasal inoculation of *K. pneumoniae* W-KP2 as 5.0×10^8 CFU/mouse (Wang et al., 2021). Similarly, the LD₁₀₀ of *K. pneumoniae* NY03 was reported as 10^7 CFU/mouse (Shi et al., 2021). To predict the potency of phage in the treatment of infectious diseases of humans, it is necessary to create models of animal infection which closely mimic the condition as it occurs in the human body.

Animals being biologically similar to humans in some regards such as susceptibility to many of the same disease conditions which afflict humans are widely used as models for study purposes (Shanks et al., 2009). Similarly, the determination of the proper dose of the infectious agent is of paramount importance. The dose administered must produce the desired diseased state before a new treatment option can be tested. From an animal welfare point of view, it is important to use as minimum animals as possible and the pain endured by the animal be kept at a low level (Festing & Wilkinson, 2007).

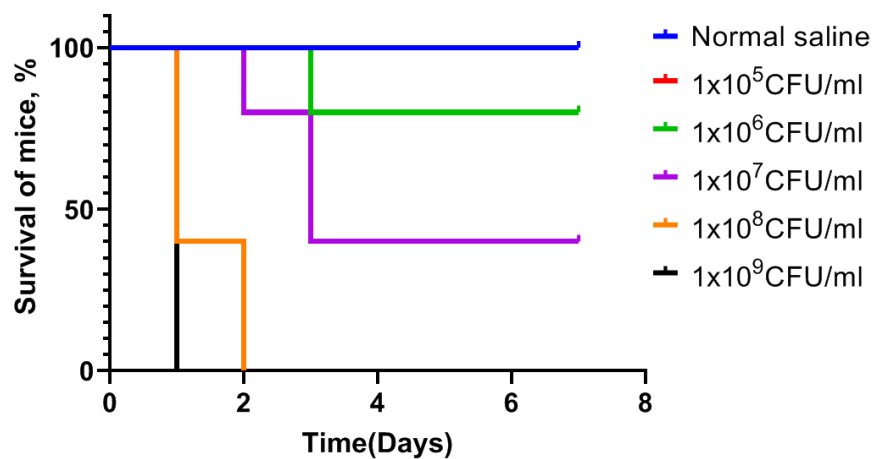


Figure 43: Determination of minimum lethal dose (MLD) of Kp56. A 200 μ L of bacterial cell suspensions ($\sim 1 \times 10^5$, $\sim 1 \times 10^6$, $\sim 1 \times 10^7$, $\sim 1 \times 10^8$ and $\sim 1 \times 10^9$ CFU/mL) were injected intraperitoneally (IP) into a group of mice (n=8 in each group) and their mortality was traced for up to 7 days. A dose of $\sim 1 \times 10^8$ CFU/mL cells was found to be fatal in >60% of mice within 24hr and 100% within 2 days of post-injection. Therefore, $\sim 1 \times 10^8$ CFU/mL was considered as LD 100.

4.6.2 Efficacy of phage therapy in the mouse model

In this study, we evaluated the efficacy of ϕ Kp_Pokalde_002 to rescue mice infected with a lethal dose of *K. pneumoniae* (Kp56) using oral and intraperitoneal (IP) routes of administration. The mice infected with the lethal dose of Kp56 were treated with the phage via IP and oral route (MOI 1.0). Both simultaneous and one-hour delay IP route treated mice were saved with the survival rate of 100% in contrast to the control group without phage therapy ($p < 0.05$). However, survivability of the oral-treated mice was decreased to 40%. Interestingly, 80% mouse survivability was recorded in the pre-treatment group (see methods) where the ϕ Kp_Pokalde_002 was administered intraperitoneally 24 hr. before the Kp56 infection. Similarly, 60% of the mice were

survived when treated with the phage via IP route after 24 hr. of Kp56 infection (Figure 44).

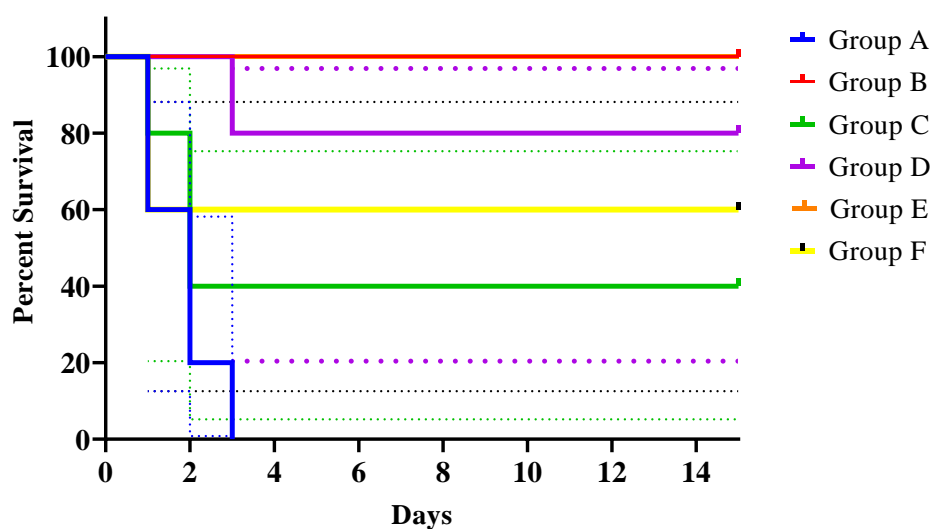


Figure 44: Efficiency of phage therapy in a mouse model. Survival curves of the infected mice (n=5/ group) treated with either SM buffer or phage ϕ Kp_Pokalde_002 at MOI 1.0 through oral and IP route. Survival curves were compared for significance with the log-rank (Mantel-Cox) test of the results obtained from comparison with the SM buffer treated (positive control) group and following parameters: A) IP route phage treated (immediate) group (P = 0.0019), B) IP route phage treated (1 hour late) group (P=0.0019), C) Oral route phage treated (immediate) group (P = 0.2019), D) Phage pre-treated (24 hr. before infection) group (P =0.0048). E) IP route phage treated 24 hr. after infection (P = 0.1181)

Previous results have also shown that mice infected with *K. pneumoniae* and *P. aeruginosa* were survived when phage administered via the both oral and IP routes (Sandra Chibani-Chennoufi et al., 2004; Hung et al., 2011). Watanabe et al.(2007) reported the survival rate of mouse was significantly higher in IP and IV routes of administration as compared to the oral route. Contrary to this, Hung et al. (2011) concluded that oral administration of phage was more efficient than the IP route during the initial infection period, while the IP route showed better therapeutic efficiency at later stage of the infection. Our result showed that the ϕ Kp_Pokalde_002 was able to cross the gut wall successfully into the blood and other tissues of mice. The survivability of oral-treated mice was decreased (40%). The possible reason for this result may be due to orally treated phage might not reached into the systemic circulation and localize into the infected site at an optimum level. This may be due to adverse

environment of the gastrointestinal tract such as gastric acidity, presence of enzymes/bile juice and poor intestinal absorption rate of the phage (Dąbrowska, 2019). It was shown that the oral route of phage delivery was efficient in the treatment of gastrointestinal infections (Wagenaar et al., 2005). Studies have shown that microencapsulation of phage protects them from the adverse gut environment and enhance the efficacy when administered orally (Singla et al., 2016). Interestingly, 80% mouse survivability was recorded in the pretreatment group ($p < 0.05$). In this group the phage Kp_Pokalde_002 was administered through IP route 24 hours prior bacterial (Kp56) infection. In this study, severely infected mice were also rescued with the phage (however survivability was decreased to 60%) where treatment was given after 24 hr. of bacteria (Kp56) infection. This result confirmed that the phage has a good pharmacokinetics and is constant within the body of mice for up to 24 hours. Successful phage therapy depends on various factors like time of phage injection, MOI (phage to bacteria ratio), host immune response and phage clearance, phage burst size, phage half-life, and bacterial resistance *in-vivo* (Ly-Chatain, 2014). Interestingly, in our study, all of the mice were rescued from the infection in an immediate and one-hour delayed phage treatment (1 hpi). Wang et al. (2018) reported that one hour delayed phage therapy led to a 56% reduced animal survival rate while others reported 100% when the phage was administrated within 4 to 7 hours post-infection. Similarly, others reported 50% of animal survivability in 24 hr. post-infection. (Pouillot et al., 2012; Shivshetty et al., 2014; Takemura-Uchiyama et al., 2014; Wang et al., 2018).

4.7 Pharmacokinetics

PK/PD are important parameters for better understanding the success of phage therapy and obtaining regulatory approval (Dąbrowska & Abedon, 2019). In this study, we focused on PK/PD of a novel phage ϕ Kp_Pokalde_002 in a mouse model. We observed the PK/PD of the phage using IP and oral routes in the presence and absence of host bacteria. A group of mice that received only phage (200 μ L of $\sim 1 \times 10^8$ PFU/mL) through IP and/or oral routes did not show any sign of illness during the experiment period (7days post phage inoculation) and the phage was detected in blood and other body tissues within the first hour of both IP and/or oral route of administrations. In the IP group and absence of host bacteria, the maximum biodistribution of the ϕ Kp_Pokalde_002 was found at 4 hr. (43% of inoculated phage titer) post phage injection (Figure 45 A and C). At 4 hr., the phage titer was

significantly higher in spleen ($6.8 \pm 0.10 \log_{10}$ PFU/mL, 6.69×10^7 PFU/mL) compared to blood ($5.3 \pm 0.12 \log_{10}$ PFU/mL, 2.22×10^5 PFU/mL), lungs ($5.6 \pm 0.4 \log_{10}$ PFU/mL, 5.78×10^5 PFU/mL), liver ($6.3 \pm 0.05 \log_{10}$ PFU/mL, 2.25×10^6 PFU/mL) and kidneys ($5.8 \pm 0.10 \log_{10}$ PFU/mL, 6.04×10^5 PFU/mL) ($p < 0.0001$, two-way ANOVA with Tukey's multiple comparisons) (Table 18). After 4 hours, there was a gradual decrease in phage titer in all organs and the phage was completely cleared within 48hr of phage inoculation except the spleen, where the complete clearance was seen at 72hr. Similarly, in an oral route and the absence of the host bacteria, the maximum biodistribution of the ϕ Kp_Pokalde_002 was found at 8hr (28%) post phage administration (Figure 45 B and D).

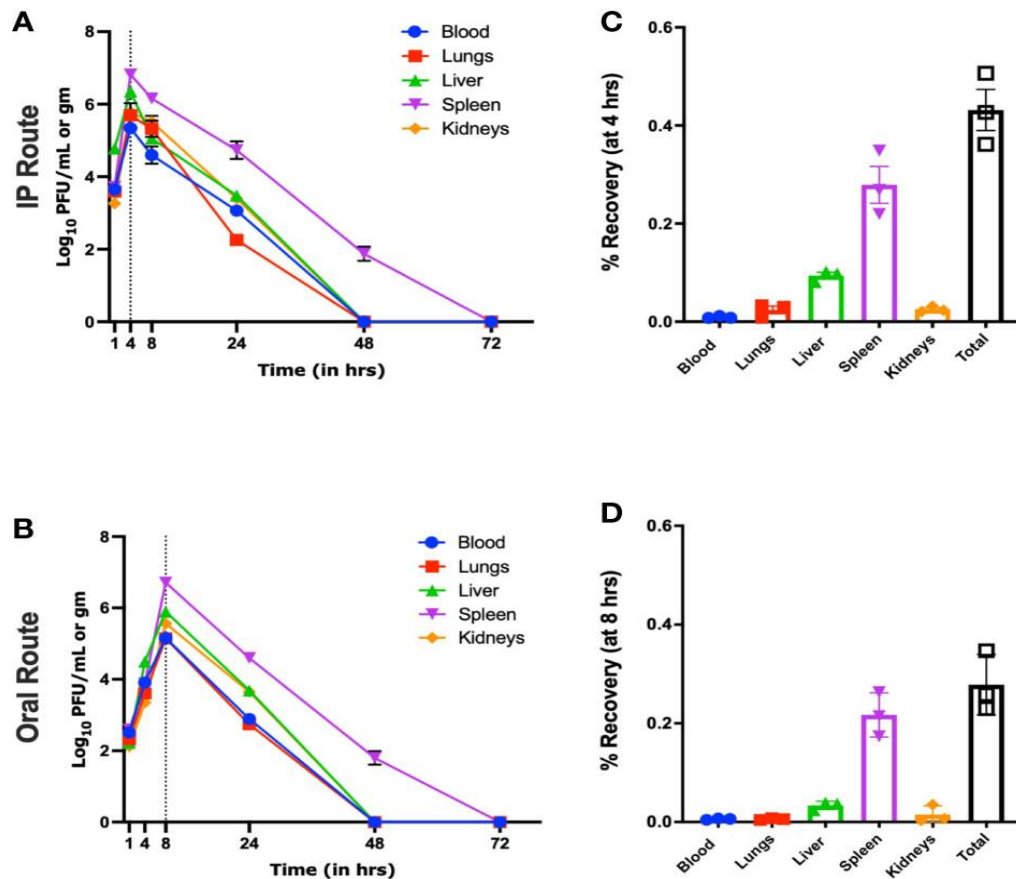


Figure 45: Pharmacokinetics of ϕ Kp_Pokalde_002 in vivo via IP and oral route in the absence of host bacteria. The phage concentration in \log_{10} PFU/mL in blood, lungs, liver, spleen, and kidney after 1, 4, 8, 24, 48, and 72 h of phage administration via IP A) and oral B) route (200 μ L of $\sim 1 \times 10^8$ PFU/mL). The result represents the mean from three independent experiments. Biodistribution of ϕ Kp_Pokalde_002 via IP C) and oral D) route at 4 h and 8 h, respectively. The dotted vertical line indicates T_{max} . Percentage recovery was calculated by dividing phage titer at the respective time-point by the administered dose ($n = 3$ mouse per time point).

At 8 hours, the phage titer was significantly higher ($p < 0.0001$, two-way ANOVA with Tukey's multiple comparisons test) in spleen ($6.7 \pm 0.09 \log_{10}$ PFU/mL, 5.21×10^6 PFU/mL) compared to blood ($4.8 \pm 0.1 \log_{10}$ PFU/mL, 1.45×10^5 PFU/mL), lungs ($5.1 \pm 0.13 \log_{10}$ PFU/mL, 1.44×10^5 PFU/mL), liver ($5.9 \pm 0.12 \log_{10}$ PFU/mL, 8.10×10^5 PFU/mL) and kidneys ($5.5 \pm 0.35 \log_{10}$ PFU/mL, 4.50×10^5 PFU/mL). After 8 hours, the phage titer gradually decreased and completely cleared from all organs within 48 hours of phage administration except the spleen, where the complete clearance was seen at 72 hr. We calculated the area under the curve (AUC) from all groups of mice to identify the phage distribution and relative bioavailability (Figure 46).

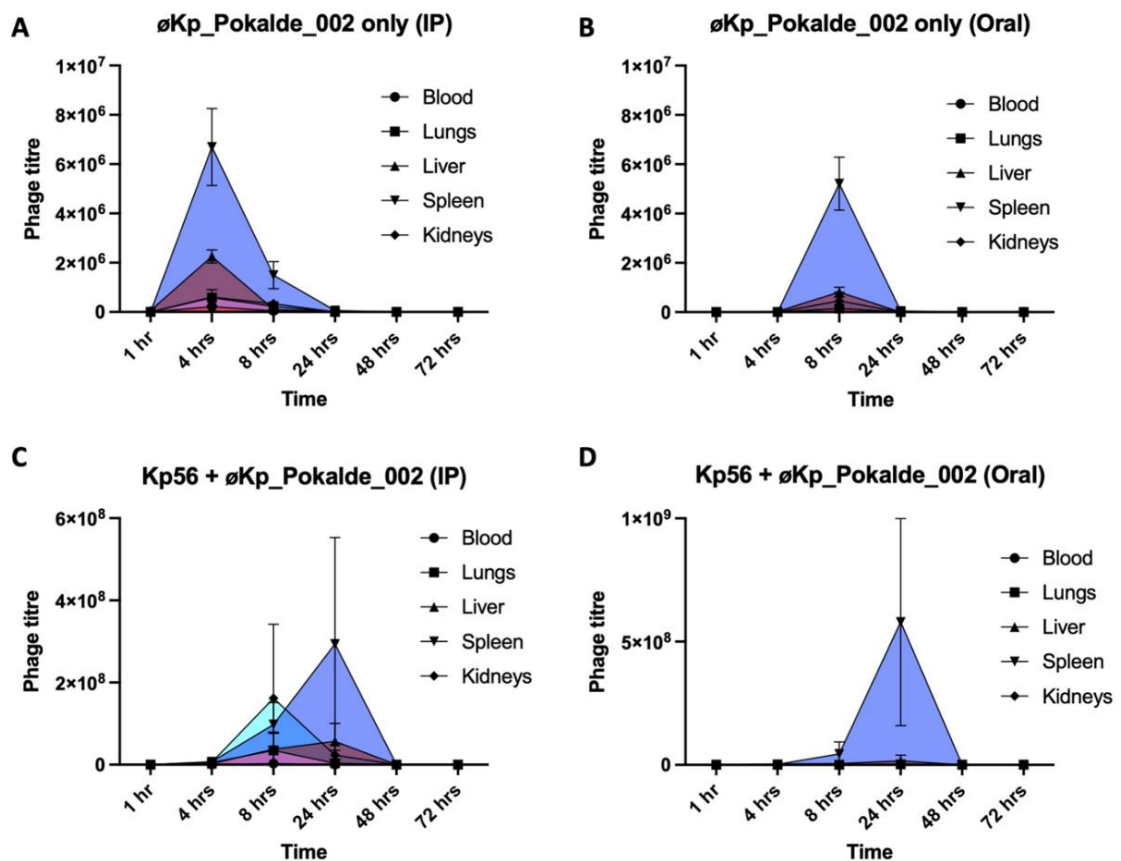


Figure 46: Area under the curve (AUC) from all groups of mice. In Figure A) Phage pharmacokinetics and AUC after administration of phage via IP route in absence of host Kp56. B) via oral route in absence of host Kp56. C) via IP route in presence of host Kp56 and D) via oral route in presence of host Kp56.

As anticipated, we also observed that relative bioavailability was found to be lower when phage was administered through oral route compared to IP in absence of host bacteria (Kp56) (Table 18). Although the results were similar in presence of host Kp56, the relative bioavailability of phage was higher in blood and spleen when administered orally compared to the IP route. Whereas, in the presence of host bacteria Kp56, a maximum titer of the ϕ Kp_Pokalde_002 was found at 8 hr. after phage injection (IP) and 24 hr. (oral) and gradually decreased after 24 hr. In both groups, maximum phage titer was found in the spleen at 24 hr. after phage administration. Though, in contrast to phage administration without host bacteria, the phage did not clear from the spleen until 72 hr. This result revealed that the phage ϕ Kp_Pokalde_002 rapidly distributed into the blood circulation within an hour of administration via both oral and IP routes. A relatively higher concentration of ϕ Kp_Pokalde_002 was recovered from plasma when injecting the phage through the IP route compared to oral (Figure 47).

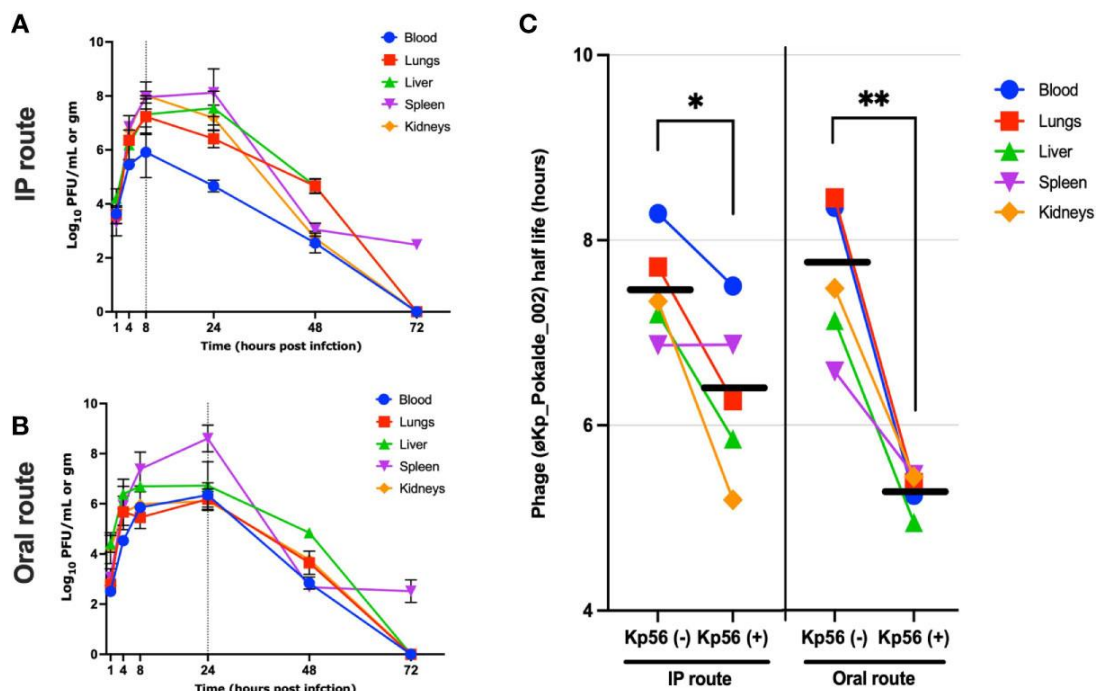


Figure 47: Half-life of ϕ Kp_Pokalde_002 in the presence and absence of host bacteria Kp56 in mice when administered via IP and oral routes. The phage concentration in \log_{10} PFU/mL in blood, lungs, liver, spleen, and kidneys after 1, 4, 8, 24, 48, and 72 h in Kp56 treatment group after administration of phage via IP A) and oral B) route (200 μ L of $\sim 1 \times 10^8$ PFU/mL). The dotted vertical line indicates T_{max} . C) The overall elimination half-life of ϕ Kp_Pokalde_002 is lower when host bacteria are present, signifying rapid clearance of phage from circulation in the presence of a susceptible host. The individual data point represents an average from three replicates from three mice. The horizontal line represents the grand mean.

Table 18: Estimated pharmacokinetic parameters of virulent phage (ϕ Kp_Pokalde_002) in the absence and in the presence of host *K. pneumoniae* (Kp56).

Organ	Blood		Lungs		Liver		Spleen		Kidneys	
	IP	Oral	IP	Oral	IP	Oral	IP	Oral	IP	Oral
Parameters										
In the absence of host bacteria (Kp56)										
Administered dose: 200 μl of 1.2 \times 10⁸ PFU/ml of ϕKp_Pokalde_002										
C_{max} (pfu/ml)	222778	72311	578611	14471	2258318	87056	6694839	521210	604444	45097
T_{max} (h)	4	8	4	8	4	8	4	8	4	8
Vd (L)	1.27	9.7	0.86	18.8	0.16	4.3	0.07	2.07	0.60	12.8
T_{1/2} (h)	8.29	8.35	7.21	8.45	7.34	7.13	6.87	6.58	7.34	7.49
CL (L/h)	0.21	1.32	0.15	2.36	0.03	0.62	0.01	0.3	0.1	1.6
AUC_{0-t} (pfu/h/ml)	269539	155155	807450	149419	2407478	848459	8248503	5262198	948204	458160
Relative bioavailability (F)	58%		19%		35%		64%		48%	
In the presence of host bacteria (Kp56)										
Administered dose: 200 μl of 1.0 \times 10⁸ CFU/ml of Kp56 + 200 μl of 1.2 \times 10⁸ PFU/ml of ϕKp_Pokalde_002										
C_{max} (pfu/ml)	2923000	3315027	34693333	2107333	56589196	16643667	293940000	579333333	23068000	1695000
T_{max} (h)	8	24	8	24	24	24	24	24	24	24
Vd (L)	0.15	0.48	0.01	0.2	0.005	0.009	0.01	0.02	0.006	0.03
T_{1/2} (h)	7.51	5.24	6.26	5.37	5.85	4.94	6.87	5.46	5.20	5.44
CL (L/h)	0.02	0.06	0.002	0.02	0.0009	0.001	0.001	0.002	0.001	0.005
AUC_{0-t} (pfu/h/ml)	3263704	4075882	43003899	2979558	97074444	25790850	399112587	626186433	190270651	3977100
Relative bioavailability (F)	125%		7%		27%		157%		2%	

C_{max}: maximum observed plasma concentration; *T_{max}*: time to the *C_{max}*; *V_d*: Volume of distribution; *T_{1/2}*: elimination half-time; *CL*: clearance; *AUC_{0-t}*: area under the concentration-time curve from time 1 h to the last quantifiable concentration. Relative bioavailability (F) was calculated using the following formula: $F = AUC_{0-t} (oral) / AUC_{0-t} (IP) \times 100\%$.

When phage was administered in mice through the IP route, the highest phage titer in the blood reached after 4hr post-administration, significantly decreased after 8hr and the negligible count was observed after 24hr. The result suggests that the phage net phage elimination is observed after 4hr if injected intraperitoneally in the absence of host bacteria. The result is consistent with other studies where it is reported that the phages take 2-4 hr. to reach their maximum count in blood and is subsequently decreased after 12hr (Capparelli et al., 2006; Kumari et al., 2010; Tiwari et al., 2011). Further, recovery of phages from blood and other tissue after oral administration shows that ϕ Kp_Pokalde_002 survived the gut environment and crossed the gut barrier to reach systemic circulation in mice subsequently reaching to different organs which is consistent with reports from other researchers (Cervený et al., 2002; Gorski & Weber-Dabrowska, 2005). Several mechanisms have been proposed for phage absorption in the gastrointestinal tracts such as intestinal permeability and intestinal transport. Although the mechanism of controlling viral translocation remains unknown, researchers suggested that the phage passage is determined by various factors, including stomach acidity, phage concentration, and interactions with gut immune cells. Micropinocytosis may be a major endocytic pathway to translocate the phage from the intestinal wall into the systemic circulation (Dąbrowska, 2019).

In our experiment, phages were recovered from blood, lungs, liver, and kidneys for up to 24 hr. and for up to 48hr in the spleen in the absence of host bacteria via both IP and oral routes. However, there was a significant difference in phage distribution, bioavailability, and elimination between IP and oral routes of administration. ϕ Kp_Pokalde_002 reached its maximum titer in blood at 4hr (2.3×10^5 PFU/mL) when administered through IP route which was relatively higher compared to administration via the oral route (4.04×10^3 PFU/mL). Similar findings have been reported previously (Cervený et al., 2002; Jun et al., 2014; Keller & Engley, 1958; Oliveira et al., 2009). Additionally, overall relative bioavailability of ϕ Kp_Pokalde_002 when administered via the oral route (at 8hr) was lower compared to IP route (at 4hr) in both absence and/or presence of host bacteria. The reason for reduced bioavailability via oral route compared to IP might be due to slow absorption of the phage in the gastrointestinal tract to reach into the systemic circulation. However, it must be noted that because of the low sampling resolution, the T_{max} could be higher than 4hr and 8hr in IP and oral administration respectively. As, ϕ Kp_Pokalde_002 was stable within a wide pH range

(3 to11) with minimal decrease in phage titer and did not show significant inactivation at 25 °C and 37 °C (as described above), the phage was well tolerated in mice gut with low acidity making it a good candidate for oral phage therapy. It, therefore, appears that the ϕ Kp_Pokalde_002 is relatively stable in the mouse body when administered via the oral route but their availability is comparatively lower and slower. Similar findings have also been reported by Otero et al. (2019) and were able to recover orally administered encapsulated as well as non-encapsulated phages from various organs.

The inter mice PK variability [coefficient of variation (%CV)] was more pronounced in oral (7-78 %) compared to IP (5-56 %) route (Table 19). The inter mice variability was profound in groups of the Kp56 infection model. In addition to differential absorption of ϕ Kp_Pokalde_002 between animals and innate immunity, the higher variability between mice in the oral group may be because of the inconsistent neutralization of phages in the gut environment caused by gut acidity (feeding habit of mice). The phage absorption in the gastrointestinal tract is affected by various factors like gut acidity, gut-permeability and is thus relatively slow. As such, lower phage particles reach into the bloodstream through the oral route compared to the IP route, which makes clinical application of phage via the oral route for systemic infection unfavorable (Wolochow et al., 1966).

Table 19: Inter mice variability (%CV) between the IP and oral groups of mice

Time	%CV (Blood)		%CV (Lungs)		%CV (Liver)		%CV (Spleen)		%CV (Kidneys)	
	IP	Oral	IP	Oral	IP	Oral	IP	Oral	IP	Oral
In absence of host bacteria (Kp56) Administered dose: 200 μL of 1.2×10^8 PFU/mL of ϕ Kp_Pokalde_002										
1 hour	15.19	27.86	5.90	37.32	23.90	14.94	20.20	7.18	8.40	19.83
4 hours	23.60	18.75	56.59	13.61	12.17	38.10	23.34	20.44	22.69	36.29
8 hours	48.48	23.49	43.12	30.07	17.93	25.01	36.97	20.64	33.71	78.44
24 hours	5.24	11.16	24.34	12.78	14.88	20.41	45.26	43.06	16.03	40.82
48 hours	0.00	0.00	0.00	0.00	0.00	0.00	46.07	73.35	0.00	0.00
72 hours	0.00	0.00	0.00	0.00	0.00	0.00	0.00	0.00	0.00	0.00

In presence of host bacteria (Kp56) Administered dose: 200 μ L of 1.2×10^8 PFU/mL of ϕ Kp_Pokalde_002

1 hour	34.12	27.86	60.47	34.77	83.76	60.53	113.81	61.03	57.62	133.91
4 hours	24.42	43.10	83.56	28.92	104.77	78.35	18.48	140.68	35.97	90.12
8 hours	151.57	22.23	128.21	68.00	100.51	41.11	54.69	106.94	111.55	116.27
24 hours	53.04	100.98	60.17	99.97	76.89	138.45	88.24	72.53	109.56	90.38
48 hours	75.14	53.42	48.14	68.35	53.63	9.50	49.37	49.66	60.09	34.94
72 hours	0.00	0.00	0.00	0.00	0.00	0.00	33.07	70.50	0.00	0.00

Further, the results suggest that the liver and spleen are the most common organs of phage accumulation suggesting phages are cleared by organs of the reticuloendothelial system such as the spleen, liver, and other filtering organs (Dąbrowska, 2019; Merrill et al., 1996). Similar results of non-homogenous biodistribution and preferential accumulation of phages in organs like the spleen and liver have also been observed in anti-pseudomonal phage in mice (Lin et al., 2020) and rabbit *in-vivo* models (Uhr & Weissman, 1965). Further, phages are also reported in the urine of humans (Hildebrand & Wolochow, 1962) and animal models like rats (Wolochow et al., 1966), rabbits (Schultz & Neva, 1965) after systemic injection which supports our finding that phages can pass through the renal filter. The role of the kidneys in the clearance of phages has also been observed in fish, where phages were detected in fish kidneys a month after phage administration (Russell et al., 1976).

The PK of phages are fundamentally different from those of chemical drugs due to the self-replicative nature of phages in the presence of susceptible bacteria, their absorption rate, and clearance by the host's immunity (Dąbrowska & Abedon, 2019) thus phage half-life cannot be estimated by the conventional approach. Although researchers have demonstrated prolonged phage half-life *in-vivo* with encapsulation of phage (Colom et al., 2015; Singla et al., 2016), the half-life of phage in the presence of a host is scarce. Using one phase decay model, our study showed that there was no significant difference in elimination half-life of ϕ Kp_Pokalde_002 when administered via IP and oral routes suggesting phage half-life to be route independent. However, the phage had a shorter elimination half-life in the blood and other organs when Kp56 was present

although phage titer was relatively higher in treatment groups compared to phage-only control groups. This suggests that phages can exponentially increase their number *in-vivo* infecting and lysing the susceptible host bacteria and is cleared more rapidly by strong immune response developed against host bacteria (nonspecific) and phage itself (anti-phage). This may explain why multiple injections of phage are required for phage therapy although theoretically, phages are self-multiplying. However, a study on *Klebsiella* phage by Soleimani Sasani and Eftekhar (2020) found half-life in blood (4hr) when phages were administered intraperitoneally [100 μ L of 10^{10} PFU/mL (*Myoviridae*)] and 8hr in lungs whereas Kumari et al. (2010) reported maximum recovery from blood, peritoneal fluid, lungs and skin at 6hr post IP injection [250 μ L of 10^{10} PFU/mL (*Podoviridae*)]. Moreover, the half-life of phage seems to be comparable to that of antibiotics in animal models (Chang et al., 1991; Griffith et al., 2003) which ranges from 0.5hr to more than 7hr which makes it a good drug candidate against bacterial infections. However, more research is required in *in-vivo* models to understand the half-life of different phages in presence of a susceptible host as this is important in designing the therapeutic dose of phage.

4.8 Pharmacodynamics

The groups of mice in the PK/PD model (not infected by Kp56) that received ϕ Kp_Pokalde_002 via IP or oral route showed only mild to moderate alveolar wall thickening and remarkably reduced neutrophil infiltration in perivascular and peribronchial areas (Figure 48). Moreover, they also did not show any significant histological changes compared to the vehicle control (SM buffer only) group at 24 hr. post phage inoculation. Further, a comparison of histological changes in the lung tissues from untreated group (Kp56 + SM buffer) and treatment group (Kp56 + ϕ Kp_Pokalde_002) revealed a noticeable interstitial infiltration by neutrophils and macrophages with severe thickening, congestion, and destruction of the alveolar wall in the lungs of the untreated group. Meanwhile, the orally treated group showed relatively increased neutrophil infiltration in the alveoli (lung tissues) compared to the IP-treated group.

The histology results also revealed that the lung tissue of the ϕ Kp_Pokalde_002 administrated mice had a similar histological picture with reference to the wild-type and SM buffer only administrated mice group. Similar results of no detrimental

histological effects were also observed by Gangwar et al. (2021) in various organs of Charles Foster rats when challenged by high (10^{15} and 10^{20} PFU/mL) of *Klebsiella* phage orally.

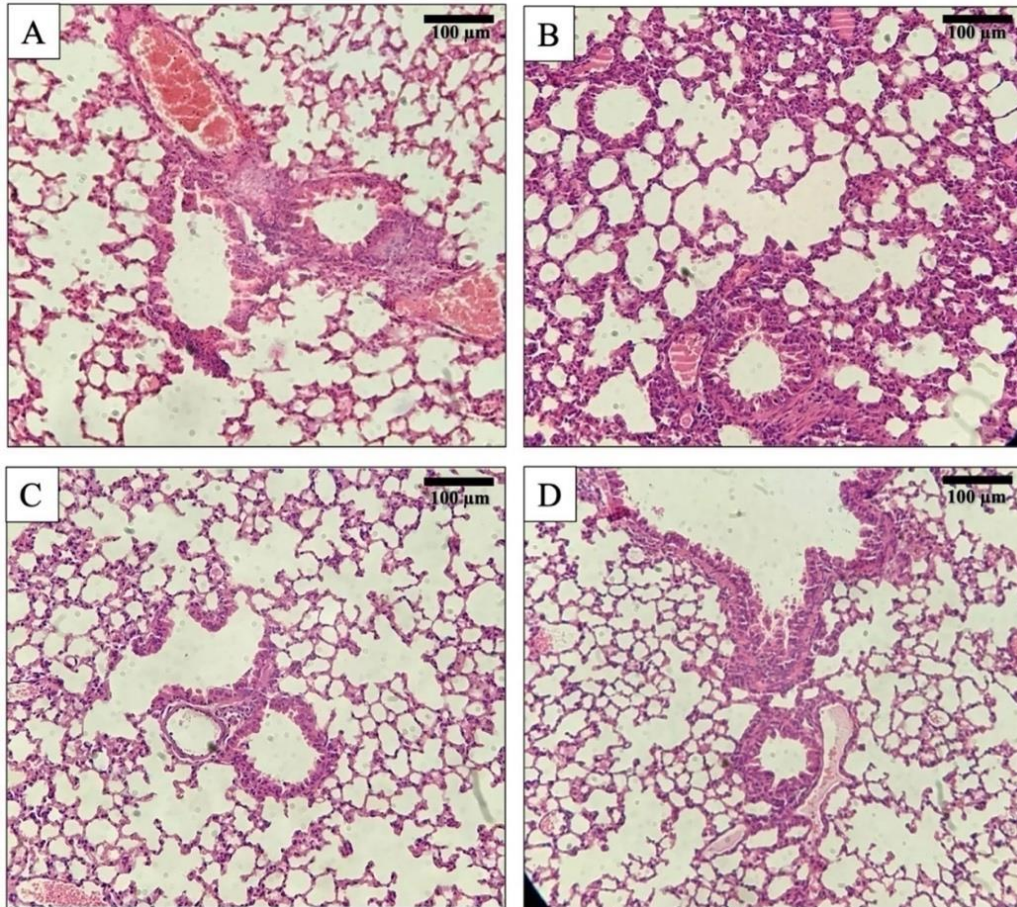


Figure 48: Histology of mouse lung tissue sections after Hematoxylin and Eosin (H&E) staining at 200x magnification. In Figure (A) Lungs' tissue of a normal mouse. (B) Lungs' tissue of bacteria K pneumoniae (Kp56) infected mouse showing interstitial infiltration by neutrophils and macrophages with rupture of alveoli. (C) Lungs' tissue of mouse treated with ϕ Kp_Pokalde_002 via IP route. (D) Lungs' tissue of mouse treated with ϕ Kp_Pokalde_002 via the oral route.

Pro-inflammatory cytokines, such as *TNF- α* , and *IL-6* are useful markers of infection severity. Upon infection, pro-inflammatory cytokines are released by the macrophages to adhere to the other inflammatory cells at the infection site (Bozza et al., 2007; Liu et al., 2016). In this study, the expression level of two pro-inflammatory cytokines (*TNF- α* and *IL-6*) in blood were analyzed to evaluate the tissue inflammation either by ϕ Kp_Pokalde_002 or by Kp56. Cytokine expression levels in the control group (SM

buffer only), phage administered group (ϕ Kp_Pokalde_002 only), Kp56 infected group (Kp56 + SM buffer) and phage-treated groups (Kp56 + ϕ Kp_Pokalde_002) were compared. A significant up-regulation of both pro-inflammatory cytokines '*TNF- α* and *IL-6* ($p < 0.0001$, Tukey's multiple comparisons test) was observed in the Kp56 infected (Kp56 + SM buffer) group compared to the control (SM buffer only) group and at 24hours post-infection, the increment in the *TNF- α* and *IL-6* were 21.0-fold and 17.1-fold respectively. Changes in *TNF- α* and *IL-6* in the phage-only administered group were 1.1-fold and 0.9-fold respectively, compared to the vehicle control (SM buffer only) arm. Interestingly, the levels of cytokine expression in the phage-treated groups via both IP and oral routes were significantly lower compared to Kp56 infected (Kp56 + SM buffer, untreated) arm ($p < 0.05$, Tukey's multiple comparisons test). The fold changes in cytokine *TNF- α* and *IL-6* expression levels in phage-treated (Kp56 + ϕ Kp_Pokalde_002) groups compared to the uninfected control (phage only) are depicted in Figure 49. The study revealed that there was negligible upregulation of pro-inflammatory cytokines (*TNF- α* , and *IL-6*) with the ϕ Kp_Pokalde_002 administered via both IP and oral routes. In contrast, there was significant upregulation of the cytokines in the mice infected with the Kp56. The expression of the cytokines was dropped after 24hr of the ϕ Kp_Pokalde_002 administration in both IP and oral routes signifying the removal of Kp56. The result supports the findings of other researchers who have reported a significant reduction in cytokines levels in phage-treated mice (Wang et al., 2016; Watanabe et al., 2007).

Phage lysates that are prepared from the gram-negative bacteria may contain bacterial endotoxins. Endotoxins are highly immunogenic, which could trigger the inflammatory response. An overexpression of cytokines leads up to aseptic shock and consequent death (Cavaillon, 2018). Phage preparation should be necessarily purified to ensure a low level of endotoxin and other bacterial contamination. However, in our study, we did not measure the level of endotoxin in the phage lysate. Although, researchers have highlighted that phage therapy causes lysis of the host bacteria within the body, thus releasing endotoxins/enterotoxins, which may induce higher levels of *TNF- α* , and *IL-6* causing septic shock (Hagens et al., 2004), the ϕ Kp_Pokalde_002 did not induce a significant inflammatory response in mice indicating a good PD efficiency. However, Chow et al. (2020) also reported that such upregulation of pro-inflammatory cytokines was transient and was diminished over time. Our results suggested that systemic

inflammation of the tissues is lower in phage-treated mice as compared to the untreated. The histological findings of the lung tissue also support these findings.

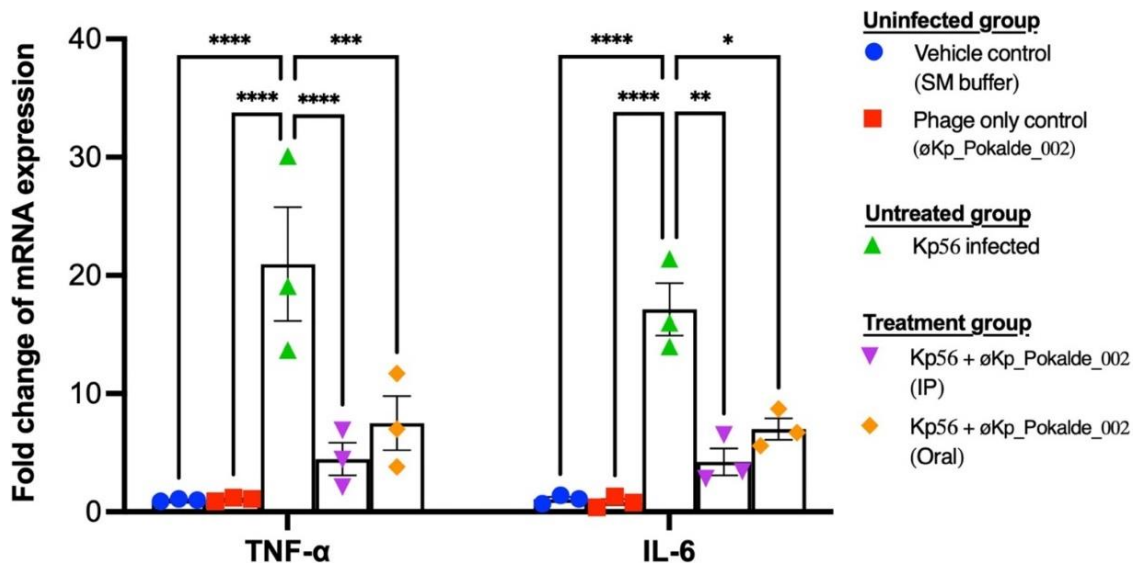


Figure 49: Pro-inflammatory cytokine TNF- α and IL-6 levels in the plasma of mice (24 h post-infection). Both TNF- α and IL-6 mRNA levels were significantly higher in Kp56 infected mice compared to uninfected and treated mice ($p < 0.05$) via both IP and oral routes. There was a negligible fold increment of TNF- α and IL-6 mRNA level in-vehicle control (SM buffer) and phage-only control (ϕ Kp_Pokalde_002). Levels of TNF- α and IL-6 mRNA were normalized to β -actin mRNA levels and were expressed as n-fold ($2^{-\Delta\Delta Ct}$) increase with reference to the control groups. Results are shown as means \pm SEM from triplicate experiments. The y-axis values represent the fold changes of mRNA relative to the β -actin mRNA in the same sample. The statistical comparison was done by two-way ANOVA. * $p < 0.05$, ** $p < 0.01$, *** $p < 0.001$, **** $p < 0.0001$.

Bacterial load was significantly reduced ($p < 0.05$) by 3-5 \log_{10} CFU/mL at 8hpi and 5-7 \log_{10} CFU/mL at 24hpi in the blood and 2.4 \log_{10} CFU/mL at 8hpi and 4-7 \log_{10} CFU/mL at 24hpi in lungs when treated with the phage via both IP and oral route. The bacterial count was completely disappeared in the blood and lung tissues after 96 hr. and 5days post-infection in the IP and oral treated group respectively. In contrast, bacterial load was lower in blood and lungs at any time point(s) when phage was administrated via IP route as compared to the oral route (Figure 50). Normal control groups survived without any symptoms of illness for 15 days. On the other hand, in the Kp56 infection model, the bacterial count increased exponentially in the blood and lungs for up to 24hr when treated with SM buffer only (untreated group), while the

bacterial count gradually decreased after 8hr when treated with ϕ Kp_Pokalde_002 (treatment group) via both IP and oral routes. The bacterial count was significantly reduced by 4-7 log₁₀ CFU/mL in the blood ($p < 0.001$) and lungs ($p < 0.05$) at 24 hr of ϕ Kp_Pokalde_002 administration compared to untreated (Kp56+SM buffer) group (two-way ANOVA with Tukey's multiple comparisons).

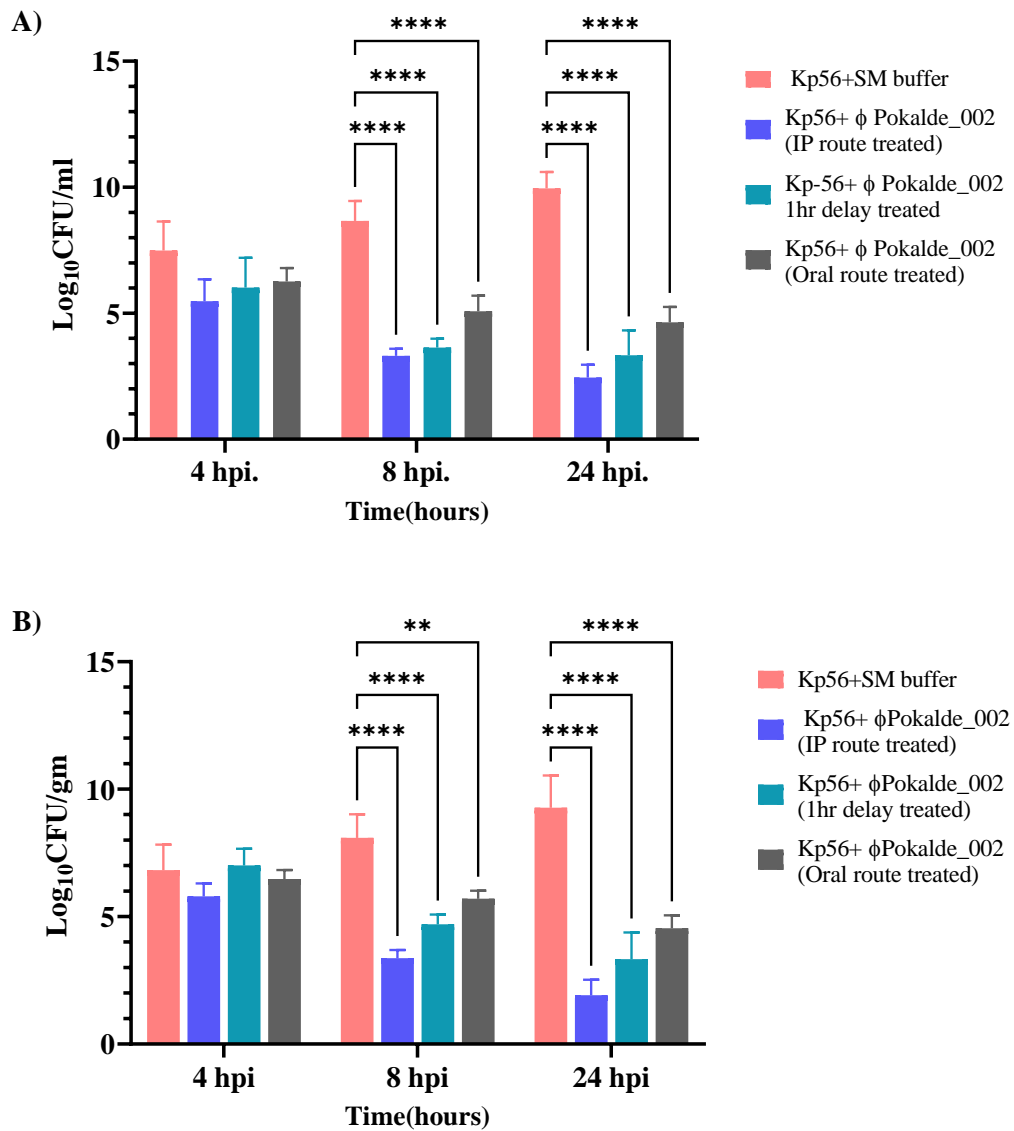


Figure 50: Bacterial load in the blood and lung tissue of mice after phage ϕ Kp_Pokalde_002 treatment via the IP and oral routes in Figures A and B respectively. The bacterial count (CFU/mL) in phage treated and untreated group was enumerated at 4hpi., 8hpi., and 24hpi. The two-way ANOVA with Dunnett's multiple comparisons test was used for statistical analysis (** $P = 0.008$, *** $P < 0.0001$).

Treatment of *K. pneumoniae* infections such as bronchopneumonia, liver abscess and burn wounds using phage has been reported in previous reports. They documented that early phage treatment is more effective for the clearance of host bacteria (Cao et al., 2015; Chhibber et al., 2008; Ellis, 1998). Intraperitoneal (IP) and intranasal routes have been utilized for phage therapy in previous studies. However, we utilized both oral and IP routes of phage administration for therapy. A significant drop in bacterial counts in the blood and lungs of animals in the phage-treated group after 8 hpi is in agreement with histopathological and cytokines marker findings. Mild lesions in the lung tissues of the treated mice group may be due to endotoxins released from the bacterial cell lysis. Continuing decreasing trend of bacterial count in both blood and lung tissue mirrors the decreasing density of bacteria in the mouse body.

CHAPTER 5

CONCLUSION AND RECOMMENDATIONS

5.1 Conclusion

Due to the increasing incidence of antibiotic resistance, humanity is pushed back towards the pre-antibiotic era where simple bacterial infections were deadly. The scientific world is therefore looking for an effective alternative to counteract this imminent crisis. Therefore, the focus of the present study was to screen, isolate, characterize potent lytic phages against multidrug-resistant clinical pathogens and evaluate the efficacy of the phage.

All of the phages exhibited excellent properties including high stability in a wide range of pH and thermal conditions and a short latent period with a high burst size making them promising therapeutic/biocontrol agents. *Myophages* showed extensive host range killing not only within its host genus *Escherichia* but also *K. pneumoniae* isolates suggesting the property of polyvalent phages. However, both *Klebsiella* phages were strictly host-specific and did not possess a wide host range.

All of the five phage genomes were sequenced, annotated, and submitted to the public database NCBI GenBank. The genomes of the five phages were composed of linear, double-stranded DNA. All of them were found to be free from genes encoding known toxins, antibiotic-resistant genes (ARGs), virulent factors (VFs) of bacterial origin, and lysogenic markers such as integrase, recombinase, repressor/anti-repressor protein, and excisionase. Thus, we can consider the phages to be strictly virulent phages and potential candidates for therapeutic applications.

Interestingly, there was a higher sequence similarity of our newly isolated *Myophages* (ϕ Ec_Makalu_001, ϕ Ec_Makalu_002, and ϕ Ec_Makalu_003) and *Podophages* (ϕ Kp_Pokalde_001 and ϕ Kp_Pokalde_002) with other phage genomes isolated from different habitats across the globe. A striking example is the >96% nucleotide identity between our *Escherichia* phages (ϕ Ec_Makalu_001, ϕ Ec_Makalu_002, and ϕ Ec_Makalu_003) with Enterobacteria phage ϕ 1, which was isolated in Georgia 50 year back. They shared conserved modular genome architecture similar to T4-like phages as they all shared a common ancestral sequence. Likewise, the

ϕ Kp_Pokalde_001 was 90% identical with *Klebsiella* phage KP34 (isolated from Poland in 2008) and phage ϕ Kp_Pokalde_002 shared 96% of the genomic identity with the *Klebsiella virus* KP32 (isolated from Russia in 2016). Based on these results, we speculate that all viral species infecting *E. coli* and *K. pneumoniae* are globally widespread, reflecting the ubiquitous nature of their host. Despite high sequence homology with each other, they had additional unique ORFs in their genomes of unknown ortholog. Based on sequence analysis of the tail spike gene (gp53) of the phage ϕ Kp_Pokalde_001 and its mutant phages, we identified that independent spontaneous mutations specific to the tail spike gene (gp53) are responsible for modulating the different plaque phenotypes. The alteration in the tail spike protein also influences the enzymatic activity and the phage adsorption kinetics. This study can provide invaluable insights in terms of engineering phage tail spike to optimize its function for broader host range applications.

On the animal model, phage ϕ Kp_Pokalde_002 successfully rescued mice infected with a lethal dose of carbapenem-resistant *K. pneumoniae* (Kp56) without any deleterious side effects. The survivability of the mice was found to be high when phage was administered through the IP route compared to the oral route. The phage therapy increased the animal survival rates, decreased bacterial counts, decreased the mRNA expression levels of pro-inflammatory cytokine markers (TNF- α and IL-6), and lesser extent of lung inflammation. In addition, the result showed that the ϕ Kp_Pokalde_002 rapidly distributed into the systemic circulation within an hour via both oral and IP routes. A higher concentration of phage in plasma was found after 4 hr (2.3×10^5 PFU/mL) through the IP route and after 8 hr (7.3×10^4 PFU/mL) through the oral route of administration. The elimination half-life of ϕ Kp_Pokalde_002 was relatively shorter in presence of host-bacteria Kp56 compared to phage only suggesting rapid clearance of phage in presence of the susceptible host.

5.2 Recommendations and future perspectives

- Our research provides preliminary pre-clinical data required for future experiments in phage therapy in humans and animals. Some of the ORFs were identified to be novel in this study. These novel phage genes without any indication of their possible role or function in phage infection have been deposited in the databases as “hypothetical proteins. Therefore, studies to

unravel unknown gene functions and ultrastructural studies elucidating the roles of individual proteins in phage should be greatly encouraged.

- Based on the result presented in this study, engineering of the tail spike protein to broaden the phage host range could be done for therapeutic/biocontrol application. Moreover, the depolymerase enzyme isolated in this study which degrades capsular polysaccharide bacterial cells could be studied further to localize the catalytic domain in the crystal structure. This enzyme may be used for therapeutic applications.
- This research provides a successful phage therapy in carbapenem-resistant *K. pneumoniae* infection in a mouse model using a novel phage ϕ Kp_Pokalde_002. Another aspect of phage therapy that must be addressed is the current legislation that regulates medicinal products, which has been written with traditional antibiotics and medicinal products. Recombinant lysin proteins, phage-encoded depolymerase enzymes, and genetically engineered phages are other potential aspects of phage therapy.
- The most straightforward application of this research is the use of well characterized phages in humans to treat terminally ill patient diagnosed with pan-drug-resistant bacterial infections.
- Further studies are suggested to improve the results presented in this research. The phage cocktail (combination of different phages) could be evaluated in pre-clinical in vivo trials using mice in a lung infection model. The combined use of phage and antibiotics is one of the attractive and feasible uses of phages. The utility of phage-antibiotic co-treatment could be explored in the pre-clinical phage therapy experiment.

5.3 Limitations

1. In this study, phages were isolated only from the samples collected within Kathmandu valley. More samples could be screened for the presence of phage against bacterial pathogens circulating throughout the country. Moreover, only lytic phages were studied at the genomic level and other temperate phages which may harbor unique ORFs in the Nepalese environment were excluded from the analysis. Therefore, both lytic and lysogenic phages should be studied at the genomic level, which may harbor unique ORFs. To maximize the chances of discovering unique phages, different types of environmental samples beyond

water from a wide variety of geographic locations and conditions could be considered.

2. Escherichia phages (ϕ Ec_Makalu_002 and ϕ Ec_Makalu_003) isolated in this study showed a multi-host killing ability, suggesting a property of polyvalent phages. However, we did not go through the detailed mechanism underlying the ability of the phages to infect the bacteria other than the primary host genus.
3. This study evaluated the PK/PD of a virulent *Klebsiella* phage that infects carbapenem-resistant clinical isolate of *K. pneumoniae* via intraperitoneal (IP) and oral routes of administration. However, more work is necessary to better understand the PK/PD of the phage using different routes, dose regimes (MOI), and time of the phage exposure in vivo model.
4. In the phage therapy experiment, bacterial endotoxin level was not measured in the phage lysate which may lead to general pathological aspects of septicemia. The future experiment should include a detailed analysis of the toxin levels of the purified phage lysates.
5. During the phage therapy experiment, there is a possibility of the emergence of phage-resistant bacterial mutants, which could hinder successful phage therapy. However, we also did not estimate the phage-induced mutants (BIM) in this study.
6. The study had a few drawbacks about the subjective scoring for the recording of clinical signs, involvement of variables like the bacterial and phage dose, time of inoculation/phage treatment, and non-testing of residual bacteria for phage susceptibility, and thus these results should be viewed with some caution. These protocols should be adjusted for more realistic disease progression, i.e., with a slow infection and no phage treatment until symptoms arise that would simulate a real-world infection scenario.

CHAPTER 6

SUMMARY

The increase of antibiotic resistance has renewed interest in the development of alternative antimicrobial agents. Phage has drawn attention to the scientific community to rediscover phage therapy in modern medicine in this antibiotic crisis. A well-characterized phage library is needed to ensure safety and prompt selection of therapeutic phages to treat extensively drug-resistant infections in humans and animals. The main aim of this Ph.D. dissertation has been to understand the genomic diversity of virulent phage infecting drug-resistant clinical strains isolated from rivers in Kathmandu valley. The other goal has also been to know the pharmacokinetic/pharmacodynamic parameters and therapeutic efficacy of the phage in carbapenem-resistant *K. pneumoniae* infection in a mouse model. The long-term goal has been to create a phage repository in Nepal that is effective against a range of clinical pathogens that would effectively use in future human phage therapy.

In the first two years of this research project, multiple rounds of phage screening, isolation resulted in the in-depth characterization of the isolated phages in terms of physicochemical and molecular level. A library of five diverse and virulent dsDNA phages, varying in genome size and infecting *E. coli* and *K. pneumoniae* clinical isolates has been established. A total of 22 phages were isolated against five carbapenem-resistant clinical isolates from the river and sewage water samples collected from different locations of Kathmandu, Nepal. Among them three *Escherichia* phages (ϕ Ec_Makalu_001, ϕ Ec_Makalu_002, ϕ Ec_Makalu_003) and two *Klebsiella* phages (ϕ Kp_Pokalde_001, ϕ Kp_Pokalde_002) were studied in detail up to genomic level, leading to the establishment of the newly defined species from Nepal. Based on the morphological features on electron microscopy and whole-genome analysis all of the *Escherichia* phages belonged to the *Myoviridae* family and both *Klebsiella* phages belonged to the *Podoviridae* family according to the International Committee on Taxonomy of Viruses (ICTV) classification guideline. All of the *Myophages* (ϕ Ec_Makalu_001, ϕ Ec_Makalu_002, and ϕ Ec_Makalu_003) and *Podophages* (ϕ Kp_Pokalde_001 and ϕ Kp_Pokalde_002) showed a wide range of pH and thermal tolerance. They survived in adverse thermal and pH conditions even below 6 and above 10 pH levels and 50 °C for up to 30 minutes. They were stable at 25 °C

and 37 °C temperature and pH 6 to 9 without significant loss in phage titer. The one-step growth curve experiment showed a similar short latent period with a high burst size clearly showing potential for phage therapy. The latent periods of all phages were between 15-20 minutes with burst sizes between 74 to 127 phage particles per cell. The host range spectrum of a phage is considered cardinal in the selection of phage for therapeutic applications and usually, phages with a broad host range are preferred. The host range of all of the isolated phages was screened by spot test followed by EoP to determine the relative efficiency of plating on 50 clinical isolates in three different genera (*Escherichia*, *Klebsiella*, and *Pseudomonas*). Interestingly, *Myophages* were found to be a wide host range of phages. They showed broad host killing not only within its host genus *Escherichia* but also *K. pneumoniae* isolates suggesting property of polyvalent phages displaying remarkable host diversity. Contrary to this, both *Klebsiella* phages were unable to lyse other bacterial isolates besides their primary host. Thus, both *Klebsiella* phages are strictly host-specific and did not possess multiple host-range. The analysis of phage proteins by SDS-polyacrylamide gel electrophoresis confirmed the differences in the protein components of these two families of the phages belonging to *Myoviridae* and *Podoviridae*.

Well-characterized phages are needed for phage therapy to ensure the genomic safety of the phage candidate. Whole-genome sequencing and bioinformatics analysis of all of the five phages was done. The genomes of the phages were submitted to NCBI GenBank under a bio project “**Development of a phage library in Nepal**” and are publicly available. The genomes of all three *Myophages* were composed of linear, double-stranded DNA of about 162 to 164 kb in length with the same G+C content about (40.6%). They had a similar number of predicted open reading frames (ORF) ranging from 272 to 274 and about 40% of ORFs are known to be functional. None of them encode any predicted tRNA gene throughout the genome. Similarly, genomes of both *Podophages* (ϕ Kp_Pokalde_001, ϕ Kp_Pokalde_002), were also found to be linear, double-stranded DNA however, smaller in size as compared to *Myophages*. They consist of about 42kb genome size with an average G+C content of about 53%. On annotation, ϕ Kp_Pokalde_001 contained 53 ORFs with 32 ORFs have assigned as predicted function, and ϕ Kp_Pokalde_002 comprised 45 ORFs with 35 predicted functional. Both genomes contained direct terminal repeats at both ends. All of the five phage genomes were found to be free from genes encoding known toxins, antibiotic-

resistant genes (ARGs), virulent factors (VFs) of bacterial origin, and lysogenic markers such as integrase, recombinase, repressor/ anti-repressor protein, and excisionase. Thus, we can consider the phages to be strictly virulent and potential candidates for therapeutic applications.

One of the most intriguing results which emerged from this analysis was the level of sequence conservation among phages within specific genera. Closely related members of these *Myophages* (ϕ Ec_Makalu_001, ϕ Ec_Makalu_002, and ϕ Ec_Makalu_003) and *Podophages* (ϕ Kp_Pokalde_001 and ϕ Kp_Pokalde_002) readily isolated from different habitats across the globe. A striking example is the >96% nucleotide identity between our *Escherichia* phages (ϕ Ec_Makalu_001, ϕ Ec_Makalu_002, and ϕ Ec_Makalu_003) and Enterobacteria phage Phi1 (which was isolated in Georgia 50 year back) despite their different geographic origins. Similarly, our *Klebsiella* phages were related to several *Podophages* isolated against *K. pneumoniae* as a host. The ϕ Kp_Pokalde_001 shared 90% genome identity with *Klebsiella* phage KP34 (isolated from Poland in 2008) and phage ϕ Kp_Pokalde_002 shared 96% of the genomic identity with the *Klebsiella* virus KP32 (isolated from Russia in 2016). The main genetic variation within each genus is largely confined to genes encoding the early phage proteins and the tail fibers, indicative of local adaptation necessary to infect specific hosts in specific environmental conditions. This finding implies that despite possible rapid phage evolution, viral genomes maintained their possessions over ecologically significant time and distance.

In this study, we observed the spontaneous loss and then recovery in the halo plaque phenotype by phage ϕ Kp_Pokalde_001. When we cored the individual plaque and performed subsequent analysis, a mixture of two types of plaques, clear with a sharp edge and a clear plaque with halo surrounding, appeared in the bacterial lawn. This heterogeneity of plaque morphology that emerged from a single plaque could be separated into distinct and uniform plaque morphology if one would subsequently purify the selected plaque without prolonging co-incubation with the host. Independent clear plaque types were isolated, purified and the whole-genome sequence of each independent isolate was compared with the original phage. All phages had a missense change/mutation within the small region of the tail spike protein (residue 81 to 208 of 571 residues long polypeptide) indicating a critical domain for the protein function.

We were then interested to understand the changes needed in the spike protein of these specific mutants to convert back to its original halo phenotype. After successful isolation and analysis of the revertant, we found that some of the phages were true revertants where M163T restored its original codon for Met but without any changes to the accompanying mutation T148A. One mutant was pseudo-revertant with non-synonymous change where the mutant L113R restored the halo phenotype by replacing the arginine (Arg) at position 113 with cysteine (Cys) but without reversion of the accompanying E48G mutation. Some of the mutants restored the phenotype by picking up additional mutation within and outside the range of the original mutation region indicating the intragenic suppressor or compensatory mutation is needed to restore the protein function. Mutation in the tail spike protein manifesting the clear phenotype with sharp edges initially led us to hypothesize that each mutant is null in hydrolyzing the capsular polysaccharide. We cloned, expressed, and purified the tail spike protein of wild-type and one of the *ClrI*_(S140N) mutants that formed the robust clear edge plaque and compare its activity with the wild-type tail spike protein. Both wild type and *ClrI*_(S140N) mutant eluted as a higher-order oligomer and of trimeric composition from the size-exclusion-chromatography. The minimal concentration of protein required for bacterial clearing activity was compared. We found an approximately eight-fold reduction in the activity of the *ClrI*_(S140N) mutant from the wild-type tail spike protein. On site-directed mutations, the single mutation in the conserved Asp223 and Asp235 reduced the enzyme activity by eight and thirty-two-fold respectively whereas mutation in Glu164 and Glu233 displayed at least three orders of reduced activity. Similarly, the adsorption efficiency of mutants from either category was poor compared to the wild-type phage. The adsorption efficiency of mutant S140N and R160H with 8-fold reduction was 86% and 93% respectively. The mutation in tail spike protein seems to be affecting the adsorption efficiency at a varying degree without its linear correlation to the enzymatic activity. These phage mutants tone down their ability to adsorb without losing their enzymatic ability to penetrate the host. But once reverted, they restore their adsorption efficiency. The result of this experiment could reveal a clearer picture of the catalytic domain and foster the mechanistic understanding of other phage tail spike proteins. This could become a valuable resource for engineering tail spikes for a broader host range application.

To date, only a few studies have been conducted to evaluate the routes of phage administration to treat systemic infection caused by carbapenem-resistant *K. pneumoniae*. In this study, we evaluated the efficacy of one of the *Klebsiella* phages ϕ Kp_Pokalde_002 to rescue mice infected with a lethal dose of carbapenem-resistant *K. pneumoniae* (Kp56) using oral and IP route of administration. The study of effectiveness and persistence of lytic phage on *K. pneumoniae* inducing bacteremia mice model showed that the lytic phage had highly curing potentiality to the lethal infection caused by *K. pneumoniae*. Both concurrent and 1-hour delay intraperitoneally treated mice were rescued with the survival rate of 100% while mouse survivability was decreased to 40% when the phage was administered orally. Interestingly, 80% of mouse survivability was when the phage administered intraperitoneally 24 hours before the Kp56 infection and 60% of mice were survived when treated 24 hr after the bacterial infection. This confirms that the phage has good pharmacokinetics properties and is stable within the body of the mice for up to 24 hours.

The pharmacokinetics of phage is primarily different from those of chemical drugs due to the self-replicative nature of phages in the presence of host bacteria, their rate of absorption, and clearance by the host's immune system. Our results showed that the phage ϕ Kp_Pokalde_002 quickly distributed into the blood circulation within an hour of administration through both oral and IP routes. A relatively higher phage titer was recovered from the blood when the phage injecting through the IP route as compared to oral. A significant difference was recorded in phage distribution, bioavailability, and elimination between IP and oral routes of administration. The phage reached its maximum titer in blood at 4 hr. (2.3×10^5 PFU/mL) when administered through the IP route which was relatively higher compared to administration via the oral route (4.04×10^3 PFU/mL). The phage showed a shorter elimination half-life in the blood and other organs in the presence of host bacteria. On comparison of histological changes in the lung tissues from the untreated group (Kp56 + SM buffer) and treatment group (Kp56 + ϕ Kp_Pokalde_002) revealed a noticeable interstitial infiltration by neutrophils and macrophages with severe thickening, congestion, and destruction of the alveolar wall in the lungs of the untreated group. The expression level of two pro-inflammatory cytokines (TNF- α and IL-6) in blood was also analyzed to evaluate the tissue inflammation either by ϕ Kp_Pokalde_002 or by Kp56. The levels of cytokine expressions in the phage-treated groups via both IP and oral routes were significantly

lower compared to the untreated group. The study revealed that there was negligible upregulation of pro-inflammatory cytokines (TNF- α , and IL-6) with the ϕ Kp_Pokalde_002 only administered group. Our results suggested that systemic inflammation of the tissues is lower in phage-treated mice as compared to untreated. Likewise, bacterial load was significantly reduced by 3-5 log₁₀ CFU/mL at 8 hours post-infection (hpi) and 5-7 log₁₀ CFU/mL at 24 hpi in the blood and 2.4 log₁₀ CFU/mL at 8 hpi and 4-7 log₁₀ CFU/mL at 24 hpi in lungs when treated with the phage. The bacterial count was completely disappeared in the blood and lung tissues after 5 days post-infection (dpi) and 7 dpi in the IP and oral treated group respectively. Intraperitoneal (IP) and intranasal routes have been utilized for phage therapy in previous studies. However, we utilized both oral and IP routes of phage therapy. A significant drop in bacterial counts in the blood and lungs of animals in the phage-treated group after 8 hpi is in agreement with histopathological and cytokines marker findings. Continuing decreasing trend of bacterial count in both blood and lung tissue mirrors the decreasing density of bacteria in the mouse body.

NEW SCIENTIFIC REPORTS OF THIS DOCTORAL RESEARCH

- To the best of our knowledge, this is the first report on isolation and characterization of lytic phages against carbapenem-resistant *E. coli* and *K. pneumoniae* from Nepal.
- To the best of our knowledge, we presented the first report of whole-genome sequencing and complete bioinformatic analysis of five novel lytic Phages that belong to the *Myoviridae* and *Podoviridae* families from Nepal.
- We registered *A Bio project* entitled **“Development of a phage library in Nepal”** in the NCBI database under a Bio project Accession number: PRJNA594990 and individual phage genomes submitted to NCBI GenBank which are publicly available.
- We presented new findings on spontaneous mutation and reversion in the tail spike gene of a *Klebsiella* phage ϕ Kp_Pokalde_001 that modulates the phage plaque behavior.
- We successfully demonstrated the phage therapy experiment with pharmacokinetics and pharmacodynamics of phage therapy via oral and IP routes using newly isolated phage ϕ Kp_Pokalde_002 in a mouse model from Nepal.

REFERENCES

- Abedon, Thomas-Abedon, C., Thomas, A., & Mazure, H. (2011). Bacteriophage prehistory: Is or is not Hankin, 1896, a phage reference? *Bacteriophage*, **1** (3): 174-178. <https://doi.org/10.4161/bact.1.3.16591>
- Abedon S.T. , Kuhl, S. J., Blasdel, B. G., & Kutter, E. M. (2011). Phage treatment of human infections. *Bacteriophage*, **1**(2): 66-85. <https://doi.org/10.4161/bact.1.2.15845>
- Abedon, S. T. (2009). Phage evolution and ecology. *Adv Appl Microbiol*, **67**(1): 1-45. [https://doi.org/10.1016/s0065-2164\(08\)01001-0](https://doi.org/10.1016/s0065-2164(08)01001-0)
- Abedon, S. T., Herschler, T. D., & Stopar, D. (2001). Bacteriophage latent-period evolution as a response to resource availability. *Applied and Environmental Microbiology*, **67**(9): 4233-4241. <https://doi.org/10.1128/aem.67.9.4233-4241.2001>
- Ackermann, H.-W. (2005). *Bacteriophages: Biology and Applications*, Boca Raton, Florida: CRC Press.
- Ackermann, H. W. (1998). Tailed bacteriophages: the order caudovirales. *Adv Virus Res*, **51**(1): 135-201. [https://doi.org/10.1016/s0065-3527\(08\)60785-x](https://doi.org/10.1016/s0065-3527(08)60785-x)
- Ackermann, H. W. (2007). 5500 Phages examined in the electron microscope. *Arch Virol*, **152**(2): 227-243. <https://doi.org/10.1007/s00705-006-0849-1>
- Adams, M. H., & Park, B. H. (1956). An enzyme produced by a phage-host cell system: II. The properties of the polysaccharide depolymerase. *Virology*, **2**(6): 719-736.
- Adriaenssens, E. M., Sullivan, M. B., Knezevic, P., van Zyl, L. J., Sarkar, B. L., Dutilh, B. E., Alfenas-Zerbini, P., Łobocka, M., Tong, Y., Brister, J. R., Moreno Switt, A. I., Klumpp, J., Aziz, R. K., Barylski, J., Uchiyama, J., Edwards, R. A., Kropinski, A. M., Petty, N. K., Clokie, M. R. J., Kushkina, A. I., Morozova, V. V., Duffy, S., Gillis, A., Rumnieks, J., Kurtböke, I., Chanishvili, N., Goodridge, L., Wittmann, J., Lavigne, R., Jang, H. B., Prangishvili, D., Enault, F., Turner, D., Poranen, M. M., Oksanen, H. M., & Krupovic, M. (2020). Taxonomy of

prokaryotic viruses: 2018-2019 update from the ICTV Bacterial and Archaeal Viruses Subcommittee. *Arch Virol*, **165(5)**: 1253-1260. <https://doi.org/10.1007/s00705-020-04577-8>

Afgan, E., Baker, D., Batut, B., van den Beek, M., Bouvier, D., Cech, M., Chilton, J., Clements, D., Coraor, N., Gruning, B. A., Guerler, A., Hillman-Jackson, J., Hiltemann, S., Jalili, V., Rasche, H., Soranzo, N., Goecks, J., Taylor, J., Nekrutenko, A., & Blankenberg, D. (2018). The Galaxy platform for accessible, reproducible and collaborative biomedical analyses: 2018 update. *Nucleic Acids Res*, **46(W1)**: W537-W544. <https://doi.org/10.1093/nar/gky379>

Aguilar-Toalá, J., Garcia-Varela, R., Garcia, H., Mata-Haro, V., González-Córdova, A., Vallejo-Cordoba, B., & Hernández-Mendoza, A. (2018). Postbiotics: An evolving term within the functional foods field. *Trends in Food Science & Technology*, **75** : 105-114.

Aleshkin, A. V., Rubalskii, E. O., Volozhantsev, N. V., Verevkin, V. V., Svetoch, E. A., Kiseleva, I. A., Bochkareva, S. S., Borisova, O. Y., Popova, A. V., Bogun, A. G., & Afanas'ev, S. S. (2015). A small-scale experiment of using phage-based probiotic dietary supplement for prevention of *E. coli* traveler's diarrhea. *Bacteriophage*, **5(3)**: e1074329. <https://doi.org/10.1080/21597081.2015.1074329>

Arndt, D., Grant, J. R., Marcu, A., Sajed, T., Pon, A., Liang, Y., & Wishart, D. S. (2016). PHASTER: a better, faster version of the PHAST phage search tool. *Nucleic Acids Res*, **44(W1)**: W16-21. <https://doi.org/10.1093/nar/gkw387>

Aslam, S., Courtwright, A. M., Koval, C., Lehman, S. M., Morales, S., Furr, C. L. L., Rosas, F., Brownstein, M. J., Fackler, J. R., & Sisson, B. M. (2019). Early clinical experience of bacteriophage therapy in 3 lung transplant recipients. *American Journal of Transplantation*, **19(9)**: 2631-2639.

Ayukekbong, J. A., Ntemgwa, M., & Atabe, A. N. (2017). The threat of antimicrobial resistance in developing countries: causes and control strategies. *Antimicrobial Resistance & Infection Control*, **6(1)**: 47. <https://doi.org/10.1186/s13756-017-0208-x>

- Azam, A. H., & Tanji, Y. (2019). Bacteriophage-host arm race: an update on the mechanism of phage resistance in bacteria and revenge of the phage with the perspective for phage therapy. *Appl Microbiol Biotechnol*, **103(5)**: 2121-2131. <https://doi.org/10.1007/s00253-019-09629-x>
- Bankevich, A., Nurk, S., Antipov, D., Gurevich, A. A., Dvorkin, M., Kulikov, A. S., Lesin, V. M., Nikolenko, S. I., Pham, S., Prjibelski, A. D., Pyshkin, A. V., Sirotkin, A. V., Vyahhi, N., Tesler, G., Alekseyev, M. A., & Pevzner, P. A. (2012). SPAdes: a new genome assembly algorithm and its applications to single-cell sequencing. *J Comput Biol*, **19(5)**: 455-477. <https://doi.org/10.1089/cmb.2012.0021>
- Barr, J. J., Auro, R., Furlan, M., Whiteson, K. L., Erb, M. L., Pogliano, J., Stotland, A., Wolkowicz, R., Cutting, A. S., Doran, K. S., Salamon, P., Youle, M., & Rohwer, F. (2013). Bacteriophage adhering to mucus provide a non-host-derived immunity. *Proc Natl Acad Sci U S A*, **110(26)**: 10771-10776. <https://doi.org/10.1073/pnas.1305923110>
- Barrow, P., Lovell, M., & Berchieri, A., Jr. (1998). Use of lytic bacteriophage for control of experimental *Escherichia coli* septicemia and meningitis in chickens and calves. *Clin Diagn Lab Immunol*, **5(3)**: 294-298.
- Barrow, P. A., & Soothill, J. S. (1997). Bacteriophage therapy and prophylaxis: rediscovery and renewed assessment of potential. *Trends in Microbiology*, **5(7)**: 268-271.
- Berti, R., Williams, A. J., Moffett, J. R., Hale, S. L., Velarde, L. C., Elliott, P. J., Yao, C., Dave, J. R., & Tortella, F. C. (2002). Quantitative real-time RT—PCR analysis of inflammatory gene expression associated with Ischemia—Reperfusion brain Injury. *Journal of Cerebral Blood Flow & Metabolism*, **22(9)**: 1068-1079.
- Betts, S., & King, J. (1999). There's a right way and a wrong way: in vivo and in vitro folding, misfolding and subunit assembly of the P22 tailspike. *Structure*, **7(6)**: R131-139. [https://doi.org/10.1016/s0969-2126\(99\)80078-1](https://doi.org/10.1016/s0969-2126(99)80078-1)

- Bhetwal, A., Maharjan, A., Shakya, S., Satyal, D., Ghimire, S., Khanal, P. R., & Parajuli, N. P. (2017). Isolation of potential phages against multidrug-resistant bacterial isolates: promising agents in the rivers of Kathmandu, Nepal. *BioMed Research International*, **2017**. <https://doi.org/10.1155/2017/3723254>
- Bielke, L., Higgins, S., Donoghue, A., Donoghue, D., & Hargis, B. M. (2007). Salmonella Host Range of Bacteriophages That Infect Multiple Genera. *Poultry Science*, **86(12)**: 2536-2540. <https://doi.org/10.3382/ps.2007-00250>
- Bikard, D., Euler, C. W., Jiang, W., Nussenzweig, P. M., Goldberg, G. W., Duportet, X., Fischetti, V. A., & Marraffini, L. A. (2014). Exploiting CRISPR-Cas nucleases to produce sequence-specific antimicrobials. *Nat Biotechnol*, **32(11)**: 1146-1150.
- Bikard, D., & Marraffini, L. A. (2012). Innate and adaptive immunity in bacteria: mechanisms of programmed genetic variation to fight bacteriophages. *Curr Opin Immunol*, **24(1)**: 15-20. <https://doi.org/10.1016/j.coi.2011.10.005>
- Blower, T. R., Short, F. L., Rao, F., Mizuguchi, K., Pei, X. Y., Fineran, P. C., Luisi, B. F., & Salmond, G. P. (2012). Identification and classification of bacterial Type III toxin-antitoxin systems encoded in chromosomal and plasmid genomes. *Nucleic Acids Research*, **40(13)**: 6158-6173.
- Bolger, A. M., Lohse, M., & Usadel, B. (2014). Trimmomatic: a flexible trimmer for Illumina sequence data. *Bioinformatics*, **30(15)**: 2114-2120. <https://doi.org/10.1093/bioinformatics/btu170>
- Bondy-Denomy, J., Pawluk, A., Maxwell, K. L., & Davidson, A. R. (2013). Bacteriophage genes that inactivate the CRISPR/Cas bacterial immune system. *Nature*, **493(7432)**: 429-432.
- Boratyński, J., Syper, D., Weber-Dabrowska, B., Łusiak-Szelachowska, M., Poźniak, G., & Górski, A. (2004). Preparation of endotoxin-free bacteriophages. *Cell Mol Biol Lett*, **9(2)**: 253-259.
- Bozza, F. A., Salluh, J. I., Japiassu, A. M., Soares, M., Assis, E. F., Gomes, R. N., Bozza, M. T., Castro-Faria-Neto, H. C., & Bozza, P. T. (2007). Cytokine profiles

- as markers of disease severity in sepsis: a multiplex analysis. *Critical Care*, **11(2)**: 1-8.
- Brabban, A., Hite, E., & Callaway, T. (2005). Evolution of foodborne pathogens via temperate bacteriophage-mediated gene transfer. *Foodborne Pathogens & Disease*, **2(4)**: 287-303.
- Brix, A., Cafora, M., Aureli, M., & Pistocchi, A. (2020). Animal models to translate phage therapy to human medicine. *International Journal of Molecular Sciences*, **21(10)**: 3715.
- Brüssow, H., Canchaya, C., & Hardt, W. D. (2004). Phages and the evolution of bacterial pathogens: from genomic rearrangements to lysogenic conversion. *Microbiol Mol Biol Rev*, **68(3)**: 560-602, table of contents. <https://doi.org/10.1128/mubr.68.3.560-602.2004>
- Cafilisch, K. M., Suh, G. A., & Patel, R. (2019). Biological challenges of phage therapy and proposed solutions: a literature review. *Expert Rev Anti Infect Ther*, **17(12)**: 1011-1041. <https://doi.org/10.1080/14787210.2019.1694905>
- Cairns, B. J., Timms, A. R., Jansen, V. A., Connerton, I. F., & Payne, R. J. (2009). Quantitative models of in vitro bacteriophage–host dynamics and their application to phage therapy. *PLoS Pathog*, **5(1)**: e1000253. <https://doi.org/10.1371/journal.ppat.1000253>
- Camacho, C., Coulouris, G., Avagyan, V., Ma, N., Papadopoulos, J., Bealer, K., & Madden, T. L. (2009). BLAST+: architecture and applications. *BMC Bioinformatics*, **10**: 421. <https://doi.org/10.1186/1471-2105-10-421>
- Campbell, A. (2003). The future of bacteriophage biology. *Nat Rev Genet*, **4(6)**: 471-477. <https://doi.org/10.1038/nrg1089>
- Cao, F., Wang, X., Wang, L., Li, Z., Che, J., Wang, L., Li, X., Cao, Z., Zhang, J., & Jin, L. (2015). Evaluation of the efficacy of a bacteriophage in the treatment of pneumonia induced by multidrug resistance *Klebsiella pneumoniae* in mice. *BioMed Research International*, **2015**. <https://doi.org/10.1155/2015/752930>

- Capparelli, R., Parlato, M., Borriello, G., Salvatore, P., & Iannelli, D. (2007). Experimental phage therapy against *Staphylococcus aureus* in mice. *Antimicrob Agents Chemother*, **51(8)**: 2765-2773. <https://doi.org/10.1128/aac.01513-06>
- Capparelli, R., Ventimiglia, I., Roperto, S., Fenizia, D., & Iannelli, D. (2006). Selection of an *Escherichia coli* O157:H7 bacteriophage for persistence in the circulatory system of mice infected experimentally. *Clin Microbiol Infect*, **12(3)**: 248-253. <https://doi.org/10.1111/j.1469-0691.2005.01340.x>
- Carey-Smith, G. V., Billington, C., Cornelius, A. J., Hudson, J. A., & Heinemann, J. A. (2006). Isolation and characterization of bacteriophages infecting *Salmonella* spp. *FEMS Microbiol Lett*, **258(2)**: 182-186. <https://doi.org/10.1111/j.1574-6968.2006.00217.x>
- Carlton, R. M. (1999). Phage therapy: past history and future prospects. *Arch Immunol Ther Exp*, **47(5)**: 267-274.
- Casjens, S. (2003). Prophages and bacterial genomics: what have we learned so far? *Mol Microbiol*, **49(2)**: 277-300. <https://doi.org/10.1046/j.1365-2958.2003.03580.x>
- Casjens, S. R., & Molineux, I. J. (2012). Short noncontractile tail machines: adsorption and DNA delivery by podoviruses. *Adv Exp Med Biol*, **726**: 143-179. https://doi.org/10.1007/978-1-4614-0980-9_7
- Cavaillon, J. M. (2018). Exotoxins and endotoxins: Inducers of inflammatory cytokines. *Toxicon*, **149**: 45-53. <https://doi.org/10.1016/j.toxicon.2017.10.016>
- Centers for Disease Control and Prevention. (2019). *Antibiotic resistance threats in the United States, 2019*: US Department of Health and Human Services, Centres for Disease Control and Prevention. <https://www.cdc.gov/drugresistance/biggest-threats.html>
- Cervený, K. E., DePaola, A., Duckworth, D. H., & Gulig, P. A. (2002). Phage therapy of local and systemic disease caused by *Vibrio vulnificus* in iron-dextran-treated mice. *Infect Immun*, **70(11)**: 6251-6262. <https://doi.org/10.1128/iai.70.11.6251-6262.2002>

- Chadha, P., Katare, O. P., & Chhibber, S. (2016). In vivo efficacy of single phage versus phage cocktail in resolving burn wound infection in BALB/c mice. *Microbial Pathogenesis*, **99**: 68-77.
- Chan, B. K., & Abedon, S. T. (2012). Phage therapy pharmacology: phage cocktails. *Advances in Applied Microbiology* **78**: 1-23. <https://doi.org/https://doi.org/10.1016/B978-0-12-394805-2.00001-4>
- Chan, B. K., Sistro, M., Wertz, J. E., Kortright, K. E., Narayan, D., & Turner, P. E. (2016). Phage selection restores antibiotic sensitivity in MDR *Pseudomonas aeruginosa*. *Sci Rep*, **6**: 26717. <https://doi.org/10.1038/srep26717>
- Chang, H. R., Comte, R., Piguet, P. F., & Pechere, J. C. (1991). Activity of minocycline against *Toxoplasma gondii* infection in mice. *J Antimicrob Chemother*, **27(5)**: 639-645. <https://doi.org/10.1093/jac/27.5.639>
- Chanishvili, N. (2012). Phage therapy--history from Twort and d'Herelle through Soviet experience to current approaches. *Adv Virus Res*, **83**: 3-40. <https://doi.org/10.1016/b978-0-12-394438-2.00001-3>
- Chereau, F., Opatowski, L., Tourdjman, M., & Vong, S. (2017). Risk assessment for antibiotic resistance in South East Asia. *BMJ*, **358**: j3393. <https://doi.org/https://doi.org/10.1136/bmj.j3393>
- Chhibber, S., Gupta, P., & Kaur, S. (2014). Bacteriophage as effective decolonising agent for elimination of MRSA from anterior nares of BALB/c mice. *BMC Microbiology*, **14(1)**: 1-13. <https://doi.org/https://doi.org/10.1186/s12866-014-0212-8>
- Chhibber, S., Kaur, S., & Kumari, S. (2008). Therapeutic potential of bacteriophage in treating *Klebsiella pneumoniae* B5055-mediated lobar pneumonia in mice. *J Med Microbiol*, **57(12)**: 1508-1513. <https://doi.org/https://doi.org/10.1099/jmm.0.2008/002873-0>
- Chibani-Chennoufi, S., Bruttin, A., Dillmann, M. L., & Brüssow, H. (2004). Phage-host interaction: an ecological perspective. *J Bacteriol*, **186(12)**: 3677-3686. <https://doi.org/10.1128/jb.186.12.3677-3686.2004>

- Chibani-Chennoufi, S., Sidoti, J., Bruttin, A., Kutter, E., Sarker, S., & Brüssow, H. (2004). In vitro and in vivo bacteriolytic activities of *Escherichia coli* phages: implications for phage therapy. *Antimicrob Agents Chemother*, **48(7)**: 2558-2569. <https://doi.org/doi:10.1128/AAC.48.7.2558-2569.2004>
- Chokshi, A., Sifri, Z., Cennimo, D., & Horng, H. (2019). Global Contributors to Antibiotic Resistance. *J Glob Infect Dis*, **11(1)**: 36-42. https://doi.org/10.4103/jgid.jgid_110_18
- Chow, M. Y. T., Chang, R. Y. K., Li, M., Wang, Y., Lin, Y., Morales, S., Mclachlan, A. J., Kutter, E., Li, J., & Chan, H.-K. (2020). Pharmacokinetics and Time-Kill Study of Inhaled Antipseudomonal Bacteriophage Therapy in Mice. *Antimicrob Agents Chemother*, **65(1)**: e01470-01420. <https://doi.org/10.1128/aac.01470-20>
- Clark, J. R., & March, J. B. (2006). Bacteriophages and biotechnology: vaccines, gene therapy and antibacterials. *Trends Biotechnol*, **24(5)**: 212-218. <https://doi.org/10.1016/j.tibtech.2006.03.003>
- Clokie, M. R., Millard, A. D., Letarov, A. V., & Heaphy, S. (2011). Phages in nature. *Bacteriophage*, **1(1)**: 31-45. <https://doi.org/10.4161/bact.1.1.14942>
- Cohen, Y., Joseph Pollock, F., Rosenberg, E., & Bourne, D. G. (2013). Phage therapy treatment of the coral pathogen *Vibrio coralliilyticus*. *Microbiology Open*, **2(1)**: 64-74. <https://doi.org/https://doi.org/10.1002/mbo3.52>
- Colom, J., Cano-Sarabia, M., Otero, J., Aríñez-Soriano, J., Cortés, P., Maspoch, D., & Llagostera, M. (2017). Microencapsulation with alginate/CaCO₃: A strategy for improved phage therapy. *Scientific Reports*, **7(1)**: 1-10. <https://doi.org/https://doi.org/10.1038/srep41441>
- Colom, J., Cano-Sarabia, M., Otero, J., Cortes, P., Maspoch, D., & Llagostera, M. (2015). Liposome-Encapsulated Bacteriophages for Enhanced Oral Phage Therapy against *Salmonella* spp. *Applied and Environmental Microbiology*, **81(14)**: 4841-4849. <https://doi.org/10.1128/aem.00812-15>
- Comeau, A. M., Bertrand, C., Letarov, A., Tetart, F., & Krisch, H. M. (2007). Modular architecture of the T4 phage superfamily: a conserved core genome and a plastic

- periphery. *Virology*, **362(2)**: 384-396. <https://doi.org/10.1016/j.virol.2006.12.031>
- Comeau, A. M., & Krisch, H. M. (2005). War is peace--dispatches from the bacterial and phage killing fields. *Curr Opin Microbiol*, **8(4)**: 488-494. <https://doi.org/10.1016/j.mib.2005.06.004>
- Comeau, A. M., Tremblay, D., Moineau, S., Rattei, T., Kushkina, A. I., Tovkach, F. I., Krisch, H. M., & Ackermann, H. W. (2012). Phage morphology recapitulates phylogeny: the comparative genomics of a new group of myoviruses. *PLoS One*, **7(7)**: e40102. <https://doi.org/10.1371/journal.pone.0040102>
- Cornelissen, A., Ceysens, P.-J., T'syen, J., Van Praet, H., Noben, J.-P., Shaburova, O. V., Krylov, V. N., Volckaert, G., & Lavigne, R. (2011). The T7-related *Pseudomonas putida* phage ϕ 15 displays virion-associated biofilm degradation properties. *PLoS One*, **6(4)**: e18597. <https://doi.org/https://doi.org/10.1371/journal.pone.0018597>
- D'Andrea, M. M., Marmo, P., Henrici De Angelis, L., Palmieri, M., Ciacci, N., Di Lallo, G., Dematte, E., Vannuccini, E., Lupetti, P., Rossolini, G. M., & Thaller, M. C. (2017). phiBO1E, a newly discovered lytic bacteriophage targeting carbapenemase-producing *Klebsiella pneumoniae* of the pandemic Clonal Group 258 clade II lineage. *Sci Rep*, **7(1)**: 2614. <https://doi.org/10.1038/s41598-017-02788-9>
- Dąbrowska, K. (2019). Phage therapy: What factors shape phage pharmacokinetics and bioavailability? Systematic and critical review. *Medicinal Research Reviews*, **39(5)**: 2000-2025. <https://doi.org/10.1002/med.21572>
- Dąbrowska, K., & Abedon, S. T. (2019). Pharmacologically Aware Phage Therapy: Pharmacodynamic and Pharmacokinetic Obstacles to Phage Antibacterial Action in Animal and Human Bodies. *Microbiology and Molecular Biology Reviews*, **83(4)**: e00012-00019. <https://doi.org/10.1128/MMBR.00012-19>
- Darling, A. E., Mau, B., & Perna, N. T. (2010). progressiveMauve: multiple genome alignment with gene gain, loss and rearrangement. *PLoS One*, **5(6)**: e11147. <https://doi.org/10.1371/journal.pone.0011147>

- De Paepe, M., Leclerc, M., Tinsley, C. R., & Petit, M.-A. (2014). Bacteriophages: an underestimated role in human and animal health? *Frontiers in Cellular and Infection Microbiology*, **4(1)**: 39. [https://doi.org/https://doi.org/10.3389/fcimb.2014.00039](https://doi.org/10.3389/fcimb.2014.00039)
- Dedrick, R. M., Guerrero-Bustamante, C. A., Garlena, R. A., Russell, D. A., Ford, K., Harris, K., Gilmour, K. C., Soothill, J., Jacobs-Sera, D., Schooley, R. T., Hatfull, G. F., & Spencer, H. (2019). Engineered bacteriophages for treatment of a patient with a disseminated drug-resistant *Mycobacterium abscessus*. *Nature Medicine*, **25(5)**: 730-733. <https://doi.org/10.1038/s41591-019-0437-z>
- Delcher, A. L., Harmon, D., Kasif, S., White, O., & Salzberg, S. L. (1999). Improved microbial gene identification with GLIMMER. *Nucleic Acids Res*, **27(23)**: 4636-4641. <https://doi.org/10.1093/nar/27.23.4636>
- Desplats, C., Dez, C., Tétart, F., Eleaume, H., & Krisch, H. M. (2002). Snapshot of the Genome of the Pseudo-T-Even Bacteriophage RB49. *J Bacteriol*, **184(10)**: 2789-2804. <https://doi.org/10.1128/JB.184.10.2789-2804.2002>
- Desplats, C., & Krisch, H. M. (2003). The diversity and evolution of the T4-type bacteriophages. *Research in Microbiology*, **154(4)**: 259-267. [https://doi.org/https://doi.org/10.1016/S0923-2508\(03\)00069-X](https://doi.org/https://doi.org/10.1016/S0923-2508(03)00069-X)
- Dhingra, S., Rahman, N. A. A., Peile, E., Rahman, M., Sartelli, M., Hassali, M. A., Islam, T., Islam, S., & Haque, M. (2020). Microbial resistance movements: an overview of global public health threats posed by antimicrobial resistance, and how best to counter. *Frontiers in Public Health*, **8**: 531. <https://doi.org/https://doi.org/10.3389/fpubh.2020.535668>
- Diaz-Munoz, S. L., & Koskella, B. (2014). Bacteria-phage interactions in natural environments. *Adv Appl Microbiol*, **89**: 135-183. <https://doi.org/10.1016/B978-0-12-800259-9.00004-4>
- Domingo-Calap, P., Beamud, B., Mora-Quilis, L., González-Candelas, F., & Sanjuán, R. (2020). Isolation and characterization of two *Klebsiella pneumoniae* phages encoding divergent depolymerases. *International Journal of Molecular Sciences*, **21(9)**: 3160. <https://doi.org/https://doi.org/10.3390/ijms21093160>

- Drulis-Kawa, Z., Mackiewicz, P., Kesik-Szeloch, A., Maciaszczyk-Dziubinska, E., Weber-Dabrowska, B., Dorotkiewicz-Jach, A., Augustyniak, D., Majkowska-Skrobek, G., Bocer, T., Empel, J., & Kropinski, A. M. (2011). Isolation and characterisation of KP34--a novel phiKMV-like bacteriophage for *Klebsiella pneumoniae*. *Appl Microbiol Biotechnol*, **90(4)**: 1333-1345. <https://doi.org/10.1007/s00253-011-3149-y>
- Drulis-Kawa, Z., Majkowska-Skrobek, G., & Maciejewska, B. (2015). Bacteriophages and phage-derived proteins--application approaches. *Current Medicinal Chemistry*, **22(14)**: 1757-1773. <https://doi.org/https://doi.org/10.2174/0929867322666150209152851>
- Dublanchet, A., & Bourne, S. (2007). The epic of phage therapy. *Canadian Journal of Infectious Diseases* **18(1)**: 15-18. <https://doi.org/https://doi.org/10.1155/2007/365761>
- Duc, H. M., Son, H. M., Honjoh, K.-i., & Miyamoto, T. (2018). Isolation and application of bacteriophages to reduce *Salmonella* contamination in raw chicken meat. *LWT: Food Science and Technology*, **91**: 353-360. <https://doi.org/https://doi.org/10.1016/j.lwt.2018.01.072>
- Duckworth, D. H. (1976). "Who discovered bacteriophage?". *Bacteriol Rev*, **40(4)**: 793-802. <https://doi.org/https://doi.org/10.1128/br.40.4.793-802.1976>
- Dufour, N., Delattre, R., & Debarbieux, L. (2018). In Vivo Bacteriophage Biodistribution. *Methods in Molecular Biology*, **2018**: 123-137. https://doi.org/10.1007/978-1-4939-7395-8_11
- Duplessis, C., Biswas, B., Hanisch, B., Perkins, M., Henry, M., Quinones, J., Wolfe, D., Estrella, L., & Hamilton, T. (2017). Refractory *Pseudomonas* Bacteremia in a 2-Year-Old Sterilized by Bacteriophage Therapy. *Journal of the Pediatric Infectious Diseases Society*, **7(3)**: 253-256. <https://doi.org/10.1093/jpids/pix056>
- Eaton, M. D., & Bayne-Jones, S. (1934). Bacteriophage therapy: review of the principles and results of the use of bacteriophage in the treatment of infections. *Journal of the American Medical Association*, **103(23)**: 1769-1776. <https://doi.org/doi:10.1001/jama.1934.72750490003007>

- Eckstein, S., Stender, J., Mzoughi, S., Vogele, K., Kühn, J., Friese, D., Bugert, C., Handrick, S., Ferjani, M., Wölfel, R., Millard, A., Ben Moussa, M., & Bugert, J. J. (2021). Isolation and characterization of lytic phage TUN1 specific for *Klebsiella pneumoniae* K64 clinical isolates from Tunisia. *BMC Microbiology*, **21(1)**: 186. <https://doi.org/10.1186/s12866-021-02251-w>
- Ellis, M. E. (1998). *Gram-negative Bacillary Pneumonia*. Cambridge: Cambridge University Press.
- Emond, E., Dion, E., Walker, S. A., Vedamuthu, E. R., Kondo, J. K., & Moineau, S. (1998). AbiQ, an abortive infection mechanism from *Lactococcus lactis*. *Applied and Environmental Microbiology*, **64(12)**: 4748-4756. <https://doi.org/https://doi.org/10.1128/AEM.64.12.4748-4756.1998>
- Eriksen, R. S., Svenningsen, S. L., Sneppen, K., & Mitarai, N. (2018). A growing microcolony can survive and support persistent propagation of virulent phages. *Proc Natl Acad Sci U S A*, **115(2)**: 337-342. <https://doi.org/10.1073/pnas.1708954115>
- Falagas, M. E., Tansarli, G. S., Karageorgopoulos, D. E., & Vardakas, K. Z. (2014). Deaths attributable to carbapenem-resistant *Enterobacteriaceae* infections. *Emerg Infect Dis*, **20(7)**: 1170-1175. <https://doi.org/10.3201/eid2007.121004>
- Farris, J. S. (1972). Estimating Phylogenetic Trees from Distance Matrices. *The American Naturalist*, **106(951)**: 645-668. www.jstor.org/stable/2459725
- Fernandes, S., & São-José, C. (2018). Enzymes and Mechanisms Employed by Tailed Bacteriophages to Breach the Bacterial Cell Barriers. *Viruses*, **10(8)**: <https://doi.org/10.3390/v10080396>
- Fernandez, L., Gutierrez, D., Garcia, P., & Rodriguez, A. (2019). The Perfect Bacteriophage for Therapeutic Applications-A Quick Guide. *Antibiotics (Basel)*, **8(3)**: <https://doi.org/10.3390/antibiotics8030126>
- Festing, S., & Wilkinson, R. (2007). The ethics of animal research. Talking Point on the use of animals in scientific research. *EMBO Rep*, **8(6)**: 526-530. <https://doi.org/10.1038/sj.embor.7400993>

- Finn, R. D., Coghill, P., Eberhardt, R. Y., Eddy, S. R., Mistry, J., Mitchell, A. L., Potter, S. C., Punta, M., Qureshi, M., Sangrador-Vegas, A., Salazar, G. A., Tate, J., & Bateman, A. (2016). The Pfam protein families database: towards a more sustainable future. *Nucleic Acids Res*, **44(D1)**: D279-285. <https://doi.org/10.1093/nar/gkv1344>
- Fischetti, V. A., Nelson, D., & Schuch, R. (2006). Reinventing phage therapy: are the parts greater than the sum? *Nat Biotechnol*, **24(12)**: 1508-1511. <https://doi.org/10.1038/nbt1206-1508>
- Fokine, A., & Rossmann, M. G. (2014). Molecular architecture of tailed double-stranded DNA phages. *Bacteriophage*, **4(1)**: e28281. <https://doi.org/10.4161/bact.28281>
- Furfaro, L. L., Payne, M. S., & Chang, B. J. (2018). Bacteriophage therapy: clinical trials and regulatory hurdles. *Frontiers in Cellular and Infection Microbiology*, **8**: 376. <https://doi.org/https://doi.org/10.3389/fcimb.2018.00376>
- Gainey, A. B., Burch, A. K., Brownstein, M. J., Brown, D. E., Fackler, J., Horne, B. A., Biswas, B., Bivens, B. N., Malagon, F., & Daniels, R. (2020). Combining bacteriophages with cefiderocol and meropenem/vaborbactam to treat a pan-drug resistant *Achromobacter* species infection in a pediatric cystic fibrosis patient. *Pediatric Pulmonology*, **55(11)**: 2990-2994. <https://doi.org/https://doi.org/10.1002/ppul.24945>
- Gallet, R., Kannoly, S., & Wang, I. N. (2011). Effects of bacteriophage traits on plaque formation. *BMC Microbiol*, **11**: 181. <https://doi.org/10.1186/1471-2180-11-181>
- Gangwar, M., Rastogi, S., Singh, D., Shukla, A., Dhameja, N., Kumar, D., Kumar, R., & Nath, G. (2021). Study on the Effect of Oral Administration of Bacteriophages in Charles Foster Rats With Special Reference to Immunological and Adverse Effects. *Frontiers in Pharmacology*, **12**: <https://doi.org/10.3389/fphar.2021.615445>
- Ghosh, C., Sarkar, P., Issa, R., & Halder, J. (2019). Alternatives to Conventional Antibiotics in the Era of Antimicrobial Resistance. *Trends Microbiol*, **27(4)**: 323-338. <https://doi.org/10.1016/j.tim.2018.12.010>

- Gibson, D. G., Young, L., Chuang, R.-Y., Venter, J. C., Hutchison, C. A., & Smith, H. O. (2009). Enzymatic assembly of DNA molecules up to several hundred kilobases. *Nature Methods*, **6(5)**: 343-345. <https://doi.org/10.1038/nmeth.1318>
- Gill, J., & Abedon, S. T. (2003). Bacteriophage ecology and plants. *APSnet Feature*, **10**: 1-17. <https://www.apsnet.org/edcenter/apsnetfeatures/Documents/2003/BacteriophageEcology.pdf>
- Gill, J. J., Pacan, J. C., Carson, M. E., Leslie, K. E., Griffiths, M. W., & Sabour, P. M. (2006). Efficacy and pharmacokinetics of bacteriophage therapy in treatment of subclinical *Staphylococcus aureus* mastitis in lactating dairy cattle. *Antimicrob Agents Chemother*, **50(9)**: 2912-2918. <https://doi.org/10.1128/aac.01630-05>
- Giulietti, A., Overbergh, L., Valckx, D., Decallonne, B., Bouillon, R., & Mathieu, C. (2001). An overview of real-time quantitative PCR: applications to quantify cytokine gene expression. *Methods (San Diego, Calif.)*, **25(4)**: 386-401. <https://doi.org/https://doi.org/10.1006/meth.2001.1261>
- Golkar, Z., Bagasra, O., & Pace, D. G. (2014). Bacteriophage therapy: a potential solution for the antibiotic resistance crisis. *J Infect Dev Ctries*, **8(2)**: 129-136. <https://doi.org/10.3855/jidc.3573>
- Gonzalez-Menendez, E., Fernandez, L., Gutierrez, D., Rodriguez, A., Martinez, B., & Garcia, P. (2018). Comparative analysis of different preservation techniques for the storage of *Staphylococcus* phages aimed for the industrial development of phage-based antimicrobial products. *PLoS One*, **13(10)**: e0205728.
- Gorski, A., Międzybrodzki, R., Borysowski, J., Dąbrowska, K., Wierzbicki, P., Ohams, M., Korczak-Kowalska, G., Olszowska-Zaremba, N., Łusiak-Szelachowska, M., & Kłak, M. (2012). Phage as a modulator of immune responses: practical implications for phage therapy. *Adv Virus Res*, **83**: 41-71. <https://doi.org/https://doi.org/10.1016/B978-0-12-394438-2.00002-5>
- Górski, A., Międzybrodzki, R., Weber-Dąbrowska, B., Fortuna, W., Letkiewicz, S., Rogóż, P., Jończyk-Matysiak, E., Dąbrowska, K., Majewska, J., & Borysowski, J. (2016). Phage Therapy: Combating Infections with Potential for Evolving

- from Merely a Treatment for Complications to Targeting Diseases. *Front Microbiol*, **7**: 1515. <https://doi.org/10.3389/fmicb.2016.01515>
- Gorski, A., & Weber-Dabrowska, B. (2005). The potential role of endogenous bacteriophages in controlling invading pathogens. *Cell Mol Life Sci*, **62(5)**: 511-519. <https://doi.org/10.1007/s00018-004-4403-6>
- Greene, J., & Goldberg, R. B. (1985). Isolation and preliminary characterization of lytic and lysogenic phages with wide host range within the *streptomycetes*. *J Gen Microbiol*, **131(09)**: 2459-2465. <https://doi.org/https://doi.org/10.1099/00221287-131-9-2459>
- Gregory, A. C., Solonenko, S. A., Ignacio-Espinoza, J. C., LaButti, K., Copeland, A., Sudek, S., Maitland, A., Chittick, L., dos Santos, F., Weitz, J. S., Worden, A. Z., Woyke, T., & Sullivan, M. B. (2016). Genomic differentiation among wild cyanophages despite widespread horizontal gene transfer. *BMC Genomics*, **17(1)**: 930. <https://doi.org/10.1186/s12864-016-3286-x>
- Griffith, D. C., Harford, L., Williams, R., Lee, V. J., & Dudley, M. N. (2003). In Vivo Antibacterial Activity of RWJ-54428, a New Cephalosporin with Activity against Gram-Positive Bacteria. *Antimicrob Agents Chemother*, **47(1)**: 43-47. <https://doi.org/10.1128/AAC.47.1.43-47.2003>
- Hagens, S., Habel, A., Von Ahsen, U., Von Gabain, A., & Bläsi, U. (2004). Therapy of experimental *Pseudomonas* infections with a nonreplicating genetically modified phage. *Antimicrob Agents Chemother*, **48(10)**: 3817-3822. <https://doi.org/https://doi.org/10.1128/AAC.48.10.3817-3822.2004>
- Hall-Stoodley, L., Costerton, J. W., & Stoodley, P. (2004). Bacterial biofilms: from the natural environment to infectious diseases. *Nature Reviews Microbiology*, **2(2)**: 95-108. <https://doi.org/https://doi.org/10.1038/nrmicro821>
- Hambly, E., & Suttle, C. A. (2005). The virosphere, diversity, and genetic exchange within phage communities. *Curr Opin Microbiol*, **8(4)**: 444-450. <https://doi.org/10.1016/j.mib.2005.06.005>

- Hampton, H. G., Watson, B. N. J., & Fineran, P. C. (2020). The arms race between bacteria and their phage foes. *Nature*, **577(7790)**: 327-336. <https://doi.org/10.1038/s41586-019-1894-8>
- Hatfull, G. F. (2008). Bacteriophage genomics. *Curr Opin Microbiol*, **11(5)**: 447-453. <https://doi.org/10.1016/j.mib.2008.09.004>
- Hatfull, G. F., & Hendrix, R. W. (2011). Bacteriophages and their genomes. *Curr Opin Virol*, **1(4)**: 298-303. <https://doi.org/10.1016/j.coviro.2011.06.009>
- Hausmann, R. (1988). *The T7 group: In The Bacteriophages*. Boston, MA: Springer Press.
- Hawkey, P. M. (1998). The origins and molecular basis of antibiotic resistance. *BMJ*, **317(7159)**: 657-660. <https://doi.org/10.1136/bmj.317.7159.657>
- Hendrix, R. W. (2002). Bacteriophages: evolution of the majority. *Theor Popul Biol*, **61(4)**: 471-480. <https://doi.org/10.1006/tpbi.2002.1590>
- Hendrix, R. W., Smith, M. C., Burns, R. N., Ford, M. E., & Hatfull, G. F. (1999). Evolutionary relationships among diverse bacteriophages and prophages: all the world's a phage. *Proc Natl Acad Sci U S A*, **96(5)**: 2192-2197. <https://doi.org/10.1073/pnas.96.5.2192>
- Heo, Y.-J., Lee, Y.-R., Jung, H.-H., Lee, J., Ko, G., & Cho, Y.-H. (2009). Antibacterial efficacy of phages against *Pseudomonas aeruginosa* infections in mice and *Drosophila melanogaster*. *Antimicrob Agents Chemother*, **53(6)**: 2469-2474. <https://doi.org/https://doi.org/10.1128/AAC.01646-08>
- Hernandez-Morales, A. C., Lessor, L. L., Wood, T. L., Migl, D., Mijalis, E. M., Cahill, J., Russell, W. K., Young, R. F., & Gill, J. J. (2018). Genomic and Biochemical Characterization of *Acinetobacter* Podophage Petty Reveals a Novel Lysis Mechanism and Tail-Associated Depolymerase Activity. *J Virol*, **92(6)**: <https://doi.org/10.1128/JVI.01064-17>
- Hesse, S., Rajaure, M., Wall, E., Johnson, J., Bliskovsky, V., Gottesman, S., & Adhya, S. (2020). Phage Resistance in Multidrug-Resistant *Klebsiella pneumoniae*

- ST258 Evolves via Diverse Mutations That Culminate in Impaired Adsorption. *mBio*, **11(1)**: <https://doi.org/10.1128/mBio.02530-19>
- Hietala, V., Horsma-Heikkinen, J., Carron, A., Skurnik, M., & Kiljunen, S. J. (2019). The removal of endo-and enterotoxins from bacteriophage preparations. *Frontiers in Microbiology*, **10**: 1674. <https://doi.org/10.3389/fmicb.2019.01674>
- Hildebrand, G. J., & Wolochow, H. (1962). Translocation of bacteriophage across the intestinal wall of the rat. *Proc Soc Exp Biol Med*, **109**: 183-185. <https://doi.org/10.3181/00379727-109-27146>
- Hill, C., Mills, S., & Ross, R. P. (2018). Phages & antibiotic resistance: are the most abundant entities on earth ready for a comeback? *Future Microbiology*, **13(06)**: 711-726. <https://doi.org/10.2217/fmb-2017-0261>
- Hodyra-Stefaniak, K., Miernikiewicz, P., Drapała, J., Drab, M., Jończyk-Matysiak, E., Lecion, D., Kaźmierczak, Z., Beta, W., Majewska, J., & Harhala, M. (2015). Mammalian Host-Versus-Phage immune response determines phage fate in vivo. *Scientific reports*, **5**: 14802.
- Howard-Varona, C., Hargreaves, K. R., Abedon, S. T., & Sullivan, M. B. (2017). Lysogeny in nature: mechanisms, impact and ecology of temperate phages. *The ISME Journal*, **11(7)**: 1511-1520. <https://doi.org/10.1038/ismej.2017.16>
- Hsu, L. Y., Apisarnthanarak, A., Khan, E., Suwantararat, N., Ghafur, A., & Tambyah, P. A. (2017). Carbapenem-Resistant *Acinetobacter baumannii* and *Enterobacteriaceae* in South and Southeast Asia. *Clin Microbiol Rev*, **30(1)**: 1-22. <https://doi.org/10.1128/cmr.00042-16>
- Hu, B., Margolin, W., Molineux, I. J., & Liu, J. (2013). The Bacteriophage T7 Virion Undergoes Extensive Structural Remodeling During Infection. *Science*, **339(6119)**: 576-579. <https://doi.org/10.1126/science.1231887>
- Hung, C.-H., Kuo, C.-F., Wang, C.-H., Wu, C.-M., & Tsao, N. (2011). Experimental Phage Therapy in Treating *Klebsiella pneumoniae*-Mediated Liver Abscesses

- and Bacteremia in Mice. *Antimicrob Agents Chemother*, **55(4)**: 1358-1365. <https://doi.org/doi:10.1128/AAC.01123-10>
- Hyman, P., & Abedon, S. T. (2010). Bacteriophage host range and bacterial resistance. *Advances in Applied Microbiology*, **70**: 217-248. [https://doi.org/https://doi.org/10.1016/S0065-2164\(10\)70007-1](https://doi.org/https://doi.org/10.1016/S0065-2164(10)70007-1)
- Hyman, P., & van Raaij, M. (2018). Bacteriophage T4 long tail fiber domains. *Biophys Rev*, **10(2)**: 463-471. <https://doi.org/10.1007/s12551-017-0348-5>
- Iida, S. (1984). Bacteriophage P1 carries two related sets of genes determining its host range in the invertible C segment of its genome. *Virology*, **134(2)**: 421-434. [https://doi.org/10.1016/0042-6822\(84\)90309-x](https://doi.org/10.1016/0042-6822(84)90309-x)
- Jain, M., Nijhawan, A., Tyagi, A. K., & Khurana, J. P. (2006). Validation of housekeeping genes as internal control for studying gene expression in rice by quantitative real-time PCR. *Biochem Biophys Res Commun*, **345(2)**: 646-651. <https://doi.org/10.1016/j.bbrc.2006.04.140>
- Jamalludeen, N., Johnson, R. P., Shewen, P. E., & Gyles, C. L. (2009). Evaluation of bacteriophages for prevention and treatment of diarrhea due to experimental enterotoxigenic *Escherichia coli* O149 infection of pigs. *Vet Microbiol*, **136(12)**: 135-141. <https://doi.org/https://doi.org/10.1016/j.vetmic.2008.10.021>
- Jassim, S. A., & Limoges, R. G. (2014). Natural solution to antibiotic resistance: bacteriophages 'The Living Drugs'. *World J Microbiol Biotechnol*, **30(8)**: 2153-2170. <https://doi.org/10.1007/s11274-014-1655-7>
- Jault, P., Leclerc, T., Jennes, S., Pirnay, J. P., Que, Y. A., Resch, G., Rousseau, A. F., Ravat, F., Carsin, H., Le Floch, R., Schaal, J. V., Soler, C., Fevre, C., Arnaud, I., Bretaudeau, L., & Gabard, J. (2019). Efficacy and tolerability of a cocktail of bacteriophages to treat burn wounds infected by *Pseudomonas aeruginosa* (PhagoBurn): a randomised, controlled, double-blind phase 1/2 trial. *Lancet Infect Dis*, **19(1)**: 35-45. [https://doi.org/10.1016/s1473-3099\(18\)30482-1](https://doi.org/10.1016/s1473-3099(18)30482-1)
- Jensen, E. C., Schrader, H. S., Rieland, B., Thompson, T. L., Lee, K. W., Nickerson, K. W., & Kokjohn, T. A. (1998). Prevalence of broad-host-range lytic

bacteriophages of *Sphaerotilus natans*, *Escherichia coli*, and *Pseudomonas aeruginosa*. *Applied and Environmental Microbiology*, **64(2)**: 575-580. <https://doi.org/10.1128/AEM.64.2.575-580.1998>

Jeon, J., Ryu, C.-M., Lee, J.-Y., Park, J.-H., Yong, D., & Lee, K. (2016). *In Vivo* Application of Bacteriophage as a Potential Therapeutic Agent To Control OXA-66-Like Carbapenemase-Producing *Acinetobacter baumannii* Strains Belonging to Sequence Type 357. *Applied and Environmental Microbiology*, **82(14)**: 4200-4208. <https://doi.org/10.1128/AEM.00526-16>

Jia, B., Raphenya, A. R., Alcock, B., Waglechner, N., Guo, P., Tsang, K. K., Lago, B. A., Dave, B. M., Pereira, S., Sharma, A. N., Doshi, S., Courtot, M., Lo, R., Williams, L. E., Frye, J. G., Elsayegh, T., Sardar, D., Westman, E. L., Pawlowski, A. C., Johnson, T. A., Brinkman, F. S., Wright, G. D., & McArthur, A. G. (2017). CARD 2017: expansion and model-centric curation of the comprehensive antibiotic resistance database. *Nucleic Acids Res*, **45(D1)**: D566-d573. <https://doi.org/10.1093/nar/gkw1004>

Johnson, J. R., & Russo, T. A. (2002). Extraintestinal pathogenic *Escherichia coli*: "the other bad *E. coli*". *The Journal of Laboratory and Clinical Medicine*, **139(3)**: 155-162. <https://doi.org/10.1067/mLc.2002.121550>

Johura, F. T., Tasnim, J., Barman, I., Biswas, S. R., Jubyda, F. T., Sultana, M., George, C. M., Camilli, A., Seed, K. D., Ahmed, N., & Alam, M. (2020). Colistin-resistant *Escherichia coli* carrying *mcr-1* in food, water, hand rinse, and healthy human gut in Bangladesh. *Gut Pathog*, **12**: 5. <https://doi.org/10.1186/s13099-020-0345-2>

Jonczyk, E., Klak, M., Miedzybrodzki, R., & Gorski, A. (2011). The influence of external factors on bacteriophages--review. *Folia Microbiol (Praha)*, **56(3)**: 191-200. <https://doi.org/10.1007/s12223-011-0039-8>

Jones, P., Binns, D., Chang, H. Y., Fraser, M., Li, W., McAnulla, C., McWilliam, H., Maslen, J., Mitchell, A., Nuka, G., Pesseat, S., Quinn, A. F., Sangrador-Vegas, A., Scheremetjew, M., Yong, S. Y., Lopez, R., & Hunter, S. (2014).

- InterProScan 5: genome-scale protein function classification. *Bioinformatics*, **30(9)**: 1236-1240. <https://doi.org/10.1093/bioinformatics/btu031>
- Jun, J. W., Shin, T. H., Kim, J. H., Shin, S. P., Han, J. E., Heo, G. J., De Zoysa, M., Shin, G. W., Chai, J. Y., & Park, S. C. (2014). Bacteriophage therapy of a *Vibrio parahaemolyticus* infection caused by a multiple-antibiotic-resistant O3:K6 pandemic clinical strain. *J Infect Dis*, **210(1)**: 72-78. <https://doi.org/10.1093/infdis/jiu059>
- Kala, S., Cumby, N., Sadowski, P. D., Hyder, B. Z., Kanelis, V., Davidson, A. R., & Maxwell, K. L. (2014). HNH proteins are a widespread component of phage DNA packaging machines. *Proc Natl Acad Sci U S A*, **111(16)**: 6022-6027. <https://doi.org/10.1073/pnas.1320952111>
- Kamp, D., Kahmann, R., Zipser, D., Broker, T. R., & Chow, L. T. (1978). Inversion of the G DNA segment of phage Mu controls phage infectivity. *Nature*, **271(5645)**: 577-580. <https://doi.org/10.1038/271577a0>
- Karaolis, D. K., Somara, S., Maneval, D. R., Johnson, J. A., & Kaper, J. B. (1999). A bacteriophage encoding a pathogenicity island, a type-IV pilus and a phage receptor in cholera bacteria. *Nature*, **399(6734)**: 375-379.
- Keen, E. C. (2015). A century of phage research: bacteriophages and the shaping of modern biology. *Bioessays*, **37(1)**: 6-9. <https://doi.org/10.1002/bies.201400152>
- Keller, R., & Engley, F. B., Jr. (1958). Fate of bacteriophage particles introduced into mice by various routes. *Proc Soc Exp Biol Med*, **98(3)**: 577-580. <https://doi.org/10.3181/00379727-98-24112>
- Kempf, M., & Rolain, J. M. (2012). Emergence of resistance to carbapenems in *Acinetobacter baumannii* in Europe: clinical impact and therapeutic options. *Int J Antimicrob Agents*, **39(2)**: 105-114. <https://doi.org/10.1016/j.ijantimicag.2011.10.004>
- Kęsik-Szeloch, A., Drulis-Kawa, Z., Weber-Dąbrowska, B., Kassner, J., Majkowska-Skrobek, G., Augustyniak, D., Łusiak-Szelachowska, M., Żaczek, M., Górski, A., & Kropinski, A. M. (2013). Characterising the biology of novel lytic

bacteriophages infecting multidrug resistant *Klebsiella pneumoniae*. *Virology Journal*, **10(1)**: 100. <https://doi.org/10.1186/1743-422X-10-100>

- Khan Mirzaei, M., & Nilsson, A. S. (2015). Isolation of phages for phage therapy: a comparison of spot tests and efficiency of plating analyses for determination of host range and efficacy. *PLoS One*, **10(3)**: e0118557. <https://doi.org/10.1371/journal.pone.0118557>
- King, A. M. Q., Lefkowitz, E. J., Mushegian, A. R., Adams, M. J., Dutilh, B. E., Gorbalenya, A. E., Harrach, B., Harrison, R. L., Junglen, S., Knowles, N. J., Kropinski, A. M., Krupovic, M., Kuhn, J. H., Nibert, M. L., Rubino, L., Sabanadzovic, S., Sanfacon, H., Siddell, S. G., Simmonds, P., Varsani, A., Zerbini, F. M., & Davison, A. J. (2018). Changes to taxonomy and the International Code of Virus Classification and Nomenclature ratified by the International Committee on Taxonomy of Viruses (2018). *Arch Virol*, **163(9)**: 2601-2631. <https://doi.org/10.1007/s00705-018-3847-1>
- Kingsford, C. L., Ayanbule, K., & Salzberg, S. L. (2007). Rapid, accurate, computational discovery of Rho-independent transcription terminators illuminates their relationship to DNA uptake. *Genome Biol*, **8(2)**: R22. <https://doi.org/10.1186/gb-2007-8-2-r22>
- Knecht, L. E., Veljkovic, M., & Fieseler, L. (2019). Diversity and Function of Phage Encoded Depolymerases. *Front Microbiol*, **10**: 2949. <https://doi.org/10.3389/fmicb.2019.02949>
- Koskella, B., & Brockhurst, M. A. (2014). Bacteria-phage coevolution as a driver of ecological and evolutionary processes in microbial communities. *FEMS Microbiol Rev*, **38(5)**: 916-931. <https://doi.org/10.1111/1574-6976.12072>
- Kostakioti, M., Hadjifrangiskou, M., & Hultgren, S. J. (2013). Bacterial biofilms: development, dispersal, and therapeutic strategies in the dawn of the postantibiotic era. *Cold Spring Harbor Perspectives in Medicine*, **3(4)**: a010306. <https://doi.org/https://doi.org/10.1101/cshperspect.a010306>
- Krogh, A., Larsson, B., von Heijne, G., & Sonnhammer, E. L. (2001). Predicting transmembrane protein topology with a hidden Markov model: application to

- complete genomes. *J Mol Biol*, **305(3)**: 567-580. <https://doi.org/10.1006/jmbi.2000.4315>
- Kropinski, A. M., Mazzocco, A., Waddell, T. E., Lingohr, E., & Johnson, R. P. (2009). Enumeration of bacteriophages by double agar overlay plaque assay. *Methods Mol Biol*, **501**: 69-76. https://doi.org/10.1007/978-1-60327-164-6_7
- Kumar, M., Sarma, D. K., Shubham, S., Kumawat, M., Verma, V., Nina, P. B., JP, D., Kumar, S., Singh, B., & Tiwari, R. R. (2021). Futuristic Non-antibiotic Therapies to Combat Antibiotic Resistance: A Review [Review]. *Frontiers in Microbiology*, **12(16)**: <https://doi.org/10.3389/fmicb.2021.609459>
- Kumari, S., Harjai, K., & Chhibber, S. (2010). Isolation and characterization of *Klebsiella pneumoniae* specific bacteriophages from sewage samples. *Folia Microbiol (Praha)*, **55(3)**: 221-227. <https://doi.org/10.1007/s12223-010-0032-7>
- Kumari, S., Harjai, K., & Chhibber, S. (2011). Bacteriophage versus antimicrobial agents for the treatment of murine burn wound infection caused by *Klebsiella pneumoniae* B5055. *J Med Microbiol*, **60(2)**: 205-210. <https://doi.org/10.1099/jmm.0.018580-0>
- Kutter, E. (2009). Phage host range and efficiency of plating. *Methods Mol Biol*, **501**: 141-149. https://doi.org/10.1007/978-1-60327-164-6_14
- Kutter, E., De Vos, D., Gvasalia, G., Alavidze, Z., Gogokhia, L., Kuhl, S., & Abedon, S. T. (2010). Phage therapy in clinical practice: treatment of human infections. *Curr Pharm Biotechnol*, **11(1)**: 69-86. <https://doi.org/10.2174/138920110790725401>
- Kutter, E., & Sulakvelidze, A. (2004). *Bacteriophages: Biology and Applications*. Boca Raton, Florida: CRC Press.
- Labrie, S. J., Samson, J. E., & Moineau, S. (2010). Bacteriophage resistance mechanisms. *Nat Rev Microbiol*, **8(5)**: 317-327. <https://doi.org/10.1038/nrmicro2315>

- Laemmli, U. K. (1970). Cleavage of structural proteins during the assembly of the head of bacteriophage T4. *Nature*, **227(5259)**: 680-685. <https://doi.org/https://doi.org/10.1038/227680a0>
- Laslett, D., & Canback, B. (2004). ARAGORN, a program to detect tRNA genes and tmRNA genes in nucleotide sequences. *Nucleic Acids Res*, **32(1)**: 11-16. <https://doi.org/10.1093/nar/gkh152>
- Latka, A., Leiman, P. G., Drulis-Kawa, Z., & Briers, Y. (2019). Modeling the Architecture of Depolymerase-Containing Receptor Binding Proteins in *Klebsiella* Phages. *Frontiers in Microbiology*, **10(2649)**: <https://doi.org/https://doi.org/10.3389/fmicb.2019.02649>
- Latka, A., Maciejewska, B., Majkowska-Skrobek, G., Briers, Y., & Drulis-Kawa, Z. (2017). Bacteriophage-encoded virion-associated enzymes to overcome the carbohydrate barriers during the infection process. *Appl Microbiol Biotechnol*, **101(8)**: 3103-3119. <https://doi.org/10.1007/s00253-017-8224-6>
- Lee, D. S., Lee, S. J., & Choe, H. S. (2018). Community-Acquired Urinary Tract Infection by *Escherichia coli* in the Era of Antibiotic Resistance. *Biomed Res Int*, **2018**: 7656752. <https://doi.org/10.1155/2018/7656752>
- Lee, E., Helt, G. A., Reese, J. T., Munoz-Torres, M. C., Childers, C. P., Buels, R. M., Stein, L., Holmes, I. H., Elsik, C. G., & Lewis, S. E. (2013). Web Apollo: a web-based genomic annotation editing platform. *Genome Biol*, **14(8)**: R93. <https://doi.org/10.1186/gb-2013-14-8-r93>
- Lefort, V., Desper, R., & Gascuel, O. (2015). FastME 2.0: A Comprehensive, Accurate, and Fast Distance-Based Phylogeny Inference Program. *Mol Biol Evol*, **32(10)**: 2798-2800. <https://doi.org/10.1093/molbev/msv150>
- Leiman, P. G., Battisti, A. J., Bowman, V. D., Stummeyer, K., Mühlenhoff, M., Gerardy-Schahn, R., Scholl, D., & Molineux, I. J. (2007). The structures of bacteriophages K1E and K1-5 explain processive degradation of polysaccharide capsules and evolution of new host specificities. *J Mol Biol*, **371(3)**: 836-849. <https://doi.org/https://doi.org/10.1016/j.jmb.2007.05.083>

- Li, B., & Webster, T. J. (2018). Bacteria antibiotic resistance: New challenges and opportunities for implant-associated orthopedic infections. *J Orthop Res*, **36(1)**: 22-32. <https://doi.org/10.1002/jor.23656>
- Lin, D. M., Koskella, B., & Lin, H. C. (2017). Phage therapy: An alternative to antibiotics in the age of multi-drug resistance. *World J Gastrointest Pharmacol Ther*, **8(3)**: 162-173. <https://doi.org/10.4292/wjgpt.v8.i3.162>
- Lin, Y. W., Chang, R. Y., Rao, G. G., Jermain, B., Han, M.-L., Zhao, J. X., Chen, K., Wang, J. P., Barr, J. J., Schooley, R. T., Kutter, E., Chan, H.-K., & Li, J. (2020). Pharmacokinetics/pharmacodynamics of antipseudomonal bacteriophage therapy in rats: a proof-of-concept study. *Clinical Microbiology and Infection*, **26(9)**: 1229-1235. <https://doi.org/10.1016/j.cmi.2020.04.039>
- Litt, P. K., & Jaroni, D. (2017). Isolation and Physiomorphological Characterization of *Escherichia coli* O157:H7-Infecting Bacteriophages Recovered from Beef Cattle Operations. *Int J Microbiol*, **2017**: 7013236. <https://doi.org/10.1155/2017/7013236>
- Liu, B., Zheng, D., Jin, Q., Chen, L., & Yang, J. (2018). VFDB 2019: a comparative pathogenomic platform with an interactive web interface. *Nucleic Acids Research*, **47(D1)**: D687-D692. <https://doi.org/10.1093/nar/gky1080> %J Nucleic Acids Research
- Liu, D., Van Belleghem, J. D., de Vries, C. R., Burgener, E., Chen, Q., Manasherob, R., Aronson, J. R., Amanatullah, D. F., Tamma, P. D., & Suh, G. A. (2021). The Safety and Toxicity of Phage Therapy: A Review of Animal and Clinical Studies. *Viruses*, **13(7)**: 1268. <https://www.mdpi.com/1999-4915/13/7/1268>
- Liu, K.-y., Yang, W.-h., Dong, X.-k., Cong, L.-m., Li, N., Li, Y., Wen, Z.-b., Yin, Z., Lan, Z.-j., & Li, W.-p. (2016). Inhalation study of mycobacteriophage D29 aerosol for mice by endotracheal route and nose-only exposure. *Journal of Aerosol Medicine and Pulmonary Drug Delivery*, **29(5)**: 393-405.
- Liu, M., Deora, R., Doulatov, S. R., Gingery, M., Eiserling, F. A., Preston, A., Maskell, D. J., Simons, R. W., Cotter, P. A., Parkhill, J., & Miller, J. F. (2002). Reverse

- transcriptase-mediated tropism switching in *Bordetella* bacteriophage. *Science*, **295(5562)**: 2091-2094. <https://doi.org/10.1126/science.1067467>
- Livak, K. J., & Schmittgen, T. D. (2001). Analysis of relative gene expression data using real-time quantitative PCR and the 2(-Delta Delta C(T)) Method. *Methods*, **25(4)**: 402-408. <https://doi.org/10.1006/meth.2001.1262>
- Low, W. L., Kenward, K., Britland, S. T., Amin, M. C., & Martin, C. (2017). Essential oils and metal ions as alternative antimicrobial agents: a focus on tea tree oil and silver. *Int Wound J*, **14(2)**: 369-384. <https://doi.org/10.1111/iwj.12611>
- Ly-Chatain, M. H. (2014). The factors affecting effectiveness of treatment in phages therapy. *Front Microbiol*, **5**: 51. <https://doi.org/10.3389/fmicb.2014.00051>
- Maddocks, S., Fabijan, A. P., Ho, J., Lin, R. C., Ben Zakour, N. L., Dugan, C., Kliman, I., Branston, S., Morales, S., & Iredell, J. R. (2019). Bacteriophage therapy of ventilator-associated pneumonia and empyema caused by *Pseudomonas aeruginosa*. *American Journal of Respiratory and Critical Care Medicine*, **200(9)**: 1179-1181. <https://doi.org/10.1164/rccm.201904-0839L>
- Madeira, F., Park, Y. M., Lee, J., Buso, N., Gur, T., Madhusoodanan, N., Basutkar, P., Tivey, A. R. N., Potter, S. C., Finn, R. D., & Lopez, R. (2019). The EMBL-EBI search and sequence analysis tools APIs in 2019. *Nucleic Acids Research*, **47(W1)**: W636-W641. <https://doi.org/10.1093/nar/gkz268>
- Magill, D. J., Kucher, P. A., Krylov, V. N., Pleteneva, E. A., Quinn, J. P., & Kulakov, L. A. (2017). Localised genetic heterogeneity provides a novel mode of evolution in dsDNA phages. *Sci Rep*, **7(1)**: 13731. <https://doi.org/10.1038/s41598-017-14285-0>
- Majkowska-Skrobek, G., Latka, A., Berisio, R., Squeglia, F., Maciejewska, B., Briers, Y., & Drulis-Kawa, Z. (2018). Phage-Borne Depolymerases Decrease *Klebsiella pneumoniae* Resistance to Innate Defense Mechanisms. *Frontiers in Microbiology*, **9(2517)**: <https://doi.org/10.3389/fmicb.2018.02>
- Malik, D. J., Sokolov, I. J., Vinner, G. K., Mancuso, F., Cinquerrui, S., Vladislavljevic, G. T., Clokie, M. R., Garton, N. J., Stapley, A. G., & Kirpichnikova, A. (2017).

Formulation, stabilisation and encapsulation of bacteriophage for phage therapy. *Advances in Colloid and Interface Science*, **249**: 100-133.

Martens, E., & Demain, A. L. (2017). The antibiotic resistance crisis, with a focus on the United States. *J Antibiot (Tokyo)*, **70(5)**: 520-526. <https://doi.org/10.1038/ja.2017.30>

Matsuzaki, S., Yasuda, M., Nishikawa, H., Kuroda, M., Ujihara, T., Shuin, T., Shen, Y., Jin, Z., Fujimoto, S., & Nasimuzzaman, M. (2003). Experimental protection of mice against lethal *Staphylococcus aureus* infection by novel bacteriophage ϕ MR11. *J Infect Dis*, **187(4)**: 613-624. <https://doi.org/https://doi.org/10.1086/374001>

Mavrich, T. N., & Hatfull, G. F. (2017). Bacteriophage evolution differs by host, lifestyle and genome. *Nature Microbiology*, **2(9)**: 17112. <https://doi.org/10.1038/nmicrobiol.2017.112>

McCarthy, S. D., Horgan, E., Ali, A., Masterson, C., Laffey, J. G., MacLoughlin, R., & O'Toole, D. (2020). Nebulized mesenchymal stem cell derived conditioned medium retains antibacterial properties against clinical pathogen isolates. *Journal of Aerosol Medicine and Pulmonary Drug Delivery*, **33(3)**: 140-152. <https://doi.org/https://doi.org/10.1089/jamp.2019.1542>

Meier-Kolthoff, J. P., Auch, A. F., Klenk, H. P., & Goker, M. (2013). Genome sequence-based species delimitation with confidence intervals and improved distance functions. *BMC Bioinformatics*, **14**: 60. <https://doi.org/10.1186/1471-2105-14-60>

Meier-Kolthoff, J. P., & Goker, M. (2017). VICTOR: genome-based phylogeny and classification of prokaryotic viruses. *Bioinformatics*, **33(21)**: 3396-3404. <https://doi.org/10.1093/bioinformatics/btx440>

Merabishvili, M., Vandenheuvel, D., Kropinski, A. M., Mast, J., De Vos, D., Verbeken, G., Noben, J.-P., Lavigne, R., Vanechoutte, M., & Pirnay, J.-P. (2014). Characterization of Newly Isolated Lytic Bacteriophages Active against *Acinetobacter baumannii*. *PLoS One*, **9(8)**: e104853. <https://doi.org/10.1371/journal.pone.0104853>

- Merril, C. R., Biswas, B., Carlton, R., Jensen, N. C., Creed, G. J., Zullo, S., & Adhya, S. (1996). Long-circulating bacteriophage as antibacterial agents. *Proc Natl Acad Sci U S A*, **93(8)**: 3188-3192. <https://doi.org/10.1073/pnas.93.8.3188>
- Messika, J., Magdoud, F., Clermont, O., Margetis, D., Gaudry, S., Roux, D., Branger, C., Dreyfuss, D., Denamur, E., & Ricard, J.-D. (2012). Pathophysiology of *Escherichia coli* ventilator-associated pneumonia: implication of highly virulent extraintestinal pathogenic strains. *Intensive Care Medicine*, **38(12)**: 2007-2016. <https://doi.org/https://doi.org/10.1007/s00134-012-2699-5>
- Molineux, G. (2004). The design and development of pegfilgrastim (PEG-rmetHuG-CSF, Neulasta). *Current Pharmaceutical Design*, **10(11)**: 1235-1244. <https://doi.org/https://doi.org/10.2174/1381612043452613>
- Monod, C., Repoila, F., Kutateladze, M., Tetart, F., & Krisch, H. M. (1997). The genome of the pseudo T-even bacteriophages, a diverse group that resembles T4. *J Mol Biol*, **267(2)**: 237-249. <https://doi.org/10.1006/jmbi.1996.0867>
- Montso, P. K., mLambo, V., & Ateba, C. N. (2019). Characterization of Lytic Bacteriophages Infecting Multidrug-Resistant Shiga Toxigenic Atypical *Escherichia coli* O177 Strains Isolated From Cattle Feces. *Frontiers in Public Health*, **7(355)**: <https://doi.org/https://doi.org/10.3389/fpubh.2019.00355>
- Mutti, M., & Corsini, L. (2019). Robust approaches for the production of active ingredient and drug product for human phage therapy. *Frontiers in Microbiology*, **10**: 2289. <https://doi.org/https://doi.org/10.3389/fmicb.2019.02289>
- Muzammil, S., Hayat, S., Fakhar-E-Alam, M., Aslam, B., Siddique, M. H., Nisar, M. A., Saqalein, M., Atif, M., Sarwar, A., & Khurshid, A. (2018). Nanoantibiotics: Future nanotechnologies to combat antibiotic resistance. *Front. Biosci*, **10**: 352-374. <https://doi.org/https://doi.org/10.2741/e827>
- Nagarjuna, D., Mittal, G., Dhanda, R., Verma, P., Gaiind, R., & Yadav, M. (2015). Faecal *Escherichia coli* isolates show potential to cause endogenous infection in patients admitted to the ICU in a tertiary care hospital. *New Microbes and New Infections*, **7**: 57-66. <https://doi.org/https://doi.org/10.1016/j.nmni.2015.05.006>

- Nale, J. Y., Spencer, J., Hargreaves, K. R., Buckley, A. M., Trzepiński, P., Douce, G. R., & Clokie, M. R. J. (2015). Bacteriophage Combinations Significantly Reduce *Clostridium difficile* Growth *In Vitro* and Proliferation *In Vivo*. *Antimicrob Agents Chemother*, **60(2)**: 968-981. <https://doi.org/10.1128/AAC.01774-15>
- National Planning Commission. (2020). *The Fifteenth Plan (Fiscal Year 2019/20 – 2023/24)*. Singha Durbar, Kathmandu: National Planning Commission. https://npc.gov.np/images/category/15th_plan_English_Version.pdf
- Nelson, D. (2004). Phage taxonomy: we agree to disagree. *J Bacteriol*, **186(21)**: 7029-7031. <https://doi.org/10.1128/jb.186.21.7029-7031.2004>
- Nepal, G., & Bhatta, S. (2018). Self-medication with Antibiotics in WHO Southeast Asian Region: A Systematic Review. *Cureus*, **10(4)**: e2428. <https://doi.org/10.7759/cureus.2428>
- Nepal, K., Pant, N. D., Neupane, B., Belbase, A., Baidhya, R., Shrestha, R. K., Lekhak, B., Bhatta, D. R., & Jha, B. (2017). Extended spectrum beta-lactamase and metallo beta-lactamase production among *Escherichia coli* and *Klebsiella pneumoniae* isolated from different clinical samples in a tertiary care hospital in Kathmandu, Nepal. *Ann Clin Microbiol Antimicrob*, **16(1)**: 62. <https://doi.org/10.1186/s12941-017-0236-7>
- Nilsson, A. S. (2019). Pharmacological limitations of phage therapy. *Ups J Med Sci*, **124(4)**: 218-227. <https://doi.org/10.1080/03009734.2019.1688433>
- Noguchi, H., Taniguchi, T., & Itoh, T. (2008). MetaGeneAnnotator: detecting species-specific patterns of ribosomal binding site for precise gene prediction in anonymous prokaryotic and phage genomes. *DNA Res*, **15(6)**: 387-396. <https://doi.org/10.1093/dnares/dsn027>
- Nolan, J. M., Petrov, V., Bertrand, C., Krisch, H. M., & Karam, J. D. (2006). Genetic diversity among five T4-like bacteriophages. *Viol J*, **3**: 30. <https://doi.org/10.1186/1743-422x-3-30>

- O'Neill, J. (2014). The Review on Antimicrobial Resistance. *Antimicrobial resistance: tackling a crisis for the health and wealth of nations*, **2014 (4)**. https://amr-review.org/sites/default/files/AMR%20Review%20Paper%20-%20Tackling%20a%20crisis%20for%20the%20health%20and%20wealth%20of%20nations_1.pdf
- Oakey, H. J., Cullen, B. R., & Owens, L. (2002). The complete nucleotide sequence of the *Vibrio harveyi* bacteriophage VHML. *J Appl Microbiol*, **93(6)**: 1089-1098. <https://doi.org/10.1046/j.1365-2672.2002.01776.x>
- Oliveira, A., Sereno, R., Nicolau, A., & Azeredo, J. (2009). The influence of the mode of administration in the dissemination of three coliphages in chickens. *Poult Sci*, **88(4)**: 728-733. <https://doi.org/10.3382/ps.2008-00378>
- Olszak, T., Shneider, M. M., Latka, A., Maciejewska, B., Browning, C., Sycheva, L. V., Cornelissen, A., Danis-Wlodarczyk, K., Senchenkova, S. N., Shashkov, A. S., Gula, G., Arabski, M., Wasik, S., Miroshnikov, K. A., Lavigne, R., Leiman, P. G., Knirel, Y. A., & Drulis-Kawa, Z. (2017). The O-specific polysaccharide lyase from the phage LKA1 tailspike reduces *Pseudomonas* virulence. *Sci Rep*, **7(1)**: 16302. <https://doi.org/10.1038/s41598-017-16411-4>
- Otero, J., García-Rodríguez, A., Cano-Sarabia, M., Maspoch, D., Marcos, R., Cortés, P., & Llagostera, M. (2019). Biodistribution of Liposome-Encapsulated Bacteriophages and Their Transcytosis During Oral Phage Therapy. *Frontiers in Microbiology*, **10(689)**. <https://doi.org/10.3389/fmicb.2019.00689>
- Pan, Y. J., Lin, T. L., Chen, C. C., Tsai, Y. T., Cheng, Y. H., Chen, Y. Y., Hsieh, P. F., Lin, Y. T., & Wang, J. T. (2017). *Klebsiella* Phage PhiK64-1 Encodes Multiple Depolymerases for Multiple Host Capsular Types. *J Virol*, **91(6)**: <https://doi.org/10.1128/JVI.02457-16>
- Pantastico-Caldas, M., Duncan, K. E., Istock, C. A., & Bell, J. A. (1992). Population dynamics of bacteriophage and *Bacillus subtilis* in soil. *Ecology*, **73(5)**: 1888-1902. <https://doi.org/https://doi.org/10.2307/1940040>

- Payne, R. J., & Jansen, V. A. (2003). Pharmacokinetic principles of bacteriophage therapy. *Clin Pharmacokinet*, **42(4)**: 315-325. <https://doi.org/10.2165/00003088-200342040-00002>
- Pedulla, M. L., Ford, M. E., Houtz, J. M., Karthikeyan, T., Wadsworth, C., Lewis, J. A., Jacobs-Sera, D., Falbo, J., Gross, J., Pannunzio, N. R., Brucker, W., Kumar, V., Kandasamy, J., Keenan, L., Bardarov, S., Kriakov, J., Lawrence, J. G., Jacobs, W. R., Jr., Hendrix, R. W., & Hatfull, G. F. (2003). Origins of highly mosaic mycobacteriophage genomes. *Cell*, **113(2)**: 171-182. [https://doi.org/10.1016/s0092-8674\(03\)00233-2](https://doi.org/10.1016/s0092-8674(03)00233-2)
- Pertics, B. Z., Cox, A., Nyúl, A., Szamek, N., Kovács, T., & Schneider, G. (2021). Isolation and Characterization of a Novel Lytic Bacteriophage against the K2 Capsule-Expressing Hypervirulent *Klebsiella pneumoniae* Strain 52145, and Identification of Its Functional Depolymerase. *Microorganisms*, **9(3)**: 650. <https://doi.org/https://doi.org/10.3390/microorganisms9030650>
- Petrov, V. M., Ratnayaka, S., Nolan, J. M., Miller, E. S., & Karam, J. D. (2010). Genomes of the T4-related bacteriophages as windows on microbial genome evolution. *Virology*, **7**: 292. <https://doi.org/10.1186/1743-422x-7-292>
- Petrovic Fabijan, A., Lin, R. C. Y., Ho, J., Maddocks, S., Ben Zakour, N. L., & Iredell, J. R. (2020). Safety of bacteriophage therapy in severe *Staphylococcus aureus* infection. *Nature Microbiology*, **5(3)**: 465-472. <https://doi.org/10.1038/s41564-019-0634-z>
- Philipson, C. W., Voegtly, L. J., Lueder, M. R., Long, K. A., Rice, G. K., Frey, K. G., Biswas, B., Cer, R. Z., Hamilton, T., & Bishop-Lilly, K. A. (2018). Characterizing Phage Genomes for Therapeutic Applications. *Viruses*, **10(4)**: <https://doi.org/10.3390/v10040188>
- Pires, D. P., Oliveira, H., Melo, L. D., Sillankorva, S., & Azeredo, J. (2016). Bacteriophage-encoded depolymerases: their diversity and biotechnological applications. *Appl Microbiol Biotechnol*, **100(5)**: 2141-2151. <https://doi.org/10.1007/s00253-015-7247-0>

- Pirnay, J.-P. (2020). Phage Therapy in the Year 2035. *Frontiers in Microbiology*, **11**.
<https://doi.org/10.3389/fmicb.2020.01171>
- Pirnay, J.-P., Verbeken, G., Ceysens, P.-J., Huys, I., De Vos, D., Ameloot, C., & Fauconnier, A. (2018). The Magistral Phage. *Viruses*, **10(2)**: 64.
<https://doi.org/10.3390/v10020064>
- Podschun, R., & Ullmann, U. (1998). *Klebsiella* spp. as nosocomial pathogens: epidemiology, taxonomy, typing methods, and pathogenicity factors. *Clin Microbiol Rev*, **11(4)**: 589-603. <https://doi.org/10.1128/cmr.11.4.589>
- Poolman, J. T., & Wacker, M. (2016). Extraintestinal Pathogenic *Escherichia coli*, a Common Human Pathogen: Challenges for Vaccine Development and Progress in the Field. *J Infect Dis*, **213(1)**: 6-13. <https://doi.org/10.1093/infdis/jiv429>
- Pouillot, F., Chomton, M., Blois, H., Courroux, C., Noelig, J., Bidet, P., Bingen, E., & Bonacorsi, S. (2012). Efficacy of bacteriophage therapy in experimental sepsis and meningitis caused by a clone O25b:H4-ST131 *Escherichia coli* strain producing CTX-M-15. *Antimicrob Agents Chemother*, **56(7)**: 3568-3575.
<https://doi.org/10.1128/aac.06330-11>
- Pyra, A., Brzozowska, E., Pawlik, K., Gamian, A., Dauter, M., & Dauter, Z. (2017). Tail tubular protein A: a dual-function tail protein of *Klebsiella pneumoniae* bacteriophage KP32. *Scientific Reports*, **7(1)**: 1-9. <https://doi.org/https://doi.org/10.1038/s41598-017-02451-3>
- Rajaure, M., Berry, J., Kongari, R., Cahill, J., & Young, R. (2015). Membrane fusion during phage lysis. *Proc Natl Acad Sci U S A*, **112(17)**: 5497-5502.
<https://doi.org/10.1073/pnas.1420588112>
- Rakhuba, D. V., Kolomiets, E. I., Dey, E. S., & Novik, G. I. (2010). Bacteriophage receptors, mechanisms of phage adsorption and penetration into host cell. *Pol J Microbiol*, **59(3)**: 145-155. <https://doi.org/DOI:10.33073/pjm-2010-023>
- Rashel, M., Uchiyama, J., Ujihara, T., Uehara, Y., Kuramoto, S., Sugihara, S., Yagyu, K.-I., Muraoka, A., Sugai, M., & Hiramatsu, K. (2007). Efficient elimination of multidrug-resistant *Staphylococcus aureus* by cloned lysin derived from

- bacteriophage ϕ MR11. *J Infect Dis*, **196(8)**: 1237-1247. <https://doi.org/https://doi.org/10.1086/521305>
- Reardon, S. (2015). Bacterial arms race revs up. *Nature*, **521(7553)**: 402-403. <https://doi.org/10.1038/521402a>
- Regulski, K., Champion-Arnaud, P., & Gabard, J. (2021). *Bacteriophages: Biology, Technology, Therapy*. Switzerland AG: Springer Nature. https://link.springer.com/referenceworkentry/10.1007%2F978-3-319-41986-2_25
- Rhoads, D. D., Wolcott, R. D., Kuskowski, M. A., Wolcott, B. M., Ward, L. S., & Sulakvelidze, A. (2009). Bacteriophage therapy of venous leg ulcers in humans: results of a phase I safety trial. *J Wound Care*, **18(6)**: 237-238, 240-233. <https://doi.org/10.12968/jowc.2009.18.6.42801>
- Rice, L. B. (2008). Federal funding for the study of antimicrobial resistance in nosocomial pathogens: no ESKAPE. *J Infect Dis*, **197(8)**: 1079-1081. <https://doi.org/10.1086/533452>
- Rice, S. A., Tan, C. H., Mikkelsen, P. J., Kung, V., Woo, J., Tay, M., Hauser, A., McDougald, D., Webb, J. S., & Kjelleberg, S. (2009). The biofilm life cycle and virulence of *Pseudomonas aeruginosa* are dependent on a filamentous prophage. *The ISME Journal*, **3(3)**: 271-282.
- Rietschel, E. T., Schade, U., Jensen, M., Wollenweber, H. W., Lüderitz, O., & Greisman, S. G. (1982). Bacterial endotoxins: chemical structure, biological activity and role in septicemia. *Scand. J. Infect. Dis. Suppl.*, **3**: 8-21. <https://cir.nii.ac.jp/crid/1571135650047078272>
- Ripp, S., & Miller, R. V. (1997). The role of pseudolysogeny in bacteriophage-host interactions in a natural freshwater environment. *Microbiology*, **143(6)**: 2065-2070. <https://doi.org/https://doi.org/10.1099/00221287-143-6-2065>
- Roach, D. R., Leung, C. Y., Henry, M., Morello, E., Singh, D., Di Santo, J. P., Weitz, J. S., & Debarbieux, L. (2017). Synergy between the host immune system and bacteriophage is essential for successful phage therapy against an acute

respiratory pathogen. *Cell Host & Microbe*, **22(1)**: 38-47.
<https://doi.org/https://doi.org/10.1016/j.chom.2017.06.018>

Romero-Calle, D., Guimaraes Benevides, R., Goes-Neto, A., & Billington, C. (2019). Bacteriophages as Alternatives to Antibiotics in Clinical Care. *Antibiotics (Basel)*, **8(3)**: <https://doi.org/10.3390/antibiotics8030138>

Ross, A., Ward, S., & Hyman, P. (2016). More Is Better: Selecting for Broad Host Range Bacteriophages. *Front Microbiol*, **7**: 1352. <https://doi.org/10.3389/fmicb.2016.01352>

Roucourt, B., & Lavigne, R. (2009). The role of interactions between phage and bacterial proteins within the infected cell: a diverse and puzzling interactome. *Environ Microbiol*, **11(11)**: 2789-2805. <https://doi.org/10.1111/j.1462-2920.2009.02029.x>

Ruska, H. (1940). Die Sichtbarmachung der bakterio-phagen lyse im übermikroskop. *Naturwissenschaften*, **28(3)**: 45-46. https://doi.org/https://ui.adsabs.harvard.edu/link_gateway/1940NW.....28...45R/doi:10.1007/BF01486931

Russell, W. J., Taylor, S. A., & Sigel, M. M. (1976). Clearance of bacteriophage in poikilothermic vertebrates and the effect of temperature. *J Reticuloendothel Soc*, **19(2)**: 91-96. <https://europepmc.org/article/med/1263185>

Saganuwan, S. A. (2011). A modified arithmetical method of Reed and Muench for determination of a relatively ideal median lethal dose (LD50). *African Journal of Pharmacy and Pharmacology*, **5(12)**: 1543-1546. <https://academicjournals.org/journal/AJPP/article-abstract/5DE665E31999>

Sambrook, H. (1989). *Molecular cloning: a laboratory manual*. New York, Cold Spring Harbor Press.

Sambrook, J., & Russell, D. J. P., NY. (2001). *Molecular cloning: A laboratory manual*. New York, Cold Spring Harbor Laboratory Press.

Sampaio, M., Rocha, M., Oliveira, H., & Dias, O. (2019). Predicting promoters in phage genomes using PhagePromoter. *Bioinformatics*, **35(24)**: 5301-5302. <https://doi.org/10.1093/bioinformatics/btz580>

- Samson, J. E., Magadán, A. H., Sabri, M., & Moineau, S. (2013). Revenge of the phages: defeating bacterial defences. *Nature reviews. Microbiology*, **11(10)**: 675-687. <https://doi.org/10.1038/nrmicro3096>
- Sanjuán, R., & Domingo-Calap, P. (2019). Genetic diversity and evolution of viral populations. *Encyclopedia of Virology*, **2021**: 53–61. <https://doi.org/10.1016/B978-0-12-809633-8.20958-8>Reference
- Sarker, S. A., Sultana, S., Reuteler, G., Moine, D., Descombes, P., Charton, F., Bourdin, G., McCallin, S., Ngom-Bru, C., Neville, T., Akter, M., Huq, S., Qadri, F., Talukdar, K., Kassam, M., Delley, M., Loiseau, C., Deng, Y., El Aidy, S., Berger, B., & Brüssow, H. (2016). Oral Phage Therapy of Acute Bacterial Diarrhea With Two Coliphage Preparations: A Randomized Trial in Children From Bangladesh. *EBioMedicine*, **4**: 124-137. <https://doi.org/10.1016/j.ebiom.2015.12.023>
- Schmidt, C. (2019). Phage therapy's latest makeover. *Nat Biotechnol*, **37(6)**: 581-586. <https://doi.org/10.1038/s41587-019-0133-z>
- Scholl, D., Rogers, S., Adhya, S., & Merrill, C. R. (2001). Bacteriophage K1-5 encodes two different tail fiber proteins, allowing it to infect and replicate on both K1 and K5 strains of *Escherichia coli*. *J Virol*, **75(6)**: 2509-2515. <https://doi.org/10.1128/JVI.75.6.2509-2515.2001>
- Schooley, R. T., Biswas, B., Gill, J. J., Hernandez-Morales, A., Lancaster, J., Lessor, L., Barr, J. J., Reed, S. L., Rohwer, F., Benler, S., Segall, A. M., Taplitz, R., Smith, D. M., Kerr, K., Kumaraswamy, M., Nizet, V., Lin, L., Mccauley, M. D., Strathdee, S. A., Benson, C. A., Pope, R. K., Leroux, B. M., Picel, A. C., Mateczun, A. J., Cilwa, K. E., Regeimbal, J. M., Estrella, L. A., Wolfe, D. M., Henry, M. S., Quinones, J., Salka, S., Bishop-Lilly, K. A., Young, R., & Hamilton, T. (2017). Development and Use of Personalized Bacteriophage-Based Therapeutic Cocktails To Treat a Patient with a Disseminated Resistant *Acinetobacter baumannii* Infection. *Antimicrob Agents Chemother*, **61(10)**: AAC.00954-00917. <https://doi.org/10.1128/aac.00954-17>

- Schultz, I., & Neva, F. A. (1965). Relationship between Blood Clearance and Viruria after Intravenous Injection of Mice and Rats with Bacteriophage and Polioviruses. *Journal of Immunology*, **94(6)**: 833-841. <https://www.jimmunol.org/content/jimmunol/94/6/833.full.pdf>
- Schwarzer, D., Buettner, F. F., Browning, C., Nazarov, S., Rabsch, W., Bethe, A., Oberbeck, A., Bowman, V. D., Stummeyer, K., Mühlenhoff, M., Leiman, P. G., & Gerardy-Schahn, R. (2012). A multivalent adsorption apparatus explains the broad host range of phage phi92: a comprehensive genomic and structural analysis. *J Virol*, **86(19)**: 10384-10398. <https://doi.org/10.1128/jvi.00801-12>
- Seckler, R. (1998). Folding and function of repetitive structure in the homotrimeric phage P22 tailspike protein. *J Struct Biol*, **122(1-2)**: 216-222. <https://doi.org/10.1006/jsbi.1998.3974>
- Shanks, N., Greek, R., & Greek, J. (2009). Are animal models predictive for humans? *Philos Ethics Humanit Med*, **4**: 2. <https://doi.org/10.1186/1747-5341-4-2>
- Shi, Y., Peng, Y., Zhang, Y., Chen, Y., Zhang, C., Luo, X., Chen, Y., Yuan, Z., Chen, J., & Gong, Y. (2021). Safety and Efficacy of a Phage, kpsk3, in an in vivo Model of Carbapenem-Resistant Hypermucoviscous *Klebsiella pneumoniae* Bacteremia. *Frontiers in Microbiology*, **2021**: 12. <https://doi.org/10.3389/fmicb.2021.613356>
- Shivshetty, N., Hosamani, R., Ahmed, L., Oli, A. K., Sannauallah, S., Sharanbassappa, S., Patil, S. A., & Kelmani, C. R. (2014). Experimental Protection of Diabetic Mice against Lethal *P. aeruginosa* Infection by Bacteriophage. *BioMed research International*, **2014**. <https://doi.org/https://doi.org/10.1155/2014/793242>
- Sidjabat, H. E., & Paterson, D. L. (2015). Multidrug-resistant *Escherichia coli* in Asia: epidemiology and management. *Expert Rev Anti Infect Ther*, **13(5)**: 575-591. <https://doi.org/10.1586/14787210.2015.1028365>
- Simoons-Smit, A., Verwey-van Vught, A., Kanis, I., & MacLaren, D. (1984). Virulence of *Klebsiella* strains in experimentally induced skin lesions in the mouse. *J Med Microbiol*, **17(1)**: 67-77. <https://doi.org/https://doi.org/10.1099/00222615-17-1-67>

- Singla, S., Harjai, K., Katare, O. P., & Chhibber, S. (2015). Bacteriophage-Loaded Nanostructured Lipid Carrier: Improved Pharmacokinetics Mediates Effective Resolution of *Klebsiella pneumoniae*-Induced Lobar Pneumonia. *J Infect Dis*, **212(2)**: 325-334. <https://doi.org/10.1093/infdis/jiv029>
- Singla, S., Harjai, K., Katare, O. P., & Chhibber, S. (2016). Encapsulation of Bacteriophage in Liposome Accentuates Its Entry in to Macrophage and Shields It from Neutralizing Antibodies. *PLoS One*, **11(4)**: e0153777. <https://doi.org/10.1371/journal.pone.0153777>
- Skurnik, M., Pajunen, M., & Kiljunen, S. (2007). Biotechnological challenges of phage therapy. *Biotechnology letters*, **29(7)**: 995-1003. <https://doi.org/10.1007/s10529-007-9346-1>
- Smith, H. W., & Huggins, M. B. (1982). Successful treatment of experimental *Escherichia coli* infections in mice using phage: its general superiority over antibiotics. *J Gen Microbiol*, **128(2)**: 307-318. <https://doi.org/10.1099/00221287-128-2-307>
- Soding, J. (2005). Protein homology detection by HMM-HMM comparison. *Bioinformatics*, **21(7)**: 951-960. <https://doi.org/10.1093/bioinformatics/bti125>
- Soleimani Sasani, M., & Eftekhari, F. (2020). Potential of a Bacteriophage Isolated from Wastewater in Treatment of Lobar Pneumonia Infection Induced by *Klebsiella pneumoniae* in Mice. *Current Microbiology*, **77(10)**: 2650-2655. <https://doi.org/10.1007/s00284-020-02041-z>
- Speck, P., & Smithyman, A. (2016). Safety and efficacy of phage therapy via the intravenous route. *FEMS Microbiol Lett*, **363(3)**. <https://doi.org/10.1093/femsle/fnv242>
- Spellberg, B. (2014). The future of antibiotics. *Crit Care*, **18(3)**: 228. <https://doi.org/10.1186/cc13948>
- Squeglia, F., Maciejewska, B., Latka, A., Ruggiero, A., Briers, Y., Drulis-Kawa, Z., & Berisio, R. (2020). Structural and Functional Studies of a *Klebsiella* Phage Capsule Depolymerase Tailspike: Mechanistic Insights into Capsular

Degradation. *Structure*, **28(6)**: 613-624 e614. <https://doi.org/10.1016/j.str.2020.04.015>

Stenvinkel, P., Ketteler, M., Johnson, R. J., Lindholm, B., Pecoits-Filho, R., Riella, M., Heimbürger, O., Cederholm, T., & Girndt, M. (2005). IL-10, IL-6, and TNF-alpha: central factors in the altered cytokine network of uremia--the good, the bad, and the ugly. *Kidney Int*, **67(4)**: 1216-1233. <https://doi.org/10.1111/j.1523-1755.2005.00200.x>

Storms, Z. J., Brown, T., Cooper, D. G., Sauvageau, D., & Leask, R. L. (2014). Impact of the cell life-cycle on bacteriophage T4 infection. *FEMS Microbiol Lett*, **353(1)**: 63-68. <https://doi.org/10.1111/1574-6968.12402>

Stothard, P., & Wishart, D. S. (2005). Circular genome visualization and exploration using CGView. *Bioinformatics*, **21(4)**: 537-539. <https://doi.org/10.1093/bioinformatics/bti054>

Straub, M. E., & Applebaum, M. (1933). Studies on commercial bacteriophage products. *Journal of the American Medical Association*, **100(2)**: 110-113.

Stummeyer, K., Schwarzer, D., Claus, H., Vogel, U., Gerardy-Schahn, R., & Mühlenhoff, M. (2006). Evolution of bacteriophages infecting encapsulated bacteria: lessons from *Escherichia coli* K1-specific phages. *Mol Microbiol*, **60(5)**: 1123-1135. <https://doi.org/10.1111/j.1365-2958.2006.05173.x>

Suay-García, B., & Pérez-Gracia, M. T. (2019). Present and Future of Carbapenem-resistant *Enterobacteriaceae* (CRE) Infections. *Antibiotics (Basel)*, **8(3)**: <https://doi.org/10.3390/antibiotics8030122>

Suez, J., Zmora, N., Zilberman-Schapira, G., Mor, U., Dori-Bachash, M., Bashardes, S., Zur, M., Regev-Lehavi, D., Brik, R. B.-Z., & Federici, S. (2018). Post-antibiotic gut mucosal microbiome reconstitution is impaired by probiotics and improved by autologous FMT. *Cell*, **174(6)**: 1406-1423. e1416.

Sui, B., Han, L., Ren, H., Liu, W., & Zhang, C. (2021). A Novel Polyvalent Bacteriophage vB_EcoM_swi3 Infects Pathogenic *Escherichia coli* and

- Salmonella enteritidis*. *Frontiers in Microbiology*, **12(1496)**. <https://doi.org/10.3389/fmicb.2021.649673>
- Sulakvelidze, A. (2011). Safety by nature: Potential bacteriophage applications- Bacteriophages offer opportunities for safely managing bacterial infections. *Microbe*, **6(3)**: 122.
- Sulakvelidze, A., Alavidze, Z., & Morris, J. G., Jr. (2001). Bacteriophage therapy. *Antimicrob Agents Chemother*, **45(3)**: 649-659. <https://doi.org/10.1128/aac.45.3.649-659.2001>
- Summers, W. (1999). *Bacteriophage discovered: Felix d'Herelle and the Origins of Molecular Biology*. New Haven, Yale University Press.
- Summers, W. C. (2012). The strange history of phage therapy. *Bacteriophage*, **2(2)**: 130-133. <https://doi.org/10.4161/bact.20757>
- Sutherland, I. W. (1976). Highly specific bacteriophage-associated polysaccharide hydrolases for *Klebsiella aerogenes* type 8. *J Gen Microbiol*, **94(1)**: 211-216. <https://doi.org/10.1099/00221287-94-1-211>
- Swanstrom, M., & Adams, M. H. (1951). Agar Layer Method for Production of High Titer Phage Stocks. *Proceedings of the Society for Experimental Biology and Medicine*, **78(2)**: 372-375. <https://doi.org/10.3181/00379727-78-19076>
- Sybesma, W., Rohde, C., Bardy, P., Pirnay, J.-P., Cooper, I., Caplin, J., Chanishvili, N., Coffey, A., De Vos, D., Scholz, A., McCallin, S., Püschner, H., Pantucek, R., Aminov, R., Doškař, J., & Kurtböke, D. (2018). Silk Route to the Acceptance and Re-Implementation of Bacteriophage Therapy—Part II. *Antibiotics*, **7(2)**: 35. <https://doi.org/10.3390/antibiotics7020035>
- Tacconelli, E., Carrara, E., Savoldi, A., Harbarth, S., Mendelson, M., Monnet, D. L., Pulcini, C., Kahlmeter, G., Kluytmans, J., & Carmeli, Y. (2018). Discovery, research, and development of new antibiotics: the WHO priority list of antibiotic-resistant bacteria and tuberculosis. *The Lancet Infectious Diseases*, **18(3)**: 318-327. [https://doi.org/https://doi.org/10.1016/S1473-3099\(17\)30753-3](https://doi.org/https://doi.org/10.1016/S1473-3099(17)30753-3)

- Takemura-Uchiyama, I., Uchiyama, J., Osanai, M., Morimoto, N., Asagiri, T., Ujihara, T., Daibata, M., Sugiura, T., & Matsuzaki, S. (2014). Experimental phage therapy against lethal lung-derived septicemia caused by *Staphylococcus aureus* in mice. *Microbes Infect*, **16(6)**: 512-517. <https://doi.org/10.1016/j.micinf.2014.02.011>
- Tanji, Y., Shimada, T., Yoichi, M., Miyana, K., Hori, K., & Unno, H. (2004). Toward rational control of *Escherichia coli* O157: H7 by a phage cocktail. *Applied Microbiology and Biotechnology*, **64(2)**: 270-274. <https://doi.org/https://doi.org/10.1007/s00253-003-1438-9>
- Temkin, E., Fallach, N., Almagor, J., Gladstone, B. P., Tacconelli, E., & Carmeli, Y. (2018). Estimating the number of infections caused by antibiotic-resistant *Escherichia coli* and *Klebsiella pneumoniae* in 2014: a modelling study. *Lancet Glob Health*, **6(9)**: e969-e979. [https://doi.org/10.1016/s2214-109x\(18\)30278-x](https://doi.org/10.1016/s2214-109x(18)30278-x)
- Thaden, J. T., Fowler, V. G., Sexton, D. J., & Anderson, D. J. (2016). Increasing Incidence of Extended-Spectrum beta-Lactamase-Producing *Escherichia coli* in Community Hospitals throughout the Southeastern United States. *Infect Control Hosp Epidemiol*, **37(1)**: 49-54. <https://doi.org/10.1017/ice.2015.239>
- Thomas, C., & Abelson, J. (1966). The isolation and characterization of DNA from bacteriophage. *Procedures in Nucleic Acid Research*, **1**: 553-561.
- Tibor, B., Roman, P., Ivana, M., Martin, B., Petr, P., Vladislava, R., Pavla, H., Varga, M., Helena, Ž., & Ivana, K. (2019). Lytic and genomic properties of spontaneous host-range Kayvirus mutants prove their suitability for upgrading phage therapeutics against *staphylococci*. *Scientific Reports*, **9(1)**: <https://doi.org/https://doi.org/10.1038/s41598-019-41868-w>
- Tiwari, B. R., Kim, S., Rahman, M., & Kim, J. (2011). Antibacterial efficacy of lytic *Pseudomonas* bacteriophage in normal and neutropenic mice models. *The Journal of Microbiology*, **49(6)**: 994-999. <https://doi.org/10.1007/s12275-011-1512-4>
- Trigo, G., Martins, T. G., Fraga, A. G., Longatto-Filho, A., Castro, A. G., Azeredo, J., & Pedrosa, J. (2013). Phage therapy is effective against infection by

- Mycobacterium ulcerans* in a murine footpad model. *PLoS Neglected Tropical Diseases*, **7(4)**: e2183. <https://doi.org/https://doi.org/10.1371/journal.pntd.0002183>
- Uhr, J. W., & Weissman, G. (1965). Intracellular Distribution and Degradation of Bacteriophage In Mammalian Tissues. *Journal of Immunology*, **94**: 544-550. <https://www.jimmunol.org/content/94/4/544.long>
- Van Belleghem, J. D., Dąbrowska, K., Vaneechoutte, M., Barr, J. J., & Bollyky, P. L. (2019). Interactions between bacteriophage, bacteria, and the mammalian immune system. *Viruses*, **11(1)**: 10. <https://doi.org/https://doi.org/10.3390/v11010010>
- Vandenheuvel, D., Lavigne, R., & Brüssow, H. (2015). Bacteriophage therapy: advances in formulation strategies and human clinical trials. *Annu Rev Virol*, **2(1)**: 599-618. <https://doi.org/https://doi.org/10.1146/annurev-virology-100114-054915>
- Veesler, D., & Cambillau, C. (2011). A common evolutionary origin for tailed-bacteriophage functional modules and bacterial machineries. *Microbiol Mol Biol Rev*, **75(3)**: 423-433, first page of table of contents. <https://doi.org/10.1128/mnbr.00014-11>
- Ventola, C. L. (2015). The antibiotic resistance crisis: part 1: causes and threats. *Pharmacy and therapeutics*, **40(4)**: 277-283.
- Verma, V., Harjai, K., & Chhibber, S. (2009). Characterization of a T7-like lytic bacteriophage of *Klebsiella pneumoniae* B5055: a potential therapeutic agent. *Curr Microbiol*, **59(3)**: 274-281. <https://doi.org/10.1007/s00284-009-9430-y>
- Vinodkumar, C. S., Kalsurmath, S., & Neelagund, Y. F. (2008). Utility of lytic bacteriophage in the treatment of multidrug-resistant *Pseudomonas aeruginosa* septicemia in mice. *Indian J Pathol Microbiol*, **51(3)**: 360-366. <https://doi.org/10.4103/0377-4929.42511>

- Wagenaar, J. A., Van Bergen, M. A., Mueller, M. A., Wassenaar, T. M., & Carlton, R. M. (2005). Phage therapy reduces *Campylobacter jejuni* colonization in broilers. *Vet Microbiol*, **109(3-4)**: 275-283. <https://doi.org/10.1016/j.vetmic.2005.06.002>
- Wahida, A., Tang, F., & Barr, J. J. (2021). Rethinking phage-bacteria-eukaryotic relationships and their influence on human health. *Cell Host & Microbe*, **29(5)**: 681–688. <https://doi.org/https://doi.org/10.1016/j.chom.2021.02.007>
- Walker, P. J., Siddell, S. G., Lefkowitz, E. J., Mushegian, A. R., Dempsey, D. M., Dutilh, B. E., Harrach, B., Harrison, R. L., Hendrickson, R. C., Junglen, S., Knowles, N. J., Kropinski, A. M., Krupovic, M., Kuhn, J. H., Nibert, M., Rubino, L., Sabanadzovic, S., Simmonds, P., Varsani, A., Zerbini, F. M., & Davison, A. J. (2019). Changes to virus taxonomy and the International Code of Virus Classification and Nomenclature ratified by the International Committee on Taxonomy of Viruses 2019. *Arch Virol*, **164(9)**: 2417-2429. <https://doi.org/10.1007/s00705-019-04306-w>
- Walter, M., Fiedler, C., Grassl, R., Biebl, M., Rachel, R., Hermo-Parrado, X. L., Llamas-Saiz, A. L., Seckler, R., Miller, S., & van Raaij, M. J. (2008). Structure of the Receptor-Binding Protein of Bacteriophage Det7: a Podoviral Tail Spike in a Myovirus. *Journal of Virology*, **82(5)**: 2265-2273. <https://doi.org/10.1128/JVI.01641-07>
- Wang, J. L., Kuo, C. F., Yeh, C. M., Chen, J. R., Cheng, M. F., & Hung, C. H. (2018). Efficacy of phikm18p phage therapy in a murine model of extensively drug-resistant *Acinetobacter baumannii* infection. *Infect Drug Resist*, **11**: 2301-2310. <https://doi.org/10.2147/idr.S179701>
- Wang, Z., Cai, R., Wang, G., Guo, Z., Liu, X., Guan, Y., Ji, Y., Zhang, H., Xi, H., Zhao, R., Bi, L., Liu, S., Yang, L., Feng, X., Sun, C., Lei, L., Han, W., & Gu, J. (2021). Combination Therapy of Phage vB_KpnM_P-KP2 and Gentamicin Combats Acute Pneumonia Caused by K47 Serotype *Klebsiella pneumoniae*. *Front Microbiol*, **12**: 674068. <https://doi.org/10.3389/fmicb.2021.674068>
- Wang, Z., Zheng, P., Ji, W., Fu, Q., Wang, H., Yan, Y., & Sun, J. (2016). SLPW: A Virulent Bacteriophage Targeting Methicillin-Resistant *Staphylococcus aureus*

In vitro and In vivo. *Front Microbiol*, **7**: 934. <https://doi.org/10.3389/fmicb.2016.00934>

Watanabe, R., Matsumoto, T., Sano, G., Ishii, Y., Tateda, K., Sumiyama, Y., Uchiyama, J., Sakurai, S., Matsuzaki, S., Imai, S., & Yamaguchi, K. (2007). Efficacy of bacteriophage therapy against gut-derived sepsis caused by *Pseudomonas aeruginosa* in mice. *Antimicrob Agents Chemother*, **51(2)**: 446-452. <https://doi.org/10.1128/aac.00635-06>

Wernicki, A., Nowaczek, A., & Urban-Chmiel, R. (2017). Bacteriophage therapy to combat bacterial infections in poultry. *Viol J*, **14(1)**: 179. <https://doi.org/10.1186/s12985-017-0849-7>

World Health Organization. (2017). *Prioritization of pathogens to guide discovery, research and development of new antibiotics for drug-resistant bacterial infections, including tuberculosis*. World Health Organization: Geneva (No. WHO/EMP/IAU/2017.12).

World Health Organization. (2019a). *Antibacterial agents in clinical development: an analysis of the antibacterial clinical development pipeline*. World Health Organization: Geneva. <https://apps.who.int/iris/handle/10665/330420>

World Health Organization. (2019b). *Antibacterial agents in preclinical development: an open access database* (No. WHO/EMP/IAU/2019.12). World Health Organization: Geneva. <https://apps.who.int/iris/handle/10665/330290>

Wienhold, S.-M., Lienau, J., & Witzentrath, M. (2019). Towards inhaled phage therapy in Western Europe. *Viruses*, **11(3)**: 295. <https://doi.org/https://doi.org/10.3390/v11030295>

Wittebole, X., De Roock, S., & Opal, S. M. (2014). A historical overview of bacteriophage therapy as an alternative to antibiotics for the treatment of bacterial pathogens. *Virulence*, **5(1)**: 226-235. <https://doi.org/10.4161/viru.25991>

Wolochow, H., Hildebrand, G. J., & Lamanna, C. (1966). Translocation of microorganisms across the intestinal wall of the rat: effect of microbial size and

concentration. *J Infect Dis*, **116(4)**: 523-528. <https://doi.org/10.1093/infdis/116.4.523>

Wright, A., Hawkins, C. H., Änggård, E. E., & Harper, D. R. (2009). A controlled clinical trial of a therapeutic bacteriophage preparation in chronic otitis due to antibiotic-resistant *Pseudomonas aeruginosa*; a preliminary report of efficacy. *Clinical otolaryngology : official journal of ENT-UK ; official journal of Netherlands Society for Oto-Rhino-Laryngology & Cervico-Facial Surgery*, **34(4)**: 349-357. <https://doi.org/https://doi.org/10.1111/j.1749-4486.2009.01973>

Wu, M., & Li, X. (2015). *Molecular medical microbiology*. Grand Forks, ND, Elsevier: Academic Press. <https://doi.org/https://doi.org/10.1016/B978-0-12-397169-2.00087-1>

Wu, Y., Wang, R., Xu, M., Liu, Y., Zhu, X., Qiu, J., Liu, Q., He, P., & Li, Q. (2019). A Novel Polysaccharide Depolymerase Encoded by the Phage SH-KP152226 Confers Specific Activity Against Multidrug-Resistant *Klebsiella pneumoniae* via Biofilm Degradation. *Front Microbiol*, **10**: 2768. <https://doi.org/10.3389/fmicb.2019.02768>

Xu, J., & Xiang, Y. (2017). Membrane Penetration by Bacterial Viruses. *J Virol*, **91(13)**: e00162-17. <https://doi.org/10.1128/JVI.00162-17>

Yam, E. L. Y., Hsu, L. Y., Yap, E. P.-H., Yeo, T. W., Lee, V., Schlundt, J., Lwin, M. O., Limmathurotsakul, D., Jit, M., Dedon, P., Turner, P., & Wilder-Smith, A. (2019). Antimicrobial Resistance in the Asia Pacific region: a meeting report. *Antimicrobial Resistance & Infection Control*, **8(1)**: 202. <https://doi.org/10.1186/s13756-019-0654-8>

Yin, J. (1993). Evolution of bacteriophage T7 in a growing plaque. *J Bacteriol*, **175(5)**: 1272-1277. <https://doi.org/10.1128/jb.175.5.1272-1277.1993>

Yin, S., Huang, G., Zhang, Y., Jiang, B., Yang, Z., Dong, Z., You, B., Yuan, Z., Hu, F., Zhao, Y., & Peng, Y. (2017). Phage Abp1 Rescues Human Cells and Mice from Infection by Pan-Drug Resistant *Acinetobacter Baumannii*. *Cell Physiol Biochem*, **44(6)**: 2337-2345. <https://doi.org/10.1159/000486117>

- Yosef, I., Goren, M. G., Globus, R., Molshanski-Mor, S., & Qimron, U. (2017). Extending the host range of bacteriophage particles for DNA transduction. *Molecular Cell*, **66(5)**: 721-728. e723.
- You, L., Suthers, P. F., & Yin, J. (2002). Effects of *Escherichia coli* physiology on growth of phage T7 in vivo and in silico. *J Bacteriol*, **184(7)**: 1888-1894. <https://doi.org/10.1128/jb.184.7.1888-1894.2002>
- Young, R. (1992). Bacteriophage lysis: mechanism and regulation. *Microbiol Rev*, **56(3)**: 430-481.
- Young, R. (2014). Phage lysis: Three steps, three choices, one outcome. *Journal of Microbiology*, **52(3)**: 243-258. <https://doi.org/10.1007/s12275-014-4087-z>
- Young, R., & Gill, J. J. (2015). Phage therapy redux—What is to be done? *Science*, **350(6265)**: 1163-1164. <https://doi.org/https://doi.org/10.1126/science.aad6791>
- Zhao, J., Zhang, Z., Tian, C., Chen, X., Hu, L., Wei, X., Li, H., Lin, W., Jiang, A., & Feng, R. (2019). Characterizing the biology of lytic bacteriophage vB_EaeM_φEap-3 infecting multidrug-resistant *Enterobacter aerogenes*. *Frontiers in Microbiology*, **10**: 420. <https://doi.org/https://doi.org/10.3389/fmicb.2019.00420>
- Zhen, X., Lundborg, C. S., Sun, X., Hu, X., & Dong, H. (2019). Economic burden of antibiotic resistance in ESKAPE organisms: a systematic review. *Antimicrob Resist Infect Control*, **8**: 137. <https://doi.org/10.1186/s13756-019-0590-7>
- Zurabov, F., & Zhilenkov, E. (2021). Characterization of four virulent *Klebsiella pneumoniae* bacteriophages, and evaluation of their potential use in complex phage preparation. *Virology Journal*, **18(1)**: 9. <https://doi.org/10.1186/s12985-020-01485-w>

APPENDIX -A

Media, Reagents, and procedures

1. Luria Bertani (LB) broth (Hi-Media India)

<u>Ingredients</u>	<u>Gram/L</u>
Casein enzymic hydrolysate	10.0
Yeast extract	5.0
Sodium chloride	10.0
Final pH (at 25°C) 7.5 ± 0.2	

2. LB broth agar

1.5% Bacto-agar to LB broth (HiMedia India)

3. Minimal Media (5X) (HiMedia India)

<u>Ingredients</u>	<u>Gram/L</u>
Potassium dihydrogen phosphate	33.9
Disodium hydrogen phosphate	15.0
Sodium chloride	2.5
Ammonium chloride	5.0

4. Tryptic Soy Broth (TSB)/Soybean-Casein Digest Medium (HiMedia India)

<u>Ingredients</u>	<u>Grams / L</u>
Pancreatic digest of casein	17.000
Papaic digest of soya bean meal	3.000
Sodium chloride	5.000
Dextrose	2.500
Dibasic potassium phosphate	2.500
Final pH (at 25°C)	7.3±0.2

5. Nutrient Broth/Agar (NB/NA) (HiMedia India)

Ingredients	Grams / L
Peptone	10.0
Beef extract	10.0
Sodium chloride	5.0
pH (after sterilization)	7.3±0.1

6. Super Optimal Broth (SOB) medium

2.0% (w/v) tryptone

0.5% (w/v) yeast extract

0.5% (w/w) NaCl

10 mM MgCl₂(1M stock)

2.5 mM KCl (1M stock)

10 mM MgSO₄(1M stock)

Add tryptone, yeast, and NaCl, make up the volume to 1.0 L with Milli-Q water and autoclave, and then add filter sterilized.

7. Super optimal broth with catabolites repression (SOC) medium

20 mM glucose added to a final concentration to the sterilized SOB medium

8. Chloramphenicol

25 mg/ml stock

250 mg of chloramphenicol (≥98%) powder added to 10 ml 100% ethanol. Store at -20°C.

9. Agrose Gel Electrophoresis

0.5 x TBE Buffer

45 mM Tris-HCl

45 mM Boric Acid

1.0 mM Na₂EDTA

10. Blue Loading Dye: 1.0 mg/mL Bromophenol blue in 20% Glycerol

11. Running buffer/Electrolysis buffer preparation: For 1000ml: pH8.4

S. No.	Constituents	Amount
i.	39mM Tris	4.724g
ii.	48mM Glycine	3.603g
iii.	0.1% SDS	0.37g

12. Reagents of Sodium dodecyl gel electrophoresis

Solution components	Resolving gel (12%)	Stacking gel (5%)
	Solution final volume: 10 ml	Solution final volume: 2.0 ml
TDW	3.3 ml	1.4 ml
30% Acrylamide	4.0 ml	0.33 ml
1.5% Tris (pH 8.8)	2.5ml	0.25 ml
10% SDS	0.1ml	0.02 ml
10% Ammonium persulfate (NH ₄) ₂ S ₂ O ₈	0.1ml	0.02 ml
TEMED	0.004 ml	0.002 ml

13. 30% Acrylamide solution

S.No.	Constituents	Amount
1	Acrylamide; C ₃ H ₅ NO: MW=71.08	29.0 g
2	Bis-Acrylamide (N, N Methylene Bisacrylamide); C ₇ H ₁₀ N ₂ O ₂ : MW=154.17	1.0 g
3	TDW	Maintain up to 100ml

14. Tris Buffer

Lower Tris buffer for 100ml (pH 8.8)			Upper Tris buffer for 50ml (pH 6.8)		
SN.	Constituents	Amount	SN.	Constituents	Amount
1	Tris (Tris base)	1.5M /18.17g	1	Tris (Tris base)	0.5M/3.03g
2	TDW	Maintain 100ml	2	TDW	Maintain 50ml

15. Loading sample buffer: pH 6.8 for 10ml

S.No.	Constituents	Amount
I.	Upper Tris pH 6.8	1.25 ml
II.	10% SDS	3.0 ml
III.	Glycerol	4.75 ml
IV.	Beta-mercaptoethanol	0.5 ml
V.	0.1% Bromophenol Blue	0.5 ml

16. Staining solution: Comassie Brilliant Blue G-250 (CBB G-250) for 500ml

S. No.	Constituents	Amount
i.	Comassie Brilliant Blue G-250	500 mg
ii.	Glacial acetic acid	25 ml
iii.	Methanol	250 ml
iv.	DW	225 ml

17. De-stain solution preparation: For 500ml

S.No.	Constituents	Amounts
i.	7.5% Glacial acetic acid	37.5 ml
ii.	5% Methanol	25 ml
iii.	DW	437.5 ml

18. Silver staining

A. Fixing solution

7.5% (v/v) glacial acetic acid

25% (v/v) propanol

B. Oxidizing solution

0.7% (w/v) periodic acid

7.5% (v/v) glacial acetic acid

C. Silver staining solution

0.0187 M NaOH

1.3% (v/v) NH₄OH

0.67% (w/v) AgNO₃

D. Developer solution

0.0222% (v/v) formaldehyde

0.005% (w/v) citric acid

E. Stop solution

1% (v/v) glacial acetic acid

19. Making Electrocompetent *E. coli* Cells (MG1655)

1. Grow an overnight culture of each strain in LB medium.
2. Prepare 25 ml of fresh LB medium in a 250 ml flask.
3. Inoculate with 100 μ l of the overnight, stationary-phase culture.
4. Grow the cells for approximately 2-3 hours, until they reach the mid-exponential phase. (OD₆₀₀ of ~0.8-1.0).
5. Transfer the cells to 15 ml Falcon conical tubes.
6. Pellet the cells by centrifugation for 5 minutes at 8,000 RPM at 4°C. Remove promptly and pour off supernatant.

7. Wash by adding 25 ml of chilled distilled water to each tube, then resuspend the pellet with a 1 ml pipette. Centrifuge for 5 minutes. Remove promptly and pour off supernatant. Repeat for at least four wash cycles with 10ml water.
8. Resuspend in approximately 100-200 μ l of d water.
9. Divide into 50 μ l aliquots in 1.7 ml tubes. Freeze or proceed directly to electroporation.

20. Transforming *E. coli* Cells by Electroporation

1. Place the electrocompetent cells on ice.
2. To the electrocompetent cells, add 1-3 μ l of DNA (<100 ng of DNA).
3. Mix by gently flicking the tube containing the electrocompetent cell + DNA mixture. Let the mixture sit on ice for 1-10 minutes.
4. Pipette the mixture into a chilled electroporation cuvette, making sure that the mixture is at the bottom of the cuvette by gently tapping the cuvette on a flat surface. (Be sure to wipe any condensation off the sides of the cuvette before electroporation)
5. Place the cuvette in the pulser and press the "Pulse" button. (*E. coli* cells, the Ec 1 / bacteria setting is fine).
6. After electroporation, add 1000 μ l of SOC media to the cuvette to recover the cells.
7. Transfer the mixture to a 1.5 mL microcentrifuge tube.
8. Incubate for ~30-60 minutes at 37°C in a shaking incubator.
9. Plate the cells (~ 50 μ l) on an LB plate containing the appropriate antibiotic.
10. Incubate overnight at 37°C or other appropriate temperature.

21. Depolymerase enzyme (gp53 of ϕ Kp Pokalde 001) extraction protocol

11. Positive clones were cultured in 25 ml LB media with 25mg/ml chloramphenicol at 37°C in the water bath (agitation at 200 rpm)

12. When OD_{600nm} reached to 0.3, a 250µl of 20% Arabinose was added and further incubated until the OD_{600nm} reached to 1.0
13. The culture was centrifuged at 8,600rpm for 10 min (4°C) and the pellet was collected.
14. Two milliliters of Tris buffer were added to the pellet to resuspend it.
15. The suspension was sonicated for 5 seconds (three times repeated) in cold.
16. Supernatant was collected by centrifuging 13000rpm at 4°C for 10 min
17. Supernatant solution containing hydrolase enzyme was stored at -20°C

22. Protein purification by HisTrap™ HP (GE Healthcare)

A. Buffer Preparation:

a. Binding/Wash buffer:

20 mM sodium phosphate

12gm Na₂HPO₄ + 100mlDW = 1M Na₂HPO₄ (stock)

2ml stock +98ml DW= 20mM Na₂HPO₄

0.5 M NaCl

10ml stock (5M NaCl, ready-made) + 90 ml DW

10 mM imidazole, pH 7.4

7gm imidazole + 100 ml DW = 1M imidazole (stock)

1ml stock + 97ml DW (pH adjusted to 7.4)

b. Elution buffer: 20 mM sodium phosphate, 0.5 M NaCl, 300 mM imidazole, pH 7.4. Filter buffers through a 0.22 µm or a 0.45 µm filter before use.

23. Sample preparation

1. Positive clone in the pBAD33 vector is grown in LB 250ml with 250 ul of 50mg/ml chloramphenicol at 37°C, 250 RPM in the shaking water bath.
2. When OD₆₀₀ reached to 0.3, 2.5ml 20% Arabinose was added and continued incubation till OD₆₀₀ reached to 1.0

3. The culture was centrifuged at 8,600rpm for 10 min (4°C) and the pellet was washed with PBS and resuspended with 10ml PBS and mixed with 10% glycerol.
4. Protease inhibitor cocktail (Roche) was added (1 tab for 20ml).
5. The suspension was French pressed at 1000 PSI two/three times
6. Supernatant was collected by centrifuging 13000rpm at 4°C for 10 min
7. Supernatant solution containing hydrolase enzyme was filter sterilized with 0.22 µm syringe filter and stored at -20°C
8. The supernatant was ultracentrifuged at 24000 rpm for 30 min.
9. Supernatant was taken and mixed with an equal volume of 2x binding buffer and kept at 4C.

24. Enzyme purification by HisTrap™ HP, 5ml column (Small scale)

1. The column was washed with 25ml distilled water to remove the ethanol.
2. The column was equilibrated with a 25 ml binding buffer (5 ml/min flow rate).
3. Pretreated sample with the binding buffer was passed through the column with a flow rate of 0.5 to 5 ml/min.
4. The column was washed with 50ml binding buffer with a flow rate of 5 to 10 ml/min.
5. The enzyme was eluted with 20ml elution buffer using a one-step or linear gradient. (Initial 4ml and last 5ml discarded and middle portion was collected as a fraction of 1ml for up to 15 ml) Maintaining a flow rate of 5 to 10 ml/min.
6. After elution, the column was washed with 25ml of binding buffer. The column is now ready for a new purification.

25. Enzyme purification by Size-exclusion chromatography (Ni Sepharose 6 Fast Flow, AKTA)

1. 5ml Nickel resin (Ni Sepharose 6 Fast Flow) was added to the gravity flow column and washed with 50 ml D water and equilibrated with 50 ml binding buffer.
2. Nickel resin was removed from the column and mixed with the pretreated sample and placed on the orbital shaking at 4C for 2 hrs.
3. The resin was transferred into the column and flow-through was collected and re-passed again and flow-through was then discarded.
4. The column was washed with 50ml binding buffer with 5mM imidazole.
5. The column was washed again with 50ml binding buffer with 10mM imidazole
6. Flow tap was closed and 5ml elution buffer with 500mM imidazole was added into the column and put on the rocker for 10 min.
7. Purified protein was collected as elution flow-through (5ml) the first fraction in (A1A2A3A4A5 1 ml each)
8. Four more fractions were collected by adding binding buffer into the column (3ml each time) B1B2B3, c1c2cc3, d1d2d3d4d5, and E 5ml.
9. All fractions were tested for the activities of Depolymerase by spot test on the host lawn and the protein concentrations were measured on the Nanodrop.
10. All fractions were checked for purity of the protein by SDS-PAGE and pure fraction was dialyzed. (Dialysis buffer: 20mM Tris HCL pH 7.5, 150 mM NaCl, 1.0 mM BME)

26. Native gel electrophoresis of phage depolymerase (gp53)

Separating Gel Preparation 10%

S. No.	Constituents	Amount
i.	D Water	2.0 ml

ii.	29: acrylamide/bisacrylamide (30% acrylamide)	3.5ml
iii.	Tris-Cl (3M pH 8.5)	3.3 ml
iv.	Glycerol	1.3ml
v.	10% ammonium persulfate	40 μ l
vi.	TEMED	30 μ l

Stacking Gel (2.89%)

S. No.	Constituents	Amount
i.	D water	3.0 ml
ii.	29: acrylamide/bisacrylamide (30% acrylamide)	700 μ l
iii.	Tris-Cl (3M pH 8.5)	1.24 ml
iv.	10% ammonium persulfate	40 μ l
v.	TEMED	15 μ l

Sample loading buffer

S. No.	Constituents	Amount
i.	0.5M Tris-Cl (pH 8.5)	1.0 ml
ii.	Glycerol (100%)	2.0 ml
iii.	Bromophenol blue (0.1%)	1.0 ml
iv.	D water	4.0 ml

Running buffer (10x)

S. No.	Constituents	Amount
i.	Tris base	15gm
ii.	Glycine	72.9 gm
iii.	D water	Up to 500ml
	pH	8.5

Working running buffer: Dilute 10x buffer to 1:10 with d water

Native gel electrophoresis of phage depolymerase (gp53) protocol

1. Thoroughly clean and dry the glass/plastic disposable plates and assemble them with bulldog clips. Clamp the chamber in an upright, level position.
2. Prepare 10 ml Separating Gel Mixture as above.
3. Mix gently and use immediately (because polymerization starts when the TEMED is added). Carefully pour the freshly mixed solution into the chamber without generating air bubbles. Pour to a level about 1 cm below where the bottom of the well-forming comb will come when it is in position.
4. Carefully overlayer the 80% isopropyl alcohol without mixing to eliminate oxygen and generate a flat top to the gel.
5. Polymerize the acrylamide for 1 hour.
6. Prepare the 4 ml Stacking Gel Solution as above.
7. Mix gently and use immediately. Pour off the 80% isopropyl alcohol from the polymerized Separating Gel, wash the gel top with water, and fill the gap remaining in the chamber with the Stacking Gel mixture.
8. Insert the comb and let it for polymerization of the acrylamide for 1 hour.
9. When the Stacking Gel has polymerized, remove the comb without distorting the shapes of the well. Remove the clips holding the plates together and install the gel in the apparatus.
10. Fill apparatus with Reservoir Buffer. Push out the bottom spacer from the gel and remove bubbles from both the top and underneath of the gel. Use the gel immediately.
11. While the gel is polymerizing, prepare samples for electrophoresis
12. Dissolve the protein sample solution in the same volume of 2 X Sample loading Buffer. (The concentration of the sample in the solution should be such as to give enough protein in a volume not greater than the size of the sample well. The bromophenol blue dye in Sample Buffer indicates when the sample solution is acidic by turning yellow. If this happens, add a little NaOH, enough to just turn blue).

13. Load the gel with 20 ul Sample Solution by pipet.
14. Start electrophoresis immediately by turning on the power. Initial voltage adjusted to 60V. When the sample entered the separating gel, the voltage increased to 110V and wait until the sample reach the bottom.
15. Remove the gel from between the glass plates and stain with SYPRO Ruby stain

Staining procedure for SYPRO Ruby stain

1. Gel was first washed in ultrapure water
2. Gel was placed in a clean container with 100 ml of fix solution (50% methanol, 7% acetic acid) and agitated on an orbital shaker for 45 mins.
3. Repeated step 2 once more with 100ml of fix solution and poured off the fix solution
4. Added 60 ml of SYPRO Ruby (Invitrogen) and agitated overnight on an orbital shaker
5. Decanted the stain for disposal and added 100 ml of wash solution (10% methanol and 7% acetic acid) and agitated for 45 mins on an orbital shaker.
6. Gel was then rinsed with ultrapure water two times for 5 minutes
7. Image was taken using a UV transilluminator.

APPENDIX-B

Ethical approval



Government of Nepal
Nepal Health Research Council (NHRC)



Ref. No.: 2682

11 May 2018

Mr. Guna Raj Dhungana
Principal Investigator
Central Department of Biotechnology
Kritipur, Kathmandu

Ref: **Approval of thesis proposal** entitled **Molecular characterization of lytic bacteriophage specific to multidrug resistant bacteria and pharmacokinetics of phage in biological model**

Dear Mr. Dhungana,

It is my pleasure to inform you that the above-mentioned proposal submitted on **23 March 2018 (Reg. no. 161/2018)** please use this Reg. No. during further correspondence) has been approved by Nepal Health Research Council (NHRC) Ethical Review Board on **9 May 2018**.

As per NHRC rules and regulations, the investigator has to strictly follow the protocol stipulated in the proposal. Any change in objective(s), problem statement, research question or hypothesis, methodology, implementation procedure, data management and budget that may be necessary in course of the implementation of the research proposal can only be made so and implemented after prior approval from this council. Thus, it is compulsory to submit the detail of such changes intended or desired with justification prior to actual change in the protocol. Expiration date of this proposal is **December 2019**.

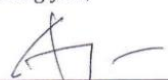
If the researcher requires transfer of the bio samples to other countries, the investigator should apply to the NHRC for the permission. The researchers will not be allowed to ship any raw/crude human biomaterial outside the country; only extracted and amplified samples can be taken to labs outside of Nepal for further study, as per the protocol submitted and approved by the NHRC. The remaining samples of the lab should be destroyed as per standard operating procedure, the process documented, and the NHRC informed.

Further, the researchers are directed to strictly abide by the National Ethical Guidelines published by NHRC during the implementation of their project proposal and **submit progress report in between and full or summary report upon completion**.

As per your thesis proposal, the total research amount is **NRs 4,95,000** and accordingly the processing fee amounts to **NRs 1,000**. It is acknowledged that the above-mentioned processing fee has been received at NHRC.

If you have any questions, please contact the Ethical Review M & E Section at NHRC.

Thanking you,


Prof. Dr. Anjani Kumar Jha
Executive Chairperson

APPENDIX-C

Identification of host bacteria using Bruker MALDI Biotyper

Run Identifier: 191104-1209-1341000369

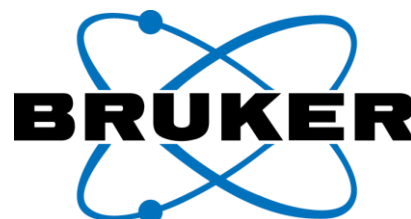
Run Creation Date/Time: 2019-11-04T12:25:19.008

Bruker MALDI

Biotyper

Identification

Results



Run Info:

Run Identifier: 191104-1209-1341000369

Operator: tof-user@FLEX-SMART

Run Creation Date/Time: 2019 11-04T12:25:19.008

Number of Tests: 25

Type: Standard

BTS-QC: passed

BTS-QC Position: C12:0

Instrument ID: 8604832.03188

Server Version: 4.1.90 (PYTH) 125 2018-09-253_08-10-24

Result Overview

SampleName	Sample ID	Organism (best match)	Score Value	Organism (second-bestmatch)	Score Value
C4 (+++) (A)	Escherichia coli M1 (standard)	Escherichia coli	2.51	Escherichia coli	2.50
C6 (+++) (A)	Klebsiella	Klebsiella	2.51	Klebsiella pneumoniae	2.43

	pneumoniae TUKp1 (standard)	pneumoniae			
C7 (+++)(A)	Klebsiella pneumoniae Kp56 (standard)	Klebsiella pneumoniae	2.57	Klebsiella pneumoniae	2.47
SampleName	Sample ID	Organism (best match)	Score Value	Organism (second-best match)	Score Value
C8 (+++)(A)	Escherichia coli M3 (standard)	Escherichia coli	2.55	Escherichia coli	2.50
C9 (+++)(A)	Escherichia coli M2 (standard)	Escherichia coli	2.55	Escherichia coli	2.52
C11 (-)(C)	NEG (standard)	No Organism Identification Possible	1.54	No Organism Identification Possible	1.46

Meaning of Score Values

Range	Interpretation	Symbols	Color
2.00 - 3.00	High-confidence identification	(+++)	Green
1.70 - 1.99	Low-confidence identification	(+)	Yellow
0.00 - 1.69	No Organism Identification Possible	(-)	Red

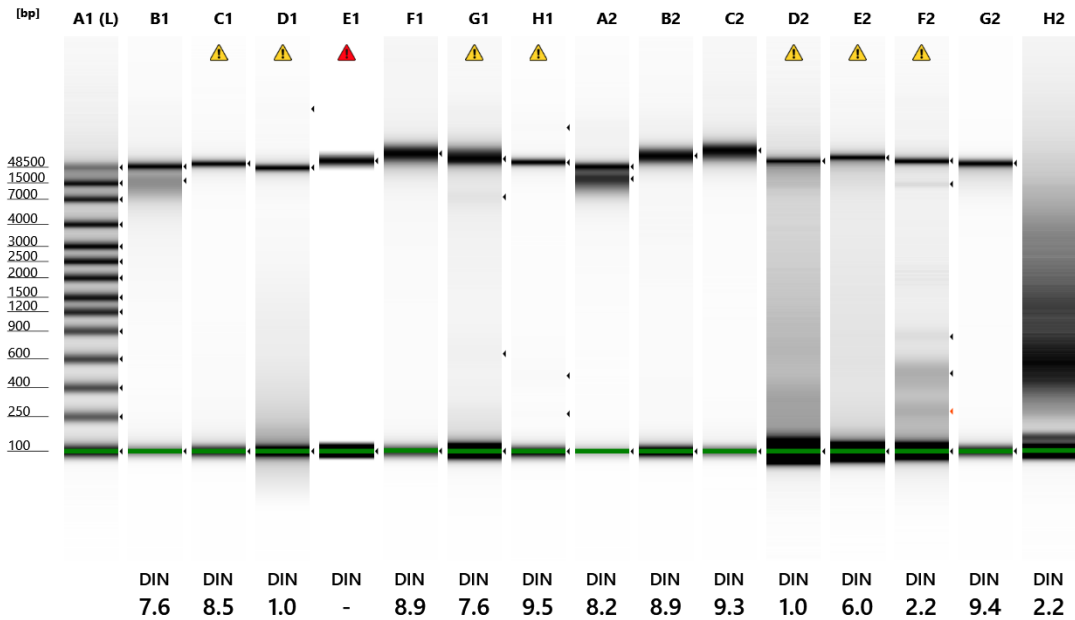
Meaning of Consistency Categories (A-C)

Category	Interpretation
(A)	High consistency: The best match is a high-confidence identification. The second-best match is (1) a high-confidence identification in which the species is identical to the best match, (2) a low-confidence identification in which the species or genus is identical to the best match, or (3) a non-identification.
(B)	Low consistency: The requirements for high consistency are not met. The best match is a high- or low-confidence identification. The second-best match is (1) a high- or low-confidence identification in which the genus is identical to the best match or (2) a non-identification.
(C)	No consistency: The requirements for high or low consistency are not met.

APPENDIX-C

Phage Genome Sequencing Data

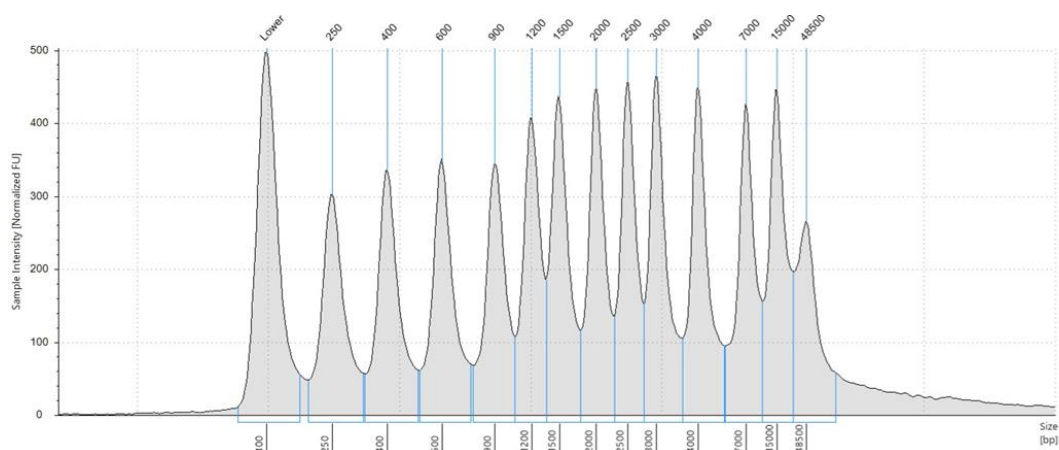
Filename: 2019-10-15 - 13.49.17. GDNA



Default image (Contrast 50%), Image is Scaled to Sample

Well	DIN	Conc. [ng/μl]	Sample Description	Observations
A1	-	77.9	Ladder	Ladder
B1	7.6	39.3	1_Pokalde_001	
C1	8.5	9.99	2_K27	Sample concentration outside recommended range
D1	1.0	9.51	3_K57	Sample concentration outside recommended range
E1	-	2.74	4_A1	Sample concentration outside the functional range for
F1	8.9	27.9	5_A4	
G1	7.6	8.79	6_Makalu_001	Sample concentration outside recommended range
H1	9.5	7.96	7_Pokalde_002	Sample concentration outside recommended range
A2	8.2	73.5	8_P4	
B2	8.9	15.2	9_Makalu_002	
C2	9.3	37.3	10Makalu_003	
D2	1.0	4.27	11_1107	Sample concentration outside the functional range for
E2	6.0	5.90	12_1151	Sample concentration outside recommended range
F2	2.2	7.80	13_1195	Sample concentration outside recommended range

A1: Ladder



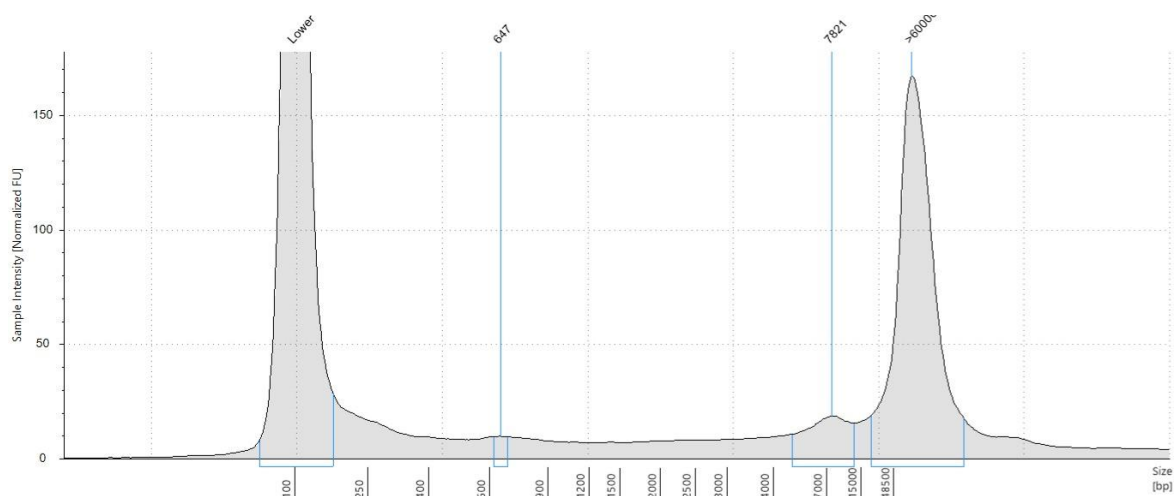
Sample Table

Well	DIN	Conc. [ng/μl]	Sample Description	Alert	Observations
A1	-	77.9	Ladder		Ladder

Peak Table

Size [bp]	Calibrated Conc.	Assigned Conc.	% Integrated Area	From [bp]	To [bp]	Observations
100	8.50	8.50	-	67	159	Lower Marker
250	5.38	-	7.21	179	326	
400	5.67	-	7.60	329	503	
600	5.80	-	7.77	507	749	
900	5.35	-	7.17	762	1054	
1200	5.53	-	7.41	1054	1348	
1500	6.17	-	8.27	1348	1773	
2000	5.86	-	7.86	1773	2275	
2500	5.68	-	7.61	2275	2781	
3000	6.26	-	8.39	2781	3595	
4000	6.10	-	8.17	3595	5442	
7000	5.63	-	7.54	5518	10552	
15000	5.92	-	7.93	10552	22622	
48500	4.50	-	6.03	22622	>60000	
-	-	-	-	-	-	Sample Well

B1: 1_Pokalde_001



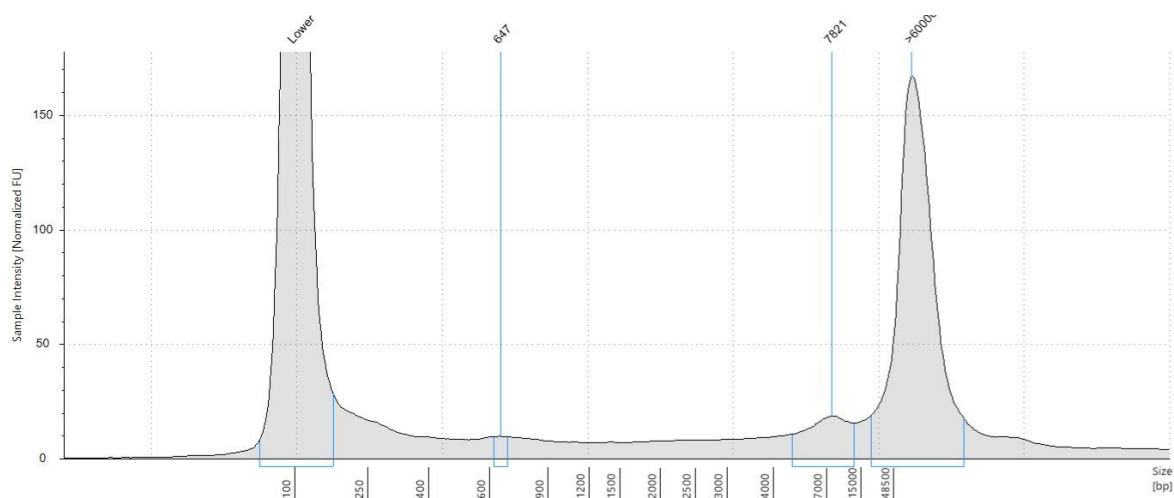
Sample Table

Well	DIN	Conc. [ng/μl]	Sample Description	Alert	Observations
B1	7	39.3	Pokalde_001		

Peak Table

Size [bp]	Calibrated Conc. [ng/μl]	Assigned Conc. [ng/μl]	% Integrated Area	From [bp]	To [bp]	Peak Comment	Observations
100	8.50	8.50	-	66	166		Lower Marker
16896	14.9	-	52.70	5299	23195		
50636	13.0	-	45.75	23195	>60000		
-	-	-	-	-	-		Sample Well

G1: 6_ Makalu_001



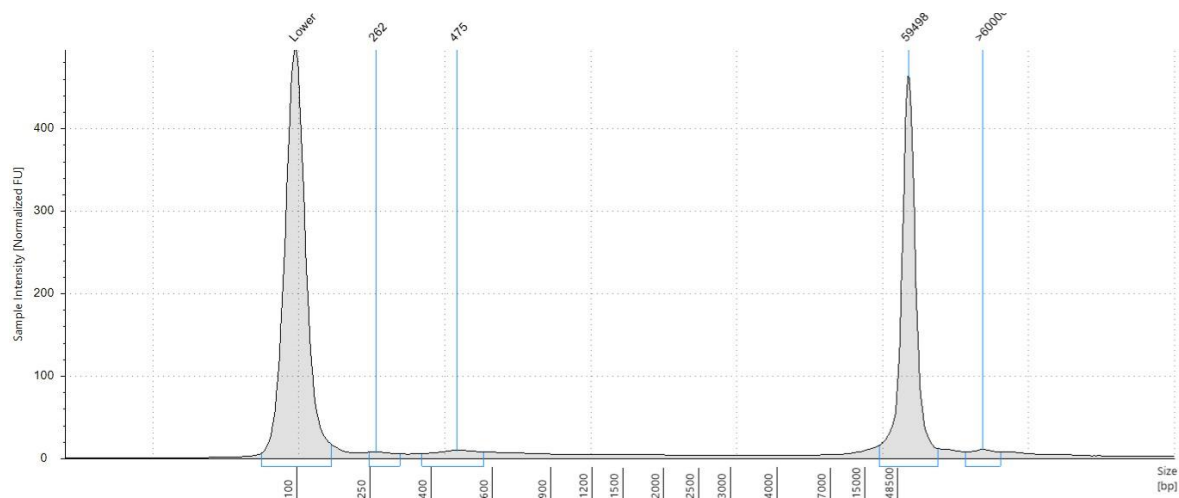
Sample Table

Well	DIN	Conc. [ng/μl]	Sample Description	Alert	Observations
G1	7.6	8.79	6_ Makalu_001	⚠	Sample concentration outside recommended range

Peak Table

Size [bp]	Calibrated Conc. [ng/μl]	Assigned Conc. [ng/μl]	% Integrated Area	From [bp]	To [bp]	Peak Comment	Observations
100	8.50	8.50	-	64	161		Lower
647	0.0874	-	1.54	616	679		
7821	0.581	-	10.28	4868	12873		
>60000	4.40	-	77.83	18705	>60000		
-	-	-	-	-	-		Sample Well

H1: 7_Pokalde_002



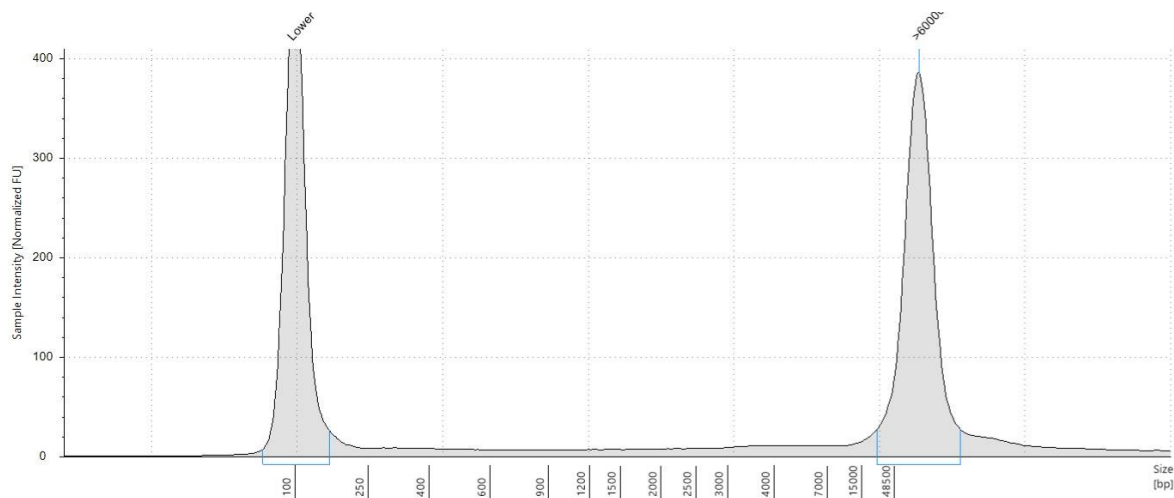
Sample Table

Well	DIN	Conc. [ng/μl]	Sample Description	Alert	Observations
H1	9.5	7.96	7_ Pokalde_002	⚠	Sample concentration outside recommended range

Peak Table

Size [bp]	Calibrated Conc. [ng/μl]	Assigned Conc. [ng/μl]	% Integrated Area	From [bp]	To [bp]	Peak Comment	Observations
100	8.50	8.50	-	65	155		Lower Marker
262	0.128	-	2.07	248	315		
475	0.309	-	5.01	374	566		
59498	5.35	-	86.84	20826	>60000		
>60000	0.200	-	3.25	>60000	>60000		
-	-	-	-	-	-		Sample Well

B2: 9_Makalu_002



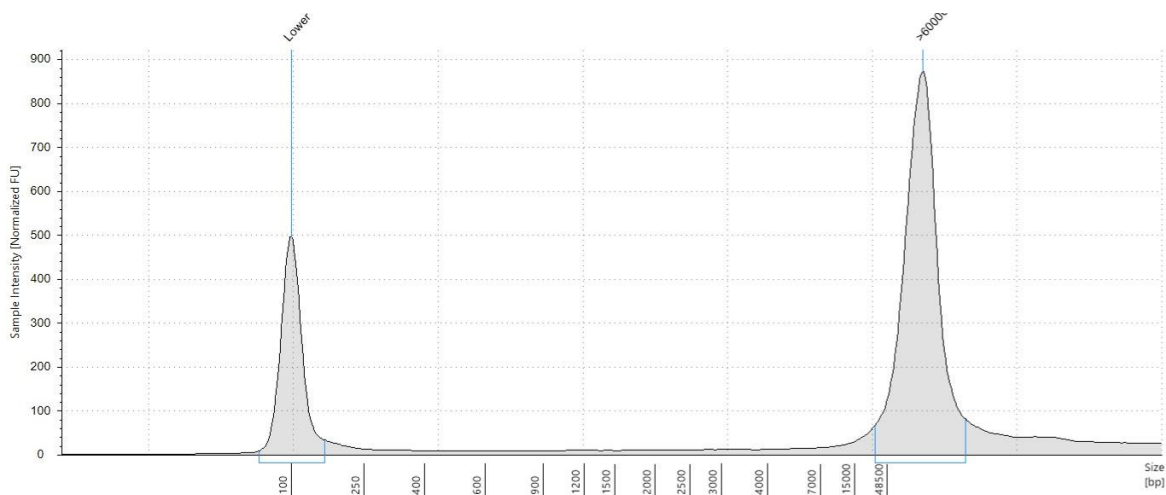
Sample Table

Well	DIN	Conc. [ng/μl]	Sample Description	Alert	Observations
B2	8.9	15.2	9_Makalu_002		

Peak Table

Size [bp]	Calibrated Conc. [ng/μl]	Assigned Conc. [ng/μl]	% Integrated Area	From [bp]	To [bp]	Peak Comment	Observations
100	8.50	8.50	-	67	154		Lower Marker
>60000	9.37	-	89.93	21221	>60000		
-	-	-	-	-	-		Sample Well

C2: 10_Makalu_003



Sample Table

Well	DIN	Conc. [ng/μl]	Sample Description	Alert	Observations
C2	9.3	37.3	10_Makalu_003		

Peak Table

Size [bp]	Calibrated Conc. [ng/μl]	Assigned Conc. [ng/μl]	% Integrated Area	From [bp]	To [bp]	Peak Comment	Observations
100	8.50	8.50	-	67	152		Lower Marker
>60000	23.7	-	86.09	24114	>60000		
	-	-	-	-	-		Sample Well

Genomic DNA ScreenTape®

TapeStation Analysis Software A.02.02 (SR1)

© Agilent Technologies, Inc. 2017

Generated: 15-Oct-2019

APPENDIX -D

NCBI GenBank Submission Records

1. NCBI, Sequence Read Archive (SRA) submission

Following GenBank entries for the Sequence Read Archive (SRA) can be retrieved from the National Center for Biotechnology Information (NCBI) using the link provided below:

<https://www.ncbi.nlm.nih.gov/sra/SRR10671636>

<https://www.ncbi.nlm.nih.gov/bioproject/PRJNA594990>

<https://www.ncbi.nlm.nih.gov/nuccore/2054245216>

<https://www.ncbi.nlm.nih.gov/nuccore/1846462340>

<https://www.ncbi.nlm.nih.gov/nuccore/1799108746>

<https://www.ncbi.nlm.nih.gov/nuccore/1780545396>

<https://www.ncbi.nlm.nih.gov/nuccore/1799108472>

2. NCBI GenBank Nucleotide sequence submission records

Following GenBank records for individual phage genome nucleotide sequences can be retrieved from the National Center for Biotechnology Information (NCBI) using the link provided below:

a) Escherichia virus Ec_Makalu_001, complete genome, GenBank: MN894885.1

b) Escherichia virus Ec_Makalu_002, complete genome, GenBank: MN709127.1

c) Escherichia virus Ec_Makalu_003, complete genome, GenBank: MN882349.1

d) Klebsiella phage Kp_Pokalde_001, complete genome, GenBank: MW590329.1

e) Klebsiella phage Kp_Pokalde_002, complete genome, GenBank: MT425185.1

APPENDIX-E

List of Primers

Primer No	Primer name	Sequences
	Genome closure PCR	
GD1	Ec_Makalu_001 F	TCGAAAGGTGTTGTCGTGTCTG
GD2	Ec_Makalu_001 R	TCTACCTCTATGCAGTTTGACAAGTG
GD3	Ec_Makalu_002 F	GCGATTGATGCTATTCAAATGCAG
GD4	Ec_Makalu_002 R	CCGATAATCTCTTTTAGACCGGACG
GD5	Ec_Makalu_003 F	TGCATCCTTCCAAACTTTCCTTG
GD6	Ec_Makalu_003R	TAAAGGGACACCAGATTGTAACCG
GD21	Kp_Pokalde_001 F	AGTGCTCTATCCTGGTCACTGAG
GD22	Kp_Pokalde_001 R	TCTGTGCGTTAGAAGTGCAGCAC
GD23	Kp_Pokalde_001(seq) F	TGCTGCTAGTCGTACCGTTAG
GD24	Kp_Pokalde_001 (seq) R	GTACCCGCTATAGCTACTGAC
GD17	Kp_Pokalde_002 F	TTTCTGCCGGATGCACCAAG
GD18	Kp_Pokalde_002 R	TGCGTTCATTGTGTGCCTCTTTG
GD19	Kp_Pokalde_002 (seq) F	GAGACGCACGAGCATTATGC
GD20	Kp_Pokalde_002 (seq) R	TTGTTCGATTGGCAACGGCTTG
	For termini end detection Primer	
GD31	Pok_001 Term F	TGA CGG AGA TTT GCG CTT CAC
GD32	Pok_001 Term R	TAG CGC TGG GAT AGT GGA TGT G
GD33	Pok_002 Term F	TTA CTG CGC CAT AGG ACT ACT TGG
GD34	Pok_002 Term R	ATG TCC GGT TGA TGA CTA CTT GAG
	For cloning (pokalde_001)	
GD09	Pok_tsFL-Vec-For	GCACTTCCACCATCACCATCACCATTAAATTAAT CAGAACGCAGAAGC
GD10	Pok_tsFL-Vec-Rev	GTGTCCCCTCTTATCGTTTCGGTACCGAGCTCGAAT TCGC
GD11	Pok_tsFL-Histag-For	GCGAATTCGAGCTCGGTACCGAAACGATAAGAGG GGACACATGG

GD12	Pok_tsFL-Histag-Rev	AATTTAATGGTGATGGTGATGGTGGAAGTGCAGCA CCAAGCTAGCCCGAG
GD13	Pok-ts-Hyd-Vec-For	CTGGGGCTGCTAGTCACCATCACCATCACCATTAA ATTAAATC
GD14	Pok-ts-Hyd-Vec-Rev	CGGAGCATGTGTCCCCTCTTATCGTTTCGGTACCG AGCTCGAATTCG
GD15	Pok-ts-Hyd-His-For	TCGGTACCGAAACGATAAGAGGGGACACATGCTC CGGCCGATTCTTC
GD16	Pok-ts-Hyd-His-Rev	TTAATGGTGATGGTGATGGTGACTAGCAGCCCCAG CCCTAAC
	For Site-Directed Mutagenesis	Sequences
GD25	D81G_For	CTGTTTATAGGTGGTGGCTTAGAGGGCGTCAAC
GD26	D81G_Rev	CTCTAAGCCACCACCTATAAACAGCATAGGGTTAG
GD27	S140N_For	CAAGTTACATCCTGGAAC TATTTGGGGTAGAG
GD28	S140N_Rev	CCAAAATAGTTCCAGGATGTAACCTGCACCATAAG
GD29	T148A_For	GTAGAGA ACTCTGCCTTTAATAACTTAGCTGGCTC
GD30	T148A_Rev	CTAAGTTATTAAGGCAGAGTTCTCTACCCAAAA TAG
GD 39	E84am,P88am_For	TGATGGCTTATAGGGCGTCAACTAGCTTGGGGCTG TATTCGTAAAC
GD 40	E84am,P88am_Rev	CTAGTTGACGCCCTATAAGCCATCACCTATAACA GCATAGG
GD 41	D161N_For	GGTGTTCGCTAACTGTATGGAGAGCCACATTTCCG GGAAC TTG
GD 42	D161N_Rev	GTGGCTCTCCATACAGTTACGCAACACCAGCGCAG AGCCAG
GD 43	E164Q_For	TGCGT GACTGTATGCAGAGCCACATTTCCGGGAAC TTGTTC
GD 44	E164Q_Rev	TCCCGGAAATGTGGCTCTGCATACAGTCACGCAAC ACCAGCGC
GD 45	D223N_For	AACAGTAACCCGAACCTGGTGTGGATTACGGATA ACAAG
GD 46	D223N_Rev	CGTAATCCACACCAGGTTCCGGTTACTGTTTGCTG TACTC

GD 47	E233Q_For	GATAACAAGTTTCAGTGGGACAGTGTACCGTACGG GGCTAAC
GD 48	E233Q_Rev	CGTACGGTACACTGTCCCACTGAAACTTGTATCC GTAATC
GD 49	D235N_For	CAAGTTTGAGTGGAACAGTGTACCGTACGGGGCTA ACAC
GD 50	D235N_Rev	CGTACGGTACACTGTTCCACTCAAACCTTGTATCC GTAATC
GD 51	Hyd35-385Vec.For	CTGGGGCTGCTAGTCACCATCACCATCACCATTAA ATTAAATC
GD 52	Hyd35-385-6Xhis.Rev	TTAATGGTGATGGTGATGGTGACTAGCAGCCCCAG CCCTAAC
GD 53	Hyd35-460Vec.For	GCCTAACGGGTGACCACCATCACCATCACCATTAA ATTAAATC
GD 54	Hyd35-460-6Xhis.Rev	TTAATGGTGATGGTGATGGTGGTCACCCGTTAGGC TGTTACC
	Pokalde_ 001 Tail spike protein	
GD35	Pok_1_TS-Seq2_For	GAA CTT GTT CCG TAG GAT GGG TG
GD36	NKCTS-Seq3_For	ATA GTC CGT TCG GCC CTG
GD37	Pok_1_TS_For	GAC TGG CGC TAT ATT AGC AAG TAC
GD38	Pok_1_TS-Seq1_For	GTG GCA GAG CAA AGC CAT TG
GD57	Pok_01_TSP1-84_Vec.F	TGGCTTAGAGCACCATCACCATCACCATTAAATTA AATCAGAAC
GD58	Pok_01_TSP1-84 R	ATTTAATGGTGATGGTGATGGTGCTCTAAGCCATC ACCTATAAACAGC

APPENDIX -F

Summary of coding sequences (CDs) and predicted functions of the phage's genomes

Table: F1 Summary of coding sequences (CDs) and predicted functions of ϕ EC_Makalu_001 complete genome GenBank ID [MN894885.1](#).

CDs	Start	End	Strand	No of amino acids	Protein Size (kDa)	Predicted function	Protein Id.
1	22	2130	-	702	81.9	rIIA protector from prophage-induced early lysis	gb QHJ73222.1
2	2145	2402	-	85	10.5	hypothetical protein	gb QHJ73223.1
3	2413	2607	-	64	7.6	hypothetical protein	gb QHJ73224.1
4	2600	2794	-	64	7.6	hypothetical protein	gb QHJ73225.1
5	2861	3160	-	99	11.7	PmgU (Putative morphogenetic function)	gb QHJ73226.1
6	3229	5052	-	607	68.6	DNA topoisomerase II large subunit	gb QHJ73227.1
7	5152	5325	-	57	6.5	FmdB family regulatory protein	gb QHJ73228.1
8	5327	5995	-	222	25.2	exonuclease	gb QHJ73229.1
9	5997	6239	-	80	9.3	hypothetical protein	gb QHJ73230.1
10	6270	6416	-	48	5.5	hypothetical protein	gb QHJ73231.1
11	6418	6585	-	55	6.6	hypothetical protein	gb QHJ73232.1
12	6596	7963	-	455	51.9	DNA helicase	gb QHJ73233.1
13	7987	8301	-	104	12.1	hypothetical protein	gb QHJ73234.1
14	8301	9056	-	251	28.7	putative Srd anti-sigma factor	gb QHJ73235.1
15	9118	9621	-	167	19.1	ADP-ribosylase	gb QHJ73236.1
16	9689	10207	-	172	19.4	dCTP pyrophosphatase	gb QHJ73237.1
17	10222	11250	-	342	40.2	DNA primase	gb QHJ73238.1
18	11260	11463	-	67	7.7	hypothetical protein	gb QHJ73239.1
19	11460	11603	-	47	5	hypothetical protein	gb QHJ73240.1
20	11611	11787	-	58	6.1	major capsid protein	gb QHJ73241.1
21	11784	12161	-	125	14.3	hypothetical protein	gb QHJ73242.1
22	12192	12827	-	211	24.1	hypothetical protein	gb QHJ73243.1
23	12878	14290	-	470	53.3	DNA primase-helicase subunit	gb QHJ73244.1

						head vertex assembly	
24	14287	14604	-	105	12.1	chaperone	gb QHJ73245.1
						RecA-like recombination	
25	14660	15730	-	356	40.1	protein	gb QHJ73246.1
26	15742	15930	-	62	7.5	hypothetical protein	gb QHJ73247.1
27	15992	18670	-	892	103.4	DNA polymerase	gb QHJ73248.1
28	18753	19115	-	120	14.4	hypothetical protein	gb QHJ73249.1
29	19117	19695	-	192	22.4	clamp loader small subunit	gb QHJ73250.1
30	19695	20669	-	324	36.9	clamp loader, small subunit	gb QHJ73251.1
						sliding clamp DNA	
31	20735	21421	-	228	25.6	polymerase accessory protein	gb QHJ73252.1
32	21452	21829	-	125	14.7	hypothetical protein	gb QHJ73253.1
						RNA polymerase-binding	
33	21834	22211	-	125	14.2	protein	gb QHJ73254.1
34	22243	22434	-	63	7.3	hypothetical protein	gb QHJ73255.1
						putative recombination	
35	22460	24142	-	560	63.6	endonuclease subunit	gb QHJ73256.1
36	24123	24386	-	87	10.2	hypothetical protein	gb QHJ73257.1
37	24383	24955	-	190	22.1	hypothetical protein	gb QHJ73258.1
38	24930	25247	-	105	12.6	hypothetical protein	gb QHJ73259.1
39	25244	25495	-	83	9.7	hypothetical protein	gb QHJ73260.1
40	25549	26574	-	341	39.1	endonuclease subunit	gb QHJ73261.1
41	26665	26952	-	95	11.1	hypothetical protein	gb QHJ73262.1
42	26954	27187	-	77	8.8	hypothetical protein	gb QHJ73263.1
						RNA polymerase sigma	
43	27171	27704	-	177	20.8	factor	gb QHJ73264.1
44	27745	29214	-	489	56.2	hypothetical protein	gb QHJ73265.1
45	29214	29501	-	95	10.8	hypothetical protein	gb QHJ73266.1
46	29523	29681	-	52	5.5	putative membrane protein	gb QHJ73267.1
47	29671	29940	-	89	10.3	thioredoxin	gb QHJ73268.1
48	29937	30419	-	160	19.1	hypothetical protein	gb QHJ73269.1
49	30421	31245	-	274	31.8	hypothetical protein	gb QHJ73270.1
50	31258	31743	-	161	18.8	hypothetical protein	gb QHJ73271.1
51	31748	32275	-	175	20	hypothetical protein	gb QHJ73272.1
						anaerobic ribonucleoside-	
						triphosphate reductase-	
52	32286	32789	-	167	19	activating protein	gb QHJ73273.1
53	32779	32931	-	50	6	hypothetical protein	gb QHJ73274.1
54	33007	33558	-	183	21.5	hypothetical protein	gb QHJ73275.1

55	33570	34112	-	180	20.9	hypothetical protein	gb QHJ73276.1
						putative anaerobic ribonucleoside-triphosphate	
56	34218	36080	-	620	69.5	reductase	gb QHJ73277.1
57	36126	36620	-	164	19.2	hypothetical protein	gb QHJ73278.1
58	36675	37853	-	392	45.5	hypothetical protein	gb QHJ73279.1
59	37910	38476	-	188	22	hypothetical protein	gb QHJ73280.1
60	38503	38763	-	86	10	hypothetical protein	gb QHJ73281.1
						recombination endonuclease	
61	38827	39315	-	162	18.6	VII	gb QHJ73282.1
62	39325	39606	-	93	10.6	thioredoxin	gb QHJ73283.1
						DNA adenine	
63	39615	40427	-	270	31.1	methyltransferase	gb QHJ73284.1
64	40427	40858	-	143	16.7	hypothetical protein	gb QHJ73285.1
65	40869	41123	-	84	9.8	hypothetical protein	gb QHJ73286.1
66	41155	41376	-	73	8.4	hypothetical protein	gb QHJ73287.1
67	41369	41662	-	97	10.9	hypothetical protein	gb QHJ73288.1
68	41677	41985	-	102	11.5	hypothetical protein	gb QHJ73289.1
69	42055	42363	-	102	11.7	hypothetical protein	gb QHJ73290.1
70	42374	42652	-	92	10.4	hypothetical protein	gb QHJ73291.1
71	42959	43297	-	112	13.3	hypothetical protein	gb QHJ73292.1
72	43297	43563	-	88	10.2	hypothetical protein	gb QHJ73293.1
73	43560	43808	-	82	9.4	hypothetical protein	gb QHJ73294.1
74	43805	44239	-	144	16.6	hypothetical protein	gb QHJ73295.1
75	44250	44468	-	72	8.4	hypothetical protein	gb QHJ73296.1
76	44479	44676	-	65	7.4	hypothetical protein	gb QHJ73297.1
77	44687	44977	-	96	11.3	hypothetical protein	gb QHJ73298.1
						tail fiber/host adhesion	
78	45079	45858	-	259	25.7	protein	gb QHJ73299.1
79	45916	46137	-	73	8.2	hypothetical protein	gb QHJ73300.1
80	46227	46511	-	94	10.3	hypothetical protein	gb QHJ73301.1
81	46508	46858	-	116	13.2	hypothetical protein	gb QHJ73302.1
82	46855	47193	-	112	12.9	hypothetical protein	gb QHJ73303.1
83	47183	47392	-	69	7.6	hypothetical protein	gb QHJ73304.1
84	47722	48120	-	132	15.1	hypothetical protein	gb QHJ73305.1
						lysis inhibition regulator	
85	48107	48409	-	100	11.4	membrane protein	gb QHJ73306.1
86	48478	49074	-	198	22.2	thymidine kinase	gb QHJ73307.1
87	49074	49367	-	97	11.3	hypothetical protein	gb QHJ73308.1

88	49360	49578	-	72	8.6	hypothetical protein	gb QHJ73309.1
89	49575	49769	-	64	7.5	hypothetical protein	gb QHJ73310.1
90	49759	50214	-	151	16.5	hypothetical protein	gb QHJ73311.1
91	50230	50589	-	119	13.7	valyl-tRNA synthetase modifier	gb QHJ73312.1
92	50597	51187	-	196	21.9	hypothetical protein	gb QHJ73313.1
93	51273	51695	-	140	16.7	site-specific RNA endonuclease	gb QHJ73314.1
94	51700	52035	-	111	13	hypothetical protein	gb QHJ73315.1
95	52098	52343	-	81	9.5	hypothetical protein	gb QHJ73316.1
96	52340	52534	-	64	7.3	hypothetical protein	gb QHJ73317.1
97	52556	53254	-	232	27	nucleotidyltransferase	gb QHJ73318.1
98	53340	53756	-	138	15.2	putative acetyltransferase- related protein	gb QHJ73319.1
99	53767	53892	-	41	4.8	hypothetical protein	gb QHJ73320.1
100	53892	54377	-	161	18.2	hypothetical protein	gb QHJ73321.1
101	54440	54829	-	129	14.8	putative endolysin	gb QHJ73322.1
102	54858	55049	-	63	6.9	hypothetical protein	gb QHJ73323.1
103	55051	55266	-	71	7.8	hypothetical protein	gb QHJ73324.1
104	55269	55448	-	59	6.5	hypothetical protein	gb QHJ73325.1
105	55530	55733	-	67	7.9	hypothetical protein	gb QHJ73326.1
106	55697	55855	-	52	5.7	hypothetical protein	gb QHJ73327.1
107	55858	56172	-	104	12.2	hypothetical protein	gb QHJ73328.1
108	56129	56449	-	106	11.9	hypothetical protein	gb QHJ73329.1
109	56468	56668	-	66	7.5	hypothetical protein	gb QHJ73330.1
110	56670	56852	-	60	6.7	hypothetical protein	gb QHJ73331.1
111	56861	57187	-	108	12.4	hypothetical protein	gb QHJ73332.1
112	57267	57455	-	62	7.2	hypothetical protein	gb QHJ73333.1
113	57478	57666	-	62	7.2	hypothetical protein	gb QHJ73334.1
114	57678	57899	-	73	8.4	hypothetical protein	gb QHJ73335.1
115	57966	58151	-	61	6.7	hypothetical protein	gb QHJ73336.1
116	58428	58646	-	72	8.5	hypothetical protein	gb QHJ73337.1
117	58643	58825	-	60	7	hypothetical protein	gb QHJ73338.1
118	58825	59046	-	73	8.7	hypothetical protein	gb QHJ73339.1
119	59043	59153	-	36	4.1	hypothetical protein	gb QHJ73340.1
120	59150	59347	-	65	7.2	hypothetical protein	gb QHJ73341.1
121	59337	59540	-	67	7.8	discriminator of mRNA degradation	gb QHJ73342.1
122	59550	59708	-	52	5.4	hypothetical protein	gb QHJ73343.1

123	59775	60152	-	125	14.8	hypothetical protein	gb QHJ73344.1
124	60266	60730	-	154	17.8	hypothetical protein	gb QHJ73345.1
125	60733	60993	-	86	9.8	chaperone for tail fiber formation	gb QHJ73346.1
126	61026	61682	-	218	24.5	putative deoxynucleotide monophosphate kinase	gb QHJ73347.1
127	61698	62288	-	196	22.2	tail completion and sheath stabilizer protein	gb QHJ73348.1
128	62732	62478	+	84	9.7	hypothetical protein	gb QHJ73349.1
129	62763	63584	-	273	31.2	DNA end protector protein	gb QHJ73350.1
130	63596	64069	-	157	19	head completion protein	gb QHJ73351.1
131	64679	64125	+	184	21.8	baseplate wedge subunit	gb QHJ73352.1
132	66490	64697	+	597	66	baseplate hub subunit and tail lysozyme	gb QHJ73353.1
133	67065	66499	+	188	21.1	hypothetical protein	gb QHJ73354.1
134	67358	67065	+	97	10.2	hypothetical protein	gb QHJ73355.1
135	69259	67355	+	634	70.7	baseplate wedge subunit	gb QHJ73356.1
136	72342	69256	+	1028	119.2	baseplate wedge subunit	gb QHJ73357.1
137	73330	72335	+	331	37.6	baseplate wedge subunit	gb QHJ73358.1
138	73697	73440	+	85	9.9	hypothetical protein	gb QHJ73359.1
139	74014	73685	+	109	13.4	hypothetical protein	gb QHJ73360.1
140	74853	74014	+	279	31.7	putative methyltransferase	gb QHJ73361.1
141	75783	74929	+	284	30.5	baseplate wedge tail fiber connector	gb QHJ73362.1
142	77582	75780	+	600	66.8	baseplate wedge subunit and tail pin	gb QHJ73363.1
143	78228	77584	+	214	23.3	baseplate wedge subunit and tail pin	gb QHJ73364.1
144	79640	78240	+	466	49.8	short tail fibers protein	gb QHJ73365.1
145	81409	79640	+	589	64.3	fibritin neck whiskers protein	gb QHJ73366.1
146	82388	81456	+	310	33.6	neck protein	gb QHJ73367.1
147	83257	82442	+	271	31.4	putative Seg-like homing endonuclease, GIY-YIG family	gb QHJ73368.1
148	84034	83294	+	246	28.5	neck protein	gb QHJ73369.1
149	84894	84106	+	262	30.4	tail sheath stabilizer and completion protein	gb QHJ73370.1
150	85405	84929	+	158	18	small terminase protein	gb QHJ73371.1
151	87225	85402	+	607	69.6	large terminase protein	gb QHJ73372.1

152	89260	87260	+	666	72.6	tail sheath protein	gb QHJ73373.1
153	89828	89334	+	164	18.4	tail tube protein	gb QHJ73374.1
154	91452	89887	+	521	60.4	portal vertex protein	gb QHJ73375.1
155	91692	91453	+	79	9.5	putative prohead core protein	gb QHJ73376.1
156	92112	91705	+	135	15.4	prohead core protein	gb QHJ73377.1
						prohead core scaffolding	
157	92819	92124	+	231	25.2	protein and protease	gb QHJ73378.1
158	93645	92851	+	264	29.4	prohead core protein	gb QHJ73379.1
159	95291	93705	+	528	56.7	major capsid protein	gb QHJ73380.1
160	95759	95631	+	42	5	hypothetical protein	gb QHJ73381.1
161	95944	95792	+	50	5.8	hypothetical protein	gb QHJ73382.1
162	97269	96028	+	413	45.6	capsid vertex protein	gb QHJ73383.1
163	97270	97857	-	195	22.3	hypothetical protein	gb QHJ73384.1
164	98271	98708	-	145	16.3	hypothetical protein	gb QHJ73385.1
165	98755	99030	-	91	10.5	hypothetical protein	gb QHJ73386.1
166	99030	99227	-	65	7.5	hypothetical protein	gb QHJ73387.1
						highly immunogenic outer	
167	99428	100630	-	400	45.2	capsid protein	gb QHJ73388.1
168	100726	100890	-	54	6.1	hypothetical protein	gb QHJ73389.1
169	100969	101694	-	241	27.5	inhibitor of prohead protease	gb QHJ73390.1
						RNA-DNA and DNA-DNA	
170	103267	101765	+	500	57.6	helicase ATPase	gb QHJ73391.1
						putative ATP-dependent	
171	103547	103311	+	78	9.1	DNA helicase	gb QHJ73392.1
172	103611	103787	-	58	6.5	hypothetical protein	gb QHJ73393.1
						recombination, repair, and	
173	103808	104215	-	135	15.8	ssDNA binding protein	gb QHJ73394.1
174	104263	104649	-	128	14.7	baseplate wedge protein	gb QHJ73395.1
						baseplate hub assembly	
175	104658	105287	-	209	23.9	protein	gb QHJ73396.1
						baseplate hub assembly	
176	106128	105358	+	256	29.6	protein	gb QHJ73397.1
						baseplate central spike	
177	107215	106106	+	369	42.2	complex protein	gb QHJ73398.1
						baseplate hub assembly	
178	107733	107215	+	172	19.4	protein	gb QHJ73399.1
						baseplate hub subunit, tail	
179	109463	107730	+	577	64.8	length determinant	gb QHJ73400.1

180	110521	109463	+	352	37.9	baseplate tail-tube junction protein	gb QHJ73401.1
181	111453	110521	+	310	34.1	baseplate tail-tube junction protein	gb QHJ73402.1
182	111486	111971	-	161	18.7	hypothetical protein	gb QHJ73403.1
183	111968	112792	-	274	32	ADP-ribosyltransferase	gb QHJ73404.1
184	112872	114923	-	683	76.4	ADP-ribosyltransferase	gb QHJ73405.1
185	114991	115203	-	70	8	hypothetical protein	gb QHJ73406.1
186	115275	115454	-	59	6.4	hypothetical protein	gb QHJ73407.1
187	115523	116041	-	172	20.5	hypothetical protein	gb QHJ73408.1
188	116043	116372	-	109	13	hypothetical protein	gb QHJ73409.1
189	116372	117088	-	238	27.4	putative C-5 cytosine DNA methylase	gb QHJ73410.1
190	117085	117330	-	81	9.6	hypothetical protein	gb QHJ73411.1
191	117327	117578	-	83	9.1	hypothetical protein	gb QHJ73412.1
192	117662	117829	-	55	6.2	hypothetical protein	gb QHJ73413.1
193	117906	118187	-	93	10.6	hypothetical protein	gb QHJ73414.1
194	118258	118527	-	89	10.5	hypothetical protein	gb QHJ73415.1
195	118654	118962	-	102	12.2	hypothetical protein	gb QHJ73416.1
196	119012	119299	-	95	11	hypothetical protein	gb QHJ73417.1
197	119383	119661	-	92	10.7	hypothetical protein	gb QHJ73418.1
198	119666	119986	-	106	12.5	hypothetical protein	gb QHJ73419.1
199	119988	120206	-	72	8.6	hypothetical protein	gb QHJ73420.1
200	120166	120423	-	85	10	hypothetical protein	gb QHJ73421.1
201	120410	120688	-	92	11	hypothetical protein	gb QHJ73422.1
202	120701	120880	-	59	6.8	hypothetical protein	gb QHJ73423.1
203	120945	121112	-	55	6.2	hypothetical protein	gb QHJ73424.1
204	121181	121474	-	97	11.3	hypothetical protein	gb QHJ73425.1
205	121491	121682	-	63	7.6	hypothetical protein	gb QHJ73426.1
206	121740	122060	-	106	12	hypothetical protein	gb QHJ73427.1
207	122078	122257	-	59	6.7	hypothetical protein	gb QHJ73428.1
208	122330	122641	-	103	11.7	hypothetical protein	gb QHJ73429.1
209	122729	123205	-	158	18.8	hypothetical protein	gb QHJ73430.1
210	123198	124694	-	498	56.2	DNA ligase	gb QHJ73431.1
211	124681	125160	-	159	18.4	hypothetical protein	gb QHJ73432.1
212	125150	125314	-	54	6.4	hypothetical protein	gb QHJ73433.1
213	125398	125721	-	107	11.7	head assembly cochaperone with GroEL	gb QHJ73434.1
214	125762	126076	-	104	11.9	hypothetical protein	gb QHJ73435.1

215	126069	126575	-	168	18.4	deoxycytidylate deaminase	gb QHJ73436.1
216	126597	126800	-	67	7.7	hypothetical protein	gb QHJ73437.1
217	126800	127678	-	292	34.5	polynucleotide kinase	gb QHJ73438.1
218	127678	128130	-	150	17.6	O-spanin	gb QHJ73439.1
219	128127	128450	-	107	12.6	I-spanin	gb QHJ73440.1
220	128495	129664	-	389	44.8	RNA ligase A	gb QHJ73441.1
221	129600	130061	-	153	17.9	endonuclease II	gb QHJ73442.1
222	130112	130510	-	132	14.8	hypothetical protein	gb QHJ73443.1
223	130581	130730	-	49	5.5	hypothetical protein	gb QHJ73444.1
224	130798	131016	-	72	8.6	hypothetical protein	gb QHJ73445.1
225	131086	131304	-	72	9.2	hypothetical protein	gb QHJ73446.1
						putative polynucleotide	
226	131405	131881	-	158	18.3	kinase/phosphatase	gb QHJ73447.1
						aerobic NDP reductase, small	
227	131878	133038	-	386	45.4	subunit	gb QHJ73448.1
228	133054	133221	-	55	6.3	hypothetical protein	gb QHJ73449.1
229	133221	133394	-	57	6.7	hypothetical protein	gb QHJ73450.1
230	133394	133594	-	66	7.5	hypothetical protein	gb QHJ73451.1
						ribonucleoside-diphosphate	
231	133630	135873	-	747	84.8	reductase subunit alpha	gb QHJ73452.1
232	135885	136187	-	100	11.7	hypothetical protein	gb QHJ73453.1
233	136224	137456	-	410	47.9	dTMP thymidylate synthase	gb QHJ73454.1
234	137428	137697	-	89	10.2	hypothetical protein	gb QHJ73455.1
235	137791	138360	-	189	21.3	dihydrofolate reductase	gb QHJ73456.1
236	138376	138705	-	109	12.8	hypothetical protein	gb QHJ73457.1
237	138761	139090	-	109	12.8	hypothetical protein	gb QHJ73458.1
238	139136	140314	-	392	45.2	hypothetical protein	gb QHJ73459.1
						single-strand DNA binding	
239	140435	141376	-	313	34.6	protein	gb QHJ73460.1
240	141437	142117	-	226	26.5	hypothetical protein	gb QHJ73461.1
						late promoter transcription	
241	142127	142381	-	84	9.5	accessory protein	gb QHJ73462.1
						double-stranded DNA	
242	142374	142649	-	91	10.7	binding protein	gb QHJ73463.1
243	142654	143253	-	199	23.2	inorganic triphosphatase	gb QHJ73464.1
244	143264	144211	-	315	36.9	RnaseH	gb QHJ73465.1
245	144214	144399	-	61	7.2	hypothetical protein	gb QHJ73466.1
						long tail fiber, proximal	
246	148212	144472	+	1246	136.6	subunit	gb QHJ73467.1

247	149385	148246	+	379	42.3	hinge connector of long-tail fiber, the proximal connector	gb QHJ73468.1
248	151078	149588	+	496	54.5	hinge connector of long-tail fiber distal connector	gb QHJ73469.1
249	154091	151149	+	980	108.5	long tail fiber distal subunit	gb QHJ73470.1
250	154371	154132	+	79	9.2	hypothetical protein	gb QHJ73471.1
251	155061	154405	+	218	25.1	holin lysis mediator	gb QHJ73472.1
252	155097	155345	-	82	9.5	hypothetical protein	gb QHJ73473.1
253	155342	155653	-	103	12.1	hypothetical protein	gb QHJ73474.1
254	155678	156010	-	110	12.8	hypothetical protein	gb QHJ73475.1
255	156019	156387	-	122	14.3	hypothetical protein	gb QHJ73476.1
256	156398	156589	-	63	7.5	hypothetical protein	gb QHJ73477.1
257	156613	156891	-	92	11.2	hypothetical protein	gb QHJ73478.1
258	156903	157661	-	252	28.5	hypothetical protein	gb QHJ73479.1
259	157732	157887	-	51	6	hypothetical protein	gb QHJ73480.1
260	157957	158169	-	70	8.1	hypothetical protein	gb QHJ73481.1
261	158235	158477	-	80	9.1	hypothetical protein	gb QHJ73482.1
262	158541	158741	-	66	7	hypothetical protein	gb QHJ73483.1
263	158738	158908	-	56	6.7	hypothetical protein	gb QHJ73484.1
264	158913	159185	-	90	10.3	hypothetical protein	gb QHJ73485.1
265	159252	159458	-	68	7.9	hypothetical protein	gb QHJ73486.1
266	159570	159965	-	131	14.8	hypothetical protein	gb QHJ73487.1
267	159969	160166	-	65	7.5	hypothetical protein	gb QHJ73488.1
268	160169	161533	-	454	51.9	DNA topoisomerase II medium subunit	gb QHJ73489.1
269	161541	161903	-	120	14.2	hypothetical protein	gb QHJ73490.1
270	161906	162199	-	97	10.8	hypothetical protein	gb QHJ73491.1
271	162245	162562	-	105	11.9	hypothetical protein	gb QHJ73492.1
272	162577	163569	-	330	37.6	rIIB protector from prophage-induced early lysis	gb QHJ73493.1

Table F2: Summary of coding sequences (CDs) and predicted functions of ϕ Ec_Maalu_002complete genome GenBank ID: [MN709127.1](#)

CDs	Start	End	Strand	No of amino acids	Protein Size (kDa)	Predictive function	Protein Id.
1	2118	10	-	702	81.9	rIIA protector from prophage-induced early lysis	"QGS83606.1"
2	2390	2133	-	85	10.5	hypothetical protein	"QGS83607.1"
3	2595	2401	-	64	7.6	hypothetical protein	"QGS83608.1"
4	2782	2588	-	64	7.6	hypothetical protein	"QGS83609.1"
5	3148	2849	-	99	11.7	hypothetical protein	"QGS83610.1"
6	5040	3217	-	607	68.5	DNA topoisomerase II large subunit	"QGS83611.1"
7	5313	5140	-	57	6.5	FmdB family regulatory protein	"QGS83612.1"
8	5983	5315	-	222	25.2	exonuclease	"QGS83613.1"
9	6227	5985	-	80	9.3	hypothetical protein	"QGS83614.1"
10	6404	6258	-	48	5.5	hypothetical protein	"QGS83615.1"
11	6573	6406	-	55	6.5	hypothetical protein	"QGS83616.1"
12	7975	6584	-	463	52.9	Dda DNA helicase	"QGS83617.1"
13	8289	7975	-	104	12	hypothetical protein	"QGS83618.1"
14	9044	8289	-	251	28.8	Srd anti-sigma factor, putative	"QGS83619.1"
15	9609	9106	-	167	19.1	ModB ADP-ribosylase	"QGS83620.1"
16	10197	9679	-	172	19.6	dCTP pyrophosphatase	"QGS83621.1"

17	11240	10212	-	342	40.2	DNA primase	"QGS83622.1"
18	11453	11250	-	67	7.7	hypothetical protein	"QGS83623.1"
19	11608	11450	-	52	5.5	hypothetical protein	"QGS83624.1"
20	11777	11601	-	58	6.1	major capsid protein	"QGS83625.1"
21	12151	11774	-	125	14.3	hypothetical protein	"QGS83626.1"
22	12817	12182	-	211	24.1	hypothetical protein	"QGS83627.1"
23	14280	12868	-	470	53.3	ATP-dependent helicase 41	"QGS83628.1"
24	14594	14277	-	105	12.1	head vertex assembly chaperone	"QGS83629.1"
25	15720	14650	-	356	40.1	UvsX RecA-like recombination protein	"QGS83630.1"
26	15920	15732	-	62	7.6	hypothetical protein	"QGS83631.1"
27	18660	15982	-	892	103.4	DNA polymerase	"QGS83632.1"
28	19105	18743	-	120	14.4	translation repressor protein	"QGS83633.1"
29	19685	19107	-	192	22.4	Sliding-clamp-loader subunit	"QGS83634.1"
30	20659	19685	-	324	37	clamp loader, small subunit	"QGS83635.1"
31	21411	20725	-	228	25.6	sliding clamp	"QGS83636.1"
32	21818	21441	-	125	14.8	hypothetical protein	"QGS83637.1"
33	22200	21823	-	125	14.2	RpbA RNA polymerase binding protein, function unknown	"QGS83638.1"
34	22422	22231	-	63	7.3	hypothetical protein	"QGS83639.1"
35	24130	22448	-	560	63.6	endonuclease subunit	"QGS83640.1"

36	24374	24111	-	87	10.1	hypothetical protein	"QGS83641.1"
37	24943	24371	-	190	22	hypothetical protein	"QGS83642.1"
38	25235	24918	-	105	12.6	hypothetical protein	"QGS83643.1"
39	25483	25232	-	83	9.7	hypothetical protein	"QGS83644.1"
40	26562	25537	-	341	39.1	endonuclease subunit	"QGS83645.1"
41	26940	26653	-	95	11.1	hypothetical protein	"QGS83646.1"
42	27175	26942	-	77	8.8	hypothetical protein	"QGS83647.1"
43	27692	27159	-	177	20.8	RNA polymerase sigma factor	"QGS83648.1"
44	29202	27712	-	496	56.9	hypothetical protein	"QGS83649.1"
45	29489	29202	-	95	10.8	conserved hypothetical protein	"QGS83650.1"
46	29669	29511	-	52	5.5	putative membrane protein	"QGS83651.1"
47	29928	29659	-	89	10.3	NrdC thioredoxin	"QGS83652.1"
48	30407	29925	-	160	19.1	hypothetical protein	"QGS83653.1"
49	31233	30409	-	274	31.8	hypothetical protein	"QGS83654.1"
50	31731	31246	-	161	18.8	hypothetical protein	"QGS83655.1"
51	32263	31736	-	175	20	hypothetical protein	"QGS83656.1"
52	32777	32274	-	167	19	M NrdG anaerobic NTP reductase, small subunit	"QGS83657.1"
53	32919	32767	-	50	6	hypothetical protein	"QGS83658.1"
54	33540	32995	-	181	21.3	hypothetical protein	"QGS83659.1"

55	34100	33558	-	180	20.8	hypothetical protein	"QGS83660.1"
56	36068	34206	-	620	69.5	putative anaerobic ribonucleoside- triphosphate reductase	"QGS83661.1"
57	36608	36114	-	164	18.9	hypothetical protein	"QGS83662.1"
58	37841	36663	-	392	45.5	conserved hypothetical protein	"QGS83663.1"
59	38464	37898	-	188	22	hypothetical protein	"QGS83664.1"
60	38751	38491	-	86	10	hypothetical protein	"QGS83665.1"
61	39288	38815	-	157	18	recombination endonuclease VII	"QGS83666.1"
62	39594	39313	-	93	10.6	NrdC thioredoxin	"QGS83667.1"
63	40415	39603	-	270	31.1	Dam DNA adenine methyltransferase	"QGS83668.1"
64	40846	40415	-	143	16.7	hypothetical protein	"QGS83669.1"
65	41111	40857	-	84	9.8	hypothetical protein	"QGS83670.1"
66	41364	41143	-	73	8.4	hypothetical protein	"QGS83671.1"
67	41650	41357	-	97	10.9	hypothetical protein	"QGS83672.1"
68	41973	41665	-	102	11.4	hypothetical protein	"QGS83673.1"
69	42353	42045	-	102	11.8	hypothetical protein	"QGS83674.1"
70	42642	42364	-	92	10.4	hypothetical protein	"QGS83675.1"
71	42938	42834	-	34	4.1	hypothetical protein	"QGS83676.1"
72	43288	42950	-	112	13.3	hypothetical protein	"QGS83677.1"
73	43554	43288	-	88	10.2	hypothetical protein	"QGS83678.1"

74	43799	43551	-	82	9.4	hypothetical protein	"QGS83679.1"
75	44230	43796	-	144	16.6	hypothetical protein	"QGS83680.1"
76	44459	44241	-	72	8.4	hypothetical protein	"QGS83681.1"
77	44667	44470	-	65	7.4	hypothetical protein	"QGS83682.1"
78	44968	44678	-	96	11.3	hypothetical protein	"QGS83683.1"
79	45849	45070	-	259	25.7	Receptor-recognizing protein	"QGS83684.1"
80	46128	45907	-	73	8.2	hypothetical protein	"QGS83685.1"
81	46502	46218	-	94	10.3	hypothetical protein	"QGS83686.1"
82	46849	46499	-	116	13.2	hypothetical protein	"QGS83687.1"
83	47184	46846	-	112	13	hypothetical protein	"QGS83688.1"
84	47383	47174	-	69	7.6	hypothetical protein	"QGS83689.1"
85	48110	47712	-	132	15.1	Mus conserved phage associated protein	"QGS83690.1"
86	48399	48097	-	100	11.4	rI lysis inhibition regulator membrane protein	"QGS83691.1"
87	49064	48468	-	198	22.2	Tk thymidine kinase	"QGS83692.1"
88	49357	49064	-	97	11.3	hypothetical protein	"QGS83693.1"
89	49568	49350	-	72	8.6	hypothetical protein	"QGS83694.1"
90	49759	49565	-	64	7.5	hypothetical protein	"QGS83695.1"
91	50204	49749	-	151	16.5	Uncharacterized 17.5 kDa protein in the tk-vs intergenic region	"QGS83696.1"

92	50579	50220	-	119	13.7	Vs valyl-tRNA synthetase modifier	"QGS83697.1"
93	51177	50587	-	196	21.9	Uncharacterized 20.7 kDa protein in vs-regB intergenic region	"QGS83698.1"
94	51685	51263	-	140	16.7	RegB site-specific RNA endonuclease	"QGS83699.1"
95	52025	51690	-	111	13.1	hypothetical protein	"QGS83700.1"
96	52331	52086	-	81	9.7	hypothetical protein	"QGS83701.1"
97	52522	52328	-	64	7.3	hypothetical protein	"QGS83702.1"
98	53242	52544	-	232	27	conserved hypothetical protein	"QGS83703.1"
99	53745	53329	-	138	15.2	conserved hypothetical protein	"QGS83704.1"
100	53881	53756	-	41	4.8	hypothetical protein	"QGS83705.1"
101	54366	53881	-	161	18.2	conserved hypothetical protein	"QGS83706.1"
102	54818	54429	-	129	14.8	putative endolysin	"QGS83707.1"
103	55038	54847	-	63	6.9	hypothetical protein	"QGS83708.1"
104	55255	55040	-	71	7.9	hypothetical protein	"QGS83709.1"
105	55437	55258	-	59	6.5	hypothetical protein	"QGS83710.1"
106	55622	55434	-	62	7.1	hypothetical protein	"QGS83711.1"
107	55843	55685	-	52	5.7	hypothetical protein	"QGS83712.1"
108	56160	55846	-	104	12.2	hypothetical protein	"QGS83713.1"
109	56437	56117	-	106	12	hypothetical protein	"QGS83714.1"
110	56656	56456	-	66	7.5	hypothetical protein	"QGS83715.1"

111	56840	56658	-	60	6.7	hypothetical protein	"QGS83716.1"
112	57175	56849	-	108	12.4	hypothetical protein	"QGS83717.1"
113	57443	57255	-	62	7.2	hypothetical protein	"QGS83718.1"
114	57654	57466	-	62	7.2	hypothetical protein	"QGS83719.1"
115	57891	57664	-	75	8.5	hypothetical protein	"QGS83720.1"
116	58143	57958	-	61	6.7	hypothetical protein	"QGS83721.1"
117	58638	58420	-	72	8.5	hypothetical protein	"QGS83722.1"
118	58817	58635	-	60	7	hypothetical protein	"QGS83723.1"
119	59038	58814	-	74	8.8	hypothetical protein	"QGS83724.1"
120	59145	59035	-	36	4.1	hypothetical protein	"QGS83725.1"
121	59339	59142	-	65	7.2	hypothetical protein	"QGS83726.1"
122	59533	59339	-	64	7.4	Dmd discriminator of mRNA degradation	"QGS83727.1"
123	59701	59543	-	52	5.4	hypothetical protein	"QGS83728.1"
124	60146	59769	-	125	14.8	hypothetical protein	"QGS83729.1"
125	60725	60261	-	154	17.8	conserved hypothetical protein	"QGS83730.1"
126	60988	60728	-	86	9.8	chaperone for tail fiber formation	"QGS83731.1"
127	61677	61021	-	218	24.5	putative deoxynucleotide monophosphate kinase	"QGS83732.1"
128	62283	61693	-	196	22.2	tail completion and sheath stabilizer protein	"QGS83733.1"
129	62473	62727	+	84	9.7	hypothetical protein	"QGS83734.1"

130	63579	62758	-	273	31.2	DNA end protector protein	"QGS83735.1"
131	63706	64728	+	340	40.9	putative homing endonuclease, HNH family	"QGS83736.1"
132	65190	64717	-	157	18.7	head completion protein	"QGS83737.1"
133	65246	65800	+	184	21.8	baseplate wedge protein	"QGS83738.1"
134	65812	67611	+	599	66.2	baseplate hub subunit and tail lysozyme	"QGS83739.1"
135	67620	68186	+	188	21.1	Uncharacterized 18.5 kDa protein in repEA-segC intergenic region	"QGS83740.1"
136	68186	68479	+	97	10.2	conserved hypothetical protein	"QGS83741.1"
137	68476	70380	+	934	70.7	baseplate wedge protein	"QGS83742.1"
138	70377	73463	+	1028	119.2	baseplate wedge protein	"QGS83743.1"
139	73456	74451	+	331	37.6	baseplate wedge protein	"QGS83744.1"
140	74561	74818	+	85	10	hypothetical protein	"QGS83745.1"
141	74806	75135	+	109	13.4	hypothetical protein	"QGS83746.1"
142	75135	75974	+	279	31.7	release factor glutamine methyltransferase	"QGS83747.1"
143	76050	76904	+	284	30.5	baseplate wedge tail fiber connector	"QGS83748.1"
144	76901	78703	+	600	66.8	baseplate wedge subunit and tail pin	"QGS83749.1"
145	78705	79349	+	214	23.3	baseplate wedge subunit and tail pin	"QGS83750.1"
146	79361	80761	+	466	49.8	short tail fibers protein	"QGS83751.1"
147	80761	82530	+	589	64.2	fibrin neck whiskers protein	"QGS83752.1"

148	82577	83509	+	310	33.6	Neck protein	"QGS83753.1"
149	83563	84378	+	271	31.4	SegB homing endonuclease	"QGS83754.1"
150	84415	85155	+	246	28.4	neck protein	"QGS83755.1"
151	85182	86015	+	277	32.4	tail sheath stabilizer and completion protein	"QGS83756.1"
152	86029	86526	+	165	18.8	small terminase protein	"QGS83757.1"
153	86523	89339	+	938	106.9	large terminase protein	"QGS83758.1"
154	89374	91374	+	666	72.6	tail sheath protein	"QGS83759.1"
155	91448	91942	+	164	18.4	tail tube protein	"QGS83760.1"
156	92001	93566	+	521	60.5	portal vertex protein	"QGS83761.1"
157	93567	93806	+	79	9.5	putative prohead core protein I	"QGS83762.1"
158	93819	94226	+	135	15.4	prohead core protein	"QGS83763.1"
159	94238	94933	+	231	25.3	prohead core scaffolding protein and protease	"QGS83764.1"
160	94965	95759	+	264	29.5	prohead core scaffold protein	"QGS83765.1"
161	95819	97405	+	528	56.7	major capsid protein	"QGS83766.1"
162	97722	97859	+	45	5.4	hypothetical protein	"QGS83767.1"
163	97892	98044	+	50	5.8	hypothetical protein	"QGS83768.1"
164	98128	99369	+	413	45.7	capsid vertex protein	"QGS83769.1"
165	99957	99370	-	195	22.3	conserved hypothetical protein	"QGS83770.1"
166	100808	100371	-	145	16.3	hypothetical protein	"QGS83771.1"

167	101130	100855	-	91	10.5	conserved hypothetical protein	"QGS83772.1"
168	101327	101130	-	65	7.5	hypothetical protein	"QGS83773.1"
169	102730	101528	-	400	45.1	hoc head outer capsid protein	"QGS83774.1"
170	102990	102826	-	54	6.1	hypothetical protein	"QGS83775.1"
171	103794	103069	-	241	27.5	Inh inhibitor of prohead protease	"QGS83776.1"
172	103865	105367	+	500	57.6	ATP-dependent DNA helicase uvsW	"QGS83777.1"
173	105411	105647	+	78	9.1	UvsW helicase	"QGS83778.1"
174	105887	105711	-	58	6.5	Uncharacterized protein in uvsW-uvsY intergenic region	"QGS83779.1"
175	106315	105908	-	135	15.8	UvsY recombination, repair, and ssDNA binding protein	"QGS83780.1"
176	106749	106363	-	128	14.7	baseplate wedge protein	"QGS83781.1"
177	107387	106758	-	209	23.9	baseplate hub assembly protein	"QGS83782.1"
178	107458	108228	+	256	29.6	baseplate hub assembly protein	"QGS83783.1"
179	108206	109315	+	369	42.2	baseplate central spike complex protein	"QGS83784.1"
180	109315	109833	+	172	19.4	baseplate hub distal subunit	"QGS83785.1"
181	109830	111563	+	577	64.8	baseplate hub subunit, tail length determinator	"QGS83786.1"
182	111563	112621	+	352	37.9	baseplate tail-tube junction protein	"QGS83787.1"
183	112621	113553	+	310	34.1	baseplate tail-tube junction protein	"QGS83788.1"
184	114072	113587	-	161	18.7	hypothetical protein	"QGS83789.1"

185	114893	114069	-	272	32	ADP-ribosyltransferase	"QGS83790.1"
186	117024	114973	-	683	76.4	ADP-ribosyltransferase	"QGS83791.1"
187	117304	117092	-	70	8	hypothetical protein	"QGS83792.1"
188	117555	117376	-	59	6.4	hypothetical protein	"QGS83793.1"
189	118142	117624	-	172	20.5	hypothetical protein	"QGS83794.1"
190	118473	118144	-	109	13	hypothetical protein	"QGS83795.1"
191	119189	118473	-	238	27.4	putative C-5 cytosine DNA methylase	"QGS83796.1"
192	119431	119186	-	81	9.6	hypothetical protein	"QGS83797.1"
193	119679	119428	-	83	9.1	hypothetical protein	"QGS83798.1"
194	119930	119763	-	55	6.2	hypothetical protein	"QGS83799.1"
195	120288	120007	-	93	10.6	hypothetical protein	"QGS83800.1"
196	120628	120359	-	89	10.5	conserved hypothetical protein	"QGS83801.1"
197	121063	120755	-	102	12.2	hypothetical protein	"QGS83802.1"
198	121400	121113	-	95	11	hypothetical protein	"QGS83803.1"
199	121762	121484	-	92	10.7	hypothetical protein	"QGS83804.1"
200	122087	121767	-	106	12.5	hypothetical protein	"QGS83805.1"
201	122307	122089	-	72	8.6	hypothetical protein	"QGS83806.1"
202	122524	122267	-	85	10	hypothetical protein	"QGS83807.1"
203	122789	122511	-	92	11	hypothetical protein	"QGS83808.1"

204	122981	122802	-	59	6.8	hypothetical protein	"QGS83809.1"
205	123213	123046	-	55	6.2	hypothetical protein	"QGS83810.1"
206	123580	123284	-	98	11.6	hypothetical protein	"QGS83811.1"
207	123757	123596	-	53	5.6	hypothetical protein	"QGS83812.1"
208	124147	123815	-	110	12.5	hypothetical protein	"QGS83813.1"
209	124344	124165	-	59	6.7	hypothetical protein	"QGS83814.1"
210	124898	124422	-	158	18.8	hypothetical protein	"QGS83815.1"
211	126387	124891	-	498	56.2	DNA ligase	"QGS83816.1"
212	126853	126374	-	159	18.4	conserved hypothetical protein	"QGS83817.1"
213	127007	126843	-	54	6.4	hypothetical protein	"QGS83818.1"
214	127414	127091	-	107	11.7	head assembly cochaperone with GroEL	"QGS83819.1"
215	127769	127455	-	104	11.8	conserved hypothetical protein	"QGS83820.1"
216	128268	127762	-	168	18.4	deoxycytidylate deaminase	"QGS83821.1"
217	128493	128290	-	67	7.7	conserved hypothetical protein	"QGS83822.1"
218	129371	128493	-	292	34.5	polynucleotide kinase	"QGS83823.1"
219	129823	129371	-	150	17.6	putative o-spanin	"QGS83824.1"
220	130143	129820	-	107	12.6	putative i-spanin	"QGS83825.1"
221	131357	130188	-	389	44.9	RNA ligase A	"QGS83826.1"
222	131754	131293	-	153	17.9	endonuclease II	"QGS83827.1"

223	132203	131805	-	132	14.8	hypothetical protein	"QGS83828.1"
224	132423	132274	-	49	5.5	hypothetical protein	"QGS83829.1"
225	132709	132491	-	72	8.6	hypothetical protein	"QGS83830.1"
226	132997	132779	-	72	9.2	hypothetical protein	"QGS83831.1"
227	133574	133098	-	158	18.2	putative polynucleotide kinase/phosphatase	"QGS83832.1"
228	134731	133571	-	386	45.4	NrdB aerobic NDP reductase, small subunit	"QGS83833.1"
229	134914	134747	-	55	6.3	hypothetical protein	"QGS83834.1"
230	135087	134914	-	57	6.7	hypothetical protein	"QGS83835.1"
231	135254	135087	-	55	6.2	hypothetical protein	"QGS83836.1"
232	137566	135323	-	747	84.8	ribonucleoside- diphosphate reductase subunit alpha	"QGS83837.1"
233	137880	137578	-	100	11.7	conserved hypothetical protein	"QGS83838.1"
234	139149	137917	-	410	47.9	dTMP (thymidylate) synthase	"QGS83839.1"
235	139390	139121	-	89	10.2	hypothetical protein	"QGS83840.1"
236	140053	139484	-	189	21.3	Frd dihydrofolate reductase	"QGS83841.1"
237	140398	140069	-	109	12.8	hypothetical protein	"QGS83842.1"
238	140783	140454	-	109	12.6	hypothetical protein	"QGS83843.1"
239	141877	140903	-	324	35.7	single-stranded DNA binding protein	"QGS83844.1"
240	142534	141938	-	198	23.1	Putative HNH endonuclease	"QGS83845.1"

241	143198	142521	-	225	26.5	similar to 59 protein of T4 needed for gp41 helicase loading	"QGS83846.1"
242	143462	143208	-	84	9.5	late promoter transcription accessory protein	"QGS83847.1"
243	143730	143455	-	91	10.7	Double-stranded DNA-binding protein	"QGS83848.1"
244	144331	143735	-	198	22.9	Inorganic triphosphatase	"QGS83849.1"
245	145289	144342	-	315	36.9	RnaseH ribonuclease	"QGS83850.1"
246	145477	145292	-	61	7.2	hypothetical protein	"QGS83851.1"
247	145552	149292	+	1246	136.7	long tail fiber, proximal subunit	"QGS83852.1"
248	149326	150465	+	379	42.3	Long-tail fiber protein	"QGS83853.1"
249	150668	152158	+	496	54.5	hinge connector of long-tail fiber distal connector	"QGS83854.1"
250	152229	154997	+	922	102.3	Long-tail fiber protein	"QGS83855.1"
251	155038	155277	+	79	9.2	hypothetical protein	"QGS83856.1"
252	155311	155967	+	218	25.1	holin lysis mediator	"QGS83857.1"
253	156251	156003	-	82	9.5	hypothetical protein	"QGS83858.1"
254	156559	156248	-	103	12.1	hypothetical protein	"QGS83859.1"
255	156916	156584	-	110	12.8	hypothetical protein	"QGS83860.1"
256	157293	156925	-	122	14.3	hypothetical protein	"QGS83861.1"
257	157495	157304	-	63	7.6	hypothetical protein	"QGS83862.1"
258	157797	157519	-	92	11.2	hypothetical protein	"QGS83863.1"

259	158567	157809	-	252	28.4	hypothetical protein	"QGS83864.1"
260	158793	158638	-	51	6	hypothetical protein	"QGS83865.1"
261	159075	158863	-	70	8	hypothetical protein	"QGS83866.1"
262	159387	159145	-	80	9	hypothetical protein	"QGS83867.1"
263	159651	159451	-	66	7	hypothetical protein	"QGS83868.1"
264	159818	159648	-	56	6.7	hypothetical protein	"QGS83869.1"
265	160095	159823	-	90	10.3	hypothetical protein	"QGS83870.1"
266	160368	160162	-	68	7.9	hypothetical protein	"QGS83871.1"
267	160875	160480	-	131	14.8	hypothetical protein	"QGS83872.1"
268	161076	160879	-	65	7.5	hypothetical protein	"QGS83873.1"
269	162443	161079	-	454	51.9	DNA topoisomerase II medium subunit	"QGS83874.1"
270	162813	162451	-	120	14.2	hypothetical protein	"QGS83875.1"
271	163109	162816	-	97	10.8	hypothetical protein	"QGS83876.1"
272	163472	163155	-	105	11.9	hypothetical protein	"QGS83877.1"
273	164479	163487	-	330	37.6	rIIB Protector from prophage-induced early lysis	"QGS83878.1"
274	164672	164541	-	43	5	hypothetical protein	"QGS83879.1"

Table F3: Summary of coding sequences (CDs) and predicted functions of ϕ EC_Makalu_003 complete genome GenBank ID: [MN882349.1](#)

CDs	Start	End	Strand	No of amino acids	Protein Size (kDa)	Predictive function	Protein Id.
1	10	2118	-	702	81.9	rIIA protector from prophage-induced early lysis	gb QHJ72949.1
2	2133	2390	-	85	10.5	hypothetical protein	gb QHJ72950.1
3	2401	2595	-	64	7.7	hypothetical protein	gb QHJ72951.1
4	2588	2782	-	64	7.6	hypothetical protein	gb QHJ72952.1
5	2849	3148	-	99	11.7	hypothetical protein	gb QHJ72953.1
6	3217	5040	-	607	68.5	DNA topoisomerase II large subunit	gb QHJ72954.1
7	5140	5313	-	57	6.5	FmdB family regulatory protein	gb QHJ72955.1
8	5315	5983	-	222	25.2	exonuclease	gb QHJ72956.1
9	5985	6227	-	80	9.3	hypothetical protein	gb QHJ72957.1
10	6258	6404	-	48	5.5	hypothetical protein	gb QHJ72958.1
11	6406	6573	-	55	6.5	hypothetical protein	gb QHJ72959.1
12	6584	7975	-	463	52.9	ATP-dependent DNA helicase	gb QHJ72960.1
13	7975	8289	-	104	12.1	hypothetical protein	gb QHJ72961.1
14	8289	9044	-	251	28.7	anti-sigma factor, putative	gb QHJ72962.1
15	9106	9609	-	167	19.1	ADP-ribosylase	gb QHJ72963.1
16	9677	10195	-	172	19.4	dCTP pyrophosphatase	gb QHJ72964.1
17	10210	11238	-	342	40.2	DNA primase	gb QHJ72965.1
18	11248	11451	-	67	7.7	hypothetical protein	gb QHJ72966.1
19	11448	11606	-	52	5.5	hypothetical protein	gb QHJ72967.1
20	11599	11775	-	58	6.2	major capsid protein	gb QHJ72968.1
21	11772	12149	-	125	14.3	hypothetical protein	gb QHJ72969.1
22	12180	12815	-	211	24.1	hypothetical protein	gb QHJ72970.1
23	12866	14278	-	470	53.3	ATP-dependent helicase	gb QHJ72971.1
24	14275	14592	-	105	12.1	head formation protein	gb QHJ72972.1
25	14648	15718	-	356	40.1	RecA-like recombination protein	gb QHJ72973.1
26	15730	15954	-	74	9	hypothetical protein	gb QHJ72974.1
27	15980	18658	-	892	103.4	DNA polymerase	gb QHJ72975.1
28	18741	19103	-	120	14.4	translation repressor protein	gb QHJ72976.1

29	19105	19683	-	192	22.4	clamp loader small subunit	gb QHJ72977.1
						DNA polymerase accessory	
30	19683	20657	-	324	36.9	protein	gb QHJ72978.1
31	20723	21409	-	228	25.6	sliding clamp holder	gb QHJ72979.1
32	21440	21817	-	125	15	hypothetical protein	gb QHJ72980.1
						RNA polymerase binding	
33	21822	22199	-	125	14.2	protein	gb QHJ72981.1
34	22230	22421	-	63	7.3	hypothetical protein	gb QHJ72982.1
35	22447	24129	-	560	63.6	endonuclease subunit	gb QHJ72983.1
36	24110	24373	-	87	10.1	hypothetical protein	gb QHJ72984.1
37	24370	24942	-	190	22.1	hypothetical protein	gb QHJ72985.1
38	24917	25234	-	105	12.6	hypothetical protein	gb QHJ72986.1
39	25231	25482	-	83	9.7	hypothetical protein	gb QHJ72987.1
40	25536	26561	-	341	39.1	endonuclease subunit	gb QHJ72988.1
41	26652	26939	-	95	11.1	hypothetical protein	gb QHJ72989.1
42	26941	27174	-	77	8.8	hypothetical protein	gb QHJ72990.1
						RNA polymerase sigma	
43	27158	27691	-	177	20.8	factor	gb QHJ72991.1
44	27732	29201	-	489	56.2	hypothetical protein	gb QHJ72992.1
45	29201	29488	-	95	10.8	hypothetical protein	gb QHJ72993.1
46	29510	29668	-	52	5.5	hypothetical protein	gb QHJ72994.1
47	29658	29927	-	89	10.3	glutaredoxin putative	gb QHJ72995.1
48	29924	30406	-	160	19.1	hypothetical protein	gb QHJ72996.1
49	30408	31232	-	274	31.8	hypothetical protein	gb QHJ72997.1
50	31245	31730	-	161	18.8	hypothetical protein	gb QHJ72998.1
51	31735	32262	-	175	20	hypothetical protein	gb QHJ72999.1
						anaerobic NTP reductase,	
52	32273	32776	-	167	19	small subunit	gb QHJ73000.1
53	32766	32918	-	50	6	hypothetical protein	gb QHJ73001.1
54	32994	33539	-	181	21.3	hypothetical protein	gb QHJ73002.1
55	33557	34099	-	180	20.9	hypothetical protein	gb QHJ73003.1
						anaerobic nucleoside	
56	34202	36064	-	620	69.5	diphosphate reductase	gb QHJ73004.1
57	36110	36604	-	164	18.9	hypothetical protein	gb QHJ73005.1
58	36659	37837	-	392	45.6	hypothetical protein	gb QHJ73006.1
59	37901	38461	-	186	21.8	hypothetical protein	gb QHJ73007.1
60	38488	38748	-	86	10	hypothetical protein	gb QHJ73008.1
						recombination endonuclease	
61	38812	39285	-	157	18	VII	gb QHJ73009.1

62	39310	39591	-	93	10.6	thioredoxin	gb QHJ73010.1
						DNA adenine	
63	39600	40412	-	270	31.3	methyltransferase	gb QHJ73011.1
64	40412	40843	-	143	16.7	hypothetical protein	gb QHJ73012.1
65	40854	41108	-	84	9.8	hypothetical protein	gb QHJ73013.1
66	41140	41361	-	73	8.3	hypothetical protein	gb QHJ73014.1
67	41354	41647	-	97	10.9	hypothetical protein	gb QHJ73015.1
68	41662	41970	-	102	11.5	hypothetical protein	gb QHJ73016.1
69	42040	42348	-	102	11.7	hypothetical protein	gb QHJ73017.1
70	42359	42637	-	92	10.4	hypothetical protein	gb QHJ73018.1
71	42724	42978	-	84	9.7	hypothetical protein	gb QHJ73019.1
72	42944	43282	-	112	13.3	hypothetical protein	gb QHJ73020.1
73	43282	43542	-	86	10	hypothetical protein	gb QHJ73021.1
74	43561	43764	-	67	7.6	hypothetical protein	gb QHJ73022.1
75	43761	44009	-	82	9.4	hypothetical protein	gb QHJ73023.1
76	44006	44440	-	144	16.6	hypothetical protein	gb QHJ73024.1
77	44451	44669	-	72	8.4	hypothetical protein	gb QHJ73025.1
78	44680	44877	-	65	7.4	hypothetical protein	gb QHJ73026.1
79	44888	45178	-	96	11.3	hypothetical protein	gb QHJ73027.1
80	45280	46059	-	259	25.7	receptor-recognizing protein	gb QHJ73028.1
81	46117	46338	-	73	8.2	hypothetical protein	gb QHJ73029.1
82	46428	46712	-	94	10.3	hypothetical protein	gb QHJ73030.1
83	46709	47059	-	116	13.2	hypothetical protein	gb QHJ73031.1
84	47056	47394	-	112	13	hypothetical protein	gb QHJ73032.1
85	47384	47593	-	69	7.6	hypothetical protein	gb QHJ73033.1
86	47922	48320	-	132	15.1	hypothetical protein	gb QHJ73034.1
						lysis inhibition regulator	
87	48307	48609	-	100	11.4	membrane protein	gb QHJ73035.1
88	48678	49274	-	198	22.2	thymidine kinase	gb QHJ73036.1
89	49274	49567	-	97	11.3	hypothetical protein	gb QHJ73037.1
90	49560	49778	-	72	8.6	hypothetical protein	gb QHJ73038.1
91	49775	49969	-	64	7.5	hypothetical protein	gb QHJ73039.1
92	49959	50414	-	151	16.5	macro domain protein	gb QHJ73040.1
						valyl-tRNA synthetase	
93	50430	50789	-	119	13.7	modifier	gb QHJ73041.1
94	50797	51387	-	196	21.8	putative 20.7 kDa protein	gb QHJ73042.1
						site-specific RNA	
95	51473	51895	-	140	16.7	endonuclease	gb QHJ73043.1
96	51900	52235	-	111	13.1	hypothetical protein	gb QHJ73044.1

97	52297	52542	-	81	9.7	hypothetical protein	gb QHJ73045.1
98	52539	52733	-	64	7.3	hypothetical protein	gb QHJ73046.1
99	52755	53453	-	232	27.1	putative 38.9 kDa protein	gb QHJ73047.1
						autonomous glycy radical	
100	53539	53955	-	138	15.2	cofactor	gb QHJ73048.1
101	53966	54091	-	41	4.8	hypothetical protein	gb QHJ73049.1
102	54091	54576	-	161	18.2	hypothetical protein	gb QHJ73050.1
103	54639	55028	-	129	14.8	putative endolysin	gb QHJ73051.1
104	55057	55248	-	63	6.9	hypothetical protein	gb QHJ73052.1
105	55250	55465	-	71	7.9	hypothetical protein	gb QHJ73053.1
106	55468	55647	-	59	6.5	hypothetical protein	gb QHJ73054.1
107	55729	55932	-	67	8	hypothetical protein	gb QHJ73055.1
108	55896	56054	-	52	5.7	hypothetical protein	gb QHJ73056.1
109	56057	56371	-	104	12.2	hypothetical protein	gb QHJ73057.1
110	56328	56648	-	106	12	hypothetical protein	gb QHJ73058.1
111	56667	56867	-	66	7.5	hypothetical protein	gb QHJ73059.1
112	56869	57051	-	60	6.7	hypothetical protein	gb QHJ73060.1
113	57060	57386	-	108	12.4	hypothetical protein	gb QHJ73061.1
114	57466	57654	-	62	7.2	hypothetical protein	gb QHJ73062.1
115	57677	57865	-	62	7.2	hypothetical protein	gb QHJ73063.1
116	57877	58098	-	73	8.5	hypothetical protein	gb QHJ73064.1
117	58165	58350	-	61	6.7	hypothetical protein	gb QHJ73065.1
118	58626	58844	-	72	8.5	hypothetical protein	gb QHJ73066.1
119	58841	59023	-	60	7	hypothetical protein	gb QHJ73067.1
120	59020	59244	-	74	8.8	hypothetical protein	gb QHJ73068.1
121	59241	59351	-	36	4	hypothetical protein	gb QHJ73069.1
122	59348	59545	-	65	7.2	hypothetical protein	gb QHJ73070.1
						discriminator of mRNA	
123	59545	59739	-	64	7.3	degradation	gb QHJ73071.1
124	59749	59907	-	52	5.4	hypothetical protein	gb QHJ73072.1
125	59975	60352	-	125	14.8	hypothetical protein	gb QHJ73073.1
126	60465	60929	-	154	17.8	hypothetical protein	gb QHJ73074.1
						chaperone for tail fiber	
127	60932	61192	-	86	9.8	formation	gb QHJ73075.1
						putative deoxynucleotide	
128	61225	61881	-	218	24.5	monophosphate kinase	gb QHJ73076.1
						tail completion and sheath	
129	61897	62487	-	196	22.2	stabilizer protein	gb QHJ73077.1
130	62677	62931	+	84	9.7	hypothetical protein	gb QHJ73078.1

131	62963	63784	-	273	31.2	DNA end protector protein	gb QHJ73079.1
132	63796	64269	-	157	19	head completion protein	gb QHJ73080.1
133	64325	64879	+	184	21.8	baseplate wedge subunit	gb QHJ73081.1
134	64891	66690	+	599	66.2	baseplate hub subunit and tail lysozyme	gb QHJ73082.1
135	66699	67268	+	189	21.3	hypothetical protein	gb QHJ73083.1
136	67270	67809	+	179	20.9	putative HNH endonuclease	gb QHJ73084.1
137	67825	68118	+	97	10.2	hypothetical protein	gb QHJ73085.1
138	68115	70019	+	634	70.7	baseplate wedge subunit	gb QHJ73086.1
139	70016	73102	+	1028	119.2	baseplate wedge subunit	gb QHJ73087.1
140	73095	74090	+	331	37.6	baseplate wedge subunit	gb QHJ73088.1
141	74200	74457	+	85	10	hypothetical protein	gb QHJ73089.1
142	74478	74774	+	98	12	hypothetical protein	gb QHJ73090.1
143	74774	75613	+	279	31.7	putative methyltransferase	gb QHJ73091.1
144	75689	76543	+	284	30.5	baseplate wedge tail fiber connector	gb QHJ73092.1
145	76540	78342	+	600	66.8	baseplate wedge subunit and tail pin	gb QHJ73093.1
146	78344	78988	+	214	23.3	baseplate wedge protein	gb QHJ73094.1
147	79000	80400	+	466	49.8	short tail fibers protein	gb QHJ73095.1
148	80400	82169	+	589	64.3	fibrin	gb QHJ73096.1
149	82216	83148	+	310	33.6	neck protein	gb QHJ73097.1
150	83185	83925	+	246	28.5	neck protein	gb QHJ73098.1
151	83954	84787	+	277	32.3	tail sheath stabilizer and completion protein	gb QHJ73099.1
152	84801	85298	+	165	18.8	small terminase protein	gb QHJ73100.1
153	85295	88111	+	938	106.9	large terminase protein	gb QHJ73101.1
154	88146	90146	+	666	72.6	tail sheath protein	gb QHJ73102.1
155	90220	90714	+	164	18.4	tail tube protein	gb QHJ73103.1
156	90773	92338	+	521	60.5	portal vertex protein	gb QHJ73104.1
157	92339	92578	+	79	9.5	putative prohead core protein I	gb QHJ73105.1
158	92591	92998	+	135	15.4	prohead assembly protein	gb QHJ73106.1
159	93010	93705	+	231	25.2	prohead core scaffolding protein and protease	gb QHJ73107.1
160	93737	94531	+	264	29.5	prohead core protein	gb QHJ73108.1
161	94591	96177	+	528	56.7	major capsid protein	gb QHJ73109.1
162	96395	96547	+	50	5.8	hypothetical protein	gb QHJ73110.1
163	96581	96733	+	50	5.8	hypothetical protein	gb QHJ73111.1

164	96817	98058	+	413	45.7	capsid vertex protein	gb QHJ73112.1
165	98059	98646	-	195	22.3	hypothetical protein	gb QHJ73113.1
166	99061	99498	-	145	16.3	hypothetical protein	gb QHJ73114.1
167	99545	99820	-	91	10.5	hypothetical protein	gb QHJ73115.1
168	99820	100017	-	65	7.5	hypothetical protein	gb QHJ73116.1
169	100218	101420	-	400	45.2	putative head outer capsid protein	gb QHJ73117.1
170	101516	101680	-	54	6.1	hypothetical protein	gb QHJ73118.1
171	101759	102475	-	238	27.2	inhibitor of prohead protease	gb QHJ73119.1
172	102546	104048	+	500	57.7	ATP-dependent DNA helicase	gb QHJ73120.1
173	104092	104328	+	78	9.1	ATP-dependent DNA helicase	gb QHJ73121.1
174	104392	104568	-	58	6.5	recombination, repair, and ssDNA binding protein	gb QHJ73122.1
175	104590	104997	-	135	15.8	recombination, repair, and ssDNA binding protein	gb QHJ73123.1
176	105045	105431	-	128	14.7	baseplate wedge subunit	gb QHJ73124.1
177	105440	106069	-	209	23.9	baseplate hub subunit	gb QHJ73125.1
178	106140	106910	+	256	29.6	baseplate hub assembly protein	gb QHJ73126.1
179	106888	107997	+	369	42.2	baseplate central spike complex protein	gb QHJ73127.1
180	107997	108515	+	172	19.4	baseplate hub assembly protein	gb QHJ73128.1
181	108512	110245	+	577	64.9	baseplate hub subunit, tail length determinator	gb QHJ73129.1
182	110245	111303	+	352	37.9	baseplate tail-tube junction protein	gb QHJ73130.1
183	111303	112235	+	310	34.1	baseplate tail-tube junction protein	gb QHJ73131.1
184	112269	112754	-	161	18.7	hypothetical protein	gb QHJ73132.1
185	112751	113575	-	274	32	ADP-ribosyltransferase	gb QHJ73133.1
186	113654	115705	-	683	76.4	ADP-ribosyltransferase exoenzyme	gb QHJ73134.1
187	115773	115985	-	70	8	hypothetical protein	gb QHJ73135.1
188	116057	116236	-	59	6.4	hypothetical protein	gb QHJ73136.1
189	116305	116823	-	172	20.5	hypothetical protein	gb QHJ73137.1
190	116825	117154	-	109	13	hypothetical protein	gb QHJ73138.1

						putative C-5 cytosine DNA	
191	117154	117870	-	238	27.4	methylase	gb QHJ73139.1
192	117867	118112	-	81	9.6	hypothetical protein	gb QHJ73140.1
193	118109	118360	-	83	9.1	hypothetical protein	gb QHJ73141.1
194	118444	118611	-	55	6.2	hypothetical protein	gb QHJ73142.1
195	118688	118969	-	93	10.6	hypothetical protein	gb QHJ73143.1
196	119040	119309	-	89	10.5	hypothetical protein	gb QHJ73144.1
197	119436	119744	-	102	12.2	hypothetical protein	gb QHJ73145.1
198	119794	120081	-	95	11	hypothetical protein	gb QHJ73146.1
199	120164	120442	-	92	10.7	hypothetical protein	gb QHJ73147.1
200	120447	120767	-	106	12.5	hypothetical protein	gb QHJ73148.1
201	120769	120987	-	72	8.6	hypothetical protein	gb QHJ73149.1
202	120947	121204	-	85	10	hypothetical protein	gb QHJ73150.1
203	121191	121469	-	92	11	hypothetical protein	gb QHJ73151.1
204	121482	121661	-	59	6.8	hypothetical protein	gb QHJ73152.1
205	121726	121893	-	55	6.2	hypothetical protein	gb QHJ73153.1
206	121962	122255	-	97	11.3	hypothetical protein	gb QHJ73154.1
207	122272	122463	-	63	7.6	hypothetical protein	gb QHJ73155.1
208	122521	122841	-	106	12	hypothetical protein	gb QHJ73156.1
209	122859	123038	-	59	6.7	hypothetical protein	gb QHJ73157.1
210	123115	123591	-	158	18.8	hypothetical protein	gb QHJ73158.1
211	123584	125080	-	498	56.2	DNA ligase	gb QHJ73159.1
212	125067	125546	-	159	18.4	hypothetical protein	gb QHJ73160.1
213	125536	125700	-	54	6.4	hypothetical protein	gb QHJ73161.1
						head assembly cochaperone	
214	125784	126107	-	107	11.7	with GroEL	gb QHJ73162.1
215	126148	126462	-	104	11.8	hypothetical protein	gb QHJ73163.1
216	126455	126961	-	168	18.4	deoxycytidylate deaminase	gb QHJ73164.1
217	126983	127186	-	67	7.7	hypothetical protein	gb QHJ73165.1
218	127186	128064	-	292	34.5	polynucleotide kinase	gb QHJ73166.1
						spanin, outer lipoprotein	
219	128064	128516	-	150	17.6	subunit	gb QHJ73167.1
						spanin, inner membrane	
220	128513	128836	-	107	12.6	subunit	gb QHJ73168.1
221	128881	130050	-	389	44.8	RNA ligase A	gb QHJ73169.1
222	129986	130447	-	153	17.9	endonuclease II	gb QHJ73170.1
223	130498	130896	-	132	14.8	hypothetical protein	gb QHJ73171.1
224	130976	131125	-	49	5.5	hypothetical protein	gb QHJ73172.1
225	131193	131411	-	72	8.6	hypothetical protein	gb QHJ73173.1

226	131481	131699	-	72	9.2	hypothetical protein	gb QHJ73174.1
						putative polynucleotide	
227	131800	132276	-	158	18.2	kinase/phosphatase	gb QHJ73175.1
						aerobic NDP reductase,	
228	132273	133433	-	386	45.4	small subunit	gb QHJ73176.1
229	133449	133616	-	55	6.3	hypothetical protein	gb QHJ73177.1
230	133616	133789	-	57	6.7	hypothetical protein	gb QHJ73178.1
231	133789	133956	-	55	6.2	hypothetical protein	gb QHJ73179.1
						ribonucleoside-diphosphate	
232	134025	136268	-	747	84.8	reductase subunit alpha	gb QHJ73180.1
233	136280	136582	-	100	11.7	hypothetical protein	gb QHJ73181.1
234	136619	137851	-	410	47.9	thymidylate synthase	gb QHJ73182.1
235	137823	138092	-	89	10.3	hypothetical protein	gb QHJ73183.1
236	138092	138184	-	30	3.4	hypothetical protein	gb QHJ73184.1
237	138186	138755	-	189	21.3	dihydrofolate reductase	gb QHJ73185.1
238	138771	139100	-	109	12.8	hypothetical protein	gb QHJ73186.1
239	139156	139485	-	109	12.6	hypothetical protein	gb QHJ73187.1
						single-stranded DNA	
240	139605	140573	-	322	35.4	binding protein	gb QHJ73188.1
						putative DNA helicase	
241	140634	141314	-	226	26.5	loader protein	gb QHJ73189.1
						late promoter transcription	
242	141324	141578	-	84	9.5	accessory protein	gb QHJ73190.1
						double-stranded DNA-	
243	141571	141846	-	91	10.7	binding protein	gb QHJ73191.1
244	141851	142450	-	199	23.2	hypothetical protein	gb QHJ73192.1
245	142461	143408	-	315	36.9	Ribonuclease H	gb QHJ73193.1
246	143411	143596	-	61	7.2	hypothetical protein	gb QHJ73194.1
						long tail fiber, proximal	
247	143669	147409	+	1246	136.6	subunit	gb QHJ73195.1
						hinge connector of long-tail	
248	147443	148582	+	379	42.3	fiber, proximal connector	gb QHJ73196.1
						hinge connector of long tail	
249	148785	150275	+	496	54.5	fiber distal connector	gb QHJ73197.1
250	150346	153288	+	980	108.5	long tail fiber distal subunit	gb QHJ73198.1
251	153329	153568	+	79	9.2	hypothetical protein	gb QHJ73199.1
252	153602	154258	+	218	25.1	holin lysis mediator	gb QHJ73200.1
253	154294	154542	-	82	9.5	hypothetical protein	gb QHJ73201.1
254	154539	154850	-	103	12.1	hypothetical protein	gb QHJ73202.1

255	154875	155207	-	110	12.8	hypothetical protein	gb QHJ73203.1
256	155216	155584	-	122	14.3	hypothetical protein	gb QHJ73204.1
257	155595	155786	-	63	7.6	hypothetical protein	gb QHJ73205.1
258	155810	156088	-	92	11.1	hypothetical protein	gb QHJ73206.1
259	156100	156858	-	252	28.4	hypothetical protein	gb QHJ73207.1
260	156929	157084	-	51	6	hypothetical protein	gb QHJ73208.1
261	157154	157366	-	70	8	hypothetical protein	gb QHJ73209.1
262	157436	157678	-	80	9	hypothetical protein	gb QHJ73210.1
263	157742	157942	-	66	7	hypothetical protein	gb QHJ73211.1
264	157939	158109	-	56	6.7	hypothetical protein	gb QHJ73212.1
265	158114	158386	-	90	10.3	hypothetical protein	gb QHJ73213.1
266	158454	158660	-	68	7.9	hypothetical protein	gb QHJ73214.1
267	158772	159167	-	131	14.9	hypothetical protein	gb QHJ73215.1
268	159171	159368	-	65	7.5	hypothetical protein	gb QHJ73216.1
DNA topoisomerase II							
269	159371	160735	-	454	51.9	medium subunit	gb QHJ73217.1
270	160743	161105	-	120	14.2	hypothetical protein	gb QHJ73218.1
271	161108	161401	-	97	10.8	hypothetical protein	gb QHJ73219.1
272	161447	161764	-	105	11.9	hypothetical protein	gb QHJ73220.1
rIIB protector from							
273	161779	162771	-	330	37.6	phage-induced early lysis	gb QHJ73221.1

Table F4: Summary of coding sequences (CDs) and predicted functions of ϕ Kp_Pokalde_001 complete genome.

CDs	Start	End	Strand	No of amino acids	Protein Size (kDa)	Predictive function	Protein Id.
1	1460	1675	+	71	8.1	hypothetical protein	gb QWT56592.1
2	1754	2329	+	191	20.8	hypothetical protein	gb QWT56593.1
3	2391	2612	+	73	8.4	DNA topoisomerase II large subunit	gb QWT56594.1
4	2605	2868	+	87	9.5	hypothetical protein	gb QWT56595.1
5	2877	3056	+	59	6.9	hypothetical protein	gb QWT56596.1
6	3068	3268	+	66	7.5	hypothetical protein	gb QWT56597.1
7	3256	3744	+	162	18	HNH endonuclease	gb QWT56598.1
8	3744	4085	+	113	13.3	hypothetical protein	gb QWT56599.1
9	4135	5817	+	560	63.5	putative structural protein	gb QWT56600.1
10	5817	6863	+	348	39	putative peptidase	gb QWT56601.1
11	6866	7306	+	146	16.5	putative membrane protein	gb QWT56602.1
12	7303	7467	+	54	6.1	hypothetical protein	gb QWT56603.1
13	7470	8261	+	263	29.5	putative DNA primase	gb QWT56604.1
14	8242	8679	+	145	16.1	putative HNH endonuclease	gb QWT56605.1
15	8680	9960	+	426	47.7	putative DNA helicase	gb QWT56606.1
16	10011	10232	+	73	8.2	putative membrane-associated initiation of head vertex	gb QWT56607.1
17	10190	10345	+	51	5.8	hypothetical protein	gb QWT56608.1
18	10336	10497	+	53	6.3	hypothetical protein	gb QWT56609.1
19	10494	12884	+	796	91.3	putative DNA directed DNA polymerase	gb QWT56610.1
20	12881	13102	+	73	8.1	hypothetical protein	gb QWT56611.1
21	13264	14253	+	329	37	putative phosphoesterase	gb QWT56612.1
22	14276	14779	+	167	18.9	hypothetical protein	gb QWT56613.1
23	14801	15625	+	274	29.2	large tegument protein	gb QWT56614.1
24	15678	15932	+	84	9.2	hypothetical protein	gb QWT56615.1
25	15936	16307	+	123	13.3	hypothetical protein	gb QWT56616.1
26	16310	16468	+	52	5.9	hypothetical protein	gb QWT56617.1
27	16534	16902	+	122	13.5	hypothetical protein	gb QWT56618.1
28	16883	17851	+	322	36.7	putative 5'-3' exonuclease	gb QWT56619.1
29	18002	18451	+	149	16.7	HNH endonuclease	gb QWT56620.1

30	18433	18855	+	140	15.7	putative DNA endonuclease VII	gb QWT56621.1
31	18852	19313	+	153	17.7	hypothetical protein	gb QWT56622.1
32	19455	21923	+	822	93.1	RNA polymerase	gb QWT56623.1
33	21947	22387	+	146	16.3	membrane-associated initiation of head vertex	gb QWT56624.1
34	22384	22647	+	87	8.7	hypothetical protein	gb QWT56625.1
35	22657	24252	+	531	58.1	head-tail connector protein	gb QWT56626.1
36	24267	25109	+	280	30	putative scaffolding protein	gb QWT56627.1
37	25135	26154	+	339	37.7	capsid protein	gb QWT56628.1
38	26166	26348	+	60	6.3	hypothetical protein	gb QWT56629.1
39	26398	26730	+	110	12.3	hypothetical protein	gb QWT56630.1
40	26896	27519	+	207	23.8	tail tubular protein A	gb QWT56631.1
41	27529	29889	+	786	86.1	tail tubular protein B	gb QWT56632.1
42	29891	30478	+	195	20.4	putative internal virion protein	gb QWT56633.1
43	30496	33180	+	894	97.3	putative internal core protein	gb QWT56634.1
44	33231	36929	+	1232	134.3	putative internal core protein	gb QWT56635.1
45	36931	38523	+	530	54.8	tail fibers protein	gb QWT56636.1
46	38523	38825	+	100	11.2	putative DNA maturase A	gb QWT56637.1
47	38825	40681	+	618	69.5	putative DNA maturase B	gb QWT56638.1
48	40681	41055	+	124	13	hypothetical protein	gb QWT56639.1
49	41067	41249	+	60	6.2	hypothetical protein	gb QWT56640.1
50	41249	41653	+	134	14	u-spanin	gb QWT56641.1
51	41646	41897	+	83	9.1	putative holin	gb QWT56642.1
52	41905	42480	+	191	20.8	endolysin	gb QWT56643.1
53	42491	44206	+	571	60.4	tail spike protein	gb QWT56644.1

Table F5: Summary of coding sequences (CDs) and predicted functions of ϕ Kp_Pokalde_002 complete genome.

CDs	Start	End	Strand	No of amino acids	Protein Size (kDa)	Predictive function	Protein Id.
1	874	1053	+	59	6.7	hypothetical protein	gb QKE60341.1
						S-adenosyl-L-methionine	
2	1118	1585	+	155	17.4	hydrolase	gb QKE60342.1
3	1709	1906	+	65	7.6	hypothetical protein	gb QKE60343.1
4	1932	2948	+	338	39.1	protein kinase	gb QKE60344.1
5	3018	5738	+	906	101.3	RNA polymerase	gb QKE60345.1
6	5837	6397	+	186	21.7	fusion protein	gb QKE60346.1
7	6487	6663	+	58	6.6	hypothetical protein	gb QKE60347.1
8	6667	6924	+	85	9.7	hypothetical protein	gb QKE60348.1
9	7025	8065	+	346	39.3	DNA ligase	gb QKE60349.1
10	8182	8445	+	87	10.1	hypothetical protein	gb QKE60350.1
11	8438	8869	+	143	16	nucleotide kinase	gb QKE60351.1
						bacterial RNA polymerase	
12	8947	9096	+	49	5.4	inhibitor	gb QKE60352.1
						single-stranded DNA-	
13	9156	9851	+	231	25.6	binding protein	gb QKE60353.1
14	9887	10270	+	127	14.2	HNH endonuclease	gb QKE60354.1
15	10251	10697	+	148	16.9	endonuclease	gb QKE60355.1
16	10700	11155	+	151	16.8	endolysin amidase	gb QKE60356.1
17	11498	13228	+	576	63.4	DNA primase/helicase	gb QKE60357.1
18	13300	13509	+	69	7.5	hypothetical protein	gb QKE60358.1
19	13509	13781	+	90	10.3	hypothetical protein	gb QKE60359.1
20	13855	14241	+	128	14.4	hypothetical protein	gb QKE60360.1
21	14258	16384	+	708	80.1	DNA polymerase	gb QKE60361.1
22	16403	16687	+	94	10.4	HNS binding protein	gb QKE60362.1
23	16684	16893	+	69	7.2	hypothetical protein	gb QKE60363.1
24	17168	18073	+	301	34.3	exonuclease	gb QKE60364.1
25	18249	18494	+	81	9.4	hypothetical protein	gb QKE60365.1
26	18720	18980	+	86	8.8	tail assembly protein	gb QKE60366.1
27	19004	20611	+	535	58.6	head-to-tail joining protein	gb QKE60367.1
28	20715	21668	+	317	35	capsid assembly protein	gb QKE60368.1
29	21849	22886	+	345	36.6	major capsid protein	gb QKE60369.1
30	22937	23158	+	73	7.8	minor capsid protein	gb QKE60370.1

31	23225	23803	+	192	21.3	tail tubular protein A	gb QKE60371.1
32	23825	24226	+	133	15.6	homing endonuclease	gb QKE60372.1
33	24192	26567	+	791	89	tail fiber protein B	gb QKE60373.1
34	26640	27053	+	137	16	internal virion protein A	gb QKE60374.1
35	27050	27436	+	128	14.5	putative DNA endonuclease VII	gb QKE60375.1
36	27441	28031	+	196	21.1	internal virion protein B	gb QKE60376.1
37	28031	30286	+	751	84.6	internal virion protein C	gb QKE60377.1
38	30303	34268	+	1321	142.6	internal virion protein D	gb QKE60378.1
39	34330	36663	+	777	84	tail fiber protein	gb QKE60379.1
40	36674	38248	+	524	55.7	tail fiber family protein	gb QKE60380.1
41	38261	38470	+	69	7.5	lysis protein	gb QKE60381.1
42	38504	38761	+	85	9.6	DNA packaging protein, small subunit	gb QKE60382.1
43	38858	39304	+	148	16.5	spanin inner membrane subunit	gb QKE60383.1
44	39301	41058	+	585	66.4	DNA packaging protein, large subunit	gb QKE60384.1
45	41303	41452	+	49	5.4	putative membrane protein	gb QKE60385.1

APPENDIX -G

Predicted promoter sequences of the phages

Phage promoter sequences were predicted by the *PhagePromoter* software. This tool searches the whole genome for promoters and identifies both types of promoters found in phage genomes and different motifs of each promoter type. A threshold was set at 0.9 for *Escherichia* phages and 0.8 for *Klebsiella* phages.

Table G1: Predicted promoter sequences of Phage_Ec_Makalu_001

S N o	Strand	Positions	Promoter Sequence	Type	Scores
1	+	(2107..2138)	TTCATTATCAATATGCATTTTCATAATATAAT	host	0.964
2	+	(3124..3150)	TTGCCATGCTCATCATCATGTTATTCT	host	0.948
3	+	(6107..6139)	TTGCCATGTATGCGCATACCCTGTTGTTAAAAT	host	0.939
4	+	(38456..38484)	TTTATACGTTTTCTGTACCATAATATAAT	host	0.909
5	+	(40742..40768)	TTGACCGTGCAATTCCCATTCTACAAT	host	0.909
6	+	(45689..45719)	TTGTAAGAGTCACTAGCGCCAATGCTATAAT	host	0.979
7	+	(49288..49313)	TTGACAATCTCAATACCCGCCATAAT	host	0.979
8	+	(49650..49679)	TGGAACACTAACAGGAGCGGTTTTTATATT	host	0.908
9	+	(62444..62451)	AATAAATA	host	0.989
10	+	(64085..64092)	TATAAATA	host	0.989
11	+	(69143..69171)	TTGACAGCTAAACCGATTGCTGATAACAT	host	0.994
12	+	(72008..72036)	TTGACAGCGGATTGCCTAGCGTGTATCCT	host	0.945
13	+	(73383..73410)	TTGACAATCTTGTCTGATAAGGTATAAT	host	1
14	+	(74086..74118)	TTGACATATGAAGAAAAGGAGTTTTGCTATAAT	host	0.997
15	+	(74599..74606)	AATAAATA	host	0.944
16	+	(74894..74901)	TATAAATA	host	0.975
17	+	(76011..76040)	TTGCCTAAAGGAAGCGCGAGTGATTATAAT	host	0.988
18	+	(78212..78241)	TCAAACGTATTGCATAAGGTGATGTATAAT	host	0.945
19	+	(82351..82378)	TTGACTTAGATCCACCATTTGGTATACT	host	1
20	+	(82389..82396)	AATAAATA	host	0.991
21	+	(82668..82699)	TTGATTTTGTCAAGAGAGAAGACACGTATAAT	host	0.978
22	+	(84033..84040)	GATAAATA	host	0.926
23	+	(87221..87228)	TATAAATA	host	0.947
24	+	(89806..89837)	TTGCTATCGATTGGGTAGAAATAAATATATTAT	host	0.973

25	+	(90616..90623)	GATAAATA	host	0.962
26	+	(91197..91204)	AATAAATA	host	0.977
27	+	(92550..92576)	TTGAAAGACTCTGGTCGCGGATACAAT	host	0.949
28	+	(92811..92818)	TATAAATA	host	0.96
29	+	(93664..93671)	TATAAATA	host	0.93
30	+	(95422..95429)	TATAAATA	host	0.988
31	+	(95983..95990)	TATAAATA	host	0.988
32	+	(98192..98219)	TTAATATTGTCCATATGTAACTAAAAT	host	0.908
33	+	(100907..100933)	ATTGCATAACGGAACACTACAATTTAAAAT	host	0.907
34	+	(101012..101039)	TTGACAGACCCATCGCGTTTGATATAAT	host	1
35	+	(101721..101728)	TATAAATA	host	0.959
36	+	(103266..103273)	AATAAATA	host	0.949
37	+	(103763..103792)	GTTTACAACAAATACAGATTTTCATAAAAAT	host	0.995
38	+	(104938..104966)	TTGATTTTTACTTGTCTAAGTCTAGAAT	host	0.941
39	+	(105136..105161)	TTGATCCCCGTACATTCGTATATAAT	host	0.916
40	+	(105330..105337)	TATAAATA	host	0.992
41	+	(106859..106885)	ATTGATTTTGTACTAAGCAGTATAAT	host	0.972
42	+	(107215..107242)	ATGACAGAACTAAACCTATGTTAAAAT	host	0.97
43	+	(110186..110208)	TATAAAAATACACTATTGAGAAA	phage	0.938
44	+	(110480..110505)	TTGACACTTTCCCGTGGTACTATATT	host	0.996
45	+	(115986..116013)	ATGACAAAGTTTTTAGTATTGGTATAGT	host	0.905
46	+	(119841..119868)	AATGATTTTCATCACTGGAGACGTATAAT	host	0.967
47	+	(120391..120416)	TTGATATGCTTTATAATCTTTAAATT	host	0.904
48	+	(121185..121212)	AATGCTTTATACGCGTATTTTCATAAATT	host	0.977
49	+	(127235..127265)	TTGACCCATATATTCTGCATCAGATAAAAAT	host	0.939
50	+	(133331..133356)	TTGACATATTTCCGTAATTATACATT	host	0.961
51	+	(140400..140422)	AAAAAAGCCTCCCCGAAGGGAGG	phage	0.906
52	+	(144436..144443)	TATAAATA	host	0.99
53	+	(149547..149554)	TATAAATA	host	0.986
54	+	(151106..151113)	TCTAAATA	host	0.915
55	+	(151699..151726)	TTGATATCGTTGACGGTATTTTAAATT	host	0.914
56	+	(153751..153781)	TTTATATTCGTTCTGATGCTCGCCTTAAAAT	host	0.959

Table G2: Predicted promoter sequences of Phage_Ec_Makalu_002

S No	Strand	Positions	Promoter Sequence	Type	Scores
1	+	(2095..2126)	TTCATTATCAATATGCATTTTCATAATATAAT	host	0.963
2	+	(3112..3138)	TTGCCATGCTCATCATCATGTTATTCT	host	0.938
3	+	(6095..6127)	TTGCCATGTATGCGCATACCTTGTTGTTAAAT	host	0.927
4	+	(18134..18162)	TAGACATTATAAACAACGCGCTCTACAAT	host	0.939
5	+	(38444..38472)	TTTATACGTTTTCTGTACCATAATATAAT	host	0.95
6	+	(45680..45710)	TTGTAAGAGTTACTAGCACCAATGCTATAAT	host	0.978
7	+	(47730..47756)	TTTATAAATTGTTTTAAAGCATAGAAT	host	0.907
8	+	(48416..48442)	TTTAAAATATTCAGTTATATTTATAAT	host	0.937
9	+	(49278..49303)	TTGACAATCTCAATACCCGCCATAAT	host	0.978
10	+	(49640..49669)	TGGAACACTAACAGGAGCGGTTTTTATATT	host	0.901
11	+	(62439..62446)	AATAAATA	host	0.989
12	+	(63614..63642)	TTGACAATCCTCTTTGCTATTGCTAAAAT	host	1
13	+	(63672..63679)	GATAAATA	host	0.973
14	+	(65206..65213)	TATAAATA	host	0.989
15	+	(70264..70292)	TTGACAGCTAAACCGATTGCTGATAACAT	host	0.994
16	+	(73129..73157)	TTGACAGCGGATTGCCTAGCGTGTATCCT	host	0.943
17	+	(74504..74531)	TTGACAATCTTGTCTGATAAGGTATAAT	host	1
18	+	(75207..75239)	TTGACATATGAAGAAAAGGAGTTTTGCTATAAT	host	0.997
19	+	(75720..75727)	AATAAATA	host	0.946
20	+	(76015..76022)	TATAAATA	host	0.975
21	+	(77132..77161)	TTGCCTAAAGGAAGCGGAGTGATTATAAT	host	0.988
22	+	(79333..79362)	TCAAACGTATTGCATAAGGTGATGTATAAT	host	0.943
23	+	(83472..83499)	TTGACTTAGATCCACCATTTGGTATACT	host	1
24	+	(83510..83517)	AATAAATA	host	0.991
25	+	(83789..83820)	TTGATTTTGTCAAGAGAGAAGACACGTATAAT	host	0.988
26	+	(85154..85161)	GATAAATA	host	0.93
27	+	(88753..88778)	TTGATATTACTGAATTTTCCTTATAAA	host	0.911
28	+	(89335..89342)	TATAAATA	host	0.958
29	+	(91920..91951)	TTGCTATCGATTGGGTAGAATAAATATATTAT	host	0.973
30	+	(91938..91945)	AATAAATA	host	0.956
31	+	(92730..92737)	GATAAATA	host	0.947
32	+	(93311..93318)	AATAAATA	host	0.995
33	+	(94664..94690)	TTGAAAGACTCTGGTCGCGGATACAAT	host	0.945
34	+	(94925..94932)	TATAAATA	host	0.962
35	+	(95778..95785)	TATAAATA	host	0.93

36	+	(97536..97543)	TATAAATA	host	0.99
37	+	(98083..98090)	TATAAATA	host	0.988
38	+	(100292..100319)	TTAATATTGTCCATATGTAAACTAAAAT	host	0.908
39	+	(103007..103033)	ATTGCATAACGGAACACTACAATTTAAAAT	host	0.907
40	+	(103112..103139)	TTGACAGACCCATCGCGTTTGATATAAT	host	1
41	+	(103821..103828)	TATAAATA	host	0.959
42	+	(105366..105373)	AATAAATA	host	0.949
43	+	(105863..105892)	GTTTACAACAAATACAGATTTTCATAAAAAT	host	0.995
44	+	(107038..107066)	TTGATTTTTACTTGTCCCTAAGTCTAGAAT	host	0.941
45	+	(107236..107261)	TTGATCCCCGTACATTCGTATATAAT	host	0.916
46	+	(107430..107437)	TATAAATA	host	0.992
47	+	(108959..108985)	ATTGATTTTTGTTACTAAGCAGTATAAT	host	0.972
48	+	(109315..109342)	ATGACAGAACTAAACCTATGTTAAAAT	host	0.97
49	+	(112286..112308)	TATAAAAATACACTATTGAGAAA	phage	0.938
50	+	(112580..112605)	TTGACACTTTCCCGTGGTACTATATT	host	0.996
51	+	(118087..118114)	ATGACAAAGTTTTTGTAGTATTGGTATAGT	host	0.905
52	+	(121942..121969)	AATGATTTTCATCACTGGAGACGTATAAT	host	0.967
53	+	(122492..122517)	TTGATATGCTTTATAATCTTTAAATT	host	0.904
54	+	(123740..123765)	TTGAAATACACCGTTCATAATATTAT	host	0.975
55	+	(128928..128958)	TTGACCCATATATTCCTGCATCAGATAAAAAT	host	0.934
56	+	(135024..135049)	TTGACATATTTCCGTAATTATACATT	host	0.965
57	+	(140868..140890)	AAAAAAGCCTCCCCGAAGGGAGG	phage	0.908
58	+	(142175..142200)	TTTATAAAGACTAACGCCGATATATT	host	0.901
59	+	(145388..145416)	GTTTAATTCGGCACGGAAATAATTATAAT	host	0.971
60	+	(145516..145523)	TATAAATA	host	0.99
61	+	(150627..150634)	TATAAATA	host	0.986
62	+	(152186..152193)	TCTAAATA	host	0.906
63	+	(152779..152806)	TTGATATCGTTGACGGTATTTTAAATT	host	0.914

Table G3: Predicted promoter sequences of Phage_Ec_Makalu_003

S No	Strand	Positions	Promoter Sequence	Type	Scores
1	+	(2095..2126)	TTCATTATCAATATGCATTTTCATAATATAAT	host	0.963
2	+	(3112..3138)	TTGCCATGCTCATCATCATGTTATTCT	host	0.938
3	+	(6095..6127)	TTGCCATGTATGCGCATACCCTGTTGTTAAAAT	host	0.927
4	+	(9047..9078)	TTGATTCTCCTTAGTTGGTATGTGTGTATTAT	host	0.917
5	+	(18132..18160)	TAGACATTATAAAACAACGCGCTCTACAAT	host	0.94
6	+	(21735..21764)	TTGATATAGTCAAACGGGATATGACATAAT	host	0.97
7	+	(38441..38469)	TTTATACGTTTTCTGTACCATAATATAAT	host	0.948
8	+	(45890..45920)	TTGTAAGAGTCACTAGCGCCAATGCTATAAT	host	0.978
9	+	(49488..49513)	TTGACAATCTCAATACCCGCCATAAT	host	0.979
10	+	(49850..49879)	TGGAACACTAACAGGAGCGGTTTTTATATT	host	0.908
11	+	(53468..53493)	TTGATTAAGAGATTGCATCATATCAT	host	0.929
12	+	(62643..62650)	AATAAATA	host	0.989
13	+	(64285..64292)	TATAAATA	host	0.989
14	+	(69903..69931)	TTGACAGCTAAACCGATTGCTGATAACAT	host	0.994
15	+	(72768..72796)	TTGACAGCGGATTGCCTAGCGTGTATCCT	host	0.945
16	+	(74143..74170)	TTGACAATCTTGTCTGATAAGGTATAAT	host	1
17	+	(74846..74878)	TTGACATATGAAGAAAAGGAGTTTTGCTATAAT	host	0.997
18	+	(75359..75366)	AATAAATA	host	0.944
19	+	(75654..75661)	TATAAATA	host	0.975
20	+	(76771..76800)	TTGCCTAAAGGAAGCGGAGTGATTATAAT	host	0.988
21	+	(78972..79001)	TCAAACGTATTGCATAAGGTGATGTATAAT	host	0.945
22	+	(87525..87550)	TTGATATTACTGAATTCCTTATAAA	host	0.903
23	+	(88107..88114)	TATAAATA	host	0.952
24	+	(90692..90723)	TTGCTATCGATTGGGTAGAATAAATATATTAT	host	0.973
25	+	(91502..91509)	GATAAATA	host	0.988
26	+	(92083..92090)	AATAAATA	host	0.994
27	+	(93436..93462)	TTGAAAGACTCTGGTTCGCGGATACAAT	host	0.948
28	+	(94550..94557)	TATAAATA	host	0.933
29	+	(96308..96315)	TATAAATA	host	0.976
30	+	(96772..96779)	TATAAATA	host	0.987
31	+	(98981..99008)	TTAATATTGTCCATATGTAAACTAAAAT	host	0.91
32	+	(101802..101829)	TTGACAGACCCATCGCGTTTGATATAAT	host	1
33	+	(102502..102509)	TATAAATA	host	0.959
34	+	(104349..104377)	TTGATGGGGCAAATAAACCAATTTAAAAT	host	0.972
35	+	(105918..105943)	TTGATTCCCGTACATTCGTATATAAT	host	0.989
36	+	(106112..106119)	TATAAATA	host	0.995

37	+	(107641..107667)	ATTGATTTTGTACTAAGCAGTATAAT	host	0.973
38	+	(107997..108024)	ATGACAGAACTAAACCTATGTAAAAT	host	0.97
39	+	(108570..108597)	TTGATAAACTTAACAAATTAGATAAACT	host	0.906
40	+	(110968..110990)	TATAAAAATACACTATTGAGAAA	phage	0.938
41	+	(111262..111287)	TTGACACTTTCCTGGTACTATATT	host	0.996
42	+	(120622..120649)	AATGATTTTCATCACTGGAGACGTATAAT	host	0.967
43	+	(121172..121197)	TTGATATGCTTTATAATCTTTAAATT	host	0.904
44	+	(121966..121993)	AATGCTTTATACGCGTATTTCATAAATT	host	0.977
45	+	(133726..133751)	TTGACATATTTCCGTAATTATACATT	host	0.961
46	+	(142105..142137)	ATGTCATTACTIONTGCATTATTGTAGTGATATAGT	host	0.905
47	+	(143633..143640)	TATAAATA	host	0.99
48	+	(148744..148751)	TATAAATA	host	0.987
49	+	(150303..150310)	TCTAAATA	host	0.943
50	+	(150896..150923)	TTGATATCGTTGACGGTTATTTTAAATT	host	0.912
51	+	(152074..152101)	TTGACTTTTCGATGCTGGTCGATTAAATT	host	0.956
52	+	(152948..152978)	TTTATATTCGTTCTGATGCTCGCCTAAAAT	host	0.956

Table G4: Predicted promoter sequences of Phage_Kp_Pokalde_001

S No	Strand	Positions	Promoter Sequence	Type	Scores
1	+	(921..949)	TTGACACCGCGAAGGGCATAAGCTAGATT	host	0.967
2	+	(1680..1711)	AGCCTATAGCATCCTATGGGGTGCTATGTGAA	phage	0.995
3	+	(2335..2366)	AGCCTATAGCGTCCTATGGGGCGCTATGTGAA	phage	1
4	+	(38338..38365)	TTGCCTAGCAACTGGTACGACTTATATT	host	0.816
5	+	(43694..43722)	TTGCCACTGCACCTTCTCGGGGCTATAGT	host	0.84

Table G5: Predicted promoter sequences of Phage_Kp_Pokalde_002

Phage_KP_pokalde_002					
Phage promoter predicted by phagepromoter (0.99)					
S No	Strand	Positions	Promoter Sequence	Type	Scores
1	-	(387..415)	TTGACAATGACCACCAATAGCCCTATAGT	host	0.99
2	+	(423..444)	TATTAGGACACACTATAGGGAGA	phage	0.99
3	+	(5749..5770)	AATTAGGGCACACTATAGGGAAC	phage	0.99
4	+	(6923..6944)	AATTAGGACACACTATAGGCAGA	phage	0.99
5	+	(8065..8086)	AATTAGGACCCACTATAGGAGAC	phage	0.99
6	+	(9091..9112)	TCATTAGGACACACTATAGGGAC	phage	0.99
7	+	(11259..11280)	AATTAGGGCACACTACAGGGAGA	phage	0.99
8	+	(18182..18203)	AATTAGGACCCACTATAGGGAAG	phage	0.99

9	+	(20610..20631)	TAATTAGGGCACA	CTATAGGGAG	ph
10	+	(21671..21692)	GAATTAGGGCACA	CTATAGGGAG	ph
11	+	(26594..26615)	AATTAGGGCACA	CTATAGGGAGA	ph
12	+	(34268..34289)	AATTAGGACACACTA		
13	+	(41139..41160)	GAATTAGGGCACA	CTA	

APPENDIX-H

- f) Multiple sequence alignment of ϕ Kp_Pokalde_001, tail-spike protein (gp53) with other three similar phage proteins using Clustal Omega.

CLUSTAL O(1.2.4) multiple sequence alignment

KP-Pokalde_001TSP	-----MALV	4
Klebsiella_phage_K64-1_TSP	MSTELTQAKGSTSRYTSRKSCAIEFNTKIDEVQYISVGLDTSIKVFDNNTQIPYVGVN	60
Klebsiella_phage_K5_TSP	-MPRFNQPKGS-----TIGVL	15
Klebsiella_phage_KP32_TSP	MLDNFNQPKGS-----TIGVL	16
	:. .	
KP-Pokalde_001TSP	ENVQTRYYSQDDLWCRVA-----DYLAKDAPVLTGLRPDSSGNYAAAIERSVAKG	54
Klebsiella_phage_K64-1_TSP	INGNVISWVSDPVKCIILTSSGTYTLFSYGLTKNIPNLLDYSDSATDDSTRFKKAILAG	120
Klebsiella_phage_K5_TSP	RDGRTIQ-----EAFDSMPRLESFEGSTP---TDKLRRAAITLG	50
Klebsiella_phage_KP32_TSP	KDGRTIQ-----EAFDSLPRLESFSGSTA---TDKLRRAAITLG	51
	: * * . . : : : . . *	
KP-Pokalde_001TSP	VKVLRVPV-----GSYYVGDCHLTNPMLFIGDGLGVNPL-GAVFVKPSTATQMFYFDG	107
Klebsiella_phage_K64-1_TSP	TESLYIPPREIY--KDVMIIGELDITSTLRLWGDSSGNIN-TGGSTKIKIASASAYGIHFNG	177
Klebsiella_phage_K5_TSP	VSEVAIGPVEGNDGSPYEFGEVVIPIYPLRIVGCGSQGINVTGKTVLKRASAGASFMFHFSG	110
Klebsiella_phage_KP32_TSP	VSEVAIGPVEGNGRPPYEFGDVVIPIYPLRIVGCGSQGINVTGKTVLKRASAGASFMFHFSG	111
	.. : : * : : : * . . : * * : : : * : : * *	
KP-Pokalde_001TSP	TG--TRLGGGFLRMHLRGAVSSDPGLMVQVTSWSYFVENSTFNNLGASALVLRDCMES	165
Klebsiella_phage_K64-1_TSP	TGQTRTPMGGGLFNLQVRGESDITGPKIKVTSWSYMRINNCIAQINISDWGIARDMMES	237
Klebsiella_phage_K5_TSP	EGQSQRPMGGGLFNINLNGDSATALGDIKVTQWSCFKAQNCSEFQNMAGWGIRLKDVMES	170
Klebsiella_phage_KP32_TSP	EGQAQRPMGGGLFNINLNGDTATALGDIKVTQWSYFKANNCAFQNMAGWGIRLKDVMES	171
	* * :***:.....* : : * :*:** : :*:..... : : * **	
KP-Pokalde_001TSP	HISGNLFRRMGASNGSVILLGDYVIGIPNNVNNLHIQNNTFGLCSGAWIKSTANSNPDLV	225
Klebsiella_phage_K64-1_TSP	SCEYTLFRRIGSDTTGILLMDDYIGTPNSVNNFHFSSNNTLGYSSGNWIKSSTNSNPDLI	297
Klebsiella_phage_K5_TSP	TITGNLFRRLGGPSGGGILFDDIRSAVTDNVLNHIEDNTFALISGPWIGSTANSNPDLI	230
Klebsiella_phage_KP32_TSP	NISGNLFRRLGGPSGGGILFDDVRSVAVTDNVLNHIEDNTFALMSGPWIGSTANSNPDLI	231
	.***:*. . . :*: * . . .***:*. . :*:.. ** ** * :*****:	
KP-Pokalde_001TSP	WITDNKFEWDSVPYGANTATQHVLDGQLSRSWITRNNGFTFRPDSAHNLYAGCIRIRSG	285
Klebsiella_phage_K64-1_TSP	WIERNKFEWDGTPSANITPKAVIDFGQMSRCRITNNGFTHTFT--DHNNYEGILRMRSG	355
Klebsiella_phage_K5_TSP	WICRNKFEYDGTAPVNPENPSYVLDFAQLSRAFISENGFTHTFT--ARNNYAGVLRIGST	288
Klebsiella_phage_KP32_TSP	WIVRNKFEFDGTPAAPNTVDSYVLDFAQLSRAFIQDNGFTHTFT--ERNRYGVLRVGGAT	289
	** ***:*. . * . * :*** :*: * ** : * * * : * : :	
KP-Pokalde_001TSP	AVGPVIVSDNKAYGCEGEFWTIEGGYVDAFDNDSNIADA-SSALSWSLSTRACRINPPR	344
Klebsiella_phage_K64-1_TSP	CAYLTKLIDNDALSCSGYFGSVEGGKLAQSGNFYNRGVVASGNMQFNVTSTRPQSIPEVI	415
Klebsiella_phage_K5_TSP	ALGTVLFDNLLFACE-SAGVINGGIVESRGNINNQGSASAATQFTNNSKVKCLQRVW	347
Klebsiella_phage_KP32_TSP	AVGTIKFDNLLFACE-SAGLIAGGIVVSRGNVNNQGSATTAIKQFTNTSSKCLKLERRVI	348
	. : ** *. : ** : : * * : * : :	
KP-Pokalde_001TSP	VYSGNMNVVRGDSPPGPGFIGQAYMRGAAAASRTVRAGAASTVALDVPAGQEMRRYQLPL	404
Klebsiella_phage_K64-1_TSP	CFTSNGNITSVGDYIDPNFISAHNMFGTSNNMFQTDTMASLYTMMNVPSLVEIRRFQLGK	475
Klebsiella_phage_K5_TSP	NIQSNGNVSVGPQLFPAGYINMAELPGNTRLSSEYDADGETTSVLRVPANTQVRQWAVPK	407
Klebsiella_phage_KP32_TSP	NVQSNGNVSVGQIILPDGYINMAELPGNTRLPSEYDADGETTSVLRVPANTQVRQWAVPK	408
	* * : . : :*. : * : : . . : * : : * : :	
KP-Pokalde_001TSP	HLLGAIVRVSLRVY----NPGATGNITLAVGSGGSSV-AAVPAGPGWFDVDFYLGNSLT	458
Klebsiella_phage_K64-1_TSP	QYLDSENTLTIQARVKVDATAGTNGELKLNIDGTTDIGSSTITASTGWQLITFQLKPSQI	535
Klebsiella_phage_K5_TSP	MYQDGLTVAKVTRANGAS---SGAI-ISLQSGSTVLSTKPIDAGVWKNYVYVYKANQL	462
Klebsiella_phage_KP32_TSP	MYKDGLTVTKVTRAKGAA---AGAI-LSLQSGSTVLSTKSIDAGVWKNYVYVYKANQL	463
	.. . : . . * : : : . : . * * : .	
KP-Pokalde_001TSP	GDGDLRFTNSTGNTLSLDGITVERARSVPFSAWTPGAVAAGTLVSPVQTLTPY--GITQ	516
Klebsiella_phage_K64-1_TSP	GAGSLRFINSQTVSILFDGIYIQRSKYIDWNFAFNPGAIAAGASITSALQSYDTIGVGTG	595
Klebsiella_phage_K5_TSP	P-ETLQLRNTGTVDALVDGMVFEKVNVIDWDFAVTPGTLAVGAKYTPSNQSYLDVAGMR-	520
Klebsiella_phage_KP32_TSP	Q-ETLQLRNTGTADVLADGMVFGKVDYIDWDFAIAPGTLAAGAKYTPSNQSYLDVAGMR-	521
	* : * : * : : : * : : : * : * : * : * : : * : *	
KP-Pokalde_001TSP	APVGLSSPVFNGSVDGLLAGVSSYSGYSSYKVTLFNPGAAAITPGATRASLVLHF-	571

https://www.ebi.ac.uk/Tools/services/rest/clustalo/result/clustalo-l20211031-103344-0633-88000893-p1m/aln-clustal_num

1/2

g) BLAST hits of ϕ Kp_Pokalde_001 gp53 tail spike protein (TSP)

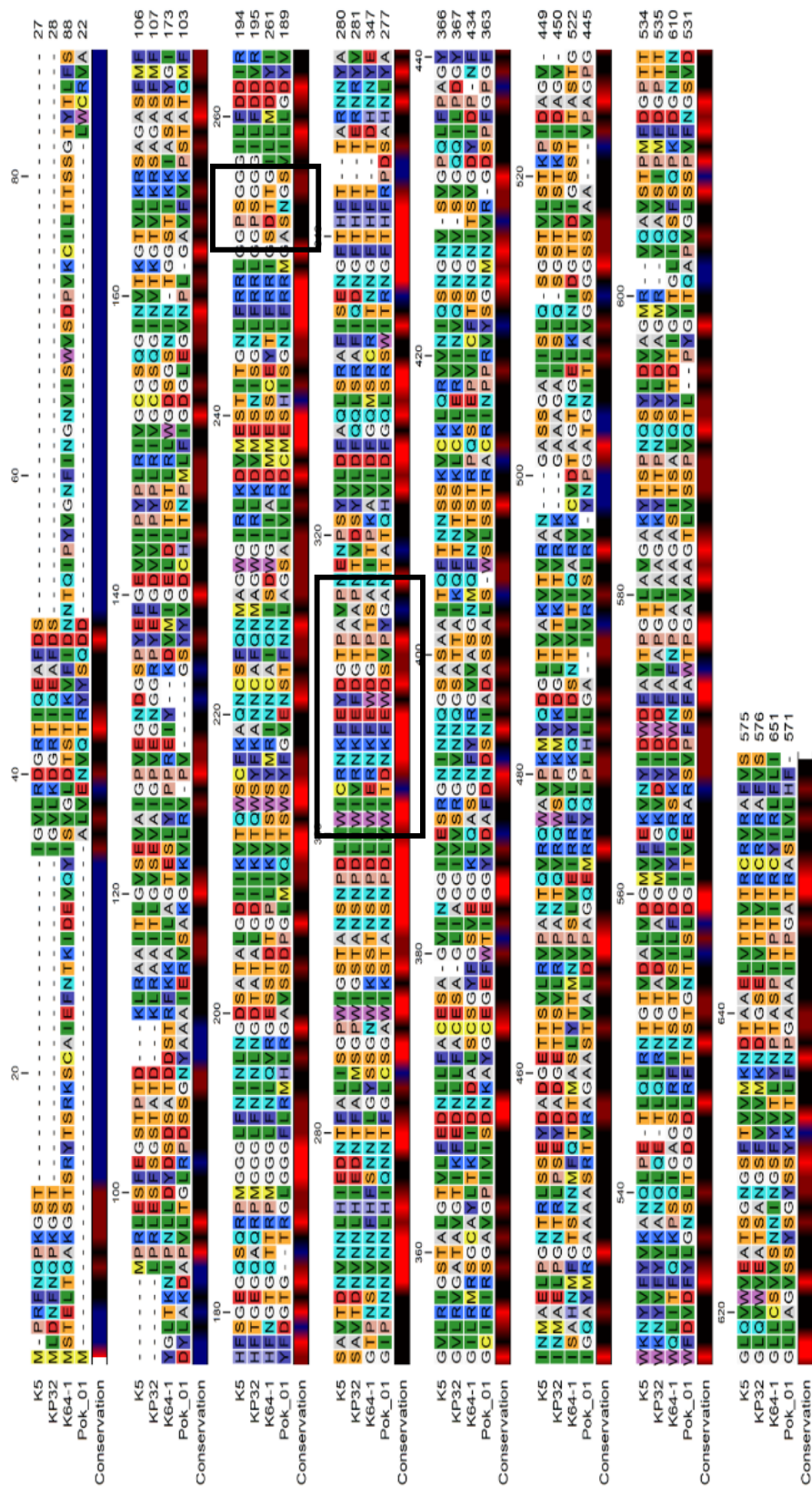


Figure 11: BLAST hits of ϕ Kp_Pokalde_001 gp53 TSP showing ~36% identities to K5, KP32, K64-1 tail-spike protein. Sequence conservation is at putative pectate lyase domain, Glu/58aa gap/ Asp/9aa gap/Glu/1aa gap/Asp.

APPENDIX: I

Scientific contributions and achievements

I. Published original articles in peer review journals:

1. **Dhungana, G.**, Regmi, M., Nepal, R., & Malla, R. (2021). Pharmacokinetics and pharmacodynamics of a novel virulent Klebsiella phage Kp_Pokalde_002 in a mouse model. *Frontiers in Cellular and Infection Microbiology*, 731. (SJR-Q1 Journal, IF-5.29). Link: <https://www.frontiersin.org/articles/10.3389/fcimb.2021.684704/full>
2. **Dhungana, G.**, Regmi, M., Paudel, P., Parajuli, A., Upadhyay, E., Gyawali, I., Upreti H., Nepal R., Pradhan P., & Malla, R. (2021). Therapeutic Efficacy of Bacteriophage Therapy to Treat Carbapenem-Resistant Klebsiella Pneumoniae in Mouse Model. *Journal of Nepal Health Research Council*, 19(1), 76-82.
Link: <https://pubmed.ncbi.nlm.nih.gov/33934137/>
3. **Dhungana, G.**, Malla, R., Rajaure, M., & Adhya, S. (2020). Complete Genome Sequence of Myophage Ec_Makalu_002, Which Infects Uropathogenic Escherichia coli. *Microbiology resource announcements*, 9(5), e01530-19.
Link: <https://www.ncbi.nlm.nih.gov/pmc/articles/PMC6992875/>
4. Archana Maharjan, Roshan Nepal, **Gunaraj Dhungana**, Apshara Parajuli, Madhav Regmi, Elisha Upadhyaya, Dipendra Mandal, Mitesh Shrestha, Pragati Pradhan, Krishna Das Manandhar, Rajani Malla (2022). “Isolation and Characterization of Lytic Bacteriophage Against Multi-drug Resistant Pseudomonas Aeruginosa” *Journal of Nepal Health Research Council*, 19 (53): 717-24
<https://doi.org/10.33314/jnhrc.v19i04.3837>
5. Nepal, R., Houtak, G., Karki, S., **Dhungana, G.**, Vreugde, S., & Malla, R. (2022). Genomic characterization of three bacteriophages targeting multidrug resistant clinical isolates of Escherichia, Klebsiella and Salmonella. *Archives of Microbiology*, 204(6), 1-9. <https://doi.org/10.1007/s00203-022-02948-0>

Manuscripts under preparation

1. Isolation and Characterization of Three Virulent Phages against Carbapenem-resistant Uropathogenic *Escherichia coli*
2. Spontaneous mutation and reversion in the tail spike protein of a Klebsiella phage Kp_Pokalde_001 modulates the phage behavior

Manuscripts reviewed

Bhargava K, Nath G, Bhargava A, Kumari R, Aseri GK and Jain N (2022) Bacterial profile and antibiotic susceptibility pattern of uropathogens causing urinary tract infection in the eastern part of Northern India. *Front. Microbiol.* 13:965053. doi: 10.3389/fmicb.2022.965053

Oral Presentation in National/International Symposium/Conferences:

1. **“Isolation and Molecular Characterization of Lytic Bacteriophage against Carbapenem-Resistant *Klebsiella pneumoniae*”**, International Conference on Bacteriophage in River Ganga (ICBRG) 2017, Varanasi, UP India, from 22 to 23 August 2017.
2. **“Therapeutic efficacy of bacteriophage therapy to treat carbapenem-resistant *Klebsiella pneumoniae* in a mouse model”** Seventh National Summit of Health and Population Scientists in Nepal, 1-2 July 2021, Kathmandu, Nepal.
3. **Bacteriophage Therapy in the Treatment of Multi-drug Resistant Bacterial Infection.** A virtual seminar organized by the Society of Nepalese Students in Korea (SONSIK) on 5th June 2022.

Poster Presentation in National/International Symposium/Conferences:

1. **Gunaraj Dhungana**, Manoj Rajaure, Rajani Malla, and Sankar Adhya, **“Assessment of Phage Therapy on Carbapenem-Resistant *Acinetobacter baumannii* Infection in Mice.”** 20th Graduate Research Symposium held on 20th Feb. 2020 in National Institute of Health, USA,
2. **Gunaraj Dhungana**, Manoj Rajaure, Phuoc Le, Meredith Showler, Rajani Malla, and Sankar Adhya **“Spontaneous mutations and reversions in the tail spike protein of a phage Kp_Pokalde_001 switch the plaque morphology”** Viruses of Microbes

2022 held on 18 – 22 July 2022, Guimaraes, Portugal, Organized by International Society for Viruses of Microorganisms and University of Minho, Portugal.

3. **Gunaraj Dhungana**, Elisha Upadhyaya, Madhav Regmi, Apshara Parajuli, Rajani Malla “**Isolation and Characterization of Novel Bacteriophage Lysing Colistin Resistant Salmonella spp., a Promising Solution to Antibiotic Crisis**”. 11th International Conference on Typhoid and Other Invasive Salmonellosis, held on March 26-28, 2019 in Hanoi, Vietnam, organized by **Coalition against Typhoid (CaT), Sabin Vaccine Institute, USA**.
4. **Dhungana G.R.**, Parajuli A, Regmi M, Upadhyaya E, Sthapit K, Maharjan A, Nepal R, Aryal P, and Malla R. “**Isolation and Characterization of Novel Bacteriophage Targeting Carbapenem-Resistant *Pseudomonas aeruginosa* Containing *bla*NDM-1 Gene in Nepal.**” EMBO/ Viruses of Microbes V: Biodiversity and future application, 9-13 July 2018, organized by Institute of Genetics and Microbiology University of Wrocław & Hirsfeld Institute of Immunology and Experimental Therapy Polish Academy of Sciences Wrocław, Poland.
5. **Dhungana GR**, Maharjan G, Parajuli A, Kafle S, Malla R., “**Biofilm Detection and Antibiotic Sensitivity Patterns of Uropathogens in Patients with Indwelling Urinary Catheter in a Tertiary Care Hospital in Nepal.**” The 2nd International Conference on Bioscience & Biotechnology (ICBB2018) from 17 to 20 February 2018, organized by the Research Institute for Bioscience & Biotechnology (RIBB) and Institute for Molecular Medicine Finland (FIMM) in Dhulikhel, Kavrepalanchowk, Nepal.
6. Madhav Regmi, Elisha Upadhyaya, Apshara Parajuli, **Guna Raj Dhungana** and Rajani Malla “**Isolation and characterization of novel lytic bacteriophages against carbapenem-resistant *Acinetobacter baumannii***” World DNA Day 2018, organized by Biotechnology Society of Nepal (BSN), at Nepal Academy of Science and Technology, Lalitpur, Nepal.
7. Apshara Parajuli, **Guna Raj Dhungana**, Madhav Regmi, Elisha Upadhyaya, Roshan Nepal, Pramod Aryal, Rajani Malla: “**Isolation and characterization of novel lytic bacteriophages against carbapenem-resistant bacteria for potential use in phage therapy**” The 2nd International Conference on Bioscience & Biotechnology

(ICBB2018) from 17 to 20 February 2018, organized by Research Institute for Bioscience & Biotechnology (RIBB) and Institute for Molecular Medicine Finland (FIMM) in Dhulikhel, Kavrepalanchowk, Nepal.

II. Fellowship, Awards, Grants & Appreciations

1. **“Best Research Paper Award 2021”** by the Nepal Health Research Council, Eighth National Summit of Health and Population Scientists in Nepal, held on 10-12 April, 2022.
2. **Pre-doctoral fellowship award** by the Department of Health and Human Services, National Institute of Health (NIH), Bethesda, Maryland 20892, the USA from September 2019 to August 2020.
3. **India Science and Research Fellowship (ISRF) Award 2019**, by the Department of Science & Technology, Government of India and the Nepal Academy of Science and Technology, Nepal.
4. **The UGC Ph.D. Fellowship and Research Support Grants (2017)** from the University Grants Commission (UGC), Sanothimi, Bhaktapur, Nepal. Award No.: Ph.D./73-74/S&T-07
5. **Ph.D. Fellowship Award** by the Nepal Academy of Science and Technology (NAST) Khumaltar, Lalitpur, Nepal.
6. **FEMS Early Career Scientist Grant, ISVM Travel Grant and SFAM Scientific Conference Abstract Scholarship** to attend the **“Viruses of Microbes 2022”**, held on 18 – 22, July 2022, in Guimaraes, Portugal.
7. **Intralytix Phage Therapy Travel award** to attend the **ASM Microbe 2019**, held on 20-24 June 2019, sponsored by Intralytix Inc. USA.
8. **Travel and Accommodation Grant Award** for the participation in **11th International Conference on Typhoid and Other Invasive Salmonellosis**, held on March 26-28, 2019 in Hanoi, Vietnam, organized by **Coalition against Typhoid (CaT), Sabin Vaccine Institute, USA.**
9. **Travel and Accommodation Grant Award** for participation in **EMBO Viruses of Microbes V: Biodiversity and future application**, Wroclaw Poland by **European Molecular Biology Organization (EMBO), 2018.**

10. **Travel and Accommodation Award** for oral presentation in “**International Conference on Bacteriophage in River Ganga (ICBRG) 2017**”, Varanasi, UP India by ICBRG 2017, IMS, BHU, India.

III. Trainings/seminars/workshops/symposia& CME

1. **As a graduate research fellow at the Laboratory of Molecular Biology, National Cancer Institute, NIH, USA:** Hands-on training on basic molecular techniques like DNA/RNA extraction, primer design, PCR, molecular cloning and downstream analysis of gene expression, protein purification techniques, next-generation sequencing and bioinformatic analysis of bacteriophage genome, comparative genome analysis, genome annotation, genome editing/ engineering, and site-directed mutagenesis, etc.
2. “**Scientists Teaching Science**” **9-week Pedagogy course, June 2020** organized by Office of Intramural Training and Education, OIR, OD, Department of Health and Human Services, National Institute of Health (NIH), Bethesda, MD, USA.
3. **Methods in Molecular Biology**, 2.8 CEUs (28 lectures/Laboratory hours) on November 2019, awarded the Foundation for Advanced Education in the Sciences (FAES), at National Institute of Health (NIH), Bethesda, MD, USA
4. **Applications of FLOW CYTOMETRY on Biotechnology**, on 14 to 17th September 2017, Organized by the Central Department of Biotechnology, TU/Ministry of Science and Technology, Kathmandu, Nepal.
5. Participated as resource person in the “**CME cum Hands-on Workshop on Medical Research and Scientific Writing – 2018**. Organized by the JF Institute of Health Sciences/LACHS and the University Grants commission Nepal from 2nd to 4th May 2018, Lalitpur, Nepal.
6. Participated in the “**Fifth International Conference of SCIENCE AND SCIENTIST-2017**”, from 18 to 19th August 2017, Nepal Pragya Pratisthan, Kamaladi, Kathmandu, Nepal.
7. Completed online course “Author AID Proposal Writing & Research Writing Course” **from 18 April to 12 June 2017, conducted by Author Aid/INASP, UK.** Completed

online course “**Author Aid Research Writing Course**” on 18th October to 28th November 2016, conducted by the Author Aid/INASP, UK.

8. Participated as delegates in “**17th international congress on infectious diseases**” on 2nd to 5th March 2016 in Hyderabad, India, organized by the **International Society for Infectious Diseases**, Brookline MA 02446-5903 USA, accredited by the **European Accreditation Council for Continuing Medical Education (EACCME) (Total 21 credit hours)**.

IV. M.Sc. thesis supervision

1. Pharmacokinetic study and assessment of cytokine expression elicited by a novel *Acinetobacter baumannii* phage in mouse model M.Sc. Thesis year (2018) by Madhav Regmi, TU Registration no: 5-2-48-1577-2010
2. Characterization, whole-genome analysis, and application of bacteriophages to control biofilm produced by carbapenem-resistant bacteria prioritized by world health organization (WHO) M.Sc. Thesis year (2018) Apshara Parajuli, Registration no: 5-2-37-299-2010
3. Molecular study of broad host range bacteriophage against colistin-resistant *Salmonella Typhi* for potential use in phage therapy M.Sc. Thesis (2019) Elisha Upadhyaya, TU Registration No.: 5-2-48-809-2011
4. Enhanced Phage Host Range by The Synergistic Effect of Newly Isolated Phage Cocktails from Rivers of Kathmandu, Nepal. M.Sc. Thesis, 2020 by Indu Gyanwali, TU Registration No. 5-2-37-168-2012
5. Experimental phage therapy in treating *Klebsiella pneumoniae* –mediated bacteremia in mouse model M.Sc. Thesis Year (2021), by Prashant Paudel, TU Registration No: 5-2-37-744-2010
6. Application of bacteriophage to control hospital-acquired infection, a new concept to disinfect hospital environment, M.Sc. Thesis, 2021, by Himani Upreti, TU registration no. 5-2-37-168-2012 (Waiting for thesis defense)
7. In-vitro assay of bacteriophage against *Salmonella* in raw food products, M.Sc. Thesis (2021) by Yujeen Chapagain, TU Registration No. 5-2-37-772-2011.

APPENDIX-J

Photographs and Certificates

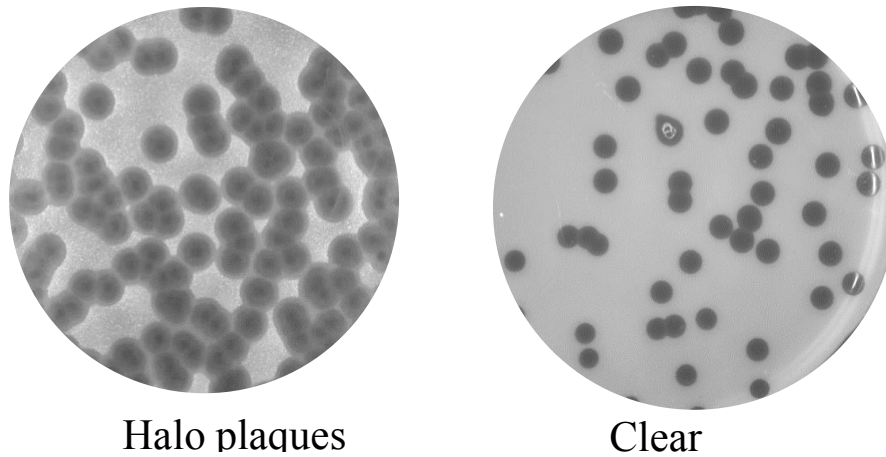


Figure J1: Halo and clear plaques formed by the phage Kp_Pokalde_001 on the lawn of the same host bacteria *Klebsiella pneumoniae* (TUKp1).

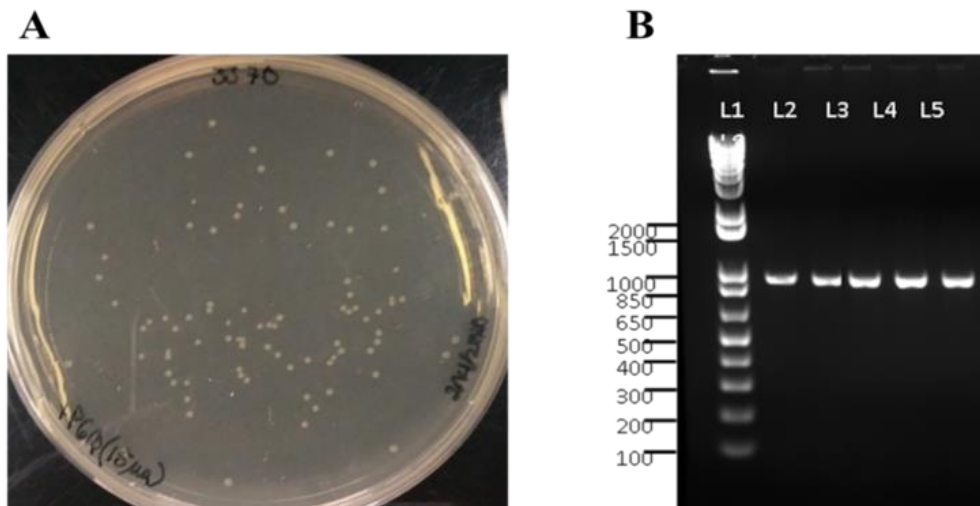


Figure J2: Positive clones of tail spike protein (gp53, Kp_Pokalde_001) in Figure A. Agarose gel electrophoresis of colony PCR from positive clones in Figure B, L1: 100 Kb Plus DNA Ladder, L2: Tail spike protein, full length, L3: Hydrolase domain, L4: Hydrolase domain S140N mutation,43371, L5: Hydrolase domain (A-G mutation,43194), L6: Hydrolase domain (A-G mutation, 43394). All clones were sequence verified.

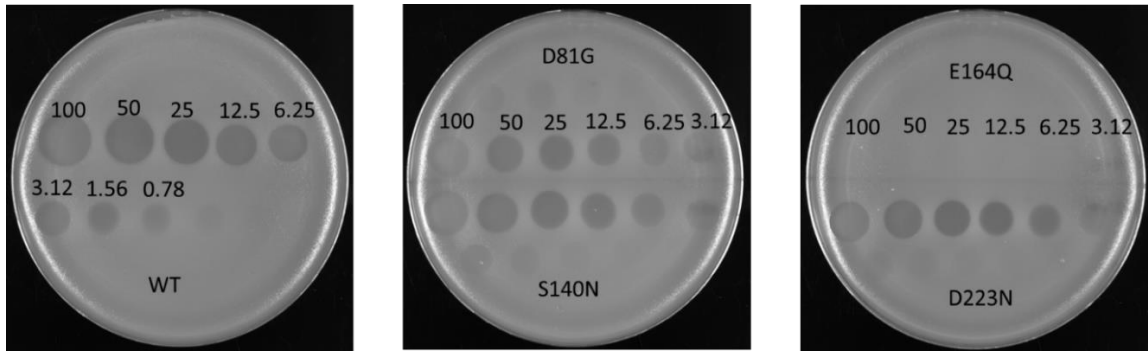


Figure J3: Spot test assay (2-fold dilution from 100 mg/ml) of the His-Trap purified depolymerase enzyme (gp53 TSP of phage Kp_Pokalde_001) on the lawn of host bacterial culture. WT- wild type phage, D81G, S140N, E164Q, and D223N mutants.

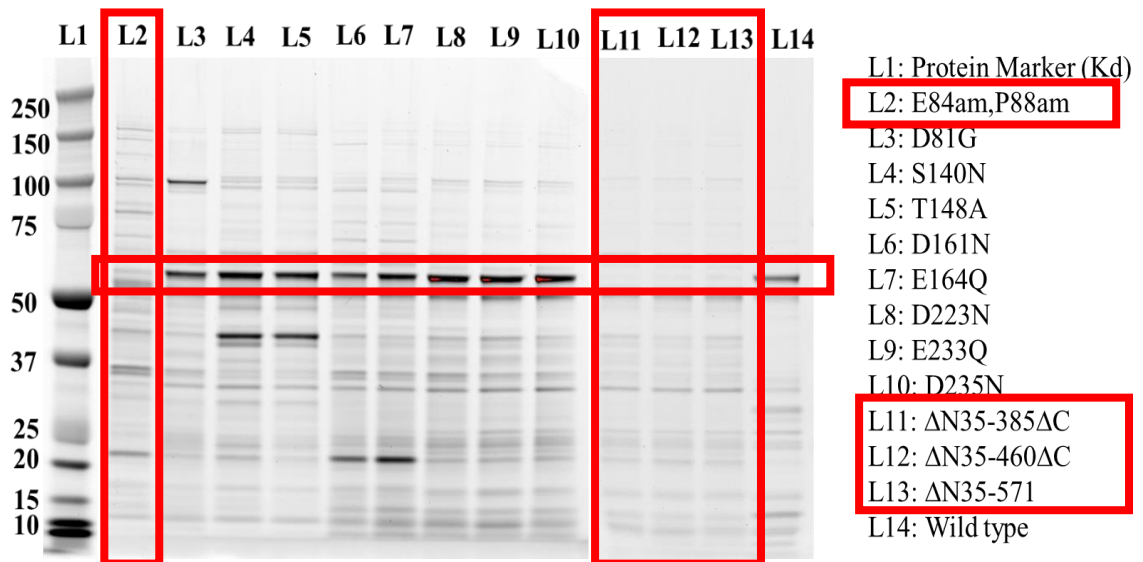


Figure J4: SDS-PAGE of Wild type, spontaneous and site-directed mutants His-Trap purified depolymerase (gp53) of Phage Kp_Pokalde_001

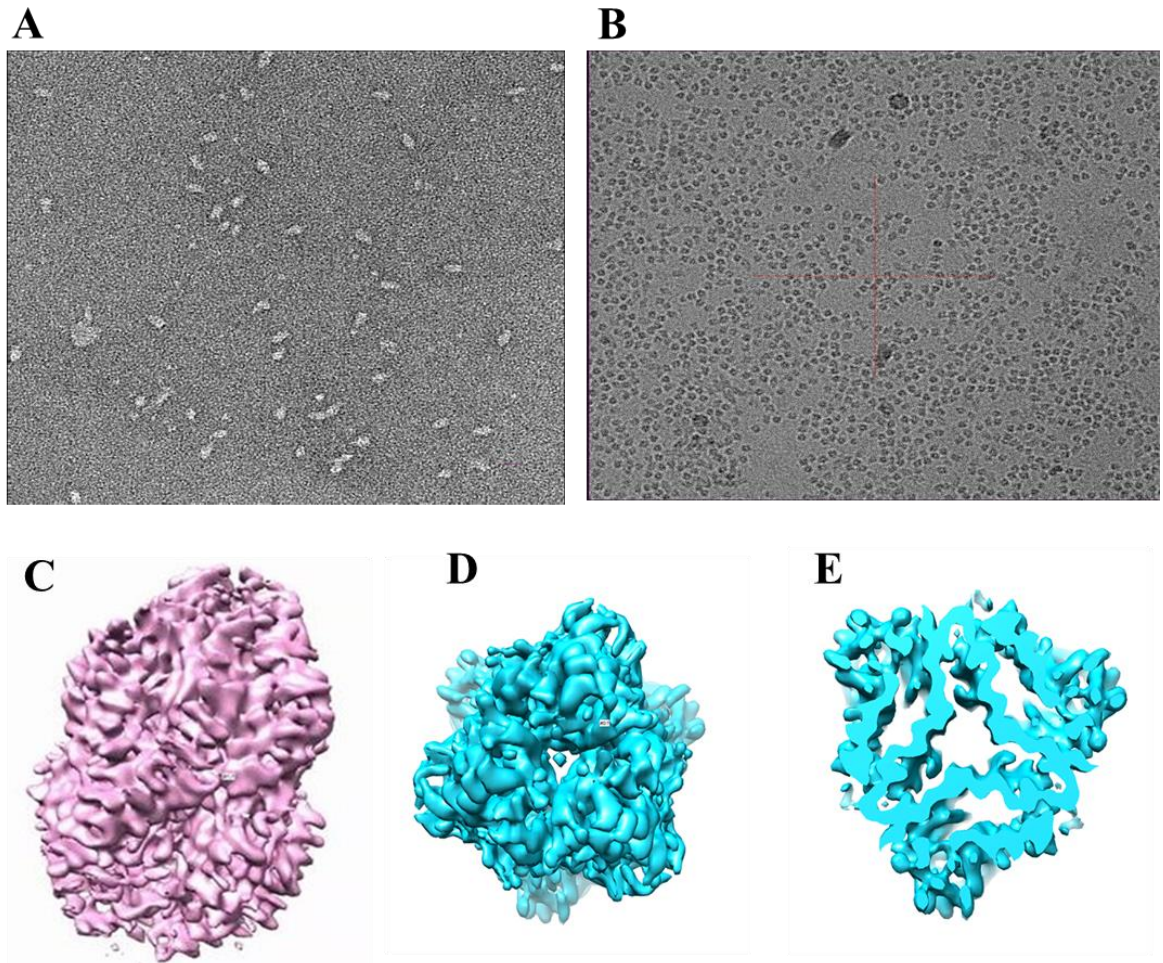


Figure J5: A) Transmission Electron Microscopy (TEM) image (10,000X) of depolymerase enzyme of Kp_Pokalde_001 (gp53) B: Cryo-Electron Microscopy (cryo-EM) image showing several images of depolymerase macro-molecules. C: Cryo-EM image of the constructed enzyme trimer, D and E are top and cross-sectional views of the enzyme respectively.



ICBRG-2017

International Conference on Bacteriophages in River Ganga 2017




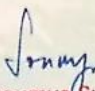
August 22-23, 2017

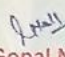
CERTIFICATE

This is to certify that Dr./Mr./Ms. Guna Raj Dhungana has participated as Chairperson/Guest Speaker/Delegate in ICBRG 2017 held on August 22-23, 2017 at Institute of Medical Sciences, Banaras Hindu University, Varanasi and presented a paper (oral/poster) on the topic. "Isolation and Molecular characterization of Lytic Bacteriophage against Carbapenem resistant Klebsiella pneumoniae."

Uttar Pradesh Medical Council has granted 08 (Eight) credit hours to delegates. (Reference No. UPMC/6602/17 Dated 18-07-2017)


Prof. V.K. Shukla
Org. Chairman
ICBRG 2017


Dr. Soumya Swaminathan
Secretary DHR & Director General
ICMR


Prof. Gopal Nath
Organizing Secretary
ICBRG 2017



CERTIFICATE OF POSTER PRESENTATION

THIS IS TO CERTIFY THAT

Guna Raj Dhungana

HAS A PRESENTATION AS A POSTER DURING
2nd INTERNATIONAL CONFERENCE ON BIOSCIENCE & BIOTECHNOLOGY
(ICBB-2018)
Dhulikhel, Nepal
February 17-20, 2018


Prajwal Rajbhandari
CO-CHAIR
President,
Research Institute for Bioscience
and Biotechnology (RIBB), Nepal


Dr. Markus Vähä-Koskela
CO-CHAIR
Senior Researcher,
Institute for Molecular Medicine Finland
(FIMM), Finland

Organizing Partner

 RESEARCH INSTITUTE
FOR BIOSCIENCE
AND BIOTECHNOLOGY


Institute for Molecular Medicine Finland
Nordic EMBL Partnership for Molecular Medicine

CERTIFICATE OF PARTICIPATION


This is to confirm that

Guna Raj Dhungana

attended the EMBO Workshop

Viruses of microbes 2018

from 09 – 13 July 2018 in Wroclaw, Poland



Gerlind Wallon, PhD
EMBO Deputy Director

**European Molecular
Biology Organization**

Meyerhofstr. 1
69117 Heidelberg
Germany

phone +49 6221 8891 0
fax +49 6221 8891 200

embo@embo.org
www.embo.org

Date and location: 13 July 2018, Heidelberg



Certificate OF Appreciation



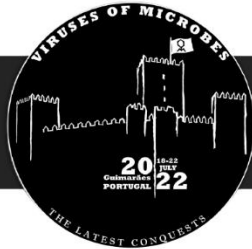
THIS CERTIFICATE IS PROUDLY AWARDED TO

Guna Raj Dhungana, PhD.
(Molecular Biology)
Tribhuvan University

For participating as guest speaker in SONSIK common forum talk, “**Bacteriophage Therapy in Treatment of Multi-Drug Resistant Bacterial Infections**”, held virtually on 05th June 2022.

We wish you every success in future and is Awarded Certificate by
Society of Nepalese Students in Korea.


Dirgha Raj Joshi
President
SONSIK



VoM 2022

18 - 22 July 2022 | Guimarães, PORTUGAL




CERTIFICATE

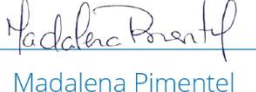
This is to certify that

GUNARAJ DHUNGANA

Attended the VoM 2022 Conference
Centro Cultural Vila Flor, Guimarães, Portugal
18 -22 July 2022

The organizers


Joana Azeredo


Madalena Pimentel

LXXXV



'Research in Public Health Emergencies: Evidence to Policy and Action'

7th
Virtual



National Summit of Health and Population Scientists in Nepal

01 – 02 July 2021 | Kathmandu, Nepal

Certificate of Oral Presentation

This is to certify that
Mr. Gunaraj Dhungana

has made a oral presentation in the Seventh national summit of health and
population scientists in Nepal

01-02 July 2021, Kathmandu, Nepal.

Organized by Nepal Health Research Council (NHRC)

Dr Pradip Gyanwali
Member-Secretary
(Executive Chief)

Prof Dr Gehanath Baral
Chairman
Nepal Health Research Council (NHRC)



Appendix-K

Published Original Articles



Pharmacokinetics and Pharmacodynamics of a Novel Virulent *Klebsiella* Phage Kp_Pokalde_002 in a Mouse Model

OPEN ACCESS

Edited by:

Jeremy J. Barr,
Monash University, Australia

Reviewed by:

Yu-Wei Lin,
Monash University, Australia
Aleksandra Petrovic Fabijan,
Westmead Institute for
Medical Research, Australia

*Correspondence:

Gunaraj Dhungana
grdhungana79@gmail.com

†Present address:

Roshan Nepal,
Adelaide Medical School,
Faculty of Health and Medical
Sciences, The University of Adelaide,
Adelaide, SA, Australia

Specialty section:

This article was submitted to
Clinical Microbiology,
a section of the journal
Frontiers in Cellular and
Infection Microbiology

Received: 23 March 2021

Accepted: 22 July 2021

Published: 16 August 2021

Citation:

Dhungana G, Nepal R, Regmi M and
Malla R (2021) Pharmacokinetics
and Pharmacodynamics of a
Novel Virulent *Klebsiella* Phage
Kp_Pokalde_002 in a Mouse Model.
Front. Cell. Infect. Microbiol. 11:684704.
doi: 10.3389/fcimb.2021.684704

Gunaraj Dhungana^{1*}, Roshan Nepal^{1,2†}, Madhav Regmi¹ and Rajani Malla¹

¹ Central Department of Biotechnology, Tribhuvan University, Kirtipur, Nepal, ² Adelaide Medical School, Faculty of Health and Medical Sciences, The University of Adelaide, Adelaide, SA, Australia

Phage therapy is one of the most promising alternatives to antibiotics as we face global antibiotic resistance crisis. However, the pharmacokinetics (PK) and pharmacodynamics (PD) of phage therapy are largely unknown. In the present study, we aimed to evaluate the PK/PD of a locally isolated virulent novel ϕ Kp_Pokalde_002 (*Podoviridae*, C1 morphotype) that infects carbapenem-resistant *Klebsiella pneumoniae* (Kp56) using oral and intraperitoneal (IP) route in a mouse model. The result showed that the ϕ Kp_Pokalde_002 rapidly distributed into the systemic circulation within an hour *via* both oral and IP routes. A higher concentration of phage in plasma was found after 4 h (2.3×10^5 PFU/ml) and 8 h (7.3×10^4 PFU/ml) of administration through IP and oral route, respectively. The phage titer significantly decreased in the blood and other tissues, liver, kidneys, and spleen after 24 h and completely cleared after 72 h of administration. In the Kp56 infection model, the bacterial count significantly decreased in the blood and other organs by 4–7 \log_{10} CFU/ml after 24 h of ϕ Kp_Pokalde_002 administration. Elimination half-life of ϕ Kp_Pokalde_002 was relatively shorter in the presence of host-bacteria Kp56 compared to phage only, suggesting rapid clearance of phage in the presence of susceptible host. Further, administration of the ϕ Kp_Pokalde_002 alone in healthy mice (*via* IP or oral) did not stimulate pro-inflammatory cytokines (TNF- α and IL-6). Also, treatment with ϕ Kp_Pokalde_002 resulted in a significant reduction of pro-inflammatory cytokines (TNF- α and IL-6) caused by bacterial infection, thereby reducing the tissue inflammation. In conclusion, the ϕ Kp_Pokalde_002 possess good PK/PD properties and can be considered as a potent therapeutic candidate for future phage therapy in carbapenem-resistant *K. pneumoniae* infections.

Keywords: bacteriophage, PK/PD, carbapenem-resistant infections, *Klebsiella pneumoniae*, phage therapy

INTRODUCTION

Antibiotic resistance has become one of the biggest challenges to the global public health. According to the World Health Organization (WHO), the world is heading towards a post-antibiotic era and it would force millions of people into extreme poverty and death by 2050 (WHO, 2017). The discovery of new class of antibiotics is often time consuming and requires tremendous investment, and as bacteria quickly become resistant to antibiotics, it will shortly be ineffective (Spellberg, 2014). As no new class of antibiotics has been discovered since the 1980s, researchers are warning about the imminent antibiotic resistance crisis of pandemic proportion if we fail to find effective alternative approaches to antibiotics in addition to development new classes of antibiotics. Recently, the ESKAPE (*Enterococcus faecium*, *Staphylococcus aureus*, *Klebsiella pneumoniae*, *Acinetobacter baumannii*, *Pseudomonas aeruginosa*, and *Enterobacter* species) pathogens are causing life-threatening infections throughout the world in both hospital and community settings with high morbidity and mortality (Paczosa and Mecsas, 2016). They are mostly multidrug-resistance (MDR) and acquire drug resistance potentially through different mechanisms such as drug inactivation, target modification, reduced permeability, or by increased efflux pump (Santajit and Indrawattana, 2016). Carbapenem-resistant *K. pneumoniae* is one of the ESKAPE pathogens categorized as critical by WHO, and research and development of new classes of antimicrobial agents is highly prioritized. A high prevalence of carbapenem-resistant *Enterobacteriaceae*, including *K. pneumoniae* infections, has also been reported in recent years in Southeast Asia including Nepal (Hsu et al., 2017; Nepal et al., 2017).

Bacteriophages (phages) are viruses that target specific bacterial species and has two distinct lifestyles: lytic and lysogenic, that dictate its role in bacterial biology. Recently, virulent phages (that strictly kill the host bacteria) have received heightened attention as a potent antimicrobial agent to treat bacterial infections, especially antibiotic resistant infections (Clokic et al., 2011). Phage therapy (using phage and its components as a therapeutic agent) has been known for more than 100 years and recently regained heightened interest as the modern understanding of phage biology, genetics, immunology, and pharmacology recognizes its use in mitigating the antibiotic resistance crisis (Young and Gill, 2015). Several studies have already demonstrated the safety and efficacy of phage therapy in systemic and tropical infections in both animal and human (Vinodkumar et al., 2008; Kumari et al., 2011; Pouillot et al., 2012; Furfaro et al., 2018; Wang et al., 2018). Phage therapy in humans is still routinely used in Georgia, Poland, and Russia, and Western countries like USA, UK, Belgium, France and Germany are using phages in therapeutics occasionally as personalized, magistral preparations and/or compassionate use to treat infections when all of the available antibiotics fail (Pirnay et al., 2018; Romero-Calle et al., 2019). Although there are more than 10 case reports published over last 10 years about phage therapy (Sybesma et al., 2018; Pirnay, 2020), and most of them showing encouraging results (Schooley et al., 2017; Dedrick et al., 2019; Petrovic Fabijan et al., 2020), it is yet to be adopted in

mainstream medicine so far. Beside regulatory hurdles, one of the possible reasons for this is poor understanding of pharmacokinetics (PK) and pharmacodynamics (PD) of phages *in vivo*. Phages possess a unique tripartite dynamic relationship between their host bacteria and human immune system (Wahida et al., 2021) as they co-evolve and self-replicate within the human body in the presence of host bacteria (Payne and Jansen, 2003). As a result, the PK/PD of phages are distinct from those of classical antimicrobials. In addition, phages have ability to pass through body barriers, potentially eliciting an immune response (Barr et al., 2013; Dąbrowska and Abedon, 2019). It is necessary to understand the PK/PD of the phage in terms of biodistribution, bioavailability, clearance, and immune response *in vivo* (Cafilisch et al., 2019). For successful phage therapy, route and dosage of phage administration must be assessed and standardized to each individual phage-bacteria combination (Payne and Jansen, 2003; Dąbrowska, 2019; Nilsson, 2019). In this study, we aimed to evaluate the PK/PD of a novel virulent (lytic) *Klebsiella* phage Kp_Pokalde_002 (GenBank ID: MT425185, hereafter referred as øKp_Pokalde_002) that infects carbapenem-resistant *K. pneumoniae* using oral and intraperitoneal (IP) route in a mouse model.

MATERIALS AND METHODS

Ethical Clearance and Animal Model

Ethical approval was obtained for the use of animal prior to the study (Ethical approval No.161/2018) from Nepal Health Research Council (NHRC), Kathmandu. The protocol was also approved by the Ethical Review Board, NHRC. Female Swiss albino mice (6–8 weeks old) weighing 23 ± 2.5 g were purchased from Natural Products Research Laboratory (NPRL), Kathmandu. The animals were housed in an animal room at Central Department of Biotechnology, Tribhuvan University and fed with normal antibiotic-free diet. Chloroform vapor was used to anesthetize the mice and then euthanized by cervical dislocation before any invasive procedures. Each experiment was performed in triplicates.

Bacterial Strain and Phage Amplification

A clinical isolate of *K. pneumoniae* (hereafter referred as Kp56) confirmed as a carbapenem-resistant strain (presence of gene *blaNDM1*, *blaKPC*) was obtained from the Microbiology Laboratory, Central Department of Biotechnology, Tribhuvan University (unpublished data). The bacteria were propagated in Luria-Bertani (LB) broth (HiMedia, India) at 37°C. A virulent øKp_Pokalde_002 (*Podoviridae*, C1 morphotype) isolated using Kp56 as a host was used in this study. The lytic-lifestyle and Gram-negative host of the phage was confirmed based on its physiochemical characteristics (Dhungana et al., 2021) and its genome analysis through PHACTS (<https://edwards.sdsu.edu/PHACTS>) (McNair et al., 2012).

The øKp_Pokalde_002 was amplified from glycerol stocks as described previously (Bourdin et al., 2014). Briefly, 1.0 ml overnight culture of the host bacteria (Kp56) was mixed with 100.0 ml LB broth and incubated at 37°C for 2.0 h with agitation

(100 rpm) to reach an exponential growth phase ($OD_{600} = 0.3$). The phage stock, acclimatized to room temperature, was then added at a multiplicity of infection (MOI) of 10, and the culture was further incubated at 37°C in a shaking incubator (250 rpm) for 5.0 h until the media was visually clear. The phage lysate was centrifuged at 3220xg (Centrifuge 5810 R, Eppendorf, Hamburg, Germany) for 15 min at 4°C, and the supernatant was filtered through a 0.22 µm pore-size Whatman™ syringe filter (Sigma-Aldrich, Missouri, United States). The phage lysate was further purified and concentrated by isopycnic cesium-chloride (CsCl) density-gradient ultracentrifugation as described elsewhere (Sambrook and Russell, 2001).

Phage/Bacteria Enumeration

Blood and homogenized tissue samples were serially diluted up to 10^{-6} in a 1.5 ml Eppendorf tubes. For bacterial count, 100 µl aliquot from each dilution was spread-plated on nutrient agar (NA) plates in duplicates and incubated at 37°C for 24 h. Similarly, for phage titer, the blood and homogenized tissue samples were centrifuged at 3220xg (Centrifuge 5810 R, Eppendorf, Hamburg, Germany) for 10 min at 4°C and filtered through a 0.22 µm pore size Whatman™ syringe filter (Sigma-Aldrich, Missouri, United States). The filtrate was serially diluted to up to 10^{-8} and phage titer was determined by Double Layer Agar (DLA) assay as described elsewhere. The phage and bacteria counts were corrected for tissue-fluid weights using following formula.

$$\frac{\# \text{ plaques or colonies/ml plated} \times \text{dilution factor}}{\# \text{ grams tissue/ml original homogenate}} = \text{PFU or CFU/gm of tissue}$$

In Vivo Pharmacokinetics of øKp_Pokalde_002 Through Oral and IP Route

In vivo PK assessment was performed as described previously (Verma et al., 2009; Pouillot et al., 2012) with modifications. Seventy-two mice were divided into four groups [2 phage only and 2 vehicle (SM buffer) control, 18 mice in each group]. In a phage only control group, the first group of mice received 200 µl (1.2×10^8 PFU/ml) of the highly purified øKp_Pokalde_002 *via* oral route while the same dosage of phage preparation was injected *via* IP route in the second group. The vehicle control group (third and fourth) received 200 µl of SM buffer only *via* oral and IP route, respectively. Three mice from each group were euthanized by cervical dislocation at 1 h, 4 h, 8 h, 24 h, 48 h, and 72 h after phage administration. Blood samples were collected in tubes containing 0.05 M EDTA anticoagulant by cardiac puncture. Tissue samples from lungs, liver, spleen, and kidneys were collected aseptically from euthanized mice and further divided into two parts. One part of each tissue was immersed in 10% formalin for histopathological examinations. Another part of tissue was weighed and homogenized in 1.0 ml PBS aseptically. The homogenized tissue was centrifuged at 10,000 rpm for 10 min at 4°C, and supernatant was filtered through a

0.22 µm pore size Whatman™ syringe filter (Sigma-Aldrich, Missouri, United States). The phage titer was determined by standard DLA technique as described elsewhere (Dhungana et al., 2021).

Klebsiella pneumoniae Infection Model

In a separate study, 54 mice (3 groups, 18 in each group) were inoculated with 200 µl (1×10^8 CFU/ml) of exponentially growing Kp56 intraperitoneally. Immediately after bacterial inoculation, 200 µl of SM buffer was injected to all mice in the first group (sepsis control) and 200 µl of øKp_Pokalde_002 (1.2×10^8 PFU/ml) was administered to all mice in second and third groups (treatment) through IP and oral routes, respectively. Three mice from each group were euthanized by cervical dislocation at 1 h, 4 h, 8 h, 24 h, 48 h, and 72 h post bacterial inoculation. Blood and tissue samples were collected and processed as described earlier to determine the phage titer and the levels of pro-inflammatory cytokines.

Histology

Histological examination of the lung tissue was done as described previously (Singla et al., 2015) with modifications. Briefly, tissues were fixed with 10% formalin and embedded in paraffin wax. Serial sections of 4–6 µm thickness were cut using microtome, de-paraffinized, rehydrated, and stained with Hematoxylin and Eosin (H&E stain). The tissue sections were examined under the light microscope for histological changes.

Cytokine Quantification

Pro-inflammatory cytokines: tumor necrosis factor alpha (TNF-α) and interleukin 6 (IL-6)] levels were measured in all Kp56 infected and øKp_Pokalde_002 treated mice. Total RNA was isolated from the blood samples using Direct-zol™ RNA MiniPrep Plus Kits (Zymo Research, USA), and cDNA was synthesized using iScript™ cDNA Synthesis Kit (Bio-Rad Laboratories, USA) following the manufacturer's instruction. DNase I (6 U/µl) was used to digest any residual DNA. Total RNA concentration was measured using NanoDrop 8000 (Thermo Fisher Scientific, USA) by spectrophotometric optical density measurement at 260/280 nm. The mRNA levels of TNF-α and IL-6 were measured by two-step relative qRT-PCR. The β-actin housekeeping gene was amplified as an internal control. Gene expressions were normalized to the expression of β-actin gene. The sequences of primers of IL-6, TNF-α, and β-actin are listed in **Supplementary Table S1**. The real time PCR was performed using SYBR® Green Master Mix (2x) Kit in CFX Connect™ RT-PCR system (Bio-Rad Laboratories, USA). Melting curve analysis was performed after the amplification phase to eliminate the possibility of nonspecific amplification or primer-dimer formation. All samples were processed in duplicate, and the output level was reported as an average. The comparative CT method was used to calculate the relative expression ratio from the real time PCR efficiency and the CT (Livak and Schmittgen, 2001; Jain et al., 2006). mRNA expression level change was calculated using double delta Ct (DDCT) method, and the change in mRNA expression levels of cytokines was expressed as fold change.

$$\text{Fold change} = 2^{-\Delta\Delta Ct}$$

where $2^{-\Delta\Delta Ct} = [(Ct \text{ of gene of interest} - Ct \text{ of internal control}) \text{ sample A} - (Ct \text{ of gene of interest} - Ct \text{ of internal control}) \text{ sample B}]$.

Data Interpretation and Statistical Analysis

Non-compartmental PK parameters: the peak plasma concentration (C_{max}) and the time to reach peak plasma concentration (T_{max}) were obtained by visual inspection of the data. The area under the plasma concentration-time curve (AUC) was calculated according to the linear trapezoidal rule up to the T_{last} phage concentration using GraphPad Prism 8 (Version 8.3.0). The half-life ($T_{1/2}$) was calculated from the one-phase exponential regression equation ($T_{1/2} = 0.693/K_{el}$) (Dufour et al., 2018; Chow et al., 2020). The elimination rate constant (K_{el}) was estimated from the slope of the elimination phase of the log transformed plasma concentration-time curve fitted by the method of least squares. All elimination phase data with associated variability were included in the estimation. Data were expressed as mean \pm standard error of mean (SEM). Comparisons of phage count and cytokine levels were performed by one-way ANOVA with Tukey's multiple-comparison test and Student's t-test. Inter mice PD variability was expressed as coefficient of variation (%CV). All statistical analysis were performed using GraphPad Prism 8 (Version 8.3.0), and differences with $p < 0.05$ were considered statistically significant.

RESULTS

Pharmacokinetics

We examined the PK/PD of $\phi Kp_Pokalde_002$ administered through IP and oral routes in mice model in the presence and absence of host bacteria Kp56 (Figure 1). Mice that received only

$\phi Kp_Pokalde_002$ through IP or oral routes did not show any sign of illness during the experimental period (72 h post phage inoculation), and $\phi Kp_Pokalde_002$ was detected in blood and other body tissues within the first hour of both IP and/or oral route of administrations.

In an IP group and in the absence of host bacteria, maximum biodistribution of the $\phi Kp_Pokalde_002$ was found at 4 h (43% of inoculated phage titer) post phage injection (Figures 2A, B). At 4 h, the phage titer was significantly higher in spleen ($6.8 \pm 0.10 \log_{10}$ PFU/ml, 6.69×10^7 PFU/ml) compared to blood ($5.3 \pm 0.12 \log_{10}$ PFU/ml, 2.22×10^5 PFU/ml), lungs ($5.6 \pm 0.4 \log_{10}$ PFU/ml, 5.78×10^5 PFU/ml), liver ($6.3 \pm 0.05 \log_{10}$ PFU/ml, 2.25×10^6 PFU/ml), and kidneys ($5.8 \pm 0.10 \log_{10}$ PFU/ml, 6.04×10^5 PFU/ml) ($p < 0.0001$, two-way ANOVA with Tukey's multiple comparisons) (Figure 2A and Supplementary Table S2). After 4 h, there was a gradual decrease in phage titer in all organs and the phage was completely cleared within 48 h of phage inoculation except from spleen, where the complete clearance was seen at 72 h.

Similarly, in an oral route and in the absence of the host bacteria, maximum biodistribution of the $\phi Kp_Pokalde_002$ was found at 8 h (28%) post phage administration (Figures 2C, D). At 8 h, the phage titer was significantly higher ($p < 0.0001$, two-way ANOVA with Tukey's multiple comparisons test) in spleen ($6.7 \pm 0.09 \log_{10}$ PFU/ml, 5.21×10^6 PFU/ml) compared to blood ($4.8 \pm 0.1 \log_{10}$ PFU/ml, 1.45×10^5 PFU/ml), lungs ($5.1 \pm 0.13 \log_{10}$ PFU/ml, 1.44×10^5 PFU/ml), liver ($5.9 \pm 0.12 \log_{10}$ PFU/ml, 8.10×10^5 PFU/ml), and kidneys ($5.5 \pm 0.35 \log_{10}$ PFU/ml, 4.50×10^5 PFU/ml) (Figure 2C). After 8 h, the phage titer gradually decreased and completely cleared from all organs within 48 h of phage administration except spleen, where the complete clearance was seen at 72 h. As expected, we further observed that relative bioavailability was lower when phage was administered through oral route compared to IP (Table 1) in the absence of host bacteria Kp56. Although the results were similar in the presence of host Kp56, the relative bioavailability of phage was higher in blood and spleen when administered orally compared to IP.

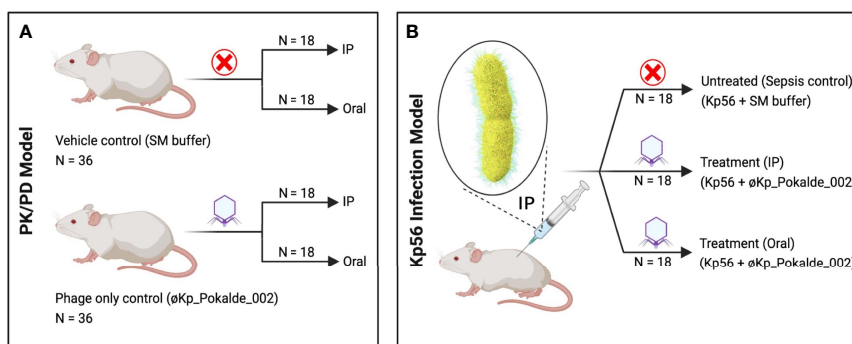


FIGURE 1 | Schematic representation of the experimental design. (A) In PK/PD model, SM buffer (vehicle control) and same dose of purified $\phi Kp_Pokalde_002$ (phage only control) was administered via both IP and oral route. (B) In Kp56 infection model, bacteria (*K. pneumoniae*) were administered via IP route only, while treatment ($\phi Kp_Pokalde_002$) was administered via both IP and oral route. Figure created in BioRender.com. PK, pharmacokinetics; PD, pharmacodynamics; SM, Sodium Magnesium; IP, intraperitoneal.

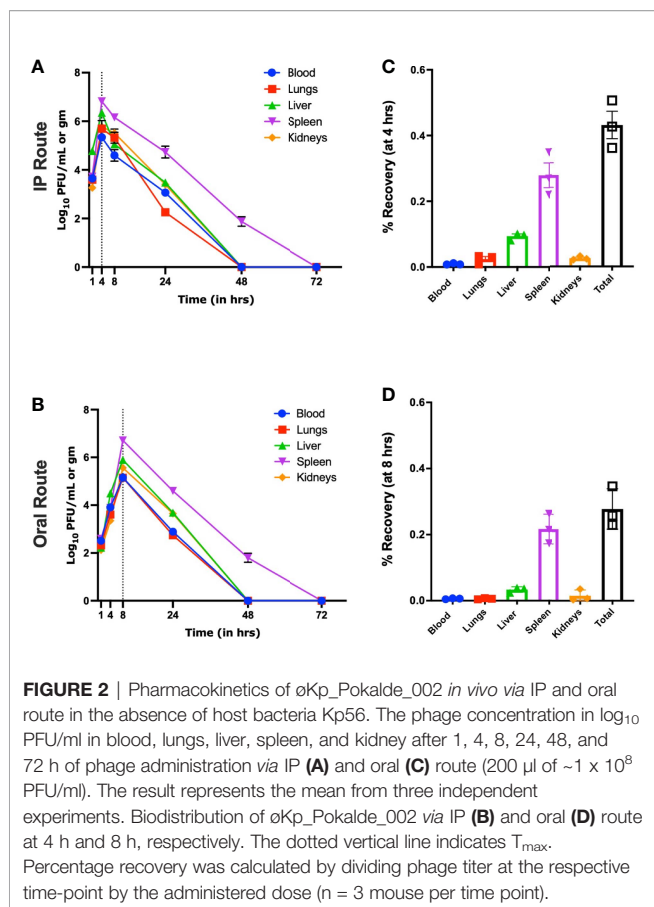


FIGURE 2 | Pharmacokinetics of øKp_Pokalde_002 *in vivo* via IP and oral route in the absence of host bacteria Kp56. The phage concentration in log₁₀ PFU/ml in blood, lungs, liver, spleen, and kidney after 1, 4, 8, 24, 48, and 72 h of phage administration via IP (A) and oral (C) route (200 µl of ~1 × 10⁸ PFU/ml). The result represents the mean from three independent experiments. Biodistribution of øKp_Pokalde_002 via IP (B) and oral (D) route at 4 h and 8 h, respectively. The dotted vertical line indicates T_{max}. Percentage recovery was calculated by dividing phage titer at the respective time-point by the administered dose (n = 3 mouse per time point).

In the presence of host bacteria Kp56, maximum titer of the øKp_Pokalde_002 was found at 8 h post phage injection (IP) and

24 h (oral) (Figures 3A, B) and gradually decreased after 24 h. In both group, maximum phage titer was found in the spleen at 24 h post phage injection. However, in contrast to phage inoculations without host, the phage did not clear from spleen until 72 h when inoculated with host Kp56.

We further report that mean elimination half-lives of øKp_Pokalde_002 in different organs were route independent [mean = 7.48 h, CV = 7.2% (IP) and mean = 7.6 h, CV = 10.5% (oral)] but the half-life was significantly lower [mean = 6.33 h, CV = 14.0% (IP) and mean = 5.3 h, CV = 4.0% (oral)] when susceptible host (Kp56) was present (Table 1) via both IP (p = 0.03, r² = 0.72, paired t-test) and oral (p = 0.0034, r² = 0.90, paired t-test) (Figure 3C) route possibly because of strong immune response from mice against bacteria and phage in the presence of Kp56 suggesting rapid clearance.

Pharmacodynamics

The groups of mice in PK/PD model (not infected by Kp56) that received øKp_Pokalde_002 via IP or oral route showed only mild to moderate alveolar wall thickening and remarkably reduced neutrophil infiltration in perivascular and peri bronchial areas (Figure 4). Moreover, they also did not show any significant histological changes compared to the vehicle control (SM buffer only) group at 24 h post phage inoculation. On the other hand, in the Kp56 infection model, bacterial count increased exponentially in the blood and lungs for up to 24 h when treated with SM buffer only (untreated group), while the bacterial count gradually decreased after 8 h when treated with øKp_Pokalde_002 (treatment group) via both IP and oral routes. The bacterial count significantly reduced by 4–7 log₁₀ CFU/ml in the blood (p < 0.001) and lungs (p < 0.05) at 24 h of øKp_Pokalde_002 administration compared to untreated (Kp56 + SM buffer) group (Supplementary Figure S3, two-

TABLE 1 | Estimated pharmacokinetic parameters of virulent phage (øKp_Pokalde_002) in the absence and in the presence of host *K. pneumoniae* (Kp56).

Organ	Blood		Lungs		Liver		Spleen		Kidneys	
	IP	Oral	IP	Oral	IP	Oral	IP	Oral	IP	Oral
Parameters										
In the absence of host bacteria (Kp56)										
Administered dose: 200 µl of 1.2 × 10⁸ PFU/ml of øKp_Pokalde_002										
C _{max} (pfu/ml)	222778	72311	578611	14471	2258318	87056	6694839	521210	604444	45097
T _{max} (h)	4	8	4	8	4	8	4	8	4	8
V _d (L)	1.27	9.7	0.86	18.8	0.16	4.3	0.07	2.07	0.60	12.8
T _{1/2} (h)	8.29	8.35	7.21	8.45	7.34	7.13	6.87	6.58	7.34	7.49
CL (L/h)	0.21	1.32	0.15	2.36	0.03	0.62	0.01	0.3	0.1	1.6
AUC _{0-t} (pfu/h/ml)	269539	155155	807450	149419	2407478	848459	8248503	5262198	948204	458160
Relative bioavailability (F)	58%		19%		35%		64%		48%	
In the presence of host bacteria (Kp56)										
Administered dose: 200 µl of 1.0 × 10⁸ CFU/ml of Kp56 + 200 µl of 1.2 × 10⁸ PFU/ml of øKp_Pokalde_002										
C _{max} (pfu/ml)	2923000	3315027	34693333	2107333	56589196	16643667	293940000	579333333	23068000	1695000
T _{max} (h)	8	24	8	24	24	24	24	24	24	24
V _d (L)	0.15	0.48	0.01	0.2	0.005	0.009	0.01	0.02	0.006	0.03
T _{1/2} (h)	7.51	5.24	6.26	5.37	5.85	4.94	6.87	5.46	5.20	5.44
CL (L/h)	0.02	0.06	0.002	0.02	0.0009	0.001	0.001	0.002	0.001	0.005
AUC _{0-t} (pfu/h/ml)	3263704	4075882	43003899	2979558	97074444	25790850	399112587	626186433	190270651	3977100
Relative bioavailability (F)	125%		7%		27%		157%		2%	

C_{max}, maximum observed plasma concentration; T_{max}, time to the C_{max}; V_d, Volume of distribution; T_{1/2}, elimination half-time; CL, clearance; AUC_{0-t}, area under the concentration-time curve from time 1 h to the last quantifiable concentration. Relative bioavailability (F) was calculated using the following formula: F, AUC_{0-t} (oral)/AUC_{0-t} (IP) × 100%.

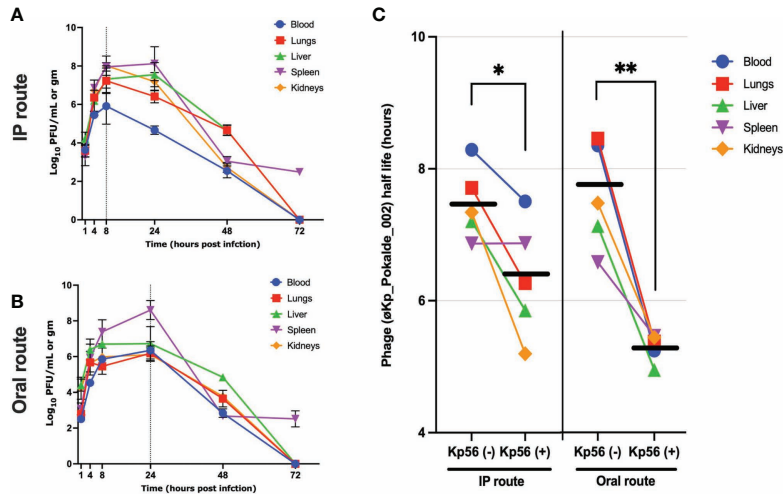


FIGURE 3 | Pharmacokinetics of ϕ Kp_Pokalde_002 *in vivo* and half-life of ϕ Kp_Pokalde_002 in the presence and absence of host bacteria Kp56 in mice when administered *via* IP and oral routes. The phage concentration in \log_{10} PFU/ml in blood, lungs, liver, spleen, and kidneys after 1, 4, 8, 24, 48, and 72 h in Kp56 treatment group after administration of phage *via* IP (A) and oral (B) route (200 μ l of $\sim 1 \times 10^8$ PFU/ml). The dotted vertical line indicates T_{max} . (C) The overall elimination half-life of ϕ Kp_Pokalde_002 is lower when host bacteria are present, signifying rapid clearance of phage from circulation in the presence of susceptible host. The individual data point represents an average from three replicates from three mouse. The horizontal line represents the grand mean.

way ANOVA with Tukey’s multiple comparisons). Further, comparison of histological changes in the lung tissues from untreated group (Kp56 + SM buffer) and treatment group (Kp56 + ϕ Kp_Pokalde_002) revealed a noticeable interstitial infiltration by neutrophils and macrophages with severe thickening, congestion, and destruction of alveolar wall in the lungs of untreated group. Meanwhile, orally treated group showed relatively increased neutrophil infiltration in the alveoli (lung tissues) compared to the IP-treated group.

The expression level of two pro-inflammatory cytokine (TNF- α and IL-6) in blood was analyzed to evaluate the tissue inflammation either by ϕ Kp_Pokalde_002 or by Kp56. Cytokine expression levels in the control group (SM buffer only), phage administered group (ϕ Kp_Pokalde_002 only), Kp56 infected group (Kp56 + SM buffer), and phage-treated groups (Kp56 + ϕ Kp_Pokalde_002) were compared. A significant upregulation of both pro-inflammatory cytokines’ TNF- α and IL-6 ($p < 0.0001$, Tukey’s multiple comparisons test) was observed in the Kp56 infected (Kp56 + SM buffer) group compared to the control (SM buffer only) group, and at 24 h post infection, the increment in the TNF- α and IL-6 was 21.0-fold and 17.1-fold, respectively. Changes in TNF- α and IL-6 in phage-only administered group were 1.1-fold and 0.9-fold, respectively, compared to vehicle control (SM buffer only) arm. Interestingly, the levels of cytokine expressions in the phage-treated groups *via* both IP and oral route were significantly lower compared to Kp56 infected (Kp56 + SM buffer, untreated) arm ($p < 0.05$, Tukey’s multiple comparisons test). The fold changes in cytokine TNF- α and IL-6 expression levels in phage-treated (Kp56 + ϕ Kp_Pokalde_002) groups compared to the uninfected control (phage only) arm are depicted in **Figure 5**.

DISCUSSION

Phage therapy is considered one of the promising alternatives to treat infections caused by MDR bacteria (Romero-Calle et al., 2019). PK/PD are fundamental parameters for better understanding the success of phage therapy and obtaining regulatory approval (Dąbrowska and Abedon, 2019). In this study, we focused on PK/PD of a novel ϕ Kp_Pokalde_002 that infects carbapenem-resistant *K. pneumoniae* using oral and IP routes of administration in a mouse model. Our results showed that ϕ Kp_Pokalde_002 rapidly distributed into the systemic circulation within an hour of administration *via* both oral and IP route. A relatively higher concentration of ϕ Kp_Pokalde_002 was recovered from plasma while injecting the phage through IP route compared to oral administration. When phage was administered in mice through the IP route, highest phage titer in the blood reached after 4 h post administration, significantly decreased after 8 h, and negligible count was observed after 24 h. The result suggests that the phage net phage elimination is observed after 4 h if injected intraperitoneally in the absence of host bacteria. The result is consistent with other studies where it is reported that the phages take 2–4 h to reach its maximum count in blood and is subsequently decreased after 12 h (Bogovazova et al., 1992; Capparelli et al., 2006; Kumari et al., 2010; Tiwari et al., 2011). Further, recovery of phages from blood and other tissue after oral administration shows that ϕ Kp_Pokalde_002 survived the gut environment and crossed the gut barrier to reach systemic circulation in mice subsequently reaching to different organs which is consistent with reports from other researchers (Cervený et al., 2002; Gorski and Weber-Dąbrowska, 2005). Several mechanisms have been proposed for phage absorption in the gastrointestinal tracts such as intestinal

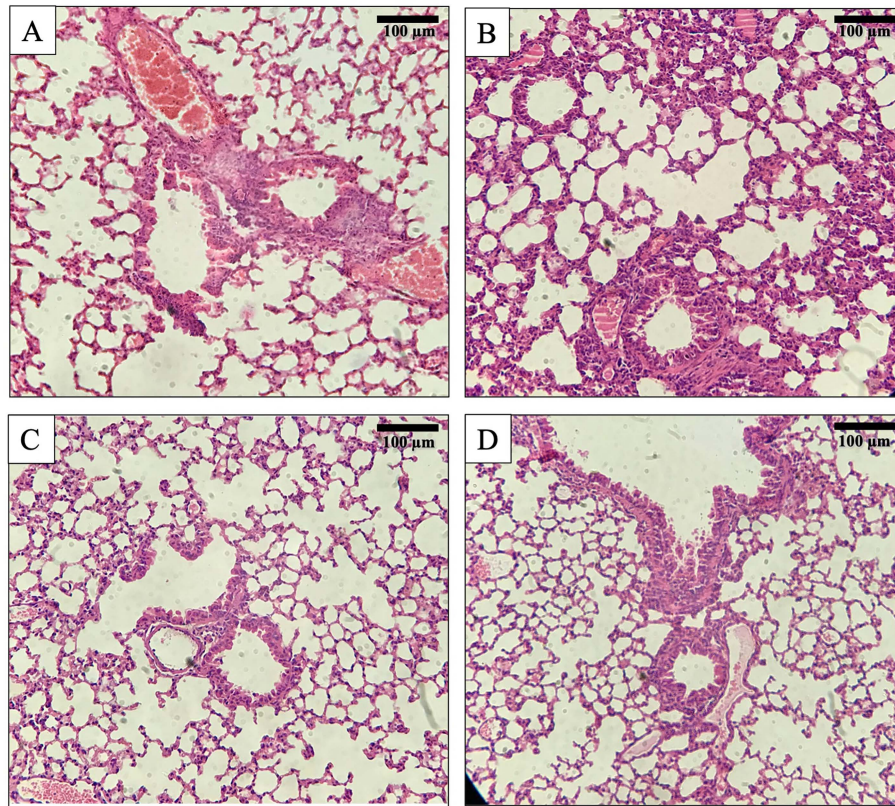


FIGURE 4 | Histology of mouse lung tissue sections after Hematoxylin and Eosin (H&E) staining at 200x magnification. **(A)** Lungs' tissue of a normal mouse. **(B)** Lungs' tissue of bacteria *K pneumoniae* (Kp56) infected mouse showing interstitial infiltration by neutrophils and macrophages with rupture of alveoli. **(C)** Lungs' tissue of mouse treated with ϕ Kp_Pokalde_002 via IP route. **(D)** Lungs' tissue of mouse treated with ϕ Kp_Pokalde_002 via oral route.

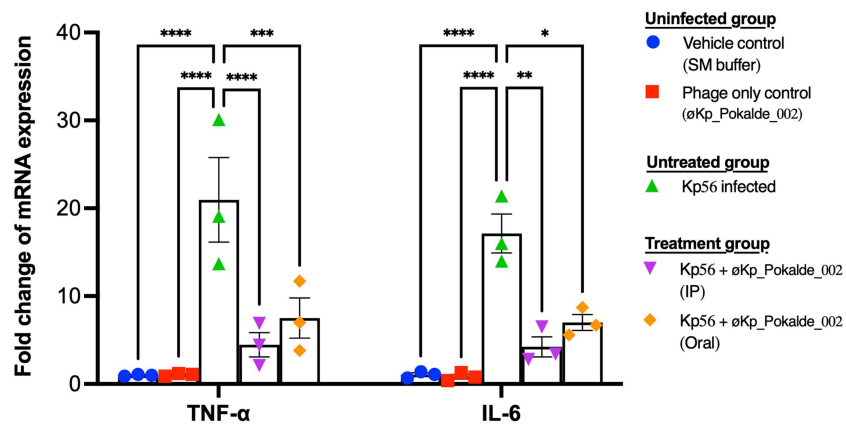


FIGURE 5 | Pro-inflammatory cytokine TNF- α and IL-6 levels in the plasma of mice (24 h post infection). Both TNF- α and IL-6 mRNA levels were significantly higher in Kp56 infected mice compared to uninfected and treated mice ($p < 0.05$) via both IP and oral routes. There was negligible fold increment of TNF- α and IL-6 mRNA level in vehicle control (SM buffer) and phage only control (ϕ Kp_Pokalde_002). Levels of TNF- α and IL-6 mRNA were normalized to β -actin mRNA levels and were expressed as n-fold ($2^{-\Delta\Delta C_t}$) increase with reference to the control groups. Results are shown as means \pm SEM from triplicate experiments. The y-axis values represent the fold changes of mRNA relative to the β -actin mRNA in the same sample. The statistical comparison was done by two-way ANOVA. * $p < 0.05$, ** $p < 0.01$, *** $p < 0.001$, **** $p < 0.0001$.

permeability and intestinal transport. Although the mechanism of controlling viral translocation remains unknown, researchers suggested that the phage passage is determined by various factors, including stomach acidity, phage concentration, and interactions with gut immune cells. Micropinocytosis may be a major endocytic pathway to translocate the phage from the intestinal wall into systemic circulation (Dąbrowska, 2019).

In our experiment, phages were recovered from blood, lungs, liver, and kidneys for up to 24 h and for up to 48 h in the spleen in the absence of host bacteria *via* both IP and oral route. However, there was significant difference in phage distribution, bioavailability, and elimination between IP and oral routes of administration. ϕ Kp_Pokalde_002 reached its maximum titer in blood at 4 h (2.3×10^5 PFU/ml) when administered through IP route which was relatively higher compared to administration *via* oral route (4.04×10^3 PFU/ml). Similar findings have been reported previously (Keller and Engley, 1958; Cervený et al., 2002; Oliveira et al., 2009; Jun et al., 2014). Additionally, overall relative bioavailability of ϕ Kp_Pokalde_002 when administered *via* oral route (at 8 h) was lower compared to IP route (at 4 h) in both the absence and/or presence of host bacteria. The reason for reduced bioavailability *via* oral route compared to IP might be due to slow absorption of the phage in the gastrointestinal tract to reach into the systemic circulation. However, it must be noted that because of the low sampling resolution, the T_{\max} could be higher than 4 h and 8 h in IP and oral administration respectively. As ϕ Kp_Pokalde_002 was stable within wide pH range (3–11) with minimal decrease in phage titer and did not show significant inactivation at 25°C and 37°C (Dhungana et al., 2021), the phage was well tolerated in mice gut with low acidity, making it a good candidate for oral phage therapy. It therefore appears that the ϕ Kp_Pokalde_002 is relatively stable in the mouse body when administered *via* the oral route but their availability is comparatively lower and slower. Similar findings have also been reported by Otero et al. (2019) and were able to recover orally administered encapsulated as well as non-encapsulated phages from various organs. Further, the inter mice PD variability [coefficient of variation (%CV)] was more pronounced in oral (7–78%) compared to IP (5–56%) route (**Supplementary Table S3**). The inter mice variability was profound in groups of Kp56 infection model. In addition to differential absorption of ϕ Kp_Pokalde_002 between animals and innate immunity, the higher variability between mice in the oral group may be because of the inconsistent neutralization of phages in the gut environment caused by gut acidity (feeding habit of mice). The phage absorption in the gastrointestinal tract is affected by various factors like gut acidity and gut permeability and is thus relatively slow. As such, lower phage particles reach into the blood stream through oral route compared to the IP route, which makes clinical application of phage *via* oral route for systemic infection unfavorable (Wolochow et al., 1966).

Further, the results suggest that liver and spleen are the most common organs of phage accumulation, suggesting phages are cleared by organs of the reticuloendothelial system such as the spleen, liver, and other filtering organs (Merril et al., 1996; Dąbrowska and Abedon, 2019). Similar results of non-homogenous biodistribution and preferential accumulation of

phages in organs like spleen and liver has also been observed in anti-pseudomonal phage in mice (Lin et al., 2020) and rabbit *in vivo* models (Uhr and Weissman, 1965). Further, phages are also reported in urine of human (Hildebrand and Wolochow, 1962) and animal models like rats (Wolochow et al., 1966) and rabbits (Schultz and Neva, 1965) after systemic injection which supports our finding that phage can pass through the renal filter. The role of the kidneys in the clearance of phages has also been observed in fish, where phages were detected in fish kidney a month after phage administration (Russell et al., 1976).

The PK of phages are fundamentally different from those of chemical drugs due to the self-replicative nature of phages in the presence of susceptible bacteria, its absorption rate, and clearance by host's immunity (Dąbrowska, 2019); thus, phage half-life cannot be estimated by conventional approach. Although researchers have demonstrated prolonged phage half-life *in vivo* with encapsulation of phage (Colom et al., 2015; Singla et al., 2016), the half-life of phage in the presence of a host is scarce. Using one phase decay model, our study showed that there was no significant difference in elimination half-life of ϕ Kp_Pokalde_002 when administered *via* IP and oral routes suggesting phage half-life to be route independent. However, the phage had a shorter elimination half-life in the blood and other organs when Kp56 was present, although phage titer was relatively higher in treatment groups compared to phage only control groups. This clearly suggests that phages can exponentially increase their number *in vivo* infecting and lysing the susceptible host bacteria and is cleared more rapidly by strong immune response developed against host bacteria (nonspecific) and phage itself (anti-phage). This may explain why multiple injections of phage is required for phage therapy, although theoretically phages are self-multiplying. However, a study on Klebsiella phage by Soleimani Sasani and Eftekhar (2020) found half-life in blood (4 h) when phages were administered intraperitoneally [100 μ l of 10^{10} PFU/ml (*Myoviridae*)] and 8 h in lungs, whereas Kumari et al. (2010) reported maximum recovery from blood, peritoneal fluid, lungs, and skin at 6 h post IP injection [250 μ l of 10^{10} PFU/ml (*Podoviridae*)]. Moreover, the half-life of phage seems to be comparable to that of antibiotics in animal models (Chang et al., 1991; Griffith et al., 2003) which ranges from 0.5 h to more than 7 h which makes it a good drug candidate against bacterial infections. However, more research is required in *in vivo* models to understand the half-life of different phages in the presence of susceptible host as this is important in designing the therapeutic dose of phage.

The histology results also revealed that the lung tissue of the ϕ Kp_Pokalde_002 administrated mice had a similar histological picture with reference to the wild-type and SM buffer only administrated mice group. Similar results of no detrimental histological effects were also observed by Gangwar et al. (2021) in various organs of Charles Foster rats when challenged by high (10^{15} and 10^{20} PFU/ml) of Klebsiella phage orally. Pro-inflammatory cytokines, TNF- α and IL-6, are useful markers of infection severity (Bozza et al., 2007). Present study revealed that there was negligible upregulation of pro-inflammatory cytokines (TNF- α , and IL-6) with the ϕ Kp_Pokalde_002 administrated *via* both IP and oral routes. In contrast, there was significant upregulation of the cytokines in the mice infected with the Kp56. Upon infection, pro-

inflammatory cytokines are released by the macrophages to adhere the other inflammatory cells at the infection site (Liu et al., 2016). The expression of the cytokines was dropped after 24 h of the ϕ Kp_Pokalde_002 administration in both IP and oral routes signifying removal of Kp56. The result supports the findings of other researchers who have reported significant reduction in cytokines levels in phage-treated mice (Watanabe et al., 2007; Wang et al., 2016). Phage lysates that are prepared from the gram-negative bacteria may contain bacterial endotoxins. Endotoxins are highly immunogenic, which could trigger the inflammatory response. An overexpression of cytokines leads to a septic shock and consecutive death (Cavaillon, 2018). Phage preparation should be necessarily purified to ensure the low level of the endotoxin and other bacterial contamination. However, in our study, we did not measure the level of endotoxin in the phage lysate. Although researchers have highlighted that phage therapy causes lysis of the host bacteria within the body, thus releasing endotoxins/enterotoxins, which may induces higher levels of TNF- α and IL-6 causing septic shock (Hagens et al., 2004), the ϕ Kp_Pokalde_002 did not induce a significant inflammatory response in mice indicating a good PD efficiency. However, Chow et al. (2020) also reported that such upregulation of pro-inflammatory cytokines was transient and was diminished over time. Our results suggested that systemic inflammation of the tissues is lower in phage-treated mice as compared to the untreated. The histological findings of the lung tissue also support these findings.

In conclusion, PK/PD of ϕ Kp_Pokalde_002 *in vivo* were assessed. Inflammatory response, half-life, and biodistribution of the phage in blood, lungs, liver, kidneys, and spleen of mouse model were determined at different time interval *via* IP and oral routes of phage administration. The ϕ Kp_Pokalde_002 distributed more rapidly into the systemic circulation *via* the IP route compared to oral route. Importantly, the ϕ Kp_Pokalde_002 did not elicit any notable inflammation in lung tissues. Further, treatment by ϕ Kp_Pokalde_002 significantly reduced the inflammations caused by bacterial infection and downregulated the levels of the pro-inflammatory cytokine (TNF- α and IL-6) expression.

To the best of our knowledge, this is the first study that evaluates the PK/PD of a virulent Klebsiella phage that infects carbapenem-resistant clinical isolate of *K. pneumoniae* *via* IP and oral routes of administration. However, more work is necessary to better understand the PK/PD of the phage using different dose regimes and time of the phage exposure in *in vivo* model.

DATA AVAILABILITY STATEMENT

The original results of the study are included in the article. Further inquiries can be directed to the corresponding author.

ETHICS STATEMENT

Ethical approval was obtained for the use of animal prior to the study from Nepal Health Research Council (NHRC), Nepal (Ethical approval No.161/2018). The protocol was also approved by the Ethical Review Board, NHRC.

AUTHOR CONTRIBUTIONS

GD and RM conceived the idea and designed the study. GD and MR performed the experiments. GD, MR, and RN analyzed the data. GD and RN drafted the manuscript. RM supervised the project. All authors contributed to the article and approved the submitted version.

FUNDING

This work was partially supported by the 'PhD Fellowship and Research Support' awarded to GD by the University Grants Commission, Nepal (UGC-Nepal) (Award Numbers: PhD/73-74/S and T-07).

ACKNOWLEDGMENTS

We gratefully acknowledge Prof. Dr. Krishna Das Manandhar, Head, Central Department of Biotechnology, Tribhuvan University, Nepal for providing consistent support in the study and members of Adhya's Laboratory, Laboratory of Molecular Biology, NCI, NIH, particularly Dr. Manoj Rajaure for guidance during the study. We also like to acknowledge Dr. Ashish Lakhey, Dr. Pooja Dhungana, Mr. Kapil Dev Neupane, Mr. Rajindra Napit, Ms. Apsara Parajuli, Ms. Elisha Upadhyay and Mr. Prashant Regmi for their valuable support during the study.

SUPPLEMENTARY MATERIAL

The Supplementary Material for this article can be found online at: <https://www.frontiersin.org/articles/10.3389/fcimb.2021.684704/full#supplementary-material>

Supplementary Figure 1 | Analysis of ϕ Kp_Pokalde_002 genome for prediction of its lifestyle and host. The lytic-lifestyle and Gram-negative host of the phage was confirmed based on its physicochemical characters (Dhungana et al., 2021) and analysis of its amino acid sequences through PHACTS (<https://edwards.sdsu.edu/PHACTS/index.php>).

Supplementary Figure 2 | Area under the curve (AUC) from all groups of mice. **(A)** Phage pharmacokinetics and AUC after administration of phage *via* IP route in the absence of host Kp56. **(B)** Phage pharmacokinetics and AUC after administration of phage *via* oral route in the absence of host Kp56. **(C)** Phage pharmacokinetics and AUC after administration of phage *via* IP route in the presence of host Kp56. **(D)** Phage pharmacokinetics and AUC after administration of phage *via* oral route in the presence of host Kp56.

Supplementary Figure 3 | Quantification of bacterial burden in lungs and blood of mice from different group. Bacterial load was significantly decreased in phage treated group compared to group that only received SM buffer as treatment control. The bacterial burden in lungs **(A)** was similar to the bacterial burden in blood of phage treated group. Although the burden of bacterial significantly decreased, it appears that oral treatment is relatively less effective compared to IP and IP-one hour delay. The color-dotted line indicates the non-linear exponential growth fit (log population).

Supplementary Table 1 | Primers used in the study.

Supplementary Table 2 | P-values at 4 h (IP administration) and 8 h (oral administration) of ϕ Kp_Pokalde_002 in the absence of host bacteria Kp56.

REFERENCES

- Barr, J. J., Auro, R., Furlan, M., Whiteson, K. L., Erb, M. L., Pogliano, J., et al. (2013). Bacteriophage Adhering to Mucus Provide a non-Host-Derived Immunity. *Proc. Natl. Acad. Sci. U.S.A.* 110 (26), 10771–10776. doi: 10.1073/pnas.1305923110
- Bogovazova, G. G., Voroshilova, N. N., Bondarenko, V. M., Gorbatkova, G. A., Afanas'eva, E. V., Kazakova, T. B., et al. (1992). Immunobiological Properties and Therapeutic Effectiveness of Preparations From Klebsiella Bacteriophages. *Zh Mikrobiol Epidemiol. Immunobiol.* (3), 30–33.
- Bourdin, G., Schmitt, B., Marvin Guy, L., Germond, J. E., Zuber, S., Michot, L., et al. (2014). Amplification and Purification of T4-Like Escherichia Coli Phages for Phage Therapy: From Laboratory to Pilot Scale. *Appl. Environ. Microbiol.* 80 (4), 1469–1476. doi: 10.1128/aem.03357-13
- Bozza, F. A., Salluh, J. I., Japiassu, A. M., Soares, M., Assis, E. F., Gomes, R. N., et al. (2007). Cytokine Profiles as Markers of Disease Severity in Sepsis: A Multiplex Analysis. *Crit. Care* 11 (2), R49. doi: 10.1186/cc5783
- Cafilisch, K. M., Suh, G. A., and Patel, R. (2019). Biological Challenges of Phage Therapy and Proposed Solutions: A Literature Review. *Expert Rev. Anti Infect. Ther.* 17 (12), 1011–1041. doi: 10.1080/14787210.2019.1694905
- Capparelli, R., Ventimiglia, I., Roperto, S., Fenizia, D., and Iannelli, D. (2006). Selection of an Escherichia Coli O157:H7 Bacteriophage for Persistence in the Circulatory System of Mice Infected Experimentally. *Clin. Microbiol. Infect.* 12 (3), 248–253. doi: 10.1111/j.1469-0691.2005.01340.x
- Cavaillon, J. M. (2018). Exotoxins and Endotoxins: Inducers of Inflammatory Cytokines. *Toxicon.* 149, 45–53. doi: 10.1016/j.toxicon.2017.10.016
- Cervený, K. E., DePaola, A., Duckworth, D. H., and Gulig, P. A. (2002). Phage Therapy of Local and Systemic Disease Caused by *Vibrio Vulnificus* in Iron-Dextran-Treated Mice. *Infect. Immun.* 70 (11), 6251–6262. doi: 10.1128/iai.70.11.6251-6262.2002
- Chang, H. R., Comte, R., Pigué, P. F., and Pechere, J. C. (1991). Activity of Minocycline Against *Toxoplasma Gondii* Infection in Mice. *J. Antimicrob. Chemother.* 27 (5), 639–645. doi: 10.1093/jac/27.5.639
- Chow, M. Y. T., Chang, R. Y. K., Li, M., Wang, Y., Lin, Y., Morales, S., et al. (2020). Pharmacokinetics and Time-Kill Study of Inhaled Antipseudomonal Bacteriophage Therapy in Mice. *Antimicrob. Agents Chemother.* 65 (1), e01470–e01470. doi: 10.1128/aac.01470-20
- Clokic, M. R., Millard, A. D., Letarov, A. V., and Heaphy, S. (2011). Phages in Nature. *Bacteriophage.* 1 (1), 31–45. doi: 10.4161/bact.1.1.14942
- Colom, J., Cano-Sarabia, M., Otero, J., Cortes, P., Maspoch, D., and Llagostera, M. (2015). Liposome-Encapsulated Bacteriophages for Enhanced Oral Phage Therapy Against *Salmonella* Spp. *Appl. Environ. Microbiol.* 81 (14), 4841–4849. doi: 10.1128/aem.00812-15
- Dąbrowska, K. (2019). Phage Therapy: What Factors Shape Phage Pharmacokinetics and Bioavailability? *Syst. Crit. Rev.* 39 (5), 2000–2025. doi: 10.1002/med.21572.
- Dąbrowska, K., and Abedon, S. T. (2019). Pharmacologically Aware Phage Therapy: Pharmacodynamic and Pharmacokinetic Obstacles to Phage Antibacterial Action in Animal and Human Bodies. *Microbiol. Mol. Biol. Rev.* 83 (4), e00012–e00019. doi: 10.1128/mmb.00012-19
- Dedrick, R. M., Guerrero-Bustamante, C. A., Garlena, R. A., Russell, D. A., Ford, K., Harris, K., et al. (2019). Engineered Bacteriophages for Treatment of a Patient With a Disseminated Drug-Resistant Mycobacterium Abscessus. *Nat. Med.* 25 (5), 730–733. doi: 10.1038/s41591-019-0437-z
- Dhungana, G., Regmi, M., Paudel, P., Parajuli, A., Upadhyay, E., Indu, G., et al. (2021). Therapeutic Efficacy of Bacteriophage Therapy to Treat Carbapenem Resistant *Klebsiella Pneumoniae* in Mouse Model. *J. Nepal Health Res. Council* 19 (1), 76–82. doi: 10.33314/jnhrc.v19i1.3282
- Dufour, N., Delattre, R., and Debarbieux, L. (2018). *In Vivo* Bacteriophage Biodistribution. *Methods Mol. Biol.* 123–137. doi: 10.1007/978-1-4939-7395-8_11
- Furfaro, L. L., Payne, M. S., and Chang, B. J. (2018). Bacteriophage Therapy: Clinical Trials and Regulatory Hurdles. *Front. Cell. Infect. Microbiol.* 8, 376. doi: 10.3389/fcimb.2018.00376
- Gangwar, M., Rastogi, S., Singh, D., Shukla, A., Dhameja, N., Kumar, D., et al. (2021). Study on the Effect of Oral Administration of Bacteriophages in Charles Foster Rats With Special Reference to Immunological and Adverse Effects. *Front. Pharmacol.* 12, 615445. doi: 10.3389/fphar.2021.615445
- Gorski, A., and Weber-Dąbrowska, B. (2005). The Potential Role of Endogenous Bacteriophages in Controlling Invading Pathogens. *Cell Mol. Life Sci.* 62 (5), 511–519. doi: 10.1007/s00018-004-4403-6
- Griffith, D. C., Harford, L., Williams, R., Lee, V. J., and Dudley, M. N. (2003). *In Vivo* Antibacterial Activity of RWJ-54428, a New Cephalosporin With Activity Against Gram-Positive Bacteria. *J. Antimicrob. Agents Chemother.* 47 (1), 43–47. doi: 10.1128/AAC.47.1.43-47.2003%
- Dhungana, G., Regmi, M., Paudel, P., Parajuli, A., Upadhyay, E., Indu, G., et al. (2021). Therapeutic Efficacy of Bacteriophage Therapy to Treat Carbapenem Resistant *Klebsiella Pneumoniae* in Mouse Model. *J. Nepal Health Res. Council* 19 (1), 76–82. doi: 10.33314/jnhrc.v19i1.3282
- Hagens, S., Habel, A., Von Ahsen, U., Von Gabain, A., and Bläsi, U. (2004). Therapy of Experimental *Pseudomonas* Infections With a Nonreplicating Genetically Modified Phage. *Antimicrob. Agents Chemother.* 48 (10), 3817–3822. doi: 10.1128/AAC.48.10.3817-3822.2004
- Hildebrand, G. J., and Wolochow, H. (1962). Translocation of Bacteriophage Across the Intestinal Wall of the Rat. *Proc. Soc. Exp. Biol. Med.* 109, 183–185. doi: 10.3181/00379727-109-27146
- Hsu, L. Y., Apisarnthanarak, A., Khan, E., Suwantararat, N., Ghafur, A., and Tambyah, P. A. (2017). Carbapenem-Resistant *Acinetobacter Baumannii* and Enterobacteriaceae in South and Southeast Asia. *Clin. Microbiol. Rev.* 30 (1), 1–22. doi: 10.1128/cmr.00042-16
- Jain, M., Nijhawan, A., Tyagi, A. K., and Khurana, J. P. (2006). Validation of Housekeeping Genes as Internal Control for Studying Gene Expression in Rice by Quantitative Real-Time PCR. *Biochem. Biophys. Res. Commun.* 345 (2), 646–651. doi: 10.1016/j.bbrc.2006.04.140
- Jun, J. W., Shin, T. H., Kim, J. H., Shin, S. P., Han, J. E., Heo, G. J., et al. (2014). Bacteriophage Therapy of a *Vibrio Parahaemolyticus* Infection Caused by a Multiple-Antibiotic-Resistant O3:K6 Pandemic Clinical Strain. *J. Infect. Dis.* 210 (1), 72–78. doi: 10.1093/infdis/jiu059
- Keller, R., and Engley, F. B. Jr. (1958). Fate of Bacteriophage Particles Introduced Into Mice by Various Routes. *Proc. Soc. Exp. Biol. Med.* 98 (3), 577–580. doi: 10.3181/00379727-98-24112
- Kumari, S., Harjai, K., and Chhibber, S. (2010). Isolation and Characterization of *Klebsiella Pneumoniae* Specific Bacteriophages From Sewage Samples. *Folia Microbiol.* 55 (3), 221–227. doi: 10.1007/s12223-010-0032-7
- Kumari, S., Harjai, K., and Chhibber, S. (2011). Bacteriophage Versus Antimicrobial Agents for the Treatment of Murine Burn Wound Infection Caused by *Klebsiella Pneumoniae* B5055. *J. Med. Microbiol.* 60 (Pt 2), 205–210. doi: 10.1099/jmm.0.018580-0
- Lin, Y. W., Chang, R. Y., Rao, G. G., Jermain, B., Han, M.-L., Zhao, J. X., et al. (2020). Pharmacokinetics/Pharmacodynamics of Antipseudomonal Bacteriophage Therapy in Rats: A Proof-of-Concept Study. *Clin. Microbiol. Infect.* 26 (9), 1229–1235. doi: 10.1016/j.cmi.2020.04.039
- Liu, K.-y., Yang, W.-h., Dong, X.-k., Cong, L.-m., Li, N., Li, Y., et al. (2016). Inhalation Study of Mycobacteriophage D29 Aerosol for Mice by Endotracheal Route and Nose-Only Exposure. *J. Aerosol Med. Pulm Drug Delivery.* 29 (5), 393–405. doi: 10.1089/jamp.2015.1233
- Livak, K. J., and Schmittgen, T. D. (2001). Analysis of Relative Gene Expression Data Using Real-Time Quantitative PCR and the 2⁻(Delta Delta C(T)) Method. *Methods.* 25 (4), 402–408. doi: 10.1006/meth.2001.1262
- Mcnair, K., Bailey, B. A., and Edwards, R. A. (2012). PHACTS, a Computational Approach to Classifying the Lifestyle of Phages. *Bioinformatics* 28 (5), 614–618. doi: 10.1093/bioinformatics/bts014
- Merrill, C. R., Biswas, B., Carlton, R., Jensen, N. C., Creed, G. J., Zullo, S., et al. (1996). Long-Circulating Bacteriophage as Antibacterial Agents. *Proc. Natl. Acad. Sci. U.S.A.* 93 (8), 3188–3192. doi: 10.1073/pnas.93.8.3188
- Nepal, K., Pant, N. D., Neupane, B., Belbase, A., Baidhya, R., Shrestha, R. K., et al. (2017). Extended Spectrum Beta-Lactamase and Metallo Beta-Lactamase Production Among *Escherichia Coli* and *Klebsiella Pneumoniae* Isolated From Different Clinical Samples in a Tertiary Care Hospital in Kathmandu, Nepal. *Ann. Clin. Microbiol. Antimicrob.* 16 (1), 62. doi: 10.1186/s12941-017-0236-7
- Nilsson, A. S. (2019). Pharmacological Limitations of Phage Therapy. *Ups J. Med. Sci.* 124 (4), 218–227. doi: 10.1080/03009734.2019.1688433
- Oliveira, A., Sereno, R., Nicolau, A., and Azeredo, J. (2009). The Influence of the Mode of Administration in the Dissemination of Three Coliphages in Chickens. *Poult Sci.* 88 (4), 728–733. doi: 10.3382/ps.2008-00378

- Otero, J., García-Rodríguez, A., Cano-Sarabia, M., Maspoch, D., Marcos, R., Cortés, P., et al. (2019). Biodistribution of Liposome-Encapsulated Bacteriophages and Their Transcytosis During Oral Phage Therapy [Original Research]. *Front. Microbiol.* 10, 689. doi: 10.3389/fmicb.2019.00689
- Paczosa, M. K., and Mecsas, J. (2016). Klebsiella Pneumoniae: Going on the Offense With a Strong Defense. *J. Microbiol. Mol. Biol. Rev.* 80 (3), 629–661. doi: 10.1128/MMBR.00078-15%
- Payne, R. J., and Jansen, V. A. (2003). Pharmacokinetic Principles of Bacteriophage Therapy. *Clin. Pharmacokinet* 42 (4), 315–325. doi: 10.2165/00003088-200342040-00002
- Petrovic Fabijan, A., Lin, R. C. Y., Ho, J., Maddocks, S., Ben Zakour, N. L., and Iredell, J. R. (2020). Safety of Bacteriophage Therapy in Severe Staphylococcus Aureus Infection. *Nat. Microbiol.* 5 (3), 465–472. doi: 10.1038/s41564-019-0634-z
- Pirnay, J.-P. (2020). Phage Therapy in the Year 2035. *Front. Microbiol.* 11, 1171. doi: 10.3389/fmicb.2020.01171
- Pirnay, J.-P., Verbeken, G., Ceysens, P.-J., Huys, I., De Vos, D., Ameloot, C., et al. (2018). The Magistral Phage. *Viruses* 10 (2), 64. doi: 10.3390/v10020064
- Pouillot, F., Chomton, M., Blois, H., Courroux, C., Noelig, J., Bidet, P., et al. (2012). Efficacy of Bacteriophage Therapy in Experimental Sepsis and Meningitis Caused by a Clone O25b:H4-ST131 Escherichia Coli Strain Producing CTX-M-15. *Antimicrob. Agents Chemother.* 56 (7), 3568–3575. doi: 10.1128/aac.06330-11
- Romero-Calle, D., Guimaraes Benevides, R., Goes-Neto, A., and Billington, C. (2019). Bacteriophages as Alternatives to Antibiotics in Clinical Care. *Antibiot (Basel)* 8 (3), 138. doi: 10.3390/antibiotics8030138
- Russell, W. J., Taylor, S. A., and Sigel, M. M. (1976). Clearance of Bacteriophage in Poikilothermic Vertebrates and the Effect of Temperature. *J. Reticuloendothel. Soc.* 19 (2), 91–96.
- Sambrook, J., and Russell, D. J. P. (2001). *Molecular Cloning: A Laboratory Manual. 3rd Ed*, vol. 620. (Cold Spring Harbor Laboratory Press), 621.
- Santajit, S., and Indrawattana, N. (2016). Mechanisms of Antimicrobial Resistance in ESKAPE Pathogens. *BioMed. Res. Int.* 2016, 2475067. doi: 10.1155/2016/2475067
- Schooley, R. T., Biswas, B., Gill, J. J., Hernandez-Morales, A., Lancaster, J., Lessor, L., et al. (2017). Development and Use of Personalized Bacteriophage-Based Therapeutic Cocktails to Treat a Patient With a Disseminated Resistant Acinetobacter Baumannii Infection. *Antimicrob. Agents Chemother.* 61 (10), AAC.00954–00917. doi: 10.1128/aac.00954-17
- Schultz, I., and Neva, F. A. (1965) *Relationship Between Blood Clearance and Viruria After Intravenous Injection of Mice and Rats With Bacteriophage and Polioviruses*. Available at: <https://www.jimmunol.org/content/jimmunol/94/6/833.full.pdf>.
- Singla, S., Harjai, K., Katara, O. P., and Chhibber, S. (2015). Bacteriophage-Loaded Nanostructured Lipid Carrier: Improved Pharmacokinetics Mediates Effective Resolution of Klebsiella Pneumoniae-Induced Lobar Pneumonia. *J. Infect. Dis.* 212 (2), 325–334. doi: 10.1093/infdis/jiv029%
- Singla, S., Harjai, K., Katara, O. P., and Chhibber, S. (2016). Encapsulation of Bacteriophage in Liposome Accentuates its Entry in to Macrophage and Shields it From Neutralizing Antibodies. *PloS One* 11 (4), e0153777. doi: 10.1371/journal.pone.0153777
- Soleimani Sasani, M., and Eftekhari, F. (2020). Potential of a Bacteriophage Isolated From Wastewater in Treatment of Lobar Pneumonia Infection Induced by Klebsiella Pneumoniae in Mice. *Curr. Microbiol.* 77 (10), 2650–2655. doi: 10.1007/s00284-020-02041-z
- Spellberg, B. (2014). The Future of Antibiotics. *Crit. Care* 18 (3), 228. doi: 10.1186/cc13948
- Sybesma, W., Rohde, C., Bardy, P., Pirnay, J.-P., Cooper, I., Caplin, J., et al. (2018). Silk Route to the Acceptance and Re-Implementation of Bacteriophage Therapy—Part II. *Antibiotics* 7 (2), 35. doi: 10.3390/antibiotics7020035
- Tiwari, B. R., Kim, S., Rahman, M., and Kim, J. (2011). Antibacterial Efficacy of Lytic Pseudomonas Bacteriophage in Normal and Neutropenic Mice Models. *J. Microbiol.* 49 (6), 994–999. doi: 10.1007/s12275-011-1512-4
- Uhr, J. W., and Weissman, G. (1965). Intracellular Distribution and Degradation of Bacteriophage in Mammalian Tissues. *J. Immunol.* 94, 544–550.
- Verma, V., Harjai, K., and Chhibber, S. (2009). Characterization of a T7-Like Lytic Bacteriophage of Klebsiella Pneumoniae B5055: A Potential Therapeutic Agent. *Curr. Microbiol.* 59 (3), 274–281. doi: 10.1007/s00284-009-9430-y
- Vinodkumar, C. S., Kalsurmath, S., and Neelagund, Y. F. (2008). Utility of Lytic Bacteriophage in the Treatment of Multidrug-Resistant Pseudomonas Aeruginosa Septicemia in Mice. *Indian J. Pathol. Microbiol.* 51 (3), 360–366. doi: 10.4103/0377-4929.42511
- Wahida, A., Tang, F., and Barr, J. J. (2021). Rethinking Phage-Bacteria-Eukaryotic Relationships and Their Influence on Human Health. *Cell Host Microbe.* 29 (5), 661–688. doi: 10.1016/j.chom.2021.02.007
- Wang, J. L., Kuo, C. F., Yeh, C. M., Chen, J. R., Cheng, M. F., and Hung, C. H. (2018). Efficacy of Phikm18p Phage Therapy in a Murine Model of Extensively Drug-Resistant Acinetobacter Baumannii Infection. *Infect. Drug Resist.* 11, 2301–2310. doi: 10.2147/idr.S179701
- Wang, Z., Zheng, P., Ji, W., Fu, Q., Wang, H., Yan, Y., et al. (2016). SLPW: A Virulent Bacteriophage Targeting Methicillin-Resistant Staphylococcus Aureus *In Vitro* and *In Vivo*. *Front. Microbiol.* 7, 934. doi: 10.3389/fmicb.2016.00934
- Watanabe, R., Matsumoto, T., Sano, G., Ishii, Y., Tateda, K., Sumiyama, Y., et al. (2007). Efficacy of Bacteriophage Therapy Against Gut-Derived Sepsis Caused by Pseudomonas Aeruginosa in Mice. *J. Antimicrob. Agents Chemother* 51 (2), 446–452. doi: 10.1128/AAC.00635-06%
- WHO (2017). *Prioritization of Pathogens to Guide Discovery, Research and Development of New Antibiotics for Drug-Resistant Bacterial Infections, Including Tuberculosis* (Geneva: S. World Health Organization).
- Wolochow, H., Hildebrand, G. J., and Lamanna, C. (1966). Translocation of Microorganisms Across the Intestinal Wall of the Rat: Effect of Microbial Size and Concentration. *J. Infect. Dis.* 116 (4), 523–528. doi: 10.1093/infdis/116.4.523
- Young, R., and Gill, J. J. (2015). Phage Therapy Redux—What is to be Done? *J. Sci.* 350 (6265), 1163–1164. doi: 10.1126/science.aad6791%

Conflict of Interest: The authors declare that the research was conducted in the absence of any commercial or financial relationships that could be construed as a potential conflict of interest.

Publisher's Note: All claims expressed in this article are solely those of the authors and do not necessarily represent those of their affiliated organizations, or those of the publisher, the editors and the reviewers. Any product that may be evaluated in this article, or claim that may be made by its manufacturer, is not guaranteed or endorsed by the publisher.

Copyright © 2021 Dhungana, Nepal, Regmi and Malla. This is an open-access article distributed under the terms of the Creative Commons Attribution License (CC BY). The use, distribution or reproduction in other forums is permitted, provided the original author(s) and the copyright owner(s) are credited and that the original publication in this journal is cited, in accordance with accepted academic practice. No use, distribution or reproduction is permitted which does not comply with these terms.

Therapeutic Efficacy of Bacteriophage Therapy to Treat Carbapenem Resistant *Klebsiella Pneumoniae* in Mouse Model

Gunaraj Dhungana,¹ Madhav Regmi,¹ Prashant Paudel,¹ Apsara Parajuli,¹ Elisha Upadhyay,¹ Indu Gyawali,¹ Himani Upreti,¹ Roshan Nepal,¹ Pragati Pradhan,¹ Rajani Malla¹

¹Central Department of Biotechnology, Tribhuvan University, Kathmandu, Nepal.

ABSTRACT

Background: Global emergence of carbapenem-resistant *Klebsiella pneumoniae* is a major public health concern. Phage therapy – application of lytic phage to kill pathogenic bacteria – is considered as one of the promising alternatives to tackle this antibiotic crisis in recent days. This study aimed to isolate, characterize and evaluate therapeutic efficacy of a novel *K. pneumoniae* phage in mouse model.

Methods: A novel lytic bacteriophage (phage) Kp_Pokalde_002 was isolated against carbapenem-resistant *K. pneumoniae* (Kp56) and characterized. Safety parameters of the phage were evaluated by bioinformatic analysis of its genome. A lethal dose ($\sim 1 \times 10^7$ CFU/mouse) of Kp56 was determined and administered in the mice. The infected mice were treated with phage Kp_Pokalde_002 at a multiplicity of infection (MOI) 1.0 ($\sim 1 \times 10^7$ PFU/mouse) via both oral and intraperitoneal (IP) routes.

Results: Isolated phage comprised an icosahedral capsid with a short tail. Based on genome analysis, the phage was strictly lytic belonging the Podoviridae family (T7-like viruses) and free from any virulent and antibiotic-resistant genes. The phage was stable up to 60 °C for 30 minutes and effective between pH 4 to 11 (optimum pH 9). The phage exhibited a short latent period (20 minutes) with burst size of 121 phage particles per infected cell. The infected mice were rescued with the phage therapy via both oral and IP route. Significant reduction of bacterial load ($3-7 \log_{10}$ CFU/ml) in the blood and lung was observed in the treatment group.

Conclusions: We provide an evidence of successful phage therapy against carbapenem-resistant *K. pneumoniae* infected mouse model using locally isolated lytic phage.

Keywords: Bacteriophage; *klebsiella pneumoniae*; phage therapy

INTRODUCTION

Klebsiella pneumoniae is one of the opportunistic pathogens, often seen as multidrug resistant including 4th generations cephalosporins. It causes a wide variety of nosocomial infections with high morbidity and mortality.¹ Due to difficulty in treating infections caused by these superbugs, an alternative approach must be sought. Among many alternatives, bacteriophage-mediated treatment or phage therapy is promising.² Phage therapy in animal models has demonstrated successful outcomes against multiple pathogens such as extended spectrum beta-lactamase (ESBL) and carbapenem-resistant bacteria like *Escherichia coli*, *Acinetobacter baumannii*, *K. pneumoniae* and *Pseudomonas aeruginosa*.³⁻⁶

Major challenges of phage therapy are poor understanding of phage-host dynamics within the body including phage

availability, stability and accessibility to the target host, development of bacteriophage resistant mutants, immune mediated phage neutralization and uncertain route and dose of administration.⁷ Till date, only few studies have been conducted to evaluate the routes of phage administration to treat systemic infection caused by carbapenem-resistant *K. pneumoniae*. Thus, this study aimed to isolate, characterize and evaluate therapeutic efficacy of bacteriophage to treat carbapenem-resistant *K. pneumoniae* in mouse model using locally isolated phage.

METHODS

The study was conducted at the Central Department of Biotechnology (CDBT), Tribhuvan University, Nepal. Phage genome sequencing and electron microscopy was performed in Xcelris Labs, Ahmedabad and Jawaharlal

Correspondence: Prof Rajani Malla, Central Department of Biotechnology, Tribhuvan University, Kathmandu, Nepal. Email: rajanimala2000@gmail.com, Phone: +9779851013734.

Nehru University, New Delhi, India. A clinical isolate of *K. pneumoniae* (Kp56) which was molecularly confirmed as a carbapenem-resistant strain from previous study, was obtained from the Microbiology Laboratory, CDBT (unpublished data). The bacterial strain was propagated in Luria-Bertani (LB) broth (HiMedia, India) at 37 °C.

A novel phage Kp_Pokalde_002 was isolated using the Kp56 as a host from the municipal wastewater canal, Kathmandu. Standard double layer agar assay (DLAA) was used for the isolation and propagation of the phage as described elsewhere.⁸ Phages were further purified by isopycnic CsCl density-gradient ultracentrifugation described previously.⁹ The phage preparation was passed through 0.22micron, syringe filter (Whatman, Sigma Aldrich, USA) and stored at 4 °C until further use. For transmission electron microscopy (TEM), the purified phage lysate was fixed with 2% paraformaldehyde and 2.5 % glutaraldehyde. Two microliters of the fixed phage lysate was spread on a carbon-coated copper grid and negatively stained with 2.0 µl of 2% (w/v) uranyl acetate (pH 4.5). The copper grid was dried completely and examined under JEM-2100F transmission electron microscope (JEOL, Japan) at 200 kV field emission.

Stability of the phage Kp_Pokalde_002 at different temperatures and pHs was determined as described previously with modifications.¹⁰ Briefly, for temperature stability, 1.0 ml phage lysate of 10⁸ PFU/ml in SM buffer (100 mM sodium chloride, 10 mM magnesium sulphate, 50 mM Tris-HCl, pH 7.5 and 0.01% (w/v) gelatin) was aliquoted in an Eppendorf tube. The aliquots were incubated at 25 °C, 37 °C, 50 °C, 60 °C and 70 °C for up to 180 minutes and titrated using DLAA. Stability of the phage at different pHs was assessed by mixing phage lysate (10⁸ PFU/ml) in SM buffer (pH 2-12) at a ratio of 1:10 (v/v) and incubated at 37 °C for 1 hour. The phage suspension was then titrated using DLAA. One-step growth experiment was performed to determine the burst size as described previously with modifications.¹¹ Briefly, 100 µl of exponentially growing Kp56 (OD₆₀₀ = 1.0) in LB broth was mixed with 100 µL of phage lysate at MOI 1.0 and incubated (without shaking) at 37 °C for 10 minutes for adsorption. The mixture was centrifuged at 11,000 rpm at 4 °C for 10 minutes and supernatant was discarded to remove un-adsorbed phage particles. The pellet was resuspended in 10 ml of LB broth and incubated at 37 °C. Aliquots of 0.1 ml were taken at intervals of 5 minutes for up to 70 minutes and its titer was estimated using DLAA. The burst-size was calculated as a ratio of the number of phage particles liberated with the initial number of infected bacterial cells.

The genomic DNA of the phage Kp_Pokalde_002 was extracted using the phenol-chloroform method described

earlier.¹² Whole-genome sequencing was performed using Illumina Nextseq500 platform. The DNA library was prepared using an Illumina Nextera XT kit. The de novo sequence assembly was performed using SPAdes 3.13.1.¹³ Structural and functional annotations of the assembled contigs were performed using tools available at the Galaxy and Web Apollo (<https://cpt.tamu.edu/galaxy-pub/>). The phage genome was screened for bacterial toxins, virulence factors and antimicrobial-resistant genes using Virulence Factors of Pathogenic Bacteria (VFDB)¹⁴, Comprehensive Antibiotic Resistance Database (CARD; <https://card.mcmaster.ca>) and Resistance Gene Identifier (RGI, v5.1.0) databases with default parameters. The complete genome sequence and associated raw data of the phage Kp_Pokalde_002 are available under GenBank accession number MT425185, BioProject accession number [PRJNA594990](https://www.ncbi.nlm.nih.gov/bioproject/PRJNA594990), and SRA accession number [SRR11570037](https://www.ncbi.nlm.nih.gov/sra/SRR11570037).

Six-eight weeks old female Swiss albino mice (23 ± 2.5 g) were purchased from the Natural Products Research Laboratory (NPRL), Kathmandu. All animal experiments followed the guidelines established by the Nepal Health Research Council, Kathmandu (ethical approval no.161/2018). Mice were anesthetized with chloroform before invasive procedures and euthanized by cervical dislocation if required. Mice were housed in the animal housing facility at the CDBT and fed with normal antibiotic-free diet. All mice were housed under identical conditions.

Minimum lethal dose (MLD) of Kp56 in mice was determined as previously described with modifications.¹⁵ One milliliter of mid-log phase bacterial suspension in LB broth (OD₆₀₀ = 1.0) was centrifuged at 4,000 rpm for 10 minutes and washed with 1.0 ml sterile phosphate buffer saline (PBS) three times. The bacterial pellet was resuspended in 1.0 ml normal saline and serially diluted to obtain bacterial count ~1×10⁶, ~1×10⁷, ~1×10⁸ and ~1×10⁹ CFU/ml. Thirty mice were divided into six groups. An aliquot of 200 µl of diluted bacterial cell suspensions (~1×10⁵, ~1×10⁶, ~1×10⁷, ~1×10⁸ and ~1×10⁹ CFU/ml) was injected into each of the five group of the mice through IP route. Two hundred microliter of normal saline was injected into the sixth (control) group. The mice were observed for signs of illness and survivability for up to 7 days.

Efficacy of phage therapy in mouse model was evaluated as previously described with several modifications.¹⁶⁻¹⁷ Briefly, mice were divided into seven groups (5 mice/group). A lethal dose (~1×10⁷ CFU/mouse) of Kp56 was injected through IP route into four of the seven groups. First group was injected with 200 µl of SM buffer via IP

route as a sepsis-positive control. The second and third groups of mice were treated with a single dose of 200 μ l of phage Kp_Pokalde_002 (1.2×10^8 PFU/ml) via either oral or IP route immediately after bacterial injection. Two hundred microliter of phage Kp_Pokalde_002 (1.2×10^8 PFU/ml) was injected through IP route after one-hour of bacterial challenge in the fourth group. In fifth group, 200 μ l of phage Kp_Pokalde_002 (1.2×10^8 PFU/ml) was injected intraperitoneally 24 hours prior Kp56 infection (pre-phage therapy group) and sixth group was a vehicle control group which was injected with 200 μ l of SM buffer only. The last, phage only group, mice were injected with 200 μ l of phage Kp_Pokalde_002 (1.2×10^8 PFU/ml) via IP route. Bacterial count was enumerated from the blood and homogenized lung tissues samples. Animals were observed for their health conditions and survivability for 15 days.

For statistical analysis, data were expressed as a mean, standard deviation (SD) of the mean and analyzed under an ordinary one-way and two-way analysis of variance (ANOVA) with Dunnett's multiple comparisons test and student's t-test using GraphPad Prism (Version 8.3.0). For phage therapy, survival curves were compared for significance using the log-rank (Mantel-Cox) test. Differences with $p < 0.05$ were considered statistically significant. Each of the experiments was performed three times. The error bars in the graphs are representative of the standard deviation in each experiment.

RESULTS

Newly isolated phage (Kp_Pokalde_002) produced a large (8-10mm), round, clear plaques surrounded by a halo zone, indicating presence of depolymerase activity on the lawn of the host Kp56 (Figure: 01-A). On TEM, the phage Kp_Pokalde_002 was found to be a tailed phage consisting of an icosahedral head measuring approximately

53 nm with a short non-contractile tail measuring approximately 13 nm in length (Figure: 01-B). According to the International Committee on Taxonomy of Viruses (ICTV) guidelines, the phage morphologically belongs to the Podoviridae family of the Caudovirales order.¹⁸

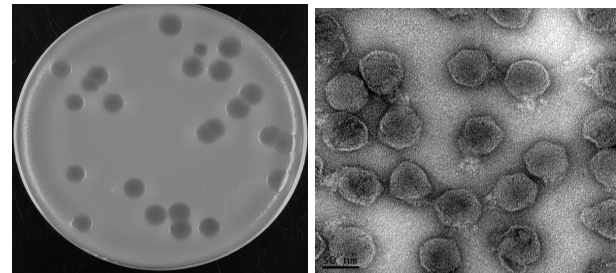


Figure 1. Morphological characterization of phage Kp_Pokalde_002.

Thermal stability of the phage Kp_Pokalde_002 was determined by incubating the phage lysate at different temperatures (25 °C, 37 °C, 50 °C, 60 °C and 70 °C) for up to 180 minutes. The phage titer did not significantly decrease ($p > 0.05$) at 25 °C and 37 °C for up to 180 minutes while the phage titer decreased rapidly after 60 minutes when incubating at 50 °C and completely lost its viability after 180 minutes (Figure 02-A). Likewise, the phage titer decreased significantly at or above 60 °C after 30 minutes. The phage viability was significantly unaffected at pH 6 to 9 ($p < 0.05$), while the phages remained viable between pH 3 to 11. The phage was completely inactivated below pH 2 and above pH 12 (Figure 02-B). The one-step growth curve showed the phage had a short latent period of 20 minutes. Similarly, the growth curve of the phage reached to the plateau at 50 minutes (Figure 02-C). The burst size was calculated based on the final titer of the phage and number of infected bacterial cells. The average burst size was found to be 121 phage particles per infected cell.

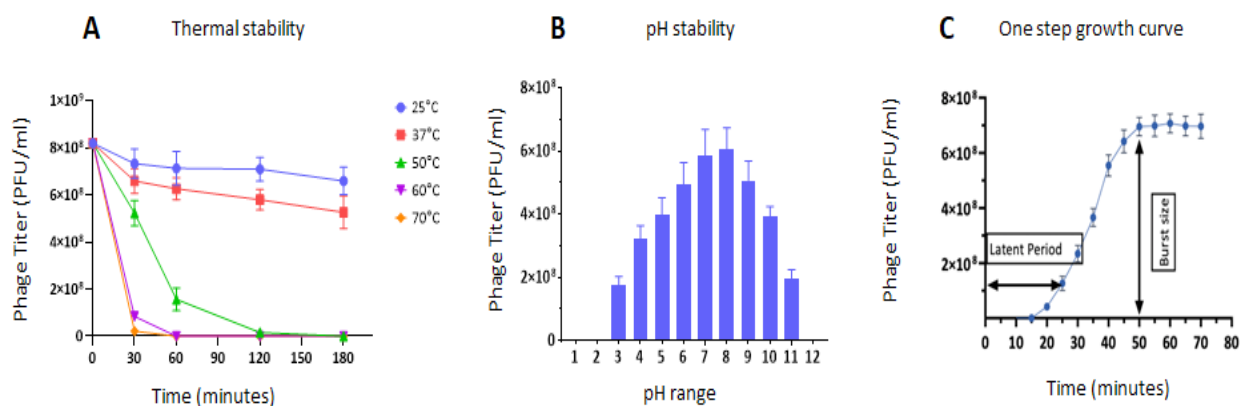


Figure 2. Thermal stability, pH stability and one step growth curve of phage Kp_Pokalde_002.

The complete genome of the phage Kp_Pokalde_002 was composed of a linear double stranded DNA of 41,816 bp in length with an average GC content of 53% (Figure: 03). The phage contained 180 bp direct terminal repeats at both ends. The phage genome comprised 45 open reading frames (ORF), one host RNAP promoter, and 12 phage promoters. Two rho-independent terminator sequences and no tRNA genes were predicted throughout the genome. All the predicted ORFs were located on the same forward strand of the DNA. Besides the predicted protein functions, the predicted amino acid size, the genomic position, the transcriptional orientation, and the GenBank protein identification numbers of the genome can be found in the GenBank accession number: MT425185. The genome of phage Kp_Pokalde_002 did not encode any known toxins and/or virulence factors (VFs) and antibiotic resistant genes.

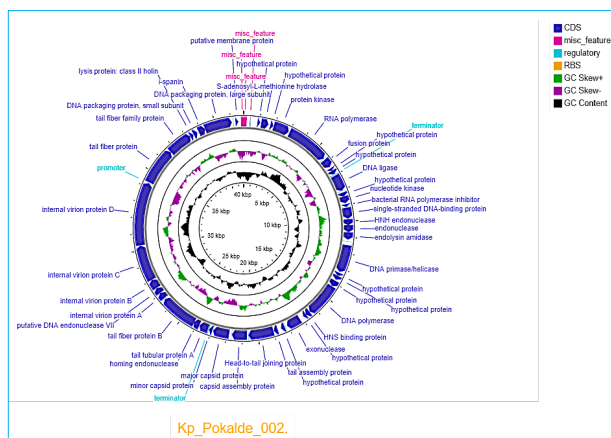


Figure 3. Circular genome view of the phage Kp_Pokalde_002.

Minimum lethal dose (MLD) experiment showed that 100% mice died within 48 hours when injected with $\sim 1 \times 10^7$ CFU/mouse of Kp56 intraperitoneally (Figure: 04). After the injections of $\sim 1 \times 10^6$ CFU/mouse, the survival rate decreased to 60% and after the injections of $\sim 1 \times 10^5$ CFU/mouse, the survival rate was 100%. Therefore, $\sim 1 \times 10^7$ CFU/mouse was considered as a lethal dose (LD_{100}) in Swiss albino mice.

For phage therapy, the mice were infected with the lethal dose of Kp56 and treated with the phage Kp_Pokalde_002 through IP and oral route at MOI 1.0. Both concurrent and 1 hour delay intraperitoneally treated

mice were rescued with the survival rate of 100% in contrast to the control group without phage therapy ($p < 0.05$). However, survivability of the oral-treated mice was decreased to 40% (Figure: 05). Interestingly, 80% mouse survivability was recorded in the pretreatment group ($p < 0.05$) where phage Kp_Pokalde_002 was administered intraperitoneally 24 hours prior to the Kp56 infection.

Bacterial load was significantly reduced ($p < 0.05$) by 3-5 \log_{10} CFU/ml at 8 hpi and 5-7 \log_{10} CFU/ml at 24 hpi in the blood and 2.4 \log_{10} CFU/ml at 8 hpi and 4-7 \log_{10} CFU/ml at 24 hpi in lungs when treated with the phage. In contrast, bacterial load was lower in blood and lungs at any time point(s) when phage was administered via IP route as compared to the oral route (Figure: 06). Normal control groups survived without any symptoms of illness for 15 days. Consistent results were obtained in three independent experiments.

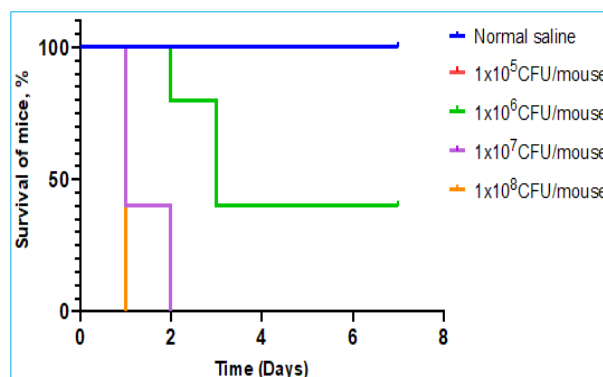


Figure 4. Determination of minimum lethal dose (MLD) of *K. pneumoniae* (Kp56).

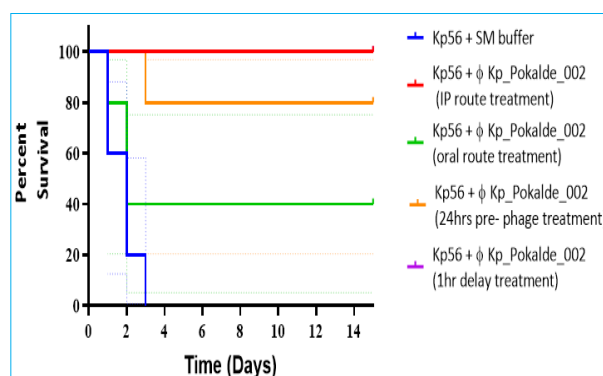


Figure 5. Efficiency of phage therapy in-vivo.

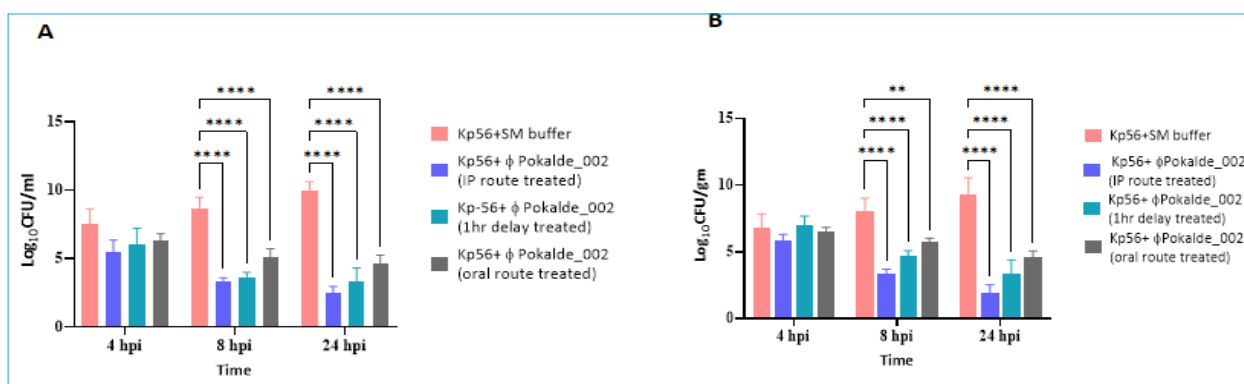


Figure 6. Bacterial load reduction by phage Pokalde_002 in blood and lung tissues.

DISCUSSION

Developing safe and effective phage therapy involves preparation of well-characterized phage library with complete information regarding its physiochemical and genomic properties to determine lysogenicity, antibiotic resistance and toxin/virulent genes.¹⁹ In this study, the morphological and genomic organization of newly isolated phage Kp_Pokalde_002 indicates that the phage was strictly lytic and shares 96% of its genomic identity with the *Klebsiella* virus KP32 (Accession No: NC_047968) belonging to the genus of T7-like viruses, Podoviridae family. Based on bioinformatic analysis, genome of phage Pokalde_002 did not have any known antibiotic resistant genes. The phage formed a round, clear plaques with distinct peripheral halo indicating the phage has depolymerase enzyme responsible for degrading capsular exopolysaccharides and biofilm produced by *K. pneumoniae*.²⁰ The phage was found to be stable in wide range of thermal and pH range make it appropriate in varying external conditions during therapy. One step growth experiment showed the phage Kp_Pokalde_002 had a short latent period with high burst size indicating rapid multiplication and high number of progeny production which further infects the hosts in its vicinity thereby eliminating host (or pathogen) efficiently within short period and unlikely to develop phage resistant mutants.²¹ Thus, we could clearly consider that the phage as a potential candidate for phage therapy.

In present study, Kp56 infected mice were rescued by a novel phage Kp_Pokalde_002 when administered via both oral and IP route. Previous results have also demonstrated that both oral and IP routes of administration protected mice from death infected with *K. pneumoniae* and *P. aeruginosa*.^{15,22} Watanabe et al. reported mouse survival rate was significantly higher in IP and IV routes of administration compared to the oral route.²³ Similarly, Hung et al. concluded that oral

administration of phage was more efficient than IP route at protecting mice infected with *K. pneumoniae* during the initial infection period, while IP route showed therapeutic efficiency during the later stage of the infection.¹⁵ Our result shown that the phage Kp_Pokalde_002 was able to cross the gut wall successfully into the blood and other tissues of mice. However, survivability of oral-treated mice was reduced to 40% as compare to IP route. The possible reason for this result may be due to orally treated phage might not have reached into the systemic circulation and localize into the infected site at an optimum concentration due to adverse environment of the gastrointestinal tract such as gastric acidity, presence of enzymes/bile juice and poor intestinal absorption rate of the phage.²⁴ It was shown that the oral route of phage delivery was efficient in the treatment of gastrointestinal infections.²⁵ Studies have shown that microencapsulation of phage protects them from the adverse gut environment and enhance the efficacy when administered orally.²⁶ Further, the phage Kp_Pokalde_002 was also able to rescue mice from the lethal infection significantly ($p < 0.05$) when administered 24 hours prior bacterial challenge. This confirms that the phage has good pharmacokinetics property and is stable within the body of the mice for up to 24 hours.

Successful phage therapy depends on various factors like time of phage injection, MOI (phage to bacteria ratio), host immune response and phage clearance, phage burst size, phage half-life, and bacterial resistance in-vivo.²⁷ Interestingly, in our study, all of the mice were rescued from the infection in an immediate and delayed phage treatment group (1 hpi). Wang et al. reported that one hour delayed phage therapy led to 56% reduced animal survival while others reported that 100% of animals survived when the phage was administered within 4 to 7 hours post infection. Similarly, 50% of animals survived when the phage was administered 24 hours post infection.^{3,4,28,29} In addition, bacteria count significantly

decreased in the phage-treated mice, which suggests that the phage effectively eliminated the bacteria in vivo. These studies demonstrated that the phage Kp_Pokalde_002 is a viable candidate for phage therapy against carbapenem resistant *K. pneumoniae* infections.

CONCLUSIONS

The results of this study provide a strong evidence of successful phage therapy in carbapenem-resistant *K. pneumoniae* infected mouse model. Based on physicochemical and genomic characters, the phage Kp_Pokalde_002 can be considered as safe therapeutic candidate. However, further research on pharmacokinetics and pharmacodynamics aspects of phage therapy and a library of well characterized phages is necessary before moving on phage therapy in human.

ACKNOWLEDGMENTS

This work was funded by the Ph.D. fellowship and research support awarded to Gunaraj Dhungana (award numbers PhD/73-74/S and T-07) by the University Grants Commission (UGC) in Nepal. Nepal Academy of Science and Technology (NAST), Prof. Dr. Krishna Das Manandhar, Head, Central Department of Biotechnology, TU, Xcelris Labs, Ahmedabad and Advanced Instrumentation Research Facility (AIRF), JNU, New Delhi.

REFERENCES

- Podschun R, Ullmann U. *Klebsiella* spp. as nosocomial pathogens: epidemiology, taxonomy, typing methods, and pathogenicity factors. *Clin Microbiol Rev*. 1998;11(4):589-603. [\[PubMed\]](#)
- Millard AD, Clokie MR, Letarov AV, Heaphy S. Phages in nature. *Bacteriophage*. 2011; 1:31-45. [\[GoogleScholar\]](#)
- Wang JL, Kuo CF, Yeh CM, Chen JR, Cheng MF, Hung CH. Efficacy of ϕ km18p phage therapy in a murine model of extensively drug-resistant *Acinetobacter baumannii* infection. *Infect Drug Resist*. 2018; 11:2301. [\[PubMed\]](#)
- Pouillot F, Chomton M, Blois H, Courroux C, Noelig J, Bidet P, et al. Efficacy of bacteriophage therapy in experimental sepsis and meningitis caused by a clone O25b:H4-ST131 *Escherichia coli* strain producing CTX-M-15. *Antimicrob Agents Chemother*. 2012;56(7):3568-75. [\[Article\]](#)
- Vinodkumar CS, Kalsurmath S, Neelagund YF. Utility of lytic bacteriophage in the treatment of multidrug-resistant *Pseudomonas aeruginosa* septicemia in mice. *Indian J Pathol Microbiol*. 2008;51(3):360-6. [\[Article\]](#)
- Kumari S, Harjai K, Chhibber S. Bacteriophage versus antimicrobial agents for the treatment of murine burn wound infection caused by *Klebsiella pneumoniae* B5055. *J Med Microbiol*. 2011;60(Pt 2):205-210. [\[Article\]](#)
- Brüssow H. Hurdles for phage therapy to become a reality—An editorial comment. *Viruses*. 2019;11(6):557. [\[Article\]](#)
- Adams MH. *Bacteriophages*. London: Interscience Publishers, Ltd.; 1959. Enumeration of bacteriophage particles; pp. 27–34. [\[Google Scholar\]](#)
- Sambrook J, Russell DJP, NY. *Molecular cloning: A laboratory manual* 3rd Ed. 620 Cold Spring Harbor Laboratory Press. 2001;621. [\[Article\]](#)
- D'Andrea MM, Marmo P, De Angelis LH, Palmieri M, Ciacci N, Di Lallo G, et al. ϕ BO1E, a newly discovered lytic bacteriophage targeting carbapenemase-producing *Klebsiella pneumoniae* of the pandemic Clonal Group 258 clade II lineage. *Sci Rep*. 2017;7(1):1-8. [\[Article\]](#)
- Merabishvili M, Vandenheuvel D, Kropinski AM, Mast J, De Vos D, Verbeken G, et al. Characterization of newly isolated lytic bacteriophages active against *Acinetobacter baumannii*. *PLoS ONE*. 2014;9(8):e104853. [\[Article\]](#)
- Sambrook H. *Molecular cloning: a laboratory manual*. Cold Spring Harbor, NY. 1989. ISBN: 0879693096 [\[Article\]](#)
- Bankevich A, Nurk S, Antipov D, Gurevich AA, Dvorkin M, Kulikov AS, et al. SPAdes: a new genome assembly algorithm and its applications to single-cell sequencing. *J Comput Biol*. 2012;19(5):455-77. [\[Article\]](#)
- Liu B, Zheng D, Jin Q, Chen L, Yang J. VFDB 2019: a comparative pathogenomic platform with an interactive web interface. *Nucleic Acids Res*. 2019;47(D1):D687-92. [\[Article\]](#)
- Hung CH, Kuo CF, Wang CH, Wu CM, Tsao N. Experimental phage therapy in treating *Klebsiella pneumoniae*-mediated liver abscesses and bacteremia in mice. *Antimicrob Agents Chemother*. 2011;55(4):1358-65. [\[Article\]](#)
- Singla S, Harjai K, Katare OP, Chhibber S. Bacteriophage-loaded nanostructured lipid carrier: improved pharmacokinetics mediates effective resolution of *Klebsiella pneumoniae*-induced lobar pneumonia. *J Infect Dis*. 2015;212(2):325-34. [\[Article\]](#)
- Merrill CR, Biswas B, Carlton R, Jensen NC, Creed GJ, Zullo S, et al. Long-circulating bacteriophage as antibacterial agents. *Proc Natl Acad Sci U S A*. 1996;93(8):3188-92. [\[Article\]](#)
- Adams MJ, Lefkowitz EJ, King AM, Harrach B, Harrison RL, Knowles NJ, et al. Changes to taxonomy and the International Code of Virus Classification and Nomenclature ratified by the International Committee on Taxonomy of Viruses (2017). *Arch Virol* 2017;162(8):2505-38.

19. Gibson SB, Green SI, Liu CG, Salazar KC, Clark JR, Terwilliger AL, et al. Constructing and characterizing bacteriophage libraries for phage therapy of human infections. *Front Microbiol.* 2019; 10:2537. [\[Article\]](#)
20. Majkowska-Skrobek G, Latka A, Berisio R, Squeglia F, Maciejewska B, Briery Y, et al. Phage-borne depolymerases decrease *Klebsiella pneumoniae* resistance to innate defense mechanisms. *Front Microbiol.* 2018;9:2517. [\[Article\]](#)
21. Mirzaei MK, Nilsson AS. Isolation of phages for phage therapy: a comparison of spot tests and efficiency of plating analyses for determination of host range and efficacy. *PLoS ONE.* 2015;10(3):e0118557. [\[Article\]](#)
22. Chibani-Chennoufi S, Sidoti J, Bruttin A, Kutter E, Sarker S, Brüssow H. In vitro and in vivo bacteriolytic activities of *Escherichia coli* phages: implications for phage therapy. *Antimicrob Agents Chemother.* 2004;48(7):2558-69. [\[Article\]](#)
23. Watanabe R, Matsumoto T, Sano G, Ishii Y, Tateda K, Sumiyama Y et al. Efficacy of Bacteriophage Therapy against *Pseudomonas aeruginosa* gut-derived Sepsis in Mice. *Antimicrob Agents Chemother.* 2007;51(2):446-52. [\[Download PDF\]](#)
24. Dąbrowska K. Phage therapy: What factors shape phage pharmacokinetics and bioavailability? Systematic and critical review. *Med Res Rev.* 2019;39(5):2000-25. [\[Article\]](#)
25. Wagenaar JA, Van Bergen MA, Mueller MA, Wassenaar TM, Carlton RM. Phage therapy reduces *Campylobacter jejuni* colonization in broilers. *Vet Microbiol.* 2005;109(3-4):275-83. [\[Article\]](#)
26. Malik DJ, Sokolov IJ, Vinner GK, Mancuso F, Cinquerrui S, Vladislavjevic GT, et al. Formulation, stabilisation and encapsulation of bacteriophage for phage therapy. *Adv Colloid Interface Sci.* 2017; 249:100-33. [\[Article\]](#)
27. Chatain-Ly Mh. The factors affecting effectiveness of treatment in phages therapy. *Front Microbiol.* 2014; 5:51. [\[Article\]](#)
28. Shivshetty N, Hosamani R, Ahmed L, Oli AK, Sannauallah S, Sharanbassappa S, et al. Experimental protection of diabetic mice against lethal *P. aeruginosa* infection by bacteriophage. *Biomed Res Int.* 2014;2014. [\[Article\]](#)
29. Takemura-Uchiyama I, Uchiyama J, Osanai M, Morimoto N, Asagiri T, Ujihara T, et al. Experimental phage therapy against lethal lung-derived septicemia caused by *Staphylococcus aureus* in mice. *Microbes Infect.* 2014;16(6):512-7. [\[Article\]](#)



Complete Genome Sequence of Myophage Ec_Makalu_002, Which Infects Uropathogenic *Escherichia coli*

 Gunaraj Dhungana,^{a,b}  Rajani Malla,^a  Manoj Rajaure,^b Sankar Adhya^b

^aCentral Department of Biotechnology, Tribhuvan University, Kirtipur, Nepal

^bLaboratory of Molecular Biology, Center for Cancer Research, National Cancer Institute, National Institutes of Health, Bethesda, Maryland, USA

ABSTRACT We isolated phage Ec_Makalu_002, which infects uropathogenic strains of *Escherichia coli*. Here, we report its complete genome sequence, annotated features, and relatedness to other phages.

One of the most common pathogens responsible for urinary tract infection (UTI) is *Escherichia coli* (1). The biggest concern about these uropathogenic strains of *E. coli* is their insensitivity to existing antibiotics and their high recurrence rates, which are linked to their ability to form both extra- and intracellular biofilm-like communities within the bladder (2, 3). To address the resistance and recurrence problem, phages are currently being suggested as an effective and alternative therapeutic (4), especially in developing countries with poor sanitation and hygiene (5). In this report, we describe the genome of Ec_Makalu_002, which was isolated from a municipal wastewater canal in Kathmandu, Nepal.

Phage Ec_Makalu_002 was originally enriched from a filtered (0.2- μ m pore size) wastewater sample by infecting an aerobically growing culture of a deidentified clinical strain of uropathogenic *E. coli* at 37°C in LB broth. The host was obtained from the National Public Health Laboratory in Nepal. A spot test demonstrated that Ec_Makalu_002 also possessed the ability to propagate on a laboratory strain of *E. coli* K-12 (MG1655), which was utilized for purification using the soft-agar overlay method (6). A high-titer phage lysate (2.3×10^9 PFU/ml) was used to extract the genomic DNA using the phenol-chloroform extraction method. The DNA library was prepared using an Illumina Nextera XT kit, and whole-genome sequencing was performed on a NextSeq 500 platform, resulting in 9,387,393 150-bp paired-end reads. Reads were inspected for overall quality using FastQC (<http://www.bioinformatics.babraham.ac.uk/projects/fastqc/>), adaptor sequence trimming was performed using Trimmomatic (7), and *de novo* sequence assembly was done using SPAdes 3.13.1 (8). All tools were run with default parameters unless otherwise specified. The largest assembled contig (164,751 bp with 4,895-fold coverage) was obtained with 77-bp identical sequences at each end, suggestive of a circularly permuted DNA packaging mechanism. The assembled genome was closed with PCR using primers (5'-GCGATTGATGCTATTCAAATGCAG-3' and 5'-CCGATAATCTCTTTAGACCG GACG-3') facing off the ends and manually corrected matching of the Sanger sequencing reads. Tools available at the Galaxy and WebApollo instances via the Center for Phage Technology (CPT) (<https://cpt.tamu.edu/galaxy-pub/>) were used for structural and functional annotation of the assembled contig (9, 10). For example, GLIMMER 3.0 (11) and MetaGeneAnnotator 1.0 (12) were used to identify coding genes, tRNA prediction was done with ARAGORN 2.36 (13), and transcriptional terminators were manually inspected based on prediction from TransTermHP (14). Gene functions were predicted largely by similarity to the Canonical Phages database based on BLASTp searches (15) and/or confirmed using InterProScan (16) and TMHMM (17), tools that were available in the CPT WebApollo interface (<https://cpt.tamu.edu/galaxy-pub/>).

Citation Dhungana G, Malla R, Rajaure M, Adhya S. 2020. Complete genome sequence of myophage Ec_Makalu_002, which infects uropathogenic *Escherichia coli*. *Microbiol Resour Announc* 9:e01530-19. <https://doi.org/10.1128/MRA.01530-19>.

Editor Catherine Putonti, Loyola University Chicago

This is a work of the U.S. Government and is not subject to copyright protection in the United States. Foreign copyrights may apply.

Address correspondence to Manoj Rajaure, manoj.rajaure@nih.gov.

Received 13 December 2019

Accepted 12 January 2020

Published 30 January 2020

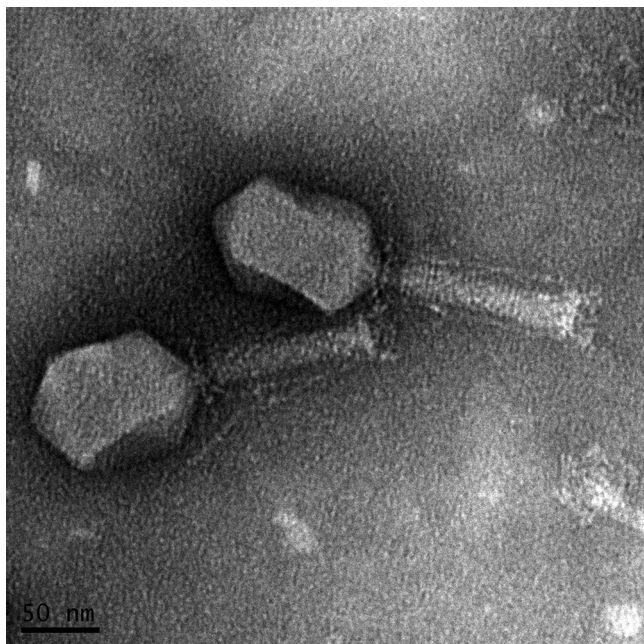


FIG 1 Transmission electron microscope image of bacteriophage Ec_Makalu_002. The phages were negatively stained with 2% uranyl acetate and observed using an FEI Tecnai T12 microscope.

The complete genome of phage Ec_Makalu_002 was 164,674 bp long with an average GC composition of 40.6%. The DNA sequence similarity of Ec_Makalu_002 was calculated using progressiveMauve 2.4.0 (18) and found to be closely related to T4-like enterobacterial phages, including ECD7 (GenBank accession number [NC_041936.1](#); 92.26%), GEC-3S ([HE978309.1](#); 92.23%), and Phi1 ([EF437941.1](#); 91.43%), all of which were isolated against virulent nonlaboratory strains of *E. coli*. Consistent with the sequence analysis, imaging using transmission electron microscopy showed that Ec_Makalu_002 belongs to the *Myoviridae* family (Fig. 1). Based on its similarity to the T4-like phages and to maintain the consistency with linear genome structure in the phage database, the genome was reopened at the *rIIA* gene homolog prior to submission. This myophage encodes 274 predicted coding sequences, but no tRNA genes were detected. Putative lysis genes, holin, endolysin, and spanins were found to be scattered throughout the genome, similar to that of the T4 phage.

Data availability. The genome sequence and associated data for phage Ec_Makalu_002 were deposited under GenBank accession number [MN709127](#), BioProject accession number [PRJNA594990](#), and SRA accession number [SRR10671636](#).

ACKNOWLEDGMENTS

This work was supported by funding from the Intramural Research Program of the NIH, National Cancer Institute, and part of the work was funded by the Ph.D. fellowship and research support awarded to Gunaraj Dhungana (award numbers PhD/73-74/S and T-07) by the University Grants Commission (UGC) in Nepal.

Genome sequencing was done at the CCR Genomics Core facility, and *de novo* sequence assembly was performed utilizing the computational resources of the NIH High-Performing Computation Biowulf Cluster. The phage was imaged at the facility of the National Institute of Biomedical Imaging and Bioengineering in Bethesda, MD.

REFERENCES

1. Flores-Mireles AL, Walker JN, Caparon M, Hultgren SJ. 2015. Urinary tract infections: epidemiology, mechanisms of infection and treatment options. *Nat Rev Microbiol* 13:269–284. <https://doi.org/10.1038/nrmicro3432>.
2. Blango MG, Mulvey MA. 2010. Persistence of uropathogenic *Escherichia coli* in the face of multiple antibiotics. *Antimicrob Agents Chemother* 54:1855–1863. <https://doi.org/10.1128/AAC.00014-10>.

3. Mulvey MA, Schilling JD, Hultgren SJ. 2001. Establishment of a persistent *Escherichia coli* reservoir during the acute phase of a bladder infection. *Infect Immun* 69:4572–4579. <https://doi.org/10.1128/IAI.69.7.4572-4579.2001>.
4. Kortright KE, Chan BK, Koff JL, Turner PE. 2019. Phage therapy: a renewed approach to combat antibiotic-resistant bacteria. *Cell Host Microbe* 25:219–232. <https://doi.org/10.1016/j.chom.2019.01.014>.
5. Nagel TE, Chan BK, De Vos D, El-Shibiny A, Kang'ethe EK, Makumi A, Pirnay J-P. 2016. The developing world urgently needs phages to combat pathogenic bacteria. *Front Microbiol* 7:882. <https://doi.org/10.3389/fmicb.2016.00882>.
6. Adams MH. 1959. *Bacteriophages*. Interscience Publishers, Inc., New York, NY.
7. Bolger AM, Lohse M, Usadel B. 2014. Trimmomatic: a flexible trimmer for Illumina sequence data. *Bioinformatics* 30:2114–2120. <https://doi.org/10.1093/bioinformatics/btu170>.
8. Bankevich A, Nurk S, Antipov D, Gurevich AA, Dvorkin M, Kulikov AS, Lesin VM, Nikolenko SI, Pham S, Prjibelski AD, Pyshkin AV, Sirotkin AV, Vyahhi N, Tesler G, Alekseyev MA, Pevzner PA. 2012. SPAdes: a new genome assembly algorithm and its applications to single-cell sequencing. *J Comput Biol* 19:455–477. <https://doi.org/10.1089/cmb.2012.0021>.
9. Afgan E, Baker D, Batut B, van den Beek M, Bouvier D, Cech M, Chilton J, Clements D, Coraor N, Gruning BA, Guerler A, Hillman-Jackson J, Hiltmann S, Jalili V, Rasche H, Soranzo N, Goecks J, Taylor J, Nekrutenko A, Blankenberg D. 2018. The Galaxy platform for accessible, reproducible and collaborative biomedical analyses: 2018 update. *Nucleic Acids Res* 46:W537–W544. <https://doi.org/10.1093/nar/gky379>.
10. Lee E, Helt GA, Reese JT, Munoz-Torres MC, Childers CP, Buels RM, Stein L, Holmes IH, Elsik CG, Lewis SE. 2013. Web Apollo: a Web-based genomic annotation editing platform. *Genome Biol* 14:R93. <https://doi.org/10.1186/gb-2013-14-8-r93>.
11. Delcher AL, Harmon D, Kasif S, White O, Salzberg SL. 1999. Improved microbial gene identification with GLIMMER. *Nucleic Acids Res* 27:4636–4641. <https://doi.org/10.1093/nar/27.23.4636>.
12. Noguchi H, Taniguchi T, Itoh T. 2008. MetaGeneAnnotator: detecting species-specific patterns of ribosomal binding site for precise gene prediction in anonymous prokaryotic and phage genomes. *DNA Res* 15:387–396. <https://doi.org/10.1093/dnares/dsn027>.
13. Laslett D, Canback B. 2004. ARAGORN, a program to detect tRNA genes and tmRNA genes in nucleotide sequences. *Nucleic Acids Res* 32:11–16. <https://doi.org/10.1093/nar/gkh152>.
14. Kingsford CL, Ayanbule K, Salzberg SL. 2007. Rapid, accurate, computational discovery of Rho-independent transcription terminators illuminates their relationship to DNA uptake. *Genome Biol* 8:R22. <https://doi.org/10.1186/gb-2007-8-2-r22>.
15. Camacho C, Coulouris G, Avagyan V, Ma N, Papadopoulos J, Bealer K, Madden TL. 2009. BLAST+: architecture and applications. *BMC Bioinformatics* 10:421. <https://doi.org/10.1186/1471-2105-10-421>.
16. Jones P, Binns D, Chang HY, Fraser M, Li W, McAnulla C, McWilliam H, Maslen J, Mitchell A, Nuka G, Pesseat S, Quinn AF, Sangrador-Vegas A, Scheremetjew M, Yong SY, Lopez R, Hunter S. 2014. InterProScan 5: genome-scale protein function classification. *Bioinformatics* 30:1236–1240. <https://doi.org/10.1093/bioinformatics/btu031>.
17. Krogh A, Larsson B, von Heijne G, Sonnhammer EL. 2001. Predicting transmembrane protein topology with a hidden Markov model: application to complete genomes. *J Mol Biol* 305:567–580. <https://doi.org/10.1006/jmbi.2000.4315>.
18. Darling AE, Mau B, Perna NT. 2010. progressiveMauve: multiple genome alignment with gene gain, loss and rearrangement. *PLoS One* 5:e11147. <https://doi.org/10.1371/journal.pone.0011147>.

See discussions, stats, and author profiles for this publication at: <https://www.researchgate.net/publication/359520299>

Isolation and Characterization of Lytic Bacteriophage Against Multi-drug Resistant *Pseudomonas aeruginosa*

Article in *Journal of Nepal Health Research Council* · March 2022

DOI: 10.333314/jnhrc.v19i04.3837

CITATION

1

READS

69

3 authors:



Gunaraj Dhungana
Tribhuvan University

22 PUBLICATIONS 64 CITATIONS

[SEE PROFILE](#)



ROSHAN NEPAL
Tribhuvan University

13 PUBLICATIONS 20 CITATIONS

[SEE PROFILE](#)



Rajani Malla

66 PUBLICATIONS 862 CITATIONS

[SEE PROFILE](#)

Some of the authors of this publication are also working on these related projects:



Bacteriophage Therapy [View project](#)



Bacteriological profile of Raw meat [View project](#)

Isolation and Characterization of Lytic Bacteriophage Against Multi-drug Resistant *Pseudomonas Aeruginosa*

Archana Maharjan,¹ Roshan Nepal,¹ Gunaraj Dhungana,¹ Apshara Parajuli,¹ Madhav Regmi,¹ Elisha Upadhyaya,¹ Dipendra Mandal,¹ Mitesh Shrestha,¹ Pragati Pradhan,¹ Krishna Das Manandhar,¹ and Rajani Malla¹

ABSTRACT

Background: *Pseudomonas aeruginosa* is a Gram-negative opportunistic pathogen frequently causing healthcare-associated infections. The apocalyptic rise of antimicrobial resistance has rekindled interest in age-old phage therapy that uses phages (viruses that infect bacteria) to kill the targeted pathogenic bacteria. Because of its specificity, phages are often considered as potential personalized therapeutic candidate for treating bacterial infections.

Methods: In this study, we isolated and purified lytic phages against multi-drug resistant *P. aeruginosa* using soft agar overlay technique. Phage characteristics like thermal and pH stability, latent period and burst size were determined using one-step growth assay while multiple host range spectrum was determined by spot assay. The phages were further characterized using protein profiling.

Results: Three *Pseudomonas* phages (øCDBT-PA31, øCDBT-PA56 and øCDBT-PA58) were isolated from the holy rivers of Kathmandu valley. Among 3 phages, øCDBT-PA31 demonstrated multiple host range and could lyse multi-drug resistant strain of *P. aeruginosa*. Further, øCDBT-PA31 showed latent period of 30 minutes with corresponding burst sizes of 423-525 PFU/cell. Interestingly, øCDBT-PA31 also tolerated a wide range of adverse conditions, such as high temperature (50°C) and pH 3-11. Further, protein profiling revealed that øCDBT-PA31 has 4 and øCDBT-PA11 had 3 distinct bands in the gradient gel ranging from approximately 3.5-29 kilodaltons (kDa) suggesting them to be morphologically distinct from each other.

Conclusions: As multi-drug resistant bacteria are emerging as a global problem, lytic phages can be an alternative treatment strategy when all available antibiotics fail.

Keywords: Antimicrobial resistance (AMR); bacteriophage; *P. aeruginosa*; phage therapy; SDS-PAGE.

INTRODUCTION

Antimicrobial resistance [AMR, also often called multi-drug resistance (MDR)] is a global problem and thus considered a burning issue all over the world with no concrete solution/alternative at sight. *Pseudomonas aeruginosa* - a common cause of hospital acquired infections (HAIs), including pneumonia and bloodstream, urinary tract, and surgical site infections.¹

Further, it is also one of the major pathogens colonizing cystic fibrosis (CF) lungs promoting an accelerated decline in pulmonary functions ultimately causing morbidity and mortality in CF. Bacteriophage (phage) is a group of viruses that infect bacteria specifically.²

Recent reports in application of phage in therapeutics has shown encouraging outcomes against difficult to

treat and/or MDR infections. In this study, we isolated three lytic *Pseudomonas* phages using *P. aeruginosa* clinical isolates (CIs) as a host from the water sample collected from various holy rivers of Kathmandu valley. We further investigated the phage dynamics (burst size, latent period), stability (temperature, pH) and the host range against wide range of *P. aeruginosa* CIs.

METHODS

P. aeruginosa CIs were collected from Tribhuvan University Teaching Hospital (TUTH), Kathmandu, Nepal and preserved at Central Department of Biotechnology, Kirtipur, Nepal. All bacterial strains were propagated in nutrient agar (NA) (HiMedia, India). Freshly prepared exponentially growing broth culture of bacteria propagated in Luria-Bertani (LB) (HiMedia, India) media was used as host for phage isolation. This was

Correspondence: Prof Rajani Malla, Central Department of Biotechnology, Institute of Science and Technology, Tribhuvan University, Kirtipur, Nepal. Email: rajanimalla2000@gmail.com.

achieved by inoculating an isolated colony of bacteria in 15.0 ml LB broth followed by incubation at 37°C with constant agitation (200 rpm) until mid-log phase ($OD_{600} = 1.0$ corresponding to 2.04×10^8 CFU/ml) was reached. Tryptic soy agar (TSA) (HiMedia, India) with varying agar concentration was used for isolation of phage using soft agar overlay technique.

Antibiotic susceptibility of collected CIs was confirmed by Kirby-Bauer disk diffusion susceptibility test protocol following Clinical & Laboratory Standards Institute (CLSI) guidelines. Different classes of antibiotics like beta-lactams, carbapenems, macrolide, fluoroquinolones, aminoglycosides were used for determining multi-drug resistant phenotype. The list of antibiotics tested, and corresponding CIs are listed in Table 1.

Isolation: Water samples were collected from rivers of Kathmandu valley [collection location: Balkhu (Bagmati river), and Kalanki (Balkhu river)] in a sterile 50.0 ml Falcon tube. Before collection, the water was mixed thoroughly, and the sediments were collected with the overlying water from collection sites. Phage isolation was performed by soft agar overlay technique as described previously.³

Purification: A completely isolated clear plaques were picked by using pipette tip and dissolved in 1.0 ml sodium chloride-magnesium sulfate (SM) buffer (5.8 g/L NaCl, 2 g/L $MgSO_4 \cdot 7H_2O$, 50 ml 1.0 M Tris, pH 7.5, 2% gelatin). The mixture was filtered through 0.2 µm syringe filter (Axiva Sichem, Haryana, India) to remove the bacterial contamination. The filtrate was further used for soft agar overlay assay as mentioned before and next day, an isolated plaque was picked. The process was repeated 3 times and the pure phage strain was collected from the plates of last round. For this, the plates from third round containing plaques were flooded with 10.0 ml of SM buffer and 2 drops of chloroform was added into it. The plates were sealed and incubated at rotating shaker (80 rpm for 30 minutes) for phage elution/diffusion from the plaques. The SM buffer was collected in a Falcon tube and centrifuged at 4000 rpm for 20 mins. Then, the supernatant was filtered through 0.2 µm syringe filter (Axiva Sichem, Haryana, India) to obtain high titer of pure phage strain. Finally, the phage lysates were stored at 4°C until further use.

Host range spectrum of purified phage was determined by spot assay on all available CIs. Briefly, 10.0 µl of serially diluted phage preparations (10^{-8} , 10^{-9} and 10^{-10} PFU/ml) was spotted on the double layered lawn cultures of the bacterial strains and allowed to absorb completely. SM

buffer was used as negative control. The plates were incubated at 37°C for 24 hours and the next day, clear lysis spots were checked. A positive spot appears as complete obliteration of the entire drop area, whereas a negative spot test will result in the bacterial lawn growing normally in the region of the spots.

The pH of the SM buffer was adjusted with either 1.0 M HCl or 0.5 M NaOH to obtain a pH range of 1-14. A total of 100 µl of known phage suspension (5×10^8 PFU/ml) was inoculated into 1.0 ml of pH-adjusted SM buffers. After incubation for 1 hour at 37°C, the surviving phage particles were enumerated immediately spotting 10.0 µl of serially diluted phage suspension on previously prepared double layer agar with host bacteria on top agar. Similarly, thermal stability of all phages at different temperatures (50, 60, 70, 80 and 90°C) was determined by incubating the known concentration of phage (10^7 PFU/ml) at indicated temperatures for 30 mins and 60 mins at pH 7.0 in SM buffer. The surviving phages were enumerated by spot assay as described earlier.

Overnight cultures of *P. aeruginosa* was adjusted to optical density (OD_{600}) of 1.0 (2.04×10^8 CFU/ml) in fresh TSB media. A single phage stock was added to give multiplicity of infection (MOI) of 100 and then the mixtures were incubated at 37°C for 1, 2, 3, 4 and 5 hrs respectively with gentle shaking. Phage-free culture (only bacteria) and bacteria-free culture (only phage) were also included as controls. Bacterial cell densities were determined at 0, 1, 2, 3, 4 and 5 hrs by spectrophotometry at 600 nm wavelength.

Phage growth cycle parameters (latent period and burst size) were determined from the dynamic change of the number of free and total phages using one-step growth assay. Briefly, 10.0 ml of a mid-exponential phase culture was harvested by centrifugation ($7,000 \times g$, 5 min, 4°C) and resuspended in 5.0 ml of LB broth and adjusted to 1.0 OD_{600} (approximately 2.04×10^8 CFU/ml) using spectrophotometer. To this suspension, appropriate volume (5.0 ml) of phage stock solution was added to have a MOI of 0.001 (2.04×10^5 PFU/ml) and left at room temperature for 5 min without snaking for phage adsorption. The mixture was then centrifuged as described above and the pellet was resuspended in 10.0 ml of fresh TSB medium. Samples were taken at every 10 min interval over a period of 2 hrs. The sample was plated immediately using soft agar overlay technique and incubated at 37°C for 24 hrs. Next day plates were monitored for plaques.

Protein profiling of two phages (øCDBT-PA31 and øCDBT-

PA11) was carried out using sodium dodecyl sulfate polyacrylamide gel electrophoresis (SDS-PAGE) using 2 different methods: acetone precipitation and direct heating. For acetone precipitation, 500 μ l of purified phage solution was precipitated with 4 volumes of ice-cold acetone for 90 minutes. Supernatant was decanted and pellet was air dried, resuspended in 100 μ l PBS (8.0 g/L NaCl, 0.2 g/L KCl, 0.2 g/L KH_2PO_4 , 1.44 g/L $\text{Na}_2\text{HPO}_4 \times 2\text{H}_2\text{O}$, pH 7.5). SDS-PAGE was carried out according to Laemmli. Briefly, 25.0 μ l of phage sample was added to 25.0 μ l of 2 \times Laemmli buffer and boiled for 10 mins. Samples were then loaded to 10% PAGEr™ Precast Gels (Lonza Inc., Rockland, USA) and electrophoresed with tris-glycine buffer. Five microliters of protein marker with 1.0 μ l of loading dye was also loaded after boiling for 5-10 mins. After electrophoresis, the gels were stained with coomassie brilliant blue R-250 (CBB) (Bio-Rad Laboratories, India) overnight and then the bands were visualized after de-staining. For direct heating, 25.0 μ l of purified *Pseudomonas* phages were mixed with equal volume of 2x sample buffer (0.125 M Tris-HCl, pH 6.8, 20% glycerol, 4% SDS, 2% mercaptoethanol, 0.02% bromophenol blue) and heated in a boiling water bath for 3-5 minutes. Protein profiles were then estimated as described earlier using the precast gel.

For transmission electron microscopy (TEM), the purified high titer phage lysate of ϕ CDBT-PA31 was fixed with 2% paraformaldehyde and 2.5 % glutaraldehyde. Two microliters of the fixed sample were spread on a carbon-coated copper grid and negatively stained with 2.0 μ l of 2% (w/v) uranyl acetate (pH 4.5). The copper grid was dried and examined under JEM-2100F transmission electron microscope (JEOL, Japan) at 200 kV field emission.

RESULTS

Three lytic *Pseudomonas* phages were isolated from the waters of Bagmati river and Balkhu river using different clinical isolates (CIs) of *P. aeruginosa* as primary host. The isolated phages were named according to the bacterial host used for phage isolation. As such, *Pseudomonas* phage CDBT-PA31 (hereafter ϕ CDBT-PA31) was isolated using PA31 as a host. Likewise, *Pseudomonas* phage CDBT-PA56 (hereafter ϕ CDBT-PA56) and *Pseudomonas* phage CDBT-PA58 (hereafter ϕ CDBT-PA58) were isolated using PA56 and PA58 as host respectively (Figure 1). ϕ CDBT-PA31 produced a well-defined sharp edged pinhead plaques of 0.1 mm (diameter) without halo whereas ϕ CDBT-PA56 produced plaques of 0.4 mm (diameter) with halo and ϕ CDBT-PA58 also produced plaques of 0.4

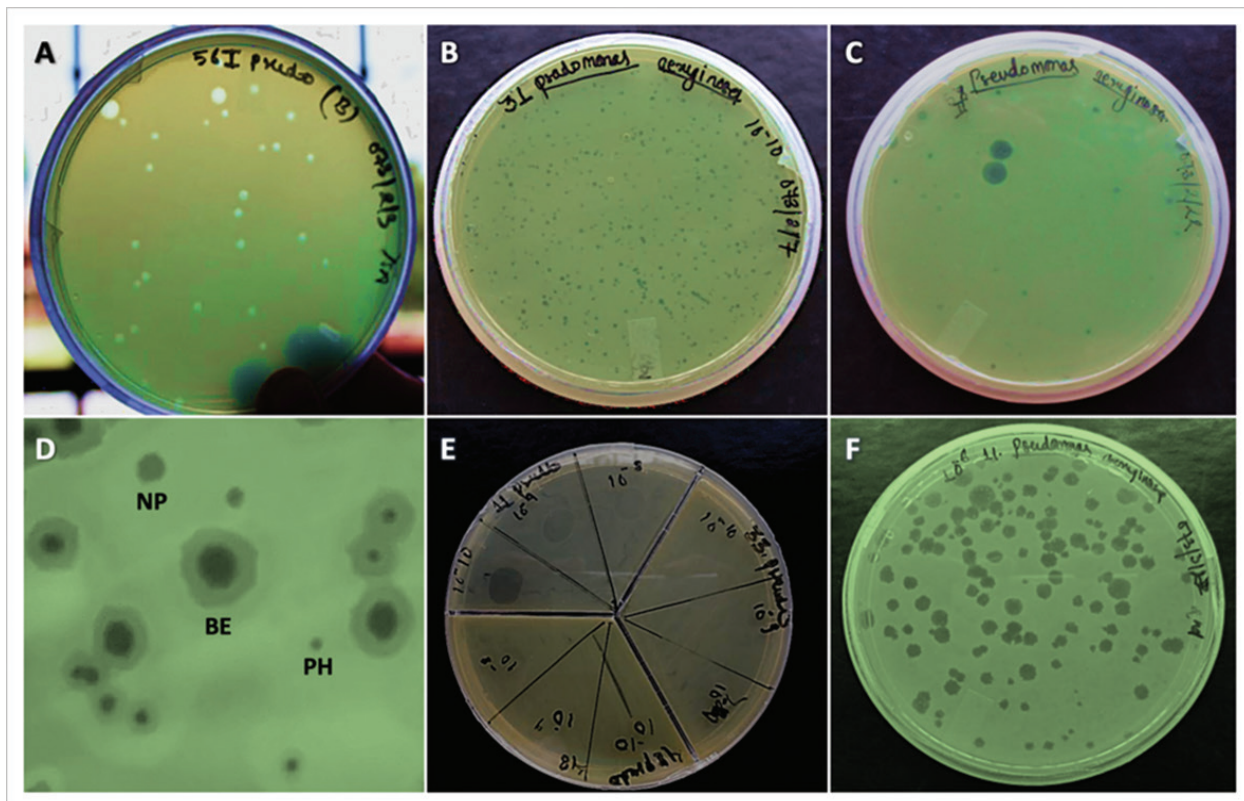


Figure 1. Isolation of lytic phages against clinical isolates of *P. aeruginosa*.

mm (diameter) with bull's eye morphology. No phages were isolated against *P. vulgaris* and other *Pseudomonas* spp. (Table 1).

Plaque morphology of isolated phages, øCDBT-PA56 (A), øCDBT-PA31 (B) and øCDBT-PA58 (C). (D) Different types of plaque morphologies: NP = normal plaque without Bull's eye, BE = plaque with Bull's eye, PH = pin-head plaques. (E) Spot assay showing intraspecies host lysis against other *P. aeruginosa* (PA11) by øCDBT-PA31 in different dilutions. (F) Intraspecies host range of øCDBT-PA31 confirmed on PA11 by DLAA method with 10^{-6} dilution.

The intra-species multi host range (MHR) spectrum of all 3 purified phages was assessed by spot assay. All 3 phages were able to lyse multiple strains other than their own host implying broad host range of isolated phages. Among them, øCDBT-PA31 showed broadest host range among the tested CIs, showed lytic activity against MDR *P. aeruginosa* (PA11) and thus was selected for further characterization. The lysis spots produced by high titer phage were larger and clearer than spots produced by lower titer indicating phage mediated lysis being dose dependent.

Table 1. Clinical isolates (CIs) of *P. aeruginosa* used as host for isolation of phage.

Bacterial strain	Strain code	Antibiotic resistance*	Phage characteristics
<i>P. aeruginosa</i>	PA11	ofloxacin, amoxyclav, bacitracin, teicoplanin, amikacin, cefotaxime, gentamycin, meropenem, penicillin G, piperacillin/tazobactam, piperacillin, methicillin, vancomycin, cloxacillin, ceftazidime	Yes (clear)
	PA31	amoxyclav, bacitracin, teicoplanin, amikacin, cefotaxime, penicillin G, methicillin, cloxacillin, ceftazidime	Yes (clear, small pin-head shaped)
	PA35	ofloxacin, amoxyclav, bacitracin, teicoplanin, cefotaxime, meropenem, piperacillin/tazobactam, piperacillin, methicillin, vancomycin, cloxacillin, ceftazidime	No
	PA37	ofloxacin, amoxyclav, bacitracin, teicoplanin, cefotaxime, piperacillin/tazobactam, piperacillin, methicillin, vancomycin, cloxacillin, ceftazidime	No
	PA56	amoxyclav, bacitracin, teicoplanin, cefotaxime, penicillin G, piperacillin, methicillin, vancomycin, cloxacillin, ceftazidime	Yes (turbid)
	PA57	ofloxacin, amoxyclav, bacitracin, teicoplanin, cefotaxime, penicillin G, methicillin, vancomycin, cloxacillin, ceftazidime.	No
	PA58	amoxyclav, bacitracin, teicoplanin, cefotaxime, penicillin G, methicillin, vancomycin, cloxacillin, ceftazidime	Yes (clear with bull's eye)
	PA36	ampicillin, cefotaxime, vancomycin, nalidixic acid	No
	PA27	ampicillin	No
<i>Pseudomonas</i> spp.	Pse13	cefotaxime, nalidixic acid, piperacillin, ampicillin	No
	Pse14	ofloxacin, cefotaxime, meropenem, piperacillin/tazobactam, piperacillin, methicillin, vancomycin, nalidixic acid, ampicillin	No
<i>P. vulgaris</i>	PV35	ampicillin, vancomycin, piperacillin	No

* Antibiotic resistance was determined by Kirby-Bauer disc diffusion method following Clinical & Laboratory Standards Institute (CLSI) guidelines. Please refer to Figure 2 for zone diameters of individual strains expressed in millimeters (mm).



Figure 2. Antibiotic susceptibility testing (AST) of various clinical isolates (CIs).

Sixteen different antibiotics were tested (y-axis) against 7 different CIs and among them *P. aeruginosa_11* (PA11) was resistant to all the antibiotics tested. The numbers inside the colored box represent lysis zone in millimeters (mm).

The effect of pH on ϕ CDBT-PA31 activity was observed by incubating known concentration (5.0×10^8 PFU/ml) of phage at different pH levels ranging from 1 to 12 for 1.0 hr. ϕ CDBT-PA31 did not lose its viability within pH 3-10 while it significantly lost its viability/activity at pH 11 (Figure 3A). The phages completely lost their activity at pH higher than 11 and lower than 3. Although, ϕ CDBT-PA31 was viable at pH 3-10, the phage titer decreased by $\sim 4 \log_{10}$ fold (initial = 5.0×10^8 PFU/ml, observed = $5.0 \pm 0.5 \times 10^4$ PFU/ml). Further, maximum stability of ϕ CDBT-PA31 was observed at pH 6 (6.51×10^4 PFU/ml). The phage titer at pH 11 was significantly decreased to 4.35×10^2 PFU/ml after an hour of incubation at 37°C .

Similarly, thermal stability of ϕ CDBT-PA31 at pH 7.0 was also determined by spot assay after incubating known concentration (5.0×10^8 PFU/ml) of phage at different temperature. The results showed that ϕ CDBT-PA31 was viable at 50°C for 30 min and 60 min (Figure 3B).

However, the viral titer significantly decreased to 6.15×10^3 PFU/ml (30 min) and to 5.63×10^3 PFU/ml (60 min). Further, the number of viable phage decreased to 3.0×10^2 PFU/ml after 30 min incubation at 60°C and to 1.0×10^2 PFU/ml after 30 min incubation at 70°C . No phage viability was observed at 80°C and higher.

In vitro phage mediated lysis of host bacteria (PA31) by ϕ CDBT-PA31 was estimated using spectrophotometry. ϕ CDBT-PA31 achieved a reduction of 1.13, 1.38, 2.05, 2.23 and 2.4 log CFU/ml after 1h, 2h, 3h, 4h and 5h respectively (Figure 3C). The reduction of bacterial cells in percentage were also calculated and is depicted in Table 2. The number of viable *P. aeruginosa* (PA31) was reduced by about 2.4 log fold (26.11%) when treated with phage at MOI of 100 compared to the phage-free control after 5.0 h incubation.

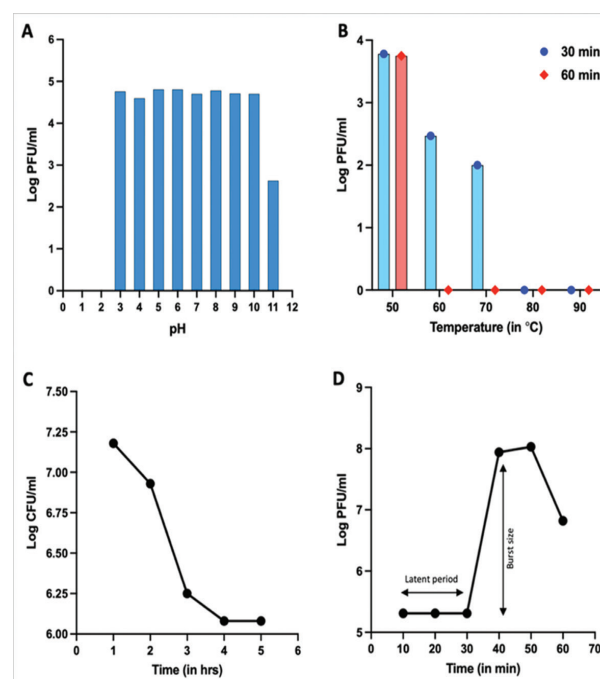


Figure 3. Stability and characterization of ϕ CDBT-PA31.

Table 2. Spectrophotometer reading of bacterial cells.

Time (hrs)	OD	CFU/ml	Log CFU/ml	Log reduction in bacterial density	Percentage reduction in bacterial density (%)
1	0.075	1.53×10^7	7.18	1.13	12.29
2	0.042	8.56×10^6	6.93	1.38	15.01
3	0.009	1.83×10^6	6.26	2.05	22.30
4	0.006	1.22×10^6	6.08	2.23	24.26
5	0.004	8.16×10^5	5.91	2.40	26.11

OD = optical density at 600 nm of wavelength, CFU = colony forming unit

(A) pH stability of ϕ CDBT-PA31: ϕ CDBT-PA31 was viable within pH range of 3-11 after 1 hr of incubation while it completely lost its viability at pH lower than 3 and higher than 11. (B) Temperature stability of ϕ CDBT-PA31: ϕ CDBT-PA31 was viable at 50°C when incubated for 30 mins and 60 mins while it gradually lost its viability at higher temperature. (C) *In vitro* phage mediated lysis by ϕ CDBT-PA31 on its parent host *P. aeruginosa*_31 (PA31): Bacterial concentration of PA31 was significantly reduced by about 2.29 log-fold (expressed in CFU/ml) when treated with ϕ CDBT-PA31 at MOI of 100. (D) One-step growth curve of ϕ CDBT-PA31 on PA31 strain: The latent period of ϕ CDBT-PA31 was 30 minutes and yielded a burst size of 423-525 PFU per infected cell.

We further characterized the growth cycle of ϕ CDBT-PA31 using one-step growth assay to identify different phases of a phage infection process. The latent period of ϕ CDBT-PA31 was 30 minutes and yielded a burst size of 423-525 PFU per infected cell (Figure 3D).

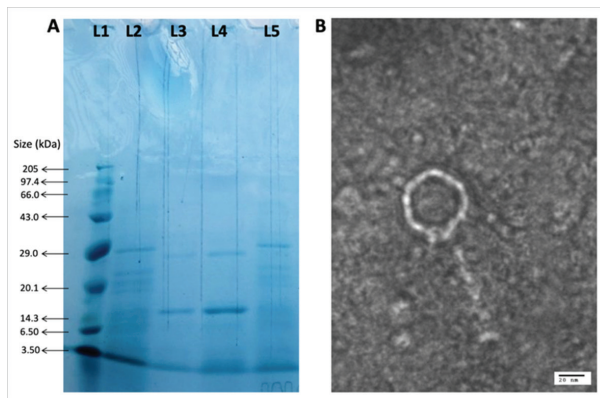


Figure 4. Phage characterization based on protein profiling and transmission electron micrograph. (A)

Protein profiling of ϕ CDBT-PA31 and ϕ CDBT-PA11. Lane 1 = Protein molecular weight marker (Genei, size = 3.5-205 kilodaltons (kDa) Lane 2 = ϕ CDBT-PA31 (acetone precipitation), Lane 3 = ϕ CDBT-PA11 (direct heating), Lane 4 = ϕ CDBT-PA11 (acetone precipitation), Lane 5 = ϕ CDBT-PA31 (direct heating). The difference in protein profiling between two phages implies that they belong to different phage family. (B) Transmission electron microscopy of ϕ CDBT-PA31. The scale bar at the bottom right corresponds to 20 nanometres (nm).

To further characterize the phages, protein profiling of ϕ CDBT-PA31 and ϕ CDBT-PA11 was carried out using sodium dodecyl sulfate polyacrylamide gel electrophoresis (SDS-PAGE). Four distinct bands of ϕ CDBT-PA31 and 3 distinct bands of ϕ CDBT-PA11 was observed in the gradient gel ranging from approximately 3.5 to 29.0 kilodaltons (kDa)

(Figure 4A). For ϕ CDBT-PA31, the most predominant polypeptide appeared at a size of approximately 29.0 kDa and could be assigned to the major capsid protein. Similarly, based on size, other three protein bands could be correlated with structural proteins: head-tail connector protein, capsid assembly protein, internal virion protein. Likewise, the major structural protein (capsid) for ϕ CDBT-PA11 appeared to be of 14.3 kDa (smaller than ϕ CDBT-PA31). The remaining two bands could be assumed as minor structural proteins. The size difference in major structural protein (capsid) implies that the two phages are not identical and possibly belongs to different families.

Transmission electron microscopy revealed that ϕ CDBT-PA31 had icosahedral capsid (54 nm) with relatively long tail (length = 95 nm, width = 8 nm) (Figure 4B). Thus, according to the ICTV classification guidelines, it belonged to *Siphoviridae* family of Caudovirales order.

DISCUSSION

Natural environment is a reservoir for variety of phages. As phages require bacteria for their multiplication, bacteria rich habitat is considered fertile niche for co-evolution of phages. Because of an unregulated antibiotic use (which accelerate emergence of AMR strains) and direct disposal of sewages, hospital waste, industrial effluents into rivers in south Asian countries like Nepal and India, possibility of finding phages against MDR bacteria is high in these regions. Previously, we've shown that phages against carbapenem-resistant *Klebsiella pneumoniae* are abundant in river waters of Kathmandu valley.³ These phages improved survival of mice without eliciting detrimental inflammatory responses.⁴ This led us to search for more therapeutic phages in rivers of Kathmandu, Nepal. Three phages potentially having strictly virulent lifestyle were isolated from the river water flowing through Balkhu (Bagmati river) and Kalanki (Balkhu river) area. Since the phages were able to effectively lyse different CIs in addition to their primary host, they can be considered as phages with wide-host-range (WHR) akin to wide-spectrum antibiotics which is a desirable character for therapeutic phages. Further, observation of bull's eye plaque in ϕ CDBT-PA58 clearly indicates that the phage has additional depolymerase activity that can further inhibit the growth of surrounding bacterial cells possibly by depolymerizing the alginic acid capsule of *P. aeruginosa*.⁵ The alginase produced by such phages may be used alone or in combination with other drug/phage to increase the well-being of CF patients by facilitating the expectoration of sputum, accelerating phagocytic

uptake of bacteria and perturbing bacterial growth in biofilms.⁵ Similar results were also observed with phage derived depolymerase enzyme alginase by Chegini, Khoshbayan⁶ and Latino, Midoux.⁷ Further, compared to bacteria, phages are four times more abundant in mucus layers because the protein shell of a phage can effectively bind mucins. This protects the underlying cells from potential bacterial pathogens, providing additional layer of non-specific immunity.⁸ As anti-*Pseudomonas* phages has been in trail against chronic otitis, ear infection, CF already, biocontrol of bacterial infection using phages is gaining traction. Also, a French team showed that a specific cocktail of ten phages was able to significantly reduce bacterial growth *P. aeruginosa*.⁹ Further, The studies on virulent phages against biofilms has shown decrease of the biomass in a biofilm but couldn't eradicate it.¹⁰ To overcome this, combination therapy (phage + antibiotics) has been proposed as phage-antibiotic synergy (PAS) has shown encouraging results. Recently, polyvalent phages were also found to conjugate with magnetic colloidal nanoparticle clusters enhancing biofilm penetration for microbial control.¹¹ In a lethal mouse model of pneumonia using an MDR *P. aeruginosa* strain from CF patients, researchers reported that a single intranasal administration of anti-*Pseudomonas* phage(s) resulted in 90%-100% survival rate and reduced pathological damage when given within 2 hrs post infection .⁹

Further, phage parameters like pH and temperature stability, latent period and burst size are cardinal in application of phage as therapeutics. øCDBT-PA31 demonstrated extended tolerance to varying pH (3-11) and to high temperature (50°C) for 60 min making it more fit for application in diverse environment and wide range of animals including human. One-step growth assay of øCDBT-PA31 showed latent period of 30 min with corresponding burst size of 423-525 PFU/infected cell. As phages with small latent period and high burst size are desirable, our phage has potential to be a therapeutic phage. Also, in *in vitro* phage mediated lysis assay, øCDBT-PA31 was able to significantly decrease bacterial population within 3.0 hrs of phage treatment with MOI 100. Protein profiling using SDS-PAGE of two phages (øCDBT-PA11 and øCDBT-PA31) clearly indicated that they had different protein components in their structure implying they are morphologically distinct from each other. Further, TEM analysis of øCDBT-PA31 confirmed that the phage belonged to *Siphoviridae* family that harbors multiple members of virulent *Pseudomonas* phage. In conclusion, we isolated and purified 3 lytic phages against 3 different MDR CIs of *P. aeruginosa*. Among them, øCDBT-PA31 showed lytic

activity against two *P. aeruginosa* CIs (PA31 and PA11) that were resistant to all tested classes of antibiotics. As the lysis spots were completely clear, we assumed øCDBT-PA31 to be virulent.

CONCLUSIONS

Based on these findings, we conclude that øCDBT-PA31 isolated from Bagmati river could be a therapeutic phage. However, genomic studies are necessary to rule out any lysogeny module and absence of other harmful (AMR, toxic, virulent) genes in the phage.

ACKNOWLEDGMENTS

We would like to thank University Grants Commission, Nepal (UGC-Nepal) for partially supporting the research through 'Thesis Support Grant' provided to AM. We would like to further acknowledge staffs at Microbiology Laboratory, Tribhuvan University Teaching Hospital, Kathmandu, Nepal for providing clinical isolates.

COMPETING INTEREST

We declare no competing interests.

Author Affiliations

¹Central Department of Biotechnology, Institute of Science and Technology, Tribhuvan University, Kirtipur, Nepal

Competing interests: None declared

REFERENCES

1. Yu X, Xu Y, Gu Y, Zhu Y, Liu X. Characterization and genomic study of "phiKMV-Like" phage PAXYB1 infecting *Pseudomonas aeruginosa*. *Sci Rep* 2017;7:13068. [Article]
2. Hagens S, Loessner MJ. Phages of *Listeria* offer novel tools for diagnostics and biocontrol. *Front Microbiol* 2014;5.[Article]
3. Dhungana G, Regmi M, Paudel P, Parajuli A, Upadhyay E, Gyawali I, et al. Therapeutic Efficacy of Bacteriophage Therapy to Treat Carbapenem Resistant *Klebsiella Pneumoniae* in Mouse Model. *Journal of Nepal Health Research Council*. 2021 Apr 23;19(1):76-82.[Article]
4. Dhungana G, Nepal R, Regmi M, Malla R. Pharmacokinetics and Pharmacodynamics of a Novel Virulent *Klebsiella* Phage Kp_Pokalde_002 in a Mouse Model. *Frontiers in Cellular and Infection Microbiology* 2021;11.[Article]

5. Glonti T, Chanishvili N, Taylor PW. Bacteriophage-derived enzyme that depolymerizes the alginic acid capsule associated with cystic fibrosis isolates of *Pseudomonas aeruginosa*. *J Appl Microbiol* 2010;108:695-702. [\[Article\]](#)
6. Chegini Z, Khoshbayan A, Taati Moghadam M, Farahani I, Jazireian P, Shariati A. Bacteriophage therapy against *Pseudomonas aeruginosa* biofilms: a review. *Annals of Clinical Microbiology and Antimicrobials* 2020;19:45. [\[Article\]](#)
7. Latino L, Midoux C, Vergnaud G, Pourcel C. Investigation of *Pseudomonas aeruginosa* strain PcyII-10 variants resisting infection by N4-like phage Ab09 in search for genes involved in phage adsorption. *PLOS ONE* 2019;14:e0215456 [\[Article\]](#)
8. Barr JJ, Auro R, Furlan M, Whiteson KL, Erb ML, Pogliano J, et al. Bacteriophage adhering to mucus provide a non-host-derived immunity. *Proceedings of the National Academy of Sciences*. 2013 Jun 25;110(26):10771-6. [\[Article\]](#)
9. Morello E, Saussereau E, Maura D, Huerre M, Touqui L, Debarbieux L. Pulmonary bacteriophage therapy on *Pseudomonas aeruginosa* cystic fibrosis strains: first steps towards treatment and prevention. *PLoS One* 2011;6:e16963. [\[Article\]](#)
10. Sulakvelidze A, Alavidze Z, Morris JG, Jr. Bacteriophage therapy. *Antimicrob Agents Chemother* 2001;45:649-59. [\[Article\]](#)
11. Li LL, Yu P, Wang X, Yu SS, Mathieu J, Yu HQ, et al. Enhanced biofilm penetration for microbial control by polyvalent phages conjugated with magnetic colloidal nanoparticle clusters (CNCs). *Environmental Science: Nano*. 2017;4(9):1817-26. [\[Article\]](#)



Genomic characterization of three bacteriophages targeting multidrug resistant clinical isolates of *Escherichia*, *Klebsiella* and *Salmonella*

Roshan Nepal^{1,2} · Ghais Houtak^{1,2} · Sumeena Karki³ · Gunaraj Dhungana³ · Sarah Vreugde^{1,2} · Rajani Malla³

Received: 1 March 2022 / Revised: 10 April 2022 / Accepted: 25 April 2022 / Published online: 19 May 2022
© The Author(s) 2022

Abstract

Application of bacteriophages (phages) to treat complex multidrug-resistant bacterial infection is gaining traction because of its efficacy and universal availability. However, as phages are specific to their host, a diverse collection of locally isolated phage from various geographical locations is required to formulate a wide host range phage cocktail. Here, we report morphological and genomic features of three newly isolated phages from river water of the urban region in Kathmandu, Nepal, targeting three different bacteria (*Escherichia coli*, *Klebsiella pneumoniae* and *Salmonella enterica*.) from the *Enterobacteriaceae* family. Morphological identification and genome analysis indicated that two phages (Escherichia phage vB_EcoM_TU01 and Klebsiella phage vB_KpnP_TU02) were strictly lytic and free from integrases, virulence factors, toxins and known antimicrobial resistance genes, whereas Salmonella phage vB_Sals_TU03 was possibly a temperate phage. The genomic features of these phages indicate that natural phages are capable of lysing pathogenic bacteria and may have potential in bacterial biocontrol.

Keywords Bacteriophage · Phage · Genomics · Phage therapy · *Enterobacteriaceae*

Abbreviations

MDR	Multidrug resistance
DLAA	Double layer agar assay
PCR	Polymerase chain reaction
CDS	Coding DNA sequence
tRNA	Transfer RNA
ARG	Antibiotic resistant gene
PATRIC	Pathosystems resource integration center
NCBI	National center for biotechnology information
TEM	Transmission electron microscopy
dsDNA	Double-strained DNA

GO	Gene ontology
G+C	Guanine and cytosine

Introduction

Enterobacteriaceae is a large family of Gram-negative rod-shaped facultatively anaerobic bacteria comprising a wide range of pathogens such as *Escherichia*, *Klebsiella*, *Salmonella*, *Enterobacter*, *Citrobacter*, *Shigella* and more. These pathogens are associated with considerable morbidity and mortality on compromised hosts and can cause life-threatening illnesses like septicaemia, haemolytic uremic syndrome, gastroenteritis, meningitis and pneumonia in healthy individuals (Donnenberg et al. 2015). These infections are usually treated with antibiotics, but lately, most human-associated pathogens are becoming increasingly resistant to antibiotics, thereby limiting the effectiveness of the antibiotic treatment. Furthermore, the emergence of carbapenem-resistant *Enterobacteriaceae* is a concern as there is no therapy or vaccines available to prevent acquisition of infection with multidrug resistant (MDR) strains. As current antibiotic therapies are ineffective to treat such infections or

Communicated by Erko Stackebrandt.

✉ Roshan Nepal
roshan.nepal@adelaide.edu.au

¹ Faculty of Health and Medical Sciences, The University of Adelaide, Adelaide, Australia

² Department of Surgery-Otolaryngology Head and Neck Surgery, The Basil Hetzel Institute for Translational Health Research, Central Adelaide Local Health Network, South Australia, Australia

³ Central Department of Biotechnology, Tribhuvan University, Kirtipur, Nepal

eliminate once infected, alternative approaches are highly sought in the management of MDR infections.

Bacteriophage (phage) is a virus that infects bacterial cells but leaves eukaryotes unscathed. Because of its host specificity, phages can be used to kill bacteria without harming untargeted cells. In the past decade, therapeutic application of phage has been gaining widespread attention because of its specificity and efficacy against MDR bacterial pathogens (Pirnay 2020). Further it is also regarded as ‘dynamic’ solution to continuously emerging MDR strains because of its co-evolving lifestyle with the bacteria. Phage therapy uses ‘strictly’ lytic phages or its derivatives to kill pathogenic bacteria. Although phage therapy is not novel and had been employed shortly after the discovery of phages around 1920s (d’Herelle 1931), invention of antibiotics curbed the widespread usage of phages therapeutically as antibiotics were more effective against a broad spectrum of bacteria. However, emergence of multidrug-resistant ‘superbugs’ has rekindled the interest in phage therapy. Studies have shown that phage therapy can be used as an alternative biocontrol agent or adjuvant therapy to antibiotics in human and animals (Petrovic Fabijan et al. 2020; Schooley et al. 2017; Ooi et al. 2019; Waters et al. 2017; Greene et al. 2021).

However, the efficacy of phage therapy targeting the pathogen of interest still has room for improvement. As phages are highly specific in regard to infecting their host, extending up to the level of bacterial strains, phages isolated from geographically same region as the bacterial host would have a higher probability of infecting the bacterial strain of interest due to the co-evolutionary adaptations (Hampton et al. 2020). Therefore, a local ‘phage bank’ comprising various phages isolated in the same region as bacterial pathogens of interest would facilitate a more effective strategy for the use of phages. Further, since most of the genes in phage genome is yet ‘hypothetical’, a comprehensive database reporting phage genome from different geolocations and clinical isolates is essential to study the co-evolution between phage and bacteria. As such, genome report provides invaluable information that can be useful in elucidating ‘conserved and unknown’ functions in phage genomes. Furthermore, the use of genomics and phenotyping of phages and their host could improve the efficacy of phage therapy in the future regarding the choice of phage for the pathogen of interest. In line with the aim of expanding phage research, previously, we reported phages exhibiting lytic activity against multidrug resistant *Pseudomonas* and *Klebsiella* (Dhungana et al. 2021a; Maharjan et al. 2022) and also studied pharmacokinetics and pharmacodynamics of our *Klebsiella* phage Kp_Pokalde_002 in a mouse model (Dhungana et al. 2021b). Here, we report the isolation, genome analysis and taxonomic position of three newly isolated phages targeting MDR human pathogens: *Escherichia coli*, *Klebsiella*

pneumoniae and *Salmonella enterica* from *Enterobacteriaceae* family.

Materials and method

Bacterial strain

Three multidrug-resistant clinical isolates of *E. coli* ($N=1$), *K. pneumoniae* ($N=1$) and *S. enterica* ($N=1$) were collected from the Microbiology Laboratory, Tribhuvan University Teaching Hospital, Kathmandu, Nepal. The clinical isolates were confirmed to be MDR by AMR testing in the microbiology department of the hospital and used as hosts for isolation and amplification of phages. The MDR status was also validated evaluating the strains against 11 different antibiotics (Supplementary table S1) using Kirby–Bauer disc-diffusion method (Hudzicki 2009). Nutrient agar (NA, agar = 1.5%, HiMedia, India) was used to grow fresh overnight culture (at 37 °C) from glycerol stock and Luria–Bertani broth (HiMedia, India) was used to propagate the host bacterium for phage isolation and amplification.

Phage manipulation: isolation, purification and amplification

A water sample was collected from the Bagmati river, Kathmandu, Nepal flowing through the urban region of the city which is heavily polluted by untreated sewers and industrial waste (Mishra et al. 2017). Phages were isolated using Double Layer Agar Assay (DLAA) as described previously with some modifications (Dhungana et al. 2021a). Briefly, the water sample was centrifuged at 3220g (Centrifuge 5810R, Eppendorf, Hamburg, Germany) for 10 min to pellet down the debris and subsequently the supernatant was filtered through a 0.45- μm and 0.22- μm pore-size Whatman™ syringe filter (Sigma-Aldrich, Missouri, United States). One millilitre filtrate was mixed with 100 μl exponentially growing host bacteria (OD_{600} 0.5) and left at room temperature (10 min) for phage adsorption. Three millilitre semisolid top agar (Tryptic Soya Agar (TSA), agar = 0.4%, stored at = 50 °C) (HiMedia, India) was added to the mixture, mixed well by swirling and poured on to the surface of previously prepared bottom agar (TSA, agar = 1.0%, HiMedia, India). After overnight incubation at 37 °C, the plates were examined for the presence of phages in the form of plaques. A single isolated clear plaque was cut and dissolved in 1.0 mL of Sodium chloride-Magnesium sulfate (SM) buffer (10 mM Tris–HCl, 10 mM $\text{MgSO}_4 \cdot 7\text{H}_2\text{O}$, 2% gelatin and 100 mM NaCl, pH 7.5). Subsequently, the phage was purified by performing three rounds of DLAA from a single isolated plaque.

Phage characterization

Transmission electron microscopy

High titre purified phage lysates were fixed with fixative (2.5% glutaraldehyde and 2% paraformaldehyde prepared in 0.1 M sodium phosphate buffer (pH 7.2)). For fixation, equal volume of phage lysate and fixative were added, mixed and left overnight. The next day, the fixed phages were subjected to high-speed centrifugation (35,000g) for 3 h. Per sample 10.0 µL fixed phage lysate was deposited on a separate 300 mesh carbon-coated copper grid. The copper grid was then flooded with 2% (w/v) uranyl acetate (pH 4.5) for 2 min. The copper grid was dried and examined in JEM-2100F Transmission Electron Microscope (JEOL, USA) at 200 kV under different magnifications. TEM micrographs were processed using ImageJ 1.50i (<https://imagej.nih.gov/ij>) (Schneider et al. 2012).

Genomic DNA extraction, sequencing and annotation

Phage genomic DNA (gDNA) was isolated using Phage DNA Isolation Kit (Norgen Biotek Corp., Ontario, Canada. Cat. #46,800) per manufacturer's instructions. Qualitative and quantitative control were performed using conventional electrophoresis and Qubit® 2.0 Fluorometer (ThermoFisher Scientific, USA), respectively. Five microliter gDNA of each sample was loaded on 1% agarose gel and run for 30 min at 110 Volt. Also, 1.0 µl of each sample was loaded in NanoDrop 8000 (ThermoFisher Scientific, USA) for determining A260/280 ratio and Qubit® 2.0 for determining concentration of gDNA.

The paired-end sequencing library was prepared using TruSeq® Nano DNA HT Library Preparation Kit (Illumina, USA). Two hundred nanograms of gDNA was fragmented by Covaris shearing that generated dsDNA fragments with 3' or 5' overhangs. The fragments were then subjected to end-repair. The ligated products were purified using SP beads supplied in the kit. The size-selected product was PCR amplified as described in the protocol. The amplified library was analyzed in Bioanalyzer 2100 (Agilent Technologies, USA) using High Sensitivity (HS) DNA chip as per manufacturer's instructions. After obtaining the Qubit®

concentration for the library and the mean peak size from Bio-analyser profile (Fig. S1A–C), the library was loaded onto Illumina HiSeq 2000/2500 (Illumina, USA) for cluster generation and sequencing. The cluster generated was assembled using CLC Genomics Workbench 6.0 (Qiagen, USA) at default parameters (Minimum contig length: 200, Automatic word size: Yes, Perform scaffolding: Yes, Mismatch cost: 2, Insertion cost: 3, Deletion cost: 3, Length fraction: 0.5, Similarity fraction: 0.8). Phage genomes were annotated for coding DNA sequences (CDS), tRNA, virulence factors, toxins, antimicrobial resistance genes (ARGs) and drug targets using the Pathosystems Resource Integration Center (PATRIC 3.6.12) webtool (<https://www.patricbrc.org/>) (Wattam et al. 2013; Brettin et al. 2015) using viruses (taxid = 10,239) as the reference database. A circular map of the phage genome was generated using CGview server (<http://cgview.ca/>) (Stothard and Wishart 2004), and a phylogenetic tree was constructed BLASTing the query sequence against NCBI database using neighbor-joining method. Only the ten most common phages were included in the phylogenetic analysis. The tree was further visualized using ggtree package in R 4.1.1 (<https://www.R-project.org/>). The lifestyle, order, family and host of the phages were computationally predicted through PhageAI (<https://phage.ai/>) (Tynecki et al. 2020).

Results and discussion

Three following phages, viz: Escherichia phage vB_EcoM_TU01 (hereafter vB_EcoM_TU01), Klebsiella phage vB_KpnM_TU02 (hereafter vB_KpnM_TU02) and Salmonella phage vB_SalS_TU03 (hereafter vB_SalS_TU03) targeting multidrug resistant clinical isolates of *E. coli*, *K. pneumoniae* and *S. enterica*. were isolated from the water sample collected from the Bagmati river (Fig. 1A, C, E). TEM revealed that among three phages, two (vB_EcoM_TU01, vB_KpnM_TU02) were from the *Myoviridae* family whereas vB_SalS_TU03 belonged to *Siphoviridae* family (Fig. 1B, D, F and Table 1). All phages were tailed phages (Order = *Caudovirales*) and consist of a linear double-stranded DNA (dsDNA) genome with gene density of approximately 1.7 genes/kilo-basepairs which is much

Table 1 Classification of phages according to ICTV* guidelines (ICTV 9th report) based on transmission electron micrograph

Phage	Capsid (in nm [^])	Tail (W×L, in nm [^])	Shape	Family (Morphotype [#])
vB_EcoM_TU01,	82×108	19×111	Elongated	Myoviridae (A2)
vB_KpnM_TU02	82×99	25×109	Elongated	Myoviridae (A2)
vB_SalS_TU03	63	9×106	Icosahedral	Siphoviridae (B1)

*ICTV = The International Committee on Taxonomy of Viruses. [^] nm = nanometre. The capsid and tail lengths are an average of three measurements of a phage electron micrograph from a purified stock.

[#]Morphotypes are based on classification by Ackermann (2001)

higher than that of the bacterial host (0.5–1.0 genes/kilo-base-pairs) (Norwood and Sands 1997). The CDS coverage of all the phages was higher than 95% whereas the average gene length ranged between 540 and 567 basepairs (Table 2).

The genome of vB_EcoM_TU01 was 169,046 bp with a G + C content of 37.42% [lower than that of its host *E. coli* (~50.6%)] encoding 286 proteins (Fig. 2). The average length of genes was 566 bp with a CDS coverage of 95.9%. Furthermore, vB_EcoM_TU01 encoded 2 transfer-RNAs (tRNA) (tRNA-Met-CAT and tRNA-Arg-TCT). Regarding the gene function, 83.2% (238/286), were functional of which 5.6% (16/286) had a Gene Ontology (GO) assigned function, and the remaining 16.8% (48/286) were hypothetical. Similarly, the genome of vB_KpnM_TU02 was 166,230 bp with a G + C content of 38.34% [lower than that of its host *K. pneumoniae* (~57%)] and encoded 294 proteins (Fig. 3). The average gene size in vB_KpnM_TU02 was 540 bp with a CDS coverage of 95.6%. The phage vB_KpnM_TU02 also encoded 15 tRNAs (tRNA-Thr-TGT, tRNA-Leu-TAA, tRNA-Arg-TCT, tRNA-Met-CAT, tRNA-Pro-TGG, tRNA-Gly-TCC, tRNA-Trp-CCA, tRNA-Ile-GAT, tRNA-Ser-TGA, tRNA-His-GTG, tRNA-Gln-TTG, tRNA-Met-CAT, tRNA-Asn-GTT, tRNA-Lys-TTT and tRNA-Tyr-GTA). Out of 294 encoded proteins, 110 (37.4%) were functional, and 184 (62.6%) were hypothetical, whereas only 11 (3.7%) encoded proteins had GO assigned function. Further,

the genome of vB_SalS_TU03 was 41,756 bp with a G + C content of 47.06% [slightly lower than that of its host *Salmonella* (~52.2%)] and encoded 71 proteins (Fig. 4). The average gene size in vB_SalS_TU03 was 562 bp with a CDS coverage of 95.7%. Out of 71 encoded proteins, 45 (63.4%) aligned with the functional protein whereas 26 (36.6%) were hypothetical. Only 2 out of 71 (2.8%) encoded proteins had GO assigned function.

Although the functions of tRNA in phages remain elusive, it is believed that more tRNA corresponds to increased virulence of the phage as it facilitates a more robust integration of the phages (Baillly-Bechet et al. 2007; Almeida et al. 2022). Since two of our phages encoded multiple tRNAs, it is more likely that these phages are virulent (lytic) and thus more suitable for therapeutic purposes. The ‘functional’ proteins include proteins involved in DNA packaging, transcription, replication, regulation, lysis and structural proteins whereas ‘hypothetical’ proteins are coding DNA sequences (CDS) with unknown functions. All the three phage genomes were free from genes encoding known toxins, antibiotic resistant genes (ARGs), virulent factors (VFs) of bacterial origin and lysogenic markers such as integrase, recombinase, repressor/anti-repressor protein, and excisionase. However, the in silico tool we used (phageAI) only categorized vB_EcoM_TU01 and vB_KpnM_02 as virulent/lytic with high confidence (96.34% and 99.27%, respectively), whereas

Table 2 Genomic and protein features of three novel phages targeting multidrug resistant *Escherichia coli*, *Klebsiella pneumoniae* and *Salmonella enterica* clinical isolates

Features	Escherichia phage vB_EcoM_TU01	Klebsiella phage vB_KpnM_TU02	Salmonella phage vB_SalS_TU03
NCBI accession	MZ560701	MZ560702	MZ560703
Genomic features			
Length (in base pairs)	169,046 bp	166,230 bp	41,756 bp
Guanine-cytosine (G + C) content	37.42%	38.34%	47.06%
Total CDS	286	294	71
tRNAs	2	15	0
Gene density (per kbp)	1.69	1.77	1.70
Average gene size (in bp)	566	540	562
CDS coverage	95.9%	95.6%	95.7%
Protein feature			
Hypothetical proteins	48 (16.78%)	184 (62.59%)	26 (36.62%)
Functional proteins	238 (83.22%)	110 (37.41%)	45 (63.38%)
Proteins with GO assignments	16 (5.60%)	11 (3.74%)	2 (2.82%)
Other features/genomes			
Transporter genes (Ref = TCDB)	5	0	0
Drug target genes (Ref = DrugBank)	3	0	0
Order	Caudovirales	Caudovirales	Caudovirales
Family	Myoviridae	Myoviridae	Siphoviridae
Genus (Ref = PhageAI, NCBI)	Mosigvirus	Jiaodavirus	Jerseyvirus
Lifestyle (Ref = PhageAI)	Virulent (C = 96%)	Virulent (C = 99%)	Temperate (C = 57%)

NCBI National Center for Biotechnology Information, CDS Coding DNA sequences, tRNA transfer RNA, kbp kilo basepairs, GO Gene ontology (<http://geneontology.org/>), TCDB Transporter classification database (<https://www.tcdb.org/>), C Confidence

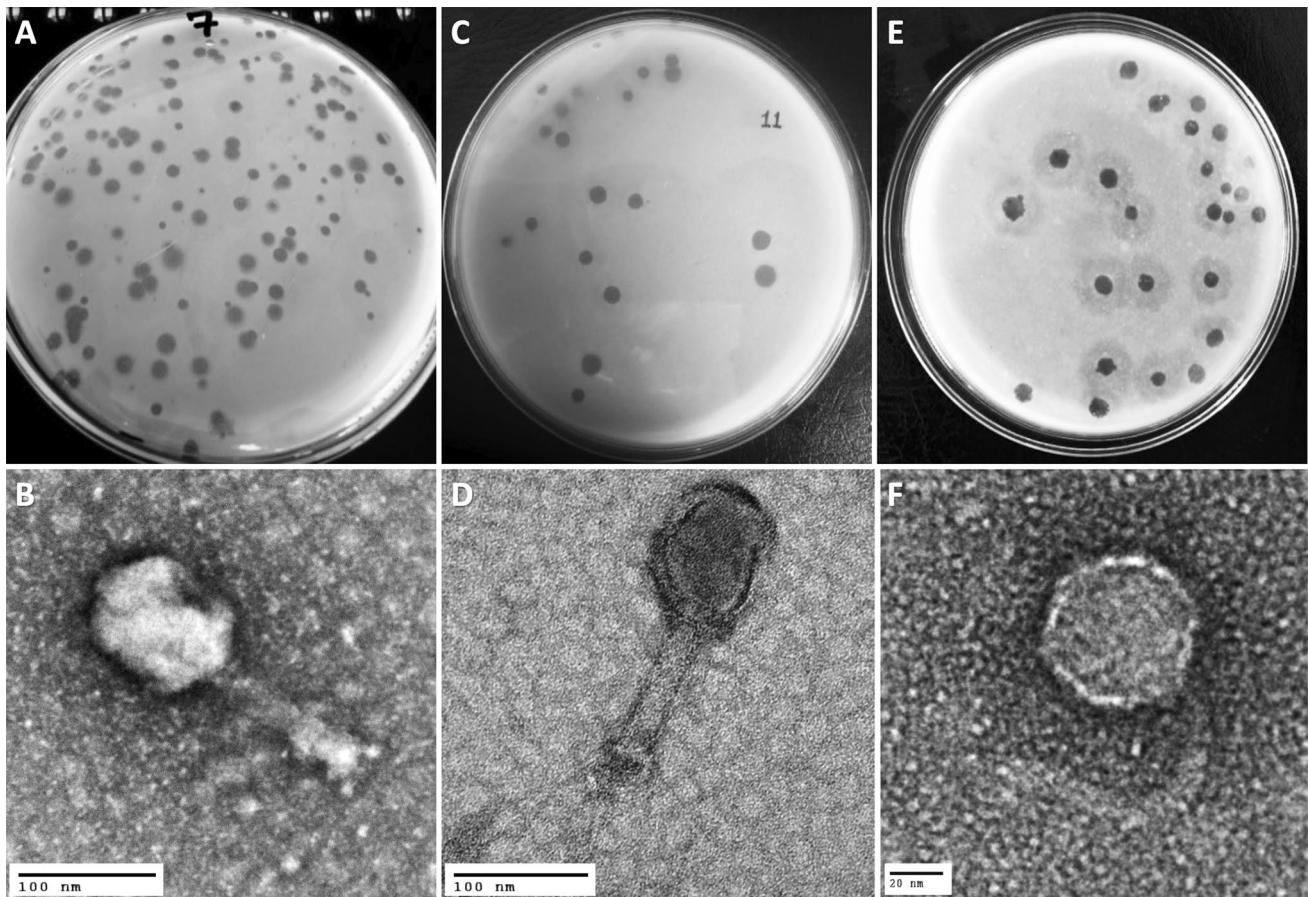


Fig. 1 Phage isolation using double layer agar assay and their transmission electron micrograph (TEM). **A, C, E** Three double layered agar plates showing different types of phage plaque morphologies isolated directly from river water. **B** TEM of Escherichia phage

vB_EcoM_TU01 (scale bar=100 nm), **D** TEM of Klebsiella phage vB_KpnM_TU02 (scale bar=100 nm), **F** TEM of Salmonella phage vB_SalS_TU03 (scale bar=20 nm)

vB_SalS_TU03 was tagged as temperate/lysogenic with a low confidence of 57%. The substantial number of hypothetical proteins in all phages clearly indicates that phages carry numerous genes that are yet to be characterized, and whose function is yet to be understood. The detailed information about the genomes of all three phages and their respective lifestyle is summarized in Table 2. These results suggest that vB_EcoM_TU01 and vB_KpnM_02 could potentially be used as therapeutic phages against multidrug resistant *E. coli* and *K. pneumoniae*, whereas vB_SalS_TU03 would less likely succeed in lysing its host as it may switch to lysogenic lifestyle and incorporate in the host genome as a prophage. Since prophages play a catalytic role in disease modulation (Nepal et al. 2022) and are known to carry genes increasing bacterial fitness which could be detrimental to humans (Balcazar 2014; Helbin et al. 2012; Khalil et al. 2016; Kondo et al. 2021; Nepal et al. 2021), such phages are not suitable for phage therapy.

Further, comparing the phage genome in the NCBI database using nucleotide BLAST (nBLAST) revealed

that the phage vB_EcoM_TU01 was closely related to a T4-like lytic Escherichia phage vB_EcoM_JS09 (NCBI accession = KF582788, query coverage = 99%, per cent identity = 98.04%) isolated in China from the sewage of a swine factory. Similarly, phage vB_KpnM_TU01 was similar to a lytic Klebsiella phage JD18 (NCBI accession = KT239446, query coverage = 96%, per cent identity = 97.89%) isolated in China. Further, phage vB_SalS_TU03 was closest to lytic Salmonella phage LSPA1 (NCBI accession = KM272358, query coverage = 93%, per cent identity = 99.17%) isolated in China from a hospital sewage (Zeng et al. 2015). These analyses indicate that our phages were novel, but highly similar to the phages isolated in neighbouring China around the same time and might have a very similar host range. Phylogenetic relatedness of all three phages against ten most common phages and their per cent identity is elaborated in Fig. 5. It is noted that, among ten most common hits, phylogenetics reveal that vB_EcoM_TU01 is also closely related to *Shigella* phages (also an *Enterobacteriaceae*). Although more

study is required, we can arbitrarily predict that phages isolated against different genus of bacteria have higher degree of similarity between them. This may explain (although not studied in this research) why some phages are polyvalent (showing inter-genus or even inter-order infectivity) and show expansive host spectrum (Gambino et al. 2020; Hamdi et al. 2017; Sui et al. 2021; Yu et al. 2016). This property thus holds immense applicability if further study is performed to determine the mechanism of phage infection and identify the factors/proteins/enzymes that determine phage-bacteria specificity.

Conclusion

Three phages infecting multidrug-resistant *E. coli*, *K. pneumoniae* and *S. enterica* were isolated, sequenced and banked. Genome analysis indicated that two of them (Escherichia phage vB_EcoM_TU01 and Klebsiella phage vB_KpnP_TU02) were strictly lytic and free from integrases, virulence factors, toxins, and antimicrobial resistance genes. Although additional studies are required, the genomic features of these phages provide valuable insights into the possibility of using natural phages as biocontrol agents against multidrug resistant human pathogens.

Supplementary Information The online version contains supplementary material available at <https://doi.org/10.1007/s00203-022-02948-0>.

Acknowledgements We are grateful to Asst/Prof. Sneha Lata Panwar and her lab members (SLS-JNU, New Delhi, India), Dr. Gajender Saini (AIRF-JNU, New Delhi, India) for assisting with the TEM analysis and Xcelris Labs Ltd., Ahmedabad, India for providing sequencing facility. We also extend our gratitude to the staffs at Microbiology Laboratory, TUTH, Kathmandu, Nepal for kindly providing MDR clinical isolates.

Author contributions RM, RN: Conceptualization and funding acquisition. RN, SK: Methodology, investigation. RN, SK, GH: Analysis and visualization. RM: Supervision. RN, SK, GH: Writing – original draft. RN, GD, GH, SV: Writing – review & editing.

Funding Open Access funding enabled and organized by CAUL and its Member Institutions. This study was partially supported by Kathmandu Center for Education and Research CAS & TU Thesis Grant for M.Sc. students-2015 granted to RN.

Data availability The annotated genome assembly of Escherichia phage vB_EcoM_TU01, Klebsiella phage vB_KpnP_TU02, Salmonella virus vB_SalS_TU03 is available through GenBank accession MZ560701, MZ560702 and MZ560703, respectively. In addition, *fastq* file pertaining to raw sequence data is deposited at NCBI and is available through BioProject accession PRJNA383466 and Sequence Read Archive (SRA) identifiers SRR5460626, SRR5460625, SRR5460624, respectively.

Declarations

Conflict of interest We declare no conflicts of interest.

Ethical approval The study does not involve any human and/or animal subjects. The clinical isolates obtained from hospital was deidentified, and no personally identifiable patient information was disclosed to the researchers.

Open Access This article is licensed under a Creative Commons Attribution 4.0 International License, which permits use, sharing, adaptation, distribution and reproduction in any medium or format, as long as you give appropriate credit to the original author(s) and the source, provide a link to the Creative Commons licence, and indicate if changes were made. The images or other third party material in this article are included in the article's Creative Commons licence, unless indicated otherwise in a credit line to the material. If material is not included in the article's Creative Commons licence and your intended use is not permitted by statutory regulation or exceeds the permitted use, you will need to obtain permission directly from the copyright holder. To view a copy of this licence, visit <http://creativecommons.org/licenses/by/4.0/>.

References

- Ackermann HW (2001) Frequency of morphological phage descriptions in the year 2000. *Adv Virol* 146:843–857. <https://doi.org/10.1007/s007050170120>
- Bailly-Bechet M, Vergassola M, Rocha E (2007) Causes for the intriguing presence of tRNAs in phages. *Genome Res* 17(10):1486–1495. <https://doi.org/10.1101/gr.6649807>
- Balcázar JL (2014) Bacteriophages as vehicles for antibiotic resistance genes in the environment. *PLoS Pathog* 10(7):e1004219. <https://doi.org/10.1371/journal.ppat.1004219>
- Brettin T, Davis JJ, Disz T, Edwards RA, Gerdes S et al (2015) RAST-Tk: a modular and extensible implementation of the RAST algorithm for building custom annotation pipelines and annotating batches of genomes. *Sci Rep* 5(1):8365. <https://doi.org/10.1038/srep08365>
- d'Herelle F (1931) Bacteriophage as a treatment in acute medical and surgical infections. *Bull N Y Acad Med* 7(5):329–348
- de Almeida ACM, Pérez-Vega C, González-Villalobos E, Borrego CM, Balcázar JL (2022) Genome analysis of a new Escherichia phage vB_EcoM_C2–3 with lytic activity against multidrug-resistant *Escherichia coli*. *Virus Res* 307:198623. <https://doi.org/10.1016/j.virusres.2021.198623>
- Dhungana G, Nepal R, Regmi M, Malla R (2021a) Pharmacokinetics and pharmacodynamics of a novel virulent klebsiella phage Kp_Pokalde_002 in a mouse model. *Front Cell Infect Microbiol*. <https://doi.org/10.3389/fcimb.2021.684704>
- Dhungana G, Regmi M, Paudel P, Parajuli A, Upadhyay E et al (2021b) Therapeutic efficacy of bacteriophage therapy to treat carbapenem-resistant *Klebsiella pneumoniae* in a mouse model. *J Nepal Health Res Council* 19(1):76–82. <https://doi.org/10.33314/jnhrc.v19i1.3282>
- Donnenberg MS (2015) Enterobacteriaceae. In: Bennett JE, Dolin R, Blaser MJ (eds) *Mandell, Douglas, and Bennett's Principles and Practice of Infectious Diseases*, 8th edn. W.B. Saunders, Philadelphia, pp 2503–2517.e2505
- Gambino M, Nørgaard Sørensen A, Ahern S, Smyrlis G, Gencay YE et al (2020) Phage S144, a new polyvalent phage infecting *Salmonella* spp. and *Cronobacter sakazakii*. *Int J Mol Sci* 21(15):5196. <https://doi.org/10.3390/ijms21155196>

- Greene W, Chan B, Bromage E, Grose JH, Walsh C et al (2021) The use of bacteriophages and immunological monitoring for the treatment of a case of chronic septicemic cutaneous ulcerative disease in a loggerhead sea turtle *Caretta caretta*. *J Aquat Anim Health* 33(3):139–154. <https://doi.org/10.1002/aah.10130>
- Hamdi S, Rousseau GM, Labrie SJ, Tremblay DM, Kourda RS et al (2017) Characterization of two polyvalent phages infecting Enterobacteriaceae. *Sci Rep* 7(1):40349. <https://doi.org/10.1038/srep40349>
- Hampton HG, Watson BNJ, Fineran PC (2020) The arms race between bacteria and their phage foes. *Nature* 577(7790):327–336. <https://doi.org/10.1038/s41586-019-1894-8>
- Helbin WM, Polakowska K, Miedzobrodzki J (2012) Phage-related virulence factors of *Staphylococcus aureus*. *Postep Mikrobiol* 51(4):291–298
- Hudzicki J (2009) Kirby-Bauer disk diffusion susceptibility test protocol. *Am Soc Microbiol* 15:55–63
- Khalil RKS, Skinner C, Patfield S, He X (2016) Phage-mediated Shiga toxin (Stx) horizontal gene transfer and expression in non-Shiga toxinigenic Enterobacter and *Escherichia coli* strains. *Pathogens Dis*. <https://doi.org/10.1093/femspd/ftw037>
- Kondo K, Kawano M, Sugai M, Castanheira M (2021) Distribution of antimicrobial resistance and virulence genes within the prophage-associated regions in nosocomial pathogens. *mSphere*. <https://doi.org/10.1128/mSphere.00452-21>
- Maharjan A, Nepal R, Dhungana G, Parajuli A, Regmi M et al (2022) Isolation and characterization of lytic bacteriophage against multi-drug resistant *Pseudomonas aeruginosa*. *J Nepal Health Res Council* <https://doi.org/10.33314/jnhrc.v19i04.3837>
- Mishra BK, Regmi RK, Masago Y, Fukushi K, Kumar P et al (2017) Assessment of Bagmati river pollution in Kathmandu Valley: scenario-based modeling and analysis for sustainable urban development. *Sustain Water Quality Ecol* 9–10:67–77. <https://doi.org/10.1016/j.swaqe.2017.06.001>
- Nepal R, Houtak G, Shaghayegh G, Bouras G, Shearwin K et al (2021) Prophages encoding human immune evasion cluster genes are enriched in *Staphylococcus aureus* isolated from chronic rhinosinusitis patients with nasal polyps. *Microb Genom*. <https://doi.org/10.1099/mgen.0.000726>
- Nepal R, Houtak G, Wormald P-J, Psaltis AJ, Vreugde S (2022) Prophage: a crucial catalyst in infectious disease modulation. *Lancet Microbe* 3(3):e162–e163. [https://doi.org/10.1016/S2666-5247\(21\)00354-2](https://doi.org/10.1016/S2666-5247(21)00354-2)
- Norwood DA, Sands JA (1997) Physical map of the *Clostridium difficile* chromosome. *Gene* 201(1):159–168. [https://doi.org/10.1016/S0378-1119\(97\)00443-5](https://doi.org/10.1016/S0378-1119(97)00443-5)
- Ooi ML, Drilling AJ, Morales S, Fong S, Moraitis S et al (2019) Safety and tolerability of bacteriophage therapy for chronic rhinosinusitis due to *Staphylococcus aureus*. *JAMA Otolaryngol Head Neck Surg* 145(8):723–729. <https://doi.org/10.1001/jamaoto.2019.1191>
- Petrovic Fabijan A, Lin RCY, Ho J, Maddocks S, Ben Zakour NL et al (2020) Safety of bacteriophage therapy in severe *Staphylococcus aureus* infection. *Nat Microbiol* 5(3):465–472. <https://doi.org/10.1038/s41564-019-0634-z>
- Pirnay J-P (2020) Phage therapy in the year 2035. *Front Microbiol*. <https://doi.org/10.3389/fmicb.2020.01171>
- Schneider CA, Rasband WS, Eliceiri KW (2012) NIH image to imageJ: 25 years of image analysis. *Nat Methods* 9(7):671–675. <https://doi.org/10.1038/nmeth.2089>
- Schooley RT, Biswas B, Gill JJ, Hernandez-Morales A, Lancaster J et al (2017) Development and use of personalized bacteriophage-based therapeutic cocktails to treat a patient with a disseminated resistant *Acinetobacter baumannii* infection. *Antimicrob Agents Chemother*. <https://doi.org/10.1128/aac.00954-17>
- Stothard P, Wishart DS (2004) Circular genome visualization and exploration using CGView. *Bioinformatics* 21(4):537–539. <https://doi.org/10.1093/bioinformatics/bti054>
- Sui B, Han L, Ren H, Liu W, Zhang C (2021) A novel polyvalent bacteriophage vB_EcoM_swi3 infects pathogenic *Escherichia coli* and *Salmonella enteritidis*. *Front Microbiol*. <https://doi.org/10.3389/fmicb.2021.649673>
- Tynecki P, Guziński A, Kazimierzczak J, Jadczyk M, Dastyk J et al (2020) PhageAI - bacteriophage life cycle recognition with machine learning and natural language processing. *bioRxiv*. <https://doi.org/10.1101/2020.07.11.198606>
- Waters EM, Neill DR, Kaman B, Sahota JS, Clokie MRJ et al (2017) Phage therapy is highly effective against chronic lung infections with *Pseudomonas aeruginosa*. *Thorax* 72(7):666. <https://doi.org/10.1136/thoraxjnl-2016-209265>
- Wattam AR, Abraham D, Dalay O, Disz TL, Driscoll T et al (2013) PATRIC, the bacterial bioinformatics database and analysis resource. *Nucleic Acids Res* 42(D1):D581–D591. <https://doi.org/10.1093/nar/gkt1099>
- Yu P, Mathieu J, Li M, Dai Z, Alvarez PJJ et al (2016) Isolation of polyvalent bacteriophages by sequential multiple-host approaches. *Appl Environ Microbiol* 82(3):808–815. <https://doi.org/10.1128/AEM.02382-15>
- Zeng W, Mao P, Hong Y, Feng M, Xu Z et al (2015) Complete genome sequence of the *Salmonella enterica* Serovar Paratyphi A bacteriophage LSPA1 isolated in China. *Genome Announc* 3(1):e01011-01014. <https://doi.org/10.1128/genomeA.01011-14>

Publisher's Note Springer Nature remains neutral with regard to jurisdictional claims in published maps and institutional affiliations.